



**1<sup>st</sup> INTERNATIONAL  
SYMPOSIUM on LIGHT ALLOYS and  
COMPOSITE MATERIALS  
ISLAC'18**

**22-24 MARCH 2018**



**22-24 MART 2018**

**Characterization  
Performance  
Application  
Production  
Recycling  
Joining  
Design**

**Aircrafts  
Biomedical  
Automotives  
Constructions  
Transportations  
Sporting Goods  
Civil Infrastructures**

**1. ULUSLARARASI  
HAFIF ALAŞIMLAR ve  
KOMPOZİT MALZEMELER  
SEMPOZYUMU  
UHAKS'18**

Genişletilmiş Özet Gönderim Son Tarihi  
Deadline for Extended Abstract Submission

**15.12.2017**

[uhaks18@karabuk.edu.tr](mailto:uhaks18@karabuk.edu.tr)

[www.uhaks18.com](http://www.uhaks18.com)

Karabuk University  
Karabuk / Turkey

# ISLAC'18

The Proceedings Book of 1st International Symposium on Light Alloys and Composite Materials March 22-24, 2018 Karabük University, Karabük, TURKEY.

**Edited by**

Prof. Dr. Bilge Demir  
Emre DEMİRCİ

**Assistant Edited by**

Yusuf GÖKALP  
Ali AKKUŞ  
Burcu ÇETİNTAŞ

Copyright

**ISBN 978-605-9554-30-5**

© 28 Aralık 2018, ISLAC'18 Karabuk University  
Karabuk, Turkey  
<http://www.uhaks18.com/>  
[uhaks18@karabuk.edu.tr](mailto:uhaks18@karabuk.edu.tr)

These proceedings include the original papers submitted to ISLAC'18. It is accessed in free of charge. All scientific and linguistic responsibilities of the published articles belong to their authors.

# **1st International Symposium on Light Alloys and Composite Materials**

**22-24 March 2018**  
**Karabük University, Karabük, TURKEY.**

## **HONORARY COMMITTEE**

Prof. Dr. Refik Polat                      Karabuk University,  
Rector

---

## **ISLAC18' CHAIR**

Prof. Dr. Bilge Demir                      Karabuk University

---

## **ORGANIZATION COMMITTEE**

Prof. Dr. Burak Dikici,	Ataturk University
Prof. Dr. Yavuz Sun,	Karabuk University
Assist. Prof. Dr. Sinan Kandemir,	Izmir Institute of Technology
Assist. Prof. Dr. Volkan Kılıçlı,	Gazi University
Assist. Prof. Dr. Nermin Demirkol,	Kocaeli University
Assist. Prof. Dr. Hakan Yılmaz,	Yildiz Technical University
Res. Assist. Dr. Faruk Mert,	Gazi University

---

## **SCIENTIFIC COMMITTEE**

Prof. Dr. Pradeep K. Rohatgi,	University of Wisconsin-Milwaukee
Prof. Dr. Anton Ficăi,	Politehnica University of Bucharest
Prof. Dr. Jufu Jiang,	Harbin Institute of Technology
Assoc. Prof. Dr. Xiaojun Yan,	Dalian University, China
Assoc. Prof. Dr. Masaaki Nakai,	Kindai University, Japan
Assist. Prof. Dr. Ajay Kumar,	Indian Institute of Science Bangalore
Assoc. Prof. Mohamed Abdel-Hady Gepreel,	Egypt-Japan University
Dr. Martin Tauber,	CRM Alliance, Belgium
Dr. Ali Ramazani,	The University of Michigan, USA
Prof. Dr. Hüseyin Çimenoglu,	Istanbul Technical University
Prof. Dr. Ali Kalkanlı,	Middle East Technical University
Prof. Dr. Mehmet Ali Arslan,	Gebze Technical University
Prof. Dr. Fevzi Bedir,	Gebze Technical University
Prof. Dr. Hayrettin Ahlatçı,	Karabuk University
Prof. Dr. Ali Güngör,	Karabuk University
Prof. Dr. Burhanettin İnem,	Gazi University

Prof. Dr. Ramazan Çıtak,	Gazi University
Prof. Dr. Adem Kurt,	Gazi University
Prof. Dr. Hakan Ateş,	Gazi University
Prof. Dr. Serkan Subaşı,	Düzce University
Prof. Dr. Yasin Kişioğlu,	Kocaeli University
Prof. Dr. Onuralp Yücel,	Istanbul Technical University
Prof. Dr. Serdar Salman,	Marmara University
Prof. Dr. Mehmet Gavgali,	Ataturk University
Prof. Dr. Nuri Ersoy,	Bagazici University
Prof. Dr. Sakin Zeytin,	Sakarya University
Prof. Dr. Mustafa Aydın,	Celal Bayar University
Prof. Dr. Bülent Kurt,	Nevsehir Haci Bektas Veli University
Prof. Dr. Mehmet Şimşir,	Cumhuriyet University
Assoc. Prof. Dr. Melik Çetin,	Karabuk University
Assoc. Prof. Dr. Yunus Türen,	Karabuk University
Assoc. Prof. Dr. Habibe Tecimer,	Karabuk University
Assoc. Prof. Dr. Derya Dışpınar,	Istanbul University
Assoc. Prof. Dr. Zafer Tatlı,	Sakarya University
Assoc. Prof. Dr. Zahide Bayer Öztürk,	Nevsehir Haci Bektas Veli University
Assoc. Prof. Dr. Serkan Özel,	Bitlis Eren University
Assist. Prof. Dr. Mehmet Ünal,	Karabuk University
Assist. Prof. Dr. Engin Çevik,	Karabuk University
Assist. Prof. Dr. Ulaş Matik,	Karabuk University
Assist. Prof. Dr. Özkan Öz,	Karabuk University
Assist. Prof. Dr. Hatice Evlen,	Karabuk University
Assist. Prof. Dr. Erkan Koç,	Karabuk University
Assist. Prof. Dr. Hüseyin Tecimer,	Karabuk University
Assist. Prof. Dr. Muhammet Uludağ,	Bursa Technical University
Assist. Prof. Dr. Hanifi Çinici,	Gazi University
Assist. Prof. Dr. Murat Alkan,	Dokuz Eylul University
Assist. Prof. Dr. M. Fatih Toksoy,	Izmir Institute of Technology
Assist. Prof. Dr. Cemal Çarboğa,	Nevsehir Haci Bektas Veli University
Assist. Prof. Dr. Arif Uzun,	Kastamonu University
Assist. Prof. Dr. Ersin Bahçeci,	Iskenderun Technical University
Assist. Prof. Dr. Abdullah Cahit Karaoğlanlı	Bartın University
Dr. Nafiz Yaşar,	Karabuk University

---

## **SECRETARY**

Assist. Prof. Dr. Yakup Kaya,	Karabuk University
Assist. Prof. Dr. Ali Kalyon,	Karabuk University
Assist. Prof. Dr. Okan Ünal,	Karabuk University
Res. Assist. Talha Sunar,	Karabuk University
Res. Assist. Yusuf Ayan,	Karabuk University
Res. Assist. Muhammed Elitaş,	Karabuk University
Res. Assist. Ahmet Serdar Güldibi,	Karabuk University
Res. Assist. Samet Nohutçu,	Karabuk University
Res. Assist. Demet Taştumur,	Karabuk University
Res. Assist. Öznur Dinçel,	Karabuk University
Res. Assist. Tuğçe Köden Yıldız,	Karabuk University
Res. Assist. Güldane Ertuğrul,	Karabuk University
Res. Assist. Muhammet Emre Turan,	Karabuk University
Res. Assist. Yasin Akgül,	Karabuk University
Res. Assist. Alper İncesu,	Karabuk University
Res. Assist. Fatih Aydın	Karabuk University
Res. Assist. Savaş Ağduk	Karabuk University
Res. Assist. Fazıl Husem	Karabuk University
Res. Assist. Safa Polat	Karabuk University
Res. Assist. Yüksel Akınay	Karabuk University

## **METALLURGY AND MATERIALS STUDENT ASSOCIATION KARABUK UNIVERSITY**

Ömür Yazıcı	Karabuk University
Yusuf Gökçalp	Karabuk University
Okan Balcı	Karabuk University
Ali Akkuş	Karabuk University
Çağrı Akı	Karabuk University
Berk Göksu	Karabuk University
Büşra Tom	Karabuk University
Serdal Han	Karabuk University
Salih Bektaş	Karabuk University
Burcu Çetintaş	Karabuk University
Emre Tuna	Karabuk University
İpek Ok	Karabuk University
Ali Emer	Karabuk University
Hakan Gaygısız	Karabuk University
Halil Ocak	Karabuk University
Oğuzhan Doğan	Karabuk University
Berna Merve Asan	Karabuk University
Ebubekir Hacı	Karabuk University
Atakan Boğa	Karabuk University
Nurettin Aydın	Karabuk University

# 1st International Symposium on Light Alloys and Composite Materials

22-24 March 2018  
Karabük University, Karabük, TURKEY.

## PREFACE

Dear governor, dear rector, dear vice rector, dear deans, dear protocol, dear participant, dear guests from either inland or abroad, you are all welcome to International symposium on light alloys and composite materials- on behalf of the committee of ISLAC18,

I salute all of you with respect. Karabük, our city has the heritage city and district of Safranbolu. In Karabük, there are lots of precious places and properties such as Hadrianapolis Ancient city and jungle. And our city Karabük is the same time industrial city with its KARDEMİR that is a first iron steel plant of TURKEY, an integrated and very important and strategic plant.

Karabük has another important precious which this is Karabük university. Karabük university is gaining lots of advantage for Karabük and has lots of nice aims for Karabük. One of these aims of the Karabük university is to make Karabük is a science, a congress and symposium city. Yes, Karabük has this potential.

Hepiniz hoş geldiniz, UHAKS18 organizasyon ekibi adına hepinizi saygı ile selamlıyorum. Yaklaşık 1 yıllık çalışmanın ve emeğin ürünü olarak hafif alaşımlar ve kompozit malzemeler sempozyumunu organize ettik. Ve şimdide açılış ve başlangıcını yapıyoruz. Hayırlara vesile olmasını hepinizin ve hepimizin istifadesini temenni ediyorum.

Sn. Rektörümüz Refik Polat beyin KARABÜK; sahip olduğu turizm potansiyeli ve sanayi şehri hüviyeti ile kongre ve sempozyum şehri olmayı hakediyor düşünceleri ile ortaya koydukları vizyon, mesleğimizin getirdiği sorumluluk ve ülkemizin ihtiyaçları doğrultusunda bir misyon üstlenerek; UHAKS18- ISLAC18'in ilk düşüncelerini Organizasyon komitemizin ilk üyesi Volkan KILIÇLI hocam ile oluşturduk ve kolları sıvadık.

Akademik yönü güçlü ve Üniversite sanayi İş birliği içerisinde bir sempozyum yapma iradesi ile yola çıktık. Sempozyum Ekibimiz kartopu misali zaman içerisinde oldukça büyük bir aileye dönüştü. Organizasyon komitesini farklı üniversitelerimizden oluşturarak yaygın ve homojen bir yapılanma sağlamaya çalıştık. Bütün ekibimizle birlikte UHAKS18 olgunlaştırdık. Sempozyumlar için üniversitelerin anlamı çok büyüktür, bunun değerini bilmemiz gerektiğini düşünüyorum. Arkamızda çok güçlü dostlarımız ve sponsorlarımız olduğunu gördük. UHAKS18- ISLAC18 İstanbul maden ve Metal İhracatçılar Birliğinin ana sponsorluğu, Leica, Mak Elektronik, İCON Kaynak'ın sponsorlukları ve KBÜ kongre koordinasyon merkezinin lojistiği ile gerçekleştirilmektedir. Kendilerine çok teşekkür ederim. ISLAC'18'e yaklaşık 17 ülkeden 397 bildiri ile 667 si Türkiye'den 70 tanesi yurt dışından olmak üzere 737 bilim insanının direkt veya dolaylı katılımı söz konusudur. Sempozyumda sunulan bildiriler ayrıca akademik uluslararası dergilerde yayınlanacaktır. Sempozyumdan sonra bu bildirilerin tam metinlerini dergi planlaması ve seçimlere göre isteyeceğiz.

Bilim insanlarını ve genç nesli teşvik etmek için ödül organize ettik, bunları vefa borcumuz olarak Sayın Prof. Dr. Süleyman SARITAŞ ve Prof. Dr. Yücel BİROL beylerin onurlarına kabul edilmesini istirham ediyorum. Onlar bu ülkeye ve alanlarına çok şey

kattılar. Alaşım ve kompozitler en az bir ortak noktaya sahiptir. Alaşım ve kompozit malzemeler, en az iki bileşenin bir karışımından oluşur. Alaşım ve kompozitler, aynı zamanda, bunları yapmak için kullanılan materyallerle ilişkili özelliklerden farklı özellikler sergilemeleri bakımından da benzerdir. Yapılan yeni çalışmalar ve sağlanan gelişmeler ile Hafif alaşım ve kompozit malzemeler dayanımın özgül ağırlığa oranı açısından çok önemli avantajlar sağlamakta bizlere yeni kapılar ve imkanlar açmakta ve insanoğlunun sınırlarını genişletmektedir. Light weight – ağırlıkta hafif malzemeler olarak ifade ettiğimiz bu malzemeler ekolojik ve tasarım harikası yapıtlar üretmemize sınırları zorlamamıza imkan vermektedirler.

Sizlerin huzurunda; Organizasyon ve bilim komitesine ve sekreteryadaki çok değerli arkadaşlarıma çok teşekkür ederim. Sempozyumu düzenlerken bizimle birlikte olan lojistiğimizi sağlayan Rektör yardımcımız Mustafa YAŞAR bey ve Üniversitemiz genel sekreteri Prof. Dr. Mücahit Coşkun beylerin şahıslarında KBÜ kongre koordinasyon merkezi yönetici ve çalışanlarına, bildiri ile akademik katkı sağlayan siz değerli katılımcılara ve görev alan değerli öğrencilerimize ve özellikle kadim dostum Demir Çelik Enstitüsü Müdürü Prof. Dr. Yavuz SUN bey ve Demir Çelik Enstitüsünün güzide ekibine, Mühendislik ve Teknoloji Fakültelerinin değerli dekan ve çalışanlarına, destek ve paydaşlıklarından dolayı teşekkürü bir borç bilirim.

Son olarak öngördüğümüz “Genç Bilim Adamı” ve “En İyi Poster” ödülleri kahraman kolluk kuvvetlerimiz, gazi ve şehitlerimiz ile üniversitelerimizde eser bırakmış aramızdan ayrılmış bütün bilim adamlarına ithaf etmek istiyorum. Özellikle rahmetli Sayın Prof. Dr. Süleyman SARITAŞ ve Prof. Dr. Yücel BİROL beylerin onurlarına kabul edilmesini istirham ediyorum. Onlar bu ülkeye ve alanlarına çok şey kattılar, yılmaz bir inançla çalıştılar değer oldular, değer ürettiler. Yarınları aydınlık ülkem, ışık saçan bilim ve olgunlaşmış mütevazı aydın bilim insanı, kendine değil topluma çalışan bilim insanı temennilerimle UHAKS18- ISLAC18 komiteleri ve sekreteryası adına hepinizi saygı ile selamlıyorum.

**Chair**

**Prof. Dr. Bilge DEMİR**

## PANELIST ASSOCIATIONS

# 1st International Symposium on Light Alloys and Composite Materials

22-24 March 2018  
Karabuk University, Karabuk, Turkey

## ACKNOWLEDGEMENTS



**Leica**

**MICROSYSTEMS**  
[www.leica-microsystems.com](http://www.leica-microsystems.com)



Malzeme Analiz ve Kalite Kontrol Cihazları Dış Tic. Ltd. Şti.

[www.makelektronik.com.tr](http://www.makelektronik.com.tr)



[www.iconendustri.com](http://www.iconendustri.com)



## INDEX

Paper Title	Page No.
Investigation of Wear and Friction Behavior of High Density Polyethylene (HDPE)/Zinc Borate Composites	1
Effect The Surfactant on The Dispersion and Mechanical Properties of Multi –Walled Carbon(MWCNT) Reinforced Polymer Composites	5
%0,2 La İÇEREN AZ31 KALİTE Mg PLAKALARININ KOROZYON DAVRANIŞINA HADDELEME PARAMETRELERİNİN VE BİLYE PÜSKÜRTME İŞLEMİNİN ETKİSİNİN İNCELENMESİ	13
Al Sıvı Metal İnfiltrasyon İçin Makro Poroz Silisyum Karbür Köpüklerin Sinterleme Davranışına Silisik Asidin Etkisi	16
Tribological Behavior of Poly-ether-ether-ketone Composite Against Unsaturated Polyester Composite and Stainless Steel Counterparts	20
Friction and Wear Performance of Short Carbon Fiber Reinforced Poly-ether-ether-ketone Thermoplastic Composite Against Polymer and Steel Material Counterparts	23
The Influence of Sliding Speed on The Tribological Behaviour of Graphite Powder Filled Polyamide-6 Composite	26
Analysis of Shear Properties of Bonded and Riveted Joints with CFRP Composite Tubes	29
Investigation of Mechanical Properties of Biodegradable PLA Composites	32
Characterization of Poly (Ethylene Terephthalate)/Poly (Butylene Terephthalate) Based Nanocomposites Reinforced with Reduced Graphene Oxide	35
Farklı Yağlayıcılarla Öğütülen Ön Karışimli Alumix 123 Tozların Sıcak Preslenmesiyle T/M Parça Üretimi	40
The Effects of Graphene Additives on the Friction and Wear Performance of Epoxy Composites	44
Sülfolanmış ZSM-5 zeolitin kullanıldığı kompozit katalitik membran üretimi ve karakterizasyonu	47
TIG Kaynağı ile Birleştirilen 7075 Alüminyum Alaşımının Kaynak Bölgesinin İncelenmesi	51
AZ31B Magnezyum Alaşımının TIG Kaynağı Yöntemi ile Kaynaklanabilirliğinin İncelenmesi	54
Titanyum Malzemelerin Patlamalı Kaynak Yöntemi ile Gerçekleştirilen Birleştirmelerin Analizi ve İncelenmesi	59
Effect of Aging Parameters on Mechanical Properties of AlSi8Cu3Fe Aluminium Alloy	64
Effect of Aging Parameters on Wear Behavior of AlSi8Cu3Fe Aluminum Alloy	66
Kendini Onarabilen/İyileştirebilen Metaller ve Metal Matrisli Kompozit Malzemeler	69
Effects of Shot Peening On The Microstructure, Hardness and Surface Roughness Properties of AZ31 and AZ31-%0.5 La Mg Alloys	72
Effect of Heat Treatment on Wear and Corrosion Resistance of Light Al-Based Al-Mg-Sb Alloy Used in Aviation and Automobile Sector	74
Alumix 123 Ön Karışimli Tozların Mekanik Alaşımınma Sürecine Yağlayıcıların Etkisi	77
Öğütülmüş Cu + SiC Takviyesiyle Al Esaslı MMKp Malzeme Üretimi ve Karakterizasyonu	82
Cu + SiC Karışım Tozun Öğütme Süresinin Metal-Seramik Etkileşimine, Toz Boyutuna ve Morfolojisine Etkisi	88
Mechanical and Corrosion Properties of Sn-Zn Alloys Used in Electronics Industry	93
Effect of Integration of Carbon Nanotubes (CNTs) on Flexural Properties of Thermoset Composites	96
Effect of Integration of Carbon Nanotubes (CNTs) on Compression after Impact Properties of Thermoset Composites	99
Effect of Integration of Carbon Nanotubes (CNTs) on Flexural Properties of Thermoplastic Composites	102
Effect of Heat Treatment on Structural, Surface and Mechanical Properties of Al-Based Al-x Mn (x = 0.1, 0.2, 0.3) Alloys	105
Finite Element Analysis of Thrust Force in Drilling of Al2014 Aluminum Alloy	109
Friction And Wear Properties Of T6 Treatment And As-Plated Duplex Ni-P/Ni-B Coatings On AZ91D Magnesium Alloy	113
Investigation of the Properties of Oxide Coating Layer TiO2 on Ti-6Al-4V Alloy by a Thermal Oxidation Method	120
Investigation of the Effect of Cementite Carbide Cutting Tips Coated by ALD Method on Machinability	123
Evaluation of low-velocity impact behaviour of epoxy nanocomposite laminates modified with silica nanoparticles at cryogenic temperatures	128
The Influence of the Grain Size of the Matrix Material on the Mechanical Properties of MMC Made Through Powder Metallurgy Route	132
Borlanmış Fe-Mg Alaşımının Aşınma Davranışının İncelenmesi	138

The Effect of Seawater Aging on the Mechanical Performance of SiO <sub>2</sub> /Epoxy Polymer Nanocomposites	142
Effect of Mg Addition on Al <sub>4</sub> Cu Powder Metallurgy Alloy	145
Preparation of Al <sub>2</sub> O <sub>3</sub> Reinforced Aluminum Matrix Composites by Powder Metallurgy	149
Electrical Conductivity and Microstructure Properties of Cu-Mo Coatings	152
Investigation of Microstructure and Biocompatibility Properties of Ceramic Based Coatings Produced by Plasma Spray Method	156
Static Analysis of Layered Functionally Graded Square Plates	159
Silikotungstik Asit Hidrat Yüklü Kitosan Hibrit Membran Sentezi Ve Sorpsiyon Performansının İncelenmesi	165
Mechanical and Microstructure Properties of Sn-Zn Alloys Used in the Electronic Industry	170
An Investigation on Hardness and Tensile-Shear Stress of Friction Stir Welded Lap Joints of AA 2014 Aluminium Alloys	173
Tufalin Çelik Plaka Yüzeylerinin Temizlenmesinde Kumlama Malzemesi Olarak Kullanılabilirliği Üzerine Bir Araştırma	178
Thermal Energy Storage Properties of Vermiculite Based-Composite PCM With Carbon Nanotubes Additive For Thermoregulation of Buildings	182
Form-Stable Attapulgit/PCM Composite For Thermal Energy Storage in Building Envelopes	186
PATERN KAYNAK YÖNTEMİ İLE 15N20 VE 1075 KALİTE ÇELİKLERİ KULLANILARAK ÜRETİLEN DAMASCUS ÇELİĞİNİN EĞMELİ YORULMA DAVRANIŞININ İNCELENMESİ	190
Comparison of Different Production Methods and Recycled CuSn10 Chips	193
Investigation of Energy Absorption Capacities of DP600 Steel with Al 2024 and AZ31 Light Metal Alloys	196
Recycling of Waste Bronze Wood Chips by Powder Metallurgy	199
PATLAMALI KAYNAK YÖNTEMİ İLE BİRLEŞTİRİLEN ALÜMİNYUM-DEMİR-ALÜMİNYUM TABAKALI KOMPOZİTİN YORULMA DAVRANIŞININ İNCELENMESİ	202
PATLAMALI KAYNAK YÖNTEMİ İLE BİRLEŞTİRİLEN ALÜMİNYUM-DEMİR-ALÜMİNYUM TABAKALI KOMPOZİTİN YORULMA DAVRANIŞININ İNCELENMESİ	205

# Investigation of Wear and Friction Behavior of High Density Polyethylene (HDPE)/Zinc Borate Composites

Mehmet Kurt<sup>#</sup>, Huseyin Unal<sup>+</sup>, Munir Tasdemir<sup>\*</sup>

<sup>#</sup> Institute of Natural and Applied Science, Sakarya University, Sakarya, 54188, Turkey

<sup>+</sup> Department of Metallurgy and Materials Engineering, Faculty of Technology, Sakarya Applied Science University, Sakarya, 54188, Turkey

<sup>\*</sup> Department of Metallurgy and Materials Engineering, Faculty of Technology, Marmara University, Sakarya, 54188, Turkey

Corresponding author: unal@sakarya.edu.tr

**Abstract**— In this experimental study, tribological behaviors of pure high density polyethylene (HDPE) and HDPE composites filled with zinc borate (ZnBr) inorganic filler material in different ratios (5%, 10% and 15%) were investigated. Friction and wear tests were carried out in dry ambient conditions at room temperature and 50% humidity conditions in a pin-on-disc wear device. The tests were carried out against AISI 316L stainless steel disc material under the load of 100N and at three different speeds (1.0, 2.0 and 3.0 m/s). The sliding distance was chosen as 2000m. As a result of the friction and wear tests, the friction coefficients and specific wear rates of the pure HDPE polymer and HDPE based polymer composite materials used in the experiments were determined. In the experiments, the effect of ZnBr filler addition ratio and sliding speed on the specific wear rate and friction coefficient values were investigated. The highest specific wear rate was determined in the HDPE+15% ZnBr polymer composite while the lowest wear rate was observed in the pure HDPE polymer. Wear surface investigations of HDPE polymer and HDPE based composite materials were examined using optical microscope.

**Keywords**— Tribology, HDPE, Zinc borate, friction, wear, composite

**Özet**— Bu deneysel çalışmada yüksek yoğunluklu polietilen (YYPE) ile farklı oranlarda (%5,%10 ve %15) çinko borat (ZnBr) katkılı YYPE kompozitlerin tribolojik davranışları incelenmiştir. Aşınma ve sürtünme deneyleri, kuru ortam, 23° oda sıcaklığında ve %50 nem şartlarında pim-disk aşınma cihazında gerçekleştirilmiştir. Deneyler 100N yük altında ve üç farklı hızda (1.0 2.0 ve 3.0 m/s gibi) AISI 316L paslanmaz çelik disk malzemeye karşı 2000m kayma yolunda yapılmıştır. Aşınma ve sürtünme deneyleri sonucunda deneylerde kullanılan polimer ve kompozit malzemelerin sürtünme katsayıları ve spesifik aşınma oranları tespit edilmiştir. Deneylerde aşınma oranı ve sürtünme katsayısına YYPE polimerine ilave edilen ZnBr katkı oranı ile birlikte kayma hızının etkisi de araştırılmıştır. Deneylerde en yüksek aşınma oranı YYPE+%15ZnBr polimer kompozitinde tespit edilirken, en düşük aşınma oranı ise saf YYPE polimerinde gözlenmiştir. YYPE polimer ve kompozit malzemelerin aşınma yüzey incelemeleri ise optik mikroskop kullanılarak incelenmiştir.

**Anahtar Kelimeler**— Triboloji, YYPE, Çinko borat, sürtünme, aşınma, kompozit

## I. INTRODUCTION

Although the use of polymer materials in the world and in our country has increased a lot, many metal and metal based materials in different areas of the industry continue to take their places and become alternative materials. However, physical, mechanical, thermal and chemical properties of pure polymers are not desirable. For this reason, glass fibers, carbon fibers, aramid fibers and wood fibers etc. can be used to improve these weak properties of polymers. such as strength enhancers, glass balls, glass spheres, wollastonite, calcite (CaCO<sub>3</sub>), talc, kaolin, zinc oxide, zinc borate, alumina, graphite and filler and cost-reducing additives are added. There are many studies in the literature on polymer based composites. Some of these are as follows. Manjunath et al. [1] studied the tribological properties of coconut shell powder reinforced and glass fiber reinforced epoxy resin has been investigated. Maysa et al. [2] investigated the effects of CaCO<sub>3</sub> mineral filler on the mechanical properties of high density polyethylene (HDPE)/ethylene propylene diene elastomer (EPDM) polymer blend. Kocabas et al. [3] produced phenolic based composite material by adding 5%, 10%, 20% and 30% by weight of mussel shell powder into the composite material consisting of copper, phenolic resin, barite, alumina and graphite investigated the effect of mussel shell powder on the tribological and mechanical properties of these composites. As a result of the tribological tests, a slight increase in the rate of wear was observed with the effect of mussel shell powder. They also found a reduction in friction coefficient. In addition, as a result of the hardness tests, it was determined that as the addition of mussel shell powder in the composite material increased, the hardness values increased. Tasdemir et al. [4] studied the effect of fillers such as talc, calcite, glass fiber and talc/calcite additives in 5%, 10%, 15% and 20% separately to the high density polyethylene polymer. The hardness, impact and tribology properties of the HDPE based composite materials were investigated. As a result of the hardness tests, it was found that all the additives added to the HDPE polymer increased the hardness of the composites. The highest hardness value was found in 20% glass fiber doped HDPE composite (60 shore D), while the lowest hardness value

## II. EXPERIMENTAL

was determined in HDPE composite with calcite/talc. In addition, the impact strength of composite materials decreased with the addition of talc, calcite, glass fiber and talc/calcite admixtures added into the HDPE polymer material. When the abrasion test results are examined, the highest wear rate is determined in 20% glass fiber reinforced HDPE polymer composite [4]. In another study, Qu et al. [5] performed copper and silicon dioxide (SiO<sub>2</sub>) in 0.1% to 0.6% by weight of poly-tetra-fluoro-ethylene (PTFE) polymer and carried out a 30-minute wear test at 3950N load at 1450 rpm. As a result of the experiments, while the rate of additive added to the PTFE polymer increased, the wear rate decreased, while the friction coefficient of SiO<sub>2</sub> filled poly-tetra-fluor-ethylene composite decreased slightly, but a slight increase was observed in the others. In recent years, the use of zinc based mineral additives in polymers has also increased. A limited number of studies on zinc additives have been studied in recent years. Some of these are as follows. Naga et al. [6] produced composite material by adding nano-sized ZnO filler at 1%, 2%, 4% and 6% by weight to the polyethylene (PE) polymer. Pin-on-disc wear test machine was used in the experiments. ZnO filled PE composite pin materials were used against steel disc and tribological tests were performed. 5-20N applied loads were used in friction and wear tests. As a result of all experiments, a slight increase was observed in the wear rate of PE based composites with addition of nano-size ZnO. The highest wear rate was determined in PE composite material with 6% ZnO content. At the same time, an increase in the specific wear rate was observed with increasing applied load. Simonsen et al. [7] investigated the mechanical properties of high density polyethylene (HDPE) composite with varying proportions of zinc borate (ZnBr) at 10% to 60% by weight. As a result of the experiments, it was observed that the specific wear rate increased with increasing applied load [6]. As a result of the experiments carried out, it was found that the tensile strength, elastic modulus and% elongation values of the composite were decreased with the increase of zinc borate additive ratio in the composite. When the results of the above literature are examined, mechanical, physical and tribological properties of many different polymer and polymer based composite materials including HDPE polymer were investigated. However, in the literature, a study on the mechanical and tribological properties of a few zinc-reinforced composite materials has been studied.

In this study, the friction and wear behaviors of zinc borate powder filled HDPE polymer composites were investigated in order to eliminate the deficiency in the literature. In the study, tribological experiments were performed under 100N load, in the sliding speed range of 1.0-3.0 m/s. The experiments were carried out at  $23 \pm 1$  °C room temperature,  $58 \pm 2\%$  humidity condition and 2000m sliding distance. As a result of the tribological experiments, zinc borate added to the HDPE polymer caused the coefficient of friction of the composite to decrease, while the specific wear rate increased. In addition, it was observed that zinc borate inorganic filler material in the composite caused abrasive wear.

### A. Materials

In this experimental study, YI666UV commercial coded high density polyethylene material was used as polymer matrix material. HDPE polymer material was obtained from PETKİM, Izmir, Turkey. Zinc borate additive SC-467 with commercial code was supplied by Jinan ShiChao Chemical Company Ltd, Shandong, China. In the study firstly, HDPE polymer composites with zinc borate were produced in a granular form by mixing in various proportions (5%, 10% and 15wt.%) in a twin screw extruder. Then, the wear test specimens were produced by Injection moulding machine using the molds prepared according to the standards. The injection molding machine is Turkish and Yonca brand and it has 400 grams capacity.

### B. Sample preparation

The friction and wear tests of HDPE polymer and HDPE based polymer composite materials which are prepared in accordance with ASTM G99 standard against AISI 316L stainless steel material have been carried out. Tribological experiments were performed on a pin-disc wear device. Pin materials used in the experiments are manufactured by injection molding method with 6 mm diameter and 50 mm length. The disc materials were first turned 100 mm in diameter and 5 mm in thickness and then surface grinded. The surface roughness of the steel disc was measured by surface profile and the surface roughness was measured as 0.35  $\mu\text{m}$ , Ra. The hardness of Brinell of stainless steel disc is maximum 217. In tribological experiments, friction coefficient and specific wear rate values were determined. The coefficient of friction is calculated by the formula  $\mu = F_s / F_n$  where  $F_s$  is friction force and  $F_n$  is normal force. The specific wear rate was calculated with the formula  $W_s = \Delta m / \rho x L x N$  where  $\Delta m$  is weight loss before and after wear test,  $\rho$  is density of polymer or composites, L is sliding distance and N is normal load applied to the polymer pin sample in the wear test.

## III. RESULTS AND DISCUSSIONS

Figure 1 shows the relationship between friction coefficient and sliding speed for pure HDPE polymer and different amount (5, 10 and 15wt.%) of zinc borate inorganic filler filled HDPE composites. The friction coefficients increased with the increment of sliding speed by 300% for pure HDPE polymer and HDPE composite materials filled with 5, 10 and 15wt.% zinc borate powder. While the ratio of increase in friction coefficient was found to be 18.9% for pure HDPE polymer, the increasing ratio in coefficient of friction for HDPE composites with 5%, 10% and 15% zinc borate powder were determined about 19.8%, 14.5% and 12.5%, respectively. The friction coefficient of the 15% ZnBr filled HDPE composite was determined to decrease by approximately 12.7% when compared to that of pure HDPE polymer.

Figure 2 shows the relationship between friction coefficient and sliding distance of pure HDPE polymer and its composites used in the experiments. When the figure is carefully examined, the coefficient of friction has stabilized approximately 400m sliding distance when the pure HDPE polymer and zinc borate powder filled HDPE composites work on a stainless steel disc. As a result of the experiments carried out at 100N load and 1.0 m/s sliding speed, the friction coefficient of HDPE composites with 15% zinc borate powder was determined to be approximately 0.17. The average friction coefficients of HDPE composites with 5% and 10% zinc borate powder were determined as 0.18 and 0.19, respectively.

Figure 3 shows the relationship between specific wear rate and the sliding speed of HDPE composites filled with different ratios of zinc borate powder under 100N applied load. As seen in this figure that the specific wear rate increased with the increase in sliding speed. By increasing the sliding speed by 300%, the specific wear rates of HDPE polymer and HDPE composites filled with 5%, 10% and 15% zinc borate powder increased by 70.6%, 105%, 108% and 113%, respectively. As shown in the figure that, the addition of zinc borate additive into the HDPE polymer composite increases the specific wear rate of the polymer composite materials. Among the materials used in the experiments, the lowest specific wear rate was obtained in the pure HDPE polymer while the highest specific wear rate was obtained in 15% zinc borate powder filled HDPE composite. The reason for the higher specific wear rate of the composite by the addition of zinc borate powder filler into the HDPE polymer can be explained by the fact that the zinc borate additive surface is unmodified or there is no surface modification to interface link the zinc borate additive with polymer such as amino-silane coupling agent.

Figure 4 presents the wear surface image of the HDPE+15% ZnBr polymer composite which shows the highest specific wear rate. As shown in the micrographs that the abrasion mechanism of the HDPE based composite material can be expressed as abrasive wear according to the results of the wear and friction test performed at high speed such as 3.0 m/s. Continuous and deep traces are observed on the composite surface. Moreover, the wear surface shows worn polymer particles, but no adhesion to the composite wear surface has been observed.

Figure 1. The relationship between friction coefficient and sliding speed of pure HDPE polymer and different amount of (5%-15wt.%) zinc borate powder filled HDPE composites (applied load: 100N)

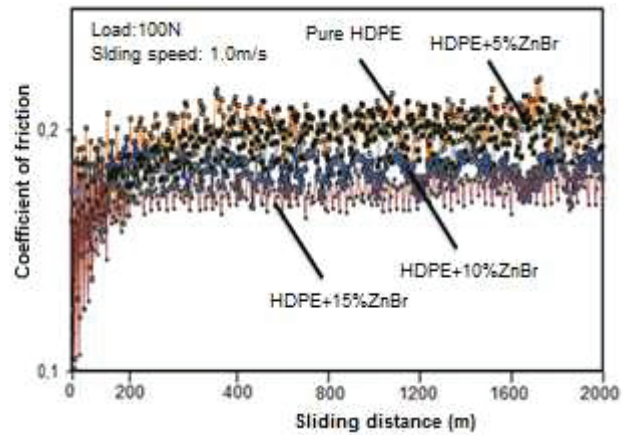


Figure 2. The relationship between friction coefficient and sliding distance of pure HDPE polymer and different amount of (5%-15wt.%) zinc borate powder filled HDPE composites (applied load: 100N and sliding speed:1.0m/s)

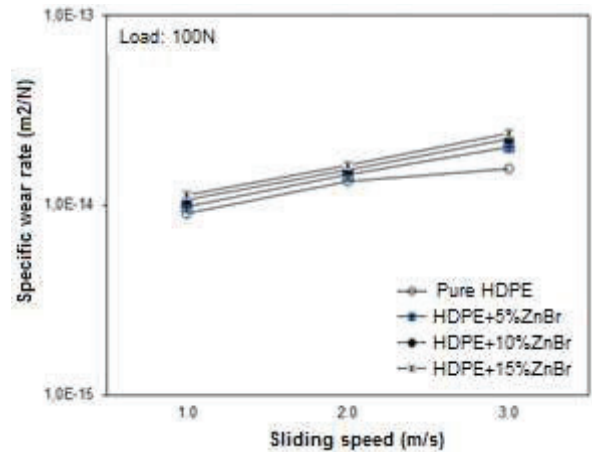


Figure 3. The relationship between specific wear rate and sliding speed of pure HDPE polymer and different amount of (5%-15wt.%) zinc borate powder filled HDPE composites (applied load: 100N)

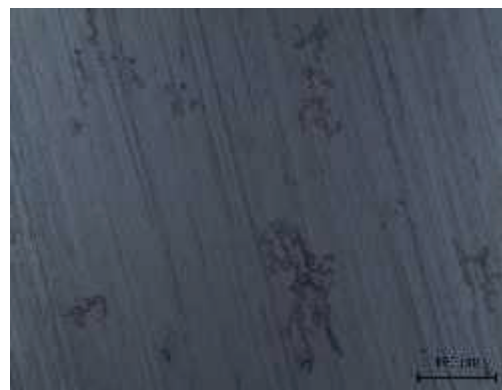
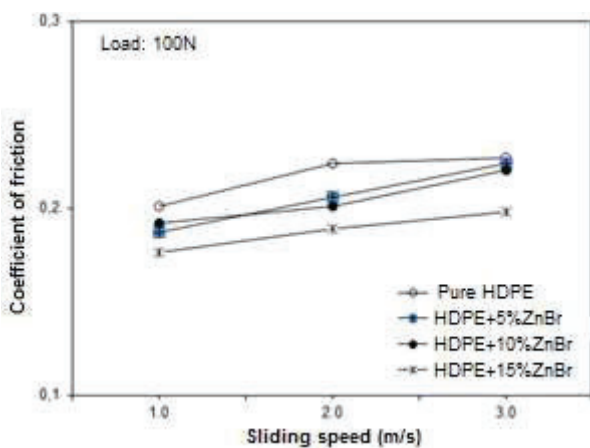


Figure 4. Microstructural images of optical microscope under the dry sliding conditions of HDPE + 15% ZnBr composite (Sliding speed: 3.0m/s, applied load: 100N)

#### IV. CONCLUSIONS

1. The specific wear rate values of both the pure HDPE polymer and the zinc borate powder filled HDPE polymer composites in different ratios (5-15% by weight) increased with increasing speed.
2. The lowest specific wear rate was obtained in pure HDPE polymer material, while the highest specific wear rate was obtained in 15wt.% ZnBr powder filled HDPE composite under the load of 100N and at the sliding speed of 3.0 m/s.
3. By increasing sliding speed, the coefficient of friction values increased with different amount of zinc borate powder filled HDPE composite.
4. The highest coefficient of friction was obtained in the pure HDPE polymer material, while the lowest coefficient of friction was determined under the load of 100 N and at the sliding speed of 3.0 m/s in the 15wt.% ZnBr powder filled HDPE polymer composite.
5. The friction coefficient and the specific wear rate are highly influenced by the material combination and the sliding speed.
6. The wear mechanism of the 15wt.% zinc borate filled HDPE composite at a sliding speed of 3.0m/s and under 100 N load can be characterized as abrasive wear.

#### REFERENCES

- [1] Manjunath, B.H., Prahlad, R.K., Dry Sliding Wear of Coconut Shell Powder Filled Glass Fiber Reinforced Polymer Composites, IRJET., 3 (6), 2395-0072, 2016.
- [2] Maysa, A., Mohamed, N.A., Shaltout, A.A., El, M., The effect of gamma irradiation and particle size of CaCO<sub>3</sub> on the properties of HDPE/EPDM blends, Arabian Journal of Chemistry., 4, 71–77, 2011
- [3] Kocabaş, I., Pıhtılı, H., An Experimental Investigation on Usability of Mussel Shells as a Candidate of Filler Material in Semi-organic Brake Linings, ICNES.,2015.
- [4] Taşdemir, M., Relation Between Microstructure and Tribological Properties of High Density Polyethylene Hybrid Composites Filled with Untreated Glass Spheres, Talc and Calcium Carbonate, Key Engineering Materials, 592-593, 655-659, 2014.
- [5] Qu, M., Yao, Y., He, J., Ma, X., Feng, J., Liu, S., Hou, L., Li, L., Tribological Study of Polytetrafluoroethylene Lubricant Additives Filled with Cu Microparticles or SiO<sub>2</sub> Nanoparticles, Tribology International., 110, 57–65, 2017.
- [6] Naga, R.B., Ramji, K., Prasad, V. S. R. K., Studies on Tribological Properties Of ZnO Filled Polymer Nanocomposites, Journal of Engineering and Applied Sciences., 6, (6), 2011.
- [7] Simonsen, J., Camille, M., Silva, A., Morrell, J.J., Wood/plastic Ratio: Effect on Performance of Borate Biocides Against a Brown Rot Fungus, Holzforschung., 58, 205–208, 2004.

# Effect The Surfactant on The Dispersion and Mechanical Properties of Multi –Walled Carbon(MWCNT) Reinforced Polymer Composites

Hatice YAKUT PEKTÜRK\*, Fatih Öz<sup>+</sup>, Sina Narimani Gharajeh<sup>+</sup>, Nuri ERSOY<sup>+</sup>, Bilge DEMİR<sup>+</sup>

\*Department of Mecanics, Gedik University Vocational High School, İstanbul, Turkey  
[hatice.yakut@gedik.edu.tr](mailto:hatice.yakut@gedik.edu.tr)

<sup>+</sup>Department of Mechanical Engineering, Boğaziçi University  
İstanbul, Country  
[faith.oz@boun.edu.tr](mailto:faith.oz@boun.edu.tr), [sinanarimani24@gmail.com](mailto:sinanarimani24@gmail.com), [nuri.ersoy@boun.edu.tr](mailto:nuri.ersoy@boun.edu.tr)

<sup>+</sup>Department of Mechanical Engineering, Karabük University  
Karabük, Turkey  
[bdemir@karabuk.edu.tr](mailto:bdemir@karabuk.edu.tr)

**Abstract**— It is well known that the homogeneous incorporation of a small concentration of carbon nanotubes (CNTs) in epoxy matrices can enhance the mechanical properties of the composites. However, CNT has a tendency to aggregate during mixing with epoxy resin due to the high van der Waals interaction energy between CNT particles. In order to overcome this problem surfactants are used during sonication to promote the homogenous dispersion of CNT in suspension. MWCNT-epoxy composites were prepared by mixing MWCNT in epoxy matrix by sonification as shown schematically in Figure 1. In this study, different surfactants were used in suspensions with different sonication time to examine their effects on homogeneous dispersion of multi-walled carbon nanotubes (MWCNT) in the epoxy matrix. Homogeneous dispersion of MWCNTs in the epoxy matrix were evaluated by optical microscope. The developed nanocomposites were also characterized mechanically by tensile test. The morphology of the fractured surfaces of neat carbon fibre reinforced polymeric (CFRP) composites and CNT reinforced CFRP nanocomposites after the tensile test was investigated using SEM. The experimental results showed that the good dispersion stability of MWCNTs is obtained with addition of BYK 9077 and BYK9076 as a surfactants and the increase of ultrasonication time improves the dispersion stability. Best result were obtained for 2 hours of sonication and 80 % sonication amplitude. It has been observed that the addition of MWCNT to CFRP composites improves the mechanical strength of the composite material. Optical images of MWCNT-epoxy nanocomposites are shown in Figure 7, and SEM images of fracture surfaces of MWCNT-epoxy-CF composites are shown in Figure 10.

**Keywords**— carbon fibre reinforced polymeric (CFRP), multi-walled carbon nanotubes (MWCNT), surfactant, BYK 9077, BYK9076

## I. INTRODUCTION

Engineering polymers are used in a wide number of applications due to their high flexibility, processability and relatively low cost. However, many polymers have low absolute strength and poor fracture toughness, limiting their applications in structural components [1]. The introduction of

CNTs into conventional fiber-reinforced polymer composites is thus assumed to significantly improve composite performance [2,3]. Paucity of structural defects in association with extraordinary high elastic modulus and strength, and exceptional high aspect ratio propels the use of carbon nanotube (CNT) in polymeric composites for applications like aerospace, automobile, sports goods, and energy [4]. Do we have to achieve a structure of completely separated CNTs homogeneously dispersed in the epoxy matrix or not? Fact is, that a good impregnation of the nanofillers is the prerequisite for an efficient exploitation of the potential benefit from CNTs as structural reinforcement. A combination of impregnated agglomerates and isolated nanotubes can be considered to be a favourable state of dispersion for at least some purposes [2].

The performance of carbon/epoxy is significantly improved if uniform dispersion of carbon nanofillers in the matrix, and strong interfacial bonding between the matrix and the filler are achieved. Weak interfacial bonding limits load transfer from the epoxy matrix to the fillers. Therefore, strong interfacial bonding and homogeneous dispersion of fillers are critical for maximizing reinforcement. However, carbon nanomaterials usually tend to re-aggregate and stack because of the strong van der Waals force and/or high surface area, restricting their applications in polymer nanocomposites [5]. To overcome these challenges, ultrasonication, high shear mixing, surfactants, chemical treatments using weak acids, and functionalization have been applied [6]. Effective strategies to improve the dispersion and interface interaction of carbon nanomaterials in a polymeric matrix have been systematically reviewed by many researchers [7]. There are two approaches for CNTs functionalization including covalent functionalization and noncovalent functionalization [8]. The covalent functionalization is usually characterized by oxidizing CNTs in an acid in order to attach carboxylic or hydroxyl groups to the end-caps or defect sites of CNTs [9]. It can dramatically improve the interfacial interaction between the nanotubes and polymer matrices via direct chemical

bonding [10]. Noncovalent functionalization is an alternative method for modifying the wall of CNTs [11]. Each method has its benefits and limitations. Mechanical methods do not permanently stabilize the dispersion and may shorten the CNTs if the excessive ultrasonication is used. Covalent methods, such as incorporating -OH or -COOH groups onto CNT surface are efficient in stabilizing the dispersions, but can result in the creation of a large number of defects on the CNT surface, and in some extreme cases, the fragmentation of CNTs. These damaging effects lead to degradation in mechanical properties of CNTs. In contrast, the physical surface treatment of CNTs is particularly attractive, as it assists in retaining the original mechanical (and electrical) properties of the CNTs. In the physical surface treatment, CNTs are dispersed in a solvent solution with the aid of dispersants and ultrasonication, prior to the addition of the epoxy resin. During the sonication, while CNT bundles break down to individual CNTs, dispersant molecules adsorb on the surface of the CNT [12].

Lukas Schlagenhauf et al. [13] observed that strong agglomeration occurred at >5% CNT content and concomitantly the mechanical properties degraded. Therefore they used the optimal concentration of around one percent.

Loos et al. [14] reported that the L 7602 and BYK 9077 copolymers were suitable for homogeneously dispersed and long-term stable suspensions of CNTs. They also investigated the combination of dispersing agents to develop the properties of CNT-epoxy systems and concluded that the combination of dispersing agents did not show any advantage over a single dispersing agent.

Zhao and Gao [15] reported high levels of stability and self-dispersion of CNTs in the presence of BYK copolymers. They believed that relatively higher dispersion degrees of CNTs in the epoxy resin could be attributed to less agglomeration of CNTs provided by the strong steric stabilization of the lengthy hydrocarbon chain on the dispersant. Although they stated that the strong steric repulsion of adsorbed dispersant molecules on the CNT surface could explain the high time dependent dispersion degree of CNT in solvent, the interaction between the dispersant molecules is not only dependent on steric repulsion. While interactions between dispersant molecules can arise from steric repulsion, the electrostatic repulsion forces can also be responsible, and little has been studied on the effect of such a repulsive force on CNT dispersion.

Koroyem et al. [13] reported that an increase in sonication energy initially leads to more CNT dispersion, although after a certain value of sonication energy, the level of dispersion remains constant. The lower interaction energy of CNTs with larger (40–60 nm) diameter, compared to those with smaller diameter (10–20 nm), the larger diameter nanotubes showed a great ability to be dispersed, while CNT length showed no significant effect on the degree of dispersion. For greater CNT dispersion additives were incorporated. Copolymers which were able to disperse the CNTs primarily by steric repulsion were found to be more influential than those which dispersed the CNTs mainly by

electrostatic repulsion, such as oleic acid. A sample of 0.1 wt.% CNT-epoxy composites demonstrates the optimal CNT dispersion for the materials and parameters investigated in this work, and lead to a modest improvement in mechanical properties. Incorporation of 0.1 wt.% CNT into epoxy lead to enhancement of about 10% and 10% in epoxy strength and Young's modulus respectively compared to that of pure epoxy without reduction at elongation at breakage.

Lin et al. [16] Reported that the good dispersion stability of MWCNTs is obtained with addition of sodium dodecylbenzene sulfonate (SDBS) as a surfactant, and the increase of ultrasonication time improves the dispersion stability. Dispersion stability of multi-walled carbon nanotubes in refrigerant with addition of surfactant.

Rezazadeh et al. Reported that The visual inspection of CNT dispersion in xylene revealed that combining the dispersant and ultrasonication may be considered as an effective method for improving nanotube dispersion and obtaining dispersion stability for at least 48 h [17].

Dhiraj Kumar et al. was prepared Workpiece specimen by using woven type glass fiber of 600 gsm. A Symmetric laminates were prepared using twelve layer of glass fiber, of stacking order [45/-45],[45/-45], [30/-60], [30/-60], [30/-60], [0/90] // [0/90], [30/-60], [30/-60], [30/-60] [45/-45], [45/-5]. For the mechanical properties of specimen, two types of test has been carried out flexural strength test and inter-laminar shear strength (ILSS) test. They reported that amount of MWCNT (%0.5,%1,%1.5) increased mechanical properties of GFRP [18].

Subhra Gantayat et al. [19] explained that Substantial enhancement of Young's modulus and tensile strength was observed with incorporation of f-MWCNT into epoxy resin. Maximum increases in both the properties were achieved at 0.6% of f-MWCNT loading.

Jeamin Cha et al. [20] reported that at 3wt% and 5wt% M-CNT/Epoxy nanocomposite, modulus and strength were reduced due to agglomeration of CNTs in epoxy matrix.

## II. EXPERIMENTAL

### A. Material

The epoxy resin and hardener (EPOSIS 120) was purchased from OMNIS composite Turkey. Resin/Hardener ratio was 100:60. The (-COOH) Functionalized Multi Walled Carbon Nano Tubes were supplied by Grafen Chemical Industries Co. Turkey with outside diameter 10-20 nm, length 5-10  $\mu\text{m}$  and purity > 96%. The dispersant (BYK9077 and BYK9076) was supplied from Pınar Kimya Co, Turkey. Ethanol as solvent was purchased from Çakır Kimya Co, Turkey. Carbon fiber fabric was supported from METXY Composite Co, Turkey.

### B. Preparation of the MWCNT-epoxy nanocomposites

In this study; Three different kind of MWCNT as %0.5,%1,%1.5 were used. Various surfactants such as BYK9077, BYK9076 were applied for mixture. The homogeneous distribution of MWCNT is the main parameters

of sonication time and the use of surfactant. In order to investigate the effect of sonication time and understand the effect of dispersant agents on the CNT dispersion, two types of surfactant and three different ratio of MWCNT were used to prepare samples.

As shown in Fig. 1; Multi-walled carbon nanotube composite were prepared in two steps. In order to obtain a plate with dimensions of 300x300 mm; at the first stage, the mixture was prepared, composed with respect to the following formulation. For sample were computed separately such as %0.5, %1 and %1.5 MWCNT (1.5 gr, 3 gr, 4,5 gr) percent of weight of 300 gr epoxy resin, besides this surfactant (3gr,6gr,9gr) of 2:1 ratio of proportion of gravity of MWCNT, all these added in 200 ml ethanol. This solution was stired for 15 min on the hot plate, subsequently. An ultrasonic mixer (UIP2000hdT, Hielscher) was used to disperse the MWCNT and disperdant into solvent. Immediately after 300 gr epoxy resin was added in the mixture and sonicated 1 more hour at fixed 80 % sonication amplitude.

At the second stage, in order to evaporate the ethanol from the solution, the mixture was hold on at room temperature at 96 hours. Hardener was added into the mixture at weight ratio to epoxy, 60:100 and stired for 10 min. The mixture was then placed in a vacuum oven at 15 min. for degassing stage. The mixture was directly transferred onto the surface of +45/-45 carbon fiber fabric by vacum infuision process and cured for 48 h at room temperature. Table I shows the details of the prepared samples with composition "specimens".

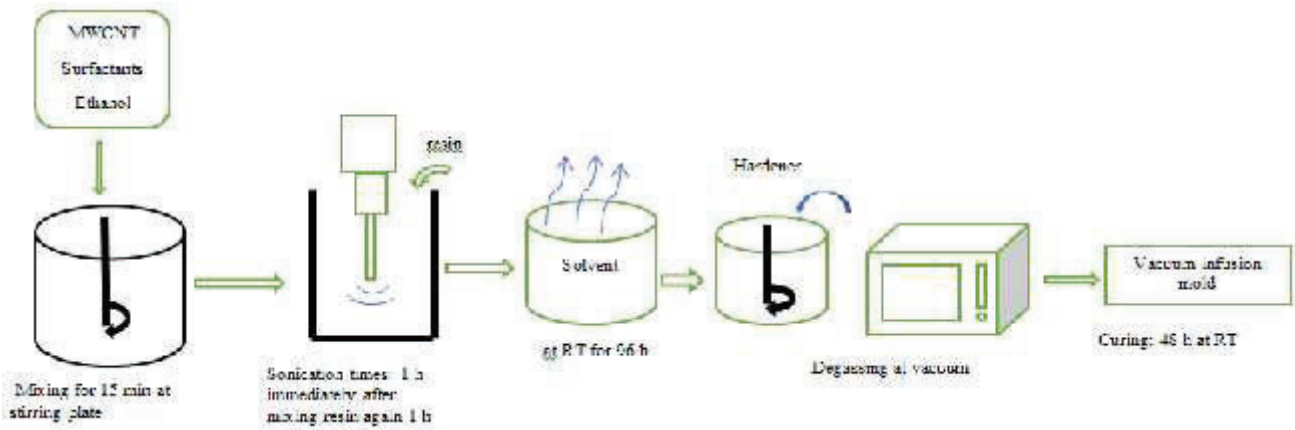


Fig. 1 Schematic diagram of the fabrication process for the MWCNT-epoxy composites

TABLE I  
 DETAILS OF THE PREPARED SAMPLES WITH COMPOSITION "SPECIMENS"

Samples Number	Samples	Matrix	MWCNT	Surfactant	Reinforcement
1	Epoxy resin.	Epoxy Resin	%0	%0	45/-45 Carbon Fabric
2	MWCNT-reinforced epoxy resin.	Epoxy Resin	%0.5	%0	45/-45 Carbon Fabric
3	MWCNT-reinforced epoxy resin.	Epoxy Resin	%0.5	BYK9077	45/-45 Carbon Fabric
4	MWCNT-reinforced epoxy resin.	Epoxy Resin	%1	BYK9077	45/-45 Carbon Fabric
5	MWCNT-reinforced epoxy resin.	Epoxy Resin	%1.5	BYK9077	45/-45 Carbon Fabric
6	MWCNT-reinforced epoxy resin.	Epoxy Resin	%0.5	BYK9076	45/-45 Carbon Fabric

Vacuum infusion technique was used to produce the fiber-reinforced composites (Fig. 2). Six laminates in dimensions of 300 mm x 300 mm x 1 mm with different MWCNT concentrations and carbon fiber orientation were manufactured according to ASTM D3039 standard (Fig.3). The laminates were cut with a water-cooled circular diamond saw; six samples with 250 mm long and 25 mm width were obtained from each composite plate in accordance with the ASTM D3039. End-tabs are attached to the prepared samples to prevent possible failure from the grip regions.



Fig. 2 Vacuum infusion technique



Fig. 3 Sample of ASTM D3039 standard

### C. Mechanical Testing

All tensile tests were conducted in an INSTRON 8801 servo-hydraulic machine, rated to 100 kN (Fig. 4). At least Five samples of specimens were tested, for reproducibility assessment. Tensile tested mechanical properties include tensile strength, tensile strain. video extensometer was used to measure the axial strain of the specimens.

### D. Results and Discussions

1) *Homogeneous Distribution of MWCNT*: This mixture was further homogenised using a variety of dispersing tools including sonication time and surfactant (Fig. 5). The effects of sonication time on MWCNT dispersion in solution as well as on the breakage of MWCNTs, are investigated using visual observation such as; optical microscope and SEM. The model IMM 901 series metallurgical microscopes are used for identification and analysis of the different structures made from composites, metals and various alloys. The IMM 901 are equipped with a 10x,20x,40x and 100x objectives lens (Fig. 6).

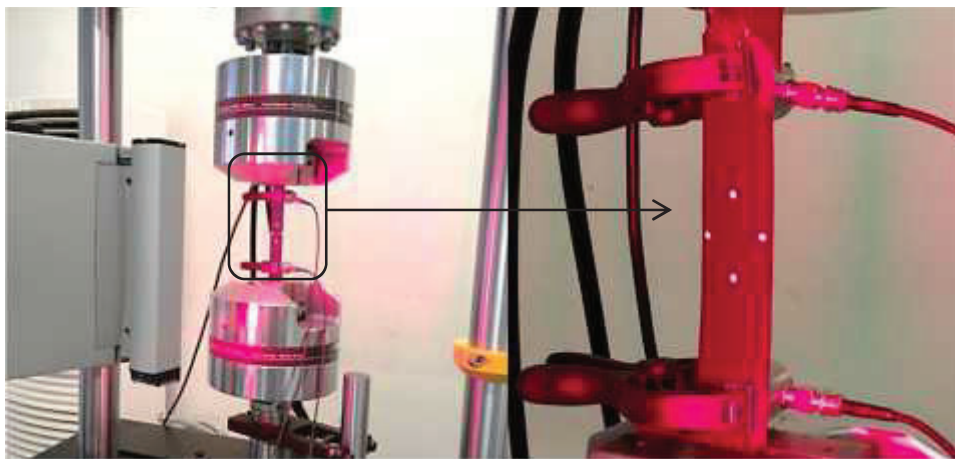


Fig. 4 Tension Tests with INSTRON 8801 servo-hydraulic test machine



Fig. 5 Stability of MWCNT dispersions a) t:1 hour b)2 hour (a:MWCNT, surfactant,ethanol b:MWCNT,surfactant,resin)

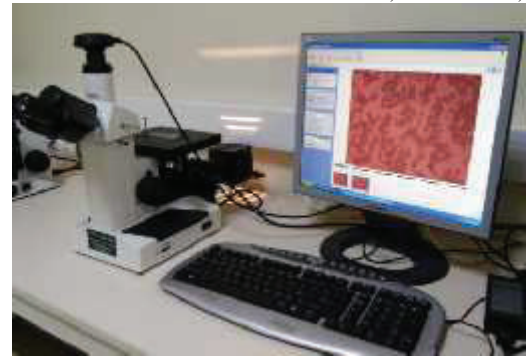


Fig. 6 Optical Microscope



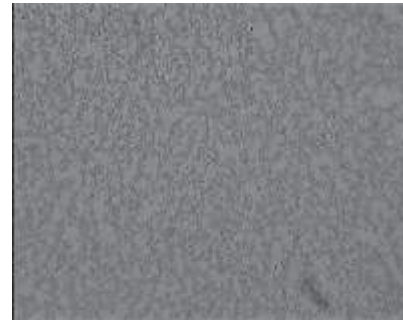
a)10x



b)10x



c)10x



d)10x



e)20x



e)20x

Fig. 7 Optical images recorded on MWCNT-dispersion a) after MWCNT and ethanol were mixed for 1 h at Hielscher Ultrasonic b) immediately after the resin was mixed for 1 h c) after the BYK9077,MWCNT,ethanol were mixed for 1 h at Hielscher Ultrasonic d)immediately after the resin was mixed for 1 h then ethanol was evaporated e) after the BYK9076,MWCNT,ethanol were mixed for 1 h at Hielscher Ultrasonic f)immediately after the resin was mixed for 1 h then ethanol was evaporated

Fig. 7 (a) shows the optical image of the microstructure of MWCNT and ethanol dispersion without surfactant that were mixed for 1 hour at Hielscher Ultrasonic sonicator. Fig. 7 (b) shows the microstructure of resin added mixture without the surfactant that was mixed for 1 hour again. It is clear that without the surfactant, MWCNTs immediately start to re-agglomerate after 2 hours due to the strong interparticle van der Waals interactions. Therefore, ultrasonication time alone is not able to provide homogeneous distribution in solution. Fig. 7(c) and (e)

illustrate the evolution of BYK 9077 and BYK 9076 in ethanol solution corresponding to 1 h sonication times, respectively. It was not sufficient for dispersion. In Fig. 7 (d) and (f), it is clearly visible that; The mixtures were homogeneously distributed after 2 hours sonication time. Thus, it seems that 2 hours sonication time is sufficient to disperse the MWCNT particles efficiently. Fig. 8 shows the SEM images of table I samples.

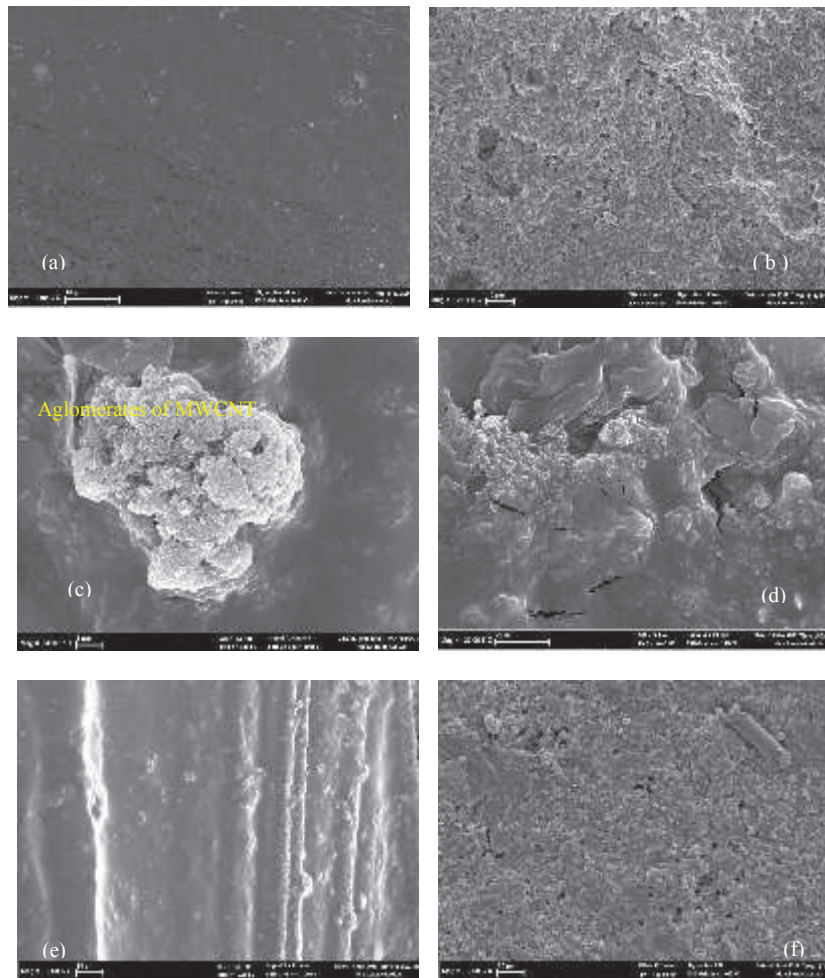


Fig. 8 SEM images of table I samples a)Sample 1 b)Sample 3 c-d)sample 2 e)sample 4 f)sample 5

### E. Mechanical Properties

The effect of MWCNT concentration on the shear strength of carbon fiber reinforced MWCNT/epoxy matrix composites is shown in Fig. 9. There is an overall increase of the shear strength with increasing MWCNT contents up to 0.5 wt%-MWCNT, with a maximum value of approximately 24 MPa (which is 50 % higher than in the absence of MWCNT). However, it was observed that there is not increase of the shear strength value by adding

surfactant (BYK9077) to solution comparing to pure epoxy. The Shear Strength of 1 wt.%MWCNT–BYK9077 epoxy composite and 1,5 wt.%MWCNT–BYK9077 epoxy composite are 14.5 MPa and 12.8 MPa respectively. As can be seen that the shear strength value decrease with increasing MWCNT contents and adding dispersant when compared with pure epoxy resin. The reinforcing efficiency of the MCNTs in this study is comparable with those reported in literature.

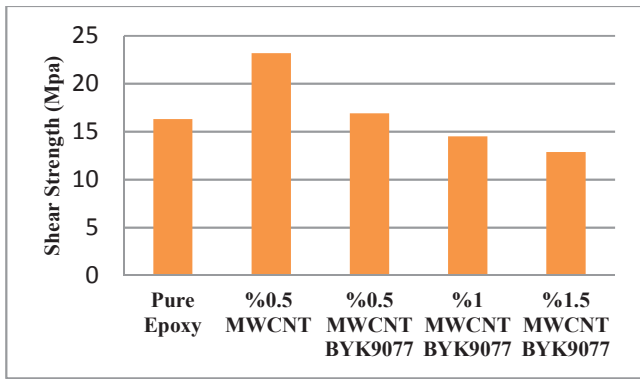


Fig. 9 The effect of MWCNT concentration on the Shear Strength of carbon fiber reinforced MWCNT/epoxy matrix composites

(Fig.10 a) shows that the fracture plane seems to have smooth surface after fracture, indicating complete debonding along the CF/epoxy interphase. Moreover, the observed interphase cracks suggest that these cracks most probably initiated in the form of debonding at the interface, propagated through the interphase, and then transferred to the matrix and eventually to final failure. These are similar with Moaseri et al's results [21]. These observations show that the onset of damaging sites at various locations along

the fiber/matrix interface suggests the presence of poor interfacial bonding [22]. Fig. 10.b shows the results of the sample containing deposition of MWCNTs. In comparison to neat epoxy deposition of MWCNTs on carbon fibers decrease the carbon fiber pull-out which may be attributed to more energy dissipation due to improved adhesion in the interphase. Addition of MWCNT in the matrix has increased the extent of fiber/polymer adhesion as can be observed in sample 2 composite.

The deposited-MWCNTs may lead to mechanical interlocking between the reinforcement and the matrix which can increase the interfacial friction and decrease the phase movements in the interphase. This is similar to the observations in a previous study [21]. Substantial area of fiber surface is still adhered with the matrix at Fig 10.b. However observations in of Fig. 10.c,d,e reveal that the matrix deformation is higher in samples 1,3,4,5 composites as compared to sample 2 composite. These composite samples showed matrix deponding and fibers pull out.

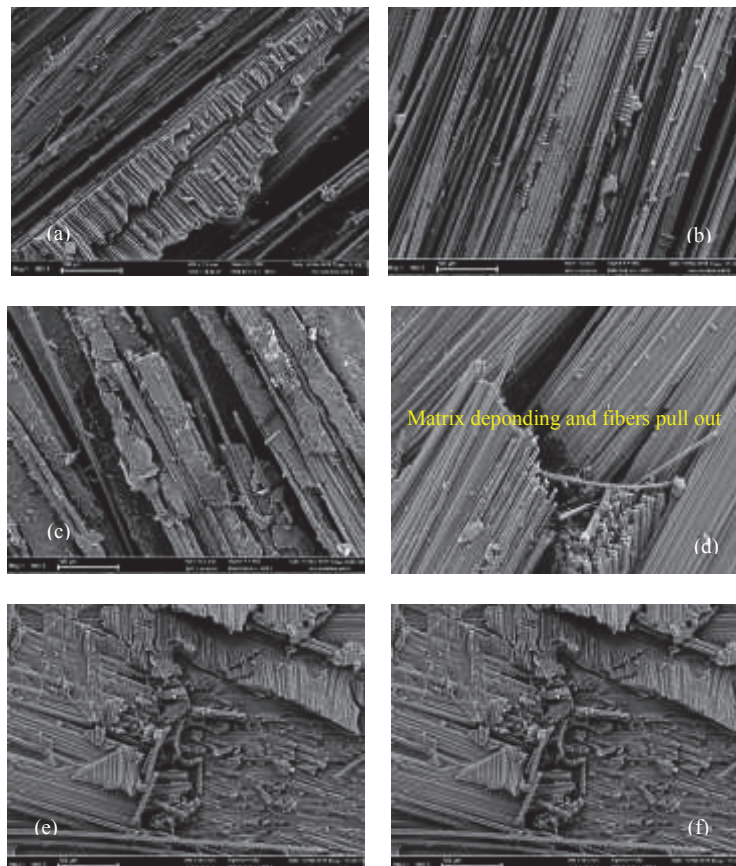


Fig. 10 SEM images of fracture surface of Table 1. samples a)Sample 1 b)Sample 2 c)sample3 d)sample 4 e-f)sample 5

### III. CONCLUSIONS

The good dispersion equality of MWCNTs in epoxy is achieved with addition of BYK9077 and BYK9076 due to their excellent adsorption capability on the MWCNT surface. In order to obtain homogeneous dispersion of MWCNT in solvent and epoxy matrices, it is important to use a set of compatible key parameters such as sufficient sonication time, a strong dispersant, together with appropriate MWCNTs. We found that the sonication time has a significant influence on the MWCNT dispersion up to a certain value of sonication time. The results of optic microscope showed that the quality of MWCNT dispersion is dependant to sonication time. Time duration of about 2 hours is efficient enough to disperse the MWCNTs. This study shows that the incorporation of %0.5 MWCNT as matrix filler in carbon fiber reinforced epoxy results in improvement on mechanical properties. 2 wt.% BYK9077 of % MWCNT reduces mechanical properties of nanocomposite. Adding of %1 and %1.5 MWCNT to solution reduce mechanical performance of BYK9077-nanocomposite. we supposed that ratio of surfactant into suspension can be excessive therefore the binding energy of the material may be reduced.

### ACKNOWLEDGMENT

This work was supported by Scientific Research Project Coordinator of Karabük University, Mechanical engineering Composite Research Laboratory of Boğaziçi University and Metallurgy Laboratory of Gedik University Vocational School. Carbon fabrics and dispersants were supplied by METYX Composites and Pınar Kimya. The authors are heartily thankful for the sponsorships of aforementioned Universities and Companies.

### REFERENCES

- [1] I. Zaman, T.T. Phan, H.C. Kuan, Q.S. Meng, L.T.B. La, L. Luong, et al., "Epoxy/graphene platelets nanocomposites with two levels of interface strength", *Polymer*, 52, 1603–1611, (2011)
- [2] F. Gojny, M. Wichmann, U. Köpke, B. Fiedler, K. Schulte "Influence of different carbon nanotubes on the mechanical properties of epoxy matrix composites" –A comparative study, *Composite Science Technology*, 65, 2300-2313, (2004)
- [3] F. Gojny, M. Wichmann, B. Fiedler, I. Kinloch, W. Bauhofer, A. Windle, et al., "Evaluation and identification of electrical and thermal conduction mechanisms in carbon nanotube/epoxy composites", *Polymer*, 47, 2036–2045, (2006)
- [4] L. Schlagenhauf, B. Kianfar, T. Buerki-Thurnherr, Y. Kuo, A. Wichser, F. Nüesch, et al., "Weathering of a carbon nanotube/epoxy nanocomposite under UV light and in water bath: impact on abraded particles", *Nanoscale*, 7, 18524–18536, (2015)
- [5] C. Bao, Y. Guo, L. Song, Y. Kan, X. Qian, Y. Hu, "In situ preparation of functionalized graphene oxide/epoxy nanocomposites with effective reinforcements", *Journal of Materials Chemistry*, 21, 13290-13298, (2011)
- [6] S. Park, D.S. Kim, "Curing behavior and physical properties of an epoxy nanocomposite with amine-functionalized graphene nanoplatelets", *Composite Interfaces*, 23, 675-687, (2016)

- [7] S. Liu, V. S. Chevali, Z. Xu, D. Hui, H. Wang, "A review of extending performance of epoxy resins using carbon nanomaterials", *Composites Part B*, 136, 197-214, (2018)
- [8] Z. Spitalsky, D. Tasis, K. Papagelis, C. Galiotis, "Carbon nanotube-polymer composites: chemistry, processing, mechanical and electrical properties", *Progress in Polymer Science*, 35, 357-401, (2010).
- [9] L. Liu, K.C. Etika, K.S. Liao, L.A. Hess, D.E. Bergbreiter, J.C. Grunlan, "Comparison of covalently and noncovalently functionalized carbon nanotubes in epoxy", *Macromolecular Rapid Communication*, 30, 627-632, (2009).
- [10] W. Zhou, S.C. Lv, W.F. Shi, "Preparation of micelle-encapsulated single-wall and multi-wall carbon nanotubes with amphiphilic hyperbranched polymer", *Macromolecular Nanotechnology*, 44, 587-601, (2008).
- [11] A. Korayem, M.R. Barati, S. J. Chen, G. P. Simon, X. L. Zhao, W. H. Duan, "Optimizing the degree of carbon nanotube dispersion in a solvent for producing reinforced epoxy matrices", *Powder Technology* 284, 541–550, (2015)
- [12] L. Schlagenhauf, B. Kianfar, T. B. Thurnher et al., "Weathering of a carbon nanotube/epoxy nanocomposite under UV light and in water bath: impact on abraded particles", *Nanoscale*, 44, (2015)
- [13] M.R. Loos, et al., "Effect of block-copolymer dispersants on properties of carbon nanotube/epoxy systems", *Composite Science Technology*, 72 482–488, (2012).
- [14] L. Zhao, L. Gao, "Stability of multi-walled carbon nanotubes dispersion with copolymer in ethanol", *Colloids Surf. A Physicochem. Eng. Asp.* 224 (1–3), 127–134, (2003).
- [15] L. Lin, H. Peng, G. Ding, "Dispersion stability of multi-walled carbon nanotubes in refrigerant with addition of surfactant", *Applied Thermal Engineering*, 91, 163-171, (2015)
- [16] V. Rezazadeh, M. R. Pourhossaini, A. Salimi, "Effect of amine-functionalized dispersant on cure and electrical properties of carbon nanotube/epoxy nanocomposites", *Progress in Organic Coatings*, 111, 389–394, (2017)
- [17] D. Kumar, K.K. Singh, "An experimental Investigation of The Effect of MWCNT on The Machinability of Glass/Epoxy Polymeric Nanocomposite Material", *Machining Science and Technology*, (2015).
- [18] S. Gantayat, D. Rout, S. K. Swain, "Mechanical properties of functionalized multiwalled carbon nanotube/epoxy nanocomposites" *Materials Today: Proceedings* 4, 4061–4064, (2017)
- [19] S. Gantayat, D. Rout, S. K. Swain, "Mechanical properties of functionalized multiwalled carbon nanotube/epoxy nanocomposites" *Materials Today: Proceedings* 4, 4061–4064, (2017)
- [20] J. Cha, G.H. Jun, J.K. Park, J.C. Kim, H.J. Ryu, "Improvement of modulus, strength and fracture toughness of CNT/ Epoxy nanocomposites through the functionalization of carbon nanotubes", *Composites Part B*, 129, 169-179, (2017)
- [21] E. Moaseri, M. Karimi, M. Maghrebi, M. Baniadam, "Two-fold enhancement in tensile strength of carbon nanotube-carbon fiber hybrid epoxy composites
- [22] R. K. Prusty, D. K. Rathore, B. C. Ray, "Evaluation of the role of functionalized CNT in glass fiber/epoxy composite at above- and sub-zero temperatures: Emphasizing interfacial microstructures", *Composites: Part A*, 101, 215–226, (2017).

# %0,2 La İÇEREN AZ31 KALİTE Mg PLAKALARININ KOROZYON DAVRANIŞINA HADDELEME PARAMETRELERİNİN VE BİLYE PÜSKÜRTME İŞLEMİNİN ETKİSİNİN İNCELENMESİ

Soner ARI, Yaren KARAUĞUZ, Medine KILINÇ, İsmail Hakkı KARA, Yavuz SUN, Yunus TÜREN  
Okan ÜNAL, Hayrettin AHLATCI\*,

Karabük Üniversitesi, Metalurji ve Malzeme Mühendisliği Bölümü, Karabük 78000 Turkey

\*Corresponding author: hahlatci@karabuk.edu.tr

**Abstract** -- In this study, the effect of shot peening process on the corrosion resistance, microstructure analysis, roughness and hardness parameters of the extruded AZ31, AZ31 + 0.2% La containing Mg alloy hot rolled plates was investigated.

## I. GİRİŞ

Düşük yoğunluğu ve sahip olduğu özel mukavemeti (mukavemet/ağırlık) sayesinde geniş kullanım alanına sahip Magnezyum (Mg) alaşımları ilgi çekici malzemeler arasındadır. Buna rağmen Mg malzemelerin düşük sertlik değerleri ve zayıf korozyon dirençleri uygulama alanlarını daraltmaktadır [1]. Sıcak haddeleme işlemi uygulanmış Mg plakaların sertlik değerlerini ve korozyon direncini arttırmak için film kaplamaları [2,3], shot peening ve alaşım elementi ilaveleri ile söz konusu olabilmektedir.



Şekil 1. AZ31 ve AZ31+%0,2 La içeren Mg plakalar

Bu çalışma da kullanılan AZ31 ve AZ31+%0,2 La içeren Mg plakalarına uygulanan shot peening ve alaşım elementi ilavesi işlemlerinin deneysel sonuçlara etkisini incelenmiştir. Aynı zamanda shot peening işleminde püskürtme süresini literatür kaynaklı çalışmalar ışığında değiştirerek yaptığımız deneysel çalışmalara etkisi gözlemlenmiştir [4].

## II. DENEYSEL ÇALIŞMALAR

Kullanılan AZ31 ve AZ31+%0,2 La içeren Mg plakalarının kimyasal analizinden elde edilen sonuçlar Tablo.1'de verilmiştir.

Tablo 1. AZ31 ve AZ31+%0,2 La Kalite Mg Plakalarının Kimyasal Kompozisyonları

	Al	Zn	Mn	La	Mg
AZ31	%2,9	%0,98	%2,13	-	Bal.
AZ31 + %0,2 La	%2,91	%1,02	%0,15	%0,22	Bal.

### A. Shot Peening

Shot peening işleminde, S110-AISI1070 standardının çelik bilya kullanılmış olup, işlem 10 dakika, 20 dakika ve 30 dakika boyunca 8 bar basınç altında, 10 cm nozul mesafesinde gerçekleştirilmiştir (Şekil 2).



Şekil 2. Kullanılan bilyalar ve Shot peening cihazı

### B. Pürüzlülük Testi

Atış işleminden sonra, yüzeyde oluşan pürüzlülüğü ölçmek için yüzey pürüzlülüğü testi SV-3100 marka test cihazıyla yapılmıştır (Şekil 3).



Şekil 3. Surface roughness (Evaluation type Surface Roughness Measurement Surface test SV-3100)

### C. Sertlik Testi

Sertlik testi sağlıklı sonuç almak amacıyla 2 ayrı test cihazı olan SHIMADZU ve QNEES marka cihazlarla 0,05 kg yük altında yapılmıştır. Sertlik ölçümleri her bir numune için yüzeyden 30 µm içerde 100 µm aralıklarla 500 µm derinliğe kadar ölçülmüştür. Her bir derinlik mesafesinden en az 5'er kez ölçüm yapılmış ve ortalamaları alınmıştır.

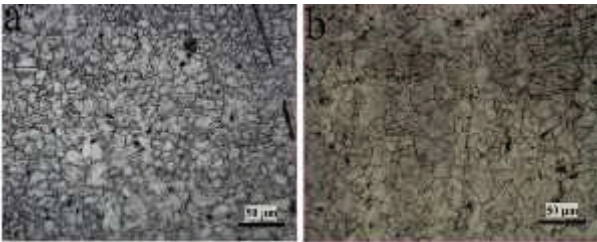
### D. Korozyon

Korozyon direncini belirlemek için daldırma yöntemi ile korozyon uygulanmıştır. Daldırma 24 saat boyunca %3,5 NaCl ve damıtılmış su ile gerçekleştirilmiştir.

## III. DENEYSEL ÇALIŞMALARIN SONUÇLARI

### A. Optik Mikroskop Sonuçları

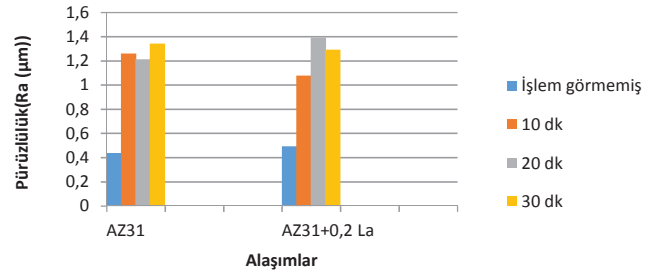
Optik mikroskop analizinde hadde sonrası alınan görüntüler de literatür kaynaklı yapılan çalışmalar baz alınarak yeniden kristalleşmiş taneler ve ikizlenmelerin olduğu tahmin edilmektedir (Şekil 4).



Şekil 4. Optik Mikroskop Görüntüleri a)AZ31 b)AZ31+%0,2 La

### B. Pürüzlülük Testi Sonuçları

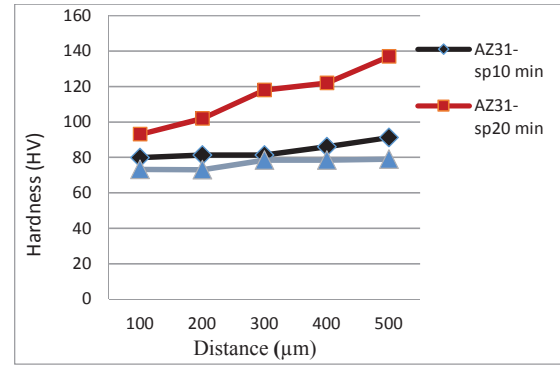
Pürüzlülük testi sonuçlarında her iki malzemede de shot peening işleminin pürüzlülüğü artırdığı görülmüştür. AZ31 kalite malzeme için 20.dk'da malzemenin tüm yüzeyinin maksimum pürüzlülüğe ulaştığı belirlenmiştir. Bu durum AZ31+%0,2 La malzeme için 30. dk'da gözlemlenmiştir (Şekil 5).



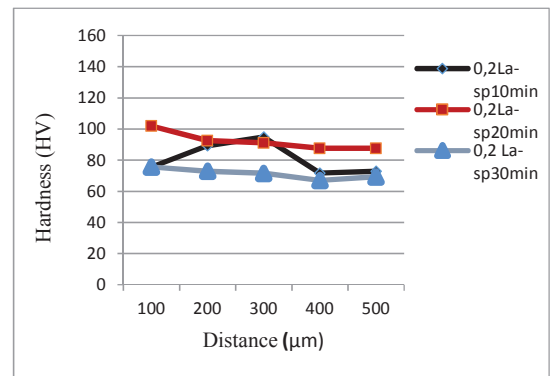
Şekil 5: Pürüzlülük testi sonuç grafiği

### C. Sertlik Testi Sonuçları

Alınan sertlik değerleri sonucunda her iki malzemede de shot peening işleminin 10.dk'sından 20.dk'sına efektif bir yükselme gözlemlenmiştir (Şekil 6). 30.dk'da bir miktar düşme görülmüştür. Bunun sebebi aşırı shot peening'den kaynaklı kısmi bir yumuşama olabileceği düşünülmektedir. Soğuk deformasyon sonrası bu kadar düşmesi beklenilmemekte olup; bu düşüş mikroyapı ile arasında ki bağımsız farklılıklardan yani tane ikizlenmesi ve/veya tane irileşmesi gibi durumlardan kaynaklanabileceği düşünülmektedir. AZ31 kalite Mg plakaya %0,2 La elementi ilaveli malzemeye yaptığımız shot peening işleminin sertliği olumsuz yönde etkilediği belirlenmiştir [6].



(a)

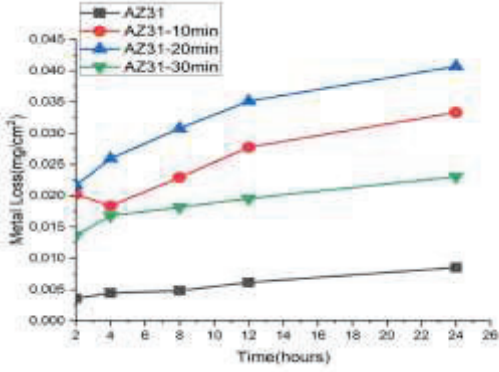


(b)

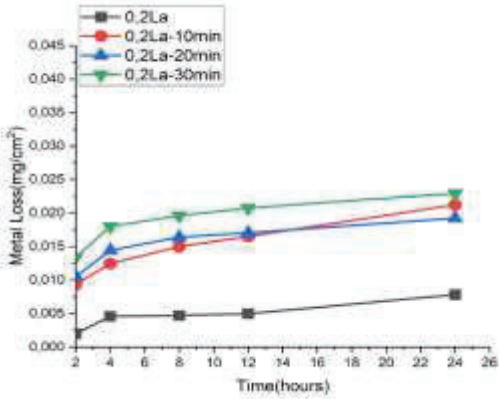
Şekil 6. Sertlik sonucu grafikleri a) Schimadzu b) Qnees test cihazında yapılan test sonuçları

#### D. Korozyon Testi Sonuçları

İncelenen alaşımların korozyon testi sonuçları Şekil 7'de gösterilmiştir. Shot peening işlemi yoğunlaştıkça korozyon olumsuz yönde etkilenmiştir. Bunun nedeni de literatür kaynaklı yaptığımız araştırmalar da shot peeningin etkisiyle pürüzlülüğün arttığı dolayısıyla yüzey alanını arttırdığı için korozyona karşı direnç azalır. 0,2 La ilaveli Mg esasl malzemenin korozyona karşı daha dirençli olduğu gözlemlenmiştir. Bu durum La elementinin ilavesinden kaynaklıdır [6,7].



(a)



(b)

Şekil 7. Korozyon testi sonuçları a) AZ31 Mg alaşımı  
b) AZ31-%0,2 La Alaşımı

#### Teşekkür

Bu çalışma TÜBİTAK 2209-A Üniversite Öğrencileri Araştırma Projeleri Destekleme Programı kapsamında 1919B011701874 numaralı proje olarak desteklenmiştir.

#### Referanslar

- [1] FuyongCao, ZhimingShi, Guang-LingSong, MingLiu, Matthew S. Dargusch, AndrejAtrens, Influence of hot rolling on the corrosion behavior of several Mg-X alloys, CorrosionScience, Volume 90, (January 2015), Pages 176-191
- [2] Dejiu SHEN, Haojie MA, Changhong GUO, Jingrui CAI, Guolong LI, Donglei HE, Qingxiang YANG, Effect of Cerium and Lanthanum additives on plasma electrolytic oxidation of AZ31 Magnesium alloy, Journal of Rare Earths, Volume 31, Issue 12, (December 2013), Pages 1208-1213
- [3] Hu, Henry, XueyuanNie, andYueyuMa. "Corrosion and Surface Treatment of Magnesium Alloys." Magnesium Alloys-Properties in Solid and Liquid States, In-Tech, Croatia (2014): 67-108
- [4] Ünal, O. (2011). Bilyalı Dövme İşleminin Tane Boyutuna Etkisinin Deneysel İncelenmesi. Bartın Üniversitesi, Fen Bilimleri Enstitüsü, Yüksek Lisans Tezi, 93s, Bartın.
- [5] A. Pardo, M.C. Merino, A.E. Coy, R. Arrabal, F. Viejo, E. M Atykina, Corrosion behaviour of Magnesium/Aluminium alloys in 3.5 wt. % NaCl, CorrosionScience, Volume 50, Issue 3, March 2008, Pages 823-834
- [6] Kara, İ. H., Ahlatçı, H., Türen, Y., & Sun, Y. (2018). Microstructure and corrosion properties of lanthanum-added AZ31 Mg alloys. Arabian Journal of Geosciences, 11(18), 535.
- [7] Seçgin G.O., İkiz Merdaneli Sürekli Döküm Yöntemi ile Üretilmiş AZ31 Magnezyum Alaşımının Korozyon Davranışının İncelenmesi, Doktora Tezi, (2012)

# Al Sıvı Metal İnfiltrasyon İçin Makro Poroz Silisyum Karbür Köpüklerin Sinterleme Davranışına Silisik Asidin Etkisi

Ebru YILMAZ<sup>1</sup> \*, Fatih ÇALIŞKAN<sup>2</sup>

Metaller ve Malzeme Mühendisliği Bölümü, Sakarya Üniversitesi, Sakarya, 54187, Türkiye

\* ylmaz.ebruu@gmail.com, fcaliskan@sakarya.edu.tr<sup>2</sup>

**Özet**—Bu çalışmada metal matrisli kompozit üretmek için alüminyum sıvı metal infiltrasyonunda kullanılacak makroporoz seramik köpüklerin üretimi hedeflenmektedir. Ana malzemesi olarak partikül formda silisyum karbür, sıvı faz oluşturuca katkı olarak MgO, Al<sub>2</sub>O<sub>3</sub>, SiO<sub>2</sub>, Na<sub>2</sub>O, stabilizör olarak silisik asit türevi solüsyon kullanılmıştır. Hazırlanan seramik çamuru kullanılarak replikasyon yöntemi ile seramik köpükler üretilmiştir. Çalışmanın odak noktasını seramik köpüğün sinterleme davranışına silisik asit türev katkısının etkisi ve nihai ürünün bağlantı kollarının morfolojisine, mukavemetine etkisinin incelenmesidir. Yapılan çalışmalarımızdan elde edilen verilere göre optimum olarak belirlenen sinterleme sıcaklığı 1200 °C' de 90 dakikadır. Sinterlenen numunelerin karakterizasyonu Makro Stereo Mikroskop kullanılarak gerçekleştirilmiş olup gözenek çapının artışı ve strut duvarlarının şekillerini koruduğu görülmüştür. Optimum elde edilen seramik köpüğün basma mukavemet değeri 145 N'dur.

**Anahtar Kelimeler**— Seramik Köpük, Metal Matrisli Kompozit, Silisyum Karbür, Polimerik Sünger, Replikasyon Yöntemi

**Abstract**—In this study, it is aimed to produce macroporous ceramic foams to be used in aluminum liquid metal infiltration for the fabrication of aluminium matrix composite. Silicon carbide in particulate form as a starting material and MgO, Al<sub>2</sub>O<sub>3</sub>, SiO<sub>2</sub>, Na<sub>2</sub>O as the liquid phase forming additives was used to obtained a strut structure. Silicic acid derivatives was added to the slurry composition as stabilizer. Ceramic foams were produced by replication method using the prepared ceramic clay. The aim of this study was to investigate the effect of silicic acid derivative on the sintering behavior of ceramic foam, and the morphology and strength of the net shape connecting arms. Results of the work showed that the optimum sintering temperature was 90 minutes at 1200°C. Investigation of Stereo Microscope was revealed that increase in the ration of silicic acid derivative in the sintered samples enhanced the pore diameter and caused a lightly change in shape of strut walls. The compression strength of optimum ceramic foam was obtained 145 N.

**Keywords**— Ceramic Foam, Metal Matrix Composite, Silicon Carbide, Polymeric Sponge, Replication Method

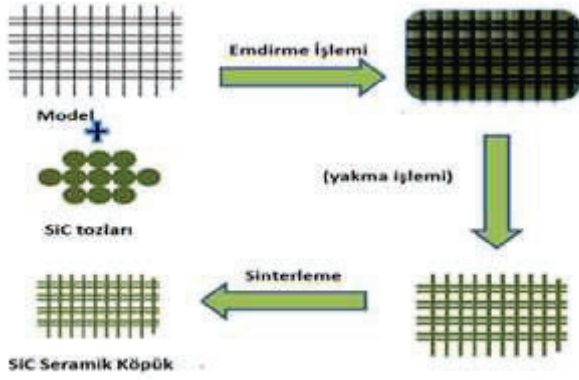
## I. GİRİŞ

Gözenekli seramikler şekillerine göre iki kategoride sınıflandırılabilir. Bunlar bal petek şekilli (honeycomb) ve

köpük (foam) şekilli seramiklerdir. Köpük seramikler birbirleriyle temas halindeki açık boşlukların devamlı bir seramik bağ ile bağlanması sonucu oluşan üç boyutlu gözenekli malzemelerdir. [1] Son yıllarda aşırı gözenekli seramik malzemelerin üretimi ve kullanımı konusunda önemli bir ilgi artışı olmaktadır. Bu tür malzemeler yüksek yüzey alanı, yüksek geçirgenlik, düşük yoğunluk, düşük özgül ısı ve yüksek ısı yalıtımı gibi özelliklerinden dolayı tercih edilmektedir. [2] Rastgele dağılmış partikül yapısına sahip köpük seramikler poroz yapıda olup metal infiltrasyonunda takviye (güçlendirici) görevi görüp kompozit malzeme üretiminde kullanılmaktadır.[3]Köpük seramik üretiminde SiC'nin tercih edilme nedeni düşük ısıl genleşme katsayısı, termal iletkenlik ve mekanik mukavemet özellikleridir.[4] Seramiklerin başka kullanım alanları; sıcak gaz filtreleri, petrokimya endüstrisinde kullanılan katalitik destekler ve dizel motor egzoz filtreleridir.[5]

Köpük seramik üretim yöntemlerinin başlıcaları; polimer sünger metodu(replikasyon yöntemi), direk köpükleştirme ve karbon preformların CVD/CVI (Chemical Vapour Deposition/ Chemical Vapour Infiltration) yöntemleriyle kaplanmasıdır. [4]

Polimer sünger metodu, 1963'te çıkarılan ilk patent olan, kontrollü makroporoziteli seramik üretimi için geliştirilen ilk imalat tekniklerinden biridir. Bununla birlikte, hala endüstride en yaygın kullanılan tekniktir.Replikasyon yönteminde birçok farklı polimer kullanılabilir; bunlar poliüretan (PU), poli (vinil klorür) (PVC), polistiren (PS) ve selüloz içerir. İşlem açık hücreli bir polimer malzemesi seramik çamurlar ile kaplanmasını içerir. Fazla çamurun polimerden uzaklaştırılması ve kurutulmasıyla, polimer yanar ve seramik tek bir aşamada sinterlenir.Akış şeması Şekil 1. ' de gösterilmektedir. [2]



Şekil 1. Replikasyon prosesinin akım şeması [8]

## II. DENEYSEL ÇALIŞMALAR

### A. Reçetenin Oluşturulması

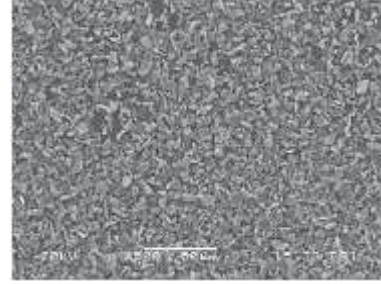
Silisyum karbür esaslı köpük seramik filtre üretiminde iskelet yapıyı teşkil edecek polimer malzemesi olarak Kurtoğlu Filtre Otomotiv Paz. San. Tic.Ltd. Şti' den temin edilen 10 PPI (Inc basına düşen por) gözenek yoğunluğundaki poliüretan süngerler kullanılmıştır. İskelet yapıyı oluşturacak ince ve kalın SiC tozları Fetaş Metalurji' den % 99.5 safiyette temin edilen tozlar, toz boyutu ölçümleri sonucunda tozların % 50' sini oluşturan toz boyut aralığı sırasıyla 5 µm ve 77 µm olarak belirlenmiştir. Şekil 2. ' de SiC tozunun SEM görüntüsü ve EDS analizi gösterilmiştir.

Seramik çamur için hazırladığımız numuneler kullanılan bağlayıcı ve malzeme cinsine ve miktarlarına göre sınıflandırılmış ve kodlar verilmiştir. Bu kodlar; hazırlanan SiC seramik çamur içinde kattığımız malzemeler bentonit, magnezyum oksit , alüminyum oksit ve silika olan malzeme cinsine göre adlandırılmaktadır. Ağırlıkça % 30 Bentonit SiC tozuna eklediğimizde 1B ve belirtilen 1B seramik çamurun içine ağırlıkça totalde % 5 magnezyum oksit, alüminyum oksit ve silika (MAS) eklediğimizde 1BMAS olduğunu belirtmektedir. Bu kodların sonunda bulunan 9, 12 ve 25 rakamları ise hazırlanan çamurun içindeki formülize edilmiş silisik asit yüzdeleri göstermektedir. Hazırlanan seramik çamurlarının bileşimleri Tablo I. de gösterilmektedir.

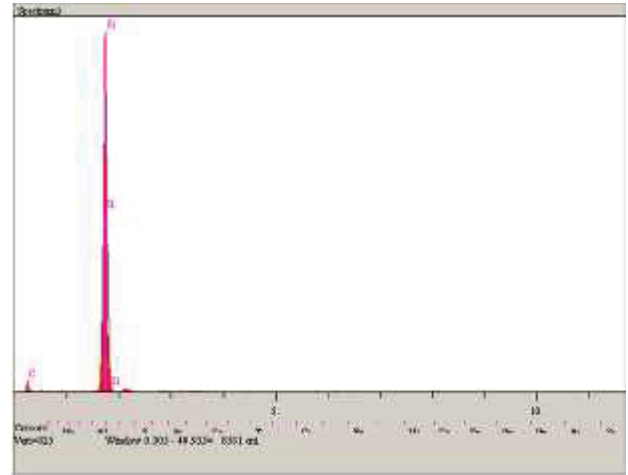
Tablo I. Formülize Ettiğimiz Silisik Asit Türevinin Ağ. % Oranı

	Bentonit	SiC	MAS	Silisik Asit Türevi
1B	30	70		
1BMAS	30	70	5	
1BMAS9	30	70	5	9
1BMAS12	30	70	5	12
1BMAS25	30	70	5	25

### B. SiC Tozun Karakterizasyonu



(a)



(b)

Şekil 2. SiC tozlarının SEM görüntüsü (a) ve EDS analizi (b)

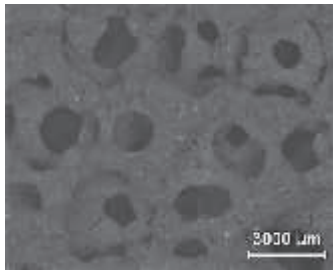
### C. Poliüretan Süngerin Emdirilmesi ve Sinterlemesi

SiC esaslı çamurun akışkanlığı SiC ve diğer katkı hammaddelerin yüksek olmasından dolayı kaplama istenildiği kalınlıkta ve eşit bir şekilde olmamıştır. Bunun için partiküllerin askıda kalması için formülize ettiğimiz silisik asit türevi katarak elde edilen bu solüsyonla, daldırma yöntemi ile polimer sünger üzerine homojen kaplama yapılarak numuneler elde edilip Şekil 3. ' de gösterilmektedir. Ayrıca kaplama kalınlığını arttırmak amacıyla aynı reçeteye hazırlanmış solüsyona sünger belli periyotlarla tekrar (2 veya 3 kez) daldırılmıştır.

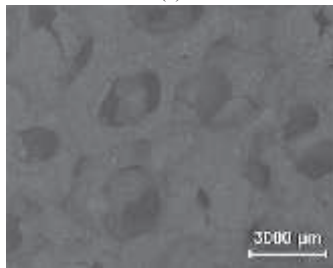


Şekil 3. Polimer süngerin seramik çamura daldırması ile oluşan yaş seramik köpük eldesi

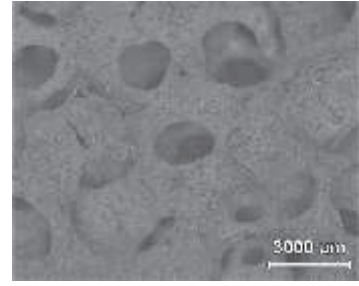
Sinterleme işlemleri yatay tüp fırınında 2 °C/ dk ısıtma hızında 450 °C' ye kadar ve bu sıcaklıkta 30 dk bekletilip 5°C/ dk ısıtma hızında 1200 °C' ye kadar ısıtılarak ve bu sıcaklıkta 90 dk bekletilerek gerçekleştirilmiştir. Altun ve arkadaşları tarafından gerçekleştirilmiş olan bir çalışmada farklı başlangıç tozları kullanılarak 1350 °C koşullarında gözenekli seramik köpük üretimi yapılmıştır. Söz konusu çalışmadan farklı olarak sadece malzeme cinsinin farklı olması seramik köpük üretimini 1350 °C sıcaklığının altında gerçekleştirilmesine sebep olmuştur. Bunun sonucunda mukavemeti bu çalışmadakinden daha az olsada başarılı bir seramik köpük elde edilmiştir.[6] Sinterleme sonrası elde edilen nihai ürünler Makro Stereo Mikroskop ile incelenip makro görüntüleri Şekil 4. ' de verilmiştir.



(a)



(b)



(c)

Şekil 4. Deney Numunelerinin sinterleme sonrası makro görüntüleri; (a) 1B MAS9, (b) 1B MAS12, (c) 1B MAS25

Alüminyum sıvı metal infiltrasyonunda kullanılmak üzere seramik filtre üretimine yönelik bu çalışmada elde edilen seramik köpüklerin mukavemetleri, silisik asit türev solüsyonlarının ağırlıkça yüzde oranlarının artması sonucu seramik köpük hücre duvarları ve kollarında homojen bir dağılıma olmadığından topaklanma olmuş bu da çatlak oluşumuna sebep vermiştir. Çatlak oluşumu sonucunda seramik köpüğün mukavemetinde azalma olduğu gözlenmektedir. Seramik köpük üretiminde optimum oran formülize silisik asit katkı oranı % 9 olan seramik köpüktür. Daha homojen bir yapı olduğundan geçişler daha düzgün ve çatlak oluşumu daha azdır. Replikasyon yönteminin yegane kusuru olan iç kısımlardaki üçgenel boş yapı bu oranda az bulunmaktadır ama bu kusurun dağılımı önlenememiştir. Koh ve arkadaşlarının yaptığı çalışmada bu polimer süngerin üzeri karbon siyahıyla kaplanarak bu yegane kusurunun dağılımı önlenmiştir. [7] Yaptığımız çalışmaya bu yöntemle daha iyi mukavemet kazandırılabilir

#### D. Seramik Köpüğün Basma Testi

Sinterlenme sonucu elde edilen % 9, % 12 ve % 25 seramik köpüklere basma testi uygulaması Şekil 5. ' de olduğu gibi gerçekleştirilmiştir.



Şekil 5. Üretilen seramik köpüklere basma testi uygulaması

Basma testi sonucu seramik köpük üretiminde optimum formülize edilmiş silisik asit katkı oranı olarak % 9 oranındaki seramik köpük olduğu Şekil 6. ' da gösterilmektedir. Elde edilen optimum seramik köpüğün basma mukavemeti ise 145 N dir. Nangrejo and Edirisinghe yaptığı çalışmaya kıyasla yaptığımız çalışmadaki solvent etkisini basma mukavemeti testinde görmekteyiz. Şekil 3' deki makro yapıda görüldüğü gibi çatlak ve topaklanma olmadan ideal kaplama kalınlığına ulaşıldı. Dolayısıyla seramik kaplama malzemesinin kalınlığı ve miktarı mukavemet değerlerinde büyük önem arz etmektedir. [8]

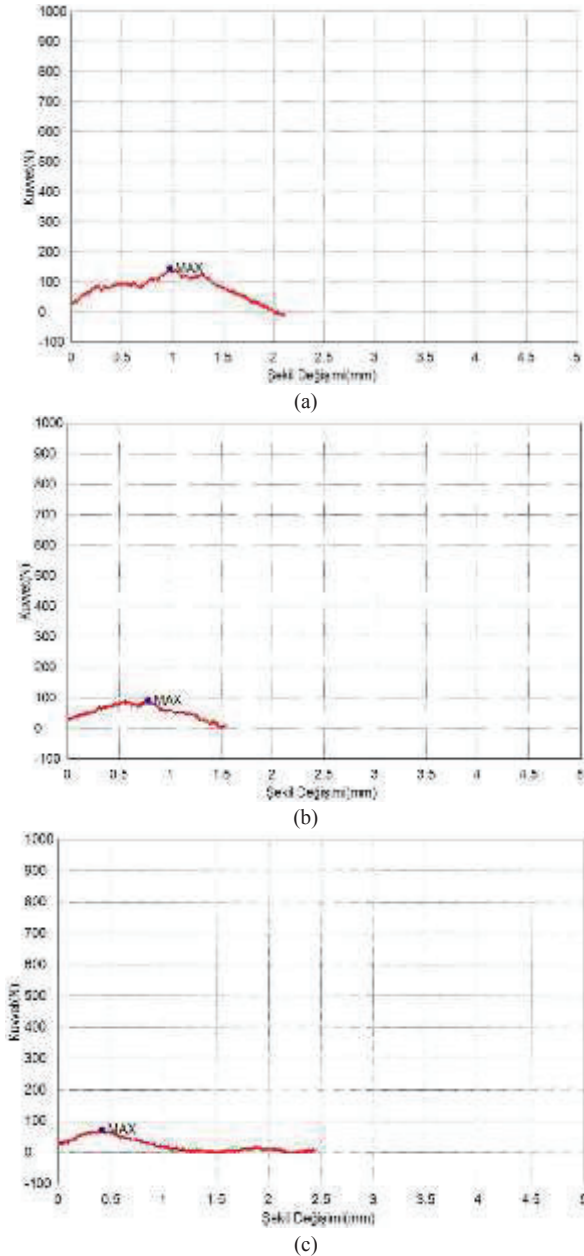
Seramik köpük üretiminde basma mukavemetlerinden iyi sonuç alınabilmesi için polimer süngerin seramik çamurla hücre duvarlarına ve kollarına eşit şekilde kaplaması yapılmalıdır. Literatürde yapılan çalışmalara bakıldığında daha önce yapılmamış olan , seramik çamura katkı hammaddelerinden formülize edilmiş silisik asit katılarak, çamurun akışkanlığını artırdığını ve topaklanmasını önlediğini % 9 katkı oranındaki seramik köpükle elde edilerek ulaşılmıştır.

### III. SONUÇLAR

Bu çalışmada replikasyon yöntemi ile kompozit malzeme yapımında kullanılmak üzere silisyum karbür esaslı seramik filtre üretimi amaçlanmıştır. SiC esaslı farklı kompozisyonlardaki seramik çamurlara reolojik özelliklerini geliştirmek ve seramik çamurun kararlılığı sağlamak için katılan formülize edilmiş silisik asit türevi kullanılmıştır. Yapılan deneysel çalışmaların sonucunda optimum seramik köpük üretiminde ağırlıkça % 9 oranındaki katkı oranı olduğu gözlenmiştir. Silisik asit türev solüsyonlarının ağırlıkça yüzde oranlarının artmasıyla beraber seramik köpük hücre duvarları ve kollarında üniform bir dağılıma olmadığından topaklanma olmuş bunun sonucunda da çatlaklar meydana gelmiştir.

### REFERANSLAR

- [1] Woyansky J. S. , Scott C. E. , Minnear W. P. , “*Processing of Porous Ceramics*”, American Ceramic Society Bulletin, Vol.71, No.11, 1992
- [2] Colombo, P. , Scheffler, M. , “*Cellular Ceramics: Structure, Manufacturing, Properties and Application*”, 2005
- [3] Çalışkan, F. , Demir, A. , Tatlı, Z. , “*Fabrication of Si<sub>3</sub>N<sub>4</sub> preforms from Si<sub>3</sub>N<sub>4</sub> produced via CRN technique*”, Journal of Porous Materials, Newyork, 2013.
- [4] Çalışkan, F. , Tatlı, Z. , Fındık, F. , “*Silisyum Karbür Esaslı Seramik Köpük Filtre Üretimi*”, ISITES 2015 ID 427. İspanya
- [5] Er, S. , “*Silisyum Karbür Esaslı Seramik Köpük Filtre Üretimi*” , Yüksek Lisans Tezi, Fen Bilimleri Enstitüsü, 2004
- [6] Altun, İ . , Akpınar, S. , Önel, K. , “*Kordiyerit esaslı silisyum karbür katkılı köpük filtrelerin karakterizasyonu ve bazı mekanik özelliklerinin belirlenmesi*” , Bilim- Teknoloji, 2009
- [7] Koh, Y. H. , Song, J. H. , Lee, S. H. , Kim, H.E, Jun, I. K. , “*Improved compressive strength of reticulated porous zirconia using carbon coated polymeric sponge as novel template*”, Materials Letters, 2006, P. 2507–2510
- [8] Raju, S. , Kim, Y- W. , Eom, J- H. , “*Processing and properties of macroporous silicon carbide ceramics: A review*”, Journal of Asian Ceramic Societies, 2013, P. 220–242



Şekil 6. Seramik köpüklerin basma mukavemetleri (a) ağırlıkça % 9 (b) ağırlıkça % 12 (c) ağırlıkça % 25

# Tribological Behavior of Poly-ether-ether-ketone Composite Against Unsaturated Polyester Composite and Stainless Steel Counterparts

Irfan Akgul #, Huseyin Unal +

# Scientific and Technological Research Center., Duzce University, Duzce, 81620, Turkey  
irfanakgul@duzce.edu.tr

+ Department of Metallurgy and Materials Engineering, Faculty of Technology, Sakarya Applied Science University, Sakarya, 54188, Turkey  
unal@sakarya.edu.tr

Corresponding author: irfanakgul@duzce.edu.tr

**Abstract**— In this experimental study, the tribological performance of glass fiber reinforced poly-ether-ketone (PEEK) composite against long glass fiber reinforced unsaturated polyester composite and steel under dry sliding condition were evaluated. Wear tests were carried out on a pin-on-disc arrangement and under 0.707, 1.41 and 2.12 MPa applied pressures and 0.5 m/s sliding speed condition. As a disc materials, AISI 316L stainless steel and 20wt.% glass fiber reinforced and 15wt.% calcium carbonate mineral filler filled unsaturated polyester (UPET+20wt.%GF+15wt.%CaCO<sub>3</sub>) composite were used. The results present that the coefficient of friction and wear rates for 30wt.% glass fibre reinforced PEEK composite (PEEK+30wt.%GF) against long glass fiber reinforced unsaturated polyester composite and stainless steel increases slightly with the increase in applied pressure values. Finally, the wear rates for PEEK polymer composite against long glass fiber reinforced unsaturated polyester composite and stainless steel under dry sliding conditions are in the order of 10<sup>-14</sup> and 10<sup>-15</sup> m<sup>2</sup>/N, respectively. The results suggested that it is more convenient to use glass fiber reinforced poly-ether-ketone composite against stainless steel for tribological applications.

**Keywords**— Polymer, composite, wear, PEEK, Thermoset, Polyester

**Özet**— Bu deneysel çalışmada cam fiber takviyeli poly-ether-ketone (PEEK) kompozitin, uzun cam fiber takviyeli doymamış poliester kompoziti ve çelik malzemeye karşı kuru kayma şartlarındaki tribolojik davranışları incelenmiştir. Tribolojik testlerde pin-on-disk aşınma test cihazı kullanılmıştır. Sürtünme ve aşınma testleri oda sıcaklığında gerçekleştirilmiştir. Tribolojik testler, 0.5 m / s kayma hızlarında ve 0.707, 1.41 and 2.12 MPa yük altında yapılmıştır. Disk olarak %20 cam fiber takviyeli ve %15 Kalsiyum karbonat dolgulu doymamış polyester kompozit(UPET+%20CF+%15CaCO<sub>3</sub>) ve AISI 316L paslanmaz çelik malzemesi kullanılmıştır. Deney sonucunda, uygulanan basıncın artması ile %30 Cam Fiber takviyeli PEEK kompozitinin Uzun Cam Fiber Takviyeli Doymamış Kompozitine ve paslanmaz çeliğe karşı çalışması durumunda artan uygulama basıncı ile Sürtünme katsayısı ve spesifik aşınma oranları arttığı görülmüştür. %30 Cam Fiber takviyeli PEEK kompozitinin Uzun Cam Fiber Takviyeli Doymamış Kompozitine ve paslanmaz çeliğe karşı kuru ortam şartlarında spesifik aşınma oranları sırasıyla

10<sup>-14</sup> ve 10<sup>-15</sup> m<sup>2</sup>/N olarak belirlenmiştir. Gerçekleştirilen aşınma deney sonuçlarından, PEEK+30CF kompozit/paslanmaz çelik çiftinin aşınma ve sürtünme uygulamalarında kullanılabilecek en iyi malzeme çifti olduğu tespit edilmiştir.

**Anahtar Kelimeler**— Polimer, kompozit, aşınma, PEEK, Termoset, Poliester

## I. INTRODUCTION

Poly-ether-ether-ketone (PEEK) is a typical high performance semi-crystalline thermoplastic polymer. It has received significant attention in recent years. PEEK polymer has high mechanical strength and chemical resistance, high stiffness, very high maximum allowable service temperature, easy processing, and excellent wear resistance and frictional properties. Due to the excellent properties making PEEK polymer the most popular advanced polymer material. So, PEEK polymer plays a more important role as a bearing and sliding material [1–2]. Many studies on the tribological properties of PEEK have been reported [3–11]. Most investigations published were in the friction and wear of polymers sliding against steels in dry conditions. The coefficient of friction can, generally, be reduced, and the wear resistance can be improved by selecting the right material combinations [12–13]. Usually, friction and wear phenomena lead to a loss of mechanical efficiency. Therefore, the accurate knowledge of the influence of sliding speed, contact temperature, and load value on the wear and friction is extremely important [13]. In the literature, there are lots of investigations about the PEEK polymer and PEEK composites against steel counterparts but there is a little study about the PEEK and its composites versus polymer counterpart materials.

The purposes of this investigation are to clarify the tribological characteristics of glass fiber reinforced PEEK composite sliding against long glass fiber reinforced and calcium carbonate mineral filler filled unsaturated polyester composite and steel under dry sliding conditions. Tribological tests versus 30wt.% glass fiber reinforced PEEK composite were carried out on a pin-on-disc arrangement. Tribological

tests were at room temperature under 0.707MPa, 1.42MPa and 2.12MPa applied pressure and at 0.5 m/s sliding speed. The specific wear rates were realized from mass loss and were reported.

## II. EXPERIMENTAL

### A. Materials

In this study, the pin material used is 30wt.% glass fiber reinforced PEEK composite. The glass fiber reinforced PEEK composite with trade name Ketron GF30 is supplied by Quadrant Engineering Plastics, Istanbul.

### B. Sample preparation

Friction and wear tests were conducted in a pin-on-disc apparatus, in which the stationary polymer pin was in contact with a rotating 316 L stainless steel disc material or 20wt.% glass fiber reinforced and 15wt.% calcium carbonate mineral filler filled unsaturated polyester composite discs. The schematic friction and wear test apparatus are shown in Figure 1. 20wt.% glass fiber reinforced and 15wt.% calcium carbonate mineral filler filled unsaturated polyester composite were firstly mixed in a mixer and then manufactured by using a hot press with a temperature of 160°C. PEEK polymer samples of six mm in diameter flat-ended pins of PEEK+30wt.%GF composite were machined by a revolver machine. The 5 mm in thickness and 100 mm in diameter disc materials are stainless steel and calcium carbonate filled and glass fiber reinforced unsaturated polyester composite material. 5 mm thick and 100 mm diameter steel disc material was first cut by saw. It is then turned and ground for proper surface roughness. Before and after each test, PEEK pin polymer and disc materials were cleaned with acetone. In this experimental study, the specific test conditions are summarized in Tables 1. All tests were repeated three times and the average values were plotted. The disc materials used in the experiments on the rotating disc with the drive of an electric motor are fixed with a screw. 6 mm in diameter polymer pin is connected to the sleeve by a mechanism on the handle. When the machine is operated, the arm apparatus to which the pin sample is connected by moving the pin sample to the disk wishes to move in the direction of rotation of the disc. This forward movement gives the frictional force. This frictional force was measured by a load cell. The received data is also stored directly in the Excel program on the computer. In the experiments, 1000 frictional load data per minute is taken and at the same time it is divided into the applied load used in the experiments and graphed in the Excel program. The coefficient of friction (COF) is expressed as the ratio of the frictional force to the normal applied force and is calculated by the following formula.

$$\text{COF} = F_s / F_N$$

where  $F_N$  is the normal load on the glass fiber reinforced PEEK composite pin material.

The specific wear rate ( $W_{sp}$ ) values were also calculated using the following formula.

$$W_{sp} = \Delta m / \rho \times L \times F_N$$

Where  $\Delta m$  is the weight loss of the sample before and after the experiment,  $\rho$  is the density of PEEK polymer pin composite material,  $L$  is the sliding distance of the pin sample during the wear test, and  $F_N$  is the normal load applied on the pin sample.

TABLE I.

TEST CONDITIONS OF THE SAMPLES

Parameters	Experimental conditions
Applied pressure (MPa)	0.707, 1.41, 2.12
Sliding speed (m/s)	0.50
Temperature (°C)	22±2
Humidity (%)	59±2
Sliding distance (m)	1000
Surface roughness ( $R_a$ , $\mu\text{m}$ )	0.35-0.40

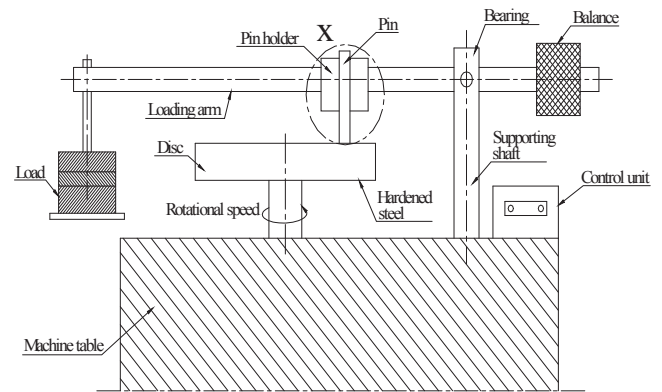


Figure 1. The schematic diagram of wear test apparatus

## III. RESULTS AND DISCUSSIONS

Figure 2 shows the variation of coefficients of friction with contact pressure for 30wt.%GF reinforced PEEK composite against AISI 316L stainless steel and 20wt.% glass fiber reinforced and 15% calcium carbonate mineral filler filled unsaturated polyester UPET+20wt.%GF+15wt.%CaCO<sub>3</sub> composite discs under dry sliding conditions, respectively. It is clear from this figure that the coefficients of friction values of 30wt.% glass fiber reinforced PEEK composite are influenced by the change in applied pressure and different rubbing surface materials. The coefficient of friction increases slightly with the increment of applied pressure values against stainless steel and UPET+20wt.%GF+15wt.%CaCO<sub>3</sub> composite discs under dry sliding conditions. By increasing the load by 200%, the coefficient of friction of 30wt.%GF reinforced PEEK composite against steel disc and UPET counter-part disc

materials increased by 8% and 30%, respectively. The results are consistent with previous studies in the literature [3,6,9,10]

Figures 3 illustrates the variation of specific wear rate with applied pressure values for 30% glass fiber reinforced PEEK composite against AISI 316L stainless steel and 20wt.% glass fiber reinforced and 15% calcium carbonate mineral filler filled unsaturated polyester UPET+20wt.%GF+15wt.%CaCO<sub>3</sub> composite discs under dry sliding conditions, respectively. The specific wear rate for PEEK+30wt.%GF increases with the increase in applied pressure values. By increasing the load by 200%, the specific wear rate value of 30wt.%GF reinforced PEEK composite against steel disc and UPET counter-part disc materials increased by 60% and 400%, respectively. The wear resistance of PEEK+30wt.%GF/AISI 316L stainless steel pair 7 times higher than that of UPET+20wt.%GF+15wt.%CaCO<sub>3</sub> composite material pair. As a result of this study, glass fiber reinforced PEEK composite/AISI 316L stainless steel pair illustrates the best tribological performance.

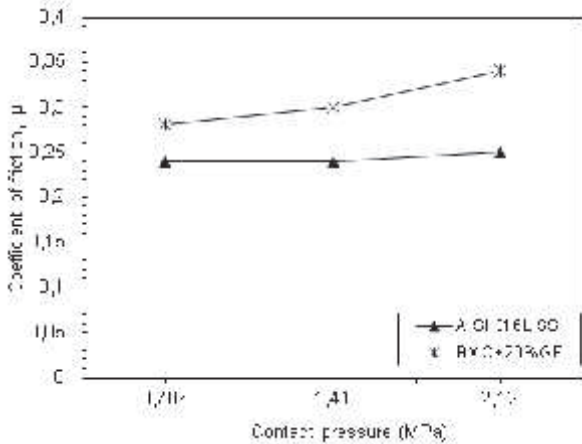


Figure 2. The relationship between coefficient of friction and contact pressure for 30% GF reinforced PEEK composites

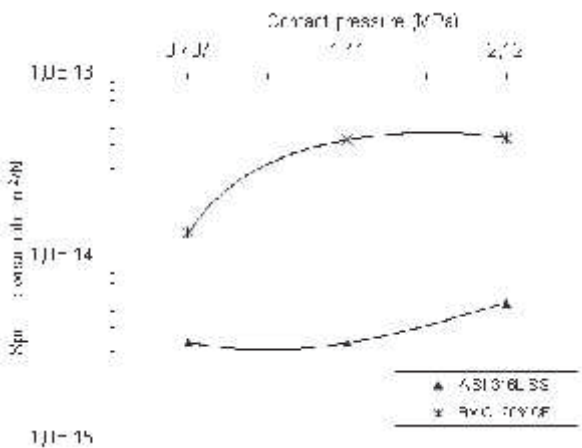


Figure 3. The variation of wear rate and contact pressure for 30%GF reinforced PEEK composites

The study of friction and wear performance of 30% glass fiber reinforced poly-ether-ether ketone polymer composite in use in electrical applications showed that:

1. The maximum friction coefficient of poly-ether-ether ketone polymer composite reinforced with 30% glass fiber against 20wt.% glass fiber reinforced and 15% calcium carbonate mineral filler filled unsaturated polyester composite (UPET+20%GF+15%CaCO<sub>3</sub>) disc material is about 0.31.
2. The friction coefficient of poly-ether-ether ketone polymer composite reinforced with 30% glass fiber against stainless steel disc is about 0.24.
3. The coefficient of friction is both large sensitive to material combinations and applied pressure.
4. The maximum specific wear rate for PEEK+30% glass fiber reinforced composite against UPET+20wt.%GF+15%CaCO<sub>3</sub> composite disc material is about  $5.0 \times 10^{-14} \text{ m}^2/\text{N}$ .
5. The minimum specific wear rate for PEEK+30wt.%glass fiber composite against AISI 316L stainless steel disc material under the applied pressure of 0.707 MPa is about  $0.5 \times 10^{-14} \text{ m}^2/\text{N}$ .
6. PEEK+30wt.%GF/AISI 316L stainless steel disc material combination showed the best tribological performance for use in tribological applications.

#### REFERENCES

- [1] Kausch, H. H. (ed.) (1993). Advanced Thermoplastic Composite, Characterization and Processing, Hanser, Munich.
- [2] Cogswell, F. N. (1992). Thermoplastic Aromatic Polymer Composites, Butterworth-Heinemann, Oxford.
- [3] Lu, Z. and Friedrich, K. (1993). On the Friction and Wear of Poly-ether-ether-ketone Composites, In:1st Balkan Conference on Tribology, Balkantrib'93, Sofia, Bulgaria, October 1-3.
- [4] Karger-Kocsis, J. and Friedrich, K. (1986). Temperature and Strain-rate Effects on the Fracture toughness of PEEK and its Short Glass Fiber Reinforced Composites, Polymer, 27(11): 1753-1760.
- [5] Talbott, M. E. and Springer, G. S. (1987). The Effect of Crystallinity on the Mechanical Properties of PEEK Polymer and Graphite Fiber Reinforced PEEK, J. Comp. Mater., 21: 1056-1081.
- [6] Voss, H. and Friedrich, K. (1987). On the Wear Behaviour of Short Fiber Reinforced PEEK Composite, Wear, 116(1): 1-18.
- [7] Voorth, J. V. and Bahadur, S. (1995). The Growth and Bonding of Transfer Film and the Role of CuS and PTFE in the Tribological Behaviour of PEEK, Wear, 181-183(1): 212-221.
- [8] Bahadur, S. and Gong, D. (1992). The Role of Copper Compounds as Fillers in the Transfer and Wear Behaviour of Polyetheretherketone, Wear, 154(1): 151-165.
- [9] Stolarski, T. A. (1992). Tribology of Polyetheretherketone, Wear, 158(1): 71-78.
- [10] Lu, Z. P. and Friedrich, K. (1995). On Sliding Friction and Wear of PEEK and its Composites, Wear, 181-183(2): 624-631.
- [11] Ovaert, T. C. and Cheng, H. S. (1991). The Unlubricated Sliding Wear Behaviour of Polyetheretherketone against Smooth Mild-steel Counterfaces, ASME J. Tribol., 113: 150-157. 1666
- [12] Yamaguchi, Y. (1990). Tribology of Plastic Materials: Their Characteristics and Applications to Sliding Components, Elsevier, Amsterdam.
- [13] Hooke, C. J., Kukureka, S. N., Liao, P., Rao, M. and Chen, Y. K. (1996). The Friction and Wear of Polymers in Non-conformal Contacts, Wear, 200(1-2): 83-94.

#### IV. CONCLUSIONS

# Friction and Wear Performance of Short Carbon Fiber Reinforced Poly-ether-ether-ketone Thermoplastic Composite Against Polymer and Steel Material Counterparts

Irfan Akgul #, Huseyin Unal +

# Scientific and Technological Research Center., Duzce University, Duzce, 81620, Turkey  
irfanakgul@duzce.edu.tr

+ Department of Metallurgy and Materials Engineering, Faculty of Technology, Sakarya Applied Science University, Sakarya, 54188, Turkey  
unal@sakarya.edu.tr

Corresponding author: irfanakgul@duzce.edu.tr

**Abstract**— In this experimental study, the tribological performance of 30wt.% short carbon fiber reinforced poly-ether-ketone (PEEK+30wt.%CF) high performance thermoplastic composite against a stainless steel (SS) and a high performance thermoplastic engineering polymer material such as 40wt.% glass fiber reinforced poly-phenylene-sulphide (PPS+40%GF) composite materials under dry sliding condition were evaluated. Tribological tests were carried out on a pin-disc wear test rig and under the sliding speed of 0.5 m/s and the applied pressures of 0.707, 1.41 and 2.12MPa conditions. The results show that the friction coefficient for carbon fiber reinforced PEEK composite against PPS+40%GF polymer composite and stainless steel materials increases slightly with the increment of applied pressure values. Furthermore, the specific wear rate for carbon fiber reinforced PEEK composite against PPS+40wt.%GF composite increases but it decreases against stainless steel with the increment of applied pressure values. Finally, the wear rates for carbon fiber reinforced PEEK polymer composite against PPS+40wt.%GF composite and stainless steel materials under dry sliding conditions are in the order of  $10^{-14}$  and  $10^{-15}$  m<sup>2</sup>/N, respectively. The results suggested that PEEK+30wt.%CF/stainless steel is the best material pair for use in friction and wear applications in the study.

**Keywords**— Polymer, tribology, PEEK, carbon fiber, PPS, composite

**Özet**— Bu deneysel çalışmada, %30 oranında kısa karbon fiber takviyeli poli-eter-eton (PEEK+%30KF) yüksek performanslı termoplastik kompozitin paslanmaz çelik (SS) ve %40 oranında cam elyaf takviyeli poli-fenilen-sülfid (PPS+%40KF) kompozit malzemesine karşı çalışması durumundaki tribolojik özellikleri kuru kayma şartlarında ve oda sıcaklığında incelenmiştir. Tribolojik testler, pim-disk aşınma test teçhizatında 0.5 m /s kayma hızında ve 0.707, 1.41 ve 2.12MPa basınçlar altında gerçekleştirilmiştir. Çalışma sonucunda, PPS +%40KF polimer kompozit malzemenin ve paslanmaz çelik malzemelere karşı çalışan karbon fiber takviyeli PEEK kompozitin sürtünme katsayısı değerleri uygulanan basınç değerlerinin artmasıyla birlikte hafif artmıştır. Ayrıca, karbon fiber takviyeli PEEK kompozitin PPS+%40KF kompozitine karşı çalışması durumundaki spesifik aşınma hızı uygulanan basınç değerinin

artmasıyla artarken paslanmaz çelik karşı disk malzemesiyle çalışması durumunda azalır. Son olarak, PPS +%40KF kompozit ve paslanmaz çelik karşı disk malzemelere, karbon fiber takviyeli PEEK polimer kompozitin spesifik aşınma hızları sırasıyla  $10^{-14}$  ve  $10^{-15}$  m<sup>2</sup>/N arasındadır. Gerçekleştirilen aşınma deney sonuçlarından, PEEK+30KE kompozit/paslanmaz çelik çiftinin elektrik endüstrisinde aşınma ve sürtünme uygulamalarında kullanılabilir en iyi malzeme çifti olduğu tespit edilmiştir.

**Anahtar Kelimeler**— Polimer, Triboloji, PEEK, Karbon Fiber, PPS, Kompozit

## I. INTRODUCTION

Unreinforced polymer material applications have been greatly limited for its mechanical properties, bad thermal properties and lower wear resistance. Therefore various reinforcements are frequently added into the unfilled polymer materials to improve the mechanical, thermal and tribological properties. Polymer composites are generally manufactured by injection molding and are valued for their good mechanical, thermal and tribological properties. So, reinforced polymer composites are preferred for many industrial applications and sectors such as electrical/electronic, automotive, aircraft, and household applications. These composites are poly-ether-ether-ketone (PEEK), poly-phenylene-sulphide (PPS), polyamides such as polyamide 6 (PA 6), polyamide 66 (PA 66), polyamide 46 (PA 46) polymers. PEEK thermoplastic polymer, a typical high performance semi-crystalline material, has received significant attention in recent years. This is due to its high mechanical strength and elastic modulus, high melting temperature, chemical inertness, high toughness, easy processing, and wear resistance. So, PEEK polymer material plays a more important role as a bearing and sliding material, especially under dry sliding and a water lubricated environment [1,2]. Many studies on the tribological properties of PEEK have been reported in previous literature [3-11]. Most investigations published were in the friction and wear of polymers sliding against steels in dry conditions. The friction coefficient can be generally reduced, and the wear rate value can be decreased by

selecting the true material combinations [12-13]. Some of the researchers observed that the friction coefficient of polymers rubbing against steel materials decreases with the increment of applied loads while other of some researchers showed that its value increases with the increment of applied load.

The purposes of this investigation are to clarify the tribological characteristics of 30wt.% carbon fiber reinforced PEEK composite sliding against stainless steel and 40wt.% glass fiber reinforced poly-phenylene-sulphide composite under dry sliding conditions. Tribological tests were at room temperature under 0.707, 1.41 and 2.12 MPa applied pressures and at 0.5 m/s sliding speed. The specific wear rates were realized from mass loss and were reported.

## II. EXPERIMENTAL

### A. Materials

In this study, the pin material used is 30wt.% carbon fiber reinforced PEEK composite. The carbon fiber reinforced PEEK composite with trade name Ketron CA30 is supplied by Quadrand Engineering Plastics, Istanbul, Turkey. The polymer composite disc material used is 40wt.% glass fiber reinforced poly-phenylene sulphide composite material. 40wt.% glass fiber reinforced PPS composite with granule form purchased from Chevron Phillips Chemical Co. Istanbul, Turkey.

### B. Sample preparation

Friction and wear tests were conducted in a pin-on-disc apparatus, in which the stationary polymer pin was in contact with a rotating AISI 316L stainless steel disc material and 40wt.% glass fiber reinforced poly-phenylene-sulphide composite discs. Samples of 6 mm in diameter flat-ended pins of 30% carbon fiber reinforced PEEK composite were machined by a revolver machine. The 100 mm in diameter and 5 mm in thickness disc materials were used. Stainless steel disc was first turned and then ground. PPS+40wt%GF composite disc material were produced by an ordinary injection molding machine. In this experimental study, the specific test conditions are summarized as follows: Test temperature and relative humidity is  $23 \pm 2$  °C and  $61 \pm 1$ %, respectively Surface roughness for steel and PPS+40wt%GF composite disc materials is about  $0,35 \mu\text{m Ra}$ . The tribological tests at 0.707, 1.41 and 2.42 MPa applied pressure and sliding speed of 0.5 m/s and a sliding distance of 1000 m. For tribological tests, a pin-on-disc wear test apparatus connected to a computer is used. During the wear tests, a transducer mounted on the loading arm measured the friction force of material pair. The friction force readings are taken an average 30 readings for every 60 seconds. A microprocessor controlled data-acquisition system was used for this purpose. Each test was done for 33 minute. Coefficient of friction and specific wear rate values were obtained from the tribological tests. The coefficient of friction values of the 30wt.% carbon fiber reinforced PEEK composites were obtained from the equipment that records the  $\mu$  value by using following relationship:

$$\mu = \frac{F_f}{F_n}$$

where  $F_f$  are frictional force and  $F_n$  is the applied load on the sample. The specific wear rate is defined as a wear volume by the normal load and the sliding distance The mass loss was measured after each set of run and volume loss ( $V$ ),  $V = m/\rho$ , was found by using density ( $\rho$ ) of PEEK composite pin sample. The following relationship was used to estimate the specific wear rate (WR) of 30wt.% carbon fiber reinforced PEEK composites;

$$W_R = \frac{V}{F \cdot L}$$

where  $L$  is the sliding distance of the pin material. Moreover, to ensure the reliability in the friction and wear results, all tests were repeated three times and the average values were plotted. Prior to the friction and wear tests, both PEEK composite pin samples and PPS+40wt.%GF composite disc, and stainless steel disc materials were cleaned with ethyl alcohol and then they dried in dry air.

## III. RESULTS AND DISCUSSIONS

Figure 1 presents the variation of coefficients of friction with applied pressure for 30wt.% carbon fiber reinforced PEEK composite against both AISI 316L stainless steel and PPS+40%GF composite discs under dry sliding conditions. It is clear from figure 1 that the coefficients of friction values of 30wt.% carbon fiber reinforced PEEK composite are influenced by the variation in applied pressure and rubbing surface materials. The coefficient of friction increases slightly with the increase in applied pressure values against both AISI 316L stainless steel disc and PPS+40wt%GF polymer composite disc under dry sliding conditions. The average friction coefficient of 30wt.% carbon fiber reinforced PEEK composite rubbing against steel and PPS composite disc materials used in the study is between 0.22 and 0.26. The average increasing ratio in coefficient of friction for carbon fiber reinforced PEEK composite against AISI 316L stainless steel is 9% while the average increasing ratio in coefficient of friction is about 18% against PPS+40wt.%GF composite discs. It is well known that the tribological behavior of polymer materials and polymer composite materials can be associated to their visco-elastic and temperature-related properties. It is known that the sliding contact of two materials results in heat generation at asperities and hence increases in temperature. The amount of rises in temperature is influenced by the amount of heat flow. If the increase in surface temperature is high in comparison to heat deformation temperature of the material, this influences the visco-elastic property which causes softening of the materials. This causes the rubbing of fibers of faced materials or fiber against polymer; therefore reflect the friction and wear performance of materials. So, the increase in the coefficient of friction occurs as rubbing carbon fiber reinforced PEEK polymer composite with both steel and polymer composite.

Figures 2 shows the variation of specific wear rate with applied pressure values for 30wt.% carbon fiber reinforced

PEEK composite against AISI 316L stainless steel and PPS+40wt.%GF composite discs under dry sliding conditions. The specific wear rate for PEEK+wt.30%CF composite against AISI 316L stainless steel disc decreases with the increase in applied pressure values. The decreasing ratio in specific wear rate from 0707 MPa to 2.12 MPa is about 30%. But the specific wear rate values for PEEK+30wt.%CF composite against PPS+40wt.%GF composite discs increases with the increase in applied pressure values. The increasing ratio in specific wear rate from 0707 MPa to 2.12 MPa is about 49%. In this study, the best tribological performance for use in electrical application is obtained for PEEK+30wt.%CF composite against AISI 316L stainless steel pair.

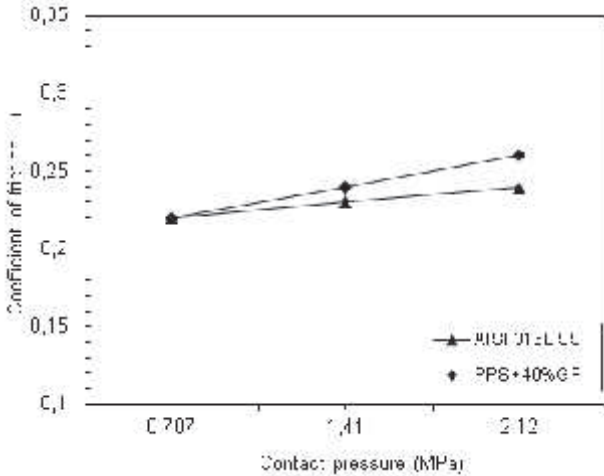


Figure 1. The variation of coefficient of friction and contact pressure for 30%CF reinforced PEEK composites

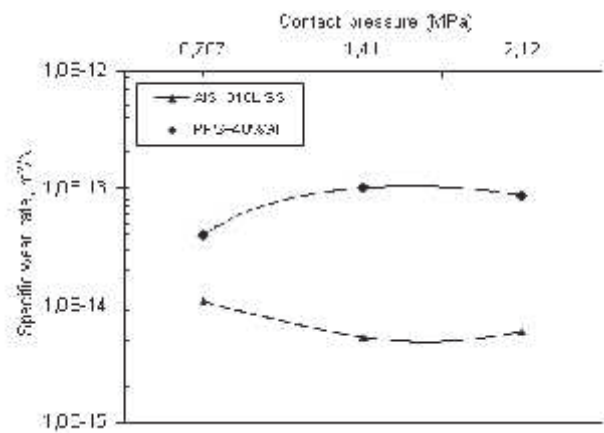


Figure 2. The variation of specific wear rate and contact pressure for 30%CF reinforced PEEK composites

#### IV. CONCLUSIONS

The study of tribological performance of PEEK+30wt.%CF composite in use in electrical applications showed that:

1. The friction coefficient of 30wt.%carbon fiber reinforced poly-ether-ether ketone polymer composite against AISI 316L stainless steel disc is about 0.222.
2. The maximum friction coefficient of 30wt.%carbon fiber reinforced poly-ether-ether ketone polymer composite against

40wt.% glass fiber reinforced poly-phenylene-sulphide composite disc is about 0.26.

3. The coefficient of friction is both large sensitive to material combinations and applied pressure.
4. The maximum specific wear rate for PEEK+30wt.%CF composite against PPS+40wt.%GF polymer composite disc material is about  $1.0 \times 10^{-13} \text{ m}^2/\text{N}$ .
5. The minimum specific wear rate for PEEK+30wt.%CF composite against AISI 316L stainless steel disc material under the applied pressure of 1.41 MPa is about  $0.6 \times 10^{-14} \text{ m}^2/\text{N}$ .
6. PEEK+30wt.%CF/AISI 316L stainless steel disc material combination showed the best tribological performance for use in electrical industry.

#### REFERENCES

- [1] Kausch, H. H. (ed.) (1993). Advanced Thermoplastic Composite, Characterization and Processing, Hanser, Munich.
- [2] Cogswell, F. N. (1992). Thermoplastic Aromatic Polymer Composites, Butterworth-Heinemann, Oxford.
- [3] Lu, Z. and Friedrich, K. (1993). On the Friction and Wear of Poly-ether-ether-ketone Composites, In:1st Balkan Conference on Tribology, Balkantrib'93, Sofia, Bulgaria, October 1-3.
- [4] Karger-Kocsis, J. and Friedrich, K. (1986). Temperature and Strain-rate Effects on the Fracture toughness of PEEK and its Short Glass Fiber Reinforced Composites, Polymer, 27(11): 1753-1760.
- [5] Talbott, M. E. and Springer, G. S. (1987). The Effect of Crystallinity on the Mechanical Properties of PEEK Polymer and Graphite Fiber Reinforced PEEK, J. Comp. Mater., 21: 1056-1081.
- [6] Voss, H. and Friedrich, K. (1987). On the Wear Behaviour of Short Fiber Reinforced PEEK Composite, Wear, 116(1): 1-18.
- [7] Voorth, J. V. and Bahadur, S. (1995). The Growth and Bonding of Transfer Film and the Role of CuS and PTFE in the Tribological Behaviour of PEEK, Wear, 181-183(1): 212-221.
- [8] Bahadur, S. and Gong, D. (1992). The Role of Copper Compounds as Fillers in the Transfer and Wear Behaviour of Polyetheretherketone, Wear, 154(1): 151-165.
- [9] Stolarski, T. A. (1992). Tribology of Polyetheretherketone, Wear, 158(1): 71-78.
- [10] Lu, Z. P. and Friedrich, K. (1995). On Sliding Friction and Wear of PEEK and its Composites, Wear, 181-183(2): 624-631.
- [11] Ovaert, T. C. and Cheng, H. S. (1991). The Unlubricated Sliding Wear Behaviour of Polyetheretherketone against Smooth Mild-steel Counterfaces, ASME J. Tribol., 113: 150-157. 1666
- [12] Yamaguchi, Y. (1990). Tribology of Plastic Materials: Their Characteristics and Applications to Sliding Components, Elsevier, Amsterdam.
- [13] Hooke, C. J., Kukureka, S. N., Liao, P., Rao, M. and Chen, Y. K. (1996). The Friction and Wear of Polymers in Non-conformal Contacts, Wear, 200(1-2): 83-94.

# The Influence of Sliding Speed on The Tribological Behaviour of Graphite Powder Filled Polyamide-6 Composite

Irfan Akgul #, Huseyin Unal +

# Scientific and Technological Research Center,, Duzce University, Duzce, 81620, Turkey  
irfanakgul@duzce.edu.tr

+ Department of Metallurgy and Materials Engineering, Faculty of Technology, Sakarya Applied Science University, Sakarya, 54188, Turkey  
unal@sakarya.edu.tr

Corresponding author: irfanakgul@duzce.edu.tr

**Abstract**— In this experimental study, the tribological behaviour of polyamide-6 (PA-6) polymer, 10wt.%graphite filled polyamide-6 (PA-6+10%G) composite, polyamide-6 with wax (PA-6+6%W) and both 10wt.% graphite and 6wt.%wax filled polyamide-6 (PA-6+10%G+6%W) composites against steel under dry sliding condition were studied. Pin-on-disc wear test rig was used for the tribological tests. Friction and wear tests were studied at room temperature. Tribological tests were done at the sliding speeds of 0.4, 0.8 and 1.6m/s and under the load of 100N. As a disc material, AISI 440C stainless steel were used. The results show that the specific wear rates for all polymer and polymer composites used against steel increases slightly with the increment of sliding speed values. In addition, the coefficient of friction for polyamide-6 with wax polymer and graphite/wax filled polyamide-6 composite increase slightly, but it is decreases slightly with the increment of sliding speed for graphite filled polyamide 6 composite. Finally, the specific wear rates for PA-6 polymer, PA-6+10%G composite, PA-6+6%W and PA-6+10%G+6%W composite against steel under dry sliding conditions are in the order of  $10^{-14}$ ,  $10^{-14}$ ,  $10^{-15}$  and  $10^{-15}$  m<sup>2</sup>/N, respectively. The results suggested that it is more convenient to use PA-6+10%G+6%W composite against steel for tribological applications in the study.

**Keywords**— Polyamide-6, composite, tribology, wax, thermoplastic, sliding speed

**Özet**—Bu deneysel çalışmada, poliamid-6 (PA-6) polimeri, ağırlıkça %10 oranında grafit tozu katkılı poliamid-6 (PA-6 +% 10 G) kompoziti, wax katkılı poliamid-6 (PA-6 +%6w) ve %10 grafit ve%6 oranında vaks katkılı poliamid-6 (PA-6+%10G+%6W) kompozitlerinin kuru kayma şartlarındaki tribolojik davranışları incelenmiştir. Tribolojik testlerde pin-on-disk aşınma test cihazı kullanılmıştır. Sürtünme ve aşınma testleri oda sıcaklığında gerçekleştirilmiştir. Tribolojik testler, 0.4, 0.8 ve 1.6m / s kayma hızlarında ve 100N yük altında yapılmıştır. Disk olarak AISI 440C paslanmaz çelik malzemesi kullanılmıştır. Deney sonucunda, kullanılan tüm polimer ve polimer kompozitlerin çeliğe karşı çalışması durumunda spesifik aşınma oranlarının artan hız ile arttığı tespit edilmiştir. Buna ilaveten, vaks katkılı poliamid-6 ile grafit ve vaks katkılı poliamid-6 katkılı kompozitlerin sürtünme katsayısı biraz artar, ancak grafit katkılı poliamid 6 kompoziti için kayma hızının hafif arttığı tespit edilmiştir. Sonuç olarak, PA-6 polimeri, PA-6+%10G kompoziti, PA-6+%6W ve PA-6+%10G+% 6W kompozitinin kuru kayma

şartlarındaki spesifik aşınma oranları sırasıyla 10-14, 10-14, 10-15 ve 10-15 m<sup>2</sup>/N olarak belirlenmiştir. Çalışmada, PA-6 +% 10G +% 6W kompoziti/paslanmaz çelik çiftinin makine endüstrisi alanında kullanılmasında en iyi malzeme olarak ifade edilebilir.

**Anahtar Kelimeler**— Polamid-6, kompozit, triboloji, wax, termoplastik, kayma hızı

## I. INTRODUCTION

Polymer and polymer composites have been widely used in various industrial applications such as aerospace, automotive, electrical/electronic, machine, textile, household and chemical industries. This is because these composite materials provide high strength/weight ratio in comparison to classic materials and self-lubricant conditions. However, applications of classic polymer materials are limited because of their bad mechanical, thermal and friction and wear performance. Therefore some additives and reinforcements are used to improve their properties. The used reinforcement and additives in polymer base materials are kaolin [1] talc [2,3], wollastonite [4], and mica [5,6] fillers and MoS<sub>2</sub>, graphite, wax and poly-tetra-fluoro-ethylene (PTFE), solid lubricants [7,8] and glass, carbon and aramid fibers. Solid lubricants were proved to be generally helpful in developing continuous transfer film between the two counterparts and accordingly reduce the coefficient of friction [9]. PA-6 polymer is an engineering plastic that is used in electrical/ electronics, automobile, packaging, textiles and consumer applications because of its excellent mechanical properties [10-12]. However, it shows some limitations in mechanical properties, thermal properties, and dimensional instability. So, the usage of pure polyamide-6 is limit for use in wide range of applications. Hence, some solid lubricants were added into the PA-6 polymer to widen and to increase its industrial application range. PA-6 filled with graphite, carbon and wax have found their application in field high velocity applications, without the need for exterior lubrication [7,8]. In fact, the friction and wear behavior of polymers is affected by environmental, operating conditions and by the type, size, amount, shape and orientation of the fiber and fillers. A relationship between the wear of the polymers composite content filler and operating parameters is desirable to obtain a

better understanding of the wear behavior. There have been some investigations exploring the influence of filler content, test conditions and environment on the friction and wear behavior of polymers. Hooke et al. [13] said that the friction coefficient can be reduced and the wear resistance increased by selecting the true material combinations. Zhang et al. [14] and Anderson [15] observed that the friction coefficient of polymers rubbing against metals decreases with the increment of load while Unal et al [16] and Shangguan et al. [17] reported that its value increases with the increment of load. In addition, some researchers showed that the coefficient of friction values and wear rate values decreased with the addition of solid lubricants.

In order to study the influence of graphite and wax on the tribological properties of polyamide-6, PA-6 composites, materials used in the study were compounded by a twin-screw extruder and then molded by using an injection molding machine. Materials contents were pure polyamide 6, PA-6+10%G, PA6+6%wax and PA6+10%G+6%wax composite. Friction and wear tests vs. AISI 440C stainless steel disc were used on a pin-on-disc wear test rig at dry conditions. Influence of graphite and wax solid lubricants, and sliding speed (0.4–1.6 m/s) was explored and evaluated.

## II. EXPERIMENTAL

### A. Materials

For this study, PA-6, graphite and wax materials were supplied from manufacturers. The matrix material polyamide 6 (Domamid) with 1.13 g cm<sup>3</sup> density and melt flow index (2.16 kg, 230 °C) 4 g per 10 min was obtained from Domopolymers in Belgium. The graphite was supplied by Sovitec and the wax was supplied by Omya Mining, Egypt.

### B. Sample preparation

In sample preparation process, the graphite and wax were added to polyamide-6 with 6 wt%, and 10 wt% ratios. The composite granules were prepared using a twin screw extruder at temperatures ranging from 220 to 255°C. The specimens of polyamide-6 and its composites were moulded by using an injection molding machine at temperatures from 220 to 250 °C. The friction and wear tests were conducted on a pin-on-disc tribometer. In this test, pin size is Ø6mmx50 mm and AISI 440C stainless steel disc was machined and prepared in Ø100 mmx5 mm size dimensions with an average surface roughness between 0.31 and 0.36 mm Ra. Before each test, PA-6 and its composite pin materials were fixed on a tribometer and rubbed against a metallographic abrasive paper placed on the rotating disc. This pre-rubbing process ensured a full contact of the pin and disc surfaces. Furthermore before each test all samples were ultrasonically cleaned in acetone and then dried. The friction and wear tests were performed at room temperature in an ambient atmosphere. Applied load of 100 N, the sliding speeds ranged from 0.4 m/s to 1.6 m/s, and sliding distance was 4000 m. All tests were repeated three times and the average

values were plotted. In this experimental study, the specific test conditions are summarized in Table 1.

TABLE I.  
 TEST CONDITIONS OF THE SAMPLES

Parameters	Experimental conditions
Sliding speed (m/s)	0.4, 0.8 and 1.6
Applied loads (N)	100
Temperature (°C)	21±2
Humidity (%)	50±7
Sliding distance (m)	4000

## III. RESULTS AND DISCUSSIONS

Figure 1 presents the variation of friction coefficient of pure PA-6, PA6+10%G, PA6+6%wax and PA-6+10%G+6%W composite under 100N applied load and at 0.4 m/s and 1.6 m/s sliding speeds, respectively. Apart from PA-6 polymer, the coefficient of friction of PA6+6%wax and PA-6+10%G+6%W composite materials increases with the increase in sliding speed values. However, the coefficient of friction of PA6+10% G composite decreases with the increment of sliding speed. As it is known polymers show a visco-elastic behavior and their deformation under applied load is visco-elastic. So, the variation of friction coefficient with load or pressure follows the equation  $\mu=K \times L^{(n-1)}$  where  $\mu$  is the coefficient of friction, K constant and n is also a constant, its value is 0.66 <n< 1 and L is the load.

Figure 2 shows the variation of specific wear rate with sliding speed for pure PA-6, PA6+10%G, PA6+6%wax and PA-6+10%G+6%W composite under 100 N load values. It is clear from this figure that the specific wear rate values increase with the increase in sliding speed values. In summary, the friction and wear of tested materials are much sensitive to change in sliding speed. The addition of graphite and wax resulted in large improvement in lowering friction coefficient and specific wear rate of polyamide based polymer composite. It is well known that graphite filler is a potential candidate which could form a transfer film on the sliding counterpart. Furthermore, graphite atoms were arranged in a hexagonal unit cell within each layer and these layers are linked by weak van der waals bonds, which may be easily broken by shear force under sliding conditions. In general, the abundant filler debris pulled out from the matrix during the sample sliding against the steel counterpart might stick together because of the repeated plastic deformation in the periodic sliding process. So, uniform film was formed on the worn sample surface and reduces the adhesion between the materials and counterparts, which led to decrease in wear rate and in friction coefficient. Again wax form a more stable and active transfer film on the counterpart disc which led to a higher drop in wear rate of the material. It is seen that among tested polyamide and polyamide composite materials, the lowest wear rate is for PA-6+6% wax with a value of  $5.5 \times 10^{-15}$  m<sup>2</sup>/N followed by PA-6+10%G+ 6% wax with  $6.9 \times 10^{-15}$  m<sup>2</sup>/N and PA-6+10%G with  $1.1 \times 10^{-14}$  m<sup>2</sup>/N and the highest value is  $2.2 \times 10^{-14}$  m<sup>2</sup>/N for pure PA-6. This means that wax and graphite filler presence in the composite shows 75% and 68% lower than that of pure polyamide-6 polymer.

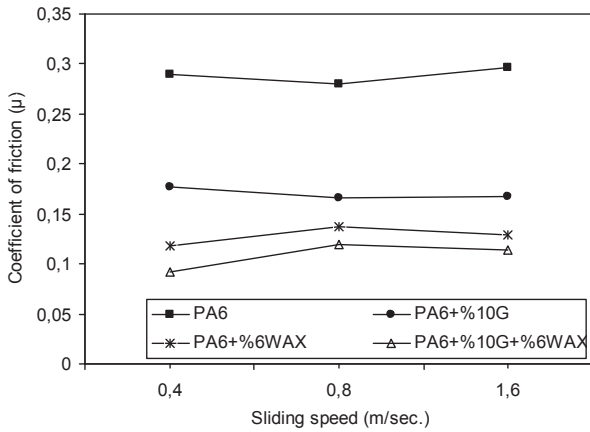


Figure 1. The variation of coefficient of friction and sliding speed for pure PA6, PA6+10%G, PA6+6%wax and PA6+10%G+6%wax polymer materials (Applied load: 100N)

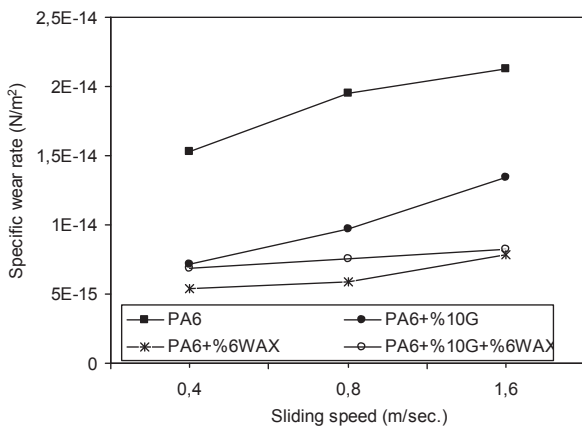


Figure 2. The variation of specific wear rate and sliding speed for pure PA6, PA6+10%G, PA6+6%wax and PA6+10%G+6%wax polymer materials (Applied load: 100N)

#### IV. CONCLUSIONS

The following items may be deduced from the results obtained from the tribological tests;

1. For PA6+6%wax and PA-6+10%G+6%W polymer materials, the coefficient of friction increase slightly with the increase in sliding speed.
2. For pure PA6, PA6+10%G, PA6+6%wax and PA6+10%G+6%wax polymer materials, the specific wear rate values increased with the increase in sliding speed.
3. The lowest wear rate is for PA6+6%wax with a value of  $5.5 \times 10^{-15} \text{ m}^2/\text{N}$ . The highest specific wear rate is for PA-6 polymer with a value of  $2.2 \times 10^{-14} \text{ m}^2/\text{N}$ .
4. From point view of tribological performance, PA6+6%wax is a more suitable polymer material for machine industry applications.
5. Finally, wax being a lot cheaper product than graphite, adding it to PA-6 means a high drop in the cost of the PA-6 composite material.

#### REFERENCES

- [1] T. Kyu, Z.I. Zhou, G.C. Zhu, Y. Tajuddin, S. Qutubiddin, Journal of Polymer Science Part B: Polymer Physics 34 (1996) 1761–1768.
- [2] K.H. Hess, Kunststoffe 73 (1983) 282–286.
- [3] H. Wiebeck, D.F. Borrelly, C. Xavier, P.S. Santos, S.A. Ascitti, M.P. Correa, Brazilian Journal of Chemical Engineering 15 (1998) 406–409.
- [4] H. Tanaka, Polymer Engineering Science 39 (1999) 817–824.
- [5] T. Watari, T. Yamane, S. Moriyama, T. Torikai, Y. Imaoka, K. Suehiro, H. Tateyama, Materials Research Bulletin 32 (1997) 719–724.
- [6] L.P. Cheng, D.J. Lin, K.C. Yang, Journal of Membrane Science 172 (2000) 157–166.
- [7] S. Choon Kang, D. Won Chung, Wear 254 (2003) 103–110.
- [8] P. Samyn, P. De Baets, G. Schoukens, B. Hendrickx, Polymer Engineering and Science 43 (2003) 1477–1487.
- [9] L. Chang., Z. Zhang, H. Zhang, A.K. Schlarb, Composites Science and Technology (2005).
- [10] U.S. Tewari, J. Bijwe, Tribological behavior of polyimides, in: M.K. Ghosh, K.L. Mittal (Eds.), Polyimides: Fundamentals and Applications, Marcel Dekker Inc. 1996.
- [11] B.B. Jia, T.S. Li, X.J. Liu, P.H. Cong, Wear 262 (2007) 1353–1359.
- [12] R.K. Goyal, A.N. Tiwari, U.P. Mulik, Y.S. Negi, Journal of Applied Polymer Science 6 (2008) 3379–3387.
- [13] C.J. Hooke, S.N. Kukureka, P. Liao, M. Rao, Y.K. Chen, Wear 200 (1996) 83–94.
- [14] X.R. Zhang, X.Q. Pei, O.H. Wang, Journal of Reinforced Plastics and Composites 27 (18) (2008) 2005–2012.
- [15] J.C. Anderson, in: K. Friedrich (Ed.), Friction and Wear and Polymer Composites, Composite Materials Series, vol. 1, Elsevier, Amsterdam, 1986, pp. 329–362.
- [16] H. Unal, A. Mimaroglu, Materials and Design 24 (2003) 183–187.
- [17] Q.Q. Shangguan, X.H. Cheng, Wear 262 (2007) 1419–1425.

# Analysis of Shear Properties of Bonded and Riveted Joints with CFRP Composite Tubes

Mustafa ASLAN<sup>#</sup>

<sup>#</sup> Ass. Prof. Dr.

Department of Metallurgical and Materials Engineering,  
Karadeniz Technical University, Trabzon, 61080, Turkey  
maslan@ktu.edu.tr

**Abstract**—The joints on tubular composites were experimentally characterised in terms material type and connection types in this study. The joints on composite tubes were manufactured with carbon fibre epoxy composite, aluminium 6061 series, and 3d printed ABS polymers in order to meet required strength in structural components. As a type of mechanical fastener, aluminium pop rivets and as an adhesive bonding material, a structural epoxy glue were applied to composite tubes. Adhesive joints have an advantage of weight and higher structural efficiency. They decrease stress concentrations with the joints which not seen in multiple rivet fasteners. In terms of shear properties under flexural and compression load, epoxy adhesive connections appear to be more favourable results when the tubes are combined. Multiple rivet fasteners showed lower results compared to results obtained with epoxy glued joints and both type connection applied joints

**Keywords**— CFRP Composite Tubes, Joints, Fasteners, Shear Properties

## I. INTRODUCTION

Carbon fibre reinforced composites are generally 30% lighter than aluminium and 50% lighter than steel [1]. Fabrication of car components with composite materials, however, needs specially designed joints in assemblies of structural components. In this respect, joints have crucial importance because they act as a transfer member where high stress concentrations and potential failures can occur during fatigue life of joined structures [2].

The design of joints strongly depends on geometrical parameters, joint materials and their properties (stiffness, strength) and properties of fasteners (rivets, bolts, pins) and adhesive materials (epoxy). Lap joints were commonly characterised by different design factors in laminar composites. However, the limited numbers of study are available with these design parameters in tubular composites. Previous studies calculated theoretical analysis of tubular lab joints in tension load and investigated the effect of adhesive layer thickness in terms of shear and normal stresses. They showed the infinite number of shear and normal stresses in overlapping ends. However, most of the study was limited to isotropic material properties in FEM and analytical results [3, 4]. Jena and

Pradhan were also applied FEM model adhesively connected joints on composite tubes in terms of thickness, overlap length and adhesive end fillets. They showed that optimum overlap length of 20-25 mm. The stress concentration values in CFRP composites were found less than isotropic material when an overlap length is more than to be of 20 mm. The optimum adhesive thickness also found to be 0,25 mm. The triangle and elliptical shape of end fillets of adhesive enhanced the joint strength [5].

## II. EXPERIMENTAL STUDY

### A. Material

The joints on tubular composites were experimentally characterised in terms material type and connection types in this study. The material selection was made by going out on the tube diameters and strength values to be used for the sections exposed to the load were determined in the automobile industry. The roll wrapped carbon fibre epoxy composite tubes in 2 mm thickness were required by Dost Kimya, Turkey. The joints on composite tubes were manufactured with carbon fibre epoxy composite, aluminium 6061 series, and 3d printed ABS polymers in order to meet required strength in structural components. The connection of the composites tubes with the different types of joints was applied with mechanical fasteners and adhesive bonding material. As a type of mechanical fastener, aluminium pop rivets and as an adhesive bonding material, a structural epoxy glue (Tiechem g550) were applied to composite tubes., the joints connected with multiple rivets, epoxy and both rivet and epoxy on composite tubes were shown in **Figure 1**. The multiple rivets in vertically applied in opposite direction (four number in total) to the joints and composite tube connection in order to provide homogeneous load distribution and magnitude. The epoxy glue was however applied to overlap area of the inner surface of the joints and the sandpapered outer surface of composite tubes considering the same overlap length size of 25 mm.



Fig. 1. Carbon epoxy composite tubes combined to different types of joint materials by multiple rivets, epoxy glue and both of them.

### B. Test Methods

Compression and flexural test experiments were carried out on an MTS Criterion model 45 brand universal testing machine. ASTM C364-99 has been used for the application of shear failure under compression loading. According to this standard, samples applied to the specimens is 2.0 mm/min. This test method includes the properties of pressing in the direction parallel to the pipe. ASTM C393-00 standard has been used for the application of interfacial short beam shear testing. According to this standard, the moving point feed rate applied to the specimens is 2 mm/min. This test method is used to determine the shear failure under the flexural load of the tubes, the maximum loads and displacement in connections between joints and composite tubes.

## III. RESULTS AND DISCUSSION

Table 1. Shear properties under compression of various type of fastener on different types of tubular structures.

Material types	Joint types	Shear strength [MPa]	Strain failure [%]	Load [N]	Maximum strain [%]
CFRP	Epoxy	1.99	1.17	4482	2.01
	Rivet	1.71	17.52	3783	24.48
	Epoxy & Rivet	1.75	12.67	3941	20.79
Aluminium 6061	Epoxy	1.43	0.48	3215	1.63
	Rivet	0.64	12.67	1432	23.77
	Epoxy & Rivet	1.28	0.95	2897	9.72
3d printed ABS	Epoxy	1.65	12.67	3711	19.96
	Rivet	1.48	8.92	3321	16.56
	Epoxy & Rivet	2.97	5.63	6616	7.82

According to the results given above in Table 1, the highest result in terms of shear strength under compressive load is obtained with application of both epoxy and multiple rivets in combination on 3d printed ABS joints with the value of 2.97 MPa. The lowest shear strength is obtained to with value of 0.64 MPa, resulting in the removal of rivets on aluminium joints on carbon epoxy composite tubes. Particularly in terms of connection elements, among three different types of connection have significantly affected on strength properties. In this respect, although multiple riveted fasteners generally exhibit higher strain ratios than those of epoxy glue, in terms of shear

strengths and maximum load, multiple rivet fasteners showed lower results compared to results obtained with epoxy glued joints and both type connection applied joints

Table 2. Shear properties flexural load of various type of fastener on different types of tubular structures.

Material types	Joint types	Maximum Load (N)	Deflection in max load (mm)	Max deflection (mm)
CFRP	Epoxy	1681	7.37	11.53
	Rivet	1177	7.81	15.33
	Epoxy & Rivet	1726	7.81	16.05
Aluminium 6061	Epoxy	4040	8.66	12.51
	Rivet	3244	4.10	19.96
	Epoxy & Rivet	3031	12.97	18.19
3d printed ABS	Epoxy	601	1.91	2.39
	Rivet	360	2.51	2.83
	Epoxy & Rivet	302	1.62	1.63

According to the flexural test results (Table 2), the highest maximum load value is 4040 N at the test sample where epoxy glue applied between the CFRP tubes and the aluminium joints. The lowest maximum stress value was determined to be 302 N in epoxy & rivet connections where ABS joints are connected to CFRP tubes. Connection elements only with epoxy and rivet joints usually give high maximum load values. However, both epoxy and rivet fastener applied connections of ABS pipes showed the lowest maximum deflection value. The test system in which aluminium joints were connected to carbon fibre epoxy composite tubes with rivet fasteners performed the maximum deflection value. The shear properties under flexural load are likely to show similar results to the shear properties under compression load. Epoxy adhesive connections appear to be more favourable results when the tubes are combined.

In terms of failure modes of the joints on composite tubes, shear out and bearing tension modes can be observed in failed test samples. Bearing type of failure mode give higher strength results and mostly observed in epoxy adhesive connections. The rivet fasteners as connection element showed shear out type of failure mode under compression and flexural load. Damaged at the contact area of joint and composite tubes induced rivet bending as well. This leads to increasing delamination of composite tubes and resulted in higher strain ratios in failure. The multiple rivets also showed complex behaviour for understanding of failure mode because the rivets were not equally shared the load and failed differently.

## IV. CONCLUSIONS

Adhesive joints have an advantage of weight and higher structural efficiency. They decrease stress concentrations with the joints which not seen in multiple rivet fasteners. Stress-strain behaviour of the adhesive and fastener joints also showed in non-uniform stress state. In future, the experimental results of this study will be supported by FEM modelling taking into

account the other design parameters such as the bonding thickness, bonding length and different shape of joints in composite connections.

#### REFERENCES

- [1] [1] The composite materials handbook MIL17 "Polymer matrix composites: materials, usage, design, and analysis, vol 2. ASTM International, West CRC press Newyork (2000)
- [2] [2] E. Patterson, D. Backman, G. Cloud Chapter 2 "Composite Materials and Joining Technologies for Composites": Proceedings of the 2012 Annual Conference on Experimental and Applied Mechanics pp. 5-9, Springer Science Media, London (2013)
- [3] [3] TA Collings Chapter 2: "Experimentally determined strength of mechanically fastened joints. In: Matthews FL (ed) Joining fibre-reinforced plastics, Elsevier Applied Science, New York (1987)
- [4] [4] A Aktas, MH Dirikolu "An experimental and numerical investigation of strength characteristics of carbon-epoxy pinned-joint plates. Compos Sci Technol 64:1605-1611(2004)
- [5] [5] B. Jena and B. Pradhan "Analysis and optimisation of bonded joints with FRP composite tubes Proceedings of the Ninth International Conference on Composite Materials Madrid Spain, 82-89 (1993)

# Investigation of Mechanical Properties of Biodegradable PLA Composites

Muhammed Dalu\*, Ertuğul Altuntaş<sup>+</sup>, Mustafa Aslan<sup>#\*</sup>, Ali Temiz\*

\*Department of Forest Industrial Engineering, Karadeniz Technical University, Trabzon, 61080, Turkey

<sup>+</sup>Department of Forest Industrial Engineering, Kahramanmaraş Sütcü İmam University, Kahramanmaraş, Turkey

<sup>#</sup>Department of Metallurgical and Materials Engineering, Karadeniz Technical University, Trabzon, 61080, Turkey

<sup>#</sup> corresponding author: [maslan@ktu.edu.tr](mailto:maslan@ktu.edu.tr)

**Abstract**— WPCs are fiber-reinforced composites produced by mixing wood components and polymers. The use of recycled chemically treated raw materials can also help to increase these properties for harsh environmental conditions. In this study, mechanical properties of treated and untreated wood flour filled polylactic acid composites were characterised. Results showed that the tensile modulus increased from 1490 MPa to 1874 MPa when the amount loading of wood flour increased from 30% to 50%. Similar trend was also observed in flexural modulus. However, the decrease in flexural and tensile strength was obtained due to the limited bonding between the cellulose fibres and the PLA matrix. The impact strength has highest value at 30% wood flour loading (2.67 kJ/m<sup>2</sup>)

**Keywords**— WPC, PLA, Treated wood, Mechanical Properties

## I. INTRODUCTION

Wood plastic composites as an alternative to traditional wood and wood based composites can be used outdoor applications with higher physical and biological properties such as durability and higher resistant to fungi, biocides. In a WPC, a polymer forms a continuous matrix that surrounds the reinforcing wood components. The low price and high stiffness of wood make it an attractive reinforcement for the commodity plastics [1]. The way of processing of WPCs is similar to the plastic, there are several appropriate manufacturing technologies available for WPCs. In spite of the fact that, the majority of WPC products are extruded, injection and compression molding are other major technologies used in WPC production [2].

Many polymers are used as the matrix material in wood plastic composites manufacturing, for examples, polyethylene (PE), polypropene (PP), polyvinyl chloride (PVC), polystyrene (PS). However, bioderived matrices, e.g. polylactide (PLA), cellulose esters and polyactates that have gained increased interest in recent years, which are made partly or fully from renewable resources [3]. In WPCs, the wood components are surrounded by the continuous polymer matrix. In general, the development of high quality WPCs is limited by two physical factors: the difference between the surface energy of the polymer matrix and wood components, and the upper temperature at which wood can be processed. There are several ways to offset or minimize these limitations and to improve the general performance of the WPC. The most common approach

involves the incorporation of different types of additives. Examples of additives used in WPCs are coupling agents, lubricants, stabilizers, inorganic fillers, biocides, and flame retardants [4-6].

## II. MATERIALS AND METHODS

### A. Materials



Figure 1. The manufactured wood plastic composites

The composite manufacturing consist of three main step; raw materials, mixture, compounding and compression molding, respectively. The raw materials formulation for the composites in this study were summarised in Table 1 and composition are given for polylactic acid (PLA) and Scotch pine (*Pinus sylverstris* L.) wood flour (30%, 40%, 50% wt) and, also maleic anhydride grafted by polyethylene (MAPE) (3%). The wood flour was dried for 24 h at 70 °C before composite preparation. Then it was mixed with the PLA and MAPE in a high-intensity laboratory mixer. This mixture was compounded in a twin-screw laboratory extruder. The seven-barrel temperature zones of the extruder were maintained from 170 °C to 195°C (from the feed zone to die zone with rising 5 °C at each barrel) during the production and the rotor speed was set at 100 rpm. Extruded samples were collected, cooled in cold water and pelletized with pelletizer. The pellets were poured into a metal frame to form the experimental composite panels via compression molding (carver) in a hot press for 4 min at 195 °C

Table 1. The compositions of the different wood plastic composites

Group ID	Wood flour (% wt)	PLA(% wt)	MAPE(% wt)
W30M3	30	70	3
W40M3	40	60	3
W50M3	50	50	3
W50M0	50	50	0

### B. Test Methods

In this experimental study, tensile and flexural test experiments were carried out on a Zwick/Roell Z010 brand universal testing machine according to ASTM D790 and ASTM D683 standards, respectively. The speed of cross head for both tests is of 5 mm/min. In tension test, elongation (strain) of the specimen was measured over a 25 mm gage length using an extensometer. In flexural testing, span length was determined as 16 times the thickness of the specimen (approximately 80 mm), as mentioned in the flexural properties standard. Moreover, the Izod impact strength was determined according to ASTM D256 standard using a HIT5.5P testing machine manufactured by Zwick Inc.. All impact samples were notched in the centre according to the standard. Six replicate samples were tested for each test group.

Morphology of the fractured composites after tensile testing was observed using a scanning electron microscope (SEM) (ZEISS EVO LS10, Germany) under an accelerating voltage of 5Kv and 250x magnification. A gold layer of a few nanometers in thickness was coated onto the fracture surfaces.

### III. RESULTS AND DISCUSSION

Table 2. Mechanical properties of wood PLA composites

Groups	Tensile strength(MPa)	Tensile modulus (MPa)	Flexural Stress	Flexural Modulus	Impact Strength
W30M3	26.32 ± 0.96	1490 ± 117	52.31 ± 2.07	3946 ± 234	2.67 ± 0.27
W40M3	19.01 ± 2.71	1568 ± 99	36.50 ± 4.60	4799 ± 131	2.13 ± 0.30
W50M3	25.03 ± 2.25	1874 ± 75	48.17 ± 6.31	5427 ± 238	2.42 ± 0.41
W50M0	16.70 ± 0.59	1714 ± 36	37.00 ± 2.58	5338 ± 294	2.28 ± 0.50

According to the results shown in **Table 2**, the tensile modulus increases with increasing loading of wood flour. The tensile modulus increased from 1490 MPa to 1874 MPa when the amount loading of wood flour increased from 30% to 50%. However, the tensile strength has the highest value of 26,32 MPa at 30% of wood flour loading and the lowest at 50% loading (16.70 MPa). As the amount of loading wood flour increased, the weak interfacial area between the filler and the matrix increased, which consequently decreased the tensile strength. The addition of MAPE coupling agent to wood flour PLA composites also showed significant increase in tensile strength of the composites by improving interfacial adhesion. Ashori & Nourbakhsh [7] also observed this. An increase in the wood content increases the micro spaces between the filler and the matrix, which weaken the filler–matrix interfacial adhesion. As a result, the values of tensile strength show a decreasing trend with increasing filler content in the composite. The flexural modulus and strength follow a similar trend as the tensile properties. The flexural modulus increased from 3946 MPa to 5427 MPa by 37.5% when wood flour increased from 30% to 50%. The flexure strength has the highest value of 52.31 MPa at 30% of wood flour loading. A similar finding was also

reported by Ndiaye et al. [8], Bhaskar et al. [9]. The decrease in flexural and tensile strength was probably due to the limited bonding between the cellulose fibres and the PLA matrix. The impact strength has highest value at 30% wood flour loading (2.67 kJ/m<sup>2</sup>) and lowest at 40% (2.13 kJ/m<sup>2</sup>) loading of the wood flour. Addition of MAPE also showed significant increase in flexural and impact properties of composites. The fracture surfaces after failed in tension test observed by SEM in Figure 2. The wood flour PLA composite samples with 3% of MAPE at 50% of wood flour content compared with wood flour PLA composites without MAPE in the same ratio of wood flour content.

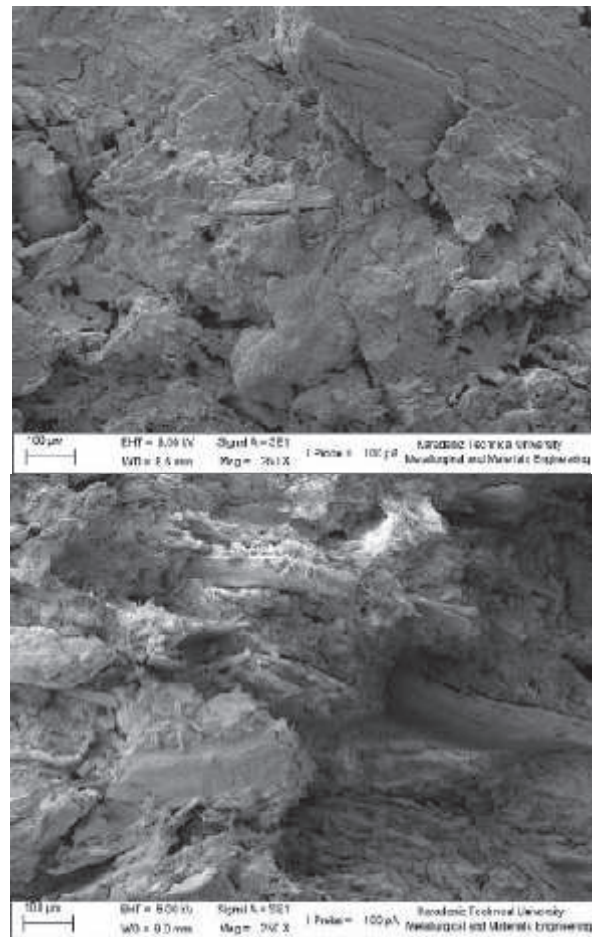


Figure 2. SEM images of wood flour-PLA composite with and without MAPE % at 250x

### REFERENCES

- [1] Clemons, C. (2008). Raw materials for wood-polymer composites. In: Oksman Niska K and Sain M (Eds.). Wood-Polymer Composites. Cambridge, CRC Press.
- [2] Godavarti, S. (2005). Thermoplastic wood fiber composites. In: Mohanty A, Misra M, and Drzal L (Eds.). Natural Fibers, Biopolymers, and Biocomposites. CRC Press, FL, US, pp. 348-386.
- [3] Faruk., O, Bledzki., K, and Nicolais L. (2012). Wood plastic composite: Present and future. Wiley Encyclopedia of Composites: 1-20.
- [4] English, W. and Falk, H. (1996). Factors that Affect the Application of Wood Fiber Plastic Composites. Wood Fiber-Plastic Composites, 7293, p.189-194.

- [5] [5] Farsi, M. (2000). Thermoplastic Matrix Reinforced with Natural Fibers: A Study on Interfacial Behavior. In *Some Critical Issues for Injection Molding*. pp. 225–247.
- [6] [6] George, J., Sreekala, M.S. and Thomas, S., 2001. A Review on Interface Modification and Characterization of Natural Fiber Reinforced Plastic Composites. *Polymer Engineering and Science*, 41(9), pp.1471–1484.
- [7] [7] Ashori, A and Nourbakhsh, A. (2009). Characteristics of wood – fiber plastic composites made of recycled materials. *Waste Management*, 29(4), pp.1291–1295.
- [8] [8] Ndiaye D, Matuana LM (2011) Thermal and mechanical properties of polypropylene/wood-flour composites *Applied polymer Sci* 119,3321-8.
- [9] [9] Bhaskar ,J., Haq.S. and Yadaw.S. (2012).Evaluation and testing of mechanical properties of wood plastic composite. *J Thermoplast Compos Mater*. 25(4), pp. 391-401.

# Characterization of Poly (Ethylene Terephthalate)/Poly (Butylene Terephthalate) Based Nanocomposites Reinforced with Reduced Graphene Oxide (ISLAC'18/UHAKS18)

Seda Hazer<sup>1</sup> Mehmet Özdemir<sup>1</sup> and Ayse Aytac<sup>1,2\*</sup>

<sup>1</sup> Department of Polymer Science and Technology, Kocaeli University, Kocaeli, 41380, Turkey

<sup>2</sup> Department of Chemical Engineering, Kocaeli University, Kocaeli, 41380, Turkey

\*Corresponding author: aaytac@kocaeli.edu.tr

**Abstract**—The blending of poly (ethylene terephthalate) (PET) and poly (butylene terephthalate) (PBT) offers the potential of improvements property between PET and PBT to obtain a new material with comprehensive properties. Considerable attention has been given to the graphene/polymer nanocomposites, which greatly improve the electrical and thermal conductivity, mechanical, thermal stability, and flame retardant properties of polymers. Similar to the other nanofillers, dispersion and interfacial interactions are the two main parameters of graphene/polymer nanocomposites. Because these parameters directly influence the properties of the prepared nanocomposites. In this work, a series of reduced graphene oxide (RGO) reinforced PET/PBT-blend based nanocomposites were prepared in a laboratory scale co-rotating extruder by melt mixing method. Two different loading level of RGO were used as 0.5 and 1 wt.%. The mechanical, thermal and thermomechanical properties of composites were characterized by using tensile tests, dynamic mechanical analyzer (DMA), differential scanning calorimeter (DSC) thermal gravimetric analysis (TGA) and scanning electron microscope (SEM). As the increased amount of reduced graphene oxide increases crystallization and melting temperature PET/PBT-blends. The elongation at break values of nanocomposites decreased and the tensile strength value of the nanocomposites slightly changed with the increasing loading level of RGO.

**Keywords**— poly (butylene terephthalate) (PBT), poly (ethylene terephthalate) (PET), reduced graphene oxide (RGO)

## I. INTRODUCTION

Poly (ethylene terephthalate) (PET) and poly (butylene terephthalate) (PBT) are the members of the most important commercial thermoplastic polyesters. PBT has the advantages of rapid crystallization rate and good mouldability properties compared with the PET, while heat-deflection temperature and rigidity of PET are superior to those of PBT. However, the processing of PET is difficult because of its low melt strength and slow rate of crystallization. PBT has the advantages of

rapid crystallization rate and good moldability. In general, the mechanical properties as well as chemical resistance characteristics are comparable for both PET and PBT. The blending of PET and PBT offers the potential of improvements property between PET and PBT to obtain a new material with comprehensive properties [1]. Theoretical compatibility of PET and PBT blends through thermodynamic considerations have been worked [2]. Also in a study indicate that PET is compatible with PBT in the amorphous phase, but in crystals phase they create separate crystal forms rather than co-crystals [3]. PBT-PET blends can have different properties than PET or PBT, according to the different blending ratio and processing conditions.

Graphene is a potential nanofiller, a single layer of carbon atoms arranged in a honeycomb network that can dramatically improve the properties of polymeric materials at a very low loading. Recently studies show that with an edition of the small amount of the graphene polymeric materials can gain better electronic [4]-[6], thermal [7], and mechanical properties [8]. More than one techniques have been improving for graphene production such as chemical [9] and mechanical exfoliation [10], alkali metals intercalation and expansion [11], microwave chemical vapor deposition, substrate-based thermal decomposition [6], and thermal exfoliation of graphite oxide [12]. The thermal exfoliation and in situ reduction method much more suitable for mass production of graphene. After thermal exfoliation of graphite oxide; graphene still contained some oxygen-containing groups [12], which will facilitate the dispersion of the nanosheets in polar polymers [13]. Graphene oxide is an oxygen enriched state of graphene. Its single layer of carbon atoms has such as epoxide and hydroxyl groups, and its edge layer with carbonyl and carboxyl groups [14]. Because of these functional groups GO gain hydrophilic character, which can improve interfacial interaction between GO and some polymers. So that GO has been extensively used for various polymer composition. Because of oxygen rich functional groups attached to the GO surface; GO is showing less electrically and thermally conductive polymer composites

than graphene. To make insulating GO conductive, an efficient reduction process must be carried out. Generally, such processes involve high temperature thermal annealing or low temperature chemical reduction. The resulting reduced graphene oxide (RGO) with higher conductivity is a promising filler for conductive composites. In this study, a series of reduced graphene oxide (RGO) reinforced PET/PBT-blend based nanocomposites were prepared in a laboratory scale co-rotating extruder by using a melt mixing method. Two different loading level of RGO were used as 0.5 and 1 wt. %. The mechanical, thermal and thermomechanical properties of composites were characterized by using tensile tests, dynamic mechanical analyzer (DMA) and differential scanning calorimeter (DSC), thermal gravimetric analysis (TGA) and scanning electron microscope (SEM).

## II. MATERIAL AND METHODS

### A. Material

Poly (ethylene terephthalate) (PET Density: ~1,38g/cm<sup>3</sup>, Melting Point: ~260 °C), poly (butylene terephthalate) (PBT Density: 1,18g/cm<sup>3</sup>, Melting Point: ~240 °C) and the reduced graphene oxide was supported from Hazerfen Kimya Malzeme ve Enerji Tek. San A.Ş for research purpose.

### B. Methods

PET and PBT were dried under vacuum oven at 160 °C for 12h before processing. PET-PBT (95:5) and (70:30) blends were prepared as control samples and after that two different RGO ratio added to these blends as 0.5 wt.% and 1 wt.% respectively. All composites were compounded on a laboratory scale co-rotating Twin-Screw Mini-Extruder (Micro-Compounder 15 ml) at 280 °C 100 rpm 3 min. The melt was directly transferred to the cylinder of DSM Xplore 10 ml laboratory-scale injection molding machine® to produce 80x10x2 mm<sup>3</sup> bars injection pressure. The prepared sample codes and a compounding ratio of blends are summarized in Table I.

TABLE I  
PREPARED SAMPLE CODES AND COMPOUNDING RATIO OF BLENDS

Element	PET%wt	PBT%wt	RGO%wt
PET	100	0	0
PBT	0	100	0
95:5 PET-PBT	95	5	0
70:30 PET-PBT	70	30	0
95:5-0.5GO	95	5	0.5
95:5-1GO	95	5	1
70:30-0.5GO	70	30	0.5
70:30-1GO	70	30	1

Tensile tests were performed by using Instron (2712-020) trademark of the universal testing machine, according to ISO 527 5 A standards. The rate of straining is 5 mm/min.

Metravib-01dB-DMA test machine was used for DMA of PET/PBT blends and composites. Storage modulus (E') was measured. The frequency of 1 Hz, ramp rate of 10°C/min temperature from 25 °C to 200 °C.

(DSC) an analysis was performed in Mettler Toledo DSC 1 machine under the nitrogen atmosphere for measuring glass transition temperature (T<sub>g</sub>), melting temperature (T<sub>m</sub>) and heat of fusion (ΔH<sub>matrix</sub>). The temperature was changed from 25 °C to 280 °C with 10°C/min heating rate. The degree of crystallinity (X<sub>c</sub>) of prepared sample was calculated according to PET by using thermal properties with the following equation (1). [15]

$$X_c(\%crystallinity) = \frac{\Delta H_m - \Delta H_c}{(\omega_f) * \Delta H_m^0} \quad (1)$$

Thermal Gravimetric Analysis (TGA) was conducted in Mettler Toledo machine under the nitrogen atmosphere. Heating rate of the samples was 10°C/min and the temperature was increased 25 °C to 750 °C.

SEM (JOEL JSM 6510) analysis was performed to investigate the fracture surfaces of tensile testing samples at an accelerating voltage 10.0 kV; zoom in 500X.

### C. RESULT AND DISCUSSION

1) *Mechanical Characteristics*: The different compositions were prepared for PET-PBT blends and RGO reinforced PET-PBT composites between 95:5 wt. % and 70:30 wt.% (Table I). The mechanical tests were performed to the prepared PET-PBT blends and composites. Tensile strength and strain values of blends and composites were obtained from tensile tests. The mechanical properties of all blends and nanocomposites are shown in Table II. In addition, the tensile stress and strain graphic of the samples are given in Fig.1. The maximum tensile stress at max. load value was observed for 95:5 PET-PBT sample as 59.7 MPa. The tensile strength value of the nanocomposites slightly decreased between 8% and 16% with the increasing loading level of RGO. The elongation at break values of nanocomposites decreased considerably.

TABLE II  
MECHANICAL PROPERTIES OF NANOCOMPOSITES

Element	Tensile Stress at Max Load (Mpa)	Elongation at Break Values (%)
PET	58.0	491
PBT	51.2	366
95:5 PET-PBT	59.7	489
70:30 PET-PBT	59.4	494
95:5-0.5RGO	54.9	6.0
95:5-1RGO	52.7	6.0
70:30-0.5RGO	51.3	5.8
70:30-1RGO	49.6	5.3

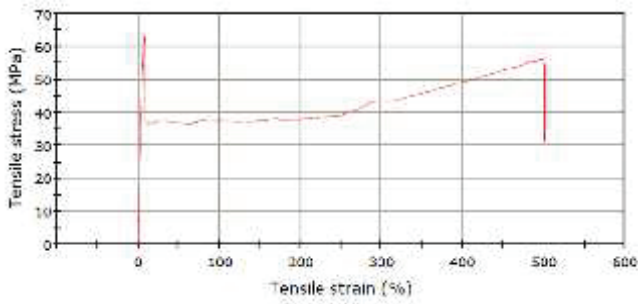


Fig. 1 The tensile stress and strain graphic of the 95:5 PET-PBT sample

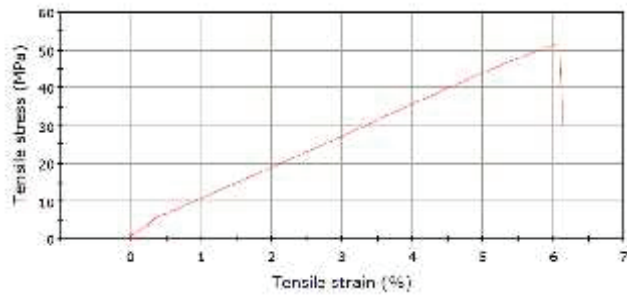


Fig. 2 The tensile stress and strain graphic of the 95:5-0.5RGO sample

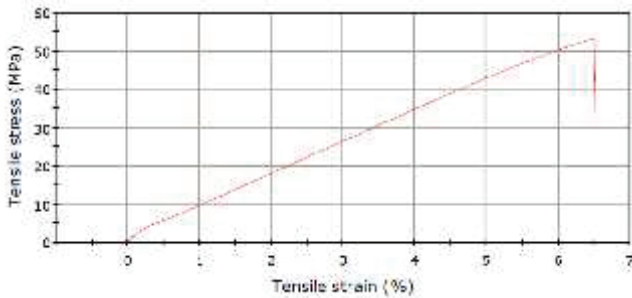


Fig.3 The tensile stress and strain graphic of the 95:5-1RGO sample

2) *Differential Scanning Calorimetry (DSC)*: Thermal properties of the blends and their nanocomposites such as glass transition temperature ( $T_g$ ) melting temperature ( $T_m$ ), crystallization enthalpy ( $\Delta H_c$ ) and melting enthalpy ( $\Delta H_m$ ) were obtained from DSC analysis. DSC results and thermograms were given in Table III and Fig.4, respectively. The glass transition temperature of PET is 70-80 °C approximately [16].  $T_g$  value of PBT is determined as 49 °C. The addition of PBT the PET caused a decrement in  $T_g$ . This reduction is slightly recovered as a result of the incorporation of RGO to the PET. The melting temperature values ( $T_m$ ) of all formulations were slightly changed. The degree of crystallinity was obtained from the melting enthalpy (melting peak areas) referred to the theoretical value of the melting enthalpy of 100% crystalline PET and PBT (12.56xJ/kg and 14.34xJ/kg) respectively [15]. Crystallinity ( $X_c$ ) value of the 95:5 PET-PBT unaffected by the addition of 5wt.% PBT. The addition of RGO to polymer system increased the crystallinity due to the nucleating agent of RGO. The maximum % crystallinity value was observed for the 1wt.% RGO including 70:30 PET-PBT composites in DSC analysis.

TABLE III  
DSC RESULTS FOR PREPARED SAMPLES

Element	$T_g$ (°C)	$T_m$ (°C)	$\Delta H_m$ (J/g)	$\Delta H_c$ (J/g)	$X_c$ %
PET	77	259	32	17	12
PBT	49	224	11	8	2
95:5 PET-PBT	66	255	22	8	11
70:30 PET-PBT	67	254	28	20	9
95:5-0.5RGO	75	259	42	24	15
95:5-1RGO	76	261	30	16	12
70:30-0.5RGO	65	258	27	10	19
70:30-1RGO	61	261	40	18	25

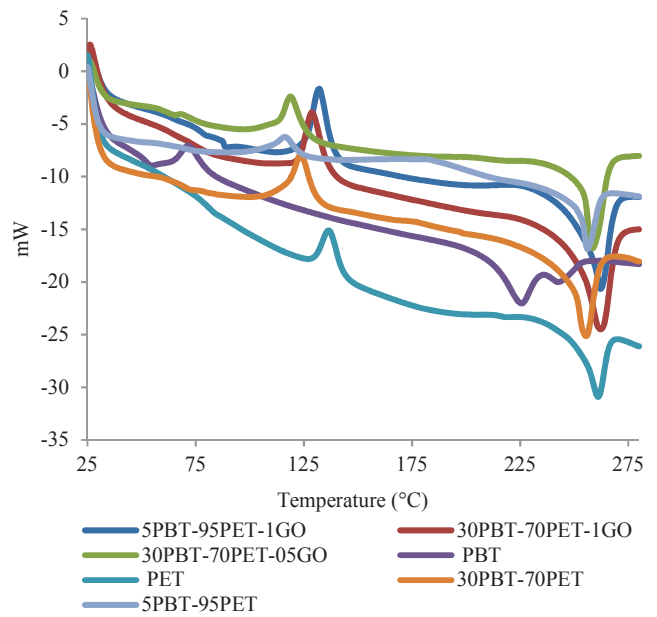


Fig. 4 DSC thermograms for all Prepared Samples

3) *Thermal Gravimetric Analysis (TGA)*: Thermal stability of the PET, PBT, PET-PBT blends and composites were conducted by TGA analysis. TGA results were summarized in Table IV. Onset temperature values for PET and PBT were measured 405 and 367 °C respectively. The similar onset values were obtained for PET-PBT blends and composites. TGA results indicate that one step degradation curve and 95:5-1GO has the most char residue. As it was expected the percentage of char residue increased with the increasing RGO ratio within the matrix.

TABLE IV  
TGA RESULTS FOR PREPARED SAMPLES

Element	Onset (°C)	%50Mass Lose Temp (°C)	Endset (°C)	%Char Residue (740°C)
PET	405	427	441	13
PBT	367	393	408	11
95:5 PET-PBT	384	412	437	12
70:30 PET-PBT	396	424	439	17
95:5-0.5GO	398	426	441	19
95:5-1GO	394	425	439	21
70:30-0.5GO	384	413	436	13
70:30-1GO	390	423	440	19

4) *Dynamic Mechanical analysis (DMA)*: The storage modulus ( $E''$ ) value of the blends and composites were given in Figure 5. According to Fig 5, among the composites, maximum storage modulus value was observed 95:5-0.5RGO. In addition, storage modulus value of nanocomposites increased compared to the blends.

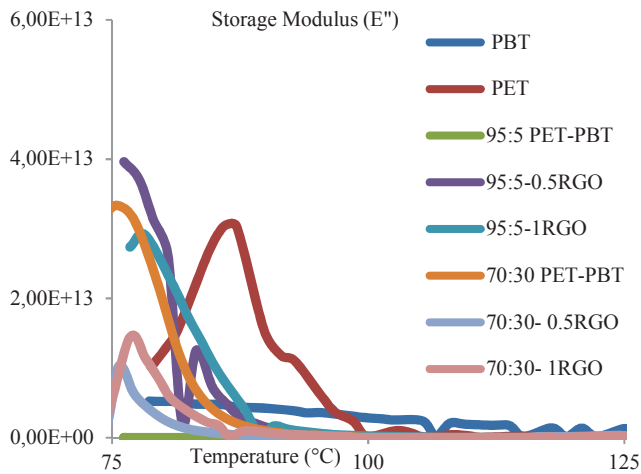


Fig. 5 DMA thermograms for all Prepared Samples

5) *Scanning Electron Microscope (SEM)*: Figure 6 shows scanning electron micrographs for the PET-PBT blends and composites. The morphology of the 95:5 and 70:30 PET-PBT blend compositions compared in Fig 6. The PET-rich 95:5 composition show slightly higher deformation on the fracture surface compared to the deformation surface of the 70:30 PET-PBT blend. It was seen that the macro cracks returned to the micro cracks. It was concluded that RGO has been changed all PET-PBT composite breaking point morphology.

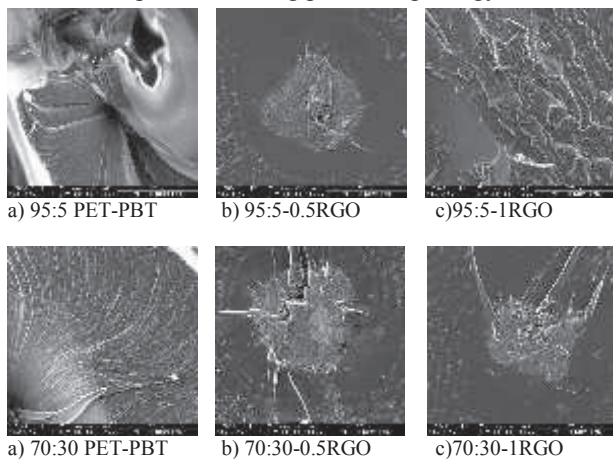


Fig. 6 Scanning electron micrographs of fracture surfaces of samples based on 95:5 PET-PBT, 70:30 PET-PBT and composites.

#### D. Figure Captions

Fig. 1 The tensile stress and strain graphic of the 95PET-5PBT sample

Fig. 2 The tensile stress and strain graphic of the 5PBT-0.5RGO sample

Fig.3 The tensile stress and strain graphic of the 5PBT-1RGO sample

Fig 4. DSC thermograms for all Prepared Samples

Fig 5. DMA thermograms for all Prepared Samples

Fig 6. Scanning electron micrographs of fracture surfaces of samples based on 95:5 PET-PBT, 70:30 PET-PBT and composites.

#### E. Table Captions

Table 1. Prepared Sample Codes Sample Codes and Compounding Ratio of Blends

Table 2. Mechanical Properties of Nanocomposites

Table 3. DSC Results for Prepared Samples

Table 4. TGA Results for Prepared Samples

### III. CONCLUSIONS

In this study, the characteristic of PET/PBT blends and RGO reinforced PET/PBT composites were investigated. Mechanical test results showed that the tensile strength value of the nanocomposites slightly changed with the increasing loading level of RGO. Elongation at break values of RGO PET-PBT composites has decreased dramatically. The maximum crystallinity was observed for the 1% RGO including 70:30 PET-PBT composites in DSC analysis. TGA results indicate that one step degradation curve and 95:5-1RGO has the most char residue. The storage modulus value of the blends increased with the addition 1wt.% RGO. As expected RGO addition on the PET-PBT composites increased the percent crystallinity. It was seen in the SEM micrographs that RGO changed all PET-PBT composite breaking point morphology.

#### ACKNOWLEDGMENT

The authors thank to Hazerfen Kimya Malzeme ve Enerji Tek. San A.Ş for providing the reduced graphene oxide.

#### REFERENCES

- [1] F. Wang, X. Meng, X. Xu, B. Wen, Z. Qian, X. Gao, Y. Ding, S. Zhang, M. Yang, "Inhibited transesterification of PET/PBT blends filled with silica nanoparticles during melt processing", *Polymer Degradation and Stability*, 93, 1397–1404, August, (2008).
- [2] S. P. Mishra and B. L. Deopura, Theoretical Prediction of Compatibility of Poly (ethylene terephthalate) and Poly (butylene terephthalate) blends, *Poly. Comm*, 26,5-7, (1985)
- [3] S. P. Mishra & B. L. Deopura, "Fibres from PET & PBT Blends," *J. Appl. Polym. Sci.*, 33,759-768, (1987).
- [4] Zhang Y, Tan YW, Stormer HL, Kim P. "Experimental observation of the quantum Hall effect and Berry's phase in graphene". *Nature* 438(7065):201–4, November, (2005)
- [5] Zhang YB, Small JP, Amori MES, Kim P. "Electric Field Modulation of Galvanomagnetic Properties of Mesoscopic Graphite", *Phys Rev Lett*, 94(17):176803, May, (2005)
- [6] Berger C, Song ZM, Li TB, Li XB, Ogbazghi AY, Feng R, et al., "Ultrathin Epitaxial Graphite: 2D Electron Gas Properties and a Route toward Graphene-based Nanoelectronics," *J Phys Chem B* 108(52):19912–6, December, (2004)
- [7] Balandin AA, Ghosh S, Bao WZ, Calizo I, Teweldebrhan D, Miao F, et al., "Superior thermal conductivity of single-layer graphene," *Nano Lett* 8(3):902–7, February, (2008)

- [8] Lee C, Wei XD, Kysar JW, Hone J. "Measurement of the elastic properties and intrinsic strength of monolayer graphene", *Science* 321(5887):385–8, July, (2008)
- [9] Stankovich S, Dikin DA, Dommett GHB, Kohlhaas KM, Zimney EJ, Stach EA, et al. "Graphene-based composite materials" *Nature*,442(7100):282–6. July, (2006)
- [10] Novoselov KS, Geim AK, Morozov SV, Jiang D, Zhang Y, Dubonos SV, et al."Electric field effect in atomically thin carbon films," *Science* ,306(5696):666–9, October, (2004)
- [11] Viculis LM, Mack JJ, Kaner RB. "A chemical route to carbon nanoscrolls," *Science*,299(5611):1361, February (2003)
- [12] McAllister MJ, Li JL, Adamson DH, Schniepp HC, Abdala AA, Liu J, et al. "Single Sheet Functionalized Graphene by Oxidation and Thermal Expansion of Graphite" *Chem Mater*,19(18):4396–404, May, (2007)
- [13] Ramanathan T, Abdala AA, Stankovich S, Dikin DA, Herrera-Alonso M, Piner RD, et al."Functionalized graphene sheets for polymer nanocomposites," *Nat Nanotechnol* 3(6):327–31. (2008)
- [14] W. Cai , R. D. Piner , F. J. Stadermann , S. Park , M. A. Shaibat , Y. Ishii , D. Yang , A. Velamakanni , S. J. An, M. Stoller, J. An , D. Chen , R. S. Ruoff , "Synthesis and solid-state NMR structural characterization of <sup>13</sup>C-labeled graphite oxide," *Science*, 321 , 1815; September, (2008)
- [15] C. Bastioli, I. Guanella, And G. Romano, "Effects of Water Sorption on the Physical Properties of PET, PBT, and Their Long Fibers Composites", *Polymer Composites*, Vol. 7 7, No. 7 February (1990)
- [16] Y.Yu And K.J Choi, "Crystallization in Blends of Poly(Ethylene Terephthalate) and Poly( Butylene Terephthalate)", *Polymer Engineering And Science*,Vol. 37, No. 1, January (1997).

# Farklı Yağlayıcılarla Öğütülen Ön Karışımli Alumix 123 Tozların Sıcak Preslenmesiyle T/M Parça Üretimi

Cankız Gizem Delibalta\*, Yusuf Özçatalbaş  
cankizdelibalta@gmail.com, yusufoz@gazi.edu.tr

*Metallerji ve Malzeme Mühendisliği, Teknoloji Fakültesi, Gazi Üniversitesi, 06560, Ankara, Türkiye*

**Özet-** Bu çalışmada ön karışımli Alumix 123 tozuna, ağırlıkça % 1,5 Çinko Stearat ve % 2 Stearik Asit katı yağlayıcısı ilave edilerek 10 saat süreyle yüksek enerjili atritörde mekanik alaşımlama (MA) işlemine tabi tutularak öğütülmüştür. Alumix 123 başlangıç tozun bileşimi ağırlıkça % 4,5 Cu, % 0,7 Si, % 0,5 Mg ve kalanı alüminyum tozu içermektedir. Azot gazı atmosferinde 10 mm çapında bilyalar kullanılarak yapılan MA işleminde bilya /toz oranı 10:1 ve devir 400 dev/dk seçilmiştir. 10 saatlik MA işlemi sonunda çinko stearat içeren ön karışımli tozun ortalama boyutu 45,2µm, stearik asitle işlem yapılan tozun ortalama boyutu ise 37µm dur. Bu tozlar bir kalıp içinde 300 MPa ön presleme basıncında oda sıcaklığında tek eksenli preslenmiştir. Daha sonra aynı kalıp içinde 300, 350, 400, 450 °C sıcaklıklarda 15'er dakika süreyle bekletilerek toplamda 1 saat yağlayıcı giderme işlemi uygulanmıştır. Yağlayıcı giderme işlemi devamında 540 °C sıcaklıkta 50 MPa basınç altında 30 dakika süreyle sıcak olarak preslenerek toz metal (T/M) numuneler üretilmiştir. Stearik asitle işlem gören tozlardan üretilen TM numunede teta fazı (CuAl<sub>2</sub>) oranının daha fazla olduğu tespit edilmiştir. Sertlik değerlerinin mekanik alaşımlama işlemiyle arttığı görülmüş, en yüksek sertlik değerine Stearik asitle işlem gören tozlarla üretilen TM numunede ulaşılmıştır.

**Anahtar Kelimeler** — Toz Metalurjisi, Sıcak presleme, Mekanik Alaşımlama, Yağlayıcı, Alumix123

## P/M Part Production by Hot Pressing of Pre-Mixed Alumix 123 Powders Milled with Different Lubricants

**Abstract** - In this study, premixed Alumix 123 powder was milled by mechanical alloying (MA) treatment in a high-energy attritors for 10 hours with 1.5 wt.% Zinc Stearate and 2 wt.% Stearic Acid solid lubricant added. The starting powder composition of Alumix 123 contains 4.5wt% Cu, 0.7wt% Si, 0.5wt% Mg and the rest of aluminum powder. MA process was performed at 400 rpm in a nitrogen gas atmosphere by using balls 10 mm in diameter and 10:1 ball/powder ratio. At the end of 10 hours MA operation, the pre-mixed powder containing zinc stearate has an average size of 45.2 µm and the average size of the powder treated with stearic acid is 37 µm. These powders were

compacted at 300 MPa pre-pressing pressure at room temperature. And then, in the same mold at 300, 350, 400, 450°C for 15 minutes, a total of 1 hour, lubricant removal process was applied. After lubricant removal process, hot pressed powder metal (P/M) samples were produced under 50 MPa pressure at 540 ° C for 30 minutes. The teta phase (CuAl<sub>2</sub>) ratio was found to be higher in the P/M sample produced from the stearic acid treated powders. The hardness values were found to increase with the mechanical alloying process and the highest hardness value was reached in the PM sample produced with stearic acid treated powders.

**Keywords**- Powder Metallurgy, Hot Pressing, Mechanical Alloying, Lubricant, Alumix123

## I. GİRİŞ

Alüminyum diğer metallere oranla düşük maliyetli, hafif bir metaldir ve ısıl işleme uygulanabilme avantajına sahiptir, özellikle yüksek performans malzemelerinden en kolay şekilde üretilenlerden biridir [1]. Alüminyum-Bakır alaşımları (2000 serisi), havacılık sanayinde kullanılan birincil alaşım türüdür ve belirli ısıl işlemler uygulanarak kullanılır [1-2]. Mekanik alaşımlama (MA) yüksek enerjili bir bilyalı değirmende katı halde toz partiküllerinin tekrarlanan kaynak, kırılma ve yeniden kaynaklanmasını içeren toz işleme tekniğidir[3-6]. Bu yöntem sonraki işlemler için daha küçük parçacık boyutu imkanı sağlar ve bu yöntemle elde edilen tozların toz metalurjisi süreci ile kompakt parçalar elde edilmesinde sıcak presleme aktif sinterleme yönteminin kullanılması ise parça yoğunluğunu %100'e yaklaştırabilir [7]. Sinterleme yöntemlerinden biri olan sıcak presleme yöntemi, aynı kalıp içerisinde hem sıkıştırma hem de sinterleme işleminin yapılmasına olanak sağlamaktadır. Bu işlemde, toz malzemenin yüksek sıcaklık deformasyon mekanizmaları, geliştirilmiş işlem sıcaklığının ve basıncın eşzamanlı uygulanmasıyla aktive edilir [7-8]. Bu yöntemde, presleme ve sinterleme işleminin birlikte yapılması soğuk presleme işlemine göre yüksek dayanım, sertlik ve yoğunluk yanında parçada düşük gözenek miktarı ve büzülmenin daha düşük

olması gibi üstünlükler sağlamaktadır [9]. Bu değerler ise başlangıç parçacık boyutlarına göre değişkenlik göstermektedir [10]. Üretilen T/M malzemelerin mikro yapısı ve mekanik özellikleri; başlangıç parça boyutuna, sinterleme sıcaklığına, presleme basıncına, sinterleme sonrası yapılan ısı işlemlere, fazların kimyasal yapısı ve mikro yapıdaki miktarına, kompakt içindeki gözenek miktarı ve geometrisine bağlı olarak da değişim gösterir [11-15].

Bu çalışmada, ön karışimli Alumix 123 tozuna ve ayrı ayrı ağırlıkça %1,5 Çinko Stearat ve % 2 oranında Stearik Asit yağlayıcıları eklenerek 10 saat süreyle yüksek enerjili atritörde mekanik alaşımlama işlemi uygulanmış, üç farklı karışım toz elde edilmiştir. Elde edilen bu tozlar ve MA işlemi uygulanmamış Alumix 123 toz karışımı, bir kalıp içinde 300 MPa ön presleme basıncında oda sıcaklığında tek eksenli preslenmiştir. Daha sonra aynı kalıp içinde 300, 350, 400, 450°C sıcaklıklarda 15'er dakika süreyle bekletilerek toplamda 1 saat yağlayıcı giderme işlemi uygulanmıştır. Yağlayıcı giderme işlemi devamında 540 °C sıcaklıkta 50 MPa basınç altında 30 dakika süreyle sıcak olarak preslenerek toz metal (T/M) numuneler üretilmiş, MA işleminin numune özelliklerine etkisi araştırılmıştır.

## II. DENEYSEL ÇALIŞMALAR

### A. Malzeme

Bu çalışmada Eckart Granulers (Almanya) tarafından üretilen Ecka Alumix 123 olarak bilinen ön-karışimli alüminyum esaslı tozlar kullanılmıştır. Alumix 123 tozuna ağırlıkça %2 stearik asit ( $\text{CH}_3(\text{CH}_2)_{16}\text{COOH}$ ) ve %1,5 çinko stearat ( $\text{Zn}(\text{C}_{18}\text{H}_{35}\text{O}_2)_2$ ) yağlayıcıları kullanılarak iki farklı karışım toz hazırlanmıştır. Alumix 123 tozunun başlangıç ortalama parçacık boyut değeri  $d_{0,5} = 114,44 \mu\text{m}$ 'dir. Kullanılan tozun içeriği % Ağırlık olarak Tablo I 'de verilmiştir.

Tablo I. Toz malzemenin kimyasal bileşimi (% ağırlık)

Alaşım Elm.	Al	Cu	Si	Mg
Alumix 123	94,3	4,5	0,7	0,5

İşlem sonrası elde edilen parçacık boyut değerleri, çinko stearat içeren ön karışimli toz için ortalama boyutu 45,2 $\mu\text{m}$ , stearik asitle işlem yapılan toz için ortalama boyutu ise 37 $\mu\text{m}$  dur.

### B. Metod

Alüminyum esaslı Alumix 123 ön karışimli tozlarına ayrı ayrı %1,5 çinko stearat ( $\text{C}_{36}\text{H}_{70}\text{O}_4\text{Zn}$ ) ve %2 stearik asit ( $\text{CH}_3(\text{CH}_2)_{16}\text{COOH}$ ) yağlayıcıları ilave edilerek; mekanik alaşımlama işlemi uygulanmıştır. Mekanik alaşımlama işlemi, su soğutmalı atritör tipi cihazda azot ( $\text{N}_2$ ) gazı atmosferinde, dev/dk hızda 4, 8 ve 10 saat süreler ile

gerçekleştirilmiştir. MA işleminde çelik kazan, Ø10 mm çapında çelik bilye, çelik karıştırıcı kol kullanılmıştır ve bilya/toz oranı 10/1'dir.

MA yöntemi ile elde edilen tozlar ve işlem görmemiş Alumix 123 toz karışımı bir kalıp içerisinde, 300 MPa ön presleme basıncında oda sıcaklığında tek eksenli preslenmiştir. Daha sonra aynı kalıp içinde 300, 350, 400, 450 °C sıcaklıklarda 15'er dakika süreyle bekletilerek toplamda 1 saat yağlayıcı giderme işlemi uygulanmıştır. Yağlayıcı giderme işlemi devamında 540 °C sıcaklıkta 50 MPa basınç altında 30 dakika süreyle sıcak olarak preslenerek toz metal numuneler üretilmiştir.

T/M parçaların fiziksel özelliklerinin belirlenmesi için Arşimed prensibine göre yoğunluk ölçümleri ve Brinell sertlik ölçümleri yapılmıştır. Numunelerin metalografik muayeneleri yapılarak optik mikroskop çalışmaları gerçekleştirilmiştir. Faz dönüşümlerini tanımlamak amacıyla XRD analizleri gerçekleştirilmiştir.

Deney numunelerinin yoğunluk ölçümleri Arşimet prensibine göre çalışan, 0,0001 g hassasiyetdeki üzerinde yoğunluk kiti bulunan Sartorius marka dijital terazide ölçülmüştür. Deney numunelerinin teorik yoğunlukları  $\rho_{\text{Alumix123}}=2,974/\text{cm}^3$  hesaplanmış ve bu çalışmadaki yoğunluk değerleri Eş.1 kullanılarak verilmiştir. Eşitlikte belirtilen " $\rho_{\text{ölçümlü}}$ " değeri, deneysel çalışmalarda elde edilen yoğunluk değerini, " $x$ " değeri yüzde yoğunluk değerini belirtmektedir.

$$\% x = \frac{\rho_{\text{ölçümlü}}}{\rho_A} \times 100 \dots \dots \dots \text{Eş.1.}$$

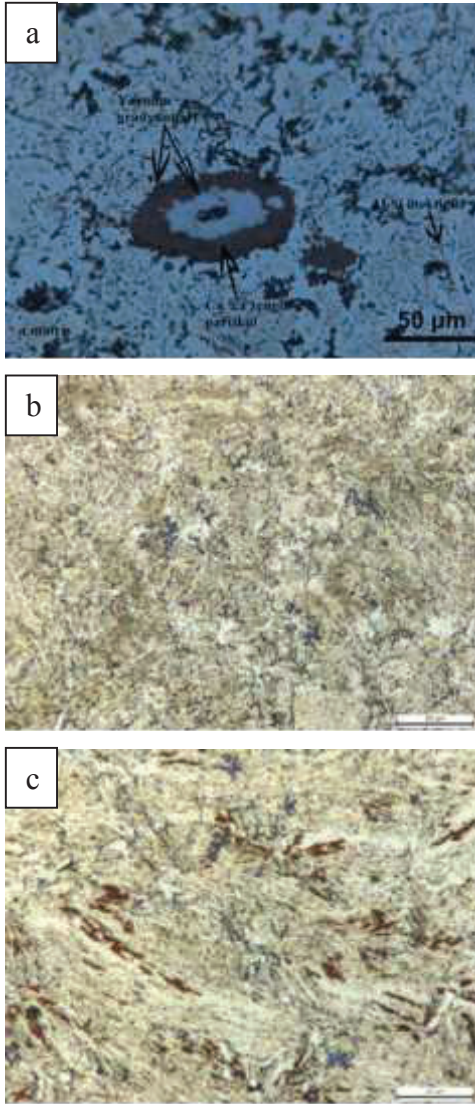
Deney numunelerinin sertlik ölçümlerinde, Brinell sertlik değerleri elde edilmiştir. Brinell sertlik testinde; 2,5 mm çaplı uç kullanılmış ve 31,25 kg yük uygulanmıştır.

## III. DENEY SONUÇLARI VE TARTIŞMA

### A. Optik Mikroskop Çalışmaları

Şekil 1'de, işlemsiz Alumix 123 ön karışimli tozdan ve sıcak presleme ile üretilen T/M malzemenin mikroyapısı (MA0), çinko stearat katkılı MA işlemi uygulanmış tozdan elde edilen numunenin (ÇSMA10) mikroyapısı ve stearik asit katkılı MA işlemi uygulanmış tozdan elde edilen numunenin (SAMA10) mikroyapısı verilmiştir.

Şekil 1a'da işlemsiz Alumix 123 ön karışimli tozdan sıcak presleme ile üretilen T/M malzemenin mikroyapısı verilmiştir. Al matris içinde tamamen çözünmemiş Cu parçacıklar açıkça görülmektedir. Ayrıca yer yer Al-Si ötektiği ve farklı geometrilere bakırca zengin fazlar mevcuttur.



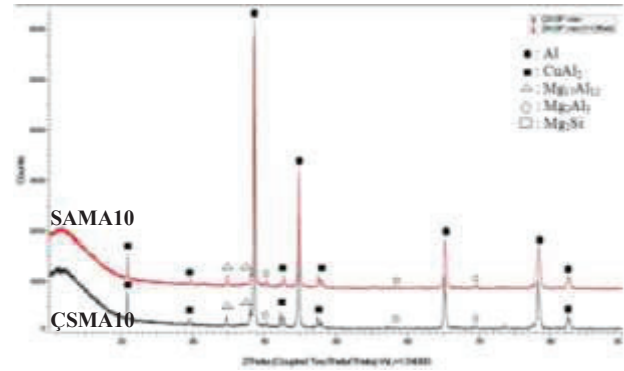
Şekil 1. Yağlayıcı türünün sıcak preslenmiş TM numune mikroyapılarına etkisi a) İşlemsiz numune (MA0) b)Çinko Stearat katkılı (ÇSMA10) c)Stearik Asit katkılı (SAMA10)

Şekil 1b ve Şekil 1c'de verilen MA işlemleriyle elde edilen mikroyapılar incelendiğinde, işlemsiz TM malzeme mikroyapısına göre faz dağılımlarının homojen olduğu söylenebilir. Bununla birlikte, MA işlemi süreci sonunda elde edilen karışım tozun morfolojisinin mikroyapıya yansıdığı görülmektedir.

Şekil 1c'de, MA sürecinde bakır parçacıklarıyla etkileşime giren Al parçacıklarının oluşturduğu bakırca zengin Al-Cu intermetalik fazlar kahverengi renk tonundadır. Beyaz renkli uzun taneler ise alüminyumca zengin bölgelerdir. Mekanik alaşımlama işleminin parçacıkların şekilleri üzerindeki etkisi, en/boy oranı artmış ve deforme olmuş pulsu taneler ile gözlemlenmiştir. Çinko stearat içeren ÇSMA10 numunesinin, stearik asit içeren SAMA10 numunesine göre daha ince taneli mikroyapıya sahip olduğu söylenebilir.

### C. XRD Analizleri

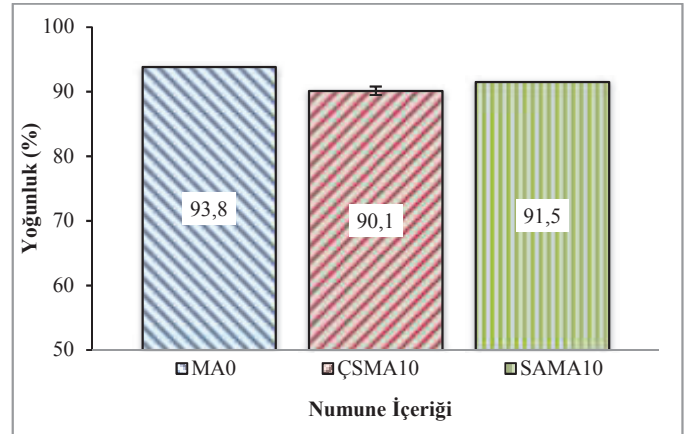
Stearik asit ve çinko stearat içeren MA işlemi uygulanmış tozlardan sıcak presleme yöntemiyle elde edilen numunelerin (SAMA10, ÇSMA10) XRD grafikleri tanımlanarak Şekil 2'de verilmiştir.



Şekil 2. ÇSMA10 ve SAMA10 numunelerinin XRD verileri

Buna göre, SAMA10 ve ÇSMA10 numunelerinin yapıları içerisinde; Al (PDF 00-004-787),  $\text{CuAl}_2(\theta)$ ,  $\text{Mg}_2\text{Si}$ ,  $\text{Mg}_2\text{Al}_3$  ve  $\text{Mg}_{17}\text{Al}_{12}$  fazlarının varlığı tespit edilmiştir [16-20]. ÇSMA10 numunesinde  $\text{CuAl}_2(\theta)$  pik şiddeti daha fazladır fakat belirgin bir fark mevcut değildir.

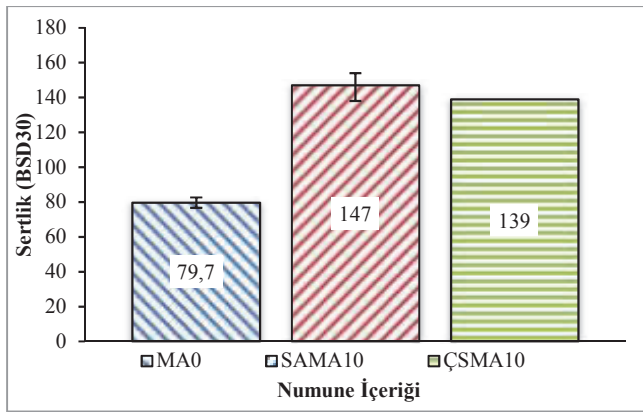
### D. Yoğunluk Ölçümleri



Şekil 3. MA işlemi ve yağlayıcı türünün T/M numune yoğunluklarına etkisi.

Teorik yoğunluk ile ölçülen yoğunlukların yüzde uygunlukları Şekil 3'deki gibidir. MA işlemiyle öğütülen tozlarla üretilen T/M parça yoğunluklarında önemli artış elde edilmesi beklenirken, bu farklılığa Alumix 123 ön karışimli tozun Al ve Cu toz parçacıklarının homojen karışımında olmayışının sebep olduğu düşünülmektedir. Zira Al'a göre özgül yoğunluğu üç kat daha fazla olan Cu parçacıklarının karışım toz yığınının altında kalma olasılığının yüksek olması ağırlıkça % 4,5 Cu içeren alaşım oranını sağlayacak teorik yoğunluk hesabının pratikte uygulanamamasına sebep olduğu söylenebilir.

### E. Sertlik Ölçümleri



Şekil 4'de MA işlemi ve yağlayıcı türünün T/M numune sertlik değerlerine etkisi.

Şekil 4'de numunelerin sertlik değerleri standart sapma değerleriyle verilmiştir. Genel olarak mekanik alaşımlama işleminin T/M parçaların sertlik değerlerinde önemli artışa yol açtığı görülmüştür. Al-Cu alaşımlarında  $CuAl_2$  fazı ile sertlik değerinde artışa yol açtığı bilinmektedir, işlem görmemiş tozlardan elde edilen MA0 numunesi ile MA işlemi uygulanmış numuneler arasındaki sertlik değeri farkının muhtemel fazın oluşumu ve miktarıyla ilgili olduğu düşünülmektedir. İki farklı yağlayıcı türü kullanılarak uygulanan işlemlerden elde edilen sertlik değerleri, stearik asit yağlayıcısının kullanımının avantaj sağladığını göstermektedir.

#### IV. SONUÇLAR

1. İşlemsiz Alumix 123 ön karışimli tozdan sıcak presleme ile üretilen T/M malzemenin mikroyapısında Al matris içinde tamamen çözünmemiş Cu parçacıklar mevcuttur.
2. Mekanik alaşımlama işlemi uygulanmış numunelerde ise bu durum söz konusu değildir. Süreç sonunda elde edilen karışım tozun morfolojisi üretilen T/M malzemenin mikroyapısına yansımıştır.
3. En yüksek yoğunluk değeri işlemsiz Alumix 123 tozundan elde edilmiştir. MA işlemi sürecinde, özgül yoğunluğu yüksek Cu parçacıkların çevreye bulaşmasıyla oluşan Cu kütle kaybının, teorik yoğunluğa göre üretilen T/M parçaların yoğunluklarını düşürdüğü söylenebilir.
4. MA işlemi ile üretilen sıcak preslenmiş T/M parçalardaki faz dönüşümlerine ve faz oranlarına yağlayıcı türünün önemli bir etkisi belirlenememiştir.
5. Stearik asit yağlayıcısı kullanılarak mekanik alaşımlama işlemi uygulanan tozlardan elde edilen T/M numuneden bu çalışma için en yüksek sertlik değerine ulaşılmıştır.

#### KAYNAKÇA

- [1] Dursun, T., Soutis, C., Recent Developments In Advanced Aircraft Aluminium Alloy, *Materials and Design*, 56, 862–871, 2014.
- [2] Callister William D., Rethwish, David G., Malzeme Bilimi ve Mühendisliği (Sekizinci Basımdan Çeviri). Türkiye: Nobel Yayınevi, 437, 2013.
- [3] J. B. Fogagnolo, D. Amador, E. M. Ruiz-Navas and J. M. Torralba, Solid solution in Al- 4,5 wt % Cu produced by mechanical alloying, *Materials Science and Engineering A*, 433, 45-49, 2006.
- [4] Koch, C.C., Whittenberger, J.D., "Mechanical Milling of Intermetallics", *Intermetallics*, 4, 339-355, 1996.
- [5] Nagesha, K.V., Rajanish M., Shivappa D.A ., "Review on Mechanical Alloying", *International Journal of Engineering Research and Applications*, Vol 3, Issue 3, 921-924, 2013.
- [6] Alamalhoda, S., "Role of Process Control Agents on Milling Behavior of Al and  $TiO_2$  Powder Mixture to Synthesize  $TiAl/Al_2O_3$  Nano Composite", *International Journal of Modern Physics: Conference Series*, Vol 5, 638-645, 2012.
- [7] Upadhyaya G. S., (2002). *Powder Metallurgy Technology* (Birinci Baskı). Hindistan: Cambridge International Science.
- [8] Şahin, T., Delibalta, C.G., Özçalbaş, Y., Sıcak Presleme ile üretilen T/M Parçaların fiziksel özelliklerine ve sıkıştırma basıncı ve yağlayıcı giderme parametrelerinin etkisi, *2nd International Conference on Material Science and Technology in Cappadocia*, 2017.
- [9] J. B. Fogagnolo, D. Amador, E. M. Ruiz-Navas and J. M. Torralba, Solid solution in Al- 4,5 wt % Cu produced by mechanical alloying, *Materials Science and Engineering A*, 433, 45-49, 2006.
- [10] Y.Y.Li, T.L. Ngai, D.T. Zhang, Y. Long, W. Xia . Effect Of Die Wall Lubrication On Warm Compaction Powder Metallurgy, *Journal of Materials Processing Technology*, 129, 354-358, 2002.
- [11] Yılmaz, R., Fe-Cu-C Kompaktlarda Presleme Basıncı ve Toz karışım Oranlarının Sertliğe ve Çekme Mukavemetine Etkisi, *4. Uluslararası Toz Metalürjisi Konferansı*, Sakarya, p: 795-806, 2005.
- [12] Güven Ş. Y. ,Toz Metalürjisi ve Metalik Köpükler, *SDU Teknik Bilimler Dergisi*, 2, 22-28, 2011 .
- [13] O. Altuntaş, *Yüksek Karbonlu Toz Metal Çeliklerin Mikro Yapı Ve Darbe Tokluğu Özelliklerine Küreselleştirme Isıl İşlemleri Etkilerinin Araştırılması*, Yüksek Lisans Tezi, Gazi Üniversitesi Fen Bilimleri Enstitüsü, Ankara, p:1-6, 2013.
- [14] Meluch, L., *Warm Compaction of Alumix 123*, PhD thesis, University of Birmingham, September, 2009.
- [15] Yılmaz, R., Fe-Cr-Mn-C Kompaktların Üretimi ve Element Miktarlarının Sertlik ve Kırılma Tokluğuna Etkisi, *4. Uluslararası Toz Metalürjisi Konferansı*, Sakarya, p: 1228-1236, 2005.
- [16] ICDD Kart numaraları; Al için PDF 00-004-787, Cu için PDF 00-003-1005, Si için PDF 00-002-0561'dir.
- [17] Chua, K. Y., Hang, M., H., Lee, C. C., Anand, T. J. S., *Advanced Materials Research*, Volume 620, 166-172, 2012.
- [18] Li, J., Luo, G., Wei, F., Efficient Production of  $Mg_2Si$  in a Fluidized-bed reactor, *Powder Technology*, Vol.229, 152-161.
- [19] Zhong, He, C. M., Liu, F. L., Chen, Y. J., Shen, B., Wu, Y. T., Deng, Y. D. Hu, W. B., Formation of an Aluminum-Alloyed Coating on AZ91D Magnesium Alloy in Molten Salts at Lower Temperature, *Surface and Coatings Technology*, Volume 205, Issue 7, 2412-2418, 2010.
- [20] Liu, T., Qin, C., Zhang, T., Cao, Y., Zhua, M., Li, X., Synthesis of  $Mg@Mg_{17}Al_{12}$  ultrafine particles with superior hydrogen storage properties by hydrogen plasma-metal reaction, *Journal of Material Chemistry*, Issue 37, 2012.

# The Effects of Graphene Additives on the Friction and Wear Performance of Epoxy Composites (ISLAC'18/UHAKS18)

Emine Feyza ŞÜKÜR<sup>1</sup>, Gürol ÖNAL<sup>2</sup>, Ahmet AVCI<sup>3</sup>

<sup>1,2</sup>Department of Mechanical Engineering, Konya Technical University, Konya, Turkey

<sup>3</sup>Department of Biomedical Engineering, Necmettin Erbakan University, Konya, Turkey

<sup>1</sup>efeyzasukur@selcuk.edu.tr, <sup>2</sup>gonal@selcuk.edu.tr

<sup>3</sup>aavci@selcuk.edu.tr

**Abstract**— In this study, the effect of graphene nanoparticles on the friction and wear of epoxy composites is examined. The tribological behavior of epoxy composites with different graphene addition ratios produced by molding technique was investigated using a pin on disc wear tester under similar test conditions. The results from the wear test indicated that GNP addition results in decrease in friction coefficient and wear. The best results were obtained with materials containing 0.5% by weight GNP compared to the epoxy matrix.

**Keywords**— Graphene nanoparticle, epoxy composite, wear

## Introduction

Today, polymers and composites are widely used as structural materials in various machine elements and engineering systems due to their superior specific properties. However, their use is restricted due to reasons related to surface properties such as tribological behavior and low wear resistance. Recent research has shown that the wear properties of composite materials can be improved by the addition of nanoparticles to composite materials and their homogeneous dispersion in the matrix [1]. To improve the tribological performance of the epoxy resins, the nanoparticles such as ZrO<sub>2</sub> [2], SiO<sub>2</sub> [3], SiC [4], TiO<sub>2</sub> [5], boron nitride [6], nanoclay [7], carbon nanotubes [6, 8] are often employed.

Graphene, which is very effective in reducing friction and protecting the surfaces from wear, is one of the most important of these nano additives with its solid lubricating property, low friction coefficient and hard structure [9, 10]. In the literature survey made on graphene added nanocomposites, changes in graphene addition ratios can be observed. These ratios generally range from 0.08% to 4% by weight. There are no rules in determining the proportions, and especially in epoxy studies, 0.05-1 ratio is preferred because the homogeneous distribution of the graphene in epoxy becomes difficult as the addition rates increase [11]. Since there is not always a direct correlation between the mechanical properties of the material and its wear properties, the additive proportions that improve the mechanical properties can deteriorate the wear properties or not improve at the same level.

In this study, the aim is to determine the most appropriate graphene additive ratio which will be applied to graphene/epoxy nanocomposites and improve wear resistance and to transfer these ratios to fiber reinforced composites in future works.

## I. MATERIALS AND METHODS

### A. Preparation of Samples

In the production of composites, as an epoxy resin, MGS H160 curing agent with Momentive's MGS L160 lamination resin was obtained from Dost Kimya Sanayi Hammaddeler San. Tic. Ltd. Sti, the graphene nanoparticles (Graphene Nanoplatelet, 99.5 +%, 6 nm, S.A.: 150 m<sup>2</sup>/g Dia: 5µm) were obtained from the Nanografi Turkey. Pure epoxy and graphene added epoxy blends with a ratio of 0.1 to 0.5% by weight were prepared and cast into 90 mm circular molds designed for the production of materials for use in pin-on-disc experiments (e.g. Fig. 1).

A tipped sonicator was used to distribute graphene particles homogeneously in epoxy. First, the amount of epoxy resin was determined, then the graphene particles were weighed in an amount corresponding to 0.1, 0.2, 0.3, 0.4 and 0.5 wt% of the epoxy resin. The mixtures were mixed in a sonicator for 20 minutes in 5 minute intervals and mixed with mechanical agitator after addition of 25% curing agent and then cast into molds. The pure epoxy and grafted admixtures poured into the mold were initially cured at room temperature for 24 hours and then at 80 ° C for 15 hours.

### B. Wear Test

Wear tests were carried out on a pin-on-disk wear tester (ASTM-G99) (e.g. Fig. 2). A steel ball with a diameter of 6 mm and a hardness of 55 HRC was used as an abrasive. Experiments were carried out at 0.75 m/s sliding velocities under constant load of 10 N over 2000 m distance.

After the tests, the weights of the samples were measured with the help of the sensitive scale and the weight losses were determined. Equation 1 was used in the calculation of the wear rate.

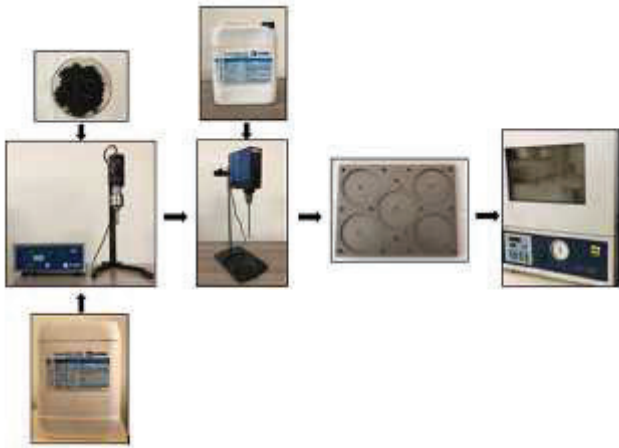


Fig. 1 Preparation of graphene/epoxy nanocomposites

$$W = \frac{\Delta m}{\rho F_N L} m^3 / N \quad (1)$$

Here;  $\Delta m$  represents the weight loss (gr) of the worn sample,  $F_N$  applied load (N),  $L$  sliding distance (m) and  $\rho$  density of the specimen in  $gr / mm^3$ .



Fig. 2 Pin-on-disk test stand

## II. RESULTS AND DISCUSSIONS

The pure epoxy sample is initially at room temperature, the polymer strength is high and accordingly it has a high coefficient of friction. As the sliding continues, the interface temperature increases, the polymer softens and the friction falls. Due to the increased contact between the sliding bodies formed due to the further softening of the epoxy, an increase in friction may be observed.

As the graphene content increased, the friction fluctuations decreased. In similar studies, the reason why the increased graphene contribution can stabilize the friction coefficient is explained by the fact that the graphene can reduce the surface temperature by increasing the thermal conductivity of the bulk material and prevent the softening and degradation of the

epoxy. For this reason, the coefficient of friction approaches a constant value as the graphene contribution increases. This behavior can be explained on the basis of the lubricity provided by the graphene, improved thermal conductivity and atomic bonding. As the graphene content increases, the epoxy thermal conductivity increases, which reduces the interface temperature.

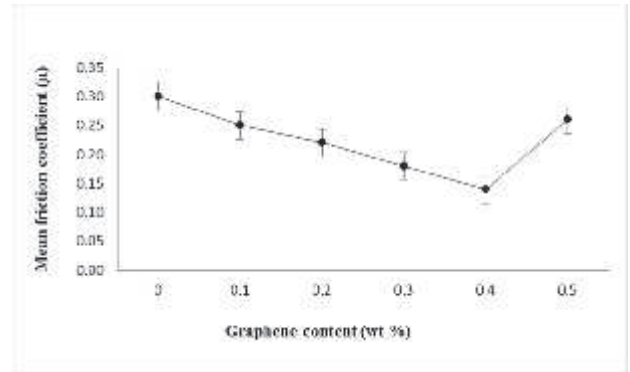


Fig. 3 Mean friction coefficient of composites

According to the results, the highest wear and weight loss occur in pure epoxy sample while this is followed by 0.5% graphene added epoxy composite. The weight loss continuously decreases until 0.4% graphene added sample and the lowest value is obtained in this ratio. When the additive ratio is increased to 0.5%, weight loss and parallelly wear increase, but the values are still below the weight loss of pure epoxy.

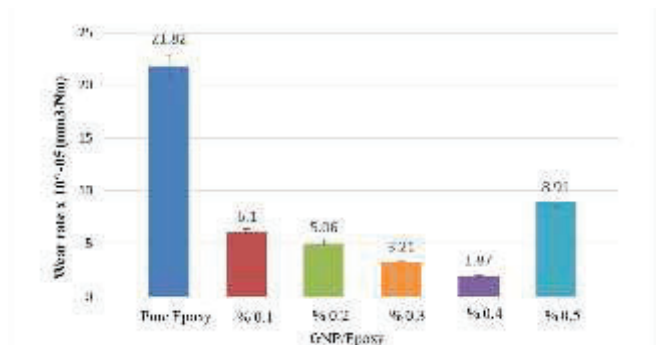


Fig. 4 Wear rates of epoxies for various graphene concentrations

In the graph in Figure 5, the wear rates of the samples are given. Wear of composites decreases as the graphene concentration increases. The greatest reduction in wear rate is seen in 0.4% graphene added composites, where wear is reduced by almost 12 times. The wear rate is lower in the other additive groups compared to pure epoxy. When the additive ratio was increased to 0.5%, the wear rate decreased by about 2.5 times compared to pure epoxy, but this was still an increase with respect to other samples. The increase in

wear rate after a certain percentage of additive is due to the inability to distribute the graphene homogeneously in epoxy. From the test results it can be clearly expressed that the graphene additive improves the wear behavior of pure epoxy and has an effect on decreasing wear.

### III. CONCLUSIONS

The effects of graphene additives on tribological behavior of epoxy composites were systematically investigated using pin-on-disk test. The wear test results indicated that the increased graphene content decreased the friction and wear of the epoxy composites due to the solid lubricating effect of graphene nanoparticles.

### REFERENCES

- [1] X. Hou, Y. Hu, X. Hu, D. Jiang, "Poly (ether ether ketone) composites reinforced by graphene oxide and silicon dioxide nanoparticles: Mechanical properties and sliding wear behavior", *High Performance Polymers*, vol. 30(4), pp. 406-417, 2017.
- [2] R.V. Kurahatti, A.O. Surendranathan, A.V.R. Kumar, C.S. Wadageri, V. Auradi, S.A. Kori, "Dry Sliding Wear Behaviour of Epoxy reinforced with nanoZrO<sub>2</sub> Particles", *Procedia Materials Science*, vol. 5, pp. 274-280, 2014.
- [3] J.T. Shen, M. Top, Y.T. Pei, J.T.M. De Hosson, "Wear and friction performance of PTFE filled epoxy composites with a high concentration of SiO<sub>2</sub> particles", *Wear*, vol. 322-323, pp. 171-180, 2015.
- [4] Q.L. Ji, M.Q. Zhang, M.Z. Rong, B. Wetzel, K. Friedrich, "Friction and Wear of Epoxy Composites Containing Surface Modified SiC Nanoparticles", *Tribology Letters*, vol. 20(2), pp. 115-123, 2005.
- [5] L. Chang, Z. Zhang, C. Breidt, K. Friedrich, "Tribological properties of epoxy nanocomposites: I. Enhancement of the wear resistance by nano-TiO<sub>2</sub> particles", *Wear*, vol. 258(1), pp. 141-148, 2005.
- [6] H. Düzcükoğlu, Ş. Ekinçi, Ö.S Şahin., A. Avcı, M. Ekrem, M. Ünalı, "Enhancement of Wear and Friction Characteristics of Epoxy Resin by Multiwalled Carbon Nanotube and Boron Nitride Nanoparticles", *Tribology Transactions*, vol. 58(4), pp. 635-642, 2015.
- [7] M. Esteves, A. Ramalho, J.A.M. Ferreira, J.P. Nobre, "Tribological and Mechanical Behaviour of Epoxy/Nanoclay Composites", 2013.
- [8] X.-J. Shen, X.-Q. Pei, Y. Liu, S.-Y. Fu, "Tribological performance of carbon nanotube-graphene oxide hybrid/epoxy composites", *Composites Part B: Engineering*, vol. 57, pp. 120-125, 2014.
- [9] A. Klemenz, L. Pastewka, S.G. Balakrishna, A. Caron, R. Bennewitz, M. Moseler, "Atomic Scale Mechanisms of Friction Reduction and Wear Protection by Graphene", *Nano Letters*, vol. 14(12), pp. 7145-7152, 2014.
- [10] D. Berman, A. Erdemir, A.V. Sumant, "Few layer graphene to reduce wear and friction on sliding steel surfaces", *Carbon*, vol. 54, pp. 454-459, 2013.
- [11] D.G. Papageorgiou, I.A. Kinloch, R.J. Young, "Mechanical properties of graphene and graphene-based nanocomposites", *Progress in Materials Science*, vol. 90, pp. 75-127, 2017.

# Sülfolanmış ZSM-5 zeolitinin kullanıldığı kompozit katalitik membran üretimi ve karakterizasyonu

Nazlı Yenihan<sup>1</sup>, Filiz Ugur Nigiz<sup>1</sup>, Nilüfer Durmaz Hilmioğlu<sup>1</sup>

<sup>1</sup> Kimya Mühendisliği Bölümü,  
Kocaeli Üniversitesi, Kocaeli, 41380, Türkiye

**Abstract**— In this study, ZSM-5 reinforced composite PVA membranes were prepared as a catalytic composite membrane and it was aimed to be used as catalyst in the production of isopropyl acetate. To improve the catalytic effect of the ZSM-5 zeolite, the sulfation was carried out. It was found that the catalytic property of the PVA

**Özet**— Bu çalışmada katalitik kompozit bir membran olarak ZSM-5 katkılı kompozit PVA membranları hazırlanarak izopropil asetat üretiminde katalizör olarak kullanılması amaçlanmıştır. ZSM-5 zeolitinin katalitik etkisini arttırmak için sülfolama işlemi gerçekleştirilmiştir. Katalizör eklenerek katalitik özellik kazandırılmış PVA kompozit membranlı reaksiyon dönüşüm değeri serbest katalizörlü reaksiyona göre daha yüksek olduğu görülmüştür.

**Anahtar Kelimeler**— Membran reaktör, esterleşme reaksiyonu, katalizör, izopropil asetat.

## 1.GİRİŞ

Membran reaktörler geleneksel ayırma yöntemlerine kıyasla düşük reaksiyon süresi, minimum reaksiyon koşulları, enerji tasarrufu, performansa göre düşük maliyet, yüksek seçicilik gibi avantajlara sahiptir. Farklı sıvı karışımları için seçici membranların kullanıldığı membran reaktörler son yıllarda enerji açısından verimli ve çevre dostu bir ayırma teknolojisi olarak kimya endüstrisinde büyük ilgi görmüştür. Pervaporasyon membran reaktörlerde sıvı karışımlar, membran yüzeyinin bir tarafına temas ederler ve buhar halinde diğer taraftan ayrılması için membran boyunca seçici olarak dağılırlar. Ayrılan buhar fazı uygun bir vakum uygulanması ya da buharın yoğunlaştırılması ile sistemden uzaklaştırılır. Böylece sistemdeki denge sınırı ürünler yönüne kaydırılmış olur. Membran reaktörlerde uygun membranlar kullanarak gerçekleştirilen esterleşme reaksiyonları esnasında, katalize edilmiş reaksiyon ortamından ürün olarak ester veya yan ürün olarak suyun uzaklaştırılması, maliyeti ve enerji tüketimini düşürür. Bu durum da geleneksel ayırma yöntemleri ile karşılaştırıldığında; reaksiyon süresinin azalması, reaksiyon

composite membrane with the addition of catalyst was higher than the free catalyst reaction.

**Key words**— Membrane Reactor, Esterification Reactions, Catalyst, Isopropyl Acetate

dönüşümün istenilen yönde artması, maliyet gibi parametreleri olumlu yönde etkiler.

Membran prosesleri endüstriyel alanlarda sıklıkla kullanılırlar. Membran esaslı denge ayırma prosesleri ultrafiltrasyon(UF), nanofiltrasyon(NF), ters osmoz(RO), mikrofiltrasyon(MF), elektrodializ(ED), pervaporasyon(PV), gaz ayırma, membran distilasyon vb. şeklindedir.<sup>[1]</sup>

Membran reaktörlerde gerçekleştirilen esterleşme reaksiyonları birçok farklı karboksilik asit-alkol sistemi için kullanılabilir. Literatürde sıklıkla yapılan bu reaksiyonlardan; oleik asit-etanol,asetik asit-etanol, asetik asit-metanol, asetik asit-izopropanol ve asetik asit-nbutanol, propiyonik asit-propanol ve 2-propanol; tartarik asit-etanol; valerik asit-etanol; laktik asit-etanol; salisilik asit-metanol bazılarıdır.

Esterleşme, kimya endüstrisinde gerçekleştirilen önemli reaksiyonlardan biridir. Esterleşme reaksiyonları temel olarak; bir asit ile bir alkolün uygun koşullarda tepkimesi ile su ve ester oluşturan reaksiyonlardır. İzopropil alkol ve asetik asitin reaksiyonu da organik sentez esaslı olan önemli bir reaksiyondur. Ancak bu reaksiyon termodinamik denge ile sınırlıdır ve reaksiyon hızı oldukça yavaştır. Termodinamik dengesizliğin üstesinden gelmek ya da dengeyi değiştirmek için reaktanlardan birinin miktarı artırılabilir gibi sistemden suyun uzaklaştırılması işlemi de yapılabilir<sup>[2]</sup>. Esterleşme reaksiyonlarında çoğunlukla killer, zeolitler, heterojen veya homojen yapıları katalizörler kullanılır. Sistem aktivitesinin artması kullanılan katalizör, kil ya da zeolit kimyasal ve fiziksel yapısına bağlıdır. Asit katalizli katalizör kullanılması reaksiyon dönüşümünü arttırabileceği gibi; hidratlı yapı bulunduran katalizör kullanılması reaksiyon dönüşümünü azaltacaktır.

Mallada R. ve ark 2007; asetik asitin etanol ile esterleşmesini zeolit katkılı membran reaktörde (mordenit ve zeolit A) ve katalizör olarak da Amberlyst15 kullanmışlardır. Mordenit katkılı membranların asetik reaksiyon ortamına karşı büyük bir direnç gösterdiğini ve reaksiyon dönüşümünü %90 seviyesine çıkardığını görmüşlerdir<sup>[3]</sup>.

Korkmaz S. Ve ark. 2009; PVMR'de PDMS membranı iki farklı katalizör kullanarak hazırlamışlar ve izobütil asetat üretimi için kullanmışlardır. Katalizör konsantrasyonunu arttırarak ve daha ince yapıda membranlar kullanarak reaksiyon dönüşüm oranının arttığını gözlemlemişlerdir. Dowex 50W-X8 ile katalize edilen reaksiyonun dönüşümü PVMR'de daha yavaş gerçekleşirken H<sub>2</sub>SO<sub>4</sub> katalizörü kullanılan reaksiyona göre dönüşümün daha uzun sürede ve daha yüksek verimde olduğu gözlemlenmiştir<sup>[4]</sup>.

Kamal A. Ve ark. 2009; Kinoksalinlerin sentezi için oldukça verimli, çevreye duyarlı, zararlı solvent içermeyen, yeşil ve geri dönüşümlü bir katalizör olan Amberlite IR-120H reçinesi kullanmışlardır. Amberlite IR-120H katalizörünün reaksiyonun tamamlanmasından sonra geri kazanılabilir ve Amberlite IR-120H katalitik özelliği dört kere tekrarlanan reaksiyon da bile bozunmadığını böylelikle de yeniden kullanılabilir özelliğinin yüksek seviyelerde olduğunu gözlemlemişlerdir<sup>[5]</sup>.

Altınokka M. R. ve ark. 2012; Amberlyst 36 varlığında asetik asidin 1-oktanol ile esterifikasyon kinetiği incelemişler ve Eley-Rediel kinetik modelini çıkarmışlardır. Bu sonuçla birlikte, Amberlyst 36'nın literatürde bildirilen titanyum tetraklorür kompleks katalizöründen daha etkili olduğunu ispatlamışlar ve sonuç olarak, Amberlyst 36'nın, katyonik iyon değiştirici bir reçine olarak, asetik asidin 1-oktanol ile esterifikasyonu için uygun bir katalizör olduğu kanısına varmışlardır<sup>[6]</sup>.

Son yıllarda kompozit membranların membran reaktörde heterojen katalizör gibi kullanıldığı ve esterleşme reaksiyonu gerçekleştirildiği birçok çalışma vardır. Kompozit membranlar genel olarak organik-inorganik kompozit membranlar şeklinde tanımlanabilirler. Endüstriyel alanda kullanılan kompozit membranlar; yüksek seçicilik ve akı, termal kararlılık gibi özellikleri iyileştirmek amacıyla geliştirilmiştir. Polimerik kompozit membranlar ise en çok tercih edilen türdür. Polimer tabanlı kompozit membranlarda sıklıkla kullanılan polimerlerden bazıları poliakrilonitril(PAN), selüloz asetat(CA), polietilen(PE), polisülfon(PS), polietersülfon(PES), polivinilalkol(PVA), polidimetilsiloksan(PDMS) v.b. şeklindedir. Hidrofilik polimerik malzemelerden polivinil alkol (PVA), üstün hidrofilik özelliği ve kimyasal stabilitesi nedeniyle kompozit membran oluşturmak amacı ile en çok çalışılan polimerlerden birisidir<sup>[7]</sup>. Membran ayırma işlemlerinde çoğunlukla zeolit katkılı polimerik kompozit malzemeler kullanılmaktadır.

Bu çalışmada katalitik kompozit bir membran olarak ZSM-5 katkılı kompozit PVA membranları hazırlanarak izopropil asetat üretiminde katalizör olarak kullanılması amaçlanmıştır.

ZSM-5 zeolitin katalitik etkisini arttırmak için sülfolama işlemi gerçekleştirilmiştir.

## 2.MATERYAL VE METHOD

### 2.1.Materyaller

Esterleşme reaksiyonu için kullanılan izopropil alkol(  $\geq$  %99.5 saflıkta) ve asetik asit (  $\geq$  %99 saflıkta) merck firmasından temin edilmiştir. Membran hazırlamada kullanılacak PVA katısı ticari adı Mowiol( Mw~125.000 ) olarak sigma-aldrich firmasından temin edilmiştir.

### 2.2. ZSM-5 Sülfolama Tekniği

ZSM-5 zeolitin katalizör etkinliğinin artırılması için kuvvetli asit alanlarına sahip H<sub>2</sub>SO<sub>4</sub> homojen katalizörü ile muameleye tabii tutulmuştur. Belirli bir orandaki zeolit önce hidratlı yapısından arındırılmak üzere 500 °C' lik kül fırınında 4 saat kurutulmuş ve sonrasında bir miktar homojen 5M'lık H<sub>2</sub>SO<sub>4</sub> emdirilmiştir.

### 2.3. Membran Hazırlama Yöntemi

Membran; çözüldüden dökme ve buharlaştırma yöntemi ile hazırlanmıştır. Bunun için öncelikle kütlece %6'lık PVA ile çözelti hazırlanmıştır. Çözücü olarak distile su kullanılmıştır. Hazırlanan çözelti dört saat süre ile 400 rpm devirde ve 85 °C karıştırılarak homojen bir çözelti elde edilmiş, sülfolanmış ZSM-5 eklenerek oluşturulan membran çözeltisi, 14cm çaplı cam petriye dökülerek kurumaya bırakılmıştır.

### 2.4.Esterleşme Reaksiyonu ve Kesikli Reaktörde Uygulanması

İzopropil alkol ile Asetik asitin esterleşme reaksiyonu Şekil 1 deki gibidir. Bu reaksiyon bir asit ve bir alkolün asit katalizli ortamda oluşan reaksiyonudur.



Şekil 1. İzopropil Asetat sentezi

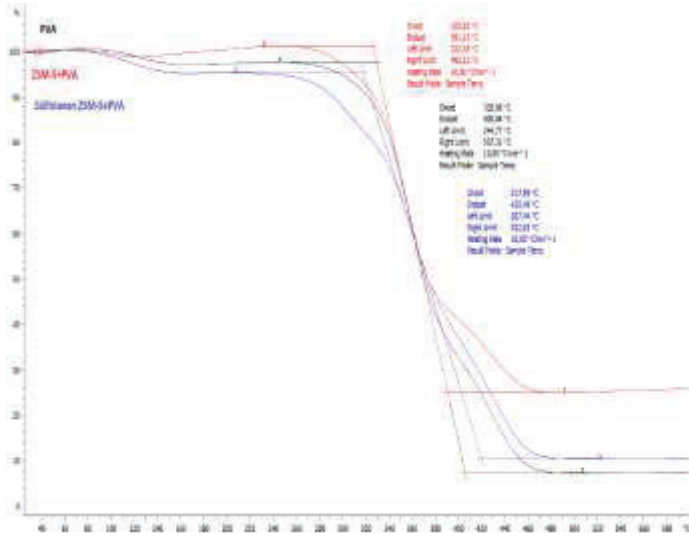
Bu reaksiyonda alkol-asit molar oranları 1:1, 2:1 ve 3:1 olacak şekilde hazırlanmıştır. Reaksiyon süreleri doğru karşılaştırma açısından altı saat olarak belirlenmiş ve reaksiyon sıcaklıkları 60°C, 70°C ve 80°C olarak seçilmiştir.

Sisteme molar oranları 1:1, 2:1 ve 3:1 olacak şekilde alkol-asit beslemesi yapılmıştır ve reaktanlar istenilen sıcaklığa ulaşınca kütlece %2'lik katalizör eklemesi ile reaksiyon başlatılmıştır. Sisteme katalizör eklemesi reaksiyon sıcaklıkları sağlandıktan sonra yapılmıştır. Bunun en önemli nedeni reaksiyondaki sıcaklığa bağlı olarak katalizör etkinliğinin belirlenmesidir. Geri soğutucu sistem reaksiyon süresi boyunca çalıştırılmıştır. Bunun başlıca nedeni buhar fazına geçebilecek olan reaktan kayıplarının önüne geçilmek istenmesidir.

### 3.SONUÇLAR VE TARTIŞMA

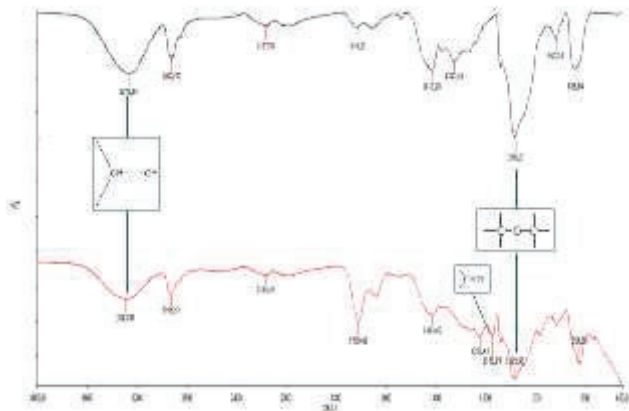
#### 2.1.Karakterizasyon Sonuçları

Şekil 2’de görüldüğü gibi ZSM-5 eklenen polimerdeki bozunma oranı azalmıştır. Eklenen sülfö grupları ise bu oranı bir miktar düşürmüştür. Ayrıca esterleşme reaksiyonunun gerçekleştiği sıcaklıkta herhangi bir kütle kaybı olmadığı için kompozit katalitik membranların reaksiyon ortamına dayanacağı ve bozulmayacağı öngörülmüştür.



Şekil 2. Saf, sülfolanmamış ve sülfolanmış kompozit membranların TGA analizi

Şekil 3’de ise 1400 cm<sup>-1</sup> bölgesinde özellikle sülfolanmış ZSM-5 içeren membranda pik alanında bir artış görülmektedir ve bunun sülfolanmış zeolitler dolayısıyla olduğu anlaşılmaktadır.

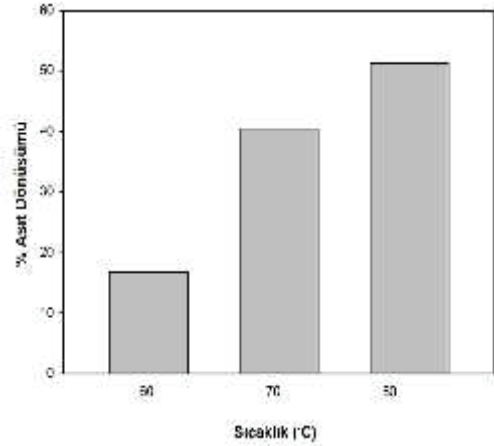


Şekil 3 . FTIR analizi ; --- PVA, ---PVA - MA – Sülfolanmış ZSM-5

Şekil 5. T= 80 °C; Katalizör miktarı %30 (PVA’ya göre)

#### 3.2.Sıcaklığın Asit Dönüşümüne Etkisi

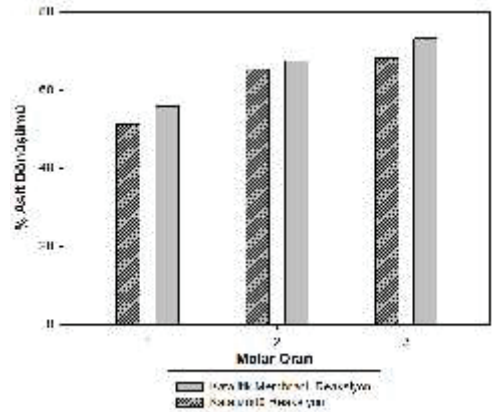
Şekil 4’de eşit molar beslemede ve ZSM-5 katalizörünün toplam çözeltiye oranı %30 iken artan sıcaklığın asetik asit dönüşümüne etkisi görülmektedir. Sıcaklık 60 °C’ den 80 °C’ ye arttıkça dönüşüm %16.7’den %51.2 ye belirgin bir şekilde arttığı görülmüştür. Endotermik ve tersinir olan bu reaksiyonun sıcaklığı arttıkça reaksiyon hız sabiti artmakta ve dönüşüm artmaktadır.



Şekil 4. M:1; Katalizör miktarı %30 (PVA’ya göre)

#### 3.3.Alkol/Asit Molar Oranının Asit Dönüşümüne Etkisi

Şekil 5’de 80 C sıcaklıkta ve ZSM-5 katalizörünün toplam çözeltiye oranı %30 iken artan alkol/asit molar besleme oranının asetik asit dönüşümüne etkisi görülmektedir. Besleme oranı 1 den 3 e arttıkça dönüşüm %51.2 den %68.2 ye artmıştır. Aynı reaksiyon aynı koşullarda membrana eklenen ZSM-5 katalizörü ile de yapılmış ve dönüşümlerin serbest katalizöre göre yüksek olduğu görülmüştür.



Hidrofilik membranın katalizör olarak kullanılmasından dolayı bir miktar da artış beklenebilmektedir. Reaksiyon

süresince esterle birlikte su oluşmaktadır. Membran suyu çektiğçe tersinir reaksiyonun dönüşümü de artmaktadır.

### SONUÇLAR

Bu çalışmada, izopropil alkol ile asetik asitin esterleşme reaksiyonu sülfolanmış ZSM-5 varlığında ve farklı sıcaklıklarda gerçekleştirilmiştir.

Elde edilen veriler neticesinde katalitik membranlı reaksiyonda gerçekleşen esterleşme reaksiyonu sırasında açığa çıkan su moleküllerinin sistemde birikmesi membranın hidrofilitesi sayesinde azaltılmış ve reaksiyon dönüşümünün serbest katalizörlü reaksiyona göre daha yüksek olduğu görülmüştür.

Sonuç olarak bu deneyde kullanılan sülfolanmış ZSM-5 katkılı PVA dan oluşan katalitik membranın etkinliğinin serbest katalizörlü reaksiyona göre daha yüksek olduğu saptanmıştır.

### KAYNAKLAR

- [1] Mulder M. 1996. Basic Principles of Membrane Technology. KLUWER ACADEMIC PUBLISHERS, pp 14-18 Netherlands.
- [2] Li W., Liu W., Xing W., Xu N. 2013. Esterification of Acetic Acid and n-Propanol with Vapor Permeation Using NaA Zeolite Membrane. Industrial And Engineering Chemistry Research, Vol.52, pp 6336-6342.
- [3] Mallada R., Iglesia O., Menendez M., Coronas J. 2007. Continuous zeolite membrane reactor for esterification of ethanol and acetic acid. Chemical Engineering Journal. Vol.131, pp 35-39.
- [4] Korkmaz S., Salt Y., Hasanoğlu A.M., Özkan S., Salt İ., Dinçer S. 2009. Pervaporation membrane reactor study for the esterification of acetic acid and isobutanol using polydimethylsiloxane membran. APPLIED CATALYSIS A-GENERAL, Vol.366, pp 102-107.
- [5] Kamal A., Babu K. S., Hussaini S. M. A. a, Mahesh R., Alarifi A. 2015. Amberlite IR-120H, an efficient and recyclable solid phase catalyst for the synthesis of quinoxalines: a greener approach. Tetrahedron Letters. Vol.56, pp 2803-2808.
- [6] Altıokka M. R., Akyalçın S. 2012. Kinetics of esterification of acetic acid with 1-octanol in the presence of Amberlyst 36. Applied Catalysis A: General. Vol.429- 430, pp 79- 84. *FLEXChip Signal Processor (MC68175/D)*, Motorola, 1996.
- [7] ] Wanqin Jin, Gongping Liu, Nanping Xu, POLYMER/CERAMIC COMPOSITE MEMBRANES, Editors: Ralph T. Yang, Organic-Inorganic Composite Membranes for Molecular Separation, 1st ed., Singapore, 18-79, 2017.

# TIG Kaynağı ile Birleştirilen 7075 Alüminyum Alaşımının Kaynak Bölgesinin İncelenmesi (ISLAC'18/UHAKS18)

Bekir Çevik\*

# Kaynak Teknolojisi Bölümü, Düzce Üniversitesi, Düzce, 81850, Türkiye  
bekircevik@duzce.edu.tr

**Özet**—Alüminyum ve alaşımlarının geleneksel kaynak yöntemleri ile birleştirilmesi oldukça zordur. Özellikle yüksek mukavemetli 7xxx serisi alüminyum alaşımları ergitmeli kaynak yöntemleri ile birleştirilmesinde güçlüklerle karşılaşmaktadır. Bu çalışmada, 3 mm kalınlığında 7075 alüminyum alaşımı malzemeler Tungsten Inert Gaz (TIG) kaynak yöntemi ile farklı kaynak akımları kullanılarak birleştirilmiştir. Elde edilen kaynaklı bağlantıların kaynak bölgesi sertlik ve mikroyapı özellikleri incelenmiştir.

**Anahtar Kelimeler**—7075 alüminyum alaşımı, TIG kaynağı, mikroyapı, sertlik

**Abstract**—Weldability of aluminium alloys are difficult by conventional welding processes. Particularly joining of the 7xxx series aluminium alloys are problematic. In this study, 3 mm thickness 7075 aluminium alloys joined by Tungsten Inert Gas (TIG) welding at the different welding current. Hardness and microstructure of the welded parts were investigated.

**Keywords**—7075 aluminium alloy, TIG welding, microstructure, hardness

## I. GİRİŞ

Alüminyum, doğada en çok bulunan metal esaslı elementtir. Günümüz endüstrisinde metal olarak çelikten sonra en fazla alüminyum kullanılmaktadır [1]. Alüminyum ve alaşımları hem endüstride hem de günlük yaşamda kullanılan birçok malzemenin yerini almaya devam etmektedir. Bunun nedeni mühendis ve tasarımcıları cazip kılan bazı üstün özellikleridir [1-4]. Özellikle hafif olmaları, iyi ısı ve elektrik iletkenlikleri, arttırılabilen mekanik özellikleri ve korozyona karşı gösterdikleri direnç en önemli ve üstün özellikleridir [1,2,5-8]. Endüstride kullanılan alüminyum alaşımları dövme ve döküm alaşımları olarak iki gruba ayrılmaktadır. Dövme alüminyum ve alüminyum alaşımları ısı işlem uygulanamayan soğuk şekil değiştirmeli ve ısı işlem uygulanabilen (çökeltme yoluyla sertleşmeli) birçok türü taşıt imalat endüstrisinde, gemi yapım endüstrisinde, havacılık ve uzay sanayinde yer

almaktadır. Endüstride en çok talep gören alüminyum alaşımları 2xxx, 5xxx, 6xxx ve 7xxx serisi alaşımlardır [5,9-12].

7075 alüminyum alaşımları havacılık sanayinde yaygın olarak kullanılan, çökeltme ile sertleştirilmiş malzemelerdir. 7075 alüminyum alaşımında ağırlık olarak % 5-6 Zn, % 2-3 Mg, yaklaşık olarak % 1,5 Cu ve çok az miktarlarda Cr, Mn, Ti ve Ag içerebilmektedir [1,5,10-12]. Bu alaşım düşük özgül yoğunlukla birlikte yüksek bir dayanıma sahiptir ve bu üstünlüklerinden dolayı uçak yapı malzemesi olarak yaygın bir şekilde kullanılmaktadır [1,11,12]. 7075 alüminyum alaşımların en yüksek sertlik değeri T6 ısıl işlemi ile elde edilir. T651 ısıl işlemi ile de çözültüye alınarak kontrollü miktarda germe ile gerilim giderme ve yapay olarak yaşlandırma yapılır [1,8,11].

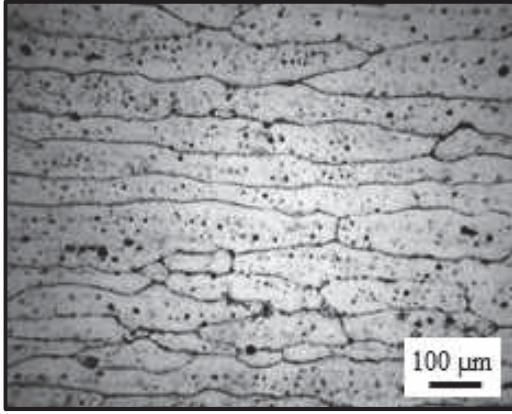
Al ve alaşımları geleneksel kaynak yöntemleri (MIG, TIG etc.) ile birleştirilebilir [2,3]. Ancak alüminyum alaşımlarının kaynak kabiliyeti çeliklerle kıyaslandığında daha kötüdür. Alüminyum ve alaşımlarının geleneksel yöntemlerle kaynağı yapılırken kendine has bazı özellikleri dikkate alınmalıdır. Alüminyum malzemeler, çeliklere göre daha yüksek ısı iletkenliğe sahiptir [2-5]. Bu özellik alüminyumun ergimesini zorlaştırdığı için kaynak kabiliyetini olumsuz etkiler. Sonuç olarak, alüminyum malzemeler geç ergiyip hızlı katılaştığı için kaynak dikişinde yetersiz ergime ve gözenekler oluşabilir [3-7].

Bu çalışmada, geleneksel ergitmeli kaynak yöntemleri ile birleştirilmesi sorunlu olan ve özellikle havacılık, uzay ve savunma sanayi gibi alanlarda yaygın olarak kullanılan 7075-T651 alüminyum alaşımı malzemeler, TIG kaynak yöntemi ile birleştirilmiştir. Elde edilen bağlantıların ara kesitinden alınan numuneler üzerinde makro ve mikroyapısal inceleme ile sertlik testi yapılmıştır. Yapılan testler sonucunda elde edilen bulgular literatür ışığında değerlendirilmiş ve yorumlanmıştır.

## II. DENEYSEL ÇALIŞMALAR

Bu çalışmada, 80×30×3 mm boyutlarındaki 7075-T651 alüminyum alaşımı malzemeler TIG kaynak yöntemi ile alın birleştirilmiştir. 7075-T651 alüminyum alaşımının

mikroyapısı Şekil 1'de kimyasal bileşimi ise Tablo 1'de verilmiştir. Kaynak öncesi numuneler hiç boşluk olmayacak şekilde alın alına getirilerek puntalanmıştır. Kaynak işlemlerinde pirinç (CuZn37) plaka altlık malzemesi olarak kullanılmıştır. Birleştirme işlemleri ilave tel kullanılmadan AC/DC pulse özellikli ve sinerjik programlanabilir TIG kaynak makinesinde Tablo 2'de verilen parametreler seçilerek AC akımda tek taraflı olarak yapılmıştır. Kaynak işleminden sonra numuneler pirinç altlık üzerinde soğumaya bırakılmıştır.



Şekil 1. 7075-T651 Al alaşımı mikroyapısı

Tablo 1. 7075 alüminyum alaşımının kimyasal kompozisyonu

Zn	Mg	Cu	Cr	Mn	Al
5,1-6,1	2,1-2,9	1,2-2	0,18-0,28	<=0,30	Kalan

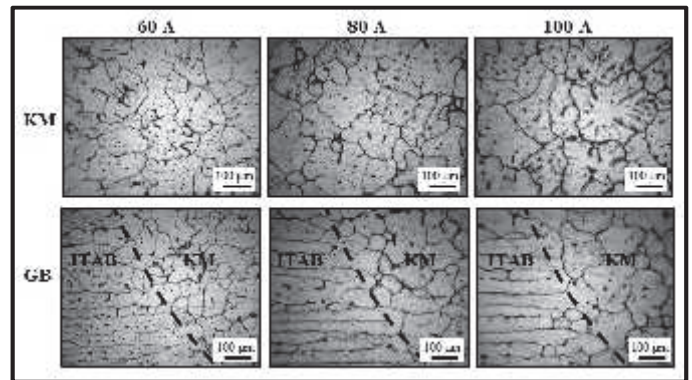
Tablo 2. Kaynak parametreleri

Tungsten elektrot çapı (mm)	Amper (A)	Voltaj (V)	Koruyucu gaz	Gaz akış debisi (lt/dak)
3.2	60	20±2	Argon	14
3.2	80	25±2	Argon	14
3.2	100	30±2	Argon	14

TIG kaynağı ile birleştirilen numuneler üzerinde mikro yapı incelemesi yapılmış ve birleşme özellikleri incelenmiştir. Bu amaçla kaynak yönüne dik kesitten alınan numuneleri 600, 800, 1000 ve 1200 nolu zımparalar ile zımparalanmıştır. Daha sonra numuneler 1µm parlatma keşesinde 3 µm'lik elmas pasta ile parlatılmıştır. Keller Reaktif (150 ml H<sub>2</sub>O, 3 ml HNO<sub>3</sub>, 6 ml HF) ile numuneler yaklaşık 60-90 saniye arasında dağlanmıştır. Mikroyapı incelemeleri, Metkon Inverted Tip Metal Mikroskopu ile yapılmıştır. Mikro görüntüler kaynak merkezi ile kaynağın geçiş bölgelerinden alınmıştır. Sertlik deneyleri kaynak yönüne dik kesitten alınan numuneler üzerinde yatay doğrultuda yapılmıştır. Deneylerde Time TH 300 marka sertlik test cihazı ile 1/16" çelik bilye ile 100 kgf yük 10 s süre ile uygulanarak ölçümler yapılmıştır. Sertlik ölçümleri kaynak merkezinden başlamak üzere malzeme kesit kalınlığının merkezi boyunca her iki tarafa 2 mm aralıklarla toplam 17 noktadan alınmıştır.

### III. SONUÇLAR VE TARTIŞMA

Şekil 2'de farklı kaynak akımlarında yapılan birleştirmelerin mikroyapıları gösterilmiştir. Kaynaklı birleştirmelerde ITAB'lar ve kaynak ergime sınırına bitişik bölgeler birbirlerine benzer görüntüler oluşmuştur. Kaynak bölgelerinin mikroyapı incelemelerinde ısının etkisiyle levhaların üst yüzeyine doğru genişleyen kaynak çekirdeği oluşmuştur. Bu duruma levhaların üst bölgesinde maksimum ısı, levhaların alt kısmında ise daha düşük ısının etkilemesi neden olmaktadır. Deformasyonla hadde doğrultusunda yönelmiş ana malzemenin yassı ve uzun mikro taneleri kaynak sırasında ergimenin ve ısı girdisinin etkisiyle daha büyük boyutlu eş eksenli tanelere dönüşmüştür. Bu durum kaynak dikişlerinin geçiş bölgelerinde (GB) net bir şekilde görülmektedir. Kaynak sürecinde akım şiddetinin artmasıyla oluşan ısı girdisi nedeniyle kaynak merkezi (KM) tane boyutunu arttırdığı belirlenmiştir.



Şekil 2. Kaynak bölgesi mikroyapıları

Kaynak dikişlerinin mikroyapı taramasında özellikle kaynak dikişlerinin kök kısımlarında levhaların birleşme yerlerinde mikro çatlakların olduğu gözlemlenmiştir. Bu çatlakları katılma sırasında alt yüzeyin birleşme bölgelerinin başlattığı düşünülmektedir. Çökelme sertleşmeli alüminyum alaşımlarının ergitmeli kaynak yöntemleriyle birleştirilmesinde çatlama ve gözenek oluşumu gibi sorunlar ortaya çıkmaktadır. Alüminyum alaşımlarının katılma sıcaklık aralıklarının geniş olması ve ısıl genleşme katsayılarının yüksek olması çatlak oluşumunun en önemli nedenidir [3,5,7-9]. Bu durum levhaların alt yüzeylerinde çatlak başlamasına ısıl genleşme nedeniyle de kaynak çekirdeğinin içine doğru ilerlemesine neden olmuştur. Alüminyum alaşımlarının kaynak dikişinde çatlak oluşumuna neden olan diğer bir faktör ark kaynaklarındaki yüksek ısı girdisidir. Ayrıca yüksek ısı girdisi, özellikle yüksek mukavemetli alüminyum alaşımlarında ısı tesiri altındaki bölgede (ITAB) tane sınırlarında düşük ergime sıcaklıklı fazların oluşumuna ve dolayısıyla bu bölgede tane sınırlarında katılma esnasında çatlama neden olabilmektedir [3,5,7].

Akım şiddetinin artması birleşme bölgesindeki sertlik dağılımına etkilemiştir. Kaynak merkezinde sertlik değeri 60

A akım değerinde 53 HRB, 80 A akım değerinde 46 HRB, 100 A akım değerinde ise 44 HRB' dir. Kaynak merkezinden 8 mm uzaklıkta (ITAB) alınan ölçümlerde 60 A akım değerinde 70 HRB, 80 A akım değerinde 66 HRB, 100 A akım değerinde ise 62 HRB olarak ölçülmüştür. Ana metalin sertlik değeri ise 85 HRB'dir. Bu sonuçlara göre kaynak bölgesinin sertlik değerlerinin artan akım şiddeti ile azaldığı görülmektedir. Bunun nedeni kaynak akım şiddetinin artmasıyla kaynak bölgesinde daha fazla ısı oluşmasındandır. Yüksek ısı girdisi çökelti fazlarını çözerek kaynak bölgesinde ve ITAB'ta sertlik düşüşüne neden olmuştur. 7075 Al alaşımlarına üretim aşamasında sertlik ve mukavemet artışı için 530 °C'lerde T6/T651 ısıl işleme uygulanmaktadır [3,5,8-10]. Lokal olarak ısınan ve ergiyen kaynak bölgesinde GP bölgeleri çözünür ve 7075 Al alaşımlarında sertleştirici η (MgZn<sub>2</sub>) çökeltileri çözünerek daha az sertleştirici özellikteki η (Mg<sub>2</sub>Al<sub>3</sub>, Al<sub>32</sub>Zn<sub>49</sub> ve Al<sub>2</sub>Cu) çökeltilerine dönüşür [1,8-13]. Literatürde kaynak bölgesindeki sertlik düşüşünün nedeni maruz kalan yüksek sıcaklıklarla birlikte dislokasyonların azalması ve mukavemetlendirici çözeltilerin sertleştirici etkilerinin azalması olarak bilinmektedir [3,5,9-14].

#### IV. SONUÇLAR

7075-T651 Al alaşımı levhalar TIG kaynak yöntemi ile farklı kaynak akımları kullanılarak birleştirilmiş ve kaynaklı bağlantıların mikroyapı ve mekanik özellikleri incelenmiş olup elde edilen sonuçlar aşağıda özetlenmiştir;

1. 7075-T651 Al alaşımı levhalar tek taraftan %100 nüfuziyet ile ilave tel kullanmadan birleştirilebilmiştir.
2. Ergime nedeniyle esas metalin yassı ve uzun taneleri kaynak çekirdeğinde daha iri ve eşeksizli tanelere dönüşmüştür. Artan kaynak akımına bağlı oluşan ısı girdisi nedeniyle kaynak çekirdeğinde daha iri taneler oluşmuştur.
3. Tüm numunelerin kaynak metali sertliğinin HAZ ve esas metalden düşük olduğu görülmüştür. Artan kaynak akımı ile kaynak merkezi sertliğinde azalma tespit edilmiştir.

#### TEŞEKKÜR

Yazar, 2018.24.03.713 nolu BAP projesi ile bu çalışmayı destekleyen Düzce Üniversitesi Rektörlüğü bilimsel Araştırma Projeleri birimine teşekkür eder.

#### REFERANSLAR

- [1] M. Erdoğan, "Mühendislik Alaşımlarının Yapı ve Özellikleri-Demir Dışı Alaşımlar", Nobel Yayınları, Ankara, pp.372-378, (2001).
- [2] Çam G and İpekoğlu G 2017 Recent developments in joining of aluminum alloys, The

- International Journal of Advanced Manufacturing Technology 91 1851-1866
- [3] C. Odabaş, Alüminyum Kaynağı, Askaynak, İstanbul, pp. 1-19, (2007).
- [4] Durgutlu A 2007 Effect of argon-hydrogen mixture on the microstructure and mechanical properties of aluminum on TIG welding Journal of Polytechnic 10 271-276.
- [5] Ç. Yeni, S. Sayer, M. Pakdil, "Comparison of mechanical and microstructural behaviour of TIG, MIG and Friction Stir welded 7075 Aluminium Alloy", Kovove Materialy, 47(5), 341-347, (2009).
- [6] Taban, E., Kaluç, E., "EN AW -5083-H321 Alüminyum Alaşımının MIG, TIG ve Sürtünen Eleman ile Birleştirmede (FSW) Kaynaklı Bağlantılarının Mekanik ve Mikroyapısal Özellikleri", Mühendis ve Makine, Cilt:46, Sayı:541, 40-51, (2005).
- [7] Çevik B and Gülenç B 2018 The effect of welding speed on mechanical and microstructural properties of 5754 Al (AlMg3) alloy joined by laser welding Materials Research Express 5(8) 086520
- [8] Z. Zhao, G.S. Frankel, "The effect of temper on the first breakdown in AA7075", Corrosion Science, 49, 3089-3111, (2007).
- [9] B. Çevik, Y. Özçatalbaş, İ. Uygur, "7075 Alüminyum Alaşımının Sürtünme Karıştırma Kaynağı ile Birleştirilmesi", 2.Uluslararası Kaynak Teknolojileri Konferansı, Ankara Türkiye, 396-374, (2012).
- [10] Çevik B, Özçatalbaş Y and Gülenç B 2016 Friction stir welding of 7075-T651 aluminium alloy Practical Metallography 53 6-23.
- [11] Çevik B, Özçatalbaş Y and Gülenç B 2016 Effect of welding speed on the mechanical properties and weld defects of 7075 Al alloy joined by FSW Kovove Materialy 54 241-247.
- [12] T. Azimzadegan, S. Serajzadeh, "An Investigation into Microstructures and Mechanical Properties of AA7075-T6 during Friction Stir Welding at Relatively High Rotational Speeds, Journal of Materials Engineering and Performance, 19,1256-1263, (2010).
- [13] Çevik, B., Özçatalbaş, Y., Gülenç, B. "SKK ile birleştirilen 7075-T651 Al Alaşımının mikroyapı ve mekanik özelliklerine devir sayısının etkisi", 3. İnt. Conference on Welding Technologies and Exhibition (ICWET'14), 658-668, May 2014, Manisa.
- [14] Çevik B, Özçatalbaş Y and Gülenç B 2016 Effect of tool material on microstructure and mechanical properties of friction stir welding Materials Testing, 58 36-42.

# AZ31B Magnezyum Alaşımının TIG Kaynağı Yöntemi ile Kaynaklanabilirliğinin İncelenmesi (ISLAC'18/UHAKS'18)

Mehmet Serkan YILDIRIM<sup>1</sup>, \*, Yakup KAYA<sup>2</sup>

<sup>1</sup>Gazi Üniversitesi, Teknik Bilimler MYO, Makina ve Metal Teknolojileri Bölümü, Ankara, 06560, Türkiye, msyildirim@gazi.edu.tr

<sup>2</sup>Karabük Üniversitesi, Teknoloji Fakültesi, İmalat Müh. Bölümü, Karabük, 78000, Türkiye, ykaya@karabuk.edu.tr

**Özet-** Bu çalışmada, hafiflik ve yüksek dayanıklılık özelliklerinden dolayı otomotiv ve elektronik endüstrisinde sıkça kullanılmakta olan AZ31B (magnezyum) levhalar TIG kaynağı yöntemi ile birleştirilmiştir. Farklı akım değerlerinde darbeli akım yöntemi kullanılarak yapılan deneysel çalışmalarda akım değeri arttıkça ana metalden kaynak metaline geçişte ve mekanik özelliklerde oluşan farklılıklar incelenmiştir. Deneysel çalışmalar sonunda, TIG kaynak yöntemiyle magnezyum malzemelerin sağlıklı bir şekilde birleştirilebildiği ve artan akım değerleriyle birlikte kaynak metali tanelerinin soğuma yönüne paralel oluştuğu görülmüştür. Magnezyumun dökümü sırasında malzeme içinde kalan gazların oluşturduğu gözeneklerin mikroyapı görüntüleri de tespit edilmiştir. Akım değerlerinin artışıyla beraber sertlik değerlerinde bir azalma meydana geldiği tespit edilmiştir. Ancak, kaynak akımının artmasıyla çekme değerlerinin de arttığı görülmüştür. Yapılan bütün çekme deneylerinin sonucunda kopmalar ITAB bölgesinde meydana gelmiştir.

**Anahtar Kelimeler-** Magnezyum, TIG kaynağı, Mikroyapı, Sertlik, Çekme deneyi.

**Abstract-** In this study, AZ31B (magnesium) plates which are mainly used in automotive and electronic industries owing to lightness and stability features were compounded with TIG welding method. During experimental studies, conducted through pulsed current method on different current values, differences in transition from base metal to welding metal and mechanic features with increasing current value were examined. After experimental studies, it was seen that magnesium materials could be compounded healthily by TIG welding method and during increasing current values welding metal grains were formed parallel as disaffection direction. In addition to this, microstructure images of pores which were composed by the gases left in the material during casting of magnesium. It was determined there were a decrease in hardness value with increase of current values. Nevertheless, it was seen that tensile values increased with increasing welding current. After all tension tests raptures occurred on HAZ area.

**Keywords-** Magnesium, TIG welding, Microstructure, Hardness, Tensile test.

## 1. GİRİŞ

İnsan vücudunun mineral olarak gereksinim duyduğu magnezyuma endüstride de bir malzeme çeşidi olarak önemli derecede gereksinim duyulmaktadır. Güneçtikçe magnezyum geleneksel olarak endüstriyel uygulamalarda kullanılan demir, alüminyum gibi metallerin yerini almaya başlamıştır [1]. Magnezyumun endüstride bu denli önemli bir yere gelmesinin en önemli sebepleri düşük yoğunluğu (1,74 g/cm<sup>3</sup>) ve yüksek dayanıklılığıdır (35-260 KNm/kg) [2,3].

Magnezyum endüstride uzay ve havacılık sektöründe uçak kanatlarında, füze parçalarında ve yakıt tanklarında; otomobil sektöründe şanzıman kutuları, motor blokları ve direksiyon simidi imalatında; laptop, televizyon, cep telefonu gibi elektronik parçaların üretiminde sıkça kullanılmaktadır [4,5].

Endüstride magnezyumun kullanılabilirliği arttıkça buna paralel olarak farklı kaynak yöntemleriyle birleştirilmesi için yapılan çalışmalarda artmıştır. Magnezyum parçaların kaynaklı birleştirilmelerinde MIG, sürtünme kaynağı, lazer kaynağı, elektro ışın kaynağı, elektrik direnç kaynağı gibi yöntemlerin yanı sıra TIG kaynağı yönteminde sıkça kullanılmaktadır [7,8].

Klasik olarak TIG kaynağı, kaynak için gerekli ısının, tükenmeyen bir elektrod (tungsten elektrod) ile iş parçası arasında oluşan ark sayesinde ortaya çıktığı bir ark kaynak yöntemidir. Koruyucu gaz olarak argon, helyum yada bu iki gazın karışımı olan soygazlar kullanılır. Koruyucu gazın görevi tungsten elektrodu, kaynak banyosunu, arki ve iş parçasının kaynağa yakın bölgelerini, atmosferin zararlı etkilerinden korumaktır [9-11].

TIG kaynak yönteminin önemli avantajlarından birisi, darbeli akım kullanılarak düşük ısı girdisiyle mükemmel kaynaklı bağlantılar elde edilebilmesidir [12]. Yüksek ve düşük akım değerleri, bu değerlerin

süresi ve darbe frekansından oluşan darbeli akım parametreleri, arkın kararlılığını, kaynak kalitesini, kaynak dikişi görünümünü ve kaynak dikiş geometrisini önemli ölçüde etkilemektedir.

Darbeli ark, kaynak akımının yüksek akım ile düşük akım arasında hızlı biçimde artıp azalmasından oluşmaktadır. Kaynak çizgisinde birbiri üstüne binmiş puntolar biçiminde görüntü elde edilmektedir. Bu parametrelerin uygunsuz seçimi düzensiz dikiş yüzeyi görünümü başta olmak üzere ergime boşluklarına, yanma oyuklarına ve yetersiz nüfuziyete neden olabilmektedir. Bu yüzden iyi bir kaynak için darbeli akım parametrelerinin uygun olarak seçimi çok önemlidir. Kaynak işleminde darbeli akım parametreleri birbirine bağlı ve karmaşık olması sebebiyle, kabul edilebilir özellikte bir kaynaklı birleştirme elde etmek için bu parametrelerin birbiriyle uyum içinde olmaları gerekmektedir [13-15].

Bu çalışmada, AZ31B magnezyum levhalar TIG kaynak yöntemi ile darbeli akım kullanılarak, farklı akım değerleri ile birleştirilmiş ve uygulanan farklı akım değerlerinin birleştirmeler üzerindeki etkisini incelemek amacıyla mikroyapı, çekme dayanımı ve sertlik özellikleri incelenmiştir.

## II. DENEYSEL METOD

TIG kaynak yönteminin kullanıldığı bu çalışmada, 1,75 mm kalınlığa sahip hadde mamulü ticari AZ31B, magnezyum levhalar darbeli akımda farklı, düşük ve yüksek akım değerleri kullanılarak birleştirilmiş ve birleştirmelerin mikroyapı, çekme dayanımı ve sertlik özellikleri araştırılmıştır. Deneysel olarak kullanılan AZ31B magnezyumun kimyasal bileşimi Tablo 1'de verilmiştir. Birleştirilecek olan magnezyum levhalar giyotin makas kullanılarak 200x50 mm ebatlarında hazırlandıktan sonra yüzeyleri temizlenmiştir. Bütün kaynak işlemlerinde ısı kaybını önlemek için magnezyum malzemeler paslanmaz çelik bir altlık kullanılarak işkence ile sabitlenip kaynağa hazır hale getirilmiştir. Kaynak işlemlerinde koruyucu gaz olarak argon gazı kullanılmış olup kaynak bölgesinin altına korunması için bir aparat yardımıyla malzemenin alt kısmına da argon gazı verilmiştir. Koruyucu gazın malzemenin alt kısmına uygulanması Şekil 1'de gösterilmiştir. Kaynak düzeneğinin hazırlanmasıyla birlikte farklı akım değerleri kullanılarak 3 adet kaynaklı birleştirme yapılmıştır. Deneyler esnasında kullanılan kaynak parametreleri Tablo 2'de verilmiştir.

TABLO 1

MAGNEZYUM AZ31B KİMYASAL BİLEŞİMİ

Kimyasal Bileşim (%)			
Al	Zn	Mn	Si
2.9	0.93	0.36	0.013
Ni	Cu	Fe	
0.00072	0.0073	0.0024	



Şekil 1 Kaynaklanan malzemeye koruyucu gazın uygulanması

TABLO 2

BİRLEŞTİRME İŞLEMİNDE KULLANILAN PARAMETRELER

PARAMETRE	Numune 1	Numune 2	Numune 3
Voltaj (V)	25		
Üst amper (A)	75	80	85
Alt amper (A)	35	40	45
Darbe frekansı (Hz)	5		
Darbe zamanı (%)	50		
Isı girdisi (kJ/mm)	9,8	9,8	9,8
Koruyucu gaz	Argon		
Gaz akış oranı (l/dk)	15		
Kaynak hızı(mm/dk)	150		
Elektrod çapı (mm)	2,4		
İlave metal (mm)	2		

Farklı kaynak akımı değerlerinin kaynak metali ve ITAB mikroyapısına olan etkilerini incelemek için kaynaklı parçalardan mikroyapı numuneleri hazırlanmıştır. Hazırlanan numuneler gömme işleminden sonra standart metalografik numune hazırlama işlemine tabi tutulmuşlardır. Bu numuneler daha sonra 10 ml asetik asit, 3 gr pikrik asit, 5 ml saf su, 50 ml etanol çözeltisinden oluşan dağlayıcı ile dağlanmış ve mikroyapı incelemesi için hazır hale getirilmişlerdir. Hazırlanan numuneler Leika DM 4000M optik mikroskopta incelenerek gerekli yerlerden mikroyapı görüntüleri alınmıştır.

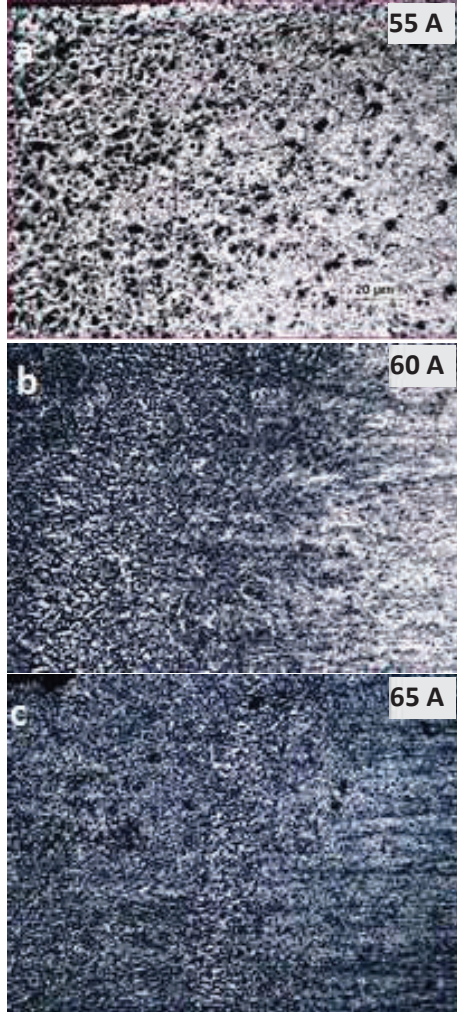
Hazırlanan mikroyapı numuneleri kullanılarak ana metal, kaynak bölgesi ve yine ana metal olacak şekilde 13 noktadan, 0,5 kg yük altında Shimadzu HVM mikrosertlik cihazı kullanılarak sertlik ölçümleri yapılmıştır.

Farklı kaynak akım değerlerinin, birleştirilen parçaların kaynak metali çekme dayanımına olan etkilerini görmek amacı ile ana malzemedan ve her akım değerinden 3 adet olmak üzere çekme deney numuneleri hazırlanmış ve teste tabi tutulmuştur. Test işlemleri oda sıcaklığında gerçekleştirilmiştir.

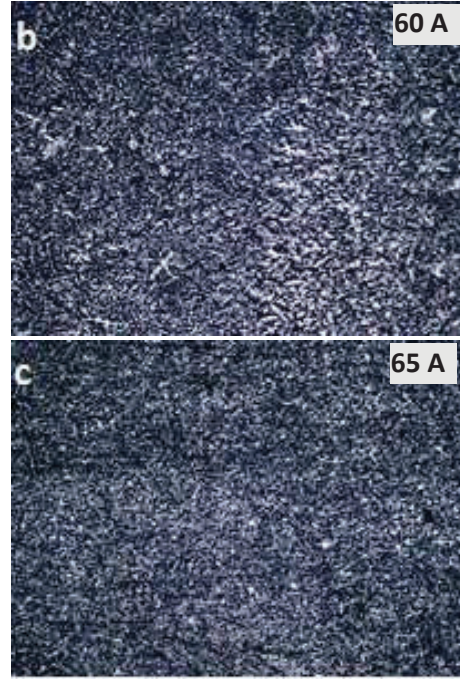
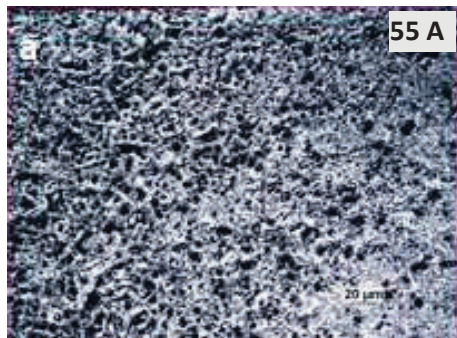
### III. DENEY SONUÇLARI VE TARTIŞMA

#### A. Mikro Yapı Sonuçları

Darbeli akım kullanılarak TIG kaynak yöntemi ile birleştirilen numunelerden aynı büyütme oranlarında elde edilen ITAB bölgesinden kaynak metaline geçişin mikroyapı görüntüleri Şekil 2 a-b-c'de verilmiştir. Yine Şekil 3 a-b-c'de kaynak metallerinin mikroyapı görüntüleri verilmiştir.



Şekil 2. Artan akım değerlerine göre kaynak metalinden ITAB'a geçişlerin mikroyapı görüntüleri

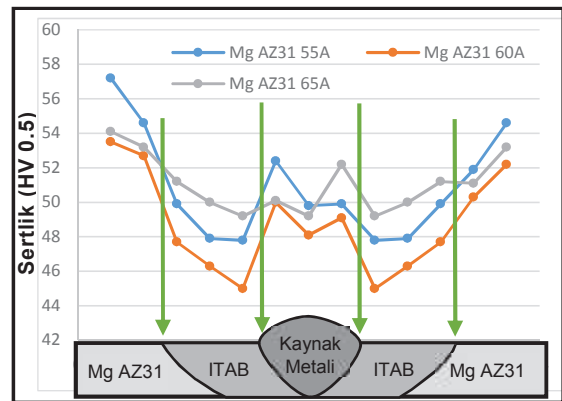


Şekil 3. Artan akım değerlerine göre kaynak metallerinin mikroyapı görüntüleri

Amper değerinin artışına paralel olarak artan ısı girdisiyle kaynak metali tanelerinin irileştiği ve soğuma yönüne paralel olarak oluştuğu görülmüştür. Mikroyapı fotoğrafları incelendiğinde gözenekli yapı dikkat çekmektedir. Gözeneklerin sebebini araştırmak için yapılan literatür araştırmasında F.Mert ve arkadaşları [16] yapmış oldukları çalışmada magnezyum alaşımli parçaların üretiminde kullanılan en yaygın yöntemin basınçlı döküm olduğunu ve bu yöntemde parçaların hızlı soğuması ile ince taneli yapı oluşması sağlanırken, gazların kaçmasını zorlaştırdığından dolayı gözenekliliğe yol açabildiği söylenmiştir.

#### B. Sertlik Sonuçları

Şekil 4'de farklı akım değerlerinde darbeli akım kullanılarak TIG kaynak yöntemi ile birleştirilen kaynaklı bağlantılar üzerinde alınan sertlik dağılım grafiği verilmiştir.

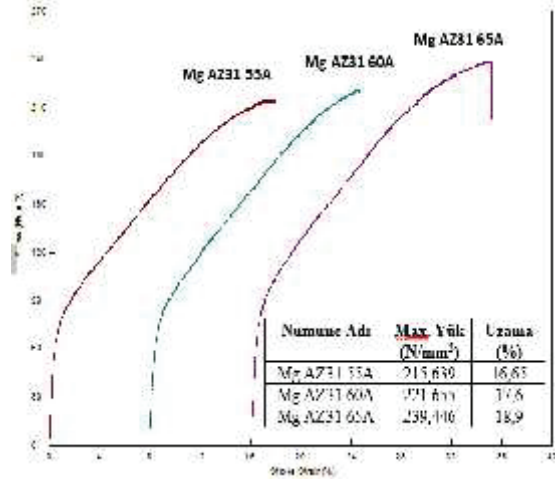


Şekil 4. Farklı amper değerlerindeki numunelerin sertlik değerleri

Sertlik grafiği incelendiğinde, en yüksek sertlik değerleri ana metalde ölçülürken, onu sırasıyla kaynak bölgesi ve ITAB bölgesinin takip ettiği görülmüştür. En düşük sertlik değerinin ITAB'da meydana gelmesinin sebebi kaynak işlemi sırasında ITAB'daki mikro yapı değişimi sırasında oluşan tane irileşmesinden kaynaklanmaktadır. Hong-tao Liu ve arkadaşlarında [17] yapmış oldukları çalışmalarda buna benzer sonuçlara ulaşılmıştır. Ayrıca farklı akım değerleriyle birleştirilen numunelerde en yüksek sertlik değeri en düşük akım değerinin kullanıldığı kaynak işleminde elde edilmiştir. Bunun nedeni akım değeri arttıkça ısı girdisinin artması ve malzemenin daha yavaş soğumasından kaynaklanmaktadır [18].

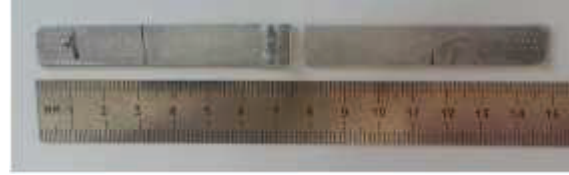
### C. Çekme Dayanımı Test Sonuçları

TIG kaynak yöntemi ile farklı akım değerlerinde darbeli akım kullanılarak birleştirilen kaynaklı bağlantılara ait çekme grafikleri Şekil 5'de verilmiştir.



Şekil 5. Farklı amper değerlerindeki numunelerin çekme grafiği

Darbeli akımda farklı akım değerleri kullanılarak yapılan birleştirmelerde kaynak bölgesinin mukavemet özellikleri, ana malzemenin mukavemet özelliklerinden düşük olduğu görülmüş olup, kaynak akımının artmasıyla çekme değerlerinin de arttığı tespit edilmiştir. Yapılan deneyler sonrasında kopmaların hepsi ITAB'dan olmuştur. Sertlik sonuçları da incelendiğinde en düşük sertliğin ITAB bölgesinde olduğu görülmüş olup bundan dolayı da kopmaların ITAB bölgesinde olduğu düşünülmektedir. Şekil 6'da çekme testi sonrası ITAB bölgesinden kopan bir numune örneği verilmiştir. Z.D. Zhang ve arkadaşları da [19] yapmış oldukları çalışmalarda bu sonuca benzer sonuçlar bildirmişlerdir.



Şekil 6. Çekme testi sonrası ITAB bölgesinden kopan numune örneği

### III. SONUÇLAR VE ÖNERİLER

Mikroyapı çalışmaları sonucunda; kaynak akımı artışına paralel olarak artan ısı girdisiyle kaynak metali tanelerinin irileştiği görülmüştür.

Sertlik grafiği incelendiğinde, en yüksek sertlik değerleri ana metalde ölçülürken, onu sırasıyla kaynak bölgesi ve ITAB bölgesinin takip ettiği görülmüştür.

Çekme testleri sonucunda ise; kaynak akımının artmasıyla çekme dayanımının da arttığı tespit edilmiştir. Ayrıca bütün numunelerde kopma ITAB'da gerçekleşmiştir.

### KAYNAKLAR

- [1] D. Sameer Kumar, C. Tara Sasanka, K. Ravindra and K.N.S. Suman, "Magnesium and its alloys in automotive applications – a review", *American Journal of Materials Science and Technology*, (2015) vol. 4 (1), pp. 12-30, 2015.
- [2] M. K. Kulekci "Magnesium and its alloys applications in automotive industry", *The International Journal of Advanced Manufacturing Technology*, vol. 39 (9-10), pp. 851-865, 2008.
- [3] M. James, J. M. Kihui, G. O. Rading and J. K. Kimotho, "Use of magnesium alloys in optimizing the weight of automobile: Current trends and opportunities", *Sustainable Research and Innovation Proceedings*, vol 3, pp. 1-3, 2011.
- [4] L. Zhi-yi, H. Tian-tian, L. Wen-juan and K. Sukbong, "Dislocation mechanism for dynamic recrystallization in twin-roll casting Mg-5.51Zn-0.49Zr magnesium alloy during hot compression at different strain rates", *Transactions of Nonferrous Metals Society of China*, vol. 26 (2), pp. 378-389, 2016.
- [5] W. Qing-liang and X. Shou-mei, "Vacuum assisted high-pressure die casting of AZ91D magnesium alloy at different slow shot speeds", *Transactions of Nonferrous Metals Society of China*, vol. 24 (10), pp. 3051-3059, 2014.
- [6] Z. Chao-yong, P. Fu-sheng and P. Hu-cheng, "Microstructures mechanical and bio-corrosion properties of as-extruded Mg-Sn-Ca alloys", *Transactions of Nonferrous Metals Society of China*, vol. 26, pp. 1574-1582, 2016.
- [7] S. Jun, W. Li-biao, L. Yang and M. Dong, "Effects of welding speed on the microstructures and mechanical properties of laser welded AZ61 magnesium alloy joints", *Materials Science and Engineering A*, vol. 578, pp. 303-309, 2013.
- [8] L. Li-ming, W. Ji-feng and S. Gang, "Hybrid laser-TIG welding, laser beam welding and gas tungsten arc welding of AZ31B magnesium alloy", *Materials Science and Engineering A*, vol. 381 (1-2), pp. 129-133, 2004.
- [9] M. L. Gour, *Principles of welding technology*, Third Edition, Edward Arnold, London Melbourne Auckland, London, 87-128, 1995.
- [10] S. C. Juang and Y. S. Tarn, "Process parameter selection for optimising the weld pool geometry in the tungsten inert gas welding of stainless steel", *Journal of Materials Processing Technology*, vol. 122 (1), pp. 33-37, 2002.
- [11] H. B. Cary, *Modern welding technology*, Second Edition, AWS, 82-85, 1981.

- [12] Y. Kaya, A. Durgutlu, N. Kahraman ve B. Gülenç, "Titanyum levhaların TIG kaynağı ile birleştirilmesinde akım türünün mikroyapı ve mekanik özellikler üzerine etkisi" *6th International Advanced Technologies Symposium (IATS'11)*, 288-293, 16-18 May 2011, Elazığ, Turkey.
- [13] P. Praveen, P. K. D. V. Yarlagadda and M. J. Kang, "Advancements in pulse gas metal arc welding", *Journal of Materials Processing Technology*, vol. 164-165, pp. 1113-1119, 2005.
- [14] S. Zhang, F. Jiang and W. Ding, "Microstructure and mechanical performance of pulsed current gas tungsten arc surface engineered composite coatings on Mg alloy reinforced by SiCp", *Materials Science and Engineering: A*, vol. 490 (1-2), pp. 208-220, 2008.
- [15] P. K. Palani and N. Murugan, "Selection of parameters of pulsed current gas metal arc welding", *Journal of Materials Processing Technology*, vol. 172 (1), pp. 1-10, 2006.
- [16] F. Mert, A. Özdemir ve Ç.Karataş, "Magnezyum Alaşımlarının Basınçlı Döküm Yöntemiyle Kalıplanabilirliğinin Değerlendirilmesi" *Politeknik Dergisi*, vol. 13 (3) pp.165-176, 2010.
- [17] L. Hong-tao, Z. Ji-xue, Z. Dong-qing, L. Yun-teng, W. Jian-hua, Y. Yuan-sheng, M. Bai-chang and Z. Hai-hua, "Characteristics of AZ31 Mg alloy joint using automatic TIG welding", *International Journal of Minerals, Metallurgy and Materials*, vol. 24 (1), pp. 102-108, 2017.
- [18] C. Çetinkaya ve U. Arabacı, "Yakma alın kaynağında yığma akım zamanının bağlantının mekanik özellikleri üzerine etkisinin incelenmesi" *Politeknik Dergisi*, vol. 7 (4), pp. 327-333, 2004.
- [19] Z. D. Zhang, L. M. Liu, Y. Shen and L. Wang, "Mechanical properties and microstructures of a magnesium alloy gas tungsten arc welded with a cadmium chloride flux" *Materials Characterization*, vol. 59 (1), pp. 40-46, 2008.

# Titanyum Malzemelerin Patlamalı Kaynak Yöntemi ile Gerçekleştirilen Birleştirmelerin Analizi ve İncelenmesi (ISLAC'18/UHAKS'18)

Kemal AYDIN<sup>1</sup>, \*, Yakup KAYA<sup>2</sup>

<sup>1</sup>Gümüşhane Üniversitesi, Gümüşhane MYO, Elektrik ve Otomasyon Bölümü, Gümüşhane, 29000, Türkiye, kemalaydin@gumushane.edu.tr

<sup>2</sup>Karabük Üniversitesi, Teknoloji Fakültesi, İmalat Müh. Bölümü, Karabük, 78000, Türkiye, ykaya@karabuk.edu.tr

**Özet-** Titanyum ve titanyum alaşımları son zamanlarda biyolojik uyumluluk nedeni ile sağlık, korozyona karşı olan dayanımı sebebi ile de endüstride kullanılan ve adından sıkça söz ettirmekte olan hafif bir malzeme türüdür. Bu nedenlerden dolayı da, titanyum ve alaşımlarının endüstride kullanımı için çeşitli kaynak yöntemlerini kullanarak birleştirme ihtiyacı doğmuştur. Bu bağlamda yapılan birleştirme yöntemlerinden patlama kaynak yöntemi ile gerçekleştirilen birleştirmeler derlenmiş olup, sonuçlar hakkında değerlendirmeler yapılmıştır.

**Anahtar Kelimeler-** Titanyum, Alaşım, Kaynak, Patlama, Korozyon

**Abstract-** Titanium and titanium alloys are a kind of light material which is used frequently in the industry due to its resistance to corrosion and corrosion due to its biological compatibility. For these reasons, there has been a need to combine various welding methods for the use of titanium and its alloys in industry. In this context, the assemblies with the explosive welding method were compiled from the joining methods and the results were evaluated.

**Keywords-** Titanium, Alloy, Welding, Explosive, Corrosion

## 1. GİRİŞ

Alüminyum ve magnezyuma genel özellikleri açısından bakıldığında genellikle hafif metaller olarak bilinse de; titanyum, demir ile karşılaştırıldığında yoğunluğunun yaklaşık % 60'ı kadarı bir yoğunluğa sahip olduğu görülmektedir. Dünyada artık çoğu ülke, titanyum malzemenin önemli olduğu kanaati oluştuğu için araştırma, geliştirme ve titanyumun uygulamaya yönelik çalışmalarına büyük bir destek vermektedir. Titanyum, mühendislik uygulamalarında kullanıldığı gibi, diş ve medikal uygulamalarda oldukça ilgi duyulan özel bir malzemedir [1,2].

Titanyum malzemelerin korozyona karşı göstermiş olduğu direnç, paslanmaz çelik ve kobalt ve alaşımları ile karşılaştırıldığında daha fazladır. Nötral pH ve izotonik tuzlu suda titanyum

malzemelerin korozyon oluşması hemen hemen yok denilecek kadar azdır. Aralık, taneler arası ve çukurcuk korozyonlarına karşı direnci oldukça yüksek olduğu görülmektedir. Titanyum malzemelerin hayvan deneylerinde ve insan hayatını kolaylaştıracak uygulamalarda biyolojik uyumlulukları konusunda şimdiye kadar olumsuz izlenimler vermemiştir [3].

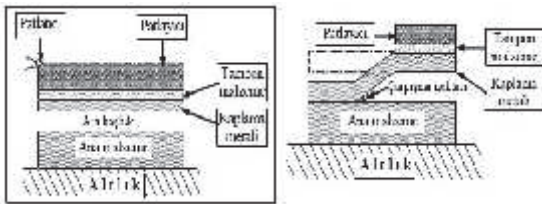
Uzay, nükleer ve kimyasal sanayii her geçen gün gelişmesiyle birlikte daha çok paslanmazlık ve aşınma direncine sahip olunan malzemelere olan ihtiyaç gün geçtikçe artmaktadır. Patlayıcının kullanılmasıyla yapılan kaynak teknolojisi, bu amaçla kullanılan modern teknoloji yöntemlerinden biridir. Patlayıcı yardımıyla yapılan kaynak uygulaması, diğer kaynak yöntemleriyle birleştirilebilmesi mümkün olmayan malzemelerin veya kompozitlerin kaynakla birleştirilebilmesinde kullanılan bir teknoloji çeşitidir [4-6].

Patlamalı kaynak yöntemi veya kaplama yöntemi iki metali patlayıcı kullanarak birleştirme işlemi ya da kaplamayı gerçekleştiren alışılmamış yani diğer kaynak yöntemleriyle karşılaştırıldığında oldukça farklı bir yöntemdir [7-9].

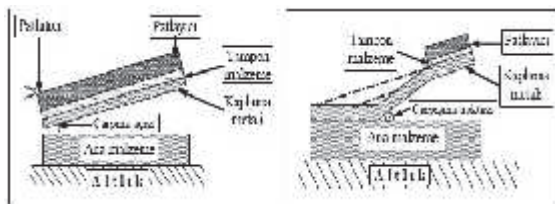
Patlamalı birleştirme olarak da bilinen patlama kaynağı, iki metal arasında patlayıcının etkisi ile oluşan yüksek hızdaki malzemelerin eğimli bir şekilde çarpışması sonucu meydana gelir. Patlama kaynağı veya kaplama yöntemi; patlayıcının etkisi ile elde edilen yüksek basınç yardımı ile iki ya da daha fazla metali birleştirmek için kullanılan bir katı hal kaynak yöntemidir. Metal yüzeylerin birbirleriyle çarpışması sonucunda yeterli bir çarpışma enerjisinin meydana gelmesiyle, bu yüzeylerde oluşan ilk temaslarını birbirleri üzerinde bir akış sergileyerek devam ettirirler ve sonuçta, katı hal birleşmesi gerçekleşmiş olur. Bu kaynak yöntemini uygularken dışarıdan herhangi ısı verilmediğinden dolayı soğuk bir teknik olarak tanımlanmasına rağmen, kaynak işleminin dinamiğinden dolayı kaynak ara yüzeyinde bölgesel yüksek sıcaklıklar meydana gelebilir. Buradaki

patlayıcının infilak edilmesiyle birlikte ısı meydana gelmesine rağmen, metal parçalar arasında ısı transferinin gerçekleşmesi için gerekli zaman yoktur ve metallerde ısı akışının olmadığı görülür [10-13].

Patlamalı kaynak veya kaplama yönteminin üç temel elemanı vardır. Bunlar; taban malzemesi, üst parça ve patlayıcıdır. Kaynak işlemi sırasında taban malzemesi sabit bir şekilde durur ve üst parça sabit duran malzemeye kaynaklanır. Aynı zamanda, taban malzemesi de büyük bir altlık yardımıyla desteklenmelidir. Üst plaka da kaynak sırasında patlayıcının etkisi ile taban malzemesi üzerine doğru hareket ettirilir. Birleştirilecek olunan üst parça genellikle taban malzemesine paralel bir konumda bulunmaktadır. Buna ilaveten bazı özel birleştirme uygulamalarında her parça için ayrı ayrı açılar oluşturularak gerçekleştirilen kaynak işlemleri vardır. Patlamalı kaynak ya da kaplama yönteminde bir altlık üzerine sırasıyla: ana malzeme (taban malzemesi), belirli bir oranda boşluk, ana metale göre eğimli ya da paralel olarak yerleştirilmiş kaplama malzemesi (üst parça), malzemelerin kaplanma sırasında hasara uğramasını önleyen tampon tabaka, patlayıcı malzeme ve patlatıcı yerleştirilmektedir. Şekil 1 ve Şekil 2' de patlamalı kaynak yönteminin paralel ve eğik düzlemlerdeki şeklini göstermektedir [14-17].



Şekil 1. Patlamalı kaynak yönteminde paralel düzlem şematik gösterimi [15].

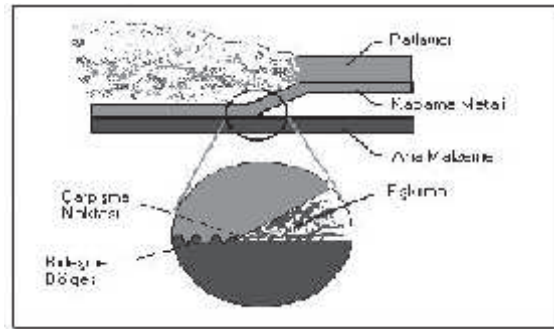


Şekil 2. Paralel kaynak yönteminde eğik düzlemde şematik gösterimi [15].

Metalik yüzeylerin çarpışması sonucunda, yeterli bir oranda çarpışma enerjisi ortaya çıktığında, bu metalik yüzeyler arasında oluşan ilk temas sonucunda birbirleri üzerinde bir akış sergileyerek devam ederler ve bu olay sonucunda bir katı hal birleşmesi meydana gelmiş olur [18-22]. Patlamalı kaynak esnasında temas yüzeylerinde oluşan basınç oldukça yüksektir ve üst tabakanın etkisiyle oluşan kinetik enerji arayüzeyde dalgalı bir birleştirme görüntüsü oluşturur. Bu darbenin oluşması ile birlikte malzemelerin iki yüzeyi birbirine mekanik olarak kilitler. Burada gerçekleşen mekanik birleşmenin etkisi ile de gerçekleşen plastik

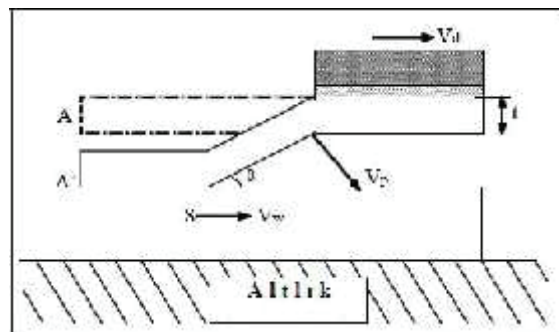
deformasyon sonucu, soğuk basınç kaynağı oluşur [14,23]. Bu işlem, kaynak esnası sırasında dışarıdan herhangi bir ısı verilmediği için soğuk teknik olarak tanımlanmasına rağmen işlemin dinamiğinden dolayı kaynak arayüzeyinde bölgesel olarak yüksek sıcaklıklar oluşabilir.

Eğimli düzlemde gerçekleşen çarpışma, metal yüzeylerden bir tabakanın metal jeti şeklinde, çarpışma arayüzey bölgesinden uzaklaşmasına sebep olur. Çarpışma sırasında yüzeyden metal jeti şeklinde fıskıran bu tabakanın kalınlığı genellikle 0,05mm'den daha azdır. Patlamanın etkisi sonucunda metal jeti dışarı atılırken, aynı zamanda çarpışan metalik yüzeylerin temizliği de gerçekleştirilmiş olunur. Kaynak yapılacak metal yüzeyinde bulunan oksit, yağ, kir, pas gibi kaynak için zararlı olan etkiler, oluşan jet ile birlikte dışarı atılmaktadırlar [24,25]. Bu olayın şematik gösterimi Şekil 3' de gösterilmiştir.



Şekil 3. Patlama kaynağında fıskırma olayı

Patlamalı kaynak yönteminde kaliteli bir birleştirme elde edebilmek için, kaynak işlemi kontrol altında tutabilecek parametrelerin belirlenmesi gerekmektedir. Birleştirme işlemi sonucunda, arayüzeyi ve kaynak kalitesini etkileyen bazı kaynak parametreleri vardır. Bu parametreler; ara boşluk mesafesi (s), eğimli düzenlemelerde başlangıç açısı (paralel düzenlemeler için bu değer  $\alpha=0$  dir) (a), patlayıcı oranı (patlayıcı kütlelerini üst levha kütlelerine oranı) (R), patlayıcının patlama hızı (Vd), üst levhanın çarpma hızı (Vp), çarpışma açısı ( $\beta$ ), kaynak hızı (çarpışma noktası hızı) (Vw) eğik düzlemlerde çarpışma açısı  $\alpha$ , altlık, füyve ve patlayıcı olarak sıralanabilir [26,27]. Şekil 4'de patlamalı kaynak yöntemi parametreleri şematik olarak gösterilmiştir.

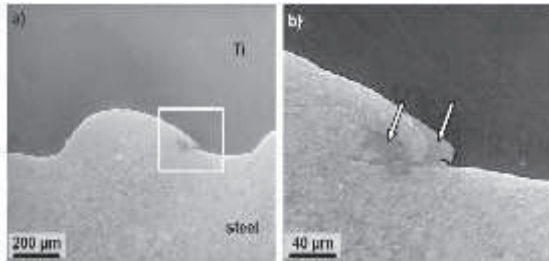


Şekil 4. Kaynak parametrelerinin şematik gösterimi

## II. YAPILAN ÇALIŞMLAR

Xia ve arkadaşları, patlamalı kaynak yöntemini kullanarak, titanyum ile alüminyum levhaları birleştirerek mekanik ve mikroyapı özelliklerini incelemişlerdir. Birleşme arayüzeyi bölgesinde dalgalı bir şekil olduğu tespit edilmiştir. 180° çift yönlü eğme testleri sonrasında, numunelerde ayrılma veya kırılma görülmediği, patlamalı kaynak yöntemi ile birleştirilen TA2/2A12 kompozit malzemelerin güvenli olduğu, X-ışını Spektrometre (EDS) sonuçlarına göre, arayüzeyde hiçbir intermetalik bileşimin görülmediği, görülmesi durumunda arayüzey bölgesinde sert ve kırılğan intermetaliklerden dolayı çatlamanın gerçekleşebileceğini bildirmişlerdir. Mikro sertlik değerlerinin arayüzeyden uzaklaştıkça azaldığı gözlenmiştir [28].

Song ve arkadaşları, titanyum ile çelik plakaları patlamalı kaynak yöntemini kullanarak kaplamış ve mikroyapısı elektron mikroskopu ile incelenerek eğme testleri gerçekleştirmişlerdir. Kaynak arayüzey bölgesinin incelemeler sonucunda dalgalı bir arayüzeye sahip olduğu belirlenmiştir. Yapılan bu mikro ölçekli incelemelerde, dalgalı arayüzey bölgesinin hemen dışarısında intermetalik inklüzyonların olduğu gözlenmiştir. Şekil 5'te oluşan inklüzyonlar (a) ve inklüzyonların etkisi ile oluşan çatlaklar (b) gösterilmiştir. 90° eğme testleri sonucunda, birleştirmelerde hiçbir ayrılma görülmediği tespit edilmiştir [29].



Şekil 5. (a) Dalgalı bölgede görülen ve çoğunlukla çelik tarafında oluşan inklüzyonlar, (b) İntermetaliklerden dolayı oluşan mikro çatlaklar

Kahraman, titanyum-paslanmaz çelik, titanyum-düşük karbonlu çelik ve titanyum-alüminyum, patlamalı kaynak yöntemi ile birleştirmiştir. Birleştirilen numunelere; sertlik, eğme ve kesme-makaslama testleri ile SEM ve mikroyapı çalışmaları gerçekleştirilmiştir. Ayrıca deniz suyu ortamında oluşan korozyon değişimlerinin belirlenmesi için çalışmalar yapılmıştır. Patlayıcı oranının R=1 kullanıldığı durumda titanyum-paslanmaz çelik ve titanyum-düşük karbonlu çelikte birleşme gerçekleşmezken, titanyum-alüminyum arasında gerekli basınç sağlandığından birleşme olumlu sonuçlanmıştır. Birleştirilen kompozitlere uygulanan çekme-makaslama testi sonucunda hiçbir kompozitte sıyrılmaya gözlenmemiştir. Optik mikroskop ile inceleme yapıldığında düşük patlayıcı oranlarında gerçekleşen birleşmede arayüzey

görüntüsü düz bir şekilde görülürken, patlayıcı oranının artmasıyla dalgalı bir arayüzey oluşmakta ve dalgaların boy ve genişliğinde artışlar gözlenmektedir. 180° çift yönlü eğme testleri sonrasında, kaynak arayüzeyinde ayrılma ya da yırtılma gibi olumsuzluklar görülmemiştir. Kaynak numunelerinin SEM ile incelenmesi sonucunda birleşme arayüzeyinde herhangi bir birleşme hatası gözlenmemiştir. Sertlik ölçüm değerlerine bakıldığında soğuk deformasyonun etkisi ile kaynaklı numunelerde olan sertlik değerlerinin orijinal malzemelere göre daha fazla olduğu tespit edilmiştir. Kompozitlere uygulanan korozyon testi sonucunda ise en dayanıklı malzeme çifti olarak titanyum-paslanmaz çelik olduğu belirlenmiştir [14].

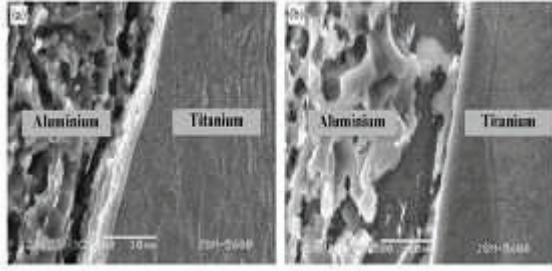
Kahraman ve arkadaşları, titanyum ile paslanmaz çeliği eğik düzlemde patlamalı kaynak yöntemini kullanarak birleştirmişlerdir. Birleştirilen kaynaklı numunelere; TEM, çekme-makaslama, bükme, sertlik ve korozyon testleri uygulanmıştır. Optik ve SEM incelemelerinde patlayıcı oranının artması ile pürüzsüz olan arayüzey bölgesinin dalgalı bir arayüzey şekline dönüştüğü gözlenmiştir. Çekme-makaslama testinde kaynaklı numunelerde sıyrılmaya tespit edilmemiştir. Patlatma oranı arttıkça sertlik değerinin arttığı ve en yüksek sertlik ölçümlerinin arayüzeyde ve arayüzeye yakın bölgelerde ölçüldüğü belirtilmiştir. Paslanmaz çelik ve titanyum malzemelerde oksit tabakası patlayıcı oranının artması ile korozyon dayanımının ters orantılı olduğu sonucuna varılmıştır. Ayrıca; eğme testi sonucunda, yırtılma, ayrılma veya kırılma gibi durumlar gözlenmemiştir (Şekil 6) [30].



Şekil 6. Eğme testi görüntüsü

Kahraman ve arkadaşları, titanium ile alüminyumu, çeşitli patlayıcı yüklerini kullanarak patlamalı kaynak yöntemi ile birleştirmiş ve birleştirilen kaynaklı numunelere; eğme, sertlik, mikroyapı, korozyon ve çekme-makaslama testleri uygulamışlardır. Çekme-makaslama testi sonucunda kaynaklı numunelerde herhangi bir ayrılma gözlenmemiştir. Eğme testi sonucunda, çatlama veya yırtılma olayı tespit edilmemiştir. Sertlik değerleri ölçüldüğünde arayüzey bölgesindeki sertlik değerlerinin orijinal malzemeye göre arttığı belirtilmiştir. SEM ve optik mikroskop çalışmasında patlayıcı oranının artmasıyla (Şekil 7) arayüzeyde oluşan dalga boyu ve genişliğinde artış olduğu tespit edilmiş olup korozyon incelemesinde ise patlayıcı

oranının artışı ile korozyon dayanımının düştüğü tespit edilmiştir [8].



Şekil 7. SEM görüntüleri (a)  $R=1$  ve (b)  $R=2.5$  patlayıcı yükü.

Yan ve arkadaşları, NiTi/NiTi şekil hafızalı alaşımları patlamalı kaynak yöntemini kullanarak birleştirmiş ve mikrosertlik testi uygulamışlardır. Kaynaklı numunelere yapılan mikrosertlik testleri sonucunda, patlamalı kaynak sırasında, patlayıcı yükünden dolayı yüksek darbe hızlarına ulaşıldığından ve bu hızın etkisi nedeni ile kaynak sırasında soğuk plastik deformasyondan olayının gerçekleştiği, sertlik değerlerinin ölçüldüğünde ise arayüze yakın bölgelerde en yüksek sertlik değerleri ve ince yapısı elde edildiği bildirilmiştir [31].

Mousavi ve arkadaşları, yapmış oldukları çalışmada Titanyum ve 304 paslanmaz çeliği patlamalı kaynak yöntemi ile birleştirmişlerdir. Kaynaklı bağlantıların arayüzeyleri incelendiğinde, düşük patlayıcı oranlarında arayüzeyin düz olduğu fakat patlayıcı oranının artmasıyla da arayüzeyin dalgalı bir yapıda olduğu belirtilmiştir. SEM ile yapılan çalışmalarda ise  $Fe_2Ti$ ,  $Fe_2Ti_4O$  ve  $Cr_2Ti$  intermetalik fazların olduğu tespit edilmiştir [32].

Manikandana ve arkadaşları, yapmış oldukları çalışmada titanyum ile paslanmaz çeliği patlamalı kaynak yöntemi ile birleştirmiştir. Yapılan incelemeler sonucunda arayüzeyde herhangi bir intermetalik olmadığı, plastik deformasyonun olduğu ve arayüzeyde dalgalı bir yapının olduğu belirtilmiştir [33].

Sakhtemanian ve arkadaşları, Titanyum ve düşük karbonlu çelik levhaları patlamalı kaynak yöntemi ile birleştirmişlerdir. Plakalar farklı düzende yerleştirilip deney yapıldığında Ti-St düzeninin St-Ti düzenine göre daha iyi bir birleşme gerçekleştirildiği belirlenmiştir [34].

Mali ve arkadaşları, yapmış oldukları çalışmada patlamalı kaynak yöntemini kullanarak Titanyum-Nikel çifti arasına Ta ve Cu tabakaları koyarak kaynak işlemini gerçekleştirerek mikroyapı ve mekanik özelliklerini incelemiştir. SEM ile yapılan inceleme de arayüzeyde dalgalı bir yapının olduğu gözlenmiştir. Kaynaklı numunelerde ölçülen sertlik değerleri başlangıçta ölçülen sertlik değerlerinden daha yüksek olduğu gözlenmiştir. Ti-Ta kısmi ergime bölgelerinde ölçülen sertlik değeri Ta-Cu arasında ölçülen sertlik değerinden daha yüksek olduğu belirlenmiştir. EDS ve SEM

çalışmalarında vorteks bölgelerinin olduğu belirlenmiştir [35].

Kahraman ve arkadaşları, titanyum ve bakır levhaları patlamalı kaynak yöntemi ile birleştirerek, mekanik ve mikroyapı özellikleri incelenmiştir. Sertlik değerleri incelendiğinde, birleşme bölgelerinde ölçülen değerlerin diğer bölgelere göre yüksek olduğu belirlenmiştir. Mikroyapı incelemelerinde patlayıcı yükünün artması ile arayüzeyde oluşan dalgalı formun büyüklüğü ve genişliği arttığı tespit edilmiştir. SEM incelemelerinde arayüzeylerde intermetalik bileşiklerin görülmediği belirtilmiştir. Patlayıcı miktarı arttığında her iki plakada da arttığı tespit edilmiştir [36].

### III. SONUÇLAR VE ÖNERİLER

Titanyumun patlamalı kaynak yöntemi ile sorunsuz bir şekilde birleştirilebildiği belirlenmiştir.

Yüksek mukavemet ve hafif yapıya ihtiyaç gün geçtikçe artmaktadır. Bunun paralelinde Titanyumun patlamalı kaynak yöntemi ile çeşitli metallerle birleştirilerek özellikle uçak ve uzay sanayisinde kullanılan kompozitlerin üretilme imkanı sağlanmış olur.

Savunma sanayiinde kullanılan füze rampalarında, füze atışına bağlı olarak oluşan iç kısımdaki aşınmaya çözüm olarak patlamalı kaynak yöntemini kullanarak incelenebilir.

### KAYNAKLAR

- [1] C. Leyens and M. Peters, "Titanium and titanium alloys", Wiley-VCH, 2003.
- [2] M. Subaşı ve Ç. Karataş, "Titanyum ve titanyum alaşımlarından yapılan implantlar üzerine inceleme" *Politeknik Dergisi*, vol. 15 (2), pp. 87-103, 2012.
- [3] K. Aydın, "Titanyum ve Bakır Mazlemelerin Difüzyon Kaynak Yöntemi İle Birleştirilebilirliğinin Araştırılması", *Yüksek Lisans Tezi*, Karabük Üniversitesi Fen Bilimleri Enstitüsü, Karabük, 1-146, 2011.
- [4] A. Blatter, and D. A. Peguiron, "Explosive joining of precious metals", *Gold Bulletin*, vol. 31 (3), pp. 93-98 1998.
- [5] F. Fındık, "Recent developments in explosive welding", *Materials and Design*, vol. 32, pp. 1081-1093, 2011.
- [6] O. Gülcan, "Metallerin patlayıcı yardımı ile kaynatılması". *Marmara Fen Bilimleri Dergisi*, vol. 24 (1), pp. 11-34, 2012.
- [7] Y. Kaya and N. Kahraman, "An investigation into the explosive welding/cladding of Grade A ship steel/AISI 316L austenitic stainless steel", *Materials and Design*, vol. 52, pp. 367-372, 2013.
- [8] N. Kahraman, B. Gülenç and F. Fındık, "Corrosion and mechanical-microstructural aspects of dissimilar joints of Ti-6Al-4V and Al plates", *International Journal of Impact Engineering*, vol. 34 (8), pp. 1423-1432, 2007.
- [9] K. Raghukandan, "Analysis of the explosive cladding of Cu-Low carbon steel plates", *Journal of Materials Processing Technology*, vol. 139 (1-3), pp. 573-577, 2003.
- [10] W. H. Kearns, "Explosion welding", *Welding Handbook*, AWS, vol. 3, 264-278, 1980.
- [11] R. A. Patterson, "Fundamentals of explosion welding", *ASM Handbook*, vol. 6, 160-164, 1993.
- [12] R. C. Gupta and G. S. Kainth, "Swinging wake mechanism for interface wave generation in explosive welding of metals", *Journal of Applied Mechanics*, vol. 57 (3), 514-521, 1990.

- [13] A. Durgutlu ve B. Gülenç, "Patlama kaynağıyla paslanmaz çelik-bakır levhaların kaynaklanabilirliği ve patlayıcı oranının birleşme arayüzüne etkisi", *Politeknik Dergisi*, vol. 5 (3), 243-247, 2002.
- [14] N. Kahraman, "Titanium levhaların patlamalı kaynak yöntemi ile farklı metallerle birleştirilmesi ve arayüzey özelliklerinin incelenmesi", *Doktora Tezi*, Gazi Üniversitesi Fen Bilimleri Enstitüsü, Ankara, 1-99, 2003.
- [15] N. Kahraman ve B. Gülenç, "Modern kaynak teknolojisi", Epa-Mat Basım Yayın Ltd. Şti., Ankara, 1-323, 2013.
- [16] M. Acarer, B. Gülenç, ve F. Fındık, "Patlamalı kaynak işlem parametrelerinin birleşme arayüzüne etkisi" 8. *Denizli Malzeme Sempozyumu*, Pamukkale Üniversitesi, Denizli, 166-171, 2000.
- [17] Y. Kaya, "Patlamalı kaynak yöntemi ile üretilen grade a gemi sacı-paslanmaz çelik kompozitlerin mikroyapı, mekanik ve korozyon özelliklerinin incelenmesi", *Doktora Tezi*, Karabük Üniversitesi Fen Bilimleri Enstitüsü, Karabük, 1-237, 2014.
- [18] A. Durgutlu, "Patlama kaynağı yöntemi ile bakır-paslanmaz çelik malzemelerinin birleştirilmesi ve ara yüzeyin mekanik-mikroyapı özelliklerinin incelenmesi", *Doktora Tezi*, Gazi Üniversitesi Fen Bilimleri Enstitüsü, Ankara, 1-111, 2003.
- [19] M. Acarer, "Patlamalı kaynaktaki patlayıcı oranı, ara boşluk mesafesi ve altlık cinsinin çelik/çelik birleştirilmesi kalitesine etkisi", *Doktora Tezi*, Sakarya Üniversitesi Fen Bilimleri Enstitüsü, Sakarya, 5-119, 2001.
- [20] B. Crossland, "Explosive welding of metals and its application", Clarendon Press, Oxford, 1-233, 1982.
- [21] J. M. Gerken "Explosion welding", *Welding Handbook*, AWS, (3): 264-278, 1980.
- [22] L. L. Richard, "Welding and welding technology", McGraw-Hill, New York, 280-284, 1973.
- [23] S. Kalpakjian, "Manufacturing processes for engineering materials", Addison-Wesley, New York, 3, 809-810, 1997.
- [24] J. G. Banker, and G. R. Edvard, "Explosion Welding" *ASM Handbook*, 6, 303-305, 1993.
- [25] A. Nobili, "The explosion bonding process", *Nobel clad Technical Bulletin*, pp. 1-6.
- [26] L. J. Bement, "Small-scale explosion seam welding", *Welding Journal*, vol. 52, pp. 147-154, 1973.
- [27] V. Balasubramanian, M. Rathinasabapathi, and K. Raghukandan, "Modelling of process parameters in explosive cladding of mild steel and aluminium", *Journal of Materials Processing Technology*, vol. 63 (1-3), pp. 83-88, 1997.
- [28] H. B. Xia, S. G. Wang, and H. F. Ben, "Microstructure and mechanical properties of Ti/Al explosive cladding", *Materials and Design*, vol. 56, pp. 1014-1019, 2014.
- [29] J. Song, A. Kostka, M. Veehmayer, and D. Raabe, "Hierarchical microstructure of explosive joints: Example of titanium to steel cladding" *Materials Science and Engineering A*, vol. 528 (6), pp. 2641-2647, 2011.
- [30] N. Kahraman, B. Gülenç and F. Fındık, "Joining of titanium/stainless steel by explosive welding and effect on interface", *Journal of Materials Processing Technology*, vol. 169 (2), pp. 127-133, 2005.
- [31] Z. Yan, L. S. Cui and Y. J. Zheng, "Microstructure and martensitic transformation behaviors of explosively welded NiTi/NiTi laminates", *Chinese Journal of Aeronautics*, vol. 20 (2), pp. 168-171, 2007.
- [32] A. A. Mousavi and P.G. F. Sartangi, "Experimental investigation of explosive welding of cp-titanium/AISI 304 stainless steel". *Materials and Design*, vol. 30 (3), pp. 459-468, 2009.
- [33] P. Manikandan, K. Hokamoto, M. Fujita, K. Raghukandan, and R. Tomoshige, "Control of energetic conditions by employing interlayer of different thickness for explosive welding of titanium/304 stainless steel". *Journal of Materials Processing Technology*, vol. 195 (1-3), pp. 232-240, 2008.
- [34] M. R. Sakhtemanian., M. Honarpisheh. and S. Amini, "Numerical and experimental study on the layer arrangement in the incremental forming process of explosive-welded low-carbon steel/CP-titanium bimetal sheet", *The International Journal of Advanced Manufacturing Technology*, vol. 95 (9-12) pp. 3781-3796, 2017.
- [35] V. I. Mali, A. A. Bataev, N. Maliutina, Kurguzov, A. Bataev, M. A. Esikoy and V. S. Lozhkin, "Microstructure and mechanical properties of Ti/Ta/Cu/Ni alloy laminate composite materials produced by explosive welding", *The International Journal of Advanced Manufacturing Technology*, vol. 93 (9-12), pp. 4285-4294, 2017.
- [36] N. Kahraman and Gülenç, B. "Microstructural and mechanical properties of Cu-Ti plates bonded through explosive welding process", *Journal of Materials Processing Technology*, vol. 169 (1), pp. 67-71, 2005.

# Effect of Aging Parameters on Mechanical Properties of AlSi8Cu3Fe Aluminium Alloy

Ebru Baser, Alper Incesu, Sedef Sismanoglu and Ali Gungor\*

Department of Metallurgical and Materials Engineering, Karabuk University, Karabük, 78050, Turkey

\*Corresponding author: agungor@karabuk.edu.tr

**Abstract**— In this study, artificial aging heat treatment was applied to Mg containing AlSi8Cu3Fe aluminium alloys at a temperature of 200 °C for 2 hrs., 4 hrs. and 8 hrs. after the solution heat treatment for 4 hrs at 540 °C. The effects of the heat treatment on the mechanical properties of the alloys were determined by the compression test. As a result of the applied compression test, it was observed that better mechanical properties were obtained at the aging duration of 4 hrs. and above.

**Keywords**— AlSi8Cu3Fe Alloy, compression test, heat treatment

## I. INTRODUCTION

Aluminium alloys have wide spread application areas from foil to wheel and also aluminium alloys have been the primary material of choice for structural components of aircraft since about 1930's [1]. AlSi8Cu3Fe is the most popular and common choice for die casting. AlSi8Cu3Fe is known for offering an ideal combination efficient material properties and production workability. In addition, this material is commonly used by industrial applications throughout the World. It is suitable for large, intricate and thin walled castings in all types of moulds, also used where corrosion resistance or ductility is required. AlSi8Cu3Fe, being a hypoeutectic alloy close to Al-Si eutectic composition [2]. The microstructure of this cast alloy is composed of primary  $\alpha$ -aluminium dendrites and eutectic islands (acicular Si crystals in aluminium) [2].

There are six property elements that compose the AlSi8Cu3Fe aluminium alloys, these include: Silicon contains the greatest impurity level in electrolytic commercial aluminium (0.01 to 0.15%). Copper will allow the alloy to react to solution heat treatment and subsequent aging with an increase in strength and hardness and a decrease in elongation. Magnesium shows an increase in the strength of aluminium without unduly decreasing the ductility. Iron has a high solubility in molten aluminium and is easily dissolved at all molten stages of production. Manganese decreases resistiveness while increasing strength in both solid solutions and precipitated intermetallic states. Zinc provides the best mix of tensile properties [3-7].

In this study, artificial aging heat treatment was applied to AlSi8Cu3Fe aluminium alloys at a temperature of 200 °C for 2 hrs., 4 hrs. and 8 hrs. after application of the heat treatment for 4 hrs at 540 °C. The effects on the mechanical properties of these heat treatment applications were also tried to be determined by the compression test.

## II. EXPERIMENTAL PROCEDURE

X-Ray Diffraction (XRD) analysis for phase identification was carried out using Rigaku ULTRA IV Diffractometer with Cu-K $\alpha$  X-ray radiation under 40-kV acceleration voltage and 40 mA current. A scan speed of the measurements was 3 deg./min. and scan range was between 30° to 90°. ICDD database was used to identify the phases of the X-ray diffraction pattern of the alloys.

Detailed microstructural investigations of alloys are carried out by Carl Zeiss ULTRA PLUS FESEM Field Emission Scanning Electron Microscopy (FESEM).

Compression tests applied to understand the effect of aging durations on the mechanical properties of the AlSi8Cu3Fe aluminum alloy. Zwick/Roell Z600 Universal Testing Machine was used for a a compression test. Test speed was 0.0005 1/min and pre-load was 20 N.

## III. RESULTS AND DISCUSSION

As can be seen from the XRD graph given in Figure 1, it was determined that the phases were composed of Al and Si phases. The reason for this is that many possible phases overlap, especially with Al and Si peaks.

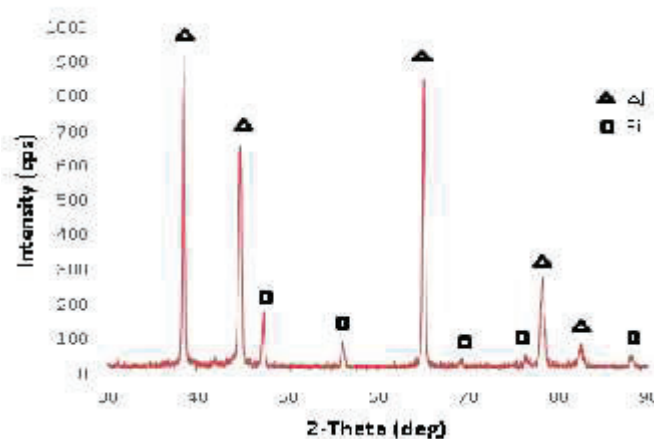


Fig 1. XRD analyses result of sample aged at 200 °C for 8 hrs.

SEM micrographs of the samples were given in Figure 2. When the SEM micrographs of the samples were analyzed, it is seen that the intermetallic particle size of 2 hrs. aged sample is smaller than the intermetallic particle size of the 4 hrs. and 8 hrs. aged samples. There is no significant difference of intermetallic particle size was observed between the 4 hrs. and 8 hrs. aged samples.

The reason is that intermetallic particles become much rougher after aging for 2 hours. The absence of such significant differences in grain size between 4 hours and 8 hours aged samples may explain the low energy difference between these two samples. This difference can be understood from the SEM images given in Figure 2.

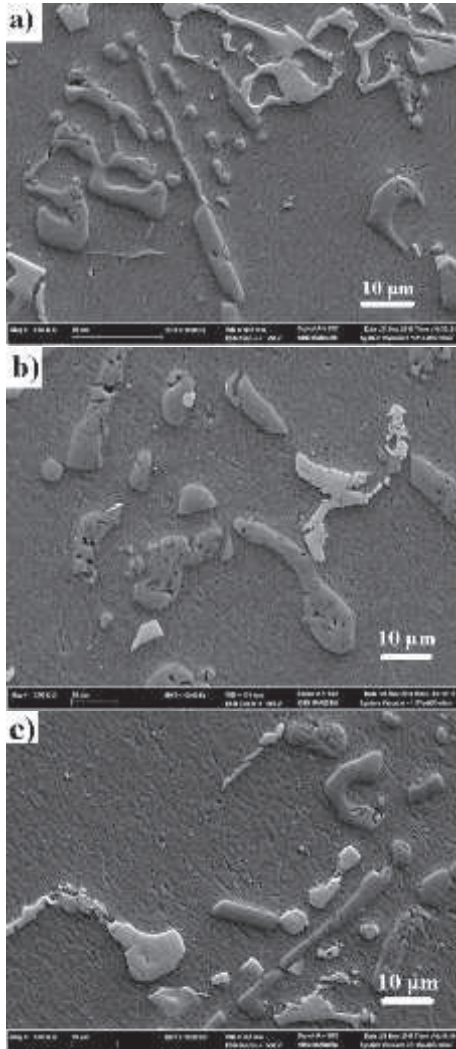


Fig 2. SEM micrographs of aged samples a) 2 hrs. b) 4 hrs. c) 8 hrs.

Compression test results were tabulated in Table 1. It can be clearly observed that 2 hrs. aged sample absorbed much less energy than the others, but there is no such obvious difference between the 4 hrs. aged and 8 hrs. aged samples.

TABLE I  
 COMPRESSION TEST PARAMETERS AND RESULTS OF AGED SAMPLES

Aging Temperature	Aging Duration	$\epsilon_{\max}$ (dL/h <sub>0</sub> )	$\sigma_0$ (N/mm <sup>2</sup> )	$\sigma_{\max}$ (N/mm <sup>2</sup> )
200 °C	2 hrs.	0,50	197,3827	483,2112
	4 hrs.	0,50	352,8853	799,7354
	8 hrs.	0,50	346,9872	647,7042

#### IV. CONCLUSIONS

In conclusion, the effects of aging parameters on the mechanical properties of the AlSi8Cu3Fe alloy were investigated. As a result of the applied compression test, it was observed that better mechanical properties were determined at the aging duration of 4 hrs. and above.

#### ACKNOWLEDGMENT

This work was supported by Scientific Research Projects Coordination Unit of Karabük University. Project Number: KBU-BAP-17-YL-198.

#### REFERENCES

- [1] E. A. Starke, Jr, and J. T. Staley, "Application of Modern Aluminum Alloys to Aircraft", *Pro 9. Aerospace Sci.*,32, 131-172, 1996.
- [2] H. E. Çamurlu and N. Unal Friction stir processing and characterization of A380 cast aluminum alloy, *International Journal of Cast Metals Research*, 24:6, 357-362, 2011.
- [3] ASM International Handbook Committee, "Metals Handbook Vol. 2: Properties and selection--nonferrous alloys and special-purpose materials", ASM International, USA, 1990.
- [4] Wang F, Liu H, Ma Y, Jin Y. Effect of Si content on the dry sliding wear properties of spray-deposited Al-Si alloy. *Mater Des* 2004;25:163-166.
- [5] Kral MV. A crystallographic identification of intermetallic phases in Al-Si alloys. *Mater Lett* 2005;59:2271-2276.
- [6] Taylor JA. Iron-containing intermetallic phases in Al-Si based casting alloys. *Procedia Mater Sci* 2012;1:19-33.
- [7] Gowri S, Samuel FH. Effect of alloying elements on the solidification characteristics and microstructure of Al-Si-Cu-Mg-Fe 380 alloy. *Metall Mater Trans A* 1994;25:437-448.

# Effect of Aging Parameters on Wear Behavior of AlSi8Cu3Fe Aluminum Alloy

Ebru Baser, Alper Incesu, Sedef Sismanoglu and Ali Gungor<sup>+</sup>

Department of Metallurgical and Materials Engineering, Karabuk University, Karabuk, 78050, Turkey

<sup>+</sup> Corresponding author: agungor@karabuk.edu.tr

**Abstract**— In this study, attempts have been made to determine wear behavior of T6 heat treatment applied to commercially produced Mg containing AlSi8Cu3Fe aluminum alloy. XRD analysis, SEM investigations, Brinell hardness and wear tests were applied to understand the effect of T6 heat treatment on the aluminum alloy. Heat treatment was applied at a temperature of 200 °C for 2, 4 and 8 hrs. after solution heat treatment for 4 hours at 540 °C. Minimum weight loss after wear test was detected in 200 °C 4 hrs aged sample. On the other hand, sample aged at 200 °C 8 hrs. has the best Brinell hardness with 120.6 HB.

**Keywords**— Al-Si alloy, T6 heat treatment, wear properties

## I. INTRODUCTION

In recent year's aluminum, magnesium and similar materials that have the high specific strength (strength/density) have become the focus of attention by the aviation and automotive industries where weight gain is important [1-3]. The weight gain in these areas will reduce fuel consumption and therefore also reduce greenhouse gasses (GHGs) emissions. It is important to improve the mechanical properties of these materials in order to increase their use. Alloying, thermo-mechanical processes, heat treatments etc. are among the methods that can be applied to develop these properties. One of the most preferred elements in the alloying of aluminum metal is silicon. Due to the high fluidity provided by the silicon, it is possible to produce parts with complex and thin sections by casting. Silicon provides fluidity to the liquid metal while also reducing the tendency to tear on the spattered part [4]. Copper can be used up to 5% as an alloying element when high strength values are required but corrosion resistance is not very important [4]. Iron, which forms intermetallic compounds with aluminum that are highly stable but have brittle nature which, negatively affects the ductility of the part and also reduces the corrosion resistance [4]. To get rid of these harmful effects that iron creates, some manganese or cobalt is added to the alloy.

The most preferred alloying method is casting. Casting is a fast and cheap method that has been utilized for long for producing structural parts in various sizes [5]. Cast products generally contain a coarse grained microstructure, particularly when the cooling rate is low. The grain morphology of gravity cast aluminium alloys is typically dendritic [6]. In addition, gas porosity is a common macro defect in cast pieces. These defects render the material vulnerable in applications that especially require mechanical strength or corrosion resistance. Heat treatment is a solution to get rid of these harmful effects

of casting. After alloying by casting, T6 heat treatment applied for the development of mechanical properties is one of the most common methods. T6 heat treatment explains as artificial aging is applied after the sample is subjected to heat treatment [4].

In this study, attempts have been made to determine wear behavior of T6 heat treatment applied to commercially produced Mg containing AlSi8Cu3Fe aluminum alloy. AlSi8Cu3Fe alloy has close eutectic composition including relatively higher Si from A356 and A357 alloys. It has good fluidity, pressure strength, hot cracking resistance, good mechanical properties and is used to produce various automotive components such as airbrake castings, gear boxes and air cooled cylinder heads [7], [8].

## II. EXPERIMENTAL PROCEDURE

Artificial aging heat treatment was applied at a temperature of 200 °C for 2, 4 and 8 hrs. after application of the heat treatment for 4 hrs. at 540 °C. The chemical composition of the alloy was given in Table 1. After the heat treatment, all specimens were cooled in water.

TABLE I  
CHEMICAL COMPOSITION OF AlSi8Cu3Fe ALUMINIUM ALLOY (IN WT.%)

ISO Norm	Fe	Si	Cu	Mn	Mg	Zn	Ni	Ti
AlSi8Cu3Fe	1.00	7.50-9.00	3.00-4.00	0.50	0.30	1.00	0.20	0.20

X-Ray Diffraction (XRD) analysis for phase identification was carried out using Rigaku ULTRA IV Diffractometer with Cu-K $\alpha$  X-ray radiation under 40-kV acceleration voltage and 40 mA current. A scan speed of the measurements was 3 deg./min. and scan range was between 30° to 90°. ICDD database was used to identify the phases of the X-ray diffraction pattern of the alloys.

Detailed microstructural investigations of alloys are carried out by Carl Zeiss ULTRA PLUS FESEM Field Emission Scanning Electron Microscopy (FESEM). Also, Energy Dispersive Spectroscopy (EDS) was performed to assess the chemical compositions of the phases.

Brinell hardness test was performed via Q250 M QNESS macro hardness test machine using 62.5 kg loads with a holding time of 20 seconds and 2.5 mm diameter indenter. Brinell hardness

values of the specimens were the averages of measurements taken at 5 different points at one indent per point.

Wear tests were conducted on UTS Tribometer T10/20 at forward and reverse movement module. AISI 52100 steel brand ball was used during the test. Wear tests were carried out at 130 mm/s. test speed with a stroke distance of 10 mm. 5 N loads were applied to the samples and 500 meters distance were taken. Lubricant was not used.

### III. RESULTS AND DISCUSSION

Figure 1 shows SEM micrographs of aged alloys. Figure 2 shows EDS analyzed the region of aged at 200 °C 8 hrs. alloy and EDS results of the phases in at.%.

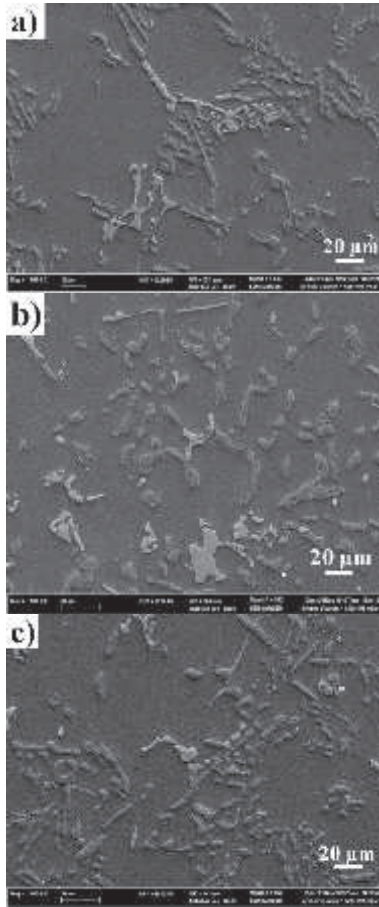


Fig 1. SEM micrographs of aged alloys 200 °C a) 2 hrs. b) 4 hrs. c) 8 hrs.

Matrix structure composed of Al, Si, Cu, and Fe. The light grey structure is Si based intermetallic and dark grey intermetallic structure is composed of Al, Si, Cu, Fe, Mg and Mn elements. It can be clearly observed EDS analyses results in Table 2, EDX spectrum points in Figure 2.

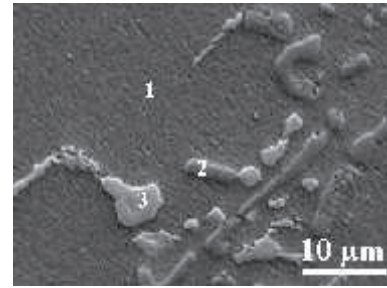


Fig 2. SEM micrograph and EDS analyses results of aged at 200 °C 8 hrs. alloy.

Table II  
 EDX SPECTRUM RESULTS OF THE POINTS

Spectrum (at.%)	Al	Si	Cu	Fe	Mg	Mn
1	94.99	1.16	2.00	0.59	0.00	0.00
2	2.17	97.61	0.00	0.10	0.00	0.00
3	63.40	11.93	4.17	15.09	5.02	5.02

Brinell hardness test was performed via Q250 M QNESS macro hardness test machine using 62.5 kg loads and a holding time of 20 seconds. Brinell hardness values of the specimens were the averages of measurements taken at 5 different points at one indent per point. Brinell hardness's of specimens are 106.8 HB, 89.2 HB, and 120.6 HB with an increasing aging duration, respectively.

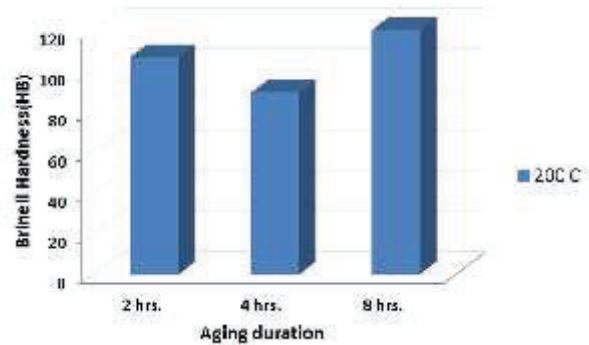


Fig 3. Graphical comparison of Brinell hardness values of the samples.

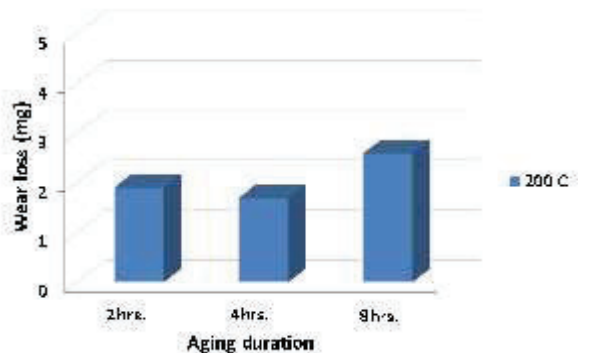


Fig 4. Graphical comparison of wear loss of the samples.

Wear tests were conducted on UTS Tribometer T10/20 at forward and reverse movement module. AISI 52100 brand ball was used during the test. Wear tests were carried out at 130 mm/s. test speed with a stroke distance of 10 mm. 5 N loads were applied to the samples and 500 meters distance were taken. Wear loss of specimens are 1.9, 1.7 and 2.6 in mg with an increasing aging duration, respectively.

While Figure 3 and Figure 4 compared, they follow a similar trend. As aging duration increased from 2 hrs to 4 hrs hardness values decreases and wear loss of the AlSi8Cu3Fe alloy decreases. Further, increase in aging duration up to 8 hrs both hardness values and wear weight losses increases as compared to previous aging durations. The reason is that intermetallic particles in the structures became larger with aging duration from 2 hrs to 4 hrs after this duration Si-based intermetallic grows faster than the other intermetallics. So, these large particles on the surface resulted in more weight loss due to the breakage during wear.

#### IV. CONCLUSIONS

In conclusion, aging heat treatment was applied at a temperature of 200 °C for 2, 4 and 8 hrs. after application of the heat treatment for 4 hours at 540 °C to the AlSi8Cu3Fe aluminum alloy. Minimum weight loss after wear test was detected in 200 °C 4 hrs aged sample. On the other hand, sample aged at 200 °C 8 hrs. has the best Brinell hardness with 120.6 HB.

#### ACKNOWLEDGMENT

This work was supported by Scientific Research Projects Coordination Unit of Karabük University. Project Number: KBU-BAP-17-YL-198.

#### REFERENCES

- [1] G. S. Cole and A. M. Sherman, "Lightweight Materials for Automotive Applications", *Materials Characterization*, 35, 3-9, 1995.
- [2] W.S. Miller, L. Zhuang, J. Bottema, A.J. Wittebrood, P. De Smet, A. Haszler, A. Vieregge, "Recent development in aluminium alloys for the Automotive industry", *Materials Science and Engineering A*, 280,37-49, 2000.
- [3] J. Hirsch, "Recent development in aluminium for automotive applications", *Trans. Nonferrous Met. Soc. China*, 24, 1995-2002, 2014.
- [4] ASM International Handbook Committee, "Metals Handbook Vol. 2: Properties and selection--nonferrous alloys and special-purpose materials", *ASM International*, USA, 1990.
- [5] E. Çamurlu and N. Ünal, "Friction stir processing and characterisation of A380 cast aluminium alloy" *International Journal of Cast Metals Research*, 24:6, 357-362, 2011.
- [6] N. Saklakoglu, S. Gencalp Irizalp, Y. Ercayhan and Y. Birol, "Investigation of wear behaviour of thixoformed and conventional gravity cast AlSi8Cu3Fe alloys", *Industrial Lubrication and Tribology*, Vol. 66 Issue: 1, pp.46-50, 2014.
- [7] S. Gencalp and N. Saklakoglu, "Effects of Low-Frequency Mechanical Vibration and Casting Temperatures on Microstructure of Semisolid AlSi8Cu3Fe Alloy", *Arabian Journal for Science and Engineering*, 37: 2255-2267, 2012.
- [8] The Aluminum Association, Inc., "Aluminum Alloy: Selection and Applications", *The Aluminum Association, Inc.*, USA, 1998.

# Kendini Onarabilen/İyileştirebilen Metaller ve Metal Matrisli Kompozit Malzemeler

Volkan Kılıçlı\*

\* Gazi Üniversitesi, Teknoloji Fakültesi, Metalurji ve Malzeme Mühendisliği, 06560, Ankara, Turkey  
vkilicli@gazi.edu.tr

**Abstract**—Self-healing materials have the ability to heal themselves when they micro damaged. Self-healing materials are receiving increasing interest and promising for the future. In this study, self-healing metals and known self-healing mechanisms are summarized.

**Keywords**—Self-healing materials, Self-healing, Self-healing metal matrix composites.

## I. GİRİŞ

Kendini onarabilen/iyileştirebilen malzemeler, doğal biyolojik malzemelerden esinlenmiş olup bu malzemeler mikro hasara uğradıklarında mikro çatlağı onarma/iyileştirme özelliğine sahiptirler [1]. Tüm biyolojik organizmalar küçük yaralanma ve kanamaları onarma yeteneğine sahiptir. Kendini onarabilen/iyileştirebilen inorganik malzemeler geliştirmek, malzeme bilimcilerinin giderek artan ilgisini görmektedir. Kendini onarabilen/iyileştirebilen malzemelerle ilgili son yıllardaki çalışmaların çoğu metalik malzemelere göre üretimi daha kolay polimerler ve seramikler üzerine yoğunlaşmıştır [2-9]. Kendini onarabilen/iyileştirebilen malzemeler otonom kendini iyileştirebilen malzemeler ve otonom olmayan kendini iyileştirebilen malzemeler olarak iki grupta sınıflandırılmaktadır. Otonom olarak kendini iyileştirebilen malzemeler şekil bellekli nano parçacık takviyeli metal matrisli kompozitler ve tane sınırlarının hareketine/göçüne dayalı metalik malzemeler olarak sınıflandırılabilir [10,11]. Otonom olmayan kendini iyileştirebilen malzemelerin sınıflandırılması Şekil 1'de verilmiştir. Otonom olmayan kendini iyileştirmede, sıcaklık, elektrik akımı, kuvvet gibi bir itici güç gerekmektedir (Tablo 1) [12,13]. Son zamanlarda kendini iyileştirebilen metaller ve metal matris kompozitler ile ilgili yapılan çalışmalar otonom olmayan kendini iyileştirme üzerine yoğunlaşmıştır [12-19]. Bu çalışmalarda sıcaklık, kuvvet veya deformasyon kendini iyileştirmeyi sağlamada tetikleyici/itici güç olarak kullanılmıştır.



Şekil 1. Kendini onarabilen/iyileştirebilen metalik malzemelerin sınıflandırılması

Kendini iyileştirebilen/onarabilen metalik malzemelerle ilgili çalışmalar; çoğunlukla Al alaşımları, Zn alaşımları ve Sn-Bi alaşımları üzerinde gerçekleştirilmiştir [17,20-23]. Kendini iyileştirebilen/onarabilen metal matris kompozitler, şekil bellekli alaşım tel takviyesi esaslı iyileştirme, mikrokapsülasyona dayalı iyileştirme olarak kategorize edilebilir (Şekil 2).

Bu çalışmada, kendini iyileştirebilen/onarabilen metalik malzemelerle ilgili çalışmalar ve bilinen kendini onarma mekanizmaları anlatılmaya çalışılmıştır.

## II. METALLERDE KENDİNİ ONARMA MEKANİZMALARINI

### A. Şekil bellekli alaşım tel takviyesi esaslı onarma

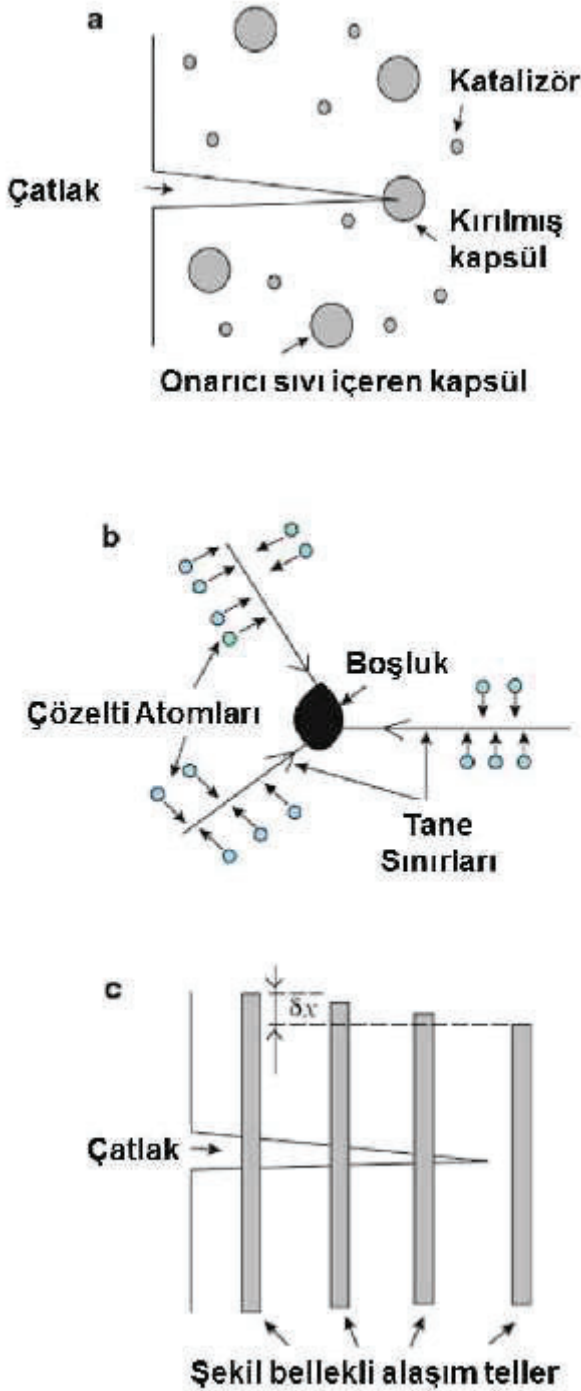
Şekil bellekli alaşım (NiTi alaşımı) telleri takviye elemanı olarak kullanarak kendini iyileştirebilen metal matrisli döküm kompozitlerin elde edilmesi hedeflenmiştir [15,21-23]. Hasarlı şekil bellekli alaşım tel takviyeli bir kompozitte, şekil bellekli alaşım tellerde deformasyon etkisiyle gerinimli bölgeler oluşmaktadır. Bu gerinimli bölgeler ısıtmanın etkisiyle martensitten östenite faz dönüşümü sayesinde tel orijinal boyutlarına dönerek çatlak kapanmasını sağlamaktadırlar (Şekil 2).

TABLE I. METALİK MALZEMELERDE BİLİLEN KENDİNİ ONARMA/İYİLEŞTİRME MEKANİZMASI VE TETİKLEYİCİLERİ

Bilinen Kendini Onarma/İyileştirme Mekanizması	Tetikleyici / İtici Güç
Şekil bellekli alaşım esaslı iyileştirme	Kuvvet / Sıcaklık
Kapsül esaslı iyileştirme	Kuvvet / Sıcaklık
Aşırı doymuş alaşımlarda çökeltme (çökeltme esaslı) iyileştirme	Sıcaklık
Elektrik akımı esaslı iyileştirme	Elektrik akımı
Kaplama esaslı iyileştirme	Sıcaklık
Ötektik tabanlı	Sıcaklık
Nano-şekil bellekli parçacık takviyesi esaslı	Deformasyon

### B. Mikrokapsül esaslı onarma

Kapsül esaslı iyileştirme mekanizması [1,24-26], yüksek ergime derecesine sahip bir alaşım içine gömülü olan içi boş seramik ( $Al_2O_3$ ) mikrokapsüller içine düşük erime noktalı bir alaşımın katılmasıdır. Büyüyen bir çatlak, seramik mikrokapsülün parçalanmasıyla, düşük erime noktalı alaşımın sıvılaştırılmasına ve mikro çatlağa akmasına izin verir. Böylelikle çatlak, iyileştirici ajan tarafından doldurularak ilerlemesi durdurulmuş olur (Şekil 2).



Şekil 2. Metalik malzemelerdeki iyi bilinen kendini iyileştirme mekanizmalarının şematik olarak gösterimi; a) Kapsül esaslı iyileştirme, b) Aşırı doymuş alaşımlarda çökeltme (çökeltme esaslı) iyileştirme ve c) Şekil bellekli alaşım tel takviyesi ile iyileştirme [1].

### C. Çökelti esaslı onarma

Çökelti esaslı iyileşmede (Şekil 2.b), aşırı doymuş ve yaşlandırılmamış alaşımlarda oluşacak çökeltiler, malzeme içerisindeki mikro çatlak veya boşluklara çekirdeklenme bölgeleri olarak görev yapar. Yaşlandırma sırasında çökecek

olan çökeltiler mikro kusurlara ve boşluklara difüze ederek bu bölgeleri onarırlar/iyileştirirler [20, 27, 28]. Bununla birlikte, bu 'iyileşme' yaşlandırma sertleşmesinin doğal sürecine benzer şekilde nanometre ölçeğinde gerçekleşir ve büyük çatlakları iyileştirme özelliği yoktur. Alaşım iyileşmeyi sağlamak için belli bir yaşlandırma sıcaklığına ısıtılır ve çökeltiler bölgesel olarak yüksek stresli ve mikro çatlakların yakınında çökeltirler [18, 19].

### D. Elektrik akımı esaslı onarma

Kontrollü elektrik akımı altında elektrolitik bir banyoda çatlak içeren bir alaşımda metal iyonlarının elektrolitik olarak çökeltmesiyle sağlanan çatlak iyileşmesi elektro-iyileşme olarak tanımlanmaktadır [29]. 100  $\mu\text{m}$ 'ye kadar olan mikrometre boyutlarındaki çatlaklar, elektro-iyileştirme prosesi ile başarılı bir şekilde onarılabilmektedir. Araştırmacılar bu işlem vasıtasıyla yaklaşık %96 çekme dayanımının geri kazanıldığını bildirmektedirler [29].

### E. Kaplama esaslı onarma

Kaplama esaslı iyileştirme/onarma yöntemi, Leser ve diğerleri [30], 2,03 mm kalınlığa sahip bir titanyum alaşımı yüzeyinde 0.005-0.015 mm kalınlığa ve 124°C erime noktasına sahip %60 In-%40 Sn (ağ.-%) alaşımdan oluşan kendini iyileştiren kaplama geliştirdi. Ti alaşımında bir yüzey çatlağı oluşması durumunda, In-Sn alaşımı erime noktasının üstünde ısıtıldığında (124°C), erimiş olan In-Sn alaşımı, titanyum alaşımının yüzeyindeki mikroçatlağı doldurur. Araştırmacılar kendini iyileştirme sürecinden sonra onarılmış çatlağın onarımından sonra, yorulma çatlak büyümesinin durdurulabileceğini ve çatlak büyüme oranının yaklaşık% 50 oranında azaltıldığını bildirmektedir [30].

### F. Ötektik esaslı onarma

Ruzek ve Rohatgi [17] tarafından geliştirilen ötektik esaslı iyileşme, katı dendritik yapının bütünlüğünü koruduğu ve dendritler arasındaki ötektik yapının iyileştirici bir yapı olarak kullanmaya dayanmaktadır. Önerilen bu yöntemde, kendini iyileştirmeyi için etkinleştirmek için, alaşım sıcaklığı, dendritler arası ötektik yapının erimesini sağlayacak bir sıcaklığa ısıtılması gerekmektedir. Böylelikle, sıvı haldeki ötektik, dendritler arasına veya yapıda bulunan herhangi bir mikro çatlak veya boşluklara akarak doldurur. Alaşımın soğutulması sonrası, dendritler arası bölgelerdeki mikro çatlakları doldurmuş olan ötektik katılacak ve böylece alaşım onarılmış olacaktır. Araştırmacılar ötektik sıvının çatlağın içine akması için yeterli miktar ve akışkanlığa sahip olması, çatlak yüzeyini ıslatması ve katılma sonrası çatlak yüzeyiyle iyi bir bağ oluşturmasının gerektiğini bildirmektedirler [17].

### G. Şekil bellekli nano parçacık takviyesi esaslı onarma

Graboswski ve Tasan [10] tarafından önerilen şekil bellekli nano parçacık takviyesi esaslı onarma matris ile nano parçacık arasında gerilme uygulandığında otonom olarak

meydana geleceği varsayılan bir onarma mekanizmasıdır. Burada, metalik matriste şekil bellekli alaşım nano parçacık çevresinde gerinme etkisiyle nanoboşluk oluşması sonucunda, şekil bellekli alaşım nano parçacığın bu gerinmenin etkisiyle östenitten martensite dönüşerek genişmesi ve nano boşluğu doldurması/kapatması varsayılmıştır. Bu onarma mekanizması halen teorik olarak bilinmemekte olup deneysel olarak ispatlanmamıştır.

### III. DEĞERLENDİRME

Kendini iyileştirebilen/onarabilen metal matrisli kompozit malzemeler araştırma aşamasındadır. Hali hazırda ticari kendini iyileştiren metal malzeme bulunmamaktadır. Şimdilik pratik uygulama için birçok kısıtlamalar bulunmaktadır. Ancak kendini iyileştirebilen metalik malzemeler gelecek için oldukça umut vericidir. Kendini iyileştirebilen/onarabilen metalik malzemelerin düşük bakım maliyeti, uzun servis ömrü ve hasarları önleme gibi birçok çekici avantajlarına rağmen, gerçek hayatta kullanılan yük taşıyıcı uygulamalarda kullanımı henüz mümkün değildir. Kendini iyileştirebilen/onarabilen metalik malzemelerde otonom iyileşme mekanizmalarının geliştirilmesi gerekmektedir. Şimdiye kadar geliştirilen iyileştirme mekanizmalarının çoğu sıcaklık, deformasyon veya elektrik akımı gibi harici tetikleyiciler gerektirmektedir. Ayrıca yüksek sıcaklıklara dayanabilecek yeni kendini iyileştirici ajanların veya mekanizmaların geliştirilmesi gerekmektedir. Ayrıca mikrohasarlı bölgenin tespiti ve görüntülenebilmesi, hasarın kendini iyileştirebilmesi için önceden belirlenmesi gereken başka bir araştırma konusudur.

### IV. KAYNAKLAR

- [1] M. Nosonovsky, P.K. Rohatgi, "Biomimetics in Materials Science: Self-healing, Self-lubricating, and Self-cleaning materials", Springer, 2011, p 1-122.
- [2] B. Aïssa, D. Therriault, E. Haddad, W. Jamroz, "Self-healing materials systems: Overview of major approaches and recent developed technologies", *Adv. Mater. Sci. Eng.*, 2012, (2012).
- [3] D. Bekas, K. Tsirka, D. Baltzis, A. Paipetis, "Self-healing materials: a review of advances in materials, evaluation, characterization and monitoring techniques", *Compos. Pt. B-Eng.*, 87, 92-119 (2016).
- [4] M. Kessler, "Self-healing: a new paradigm in materials design", *Proc. Inst. Mech. Eng. Part G-J. Aerosp. Eng.*, 221(4), 479-495 (2007).
- [5] M. Samadzadeh, S.H. Boura, M. Peikari, S. Kasiriha, A. Ashrafi, "A review on self-healing coatings based on micro/nanocapsules", *Prog. Org. Coat.*, 68(3), 159-164 (2010).
- [6] R.P. Wool, "Self-healing materials: a review", *Soft Matter*, 4(3), 400-418 (2008).
- [7] D.Y. Wu, S. Meure, D. Solomon, "Self-healing polymeric materials: a review of recent developments", *Prog. Polym. Sci.*, 33(5), 479-522 (2008).
- [8] Y. Yuan, T. Yin, M. Rong, M. Zhang, "Self healing in polymers and polymer composites. Concepts, realization and outlook: a review", *Express Polym. Lett.*, 2(4), 238-250 (2008).
- [9] P. Zhang, G. Li, "Advances in healing-on-demand polymers and polymer composites", *Prog. Polym. Sc.*, 57, 32-63 (2016).
- [10] B. Grabowski, C.C. Tasan, Self-Healing Metals, "Self-Healing Materials"ed., M.D. Hager, S. van der Zwaag, U.S. Schubert, Eds., Springer, 2016, p 387-407.
- [11] G. Xu, M. Demkowicz, "Healing of nanocracks by disclinations", *Phys. Rev. Lett.*, 111(14), 145501 (2013).
- [12] J. Ferguson, B.F. Schultz, P.K. Rohatgi, "Self-healing metals and metal matrix composites", *JOM*, 66(6), 866-871 (2014).
- [13] A.D. Moghadam, B.F. Schultz, J. Ferguson, E. Omrani, P.K. Rohatgi, N. Gupta, "Functional metal matrix composites: self-lubricating, self-healing, and nanocomposites-an outlook", *JOM*, 66(6), 872-881 (2014).
- [14] K. Alaneme, M. Bodunrin, "Self-healing using metallic material systems-A review", *Applied Mater. Today*, 6, 9-15 (2017).
- [15] M. Manuel, Principles of Self-healing in Metals and Alloys: An Introduction, "Self-healing Materials: Fundamentals, Design Strategies, and Applications"ed., S.K. Ghosh, Ed., Wiley-VCH Verlag 2009, p 251-265.
- [16] S.K. Misra, "Shape Memory Alloy Reinforced Self-healing Metal Matrix Composites," University of Wisconsin-Milwaukee, 2013.
- [17] A.C. Ruzek, "Synthesis and Characterization of Metallic Systems with Potential for Self-healing," University of Wisconsin-Milwaukee, 2009.
- [18] S.K. Ghosh, "Self-healing Materials: Fundamentals, Design Strategies, and Applications", John Wiley-VCH, 2009, p 1-28.
- [19] S. van der Zwaag, "Self Healing Materials: An Alternative Approach to 20 Centuries of Materials Science", Springer, 2008, p 1-18.
- [20] K.K. Alaneme, O.I. Omosule, "Experimental Studies of Self Healing Behaviour of Under-Aged Al-Mg-Si Alloys and 60Sn-40Pb Alloy Reinforced Aluminium Metal-Metal Composites", *J. Minerals Mater. Charac. Eng.*, 3(01), 1 (2014).
- [21] J. Ferguson, B. Schultz, P. Rohatgi, "Zinc alloy ZA-8/shape memory alloy self-healing metal matrix composite", *Mater. Sci. Eng. A*, 620, 85-88 (2015).
- [22] M.V. Manuel, G.B. Olson, Biomimetic Self-healing Metals, 1<sup>st</sup> International Conference on Self-Healing Materialsed., 2007, p 1-8.
- [23] P. Rohatgi, "Al-shape memory alloy self-healing metal matrix composite", *Mater. Sci. Eng. A*, 619, 73-76 (2014).
- [24] J. Martinez-Lucci, R. Amano, P. Rohatgi, B. Schultz, Self-healing in an Aluminum Alloy Reinforced with Microtubes, 3<sup>rd</sup> Energy Nanotechnology International Conference-ENIC2008ed., 2008, p 1-10.
- [25] J. Martinez-Lucci, R. Amano, P. Rohatgi, B. Schultz, A. Ruzek, Design and Demonstration of Self-Healing Behavior in a Lead-Free Solder Alloy, 7<sup>th</sup> International Energy Conversion Engineering Conference., 2009, p 1-7.
- [26] J. Martinez-Lucci, A. Ruzek, S.K. Misra, P.K. Rohatgi, R.S. Amano, "Self-healing in Metal Castings", *AFS Trans.*, 101, 187-195 (2011).
- [27] S. Van der Zwaag, "Routes and mechanisms towards self healing behaviour in engineering materials", *Bull. Pol. Acad. Sci.-Chem.*, 58(2), 227-236 (2010).
- [28] S. Van der Zwaag, N. Van Dijk, H. Jonkers, S. Mookhoek, W. Sloof, "Self-healing behaviour in man-made engineering materials: bioinspired but taking into account their intrinsic character", *Philos. Trans. R. Soc. A-Math. Phys. Eng. Sci.*, 367(1894), 1689-1704 (2009).
- [29] X. Zheng, Y.-N. Shi, K. Lu, "Electro-healing cracks in nickel", *Mater. Sci. Eng. A*, 561, 52-59 (2013).
- [30] P.E. Leser, J.A. Newman, S.W. Smith, W.P. Leser, R.A. Wincheski, T.A. Wallace, E.H. Glaessgen, R.S. Piascik, Mitigation of crack damage in metallic materials, ed., NASA Technical Reports Server-NTRS, 2014.

# Effects of Shot Peening On The Microstructure, Hardness and Surface Roughness Properties of AZ31 and AZ31-0.5 La Mg Alloys

Nihal Kanca, Özlem Keleş, Canan Dursun, İsmail Hakkı KARA, Yavuz SUN, Yunus TÜREN, Okan ÜNAL, Hayrettin AHLATCI\*, Galal Ahmed EL-MENSOURI,

Karabuk University, Department of Metallurgy and Materials Engineering<sup>1</sup> and Department of Mechanical Engineering Turkey

\*Corresponding author: hahlatci@karabuk.edu.tr

The use of magnesium alloys in aerospace, space, and automotive industry as structural materials has gradually been increased. Magnesium alloys producers are much less than the iron and steel producers in number due to the alloys are still not widely used and their production cost are high. This is one of main reasons that the prices of the alloys are expensive. In this study, adding La element to AZ31 and compare to mechanical properties and surface roughness behaviour..

## I. INTRODUCTION

Due to its low density and its special strength (strength/weight), magnesium (mg) alloys with wide application area are among the most attractive materials. In spite of this, the low hardness values of Mg materials and poor corrosion resistance narrow the application areas. In order to increase the hardness values and corrosion resistance of hot rolled mg plates, film coatings, shot peening and alloying elements may be involved [1,2].

In this study, the effects of the addition of peening and alloy elements on AZ31 and AZ31 + 0.5% La containing Mg plates were investigated. At the same time, the effect of spraying time in the light of literature studies in the shot peening process has been observed.

## II. EXPERIMENTAL STUDIES

The material used in this study are showed in Figure 1. The compositions of the investigated AZ31 and AZ31+0.5 La alloys are given Table 1.



Figure 1. Plates of the AZ31 and AZ31+0,5% La investigated in this study.

Table 1. The composition of the AZ31 and AZ31+0,5% La investigated in this study.

	Al	Zn	Mn	La	Mg
AZ31	%2,9	%0,98	%0,13	-	Bal.
AZ31 + %0,5 La	%2,91	%1,02	%0,15	%0,51	Bal.

### A. Shot Peening

In the shot peening process, steel ball of S110-AISI1070 quality standard was used and the process was performed at 10 cm nozzle distance under 10 bar, 20 min and 8 bar pressure for 30 min. (Figure 2).



Figure 2. Used balls and shot peening device

### B. Roughness Test

Roughness measurements of the original and shot peened samples were done by using SV 3100 model Measurement Surface Test Machine (Figure 3.).



Figure 3. Surface roughness (Evaluation type Surface Roughness Measurement Surface test SV-3100)

### C. Hardness Test

The hardness test was carried out under 0.05 kg load. The measurements were performed at least 5 times at each depth and on average. Hardness measurements were measured from the surface for each sample to the depth of 500  $\mu\text{m}$  at 100  $\mu\text{m}$  intervals.

## III. RESULTS OF EXPERIMENTAL STUDIES

### A. Optical Microscope Results

In the optical microscope analysis, the images taken after the rolling process were estimated to be recrystallized grain and twins based on [3,4] (Figure 4).

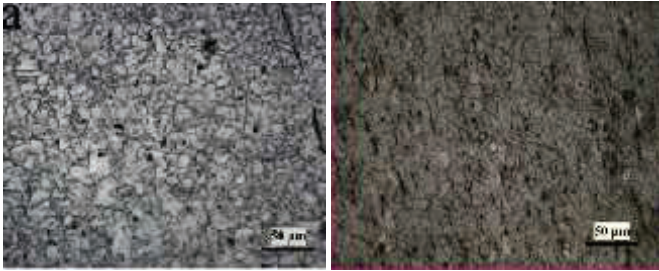


Figure 4. Optical Microscope Images a)AZ31 b)AZ31+0,5La

### B. Roughness Test Results

Roughness test results show that both materials increase the roughness of shot-peening process [5]. It was determined that the entire surface of the material reached the maximum roughness at 20 minutes for AZ31 quality material. This was observed at 30 min for AZ31+0.5 La material (Figure 5).

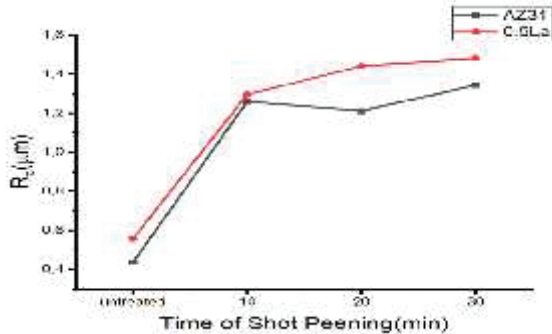
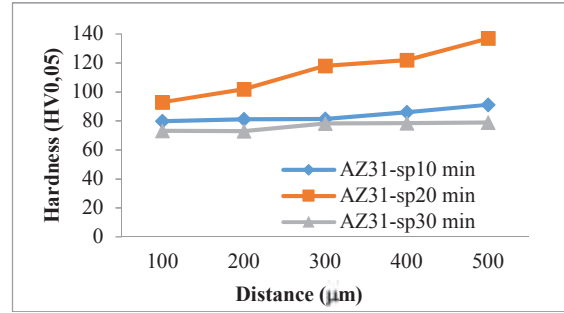


Figure 5. Roughness Test Results.

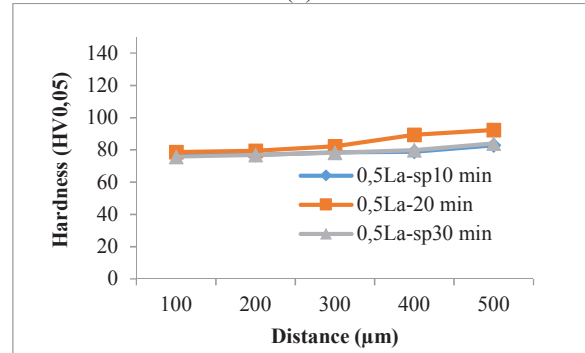
### C. Hardness Test Results

As a result of the hardness values obtained, an effective increase was observed from the 10th minutes of the shot peening process to the 20th minutes in both materials (Figure 6). There was a little bit of fall in the 30's minutes. This may be due to a partial softening caused by excessive shot peening [5]. It has been determined that the shot peening process which

we made with 0.5% La element added material to AZ31 quality Mg plate adversely affects the hardness.



(a)



(b)

Figure 6. Hardness Test Results of (a) AZ31 and (b) AZ31+0,5 % La alloys.

### Acknowledgement

In this study, when I consulted with him, when I consulted him, he gave me more than his precious time and he offered me more than he could to be useful to me with great interest. I would like to take advantage of my precious teacher Prof.Dr.Hayrettin Ahlatçı and Prof.Dr.Yavuz Sun, thanks to my teachers, I owe my gratitude.

In our support no.2209A, we would like to express our respect and gratitude to TÜBİTAK, who has provided us with any kind of material and moral assistance

### References

- 1) F. Öztürk ve İ. Kaçar, Magnezyum Alaşımları Ve Kullanım Alanlarının İncelenmesi, Niğde Üniversitesi Mühendislik Bilimleri Dergisi, Cilt 1 Sayı 1, (2012), 12-20.
- 2) A. Akdoğan, Magnezyum ve Magnezyum Alaşımları Ders Notu, [http://www.yildiz.edu.tr/~akdogan/lessons/malzeme2/Magnezyum\\_ve\\_Magnezyum\\_Alasimlari.pdf](http://www.yildiz.edu.tr/~akdogan/lessons/malzeme2/Magnezyum_ve_Magnezyum_Alasimlari.pdf)
- 2) C. Zhang, J. Zhang, S. Zhang, Z. Wang, Comparison of calcium phosphate coatings on AZ31 and fluoride-treated AZ31 alloy prepared by hydrothermal method and their electrochemical corrosion behaviour, Materials Chemistry and Physics, Volume 220, 1 December 2018, Pages 395-401.
- 3) C. Liu, H. Zheng, X. Gu, B. Jiang, Effect of severe shot peening on corrosion behavior of AZ31 and AZ91 magnesium alloys, Journal of Alloys and Compounds, Volume 770, 5 January 2019, Pages 500-506
- 5) O. Ünal, (2011). Bilyalı Dövme İşleminin Tane Boyutuna Etkisinin Deneysel İncelenmesi. Bartın Üniversitesi, Fen Bilimleri Enstitüsü, Yüksek Lisans Tezi, 93s, Bartın.

# Effect of Heat Treatment on Wear and Corrosion Resistance of Light Al-Based Al-Mg-Sb Alloy Used in Aviation and Automobile Sector

Fatma MEYDANERİ TEZEL\*<sup>1</sup>, Çağla Elçin YAĞCIOĞLU<sup>1</sup>, Berkay ARAS<sup>1</sup>, Ozan AKYOL<sup>1</sup>

<sup>1</sup>Department of Metallurgy and Materials Engineering, Faculty of Engineering, Karabük University, 78050, Karabük, Turkey.

\*Corresponding author: [fatmameydaneri@karabuk.edu.tr](mailto:fatmameydaneri@karabuk.edu.tr)

**Abstract**— With the development of technology, light engineering alloys have recently become a popular group of material. The most important consideration in the development of these alloys is production cost, applicability in technology, temperature and composition. For this reason, in this study, the effects on corrosion resistance of composition and annealing parameters in light Al-based Al-Mg-Sb eutectic alloy systems with commercial and industrial design were investigated depending on precipitation and intermetallic phase distribution in microstructure. Al based Mg-Al-Sb eutectic alloys were melted by induction furnace, and were casted into kokil mould. Then, samples were annealed at 573 K with vacuum furnace. Cyclic Potentiostatic test was applied with the PARSTAT 4000 device for corrosion rate. In the experiment, firstly, the change in corrosion potentials between the working electrode and the reference electrode since the dipped reference electrode and working electrode into the 3.5% NaCl solution was measured as mV versus time without passing current on the system. After reaching the equilibrium potential ( $E_{kor}$ ), potentiodynamic polarization curves were recorded from the cathodic to anodic direction. Measurements were carried out at open circuit potential (15 min), and the graphs of the change of the potential versus the current density were obtained, and the corrosion rates were determined for the heat treatment and heat-free samples.

**Keywords**— Heat treatment, microstructure, corrosion rate, wear

## I. INTRODUCTION

The second most common metal element in the land is aluminum. Aluminum is recycled by the recycling circle. Aluminum can be re-melted with only 5% of the energy required for raw material production and can be used for brand new products. The most commonly used aluminum and aluminum alloys after steel in today's industry are; they are now an important material for engineers and designers due to their low strength, good thermal and electrical conductivity, increased strength properties and corrosion resistance. Particularly in recent years, energy-saving efforts have been the preferred materials in aluminum alloys, cars, buses, trains, marine crafts, making the production of less fuel-efficient lightweight and economical vehicles a priority. In fact, these alloys have been used in the aviation industry for many years and have been used in the defense industry due to their increased strength and impact properties. For these reasons, it is frequently used, especially where lightweight material is

needed. Aluminum; high corrosion resistance in the environment of many chemicals including air, water, salt water and petrochemicals [1,2].

The very low solids (<0.01%) antimony is used as an alloy to prevent hot fracture [9]. According to the investigations conducted, grain contents of Al alloys were thinned by using Sb in the amount of about 0.5%, which resulted in improvement of mechanical properties, but more than 1% resulted in negative results [3, 4]. According to another research, it has been observed that it causes an increase in magnetization [5]. In another study, antimony was added to Mg-based Al alloys and it was found that the corrosion layer of the oxide layer formed is very good against sea salt. The eutectic point of Al-Sb systems is known as 1% Sb, 930 K [6]. In another study, the thermodynamic modeling of the Mg-Al-Sb system is performed for the first time. Only Al-Sb and Mg-Sb are reoptimized among these binary systems. While the liquid phases are identified by the Redlich-Kister polynomial model, the high temperature modification of the  $Mg_3Sb_2$  compound in the Mg-Sb system is defined by the sub-partitioning model. The generated database thermodynamic properties are used to calculate and predict the binary phase diagrams of Al-Sb and Mg-Sb and the liquid states of the triplet derivative. The obtained Mg-Al-Sb database estimated the closed triple liquid mix interval, six triple eutectic, two triple peritectic, four E point and critical point. [4].

Mg-Al-Sb alloy is manufactured by arc melting system. When microstructural analyzes was carried out, only  $Mg_3Sb_2$  and AlSb phases were found for different heat treatment conditions. Phase transitions were determined to be 580 °C, partial melting according to DTA analysis and supported by literature studies. Resistance results have shown that metallic and semiconductor type behavior is dependent on the heat treatment temperatures. Heat conductivity measurements were carried out at 2-300 K and the data were analyzed by sum of cage and carrier. The thermo-force data are negative and positive, indicating the sign of total carriers. The linear dependence of the thermo-power on temperature was shown to be the metallic type characteristics of the samples. The mechanical properties of the samples showed two types of hardness values depending on the heat treatment temperature. [7].

In this study; the effects of composition and annealing parameters on the corrosion resistance and wear properties of Al-Mg-Sb eutectic alloy systems with lightweight Al base with commercial and industrial design have been investigated depending on the precipitate and intermetallic phase distribution in the microstructure.

## II. EXPERIMENTAL PROCEDURE

Alloys with Al-Mg-Sb eutectic composition with Al based will be melted in SiC pot by using vacuum melting furnace, melted cocil mold will be poured and samples will be obtained. Then a portion of the specimen will be annealed for 1.5 hours in the annealing furnace.

For Corrosion Resistance Cyclic Potentiostatic test with PARSTAT 4000 device will be applied. Cold bakalite will be taken before the sample. After peeling, the sample will have "bottom surface" and "top surface" areas. The bottom surface is the surface that will undergo corrosion. On the upper surface, a hole corresponding to a 2.5 mm (or 3 mm) flat-bottomed screw inlet shall be drilled to keep the sample stable during the test. The surface (bottom surface) area to be subjected to corrosion must have a highly measurable high symmetry. 400, 800, 1200 and 3000 grid silicon carbide (SiC) sanding will be applied on the surface which will be subject to corrosion. The sample holder electrode with a flat base screw end is screwed into the sample. The test is then placed in the cell. Two graphite electrodes and one reference electrode (SCE: Saturated Calomel Electrode or Ag / AgC electrode) are placed in the cell. Then add enough solution (%3,5 NaCl solution) to cover half of the sample. Before all tests, the surface of the sample is measured at the open circuit potential in the corrosive environment. Then a corrosion test is carried out.

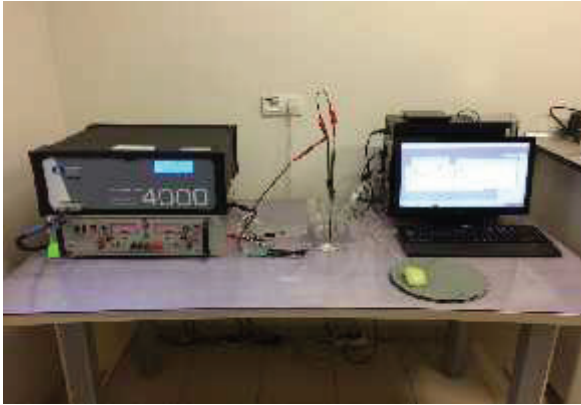


Fig. 1 PARSTAT 4000 Corrosion Test Devices and Corrosion Tubes

Using the UTS TRIBOMETER T10 / 20 device (Fig. 2), abrasion test was applied to the samples prepared on the surface of the mirror under 10N and 20N loads. After the test, the loss of wear in the material was calculated by calculating the mass and volume loss.



Fig. 2. UTS TRIBOMETER T10/20 Cihazı

## III. CONCLUSIONS

Six samples as 62.86% Al-37.13% Mg-0.01% Sb (% wt.); 57.6% Al-42.4% Mg-0.001% Sb (% wt.) and 90.2% Al-9.3% -Gg- 0.5% Sb. are applied for corrosion test for both heat treated and non-heat treated. The potentiodynamic graphs of all samples are given in fig. 3.

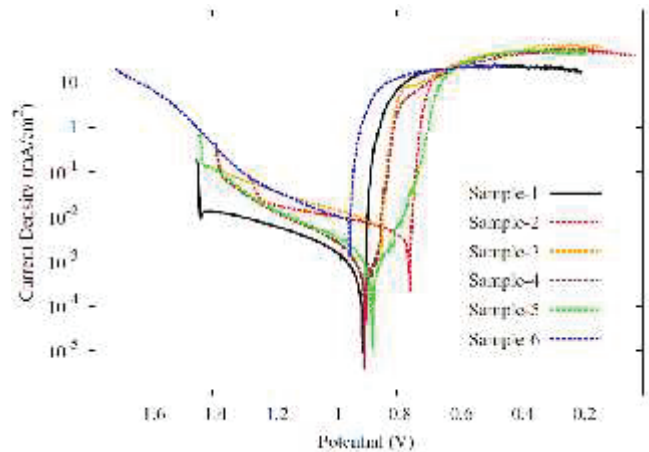


Fig. 1 Potentiodynamic Test Results for all of samples.

For %62.86Al-%37.13Mg-%0.01Sb (%wt.); %57.6 Al-%42.4 Mg-%0.001 Sb (%wt.) ve %90.2Al-%9.3Mg-%0.5Sb(%wt.), Corrosion test data on 6 samples with heat treatment and non-heat treatment of alloy alloys given in Table 1.

Table 1. Corrosion current and corrosion versus areas of samples prepared for corrosion testing

Samples	Surface Area (cm <sup>2</sup> )	Corrosion Current (μA)	Corrosion Rate (μm/year)
Sample 1- Heat Treated-(%62.86Al-%37.13Mg-%0.01Sb)	1.06	1.55	21.80
Sample 6- Heat Free-(%62.86Al-%37.13Mg-%0.01Sb)	1.02	8.21	121.52
Sample 2- Heat Free-(%62.86Al-%42.4Mg-%0.001 Sb)	1.02	5.34	58.85
Sample 5- Heat Treated -(%57,6Al-%42,4Mg-%0,001 Sb)	0.66	0.94	15.80
Sample 3- Heat Free-(%90.2Al-%9.3Mg-%0.5Sb)	0.37	2.65	155.70
Sample 4- Heat Treated-(%90.2Al-%9.3Mg-%0.5Sb)	0.8	1.10	29.89

According to the results of the corrosion test, the mass loss in the heat treated samples and the samples with less antimony content was less and the oxidation increased in the structure as a result of the test.

Abrasion test was carried out under two loads, 10 N and 20 N. The pressure applied in the abrasion test increases as wear increases. It has been observed that the applied heat treatment has a positive effect on wear. As a result of the heat treatment applied, it was observed that the amount of wear decreased and the wear lines were more prominent. Reductions in tears and ruptures occur. Al ratio has gained more importance on the amount of abrasion, increase in Mg and Sb amount caused by tearing and ruptures in abrasions.

#### REFERENCES

- [1] Akdoğan, A. "Al ve alaşımları ders notları", Yıldız Teknik Üniversitesi, [http://www.yildiz.edu.tr/~akdogan/lessons/malzeme2/Aluminyum\\_ve\\_Aluminyum\\_Alasimlari.pdf](http://www.yildiz.edu.tr/~akdogan/lessons/malzeme2/Aluminyum_ve_Aluminyum_Alasimlari.pdf), Son erişim tarihi: 17 Ocak 2017.
- [2] Aluminiumdesign.net. "Aluminium alloys". <http://www.aluminiumdesign.net/design-support/aluminium-alloys>, Son erişim tarihi 17 Ocak 2017.
- [3] Ren, B / Liu, Z. / Zhao, R. / Zhang, T. / Liu, Z. / Wang, M. / Weng, Y. "Effect of Sb on microstructure and mechanical properties of Mg2Si/Al-Si composites", *Transactions of Nonferrous Metals Society of China*, 20, 1367-1373, 2010.
- [4] Uzun, O. / Yılmaz, F. / Kolemen, U. / Basman, N. "Sb effect on micro structural and mechanical properties of rapidly solidified Al-12Si alloy", *Journal of Alloys and Compounds*, 509, Page 21-26, 2011.
- [5] Agarwal, S., Mukhopadhyay "Effect of Sn and Sb element on the magnetism and functional properties of Ni-Mn-Al ferromagnetic shape memory alloys", *Journal of Magnetism and Magnetic Materials*, 402, Page, 161-165, 2016.
- [6] Mondolfo, L. F. "Aluminium Alloys: Structure and Properties", Butterworth & Co (Publishers) Ltd. London 1976.
- [7] Balakumar T, Medraj, "Thermodynamic Modeling of Al-Mg-Sb System, Computer Coupling of Phase Diagrams and Thermochemistry", 29, Page 24-36, 2005.

# Alumix 123 Ön Karışımli Tozların Mekanik Alaşım Lanma Sürecine Yağlayıcıların Etkisi

Cankız Gizem Delibalta\*, Yusuf Özçatalbaş  
cankizdelibalta@gmail.com, yusufoz@gazi.edu.tr

*Metallerji ve Malzeme Mühendisliđi, Teknoloji Fakültesi, Gazi Üniversitesi, 06560, Ankara, Türkiye*

**Özet-** Bu çalışmada, ön karışımli Al + Cu tozlarının mekanik alaşım lanma (MA) sürecine % 1,5 Çinko Stearat ve % 2 Stearik Asit katı yağlayıcıların etkisi araştırılmıştır. Ağırlıkça % 4,5 Cu, % 0,7 Si, % 0,5 Mg içeren ön karışım oranındaki ticari Alumix 123 yağlayıcı ilave edilerek, dikey tip yüksek hızlı atritörde Azot gazı ortamında mekanik alaşım lanmaya çalışılmıştır. Paslanmaz çelik tank, çelik karıştırıcı kol ve 10 mm çapında çelik bilyalar kullanılarak mekanik alaşım lanma işlemi uygulanmıştır. Bilya/toz oranı 10:1 olarak yapılan MA işlemi, 400 dev/dk hızda 4 saat (MA4), 8 saat (MA8) ve 10 saat (MA10) sürelerle gerçekleştirilmiştir. Öğütülen karışım tozların boyutları lazer parçacık boyut ölçüm cihazı ile öğütülen toz morfolojisi, Al-Cu faz etkileşimleri ise optik ve tarama elektron mikroskop (SEM) çalışmaları ile karakterize edilmiştir. 10 saatlik MA sürecinde yağlayıcı türünün faz dönüşümlerine etkisi x-ışınları kırınımı (XRD) analizi ile incelenmiştir. Ancak her iki yağlayıcı ile yapılan 10 saatlik MA sonunda oluşmuş yeni bir faz belirlenmemiştir. Bu durumda tozların öğütülme işlemi incelendiğinde, karışım tozların başlangıç parçacık boyutu ortalaması  $d_{0,5} = 114,4 \mu\text{m}$  dir. Bu tozların 4 saatlik süre sonundaki parçacık boyutu Çinko Stearat içeren numune için  $d_{0,5} = 151,2 \mu\text{m}$ , Stearik Asit içeren numune için  $d_{0,5} = 85,1 \mu\text{m}$ 'dir. Çinko Stearat içeren numunenin parçacık boyutunda kaynaklanmalar sonucunda 4 ve 8 saatlerde artış gözlenmiş, 10 saatlik süreç sonucunda daha düşük değere ulaşılmıştır. Stearik asit içeren numunenin parçacık boyutunda ise süreye bağılı olarak lineer düşüş gözlemlenmiş, başlangıç parçacık boyutlarına göre ise sonuçta Stearik Asit içeren numunede daha küçük parçacık boyutu elde edilmiştir.

**Anahtar Kelimeler** — Toz Metalurjisi, Alumix123, Mekanik Alaşım Lanma, Yağlayıcı

## The Effect of Lubricants on Mechanical Alloying Process of Alumix123 Pre-Mixed Powders

**Abstract-** In this study, the effects of 1.5% Zinc Stearate and 2% Stearic Acid solid lubricants on the mechanical alloying (MA) process of premixed Al + Cu powders were investigated. By adding a commercial Alumix-123 lubricant with a pre-mix ratio of 4.5% Cu, 0.7% Si, 0.5% Mg by weight, vertical type high-speed atomizer tried to alloy the mechanics in the atmosphere of nitrogen gas. Mechanical alloying was applied using a stainless steel tank, a steel stirrer arm and steel balls with a diameter of 10 mm. The MA process with the ball-to-powder weight ratio (BPR) was 10/1 was carried out for 4 hours (MA4), 8 hours (MA8) and 10 hours (MA10) at 400 rpm. size of the milled powder mixture with a laser particle size analyzer, the milled powder morphology of the Al-Cu phase interaction of optical and scanning electron microscopy (SEM) were characterized by studies. The effect of phase transformation on the lubricant species in the 10 hour MA

process was investigated by x-ray diffraction (XRD) analysis. However, a new phase formed at the end of 10 hours of MA with both lubricants could not be detected. When the grinding process of powders is examined in this case, the average particle size of the mixture powders is  $d_{0,5} = 114,4 \mu\text{m}$ . This is the grain size of the powders at the end of 4 hour period for the sample containing Zinc Stearate  $d_{0,5} = 151,2 \mu\text{m}$  is  $d_{0,5} = 85,1 \mu\text{m}$  for the samples containing stearic acid. As a result of grain size welding of the sample containing zinc stearate, an increase was observed at 4 and 8 hours and a lower value was reached as a result of the 10 hour process. In the samples containing stearic acid was observed grain size decreases linearly depending on the time and according to the initial grain size of the resulting samples containing stearic acid as a smaller particle size.

**Keywords-** Powder Metallurgy, Mechanical Alloying, Alumix123, Lubricant

## I. GİRİŞ

Mekanik alaşım lanma (MA) yüksek enerjili bir bilyalı değirmende katı halde toz partiküllerinin tekrarlanan kaynak, kırılma ve yeniden kaynaklanmasını içeren toz işleme tekniğidir [1-4]. MA; oda sıcaklığında uygulanabilir olmasının yanısıra, başlangıç tane boyutundan bağımsız olarak ince tozları homojen bir şekilde üretmeyi de mümkün kılan avantajlara sahiptir [5]. Başlangıçta ve sonrasında parçacıklarda farklı şekillerde değişimler görmek mümkündür. MA işleminin başlangıcında, tekrar eden kırılma ve soğuk kaynaklanma tekrarlı mekanizmaların sonucunda çoklu katmanlardan oluşan bir toz oluşur. Bu kuvvetin oluşturduğu plastik deformasyonun etkisiyle, toz partikülleri sertleşir ve kırılmalarına neden olur [6,7]. İlerleyen sürelerle birlikte parçacık boyut ve morfolojilerinde değişim gözlemlenmektedir. Bu süreçte yağlayıcı ilavesi ise çarpışma sırasında parçacıklar arasındaki kaynaklanmaları önleyerek reaksiyon hızını yavaşlatır ve parçacık boyutunu düşürür [6-8]. MA sürecinde kullanılan bu yağlayıcılar, özellikle soğuk kaynaklanma etkisini azaltır [5-10]. Partiküller arasındaki topaklanmayı engeller ve kullanılan yağlayıcı türü, miktarı ve öğütme şekli; tozların son tane boyutunu, şeklini ve saflık derecesini belirlemede önemli rol oynar. Birçok yağlayıcısının kullanımı da MA sürecinde son tane boyutunu azaltır [6].

Bu çalışmada, mekanik alaşım lanma sürecine yağlayıcıların etkisini araştırmak amacıyla aynı parametreler ile iki farklı yağlayıcı ile işlem uygulanmış yağlayıcı türünün sürece etkisi araştırılmıştır. Bunun için, ön karışımli Alumix 123 tozuna ayrı

ayrı ağırlıkça %1,5 Çinko Stearat ve %2 oranında Stearik Asit yağlayıcıları eklenerek mekanik alaşımlama sürecine etkileri araştırılmıştır. Bu çalışmada da kullanılan yağlayıcılar, MA sürecinde yaygın olarak kullanılan yağlayıcılardandır [11]. Mekanik alaşımlama işlemi su soğutmalı atritör tipi cihazda azot (N<sub>2</sub>) gazı atmosferinde gerçekleştirilmiştir. Mekanik alaşımlama işlemi, 400 dev/dk hızda 4, 8 ve 10 saat süreler ile gerçekleştirilmiştir. MA işleminde çelik kazan, Ø10 mm çapında çelik bilye, çelik karıştırıcı kol kullanılmıştır ve bilye/toz oranı 10/1'dir. Öğütülen karışım tozların boyutları lazer parçacık boyut ölçüm cihazı ile ölçülmüş, öğütülen toz morfolojisi ve Al-Cu faz etkileşimleri ise optik ve tarama elektron mikroskop (SEM) çalışmaları ile karakterize edilmiştir. 10 saatlik MA sürecinde yağlayıcı türünün faz dönüşümlerine etkisi X-ışınları kırınımı (XRD) analizi ile incelenmiştir.

## II. DENEYSEL ÇALIŞMALAR

### A. Malzeme

Bu çalışmada Eckart Granulers (Almanya) tarafından üretilen Ecka Alumix 123 olarak bilinen ön-karışimli alüminyum esaslı tozlar kullanılmıştır. Alumix 123 tozuna ağırlıkça %2 stearik asit(CH<sub>3</sub>(CH<sub>2</sub>)<sub>16</sub>COOH ) ve %1,5 çinko stearat( Zn(C<sub>18</sub>H<sub>35</sub>O<sub>2</sub>)<sub>2</sub> ) yağlayıcıları kullanılarak iki farklı karışım toz hazırlanmıştır. Alumix 123 tozunun başlangıç ortalama parçacık boyut değeri d<sub>0,5</sub> = 114,44 µm'dir. Kullanılan tozun içeriği % Ağırlık olarak Tablo I 'de verilmiştir.

Tablo I. Alumix123 malzemenin kimyasal bileşimi (% ağırlık)

Alaşım	Al	Cu	Si	Mg
Alumix 123	94,3	4,5	0,7	0,5

### B. Metod

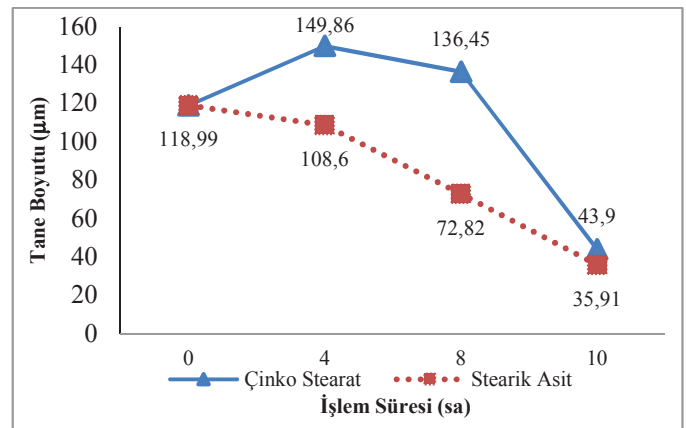
Alüminyum esaslı Alumix 123 ön karışimli tozlarına ayrı ayrı %1,5 çinko stearat (C<sub>36</sub>H<sub>70</sub>O<sub>4</sub>Zn) ve %2 stearik asit (CH<sub>3</sub>(CH<sub>2</sub>)<sub>16</sub>COOH) yağlayıcıları ilave edilerek Turbula cihazında 30 dakika karıştırma işlemine tabi tutulmuştur. Bu karışım tozlara dikey tip Union Process Marka Patch HD01 model su soğutmalı yüksek hızlı atritörde Azot (N<sub>2</sub>) gazı ortamında mekanik alaşımlama işlemi uygulanmıştır. Mekanik alaşımlama işlemi paslanmaz çelik tank, çelik karıştırıcı kol ve 10 mm çapında çelik bilyeler kullanılarak gerçekleştirilmiştir. Bilye/toz oranı 10:1 olarak yapılan MA işlemi her iki karışım içinde, 400 dev/dk hızda 4 saat (MA4), 8 saat (MA8) ve 10 saat (MA10) sürelerle gerçekleştirilmiştir. Deneydeki numuneler çinko stearat katkılı 10 saat süreyle mekanik alaşımlama işlemi uygulanan karışım için "ÇSMA10", stearik katkılı olan için ise "SAMA10" olarak kodlanmıştır. Bu çalışmada kullanılan bütün karışım tozlara uygulanacak işlemler öncesinde ve sonrasında parçacık boyut ölçümü uygulanmıştır. Alumix 123 başlangıç tozunu, yağlayıcıları ve mekanik alaşımlama işlemi sonrası toz karışımını karakterize etmek amacıyla sterio mikroskop, optik mikroskop ve taramalı elektron mikroskopunda incelemeler gerçekleştirilmiştir. Bu işlemler ile tozu genel karakterize etmek ve faz tanımlamalarına yardımcı olması amaçlanmıştır. 10 saat mekanik alaşımlama

işlemi sonrasında toz karışımlarına XRD analizi uygulanmıştır.

## III. DENEY SONUÇLARI VE TARTIŞMA

### A. Parçacık Boyut Analizleri

Şekil-1'de farklı yağlayıcı içeren Alumix 123 tozların MA süresine bağlı parçacık boyut değişimleri verilmiştir. Şekil 1.'de verilen grafiğe göre yağlayıcı türlerinin toz parçacık boyutuna etkisi incelendiğinde, karışım tozların başlangıç parçacık boyutu ortalaması d<sub>0,5</sub>= 114,4 µm 'dir. Bu tozların 4 saatlik süre sonundaki parçacık boyutu Çinko Stearat içeren numune için d<sub>0,5</sub>=151,2 µm, Stearik Asit içeren numune için d<sub>0,5</sub>=85,1 µm'dir. 4 saatlik süreç için, çinko stearat içeren numunenin parçacık boyutunda muhtemel kaynaklanmalar sonucunda artış gözlemlenmiştir(Şekil 1). Stearik asit içeren numunede ise; kaynaklanma süreci gösteren parçacık boyut artışı yerine azalma görülmektedir.

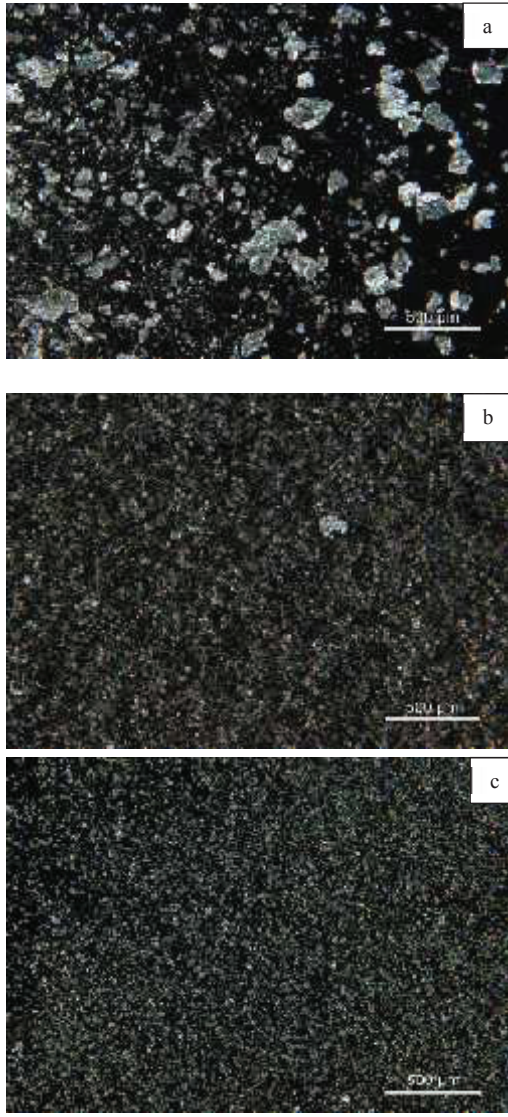


Şekil 1. Katı yağlayıcı türü ve MA süresinin toz boyutuna etkisi

Başlangıç parçacık boyutlarına göre ise 10 saatlik süreç sonucunda stearik asit içeren numunede daha düşük değere ulaşılmıştır. Stearik asit içeren numunenin parçacık boyutunda ise süreye bağlı olarak lineer düşüş gözlemlenmiştir, çinko stearat içeren numune için ise bu durum geçerli değildir. Süreç sonucunda ulaşılan değerler ise; Çinko Stearat içeren numune için d<sub>0,5</sub>=45,2 µm, Stearik Asit içeren numune için d<sub>0,5</sub>=37 µm'dir. MA işlemi sürecinde stearik asidin, toz öğütme işlemine olumlu etkisi olduğu söylenebilir.

### B. Sterio Mikroskop Çalışmaları

Şekil 2'de aynı büyütme değerlerinde işlemsiz Alumix 123, 10 sa öğütülmüş Çinko Stearat içeren(ÇSMA10) ve Stearik Asit içeren(SAMA10) toz karışımlarının sterio mikroskop görüntüleri verilmiştir.

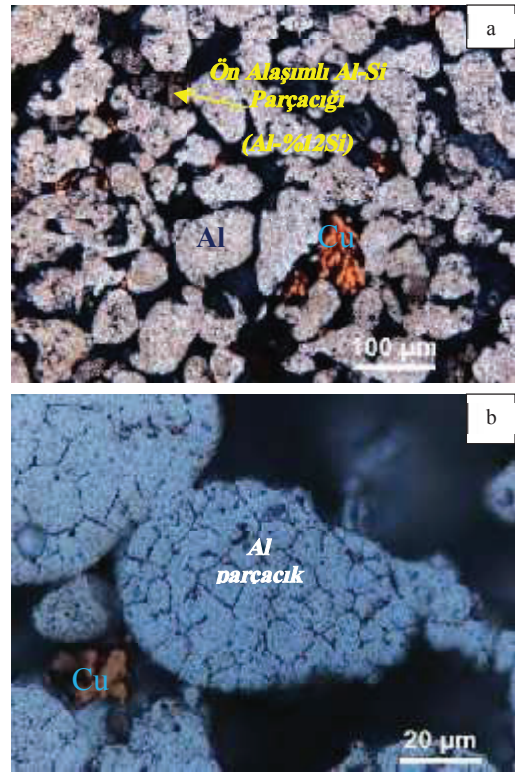


Şekil 2. Karışım tozların stereo ışık mikroskobu görüntüleri  
a) İşlemsiz Alumix 123 b) ÇSMA10 c) SAMA10

Şekil 2a'da görüntüsü verilen işlemsiz Alumix 123 numunesinde toz boyut dağılımı çok değişkendir ve özellikle iri Al parçacıkları görülmektedir. Şekil 2.b.'de verilen ÇSMA10 numunesinde ise halen kırılmamış kaynaklı iri parçacıklar mevcuttur. Şekil 2c'deki SAMA10 numunesinde ise genel olarak ince ve homojen toz boyut dağılımı görülmektedir. Ayrıca stearik asit numunesi ile işlem gören toz karışımında daha küçük boyutlara ulaşıldığı gözlemlenmiştir.

#### C. Optik Mikroskop Çalışmaları

Şekil-3'de mekanik alaşımlama işlemi uygulanmamış işlemsiz tozun farklı büyütme ölçeklerinde optik mikroskop görüntüleri verilmiştir.

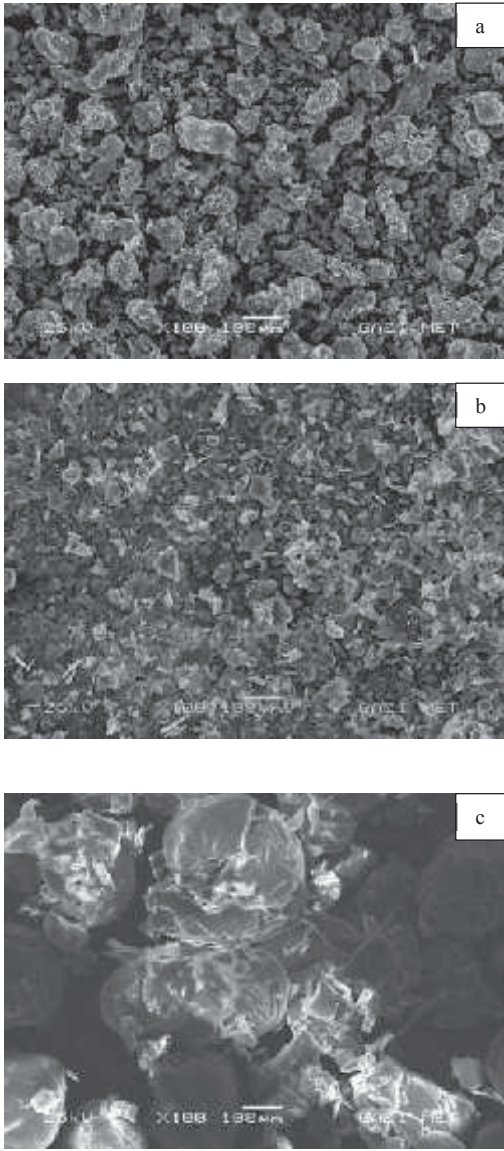


Şekil 3. İşlemsiz tozun (Alumix 123) farklı büyütme ölçeklerinde optik mikroskop görüntüleri. a) Genel Görünüm b) Al parçacık mikroyapısı

Şekil 3a'da verilen mikroyapı görüntüsünde ön karışımli Alumix 123 tozunun büyük bir bölümünü muhtemelen su atomizasyonu ile üretilen Alüminyum toz parçacık oranının fazla olduğu görülürken, elektroliz ile üretilen Cu parçacıklarının dendritik halde bulunduğu ve yüksek saflıkta olduğu bilinmektedir. Şekil üzerinde belirtildiği şekilde, Al-Si alaşımı parçacık görülmektedir. Alumix 123 tozuna yapılan optik mikroskop incelemeleri ve EDS analizleri ile yapıdaki silisyum alaşım oranının ağırlıkça % 15 Si içeren ön alaşımli olarak karışım toz içinde bulunduğu, magnezyumun ise Al-40Mg ön alaşımli halde bulunduğu tespit edilmiştir. Şekil 3b'de ise ortalama 60 µm boyutundaki bir Al parçacığın mikroyapısı görülmektedir. Bu parçacığın ise ortalama 8 µm boyutlarında çok sayıda taneden meydana geldiği açıkça görülmektedir. Hızlı katılaşma ile oluşan bu tane yapısı ve parçacığın yumrusal formu, Al parçacıkların su atomizasyonu ile üretilme ihtimalini artırmaktadır.

#### D. Elektron Mikroskobu Çalışmaları

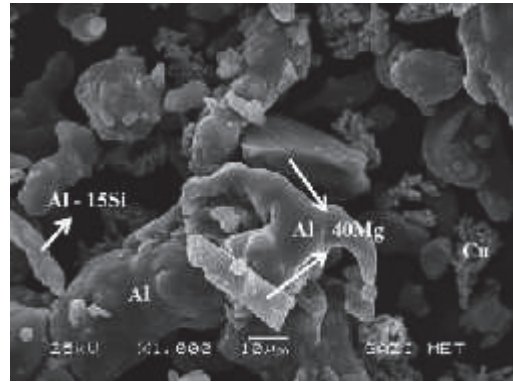
Şekil 4'te işlemsiz Alumix 123 tozunun ve yağlayıcı türlerinin elektron mikroskobu görüntüleri verilmiştir.



Şekil 4. İşlemsiz tozun ve yağlayıcı türlerinin SEM görüntüleri (a) Alumix123 (b) Çinko Stearat (c) Stearik Asit

Şekil 3a'da işlemsiz Alumix 123 tozunun genel olarak boyut dağılımının değişken olduğu görülmüştür. Şekil 3b ve Şekil 3c'de verilen görüntülerde çinko stearat yağlayıcısının parçacık boyutu olarak stearik asit yağlayıcısından daha küçük parçacıklara sahip olduğu ve daha farklı boyut aralıkları içerdiği, stearik asidin ise neredeyse küresel şekle yakın olduğu görülmüştür.

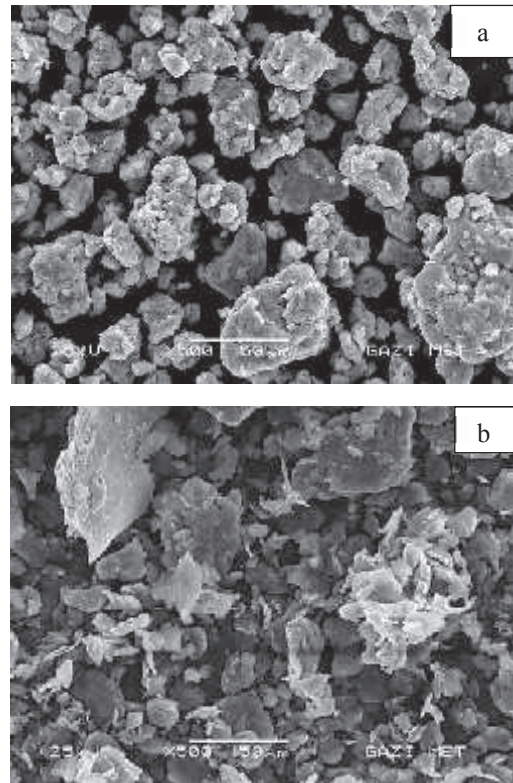
Alumix 123 tozunda ön alaşımlanmış Al-12Si tozları olduğu bilinmektedir [12] ve Alumix 123 ön karışım tozuna EDS analizleri yapılarak tanımlanmıştır. Şekil 5'de EDS analizi yapılan parçacıklar ve görüntü üzerinde yüzdesel olarak EDS analizi sonuçları verilmiştir.



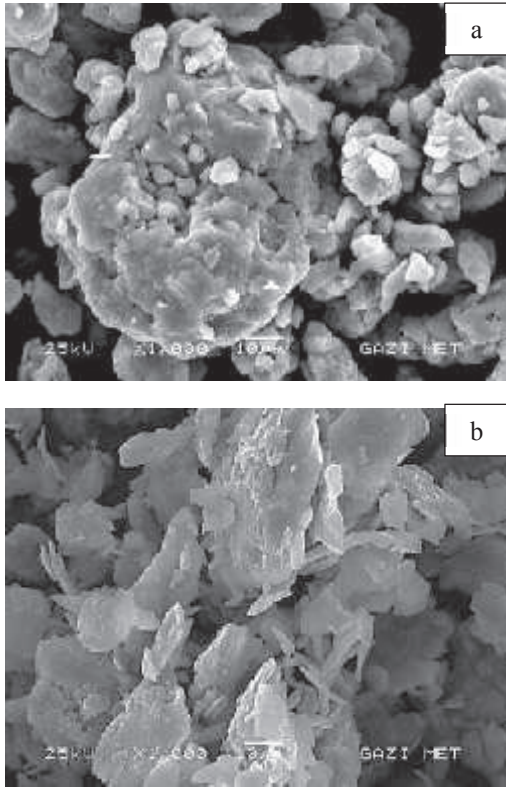
Şekil 5. Alumix 123 tozunun genel görünümü SEM/EDS görüntüsü

EDS analizlerinin sonuçlarına göre Resim 5.4' de gösterilen Alumix 123 karışım tozu oluşturan parçacıklar analiz edildiğinde, iri ve yumrusal formda olan parçacıkların alüminyum toz parçacıkları olduğu, dendritik biçimde olan parçacıkların bakır toz parçacıkları olduğu, köşeli prizmatik olan parçacıkların Al-Mg alaşımı olduğu ve yaklaşık %40 Mg içeren ön alaşımlı toz parçacıkları olduğu, yine köşeli biçimdeki parçacıkların ise yaklaşık % 15 Si içeren, Al-Si ön alaşımlı toz parçacıklar olduğu belirlenmiştir.

10 sa mekanik alaşımlama işlemi uygulanmış toz karışımların (ÇSMA10 ve SAMA10) SEM görüntüleri Şekil 6 ve Şekil 7'de verilmiştir.



Şekil 6. 10 sa MA işlemi sonrası tozların sem görüntüleri (a) Çinko stearat içeren (b) Stearik asit içeren



Şekil 7. 10 sa MA işlemi sonrası tozların SEM görüntüleri (a) Çinko stearat içeren (b) Stearik asit içeren

Şekil 6a'da verilen ÇSMA10 numunesinin genel görünümü incelendiğinde, tane boyutlarının farklı aralıklar içerdiği ve yumrusal biçimlerde olduğu görülmüştür. MA etkisini ise gerek boyut dağılım değişkenliği, gerekse Şekil 7a'daki görüntüde görmek mümkündür. SEM görüntüleri verilen tozların genel olarak hala öğütme sürecinin tamamlanmadığı görülmüştür. Tozların henüz kaynaklanma sürecinde olduğu ancak kaynaklanma sürecinde iri parçacıkların üzerine küçük parçacıkların sıvanma şeklinde yapıldığı belirlenmiştir. MA işlemi sürecinde beklenen deformasyonla pulsu yapılar yerine yumrusal formlardaki başlangıç parçacıklarının biçimlerini genel olarak koruduğu görülmektedir. Şekil 6b'de verilen SAMA10 numunesinin genel görünümünü incelendiğinde, öğütme işleminin gerçekleştiği, plastik deformasyonla farklı boyutlarda ve geometrilerde parçacıkların oluştuğu görülmüştür. Şekil 7b'de kaynaklanmış, yassılaştı ve pulsu geometride toz parçacıkları görülmektedir.

#### IV. SONUÇLAR

1. Tozların öğütülme işlemi incelendiğinde, 4 saatlik süre sonundaki tane boyutu Çinko Stearat içeren numune için  $d_{0,5}=151,2 \mu\text{m}$ , Stearik Asit içeren numune için  $d_{0,5}=85,1 \mu\text{m}$ 'dir. Bu durum kısa süreli MA işleminde dahi toz öğütme sürecine sterarik asit yağlayıcısının önemli etkisi olduğunu göstermektedir.

2. Çinko Stearat içeren numunenin toz parçacık boyutunda kaynaklanmalar sonucunda 4 ve 8 saatlere kadar artış gözlenmiş, 10 saatlik süreç sonucunda ancak toz boyutları önemli oranda küçülmeye başlamıştır.
3. Stearik asit içeren numunenin parçacık boyutunda ise süreye bağlı olarak lineer düşüş gözlemlenmiş, başlangıç tane boyutlarına göre ise sonuçta Stearik Asit içeren numunede daha küçük tane boyutu elde edilmiştir.
4. Genel olarak çinko stearatın aksine, stearik asit katkılı MA işleminde kaynaklanma ve parçacık irileşme süreci olmaksızın öğütme işlemi gerçekleşmiştir. Bu durumda stearik asit'in, Al parçacıkların kaynaklanmalarına engel olabileceği söylenebilir.

#### V. KAYNAKÇA

- [1] J. B. Fogagnolo, D. Amador, E. M. Ruiz-Navas and J. M. Torralba, Solid solution in Al-4,5 wt % Cu produced by mechanical alloying, *Materials Science and Engineering A*, 433, (45-49), (2006).
- [2] Koch, C.C., Whittenberger, J.D. (1996). Mechanical Milling of Intermetallics, *Intermetallics*, 4, 339-355.
- [3] Nagesha, K.V., Rajanish M., Shivappa D.(2013). A Review on Mechanical Alloying, *International Journal of Engineering Research and Applications*, Vol 3, Issue 3, 921-924.
- [4] Alamolhoda, S. (2012). Role of Process Control Agents on Milling Behavior of Al and TiO<sub>2</sub> Powder Mixture to Synthesize TiAl/Al<sub>2</sub>O<sub>3</sub> Nano Composite, *International Journal of Modern Physics: Conference Series*, Vol 5, 638-645.
- [5] Soni, P.R. (2001). *Mechanical Alloying Fundamentals and Applications*, (Dijital Kitap). İngiltere: Cambridge International Science Publishing, 1-3.
- [6] C. Suryanarayana, *Progress in Material Science*, 46, (1-184), (2001).
- [7] Zhang, D. L., Massalski, T. B., Paruchuri, M. R. (1994). Formation of Metastable and Equilibrium Phases During Mechanical Alloying Of Al and Mg Powders. *Metallurgical and Materials Transactions A*, Vol 25, Issue 1, 73-79.
- [8] Zolriasatein, A., Yan, X., Bauer, E., Rogl, P. Shokuhfar, A., Paschen, S. (2015). Influence of PCA on Thermoelectric Properties and Hardness of Nanostructured Ba-Cu-Si Clathrates, *Materials and Design*, 87, 883-890.
- [9] Shaw, L., Zawrah, J., Villegas, H., Luo, H., Miracle, D. (2003). Effect of Process-Control Agents on Mechanical Alloying of Nanostructured Aluminum Alloys, *Metallurgical and Materials Transactions A*, Vol 34A, 159-170.
- [10] Neamt, B.V., Chicinas, H.F., Marinca, T.F., Isnard, O. Pan, O., Chicinas, I. (2016). Amorphisation of Fe-based Alloy via Wet Mechanical Alloying Assisted by PCA Decomposition. *Materials Chemistry and Physics*, 183, 83-92.
- [11] Alamolhoda, S. (2012). Role of Process Control Agents on Milling Behavior of Al and TiO<sub>2</sub> Powder Mixture To Synthesize TiAl/Al<sub>2</sub>O<sub>3</sub> Nano Composite. *International Journal of Modern Physics: Conference Series*, Vol. 5, 638-645.
- [12] Meluch, L., "Warm Compaction of Alumix 123", *PhD thesis*, (88-89), University of Birmingham, (2009).

# Öğütülmüş Cu + SiC Takviyesiyle Al Esaslı MMC<sub>p</sub> Malzeme Üretimi ve Karakterizasyonu

Ezgican Atar\*, Damla Sarıdemir ve Yusuf Özçatalbaş  
[ezgican.atar@gazi.edu.tr](mailto:ezgican.atar@gazi.edu.tr), [yusufoz@gazi.edu.tr](mailto:yusufoz@gazi.edu.tr)

*Metalurji ve Malzeme Mühendisliği, Teknoloji Fakültesi, Gazi Üniversitesi, 06560, Ankara, Türkiye*

**Özet-** Bu çalışmada farklı sürelerde öğütülen Cu + SiC karışım tozların, Al-Cu alaşımı matris ve SiC takviye içeren metal matrisli kompozit (MMC<sub>p</sub>) malzeme üretimine etkisi araştırılmıştır. Bu amaçla, ağırlıkça % 67 Cu ve %33 SiC tozları üç boyutlu karıştırma cihazında (Turbula) paslanmaz çelik kap içinde 15 mm çapında zirkonya bilyeler vasıtasıyla 5 (M5), 10 (M10) ve 15 (M15) saat sürelerle öğütülmüştür. Öğütülen karışım tozlar ağırlıkça % 4,7 Cu + % 2,3 SiC içeren oranda Al tozu ile 45 dakika Turbula'da karıştırılmıştır. Bu toz karışımı 20 MPa basınçta soğuk preslendikten sonra, 500°C 'de 200 MPa basınçta 30 dakika süreyle sıcak preslenerek MMC<sub>p</sub> malzemeler üretilmiştir. Toz metalürjisi (TM) yöntemiyle üretilen MMC<sub>p</sub> malzemelerin mikroyapıları ve fazları SEM/EDS analizleri ile XRD çalışmaları yapılarak tanımlanmıştır. Mekanik ve fiziksel özellikleri ise sertlik, çapraz kırılma deneyi ve yoğunluk ölçümleri ile karakterize edilmiştir. Genel olarak, uzun süreli öğütülmüş Cu+SiC tozlarıyla takviyelendirilen MMC<sub>p</sub> malzemelerin yoğunluğunda kısmi düşüş olmasına rağmen mekanik özelliklerinde artış belirlenmiştir. İşlemsiz (M0) MMC<sub>p</sub> malzemenin gerçek yoğunluğunun teorik yoğunluğa oranı %99,5 dir. Ancak, M10 ve M15 katkılı MMC<sub>p</sub>'lerdeki yoğunluk oranı sırasıyla %96,3 ve %98,6 olarak ölçülmüştür. M15 katkılı MMC<sub>p</sub>'de en yüksek çapraz kırılma dayanımı (212 MPa) belirlenmiş ve işlemsiz MMC<sub>p</sub>'ye göre yaklaşık %20 oranında artış sağlanmıştır. Üretilen kompozit malzeme sertliklerinde ise işlemsiz malzemeye oranla M15 malzemede % 46 artışı sağlanmıştır.

**Anahtar Kelimeler** — Toz Metalurjisi, Mekanik Öğütme, Metal Matrisli Kompozit, Karakterizasyon

## Production and Characterization of Al-Based MMC Materials Reinforced By Milled Cu + SiC Powders

**Abstract** - In this study, the effects of Cu + SiC mixture powders milled at different times on the production of metal matrix composite (MMC<sub>p</sub>) materials containing Al-Cu Alloyed matrix and SiC reinforcement were investigated. For this purpose, 67 wt.% Cu and 33 wt.% SiC powders were milled in a three-dimensional mixing apparatus (Turbula) in a stainless steel vessel with zirconia balls of 15 mm diameter for 5 (M5), 10 (M10) and 15 (M15) hours. The milled mixture powders were mixed in a Turbula for 45 minutes with aluminum powder containing 4.7 wt.% Cu + 2.3 wt.% SiC. This mixture powder was cold compacted at 20 MPa Pressure and then hot pressed at 500 °C under 200 MPa pressure for 30 minutes to produce MMC<sub>p</sub>

materials. Microstructures and phases of MMC<sub>p</sub> materials produced by powder metallurgy (PM) route were determined by XRD analyzes with SEM / EDS studies. Mechanical and physical properties of MMC<sub>p</sub> materials were characterized by Brinell hardness, transverse rupture strength (TRS) tests and density measurements. In general, an increase in the mechanical properties has been determined although there is a partial reduction in the density of MMC<sub>p</sub> materials reinforced with M15 powders. The ratio of the actual density of unprocessed (M0) MMC<sub>p</sub> material to the theoretical density is 99.5%. However, the density ratios in MMC<sub>p</sub> reinforced with M10 and M15 were measured as 96.3% and 98.6% respectively. The highest transverse rupture strength (212 MPa) was determined in M15 reinforced MMC<sub>p</sub> and an increase of about 20% was achieved. The hardness of the produced composite materials doped M15 was increased by 46% compared with the M0 material.

**Keywords-** Powder Metallurgy, Milling, MMC<sub>p</sub>, Characterization

### I. GİRİŞ

Kompozit malzemeler, kimyasal bileşimi ve özellikleri farklı olan iki veya daha fazla malzemenin makro düzeyde birleştirilmesiyle elde edilen malzemeler olarak tanımlanmaktadır.[1] Kompoziti oluşturan malzemeler ara yüzeylerle birbirlerinden ayrılır ve yapı içinde kendi özelliklerini korurlar. Ancak kompozit malzemenin özellikleri, kendisini oluşturan malzemelerin özelliklerinden üstündür.[2]

Malzeme üretim yöntemlerindeki gelişmelerle birlikte değişik uygulama alanlarında kullanılmak üzere farklı özelliklerde malzemelerin geliştirilmesi süreci de devam etmektedir. Toz metalürjisi yöntemi de halen gelişme süreci devam eden üretim yöntemlerinden biridir [3-4].

Son zamanlarda TM ile malzeme üretimi en hızlı gelişen imalat yöntemlerinden birisi olmuştur. TM ile üretim yöntemi, karıştırılmış metal tozlarının, oda sıcaklığında veya yüksek sıcaklıklarda, üretilecek parça şekli ve boyutlarına sahip kalıp içinde preslenerek şekillendirme ve ardından belirli bir sıcaklıkta sinterleme ile gerçekleştirilen bir imalat yöntemidir [5]. Toz metal parçalar haddeleme, döküm gibi geleneksel imalat yöntemleri ile üretilen malzemelere göre bazı değişik ve avantajlı özelliklere sahiptir. Bu avantajlar, üretimi zor olan alaşımları daha kolay üretme, karmaşık şekilli parçaların imalat kolaylığı, yoğunluk kontrolü ve ekonomiklik gibi özelliklerdir [6].

Alüminyum ve alaşımları, bazı korozif ortamlarda bozulmaya karşı iyi mekanik özellik direnci ile düşük

yoğunluklarından dolayı kimya, otomotiv, gıda, havacılık ve denizcilik endüstrisindeki birçok uygulamada istenen ve kullanılan malzemelerdir [7]. Al matrisli partikül takviyeli kompozitlerin, ticari Al alaşımları ile kıyaslandığında artan sertlik, yüksek aşınma direnci, mukavemetinin uygunluğu, titreşim azaltıcı ve düşük ısı yayılım katsayısı gibi malzemelerde istenilen üstün özellikleri bir arada bulundurmaları nedeniyle bu malzemeler daha da önemli olmuştur [8]. Alüminyum alaşımları günümüzde çelikten sonra en çok kullanılan metalik mühendislik malzemeleridir [9].

Kompozit malzemelerin üretiminde karşılaşılan temel problem, matris ile takviye malzemeleri arasında etkili bir bağlanmanın elde edilememesidir. Nispeten düşük sıcaklıklarda yapılan TM üretim yöntemi, teorik olarak arayüz kinetiğinin daha iyi kontrol edilmesini sağlar [7].

Mekanik öğütme (MÖ) yöntemi kullanarak matrisi oluşturan metal ile seramik partikülleri, mekanik olarak birbirine bağlayacak prosesin uygulanmasının, ara yüzey bağ kuvvetlerini arttırdığına dair çalışmalar mevcuttur. Uygulanan mekanik öğütme prosesinin MMKp üretiminde kullanılması, üretilen kompozit malzemenin mekanik özelliklerini arttırdığı yapılan çalışmalarda gözlemlenmektedir.

Bu amaç doğrultusunda matris partikül ara yüzey bağlarını kuvvetlendirmek için mekanik öğütme yöntemi kullanılmıştır. Al'u alaşımlandırmak amacıyla kullanılan Cu tozları ile seramik SiC tozları belli süreler ile öğütülmüştür. Cu takviye elemanı ile SiC-Al ara yüzeyinde adhesiv etkileri artırılmaya çalışılmıştır. SiC parçacıklarının yüzeylerini Cu sünek faz ile kaplamaya çalışılmıştır.

SiC+Al alaşımı matrisli kompozit malzeme üretim sürecinde; Cu ve SiC parçacıkları üç boyutlu karıştırıcıda (Turbola) mekanik olarak 45 dakika bilyasız, 5, 10, 15 saat bilyalı karıştırılmıştır. Ardından bu karışım tozlar Al tozlar ile karıştırılarak Cu'ın Al'u difüze olarak alaşımlandırması aynı zamanda seramik partiküllerin yüzeyinde mekanik bağlantılı Cu kaplanması ve kompozit malzemenin bağlarının artırılması hedeflenmiştir. TM yöntemi ve sıcak presleme ile Al+%4,7Cu Matris alaşımında %2,3SiC takviye içeren MMKp üretimi gerçekleştirilmeye çalışılmıştır.

## II. DENEYSEL ÇALIŞMALAR

### A. Malzeme

Deneysel çalışmalarda, atomizasyon yöntemiyle üretilmiş %99,7 saflıkta alüminyum ve %99 saflıkta elektroliz yöntemi ile üretilmiş dentiritik bakır tozları kullanılmıştır. Al-%4,7Cu toz karışımında Al toz tane boyutu 160 µm altında, Cu toz tane boyutu ise 140 µm altında ve ortalama olarak 40 µm'dur.

### B. Metod

Ağırlıkça %67 Cu ve %33 SiC toz karışımı 45 dakika süreyle turbula cihazında ön karıştırma yapılmıştır. Devamında bu karışım toz, 5, 10, 15 saat sürelerde paslanmaz çelik kap içinde 10 mm çapında zirkonya bilyalar kullanılarak turbulada mekanik öğütme işlemine tabi tutulmuştur. Bu sayede mekanik

öğütülmüş Cu+SiC toz karışımları elde edilmiştir. Devamında ağırlıkça %7 oranında Cu+SiC öğütülmüş toz ile %93 Al tozu turbula da 45 dakika karıştırılarak ağırlıkça %4,7Cu, %2,3 SiC ve %93Al karışım tozu elde edilmiştir. Bu toz karışımı 30x50 mm<sup>2</sup> lik kalıp içerisinde alınarak oda sıcaklığında ön şekillendirme için 20MPa ön yük uygulanmış ve devamında 500 °C kalıp sıcaklığında ve 200 MPa basınç altında 30 dk süre ile tek yönlü sıcak preslenerek kompozit numune haline getirilmiştir. Bu sayede 30x50x13 mm<sup>3</sup> kesitli MMK<sub>p</sub> blok numuneler üretilmiştir. Sadece ön karıştırılmış tozlardan üretilmiş MMK<sub>p</sub> ile birlikte 5, 10 ve 15 saat öğütme süreleriyle elde edilen öğütülmüş tozlardan üretilen MMK<sub>p</sub> numuneler M5, M10 ve M15 olarak kodlanmıştır.

Numuneler tel erezyon kesim yöntemi ile dikey olarak kesilip 6,5x50x13mm<sup>3</sup> kesitli her numuneden 4'er blok numuneler elde edilmiştir.

Parçaların makro sertlik ölçümleri ASTM E 10'a uygun olarak alınmıştır. Emco marka DuraVision 200 model sertlik ölçüm cihazında BSD30 sertlik değerleri ölçülmüştür. Yapılan sertlik değerlerindeki güvenilirliği sağlayabilmek amacı ile üç noktadan ölçüm yapılmıştır. Alınan bu değerlerin aritmetik ortalamaları hesaplanarak sertlik değerleri belirlenmiştir. Sertlik ölçümleri numunelere presleme yönüne dik yüzeyden yapılmıştır.

Kompozitlerin çapraz kırılma dayanımları aşağıda verilen ASTM B528-05'de belirtilen eşitlik kullanılarak hesaplandı. Deneysel GÜTF Metalürji ve Malzeme Mühendisliği Mekanik Testler Laboratuvarında INSTRON marka, 50 kN kapasiteli, çekme ve eğme testi yapabilen bilgisayar kontrollü cihazda yapılmıştır.

$$\text{Çapraz Kırılma Dayanımı (TRS)} = \frac{3 \cdot P \cdot L}{2 \cdot t^2 \cdot w} \text{ MPa}$$

MMK<sub>p</sub> numunelerinin yoğunluk ölçümleri Arşimet prensibine göre çalışan, 0,0001 g hassasiyetdeki üzerinde yoğunluk kiti bulunan Sartorius marka dijital terazide ölçülmüştür. Aşağıdaki aşamalar uygulanarak yoğunluk hesaplanmıştır.

- Numunenin havadaki ağırlığının ölçümü ( W )
- Dara alma
- Su içinde ağırlık ölçümü ( G )
- Malzemenin yoğunluğu ( g )
- Yüzde yoğunluk ( % g )

Deneysel numunelerinin yoğunluk ölçümleri Arşimet prensibine göre çalışan, 0,0001 g hassasiyetdeki üzerinde yoğunluk kiti bulunan Sartorius marka dijital terazide ölçülmüştür.

Ağırlıkça %93Al +%4,7 Cu+%2,3 SiC tozları ile üretilen MMK<sub>p</sub> malzemenin teorik yoğunluğu;

$$\text{➤ } d_{Cu} = 8,92 \times \%4,7 = 0,41924 \text{ .....(1)}$$

$$\text{➤ } d_{Al} = 2,7 \times \%93 = 2,511 \text{ ..... (2)}$$

$$\text{➤ } d_{SiC} = 3,20 \times \%2,3 = 0,0736 \text{ .....(3)}$$

$$+ \text{-----}$$

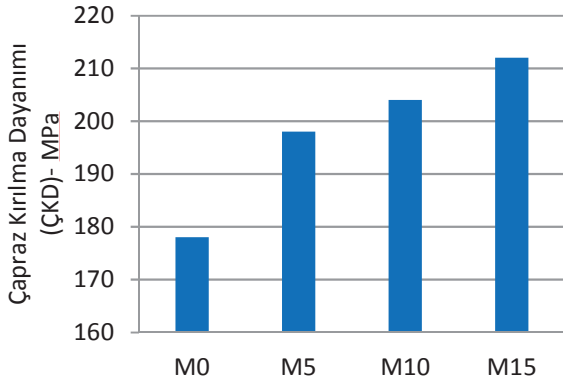
$$\text{➤ } d_{Cu} + d_{Al} + d_{SiC} = 3,004 \text{ g/cm}^3 \text{ .....(4)}$$

Deneysel numunelerinin teorik yoğunlukları  $d_t=3,004\text{g/cm}^3$  olarak hesaplanmıştır.

### III. DENEY SONUÇLARI VE TARTIŞMA

#### A. Çapraz Kırılma Dayanımı (ÇKD)

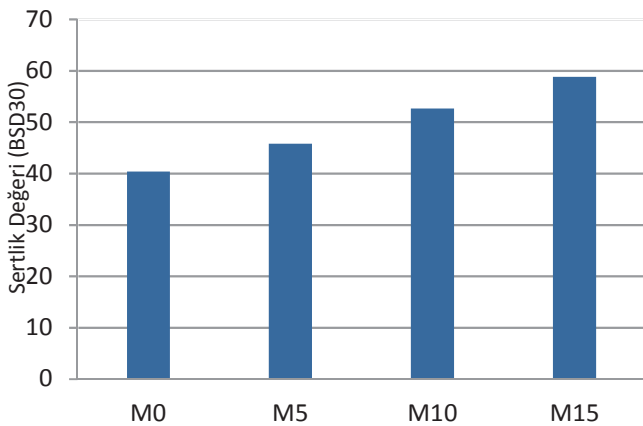
Şekil 1' de üretilen MMK<sub>p</sub> malzemelerin çapraz kırılma dayanımları (ÇKD) gösterilmiştir. Mekanik öğütme yapılmadan üretilen kompozit malzemenin (M0) çapraz kırılma dayanımının 178 MPa ile en düşük olduğu, öğütme süresinin artırılması ile çapraz kırılma dayanımında artış olduğu ve en yüksek dayanımın 15 saat öğütülen M15 numunesinde 212 MPa'a artış gösterdiği belirlenmiştir. Çapraz kırılma dayanımının öğütme süresi ile artış gösterdiği ve bu durumun azalan Cu parçacık boyutu ile artan SiC ve Cu girişimine bağlandığı söylenebilir.



Şekil 1. Karışım toz öğütme süresinin MMK<sub>p</sub> malzemelerin çapraz kırılma dayanımına etkisi

#### B. Sertlik Değişimi

Şekil 1 ve Şekil 2'de verilen her iki grafikten de anlaşılacağı gibi, ağırlıkça aynı Cu ve SiC<sub>p</sub> içeriğine rağmen, artan öğütme süresiyle elde edilen karışım tozun katkısı, üretilen metal matrisli kompozitin gerek sertliğini ve gerekse çapraz kırılma dayanımını arttırmıştır [7,8].



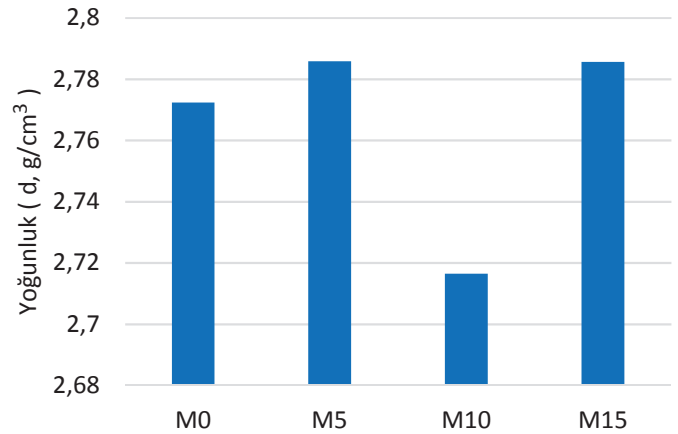
Şekil 2. Karışım toz öğütme süresinin MMK<sub>p</sub> malzemelerin sertliklerine etkisi

Öğütme süresindeki artışla mekanik özelliklerde sağlanan bu avantajın, artan öğütme süresiyle azalan SiC ve Cu parçacık

boyutlarından kaynaklandığı söylenebilir. Zira küçük Cu parçacık boyutu, sinter sürecinde Al-Cu alaşımlanma oranını artırırken, daha küçük SiC boyutu ise matrisin dayanımını MMK<sub>p</sub> malzemenin dayanımını arttırmada katkı sağlamıştır. Kurt ve arkadaşları, Mg katkısı ve Si katkısının Al-Cu elementel karışımlarının mekanik özelliklerine artışa sebep olduğunu rapor etmişlerdir. [10-15].

Gupta ve Ling, alüminyuma yapılan silisyum ilavesinin mikroyapı ve mekanik özelliklere etkisini incelemişler ve ötektik-üstü ve ötektik-altı alaşımların metalürjik karakterizasyonunu gerçekleştirmişlerdir. Elde ettikleri sonuçlara göre, silisyum ilavesi sertlik ve yaşlanma kabiliyetinde artışa neden olmuştur. [16]

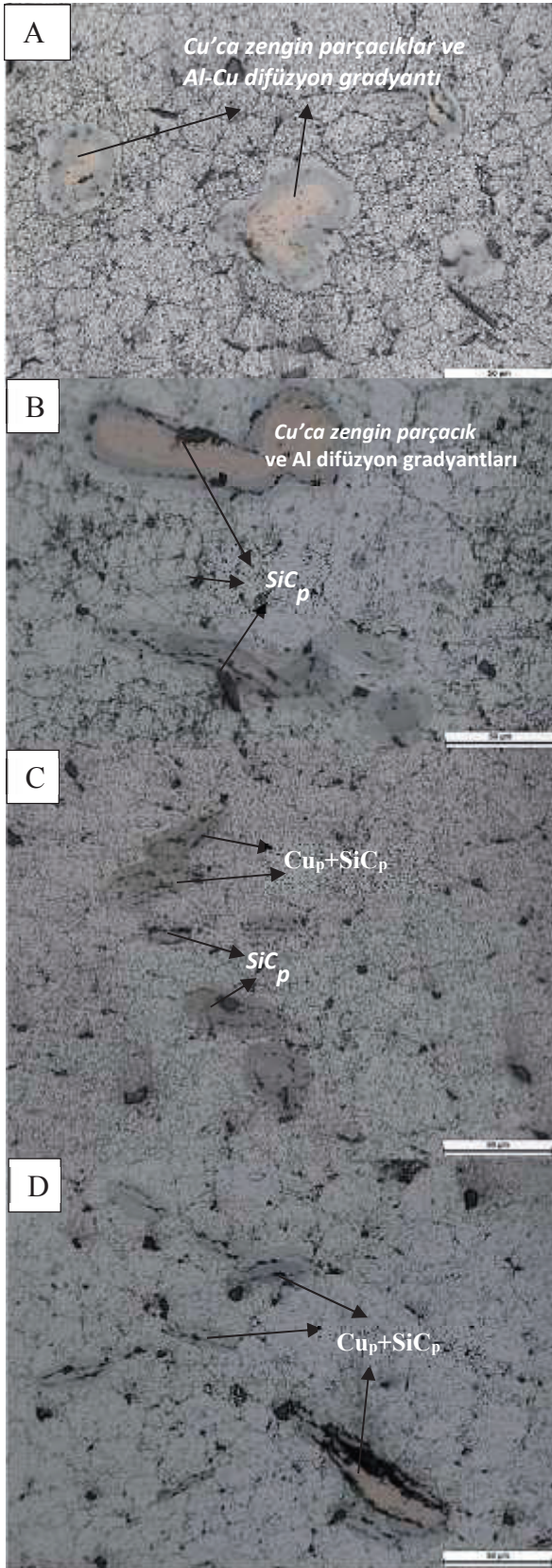
#### C. Yoğunluk Değişimleri



Şekil 3. Karışım toz öğütme süresinin MMK<sub>p</sub> malzemelerin yoğunluklarına etkisi

Teorik yoğunluk ile ölçülen yoğunlukların yüzde uygunlukları Şekil 3'deki gibidir. Üretilen MMK<sub>p</sub> malzemelerin teorik yoğunlukları  $d_t=3 \text{ g/cm}^3$  olarak dört nolu eşitlikle hesaplanmış olmasına rağmen, ölçülen en fazla yoğunluk  $2,787 \text{ g/cm}^3$  civarında M5 ve M15 numunelerinde belirlenmiştir. M10 numunesi yoğunluğu ise  $2,72 \text{ g/cm}^3$  civarındadır. Bu durumda ulaşılan en yüksek yoğunluk oranı %93 en düşük ise %91 civarındadır ve bu oranlar sıcak presleme ile üretilen MMK<sub>p</sub> malzemeler için düşüktür. Zira sıcak presleme aktif sinterleme işlemi ile %99 yoğunluklara ulaşılabilir. Yoğunluğun artması ise mekanik özellikleri iyileştirmektedir [17]. Mekanik öğütme öncesi veya çeşitli sürelerdeki öğütme sonrası ağırlıkça %93 oranında Al tozları ile karıştırılan ağırlıkça %7 oranında Cu+SiC karışım tozu içeriğinden kaynaklandığı düşünülmektedir. Karışım tozun aslında %67 Cu ve %33 SiC içeriğinde olması gerekirken 7 g alınan toz içeriğinde Cu oranının daha olması muhtemeldir. Zira, Cu+SiC karışımı belirtilen oranda homojen karışmamıştır ve Cu parçacıklara girişim yapmış yoğun SiC parçacıkları bulunmaktadır. Bu durum ise karışımındaki Cu oranını azaltmaktadır. Ayrıca Cu özgül yoğunluğunun fazla olması sebebiyle karışım toz kütlelerinin altında kalarak bir nolu eşitlikte hesaba katılan Cu oranının sağlanmadığını göstermektedir.

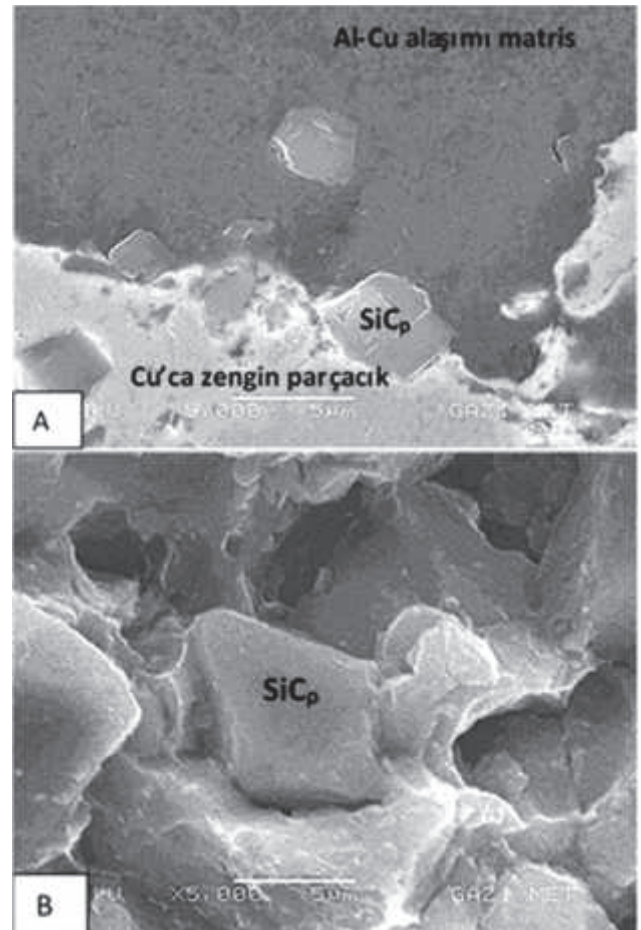
#### D. MMK<sub>p</sub> Numunelerin Optik Mikroskop Görüntüleri



Şekil 4. A)M0, B)M5, C)M10, D)M15 Mikroyapıları

Şekil 4.'de öğütme prosesinin tozların boyutlarına, Cu+SiC etkileşimlerine ve malzemenin morfolojisine etkisi açıkça görülmektedir. Şekil 4.A'da görülen mikroyapıda Al-Cu yayınımları ile oluşmuş yayınımlar (difüzyon) gradyanlarının farklı renk tonlamalarındaki Cu'ca zengin parçacıkları ve SiC'ün iri parçacıkları görülmektedir. Şekil 4.B'de ise beş saatlik öğütme sürecinde deforme olmuş ve Cu parçacığı etrafına yapışmış öğütülmüş SiC parçacıkları görülmektedir. 15 saatlik öğütme ile sağlanan Cu+SiC etkileşiminde daha ince dağılımlı SiC parçacıkların, öğütme sürecinde deforme olan Cu çevresinde sıralandığı belirlenmiştir. Al matris içinde de yer yer homojen denebilecek dağılımda SiC mevcuttur (Şekil 4.C). Şekil 4.D'de ise 15 saat öğütmenin etkisiyle genel olarak daha küçük boyutlu Cu ve SiC etkileşimleri mevcuttur. Daha ince SiC parçacıkların Cu ile etkileşimi ile oluşan karışımla birlikte daha iri SiC parçacıkların Al matriste dağıldığı görülmektedir. Bununla birlikte M0 ve M5 metal matris kompozit malzemelerdeki Cu parçacıklarda görülen Al-Cu yayınımlarındaki gradyanları M10 ve M15 malzemelerde genel olarak mevcut değildir. Ancak iri Cu parçacıklarda bu etki halen mevcuttur. Bu durum, sıcak presleme sürecinde Al-Cu ve Cu-Al yayınımlarının tamamlanmadığının belirtisi olarak görülebilir[18, 19].

#### E. MMK<sub>p</sub> Malzeme ve Kırık Yüzey SEM İncelemeleri



Şekil 5. M15 katkılı metal matrisli kompozit malzemenin ve kırık yüzeyin SEM görüntüsü.

Şekil 5.A)'daki 15 saatlik öğütmeyle hazırlanmış karışım katkısıyla üretilen MMK<sub>p</sub> malzemenin SEM görüntüsünde, Al-Cu alaşımı matris içindeki SiC<sub>p</sub> görülmektedir. Bununla birlikte M15 öğütme sürecinde Cu parçacık içinde yerleşmiş ve sıcak presleme sürecinde Al matriste tamamen çözünmemiş Cu'ca zengin parçacıktaki [9,21] seramik parçacıklar da dikkat çekmektedir. Ayrıca, Cu-Al arayüzeyinde, öğütme sürecinde Cu parçacığa yapışmış farklı boyutlarda çok sayıda seramik parçacıklar mevcuttur. Öğütme işlemi sonucunda SiC partikülleri Cu parçacık etrafını neredeyse kaplamış durumdadır. Cu'nin etrafını saran SiC partiküllerinin Al-Cu yayılımını engellediği veya yavaşlattığı düşünülmektedir. Sıcak presleme sürecine rağmen Al matris içinde Cu oranının düşük çıkmasının sebebinin bu etki olabilir. Cu ve SiC parçacıkların mekanik karıştırılıp öğütülmesindeki amaç, SiC parçacıkların Cu ca zengin bir katmanla kaplanmasını sağlamak ve bu sayede Al matrisle seramik parçacık-aluminyum metal matris arayüzey bağı arttırmaktır. Bununla birlikte, yaşlandırma ısıl işlemi ile çökelti sertleşmesi sağlayabilecek Al-Cu alaşımı matris oluşturmak diğer bir hedefdir. Ancak ulaşılabilen en fazla 15 saatlik öğütme işleminde, Cu parçacıkların yoğun olarak SiC parçacıklarla adeta kaplandığı söylenebilir. Ancak arttırılan daha uzun süreyle öğütme işlemi ile belirtilen hedeflere ulaşılabileceği söylenebilir.

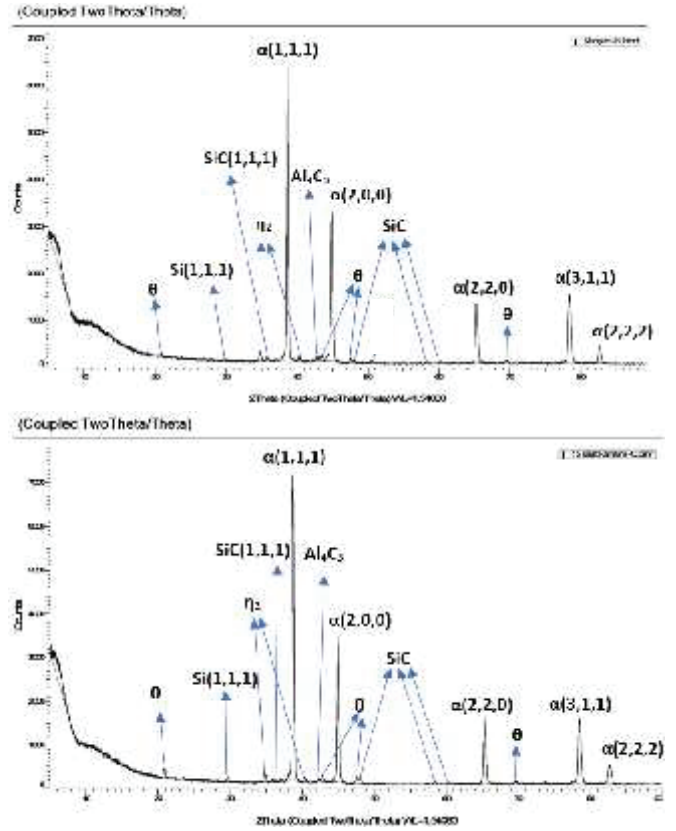
Şekil 5.B'de üretilen MMK<sub>p</sub> malzemenin ÇKD sonundaki kırık yüzey SEM görüntüsü verilmiştir. Burada görülen SiC parçacığın Al-Cu alaşımı matrisle yer yer güçlü adhesiv bağla bağlandığı söylenebilir. Bu durum, çalışmanın hedefleri bakımında olumlu etkiler oluşturabileceğini göstermektedir.

#### F. XRD Analizi

Şekil 6'da verilen XRD çalışmaları, öğütmesiz (M0), 15 saatlik öğütme ile elde edilen Cu+SiC karışım tozlar kullanılarak üretilen Al-Cu alaşımı matrisli ve SiC takviyeli MMK<sub>p</sub> malzemesinde (M15) oluşan fazlar tanımlanmıştır.

XRD analiz sonuçlarının yorumlarında yola çıkarak çalışmamızda muhtemel fazlar kesinleştirilmiştir. Norbert ve arkadaşları yaptıkları çalışmada Al-Cu faz dengesini incelemiş ve Al-Cu intermetaliklerinin XRD üzerindeki bölgelerinden bahsetmişlerdir. [22]. T/M ile üretilmiş Al-%4,7 Cu alaşımında mevcut fazlar :  $\theta$ -CuAl<sub>2</sub> ,  $\alpha$ -Al,  $\eta_2$ -Cu<sub>9</sub>Al<sub>4</sub> olarak belirlenmiştir.

M15 saat öğütme sonucunda üretilen metal matrisli kompozitlerin  $\theta$  - CuAl<sub>2</sub> fazı oranının M0 numunesine göre arttığı pik şiddetlerinden görülmektedir. Elementel Si pikinin varlığı ilgi çekici olmakla birlikte, M15 numunesinde M0 numunesine oranla daha belirgin olduğu görülmektedir.



Şekil 6. Karışım M0 Numunesi ve M15 Numunesinin XRD sonuçları

#### IV. SONUÇLAR

1. Tozların başlangıç boyutlarına göre, artan öğütme süresi ile toz boyutları azalırken, deforme olmuş pulsu parçacıkların oranı artmıştır. Öğütme işlemi sonrası Cu parçacık yüzeylerine SiC seramik parçacıkların yapıştığı belirlenmiştir.
2. Öğütme işlemi ile elde edilen karışım tozlarla üretilen kompozitlerin sertlikleri, işlemsiz (M0) kompozitlere göre daha yüksektir. Artan öğütme süresiyle hazırlanmış Cu+SiC karışım tozla üretilen kompozitlerin sertlikleri öğütme süresiyle artmıştır.
3. Yine artan öğütme süresi ile üretilen MMK<sub>p</sub>' lerin çapraz kırılma dayanımının da arttığı gözlenmiştir.
4. Onbeş saat öğütülmüş (M15) Cu+SiC karışımla üretilen Al matrisli MMK'lerdeki kırık yüzey incelemeleri, SiC takviye parçacıklarının Al-Cu alaşımı matris ile arayüzey bağının yeterince güçlü olduğunu göstermiştir.

#### V. KAYNAKÇA

- [1] Kaw, A.K., "Mechanics of Composite Materials", Crc Press, Washington, 3: 61-65 (1997).

- [2] Hull, D. ve Clyne, T.W., “An Introduction to Composite Materials”, 2nd Edition, Cambridge University Press, Cambridge, (1996).
- [3] Ateş E.A., “Toz Metalurjisi ile Üretilen AA 2024-Al<sub>3</sub>Cu Sistemlerine Yaşlandırma Isıl İşleminin Uygulanması ve Mikroyapısal Özelliklerin Araştırılması”, Yüksek Lisans Tezi, G.Ü.F.B.E, Eylül, (2012).
- [4] German, R.M., “Toz Metalurjisi ve Parçacıklı Malzeme İşlemleri”, Süleyman Sarıtaş, Mehmet Türker, Nuri Durlu, Ankara, (2007).
- [5] Ibrahim, I. A., Mohamed, F. A. And Lavernia, E. J., Particulate Reinforced Metal Matrix Composites- a review, *Journal of Materials Science*, 26, 1137-1156, (1991)
- [6] Varol, T., Pamukkale Univ Muh Bilim Derg. Baskıdaki Makaleler: PAJES-56255 |DOI: 10.5505/pajes.2017.56255
- [7] Ekinci, V. Ş. Bağcı C. Arık, H., “Effect of Al<sub>2</sub>O<sub>3</sub> Content and Milling Time on Microstructure and Mechanical Properties of Aluminum Metal Matrix”, *Experimental Techniques*, 10.1111(1747-1597), (2011).
- [8] Gazawil A. A., Gabbitas, B. Zhang D., Kong C. and Munroe, P., “Microstructure and Mechanical Properties of Ultrafine Structured Al-4wt%Cu-(2.5-10) vol.%SiC Nanocomposites Produced by Powder Consolidation Using Powder Compact Extrusion”, *Journal of Research in Nanotechnology*, Vol. 2015, Article ID 928417, (2015).
- [9] Altenpohl, D. G. “Present Structure and Future Trends in Key Materials Industries. Materials in World Perspective”: Assessment of Resources, Technologies and Trends for Key Materials Industries, Springer Berlin Heidelberg, Berlin, Heidelberg, Heidelberg p. 21–126, (1980).
- [10] Gökçe, A.. “Toz Metalurjisi Yöntemiyle Üretilen Al-Cu Alaşımlarının Mekanik Özelliklerinin Geliştirilmesi,” PhD Thesis, Sakarya University, Sakarya. (2013).
- [11] Gökçe, A., Findik, F., Kurt, A. O.. “Effects of Mg Content on Aging Behavior of Al<sub>4</sub>CuXMg PM Alloy,” *Materials and Design*, vol. 46, p. 524–31. (2013).
- [12] Gökçe, A., Findik, F., Kurt, A.O. “Sintering and Aging Behaviours of Al<sub>4</sub>CuXMg PM Alloy,” *Canadian Metallurgical Quarterly*, vol. 55, no. 4, p. 391–401. (2016).
- [13] Gökçe, A., Findik, F., Kurt, A. O. “Microstructural Examination and Properties of Premixed Al-Cu-Mg Powder Metallurgy Alloy,” *Materials Characterization*, vol. 62, no. 7, p. 730–5. (2011).
- [14] Gökçe, A., Findik, F., Kurt, A. O. Effects of Sintering Temperature and Time on the Properties of Al-Cu PM Alloy. In 7th International Powder Metallurgy Conference and Exhibition (Editors: Rahmi, Ü., Yusuf, U., Mehmet, T.), Turkish Powder Metallurgy Association, Ankara. 2014.
- [15] Toyran, O., Gökçe, A., Kurt, A. O. “Effects of Micro Level Si Addition on The Properties of Aluminium PM Alloy,” In Proceedings of The 6th International Powder Metallurgy Conference and Exhibition (Editors: Türker, M., Kalkanlı, A., Uslan, İ., Demir, T., Usta, Y., Dericioğlu, A.), Turkish Powder Metallurgy Association, Ankara. 2011.
- [16] Gupta, M., Ling, S. “Microstructure and Mechanical Properties of Hypo/Hypereutectic Al–Si Alloys Synthesized Using a Near-Net Shape Forming Technique,” *Journal of Alloys and Compounds*, vol. 287, no. 1, p. 284–94. 1999.
- [17] YILMAZ, R. “Fe-Cu-C Kompaktlarda Presleme Basıncı ve Toz Karışım Oranlarının Sertliğe ve Çekme Mukavemetine Etkisi” 4. Uluslararası Toz Metalurjisi Konferansı, 1228-1236, Sakarya, Türkiye, (2005).
- [18]Ekici, E., Gülesin, M., ve Özçatalbaş, Y., “Ön Karıştırılmış ve Sıcak Preslenmiş Al-Cu Alaşımı Toz Metal Parçalarda Kirkendall Etkisi ve Fiziksel Özelliklerinin Araştırılması”, 456-460, 6. Uluslar arası Toz Metalurjisi Konferansı ve Sergisi 05-09 Ekim ODTÜ, Ankara. 2011
- [19] Mutlu, N., Kurt, A., Özçatalbaş, Y., “Ön Karışım Al+%4,5Cu Tozlarının Alaşımlanması ve T6 Isıl İşleminin Uygulanabilirliği”, 4th International conference on materials science and nanotechnology for next generation (MSNG2017), June 28-30, Sarajevo, BOSNIA, 2017.
- [20] A Ozer, “ The microstructures and mechanical properties of Al-15Si-2.5Cu-0.5Mg/(wt.%)B<sub>4</sub>C composites produced through hot pressing technique and subjected to hot extrusion”, *Materials Chemistry and Physic*, 183, 288-296, (2016)
- [21] K. Köprülü, N. Mutlu, A. Kurt, B. Gülenç, Y. Özçatalbaş, “Al + % 4,5 Cu Ön Karışım Tozların Alaşımına Isıl İşlemlerin Etkisi, *GU J Sci, Part C, Cilt 6, Sayı 2, Sayfalar 283 – 293, 2018.*
- [22] Norbert Ponweiser, Klaus W. Richter, “New investigation of phase equilibria in the system Al–Cu–Si” [*J. Alloys Compd.* 512, 252–263, (2012).

# Cu + SiC Karışım Tozun Öğütme Süresinin Metal-Seramik Etkileşimine, Toz Boyutuna ve Morfolojisine Etkisi

Ezgican Atar \*, Damla Sarıdemir ve Yusuf Özçatalbaş  
[ezgican.atar@gazi.edu.tr](mailto:ezgican.atar@gazi.edu.tr), [damla.saridemir06@hotmail.com](mailto:damla.saridemir06@hotmail.com), [yusufoz@gazi.edu.tr](mailto:yusufoz@gazi.edu.tr)

*Metallerji ve Malzeme Mühendisliği, Teknoloji Fakültesi, Gazi Üniversitesi, 06560, Ankara, Türkiye*

**Özet-** Bu çalışmada, Cu + SiC karışım tozların öğütülme süresinin, tozların yapısına, morfolojisine ve boyutlarına etkisi araştırıldı. Bu amaçla, ağırlıkça %67 Cu ve %33 SiC tozları üç boyutlu karıştırma cihazında (Turbula) paslanmaz çelik kap içinde 15 mm çapında zirkonya bilyeler vasıtasıyla öğütülmüştür. Ortalama bilye/toz oranı 10:1 olarak yapılan öğütme işlemi, 80 dev/dak hızda ve 5 (M5), 10 (M10) ve 15 (M15) saat sürelerle gerçekleştirilmiştir. Öğütülen karışım tozların boyutları lazer parçacık boyut ölçüm cihazı ile morfolojisi ve CuSiC etkileşimleri ise optik ve tarama elektron mikroskop (SEM) çalışmaları ile karakterize edilmiştir. Bakır ve silisyum karbür tozlarının başlangıç ortalama tane boyutu ( $d_{0,5}$ ) sırasıyla 44,8 $\mu$ m ve 13,4 $\mu$ m olarak belirlenmiştir. Bu tozların belirtilen karışım oranlarındaki tane boyutu ise  $d_{0,5}=21,9$   $\mu$ m dur. Beş saatlik öğütme sonunda karışım toz tane boyutu  $d_{0,5}=14,6$   $\mu$ m'ye düşerken artan öğütme süresiyle 10 saatte  $d_{0,5}=30,8$   $\mu$ m yükselmiştir. Öğütme süresi 15 saate ulaştığında ise karışım toz tane boyutu  $d_{0,5}=26$   $\mu$ m düşüş göstermiştir. Düşük öğütme süresinde, iri Cu parçacıklara ( $Cu_p$ ) mekanik olarak girişim yapmış küçük tane boyutunda SiC parçacıkları ( $SiC_p$ ) belirlenmiştir. 15 saatlik öğütme sonunda ise Cu parçacıkların kısmen pulcuksu şekle dönüştüğü ve Cu-SiC girişim oranının azaldığı belirlenmiştir. 15 saatlik öğütülmüş tozun SEM incelemesinde ise  $SiC_p$ 'lerin yüzeylerine yapışmış mikron altı ve birkaç mikron boyutlarında  $Cu_p$ 'lerle kaplandığı belirlenmiştir.

**Anahtar Kelimeler** — Toz Metalurjisi, Öğütme, Cu+SiC, Metal-Seramik Etkileşimi

## The Effect of Milling Time of Cu + SiC Mixed Powders on Powder Size, Morphology and Metal-Ceramic Interaction

**Abstract** -In the current research, effect of milling time on the structure, particle size and morphology of Cu + SiC mixed powders was investigated. For this purpose, 67 wt% Cu and 33 wt% SiC powders were milled in zirconia balls with a diameter of 15 mm in a stainless steel vessel at a three-dimensional mixing apparatus (Turbula). The milling operation at ball-to-powder ratio of 10:1 was carried out at 80 rpm for 5 (M5), 10 (M10) and 15 (M15) hours. The dimensions of the milled mixture powders were characterized by laser particle size meter and, morphology and Cu-SiC interactions of milled powders were investigated by optical and scanning electron microscope (SEM). The initial average particle size ( $d_{0,5}$ ) of copper and silicon carbide powders was determined as 44.8 $\mu$ m and 13.4 $\mu$ m, respectively. The particle

size of these powders at the specified mixing ratios was  $d_{0,5} = 21.9$   $\mu$ m. At the end of the five-hours milling, the powder particle size decreased to  $d_{0,5} = 14.6$   $\mu$ m and then particle size increased ( $d_{0,5} = 30.8$   $\mu$ m for 10 hours) with increasing milling time. When the milling time reached 15 hours, the mixed powder particle size decreased to  $d_{0,5} = 26$   $\mu$ m. At the low milling time, smaller SiC particles ( $SiC_p$ ) were mechanically penetrated to coarse Cu particles ( $Cu_p$ ). At the end of the 15-hour milling, Cu particles were partially converted to flake-like shape and Cu-SiC penetration ratio decreased. In the SEM study of the 15-hours milled powder, it was determined that the Cu particles with submicron and several micron sizes were deposited on the surfaces of the SiC particles.

**Keywords-** Powder Metallurgy, Milling, Cu+SiC, Metal-Ceramic Interaction

### I. GİRİŞ

Metal Matrisli Kompozit (MMK) malzemeler mühendislik uygulamalarında yüksek dayanç ve düşük özgül yoğunluk istenen yerlerde yaygın olarak kullanılmaktadır. Özellikle parçacık takviyeli ve Alüminyum alaşımı metal matris yapıyla üretilen kompozit malzemeler, yüksek aşınma direnci ve özgül dayanım gerektiren mühendislik uygulamalarında kullanılır. Metal matrisli parçacık takviyeli kompozit ( $MMK_p$ ) malzemelerde seramik parçacık ve metal matris arayüzünde yeterince bağ oluşturmak üretilen  $MMK_p$  malzemenin performansı bakımından önem arz eder [1-3].

Metal matris ve seramik takviye parçacığı arayüzey bağının geliştirilmesi halen çalışılan araştırma konularındandır. Bu amaç doğrultusunda seramik parçacıkların matrisle metalurjij bağ kurabilecek Cu, Ni vb. Metallerin elektroliz vb. Yöntemlerle kaplanması [4], seramik parçacıkların yüzeylerinin kimyasal aktivasyonunu artırma işlemleri, üretilen  $MMK_p$  malzemeye uygulanan ekstrüzyon, haddeleme gibi sıcak deformasyon işlemlerinin uygulanması gibi işlemler uygulanır. Bununla birlikte in-situ yöntemi ile kompozit malzeme üretimi [1] bu amaçla uygulanan diğer bir  $MMK_p$  üretim yöntemidir. Yapılan uygulamada genellikle seramik parçacık ile metal matris arasında adhesive bağ oluşur. Bu bağın özellikleri, bağlanan malzemelerin özellikleriyle ilgilidir [5-7].  $MMK$  malzeme üretiminde bu arayüzeyde genellikle kimyasal reaksiyonlarla ve her iki parçacığın atomlarından

oluşan intermetalikler ise kırılganlıkları sebebiyle istenmezler [8, 9].

Son zamanlarda Toz Metalurjisi (T/M) yöntemi ile MMKp malzeme üretimi en hızlı gelişen imalat yöntemlerinden birisi olmuştur. TM ile üretim yöntemi, karıştırılmış metal tozlarının, oda sıcaklığında veya yüksek sıcaklıklarda, üretilecek parça şekli ve boyutlarına sahip kalıp içinde preslenerek şekillendirme ve ardından belirli bir sıcaklıkta sinterleme ile gerçekleştirilen bir imalat yöntemidir. Toz metal parçalar haddeleme, döküm gibi geleneksel imalat yöntemleri ile üretilen malzemelere göre bazı değişik ve avantajlı özelliklere sahiptir. Bu avantajlar, üretimi zor olan alaşımları daha kolay üretme, karmaşık şekilli parçaların imalat kolaylığı, yoğunluk kontrolü ve ekonomiklik gibi özelliklerdir [10-12].

Alüminyum ve alaşımları, bazı korozif ortamlarda bozulmaya karşı iyi mekanik özellik direnci ile düşük yoğunluklarından dolayı kimya, otomotiv, gıda, havacılık ve denizcilik endüstrisindeki birçok uygulamada istenen ve kullanılan malzemelerdir [13]. Al matrisli partikül takviyeli kompozitlerin, ticari Al alaşımları ile kıyaslandığında artan sertlik, yüksek aşınma direnci, mukavemetinin uygunluğu, titreşim azaltıcı ve düşük ısı yayılım katsayısı gibi malzemelerde istenilen üstün özellikleri bir arada bulundurması nedeniyle bu malzemeler daha da önemli olmuştur. Kompozit malzemelerin üretiminde karşılaşılan temel problem, matris ile takviye malzemeleri arasında etkili bir bağlanmanın elde edilememesidir. Nispeten düşük sıcaklıklarda yapılan TM üretim yöntemi, teorik olarak arayüzey kinetiğinin daha iyi kontrol edilmesini sağlar [14,15].

Mekanik öğütme (MÖ) yöntemi kullanarak matrisi oluşturan metal ile seramik partikülleri, mekanik ve adhesiv bağ ile birbirine bağlayacak prosesin uygulanmasının, ara yüzey bağını arttırdığına dair çalışmalar mevcuttur. Uygulanan mekanik öğütme prosesinin MMKp üretiminde kullanılması, üretilen kompozit malzemenin mekanik özelliklerini arttırdığı yapılan çalışmalarda gözlemlenmektedir [16,17].

Bu çalışmanın amacı doğrultusunda matris partikül ara yüzey bağlarını kuvvetlendirmek için Cu+SiC karışımına belirli sürelerde mekanik öğütme uygulanmıştır. Bu sayede öğütülen ve kırılan SiC yüzeylerindeki aktiflikten de yararlanarak Cu parçacıklarla kaplanmaya (sıvanmaya) çalışılmıştır. Bu yöntemle Cu kaplanmış SiC seramik parçacıklar ile Al matris arasında ise sinter sürecinde Al+Cu alımı matris oluşturulmak istenmiştir.

## II. DENEYSEL ÇALIŞMALAR

### A. Malzeme

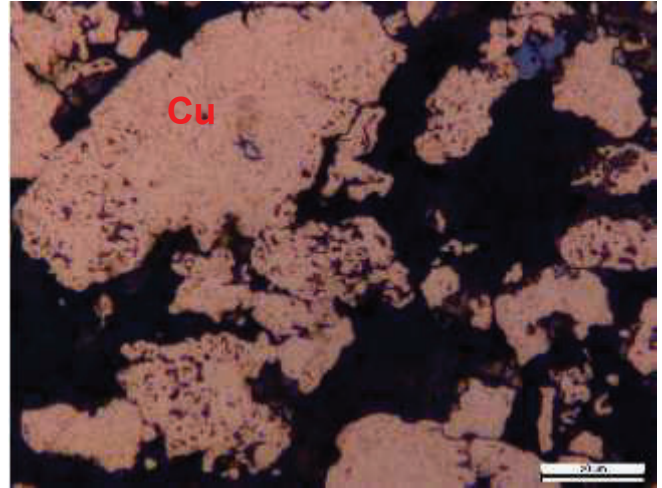
Deneysel çalışmalarda, atomizasyon yöntemiyle üretilmiş %99,7 saflıkta alüminyum ve %99,6 saflıkta elektroliz yöntemi ile üretilmiş dentiritik bakır tozları kullanılmıştır. Cu toz tane boyutu ise 140 µm altında ve ortalama olarak  $d_{0,5}=45$  µm'dur. SiC tozu ise 90 µm altı ve ortalama  $d_{0,5}=13$  µm dir.

### B. Metot

Bu amaçla, ağırlıkça %67 Cu ve %33 SiC tozları üç boyutlu karıştırma cihazında (Turbula) paslanmaz çelik kap içinde 15 mm çapında zirkonya bilyeler vasıtasıyla öğütülmüştür. Ortalama bilye/toz oranı 10:1 olarak yapılan öğütme işlemi, 80 dev/dak hızda ve 5 (M5), 10 (M10) ve 15 (M15) saat sürelerle gerçekleştirilmiştir. Öğütülen karışım tozların boyutları lazer parçacık boyut ölçüm cihazı ile morfolojisi ve Cu-SiC etkileşimleri ise optik ve tarama elektron mikroskop (SEM) çalışmaları ile karakterize edilmiştir.

## III. DENEY SONUÇLARI VE TARTIŞMA

### A. Başlangıç Tozların Karakterizasyonu

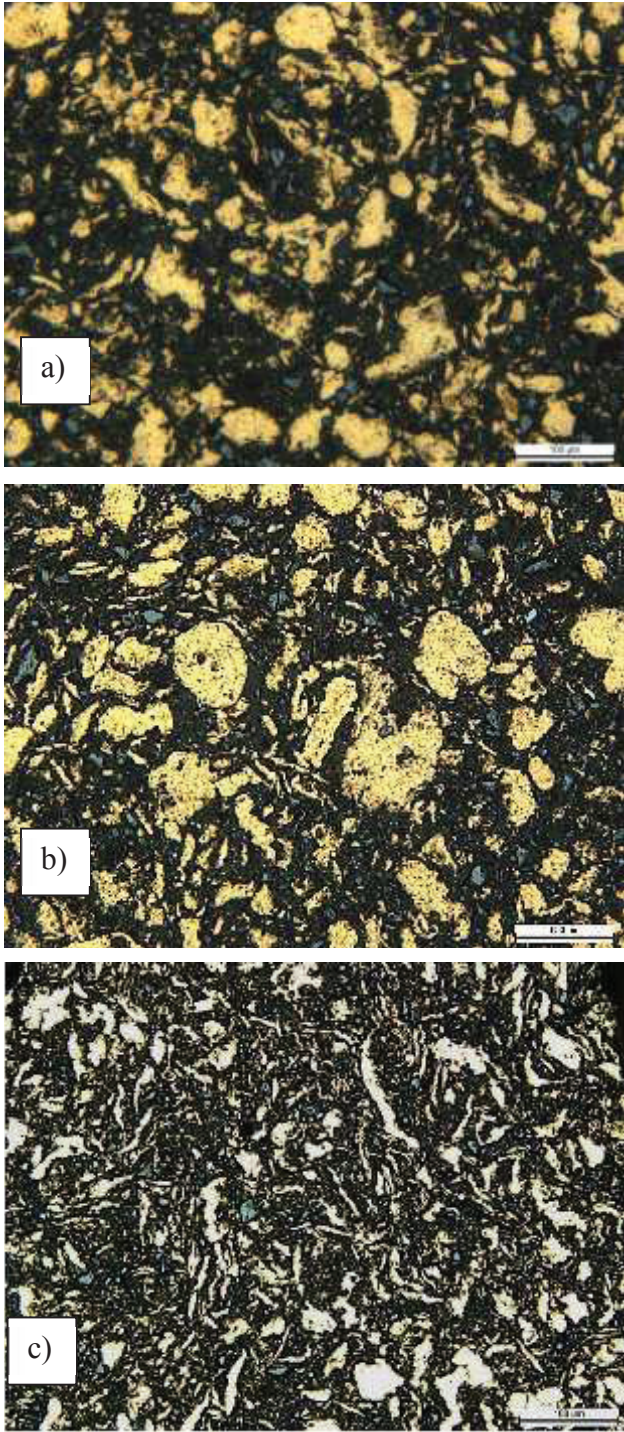


Şekil 1. Öğütmede kullanılan Cu toz parçacıklar

Şekil 1'de öğütme öncesi Cu parçacıkların optik mikroskop görüntüleri verilmiştir. Epoksi reçineye gömülerek yapılan parlatma sonrası görüntüde, yer yer Cu parçacık dentiritleri arası boşluklar koyu renk tonunda görülmektedir.

### B. Cu+SiC Karışım Tozun Öğütme Süresine Bağlı Toz Morfolojisindeki Değişim

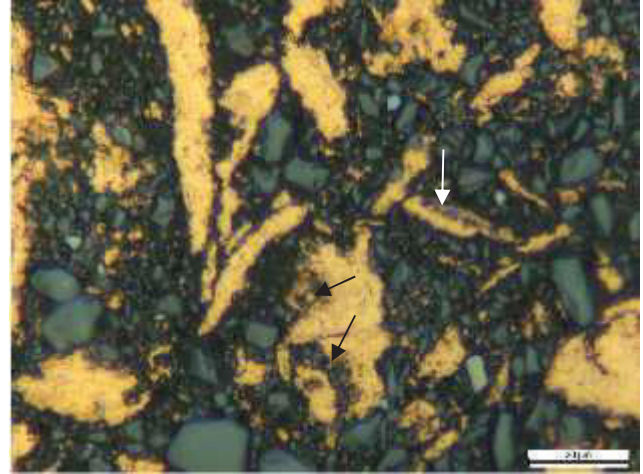
Şekil.2'de ağırlıkça %67 Cu ve %33 SiC içeren toz karışımın, 5, 10 ve 15 saat süresince öğütülmesi sonucu elde edilen tozların optik mikroskop görüntüleri verilmiştir. Beş saat öğütme yapılan (M5) karışımında henüz belirgin öğütme etkisi mevcut değildir. Özellikle Cu parçacıklar genel olarak iri ve yumrusal formdadır. Bununla birlikte az oranda da olsa deforme olmuş yassı parçacıklar da mevcuttur. Artan öğütme süresiyle birlikte (M10) yassı küçük Cu parçacıkların oranı artmaktadır. Ayrıca SiC parçacıklarında (koyu gri) öğütmenin daha etkin olduğu görülmektedir. Zira M10 işlemi ile daha küçük boyuttaki SiC oranında artış olmuştur. Onbeş saatlik öğütme (M15) sonunda ise özellikle Cu parçacık morfolojisinin başlangıç toz biçim ve boyutuna göre önemli oranda değiştiği ve yassı küçük Cu parçacıklara dönüştüğü açıkça görülmektedir. Bu öğütme süresinde SiC parçacıklarının da önemli oranda öğütmeden etkilendiği ve parçacık boyutunun önemli oranda küçüldüğü görülmektedir.



Şekil 2. Cu+SiC Karışım tozun öğütme süresine bağlı morfolojisindeki değişim a)M5 b)M10 ve c)M15

Artan öğütme süresiyle birlikte zirkonya bilyaların kinetik enerjisine maruz kalan ve bu sayede plastik deforme olan Cu parçacıkların birlikte SiC parçacıkların da kırılarak öğütüldüğü görülmüştür. Bu süreç içinde Cu/SiC/Cu, Cu/Cu ve Cu/SiC

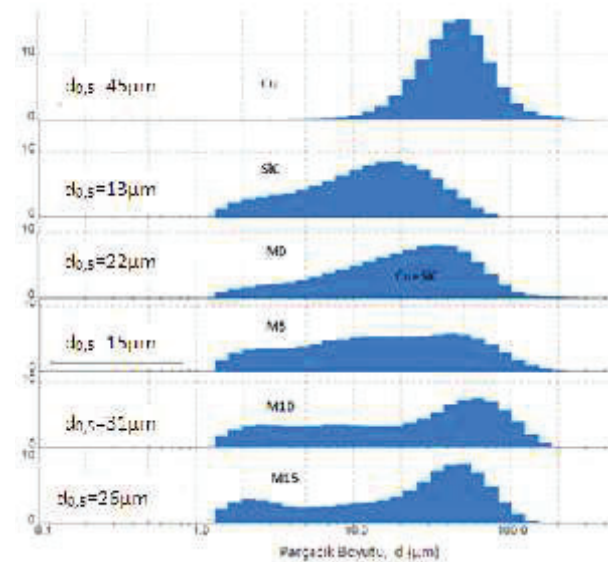
etkileşimleri belirlenmiştir. Elektroliz yöntemiyle üretilmiş Cu parçacıkların dentirit kolları arasında yerleşen özellikle küçük boyutlu SiC parçacıklarının Cu/SiC/Cu etkileşimi gösterdiği Şekil 3'de oklarla gösterilmiştir. Bunun dışında yoğun olarak Cu parçacıkların yüzeyine mekanik girişim yapmış bir dizi küçük boyutlu SiC parçacıklarının ise Cu/SiC etkileşimi gösterdiği ve bu durumun daha yaygın olduğu belirlenmiştir (Şekil 3).



Şekil 3. 15 saat öğütme işlemi sonunda Cu/SiC etkileşimi

#### C. Öğütme Süresine Bağlı Toz Tane Boyut Değişimi

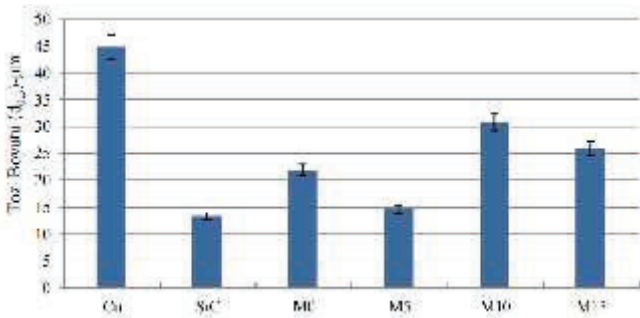
Şekil 4'de başlangıç tozların, karışım tozların ve öğütme süresinin Cu+SiC karışım tozun tane boyut dağılımları verilmiştir.



Şekil 4. Öğütme süresinin toz tane boyut dağılımına etkisi

Burada, en büyük parçacık dağılımının Cu tozlarda olduğu ve  $d_{0,5}$  ortalama toz dağılımının 45µm civarında olduğu görülmektedir. SiC toz ilavesi ile öğütmesiz karışım tozun (M0)

toz dağılımının, ağırlıkça Cu tozu etkin olmasına rağmen, SiC tozun düşük özgül yoğunluğu sebebiyle artan hacimce SiC oranı, Cu+SiC karışım tozunda toz boyut dağılımını sola doğru kaydırmıştır (Şekil 4). Bu sayede M0 tozun ortalama toz boyutu 22µm civarındadır. Bu karışımın beş saatlik öğütme işlemi sonunda, iri toz oranının azaldığı küçük toz oranının ise artarak ortalama toz boyutunun 15µm'a düştüğü görülmektedir (Şekil 4 ve Şekil 5). Bu durumun muhtemel olarak iri SiC parçacıkların öğütülmesinden kaynaklandığı düşünülmektedir. Artan öğütme süresiyle birlikte (M10) kaynaklanan Cu tozları sebebiyle iri toz oranında artış gözlenirken yaklaşık 20µm altı toz oranında azalma görülmüştür. 15 saatlik öğütme sonunda ise, iri toz oranı artarken iri toz boyutunun küçüldüğü görülmektedir. Bu süreç ise öğütmede kırılma süreci olarak değerlendirilebilir.

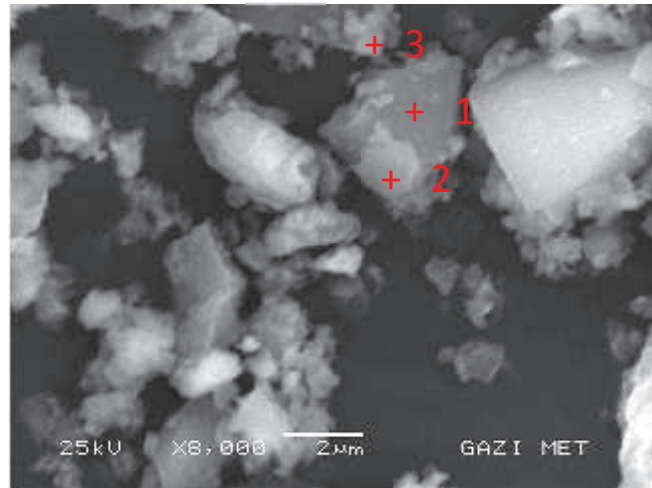


Şekil 5. Başlangıç ve karışım öğütülmüş tozların ortalama toz tane boyut dağılımı.

#### D. Öğütülmüş Tozların SEM/EDS İncelemeleri

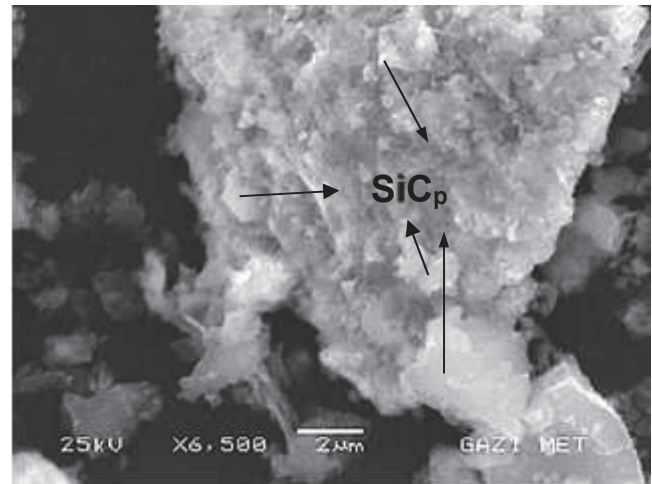
Şekil 6'da 15 saat öğütülmüş Cu+SiC karışım tozların SEM görüntüsü ve bazı parçacıkların EDS analizleri verilmiştir. Genel olarak burada dikkat çeken esas husus, SiC parçacıklarında belirli oranlarda Cu içeriği bulunmasıdır. 1 nolu analiz noktasında yaklaşık %13 Cu belirlenmiştir. Bu bölgede SiC parçacığı tamamen Cu'la kaplanmamış dahi olsa, mikron altı boyutlarda Cu varlığı mevcuttur. SiC parçacığın daha kalın ve belirgin miktarda Cu'la kaplandığı bölge 2 numaralı analiz bölgesidir. Buradaki açık gri tonlamalı parçacık muhtemel Cu'ca zengin parçacıktır ve adhesiv etkiyle SiC parçacık yüzeyine bağlanmıştır.

Bununla birlikte iri Cu parçacıkların yüzeylerine mekanik veya adhesiv etkiyle bağlanmış SiC parçacıkları Cu/SiC etkileşimi yapmıştır. Şekil 7'de gösterilen durum, birkaç mikrometreden mikron altı boyutlara kadar farklı boyut aralığındaki SiC parçacıkların Cu yüzeyinde yoğun olarak tutunduğu görülmektedir. Öğütme sürecinde bu tür Cu parçacıklardan kopan veya ayrılan SiC parçacıkların oluşturduğu adhesiv etkiye göre, belirli oranlarda Cu içeriyor olması muhtemeldir.



Bölge	Ağırlıkça %Cu	Ağırlıkça %SiC
1	%12,897	%87,103
2	%7,819	%91,333
3	%3,504	%96,497

Şekil 6. M15 öğütülmüş tozun SEM/EDS analizleri



Şekil 7. M15 öğütülmüş tozda Cu/SiC etkileşimi

#### IV. SONUÇLAR

- Öğütmenin ilk sürecinde özellikle iri SiC parçacıkların kırılarak karışım tozun ortalama tane boyutunun azaldığı belirlenmiştir. Artan öğütme süreciyle birlikte, özellikle Cu parçacıkların kaynaşması ve/veya iri Cu parçacıkların yüzeyine ince SiC parçacıkların yapışması ile ortalama parçacık tane boyutu artmıştır.

- Tozların başlangıç boyutlarına göre; artan öğütme süresi ile toz boyutlarının azaldığı görülmüştür. Onbeş saate kadar artan öğütme süreci sonunda ortalama tane boyutunun azalmaya başladığı, Cu parçacıklarda pulcuksu formların oluştuğu görülmüştür.
- 15 saat öğütme işleminde SiC parçacıkların yüzeyine yapışmış birkaç mikrometre boyutlarında Cu tabakacıklara veya SiC parçacıklarda Cu'ca zengin yüzeylere rastlanmıştır.

## V. KAYNAKÇA

[1] Ozcatalbas Y., "Investigation of The Machinability Behaviour of Al4C3 Reinforced Al Based Composite Produced by Mechanical Alloying Technique", *Composites Science and Technology*, Vol.63, pp.53-61, (2003).

[2] Kaw, A.K., "Mechanics of Composite Materials", Crc Press, Washington, 3: 61-65 (1997).

[3] Hull, D. ve Clyne, T.W., "An Introduction to Composite Materials", 2nd Edition, Cambridge University Press, Cambridge, (1996).

[4] Ibrahim, I. A., Mohamed, F. A. And Lavernia, E. J., Particulate Reinforced Metal Matrix Composites- a review, *Journal of Materials Science*, 26, 1137-1156, (1991).

[5] Dariusz M. J., Chmielewsk M., Agata S. N., "The Influence of the Particle Size on the Adhesion Between Ceramic Particles and Metal Matrix in MMC Composites", *Journal of Materials Engineering and Performance*, Volume 25, Issue 8, pp 3139–3145, (2016).

[6] Chmielewski, M. Nosewicz, S. Pietrzak, K. J. Rojek, A. "Sintering Behavior and Mechanical Properties of NiAl, Al<sub>2</sub>O<sub>3</sub>, and NiAl-Al<sub>2</sub>O<sub>3</sub> Composites", *J. Mater. Eng. Perform.*, 23, p 3875–3886 , (2014).

[7] Weglewski, W. Basista M., Manescu, Chmielewski, A. "Effect of Grain Size on Thermal Residual Stresses and Damage in Sintered Chromium–Alumina Composites", *Measurement and Modeling, Compos. Part B*, 67, p 119–124, (2014).

[8] Olesinska, W. Kalinski, D. Chmielewski, M. Diduszko, R. "Influence of Titanium on the Formation of a Barrier Layer During Joining an AlN Ceramic with Copper by the CDB Technique", *J. Mater. Sci.*, 2006, 17, p 781–788

[9] Finnis, M.W., "The Theory of Metal-Ceramic Interfaces", *J. Phys.*, 8, p 5811–5836, (1996).

[10] German, R. M., Sarıtaş S., Türker M., "Toz Metalurjisi ve Parçacıklı Malzeme İşlemleri" ISBN: 978-975-92463-2-7, Uyum Ajans, Ankara.

[11] Gökçe, A., Findik, F., Kurt, A. O. "Microstructural Examination and Properties of Premixed Al-Cu-Mg Powder Metallurgy Alloy," *Materials Characterization*, vol. 62, no. 7, p. 730–5. (2011).

[12] Köprülü, K. Mutlu, N. Kurt, A. Gülenç, B. Özçatalbaş, Y., "Al + % 4,5 Cu Ön Karışimli Tozların Alaşımına Isıl İşlemlerin Etkisi, GU J Sci, Part C, 6(2): 283-293 (2018)

[13] Özçatalbaş, Y. Arık, H. "Mekanik Alaşımlama Yöntemi ile Üretilen Al-Al4C3 Kompozit Malzemenin İşlenmesinde

Talaş Oluşumu", 3. Uluslararası Toz Metalurjisi Konferansı, Türkiye/Ankara, (2002).

[14] Gazawi, A. A. Gabbitas, B. Zhang, D. Kong C., "Microstructure and Mechanical Properties of Ultrafine Structured Al-4wt%Cu-(2.5-10) vol.%SiC Nanocomposites Produced by Powder Consolidation Using Powder Compact Extrusion", *Journal of Research in Nanotechnology*, Vol. 2015, Article ID 928417, (2015).

[15] Ekinci, V. Ş. Bağcı, C. Arık, H. "Effect of Al<sub>2</sub>O<sub>3</sub> Content and Milling Time on Microstructure and Mechanical Properties of Aluminum Metal Matrix", *Experimental Techniques*, 10.1111, (1747-1597), (2011).

[16] Alam S. N., Singh, H. "Development of copper-based metal matrix composites: An analysis by SEM, EDS and XRD", *Compositional Analysis Supplement*, 8-12, (2014)

[17] Ozer, A., "The microstructures and mechanical properties of Al-15Si-2.5Cu-0.5Mg/(wt.%)B<sub>4</sub>C composites produced through hot pressing technique and subjected to hot extrusion", *Materials Chemistry and Physics*, 183, 288-296, (2016)

# Mechanical and Corrosion Properties of Sn-Zn Alloys Used in Electronics Industry

Fazıl HÜSEM<sup>1\*</sup>, Fatma MEYDANERİ TEZEL<sup>1\*</sup> and Salih BEKTAŞ<sup>1\*</sup>

<sup>1</sup>Department of Metallurgy and Materials Engineering, Faculty of Engineering, Karabük University, 78050, Karabük, Turkey

\*Corresponding author: fazilhusem@karabuk.edu.tr; fatmameydaneri@karabuk.edu.tr; bektassalih25@gmail.com

**Abstract**— In this study, it is aimed to form alloys by combining Sn and Zn elements by casting method. Microstructural properties of Sn-50 wt.% Zn and Sn-80 wt.% Zn alloys were examined with SEM, EDX, XRD devices. Average micro hardness values of Sn-[x] wt. % Zn [x=50 and 80] alloys were measured to be 62.1 and 49.2 (Hv<sub>0.05</sub>). According to these results, micro hardness values only depend on the composition, and decrease with increasing of Zn composition. Mechanical properties (yield, elongation, elongation) were also obtained by using a tensile tester. The tensile test results for Sn-50 wt.% Zn and Sn-80 wt.% Zn indicating that the sample with the best mechanical properties is Sn-50 wt.% Zn. In addition, the tensile value obtained for the Sn-50 wt.% Zn sample is 78.26 MPa, the unit strain is 5.8% and the yield stress is 53.76 MPa. Also, the corrosion behavior of Sn-50 wt.% Zn and Sn-80 wt.% Zn alloys was determined by applying the mass loss corrosion test.

**Keywords**— Mechanical properties, Microstructure, Corrosion

## I. INTRODUCTION

Sn-Zn based alloys are an alloy group of particular interest as lead-free solder in the electronics industry. Considering the characteristics of solder alloys, they are producible, their reliability and environmental suitability are remarkable; such as melting temperatures, solder ability, flow ability, density, thermal and electrical properties, corrosion and oxidation behaviour, surface tension, rework ability and cost. Lead-free solder alloys are also sensitive to environmental and human health and are among the main reasons for preferring these alloys. Sn-Zn solders have a variety of fascinating properties such as low melting temperature at 198 °C. In addition to these, it includes most of the physical properties of the solder alloy related to soldering, such as melting degree, solderability, flowability, density, thermal and electrical properties, corrosion and oxidation behaviour, surface tension, rework ability and cost. The reliability of a solder alloy to be first and second level packaging is based on the elastic modulus, tensile stress, and shear strength, fatigue and creep behaviour, mainly the coefficient of thermal expansion.

In addition, in the metal coating industry, Zn-Sn alloys are now used as protective coatings on ferrous base metals. Low cost Zn-Sn coatings show high corrosion resistance and are seen as promising candidates to replace toxic cadmium and allergenic nickel coatings [1-3].

## II. EXPERIMENTAL PROCEDURE

The cavity mould cavity is set for four cylindrical samples. The mould cavity dimensions for each sample are  $\varnothing = 20$  mm,  $h = 170$  mm. The amounts of the tin (Sn) and zinc (Zn) metals were calculated and melted in the melting furnace in the graphite crucible. The melting was heated to about 100 °C from the melting temperature of the sample. After mixing several times, the homogenous molten obtained was poured into the mould.

### A. Microstructure Properties

Surface morphology and composition analysis of the samples were investigated (Zeiss Ultra Plus SEM) and (EDX) spectrometer, respectively. To obtain the SEM images, Struers brand Discotom 100 and Secotom 50 devices were used to cut the samples. With Tegramin 30 automatic sanding and polishing device, transverse sections were ground flat with SiC papers and mechanically polished using 6  $\mu\text{m}$ , 3  $\mu\text{m}$ , 1  $\mu\text{m}$ , and 1/4  $\mu\text{m}$  diamond paste. Then, etching was carried out with a mixture of 49% H<sub>2</sub>O, 1% H<sub>2</sub>SO<sub>4</sub> and 2 g CrO<sub>3</sub>. Ratio of chemical compositions was measured by an EDX spectrometer attached to the SEM.

### B. Mechanical and Microhardness Properties

The axial and variable forces are applied to circle or rectangular test piece with dimensions compatible with standards by installing to the traction device. The pulling device is mainly; It consists of two jaws that can move up and down relative to each other, two jaws to which the test piece is connected, and units that measure these two sizes, which give them movement or strength. In order to apply the tensile test to the samples, firstly, the specimen was processed to be a specimen of the tensile test, which has a diameter of ( $d_0$ ) = 10.2 mm, cross-sectional area ( $A_0$ ) = 81.71 mm<sup>2</sup>, length ( $L_t$ ) = 160 mm and round section according to the standards in the CNC machine. The tensile test of the specimen prepared according to the standards was carried out at room temperature (25 °C) with a Zwick / Roell Z600 tensile testing device.

The Vickers hardness value is the portion of the test load expressed in kg (mm<sup>2</sup>) to the trace area. Vickers hardness values of the samples were determined by QNESS Q10 A + brand Hardness Tester. After the load is removed, the hardness value is calculated by making the measurement diagonal.

$$H_V = \frac{2F \sin(\phi/2)}{d^2} \quad (1)$$

where  $\phi$  is the indenter apex angle, F is the applied load and d is the average length of diagonals. For micro hardness measurements, 100 g load was applied for 15 seconds.

### C. Corrosion Properties

Firstly, the initial mass and area of the samples are calculated. Then, 3.5% salt is added to the pure water and saline solution is prepared. Samples prepared for corrosion are immersed in solution and removed every 2 days. It is dried after removal. In order to attenuate the corrosion particles present on the surface, it is first kept in 250 ml of ethyl alcohol for 1 minute, then kept in 250 ml of acetone for 1 minute and removed. After removal, the sample surface is cleaned with a toothbrush. Then all these operations are applied every 2 days for 10 days. At the end of every 2 days, the weight is measured and the mass loss is calculated.

### III. CONCLUSIONS

The microstructures of Sn- [x] wt.% Zn [x = 50 and 80] were visualized with SEM and SEM images with a magnification factor of 2,000x. are given in Fig.1. According to the Zn ratio, Zn grains are formed as islets. The composition analysis was determined from light grey (1) and dark grey (2) regions. However, Zn was activated by oxygen in the casting stage and some oxygen was mixed in the structure and showed accumulation in the grain boundaries.

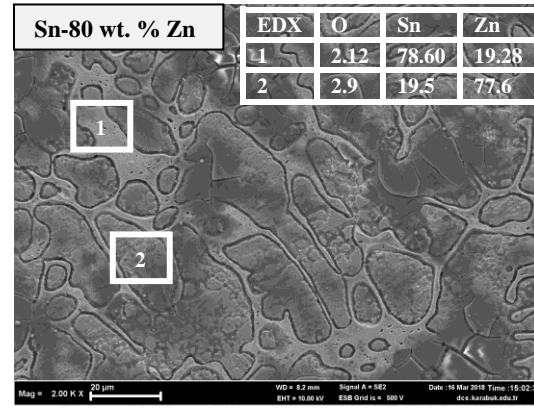
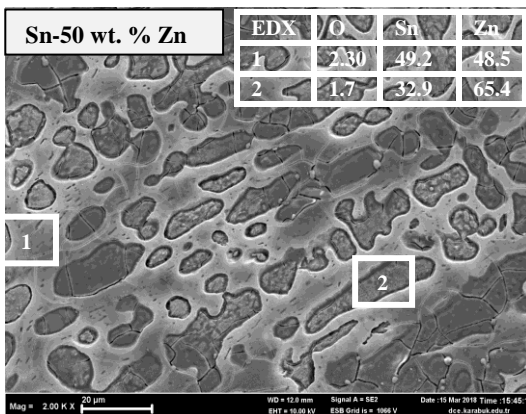


Fig. 1 SEM images and EDX analyses of Sn-x wt. % Zn [x= 50, 80] alloys.

Two tensile samples were prepared for each composition of Sn-x wt. % Zn [x=50 and 80] and subjected to tensile testing. The average values of 2 separate results were determined and the applied load, tensile strength, elongation amount and yield strength of the alloys were determined and given in Table 1. Accordingly, the tensile and yield strength of the Sn-50% wt. Zn alloy is higher than the tensile and yield strength of the Sn-80% alloy. That is, as the amount of Zn in the alloy increases, the tensile strength and yield strength of the alloy are reduced.

Table 1. Mechanical Properties of Sn-x wt. % Zn [x=50 and 80] alloys.

Samples	Peak Load (kN)	Peak Stress (MPa)	Elongation	Yield
Sn-50 wt.% Zn	5.60	71.4	0.030	47.02
Sn-80 wt.% Zn	4.36	55.5	0.016	39.45

Micro hardness measurements of Sn-[x] wt.% Zn [x=50 and 80] alloys were calculated to be average values of micro hardness measurements of Sn and Zn phases, and Sn-Zn grain boundaries in microstructures. Solidification conditions of Sn-[x] wt.% Zn [x=50 and 80] alloys are same. So, micro hardness values only depend on the composition, and increase with increasing of Zn composition. Vickers micro hardness values were calculated by taking 5 measurements for each sample and given in Table 2.

Table 2. Microhardness values of Sn-[x] wt.% Zn [x=50 and 80] alloys.

	Micro Hardness Scale	Hardness
Sn-50 wt.% Zn	Hv 0.05	62.7
Sn-80 wt.% Zn	Hv 0.05	49.1

For Sn-50 wt.% Zn alloy, we initially weighed 1.9623 g and have 1.8378 cm<sup>2</sup> area, for Sn-80 wt.% Zn alloy, initially 2.0553 g weight and 2.1205 cm<sup>2</sup> area samples. Corrosion rates were calculated by measuring the mass losses of the samples in %3.5 salt water for every 2 days and are given in Fig.2. According to this, Sn-80 wt.% Zn alloy has a higher resistance to corrosion than Sn-50 wt.% Zn alloy. That is, as the amount of Zn in the alloy increases, the corrosion resistance of the alloy increases.

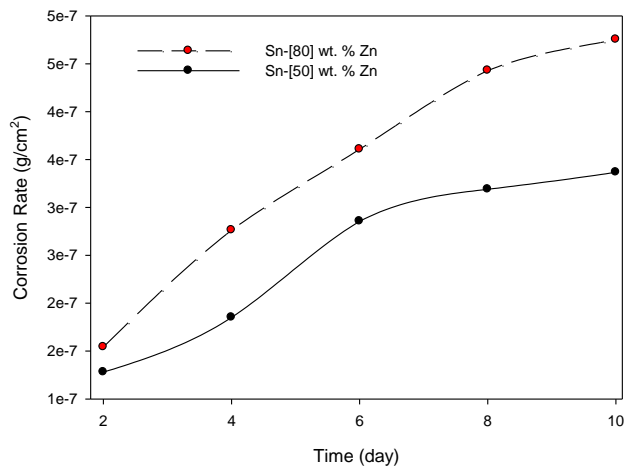


Fig. 2. Corrosion Rates of Sn-x wt.% Zn [x= 50, 80] alloys.

#### REFERENCES

- [1] K. Suganuma, S.H. Huh, K. Kim, H. Nakase, Y. Nakamura, *Materials Transactions*, 42 (2) (2001) 286–291.
- [2] M.O. Alam, Y.C. Chan, K.N. Tu, *Chemistry of Materials*, 15 (23) (2003) 4340–4342.
- [3] M.O. Alam, Y.C. Chan, K.N. Tu, *Journal of Applied Physics*, 94 (12) (2003) 7904–7909.

# Effect of Integration of Carbon Nanotubes (CNTs) on Flexural Properties of Thermoset Composites (ISLAC'18/UHAKS18)

Pınar Çolak, Erdinç Günaydin, Kemal Kadioğlu, Özgür Demircan\*

\* Department of Metallurgical and Materials Engineering, Ondokuz Mayıs University, Samsun, 55000, Turkey

\* Corresponding author: ozgur.demircan@omu.edu.tr

**Abstract**—In this study, the effect of carbon nanotubes (CNTs) addition on the mechanical properties of glass fiber reinforced composite materials was investigated. Multi walled carbon nanotubes (MWCNTs)/glass fiber/epoxy resin were used to fabricate the thermoset composites using resin transfer molding (RTM) method. As a result of this study, it was observed that samples containing of MWCNTs in the 0° direction had a higher tensile strength of 14% compared to those without MWCNTs. At the same time, samples with MWCNTs in the 90° direction were found to have the best bending modulus, strength, and 97% and 58% increase in flexural modulus and strength compared to samples without MWCNTs.

**Keywords**— Glass fiber, carbon nanotube, mechanical properties, composite materials

## I. INTRODUCTION

Nanocomposite materials are obtained as a dispersion in a nanometer dimension within one second phase and are defined as at least two phase material groups. Carbon nanotube is an allotropic form of carbon element [1]. In other words, they are obtained by cylindrical wrapping of plates in the form of honey pellets. In shapely carbon nanotube structures, atoms are connected to each other by sp<sup>2</sup> (like graphite), atoms form hexagonal geometry, and each atom has only three neighbours. Carbon nanotubes have high resistance to impacts such as compression, bending, twisting due to hole structures and high length / diameter ratios [2]. Nanotubes can have diameters changing from 1 to 100 nm and lengths in micrometers [3]. There are single-layer (single-walled) or multi-layer (multi-walled) carbon nanotubes. Previous scientific investigations have demonstrated that multi-walled carbon nanotubes (MWCNTs) have higher resistance to chemicals than single-walled carbon nanotubes (SWCNTs) [4]. Carbon nanotubes are one hundred times stronger than steel, and weight is one sixth. Steel is harder at the same time, but as flexible as plastic. Therefore, it is the most robust material known to have high corrosion resistance [5]. The measured specific tensile strength of a single layer of a multi-walled carbon nanotube can be as high as 100 times compared to steel [6]. Because of these properties, CNTs have been used. In addition, if we look at the structure and properties of Epoxy; the low molecular weight of liquid immature epoxy resins gives them superior molecular mobility during processing. High strength thermoset polymers

such as epoxy are added to glass fiber to increase mechanical strength and thermal stability. The addition of nanoparticles lead to increases in inter fibre fracture strength of up to 16% [7]. This important feature allows the liquid epoxy resins to be quickly wetted to the surface. Fiber reinforced materials generally have more resistant structure than unreinforced materials. As the glass fiber ratio increases, the strength of the material increases. The addition of MWCNTs not only increases the tensile strength of the epoxy matrix but also increases fracture toughness [8]. Furthermore, it has been demonstrated that the inner layers of an MWCNT can be effectively deformed only through the direct application of tensile or shear forces, not through van der Waals interactions [4]. There are some studies on the improvement of interfacial and mechanical properties of thermoset composites by incorporating of CNTs into composites by fiber coating.

In the literature, it was found no research about the mechanical properties of the glass fiber/epoxy resin/MWCNTs integrated thermoset composites. The purpose of this research was to study the effect of the MWCNTs incorporation on the flexural properties of the thermoset composites fabricated by the resin transfer method (RTM). The tensile and flexural properties of 0.0 wt% and 0.2 wt% MWCNTs incorporated specimens in the 0° and 90° directions were investigated.

## II. EXPERIMENTAL PROCEDURE

Multi-walled carbon nanotubes (MWCNTs) were supplied by Ege Nanotek Kimya Sanayi Limited Şirketi, Izmir/TURKEY. Biaxial warp-knitted fabrics were supplied by Metyx Composites Corporation, Istanbul/Turkey. Epoxy resin (Araldite LY 3598) and hardener (Aradur 349) were supplied by Huntsman from Germany. The fibers were cut to size of 750 mm x 350 mm. Both faces of the four layers of the fabrics were coated by the prepared solution of ethanol and MWCNTs (i.e. four faces of the fabrics were coated with each prepared solution). Figure 1 shows the fabrics after coating, respectively. The cut glass fibers were placed in the mold cavity of resin transfer molding (RTM) device in a symmetrical stacking sequence ([90<sub>wa</sub>/0<sub>we</sub>/90<sub>wa</sub>/0<sub>we</sub>]<sub>s</sub>) (Figure 2). Epoxy and hardener were mixed at a ratio of 100/22. The CNT integrated composite materials with biaxial warp-knitted fabric were fabricated by the RTM. The CNTs weight percentages were 0.2 wt% in

fabricated composite panels. The produced composites were tested by using the INSTRON 5982 100 KN flexural tests at Ondokuz Mayıs University (OMU) Central Laboratory (KITAM). Test span lengths for flexural tests are 48 and 64 mm depending on the specimen thickness utilized. In the flexural tests three specimens were tested both in 0° and 90° directions for each type of composite panels.

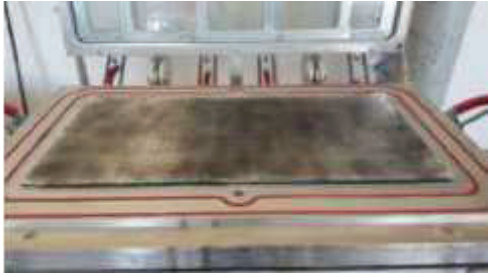


Fig. 1 Four layers 0.2% CNT integrated fabrics

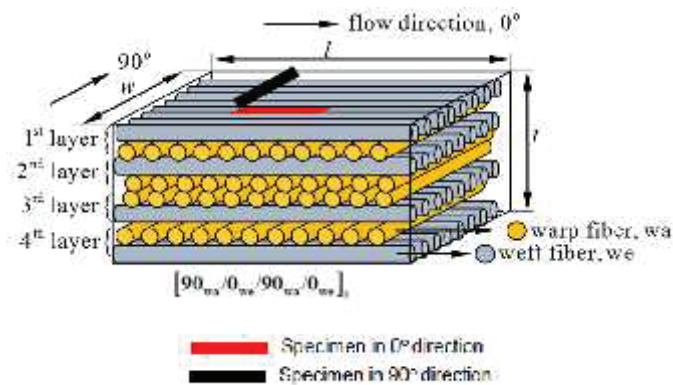


Fig. 2 Schematic drawing of four layers fabrics

After fabricating of the composites, burn off method in a muffle furnace was performed in order to determine the percentages of each of the constituents (volume fraction of fibers) in the thermoset composites. Table I and Table II shows parameters of the biaxial warp-knitted (BWK) fabric reinforcements and Table III shows the volume fraction of the fibers.

Table I Parameters of the biaxial warp-knitted (BWK) fabric

E Glass Sample	0° (Warp) Fiber (Tex)	90° (Weft) Fiber (Tex)
LT1200 (0 wt% CNT)	2400	1200
LT1200 (0.2 wt% CNT)	2400	1200

Table II Parameters of the biaxial warp-knitted (BWK) fabric

Area weight of 0° warp fibers (gr/m <sup>2</sup> )	Area weight of 90° weft fiber (gr/m <sup>2</sup> )	Fabric weight (gr/m <sup>2</sup> )
614 (0 wt% CNT)	7	1187
614 (0.2 wt% CNT)	7	1187

Table III The volume fraction of the fibers in composites

Weft fiber volume fraction (Vf %)	Warp fiber volume fraction (Vf %)	Stitch fiber volume fraction (Vf %)

18.5 (0 wt% CNT)	17.1	0.70
19.8 (0.2 wt% CNT)	18.2	0.30

Figure 3 and 4 show the scanning electron microscope (SEM) images of morphology of MWCNTs and MWCNTs coated fabrics. Figure 4 proved how the nanotubes were homogeneously distributed on the surface of the reinforcement.

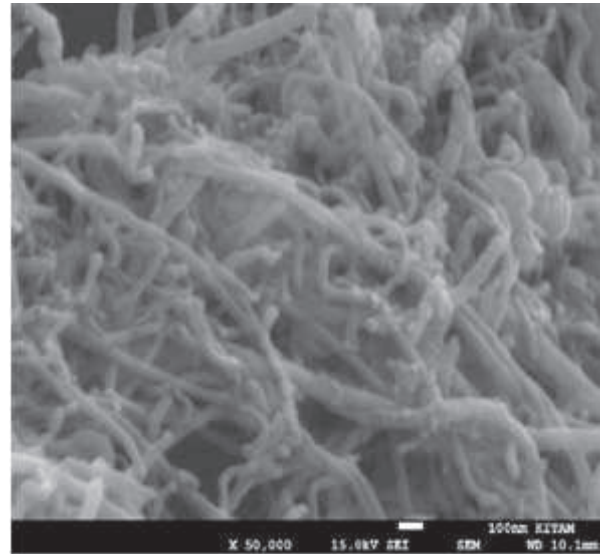


Fig. 3 SEM image of 0.2% CNTs coated BWK fabric (X50.000)

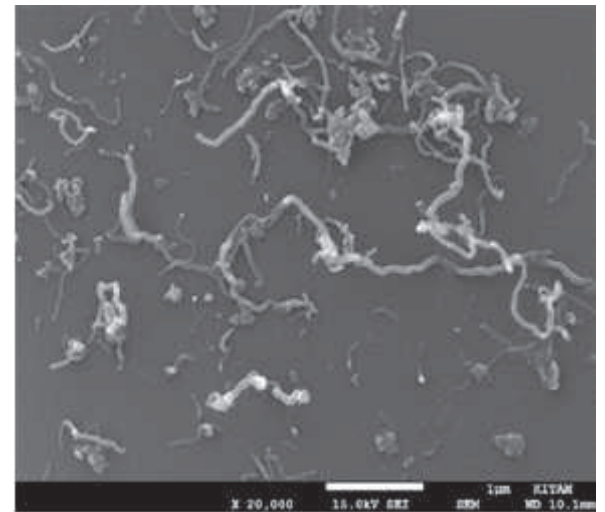


Fig. 4 SEM of 0.2% CNTs coated BWK fabric (X20.000)

### III. RESULTS AND DISCUSSIONS

Figure 5 represents the results of the flexural modulus and strength of the specimens. The composites without CNTs in 0° direction had higher flexural modulus and strength (15.5 GPa and 433.1 MPa) compared to that was in 90° direction (12.1 GPa and 356.5 MPa). Since the volume fraction of weft fibers (18.5%) is higher than warp fibers (17.1%), for composites without CNTs, the specimen tested in 0° direction has a greater flexural modulus and strength than those in 90° direction. Furthermore, composites with CNTs in both 0° and 90°

directions showed higher flexural modulus and strength compared to that was without CNT. The interfacial properties between fiber and epoxy matrix could be improved by coating of the fiber surface with CNTs nano particles and this might be the possible reason of the improvement of the flexural properties of composites.

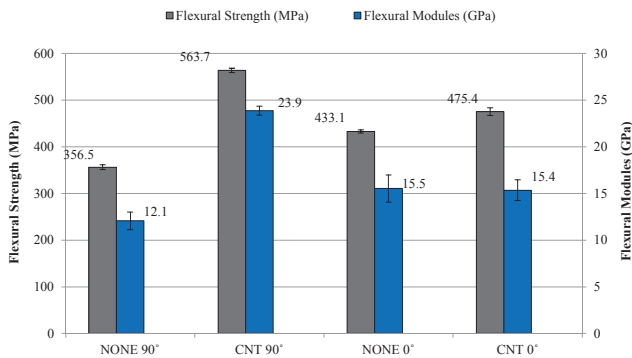


Fig. 5 The results of the flexural modulus and strength of the specimens

#### IV. CONCLUSIONS

In thermoset composites, the effect of MWCNTs integration on the mechanical properties of the samples were evaluated. Our study revealed that the three-point flexural properties of the thermoset composites with glass fiber reinforcements could be improved by incorporating 0.2 wt% percentages of the MWCNTs at the interface of fabric layers. The specimens with 0.2 wt% MWCNTs in 90 direction showed the best results in terms of the flexural modulus and strength among the other specimens. In particular, the thickness values of epoxy/fiber/MWCNT added composite samples have less thickness when compared to the epoxy/fiber composite. Thus, it has shown us that the interfacial alignment in CNT samples has improved. Our study showed that the bending properties of thermosetting composites with glass fiber reinforcements can be improved by adding nano materials.

#### ACKNOWLEDGMENT

This study has been granted by Research fund of OMU (Project No: PYO.MUH.1904.16.004)

#### REFERENCES

- [1] P. Bondavalli, "Graphene and related nanomaterials", *A volume in Micro and Nano Technologies*, pp. 1–40, 2018.
- [2] D. Özyurt, "Sıcak filament destekli kimyasal buhar biriktirme yöntemi ile karbon nanotüp yüzey modifikasyonu". Yüksek Lisans Tezi, Selçuk Üniversitesi, Konya. pp. 1- 4. 2012.
- [3] B. K. Kaushik, and M. K. Majumder, Carbon nanotube based VLSI interconnects, *Springer Briefs in Applied Sciences and Technology*, Pages 17-37. Doi:10.1007/978-81-322-2047-3\_2., 2015.
- [4] T. W. Chou and C. Li., Elastic moduli of multi-walled carbon nanotubes and the effect of van der waals forces, *Composite Science Technology*. doi: 10.1016/S02663538(03)00072-1., pp. 1517-1524, 2003.
- [5] R. Donald – R. Dominick, *Reinforced Plastics Handbook 3rd Edition*, Elsevier Science & Technology Books, pp. 24–108, 2005.
- [6] R. S. Ruoff, D. Qian and K. W. Liu., "Mechanical properties of carbon nanotubes: theoretical predictions and experimental measurements",

Published by Elsevier SAS, *Comptes Rendus Physique*, vol. 4, 993–1008, 2003.

- [7] L. Böger, J Sumfleth, H. Hedemann and K. Schulte, "Improvement of fatigue life by incorporation of nanoparticles in glass fibre reinforced epoxy", *Composites: Part A*, vol. 41, pp. 1419–1424, 2010.
- [8] P. Guo, X Chen, X. Gao, H. Song and H. Shen, "Fabrication and mechanical properties of well-dispersed multiwalled carbon nanotubes/epoxy composites", *Composites Science and Technology*, vol. 67, pp. 3331–3337, 2007.

# Effect of Integration of Carbon Nanotubes (CNTs) on Compression after Impact Properties of Thermoset Composites (ISLAC'18/UHAKS18)

Erdinç Günaydin, Pinar Çolak, Kemal Kadioğlu, Özgür Demircan\*

\* Department of Metallurgical and Materials Engineering, Ondokuz Mayıs University, Samsun, 55000, Turkey

\* Corresponding author: ozgur.demircan@omu.edu.tr

**Abstract**—In this study, glass fiber/epoxy resin/multi-walled carbon nanotubes (MWCNTs) were used to fabricate the thermoset composite materials with biaxial warp-knitted fabrics. Thermoset composites were fabricated using resin transfer molding (RTM) methods. The fabricated samples were tested with compression after impact (CAI) tests. CNT integrated specimens showed 17% improvement of CAI strength against specimens without CNTs from CAI tests.

**Keywords**— Non-crimp fabric, thermosets composites, carbon nanotubes, compression after impact properties.

## I. INTRODUCTION

Nanocomposite materials are obtained as a dispersion in a nanometer dimension within one second phase and are defined as at least two phase material groups. Carbon Nanotube is an allotropic of carbon element [1]. In other words, they are obtained by cylindrical wrapping of plates in the form of honey pellets. In shapely carbon nanotube structures, atoms are connected to each other by sp<sup>2</sup> (like graphite), atoms form hexagonal geometry, and each atom has only three neighbours. Carbon nanotubes have high resistance to impacts such as compression, bending, twisting due to hole structures and high length / diameter ratios [2]. There are single-layer (single-walled) or multi-layer (multi-walled) carbon nanotubes. Previous scientific investigations have demonstrated that multi-walled CNTs (MWCNTs) have higher resistance to chemicals than single-walled CNTs (SWCNTs). Carbon nanotubes are one hundred times stronger than steel, and weight is one sixth. Steel is harder at the same time, but as flexible as plastic. Therefore, it is the most robust material known to have high corrosion resistance [3]

Because of these properties, CNTs have been used. In addition, if we look at the structure and properties of Epoxy; the low molecular weight of liquid immature epoxy resins gives them superior molecular mobility during processing. High strength thermoset polymers such as epoxy are added to glass fiber to increase mechanical strength and thermal stability [4].

This important feature allows the liquid epoxy resins to be quickly wetted to the surface. Fiber reinforced materials generally have more resistant structure than unreinforced materials. As the glass fiber ratio increases, the strength of the

material increases [5]. Adding more fibers can increase tensile and impact strength, while layer delamination occurs under tensile, compressive and shear loading [4].

There are some studies on the improvement of interfacial and mechanical properties of thermoset composites by incorporating CNT into composites by fiber coating. From here it is aimed to increase the compression after impact (CAI) properties of the new nanocomposites, which we will produce by improving the interface between resin and fiber, thus reaching new areas of use.

## II. EXPERIMENTAL PROCEDURE

Multi-walled carbon nanotubes (MWCNTs) were supplied by Ege Nanotek Kimya Sanayi Limited Şirketi, Izmir/TURKEY. Biaxial warp-knitted fabrics were supplied by Metyx Composites Corporation, Istanbul/Turkey. Epoxy resin (Araldite LY 3598) and hardener (Aradur 349) were supplied by Huntsman from Germany. The fibers were cut to size of 750 mm x 350 mm. Both faces of the four layers of the fabrics were coated by the prepared solution of ethanol and MWCNTs (i.e. four faces of the fabrics were coated with each prepared solution). Figure 1 shows the fabrics after coating, respectively. The cut glass fibers were placed in the mold cavity of resin transfer molding (RTM) device in a symmetrical stacking sequence ([90<sub>wa</sub>/0<sub>we</sub>/90<sub>wa</sub>/0<sub>we</sub>]<sub>s</sub>) (Figure 2). Epoxy and hardener were mixed at a ratio of 100/22. The CNT integrated composite materials with biaxial warp-knitted fabric were fabricated by the RTM. The CNTs weight percentages were 0.2% in fabricated composite panels.

The produced composites were tested by using the Zwick in Mirarge Laboratory, Istanbul/Turkey. The size of the specimens was 100 mm x 150 mm. In order to characterize the thermoset composites, low energy impact tests were conducted at 43 J to evaluate the damage resistance of composites. Zwick Roell Z250 KN Universal test equipment was used for CAI tests. Once the low energy impacts were completed, the damaged samples were used for the CAI tests with constant displacement of 0.5 mm/min and a 250 kN unit cell. The EN 6038 test standard was used to perform the CAI tests and three specimens were tested.

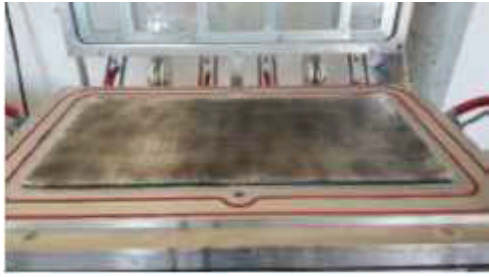


Fig. 1 four layers 0.2% CNT integrated fabrics.

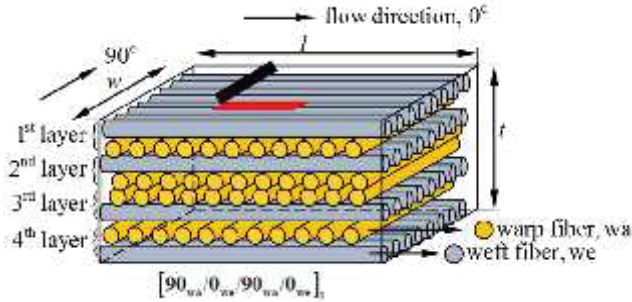


Fig. 2 Schematic drawing of four layers fabrics.

After fabricating of the composites, burn off method in a muffle furnace was performed in order to determine the percentages of each of the constituents (volume fraction of fibers) in the thermoset composites. Table 1 and 2 shows parameters of the biaxial warp knitted (BWK) fabric reinforcements and Table 3 shows volume fraction of the fibers in composites.

Table 1 Parameters of the biaxial warp-knitted (BWK) fabric

E Glass Sample	0° (Warp) Fiber (Tex)	90° (Weft) Fiber (Tex)
LT1200 (0 wt% CNT)	2400	1200
LT1200 (0.2 wt% CNT)	2400	1200

Table II Parameters of the biaxial warp-knitted (BWK) fabric

Area weight of 0° warp fibers (gr/m²)	Area weight of 90° weft fiber (gr/m²)	Fabric weight (gr/m²)
614 (0 wt% CNT)	7	1187
614 (0.2 wt% CNT)	7	1187

Table III The volume fraction of the fibers in composites

E Glass Sample	Weft Vf%	Warp Vf%	Stitch Vf%	Total Vf%	Thickness (mm)
LT1200 (0 wt% CNT)	18.5	17.1	0.7	36.3	5.0
LT1200 (0.2 wt% CNT)	19.8	18.2	0.3	38.3	4.8

Figure 3 and 4 show the scanning electron microscope (SEM) images of morphology of MWCNTs and MWCNTs coated fabrics. Figure 4 proved how the nanotubes were homogeneously distributed on the surface of the reinforcement.

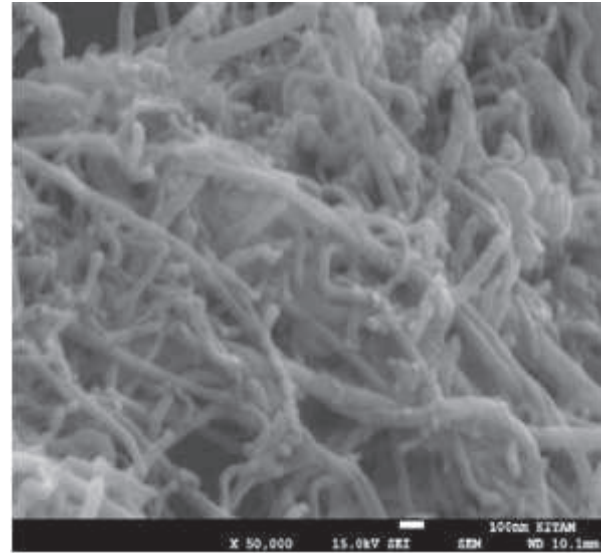


Fig. 3 SEM image of 0.2% CNTs coated BWK fabric (X50.000)

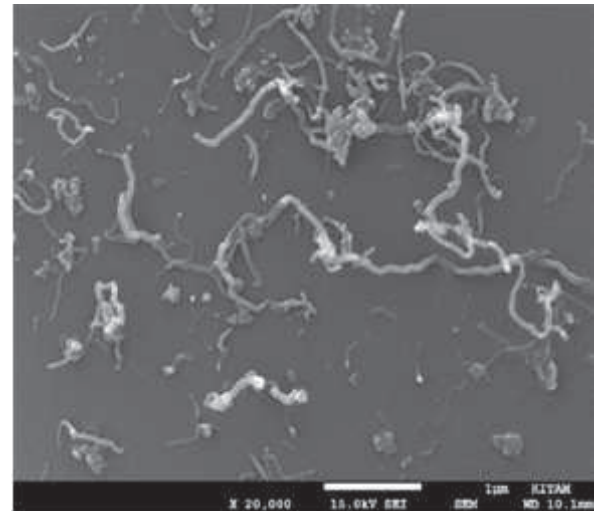


Fig. 4 SEM of 0.2% CNTs coated BWK fabric (X20.000)

### III. RESULTS AND DISCUSSION

It was expected that composites with CNTs could represent higher compression after impact properties compared to that was without CNT. Figure 5 shows the results of the CAI test on thermoset composites with 0 wt% and 0.2 wt% CNTs. The CAI strength of the specimens with 0 wt% and 0.2 wt% MWCNTs were 142.8 MPa and 172.8 MPa. CNT integrated specimens showed 17% improvement of CAI strength against specimens without CNTs from CAI tests.

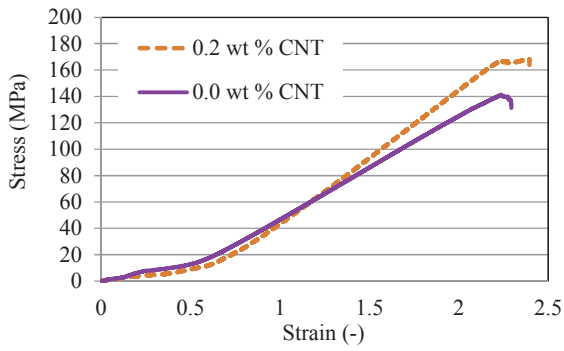


Fig. 5 Results of the CAI test on thermoset composites with 0 wt% and 0.2 wt% CNTs

The interfacial properties between fiber and epoxy matrix could be improved by coating of the fiber surface with CNTs nano particles and this might be the possible reason of the improvement of the compression after impact properties of composites.

#### IV. CONCLUSIONS

Our study showed that composites with CNTs could represent higher compression after impact properties compared to that was without CNTs. Addition of CNTs on the surface of the reinforcements improved CAI test results of the specimens. CNT integrated specimens showed 17% improvement of CAI strength against specimens without CNTs from CAI tests.

#### ACKNOWLEDGMENT

This study has been granted by Research fund of OMU (PYO.MUH.1904.16.005)

#### REFERENCES

- [1] <http://www.kimyakongreleri.org/P2012/P2012-079.pdf>
- [2] D. Özyurt, *Sıcak filament destekli kimyasal buhar biriktirme yöntemi ile karbon nanotüp yüzey modifikasyonu*. Yüksek Lisans Tezi, Selçuk Üniversitesi, Konya, 2012.
- [3] D. Rosato, D. Rosato, *Reinforced Plastics Handbook*, 3rd Edition, Elsevier Science & Technology Books, 2004.
- [4] R. B. Seymour, *Plastics Technology*, Encyclopedia of Chemical Technology, Wiley, 1968.
- [5] N. L. Hancox, R. M. Mayer, *Design Data for Reinforced Plastics*, Chapman & Hall, London, 1994.

# Effect of Integration of Carbon Nanotubes (CNTs) on Flexural Properties of Thermoplastic Composites (ISLAC'18/UHAKS18)

Abdurrahman Yildiz<sup>1</sup> and Özgür Demircan<sup>1,\*</sup>

<sup>1</sup> Department of Metallurgical and Materials Engineering, Ondokuz Mayıs University, Samsun, 55000, Turkey

\*Corresponding author: ozgur.demircan@omu.edu.tr

**Abstract**— In this study, the effect of carbon nanotubes (CNTs) addition on the mechanical properties of glass fiber reinforced thermoplastic composite materials was investigated. Composites have been obtained from biaxial weft-knitted (BWK) fabrics with different knit structures (interlock, tuck and tuck-miss) and with CNTs. Multi walled carbon nanotubes (MWCNT) were used in 0.4 wt% in glass fiber/polypropylene thermoplastic composites. Thermoplastic composites were fabricated by using hot press method. As a result of this study, with the contribution of MWCNT, the highest bending strength and modulus were obtained from interlock and tuck-miss.

**Keywords**— Biaxial weft-knitted fabric, carbon nanotube, thermoplastic composite, bending properties

## I. INTRODUCTION

Thermoplastics materials can be melted and shaped when heated. The thermoplastic polymers do not have covalent bonds as compared to the thermosets. In structural polymeric composite applications, textiles (e.g., unidirectional, woven fabrics) are commonly applied as reinforcement because of the high fiber volume fractions and the possibility to tailor the load bearing capacity through the fiber lay-up. Nowadays, thermoplastic composites are being used in various industries such as automotive, wind turbines, and so on. Thermoplastic polymers have potential for rapid, low cost, and mass production of reinforced composites. The very high viscosity of thermoplastic composites makes the processing of thermoplastic matrix composites difficult. Therefore, some techniques, such as commingled yarns, were developed in order to improve processability of thermoplastic composites [1]. The commingled yarn consists of a blended combination of reinforcement fibers and matrix filaments spun from the bulk polymers. In the commingled state, the different filaments scatter amongst one another, as a result, the resin flow distance for impregnation and consequently the applied pressure and time are limited, leading to a saving in manufacturing cost [2], [3]. The attractive properties, such as those requiring high-energy absorption or good impact resistance, or in cases where the component is complex in shape and demands exceptional formability, can be achieved by using knitted composites [4]. Additional yarns can be added to increase the mechanical properties of the fabrics. With the additional yarns, the fabrics can take forms and shapes. Reinforcing yarns, for example, glass fiber (GF) or aramid fiber, can be used within all yarn systems in biaxial weft-knitted (BWK) fabrics [5]. The tensile

properties of the BWK thermoset composites was reported by Demircan et al. [6]. Knitted fabric-reinforced thermoplastic composites with commingled fibers were studied by some researchers. Tensile properties of multilayer-connected biaxial weft knitted fabric reinforced composites for carbon fibers investigated by Yexiong et al. [7]. They found that the carbon fiber volume fraction has significant effect on tensile strength of MBWK fabrics reinforced composites. The tensile properties of knitted fabric-reinforced composites made from GF/PP commingled yarn with different loop densities were investigated by Zaixia et al. [8]. The ballistic impact behavior of biaxial weft-knitted UHMWPE composites has been investigated by Liang et al. [9]. It was found that ballistic performances were influenced by the pressing pressure. Effects of biaxial deformation of the knitted glass preform on the in-plane mechanical properties of the composite investigated by Khondker et al. [10]. They found that the tensile properties were affected by the stretching of the knitted fabric.

In this study, the bending properties of MWCNTs integrated thermoplastic composites with biaxial weft-knitted fabrics (BWK) were investigated. In the literature, some studies on the effect of MWCNTs integration in the mechanical properties of thermoplastic composites were reported. However, to the best of the authors' knowledge, it was found no work the addition of MWSNTs on the effect of bending properties of thermoplastic composites reinforced with biaxial weft-knitting fabric.

## II. EXPERIMENTAL PROCEDURE

Materials, multi-walled carbon nanotubes (MWCNT) supplied by Ege Nanotek Kimya Sanayi Limited Şirketi, İzmir TURKEY. Biaxial-weft knitted fabrics with glass and Polypropylene (PP) commingled fibers were supplied by Shima Seiki, Wakayama / JAPAN. The fibers were cut to size of 230 mm x 160 mm. Both faces of the eight layers of the fabrics were coated by the prepared solution of ethanol and 0.4 wt% MWCNTs (i.e. 16 faces of the fabrics will be coated with each prepared solution). In this study, the BWK fabrics of interlock, tuck and tuck&miss were used as a reinforcement. MWCNT was sprayed on the fabrics, which had size of 230x160 mm<sup>2</sup>. It was mixed by adding 0.4 wt% MWCNT to 400 g ethanol. This ratio was sprayed evenly on a total of 16 surfaces.

The GF/PP-commingled yarns were used as warp (410 tex), weft (410 tex), and stitch yarns (138 tex) in the BWK fabrics.

The volume content of the GFs was 52% and that was for the PP fibers 48% in the warp and weft commingled yarns. The volume content of the GFs was 27% and that was 73% for the PP fibers in the stitch commingled yarns.

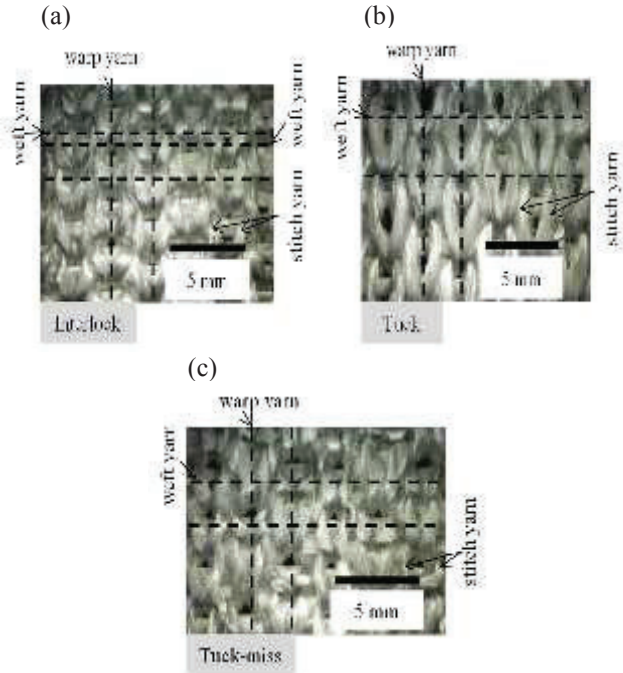


Fig. 1 Photographs of the BWK fabrics: (a) interlock, (b) tuck, (c) tuck-miss

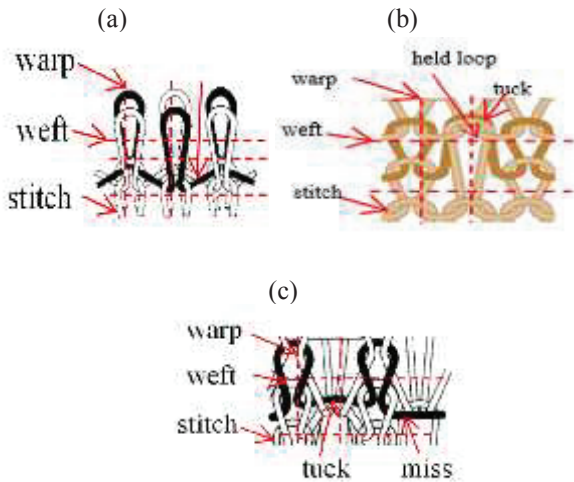


Fig. 2 Schematic drawings of the BWK fabrics: (a) interlock, (b) tuck, (c) tuck-miss

Figure 1a-c shows the photographs of the BWK fabrics. The schematic drawings of the BWK fabrics are shown in Figure 2a-c.

Interlock fabrics are obtained by interconnecting two separate 1x1 rib structures. The looped legs are clearly visible on the anterior and posterior sides of the interlock. The appearance of both sides of the fabric is like the front of the plain fabric. Tuck, the characteristic appearance of the hanger is the yarn which is folded in the direction of the elongated loop. Hangers increase the weight and thickness of the fabric as the

straps are placed on normal loops without creating a new row. Tuck-miss, pattern can be created by repeating a jumping structure, a single needle or a pair of needles next to each other in the form of a transverse yarn investment in the middle of a fabric that is elongated in the fabric.

The eight layers fabric with symmetric laminate sequence (Figure 3) were placed in the mold of hot press machine. CNT integrated thermoplastic composite materials with biaxial weft-knitted fabric were fabricated by the Compression Molding Method (Figure 4). The produced composites were tested by using the INSTRON 5982 100KN Flexural Tests at Ondokuz Mayıs University (OMU) Central Laboratory (KITAM). In the flexural tests three specimens were tested in weft directions for each type of composite panels. The fabricated plates were cut in 80x15 mm<sup>2</sup> dimensions in the weft direction.

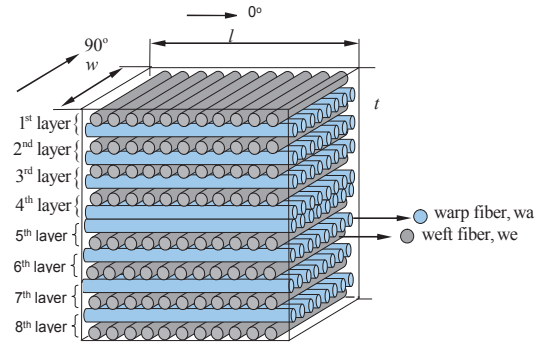


Fig. 3 Schematic drawing of eight layers fabrics.

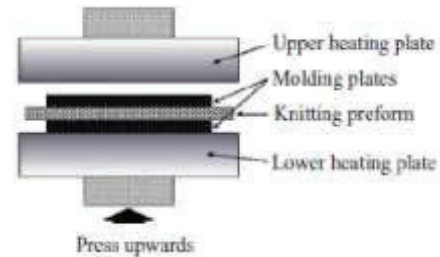


Fig. 4 Schematic drawing of compression molding method

The molding pressure, temperature, and time were 4 MPa, 165 °C, and 30 min. Later, mold was cooled until it comes to the room temperature around 40°C. Fiber Vfs were found out by performing burn-out tests. In the combustion test, three samples of each composite were sampled. The dimensions of the specimens were 1x1 cm. The specimens were weighed at 625 °C for 4 hours. The fiber volume ratio was determined after burn-out tests. Table 1 shows the fiber Vf and thickness of 8 layers-BWK composites.

Table 1 Fiber Vf and thickness of 8 layers-BWK composites

Samples	Weft Vf (%)	Warp Vf (%)	Stitch Vf (%)	Total Vf (%)	Thickness (mm)
0.4 wt% MWCNTs Interlock	18.3	7.89	14.2	40.4	3.11
0.4 wt% MWCNTs Tuck	9.08	8.21	14.7	31.9	3.48

0.4 wt% MWCNTs Tuck-miss	12.3	7.03	17.2	36.6	3.68
--------------------------	------	------	------	------	------

### III. RESULTS AND DISCUSSION

Figures 5 (a) and (b) shows the results from the three-point bending test with various knitting types with MWCNT and without MWCNT. According to the test results (Figures 5 (a)), the interlock and tuck-miss composites with 0.4 wt% MWCNTs had almost same bending strength (about 199.9 MPa). The tuck with 0.4 wt% MWCNTs composites had the lowest bending strength (141.8 MPa). Since the knitting structures of fabrics were changed, they had different mechanical properties with the same amount of the MWCNTs. By changing knitting structures, the volume fraction of the fibers were changed. According to the results of burning test, the BWK composites with 0.4 wt% MWCNTs with the interlock and tuck-miss had higher weft fiber Vf (18.3% and 12.3 %) compared to the BWK composites with 0.4 wt% MWCNTs with the tuck (9.08 %).

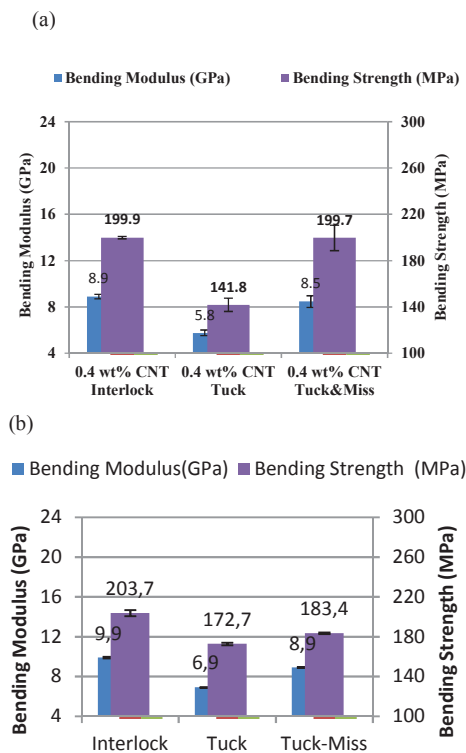


Fig. 5 Results from three-point bending tests: (a) with MWCNT, (b) without MWCNT [1]

Due to had a higher fiber volume fractions of the composites with interlock and tuck-miss with 0.4 wt% MWCNTs, they had higher bending properties compared to the that was with tuck composites. Almost same bending strength and modulus were obtained from eight layers with MWCNTs (Figures 5 (a)) compared to that was ten layers without MWCNTs [1] (Figures 5 (b)).

### IV. CONCLUSIONS

In our study, we investigated the bending properties of biaxial weft-knitted fabrics with different knitting structures and with MWCNTs. The effect of MWCNTs on the strength of the materials was observed. The effect of fiber volume ratio was observed as a result of the three point bending test. According to the result of the test the samples with the highest bending resistances was obtained with interlock and tuck & miss. The bending strength obtained from ten layers of BWK fabrics according to the works done in the literature was obtained by using eight layers of BWK fabrics in our work.

### ACKNOWLEDGMENT

This study has been supported by Research fund of OMU (Project No: PYO.MUH.1901.16.001). The authors thank to Mr. Shinsuke Ashibe, Mr. Tatsuya Kosui (R&D New Technology Applications, Shima Seiki, Wakayama, Japan) and Prof Asami Nakai (Gifu University, Gifu City, Japan).

### REFERENCES

- O. Demircan, S. Ashibe, T. Kosui and A. Nakai, "Effect of various knitting techniques on mechanical properties of biaxial weft-knitted thermoplastic composites", *Journal of Thermoplastic Composite Materials*, vol. 28(6), pp. 896-910, 2015.
- E. Mäder, J. Rausch and N. Schmidt, "Commingled yarns – processing aspects and tailored surfaces of polypropylene/glass composites", *Composites Part A*, vol. 39, pp. 612-623, 2008.
- N. Bernet, V. Michaud, P. E. Bourban and J. A. E. Manson, "Commingled yarn composites for rapid processing of complex shapes", *Composites Part A*, vol. 32, pp. 1613-1626, 2001.
- O. A. Khondker, T. Fukui and A. Nakai, et al. "Initial fracture of the weft weft-knitted textile composites." *Composites Part A*, vol. 35: pp. 1185-1194, 2004
- P. Haller, T. Birk and P. Offermann, et al. "Fully fashioned biaxial weft knitted and stitch bonded textile reinforcements for wood connections", *Composites Part B*, vol. 37, pp. 278-285, 2006.
- O. Demircan, AR. Torun and T. Kosui, et al. "Effect of stitch and reinforcement yarn types on tensile properties of biaxial weft knitted composites," Tokyo, Japan: Japan Sampe, 2011.
- Y. Qi, J. Li and L. Liu, "Tensile properties of multilayer-connected biaxial weft knitted fabric reinforced composites for carbon fibers", *Materials & Design*, vol.54, pp. 678-685, 2014.
- F. Zaixia, Zhangyu and C. Yanmo, "Investigation on the tensile properties of knitted fabric reinforced composites made from GF-PP commingled yarn preforms with different loop densities", *Journal Thermoplastic Composites Mater*; vol. 19, pp. 113-125, 2006.
- Z. Liang, G. Qiu, and X. Yi, "The ballistic impact behavior of composites reinforced by biaxial weft knitted uhmwpe fabrics" *Composite Technologies for 2020, Proceedings of the Fourth Asian-Australasian Conference on Composite Materials (ACCM 4)*
- O. A. Khondker, K. H. Leong and I. Herszberg, "Effects of biaxial deformation of the knitted glass preform on the in-plane mechanical properties of the composite", *Composites Part A: Applied Science and Manufacturing*, vol. 32, pp. 1513-1523, 2001.

# Effect of Heat Treatment on Structural, Surface and Mechanical Properties of Al-Based Al-x Mn (x = 0.1, 0.2, 0.3) Alloys

Fazıl HÜSEM, Fatma MEYDANERİ TEZEL, Atakan BOĞA\*, Serdal HAN, Melih SEMERÇİ

Department of Metallurgy and Materials Engineering, Faculty of Engineering, Karabük University, 78050, Karabük, Turkey  
\*Corresponding author: atakanbga@gmail.com

**Abstract—** In this study, the mechanical properties of alloys with different compositions of Al-based Al-Mn alloys were determined by Vickers Hardness Tester, Tensile Test and the effect of heat treatment was discussed. Accordingly, the average hardness values of Al-x Mn (x = 0.1, 0.2, 0.3) alloys were measured as 47.7, 50.8 and 53.3 for the samples not subjected to heat treatment and 50.2, 54.1 and 81 for the samples subjected to heat treatment, respectively. According to the tensile test results, the order of Al-x Mn (x = 0.1, 0.2, 0.3) alloys is max. tensile strength 87.9, 97.4, 101.23 MPa, heat treated samples 101.15, 106.6, 125.4. SEM, EDX and XRD and microstructural and surface morphologies related to the composition were investigated.

**Keywords—** Heat treatment, Tensile strength, microstructure, micro hardness

## I. INTRODUCTION

Aluminum, which is in the light metal category due to the development of technology and the technical features it possesses, is widely used in many fields of industry. In practice, the ratio of the strength to the weight (specific strength property) is very large; the soft and one-third the weight of steel. When alloying elements are added, the mechanical properties can be increased to be comparable to steel; this makes aluminum usable for medicine, construction, food, automotive and aerospace industries [1-5].

Aluminum alloys have a wide range of light structural properties. Addition of secondary elements has become an inevitable way to become a commercially available material because of its density, tensile strength, lightweight structural properties in terms of ductility. All the hardening elements added to aluminum reduce thermal and electrical conductivity and elongation. The applied heat treatments change plasticize and hardness. The manganese has an effect of increasing the toughness and ductility properties, but it has become an

essential element in the secondary additions by increasing the tensile strength without reducing the corrosion resistance [5-8].

## II. EXPERIMENTAL PROCEDURE

For Al-Mn alloy, Al and Mn ingots with 99% purity were used. The composition of Al-x Mn (x = 0.1, 0.2, 0.3) was prepared and in the Protherm brand oven, after melting the aluminum for two hours at 670 °C, the manganese was added to the aluminum at a certain rate and the temperature of the oven was increased to 1350 °C and kept for two and a half hours. The casting process was then carried out in the mold. This track is repeated for each alloy. Samples for heat treatment were heat treated at 450 °C in Protherm brand heat treatment furnace for 4.5 hours. After heat treatment, all samples were taken with the help of lathe machine. Secotom 50 brand spiral cutting device with samples of the test in the desired standards tensile test, microhardness, SEM + EDX, XRD samples were prepared. Samples prepared for XRD and micro hardness tests were polished and sanded with Tegramin 30 branded device, and samples prepared for SEM and EDX analysis were made by polishing with CitoPress 10 brand balancing device.

## III. CONCLUSION

The tensile test was divided into two as heat treatment and heat treatment and a total of 6 samples were examined, respectively, 0.1, 0.2, 0.3. According to the tensile test results, the order of Al-x Mn (x = 0.1, 0.2, 0.3) alloys is max. tensile strength 87.9, 97.4, 101.23 MPa, for heat-treated samples 101.15, 106.6, 125.4. The mean stress values of Al-x Mn (x = 0.1, 0.2, 0.3) alloys were measured as 4.3, 16.2 and 21.5 for non-heat treated samples, and 18.7, 16.4 and 12.6 for heat treated samples, respectively. The mean peak voltage of the Al-x Mn (x = 0.1, 0.2, 0.3) alloys was 87.9, 125.4 and 106.6 for non-heat-treated samples, and 101.15, 97.4 and 101.23 for heat-treated samples, respectively. The increasing manganese content and the increase in tensile and elongation values of the sample after the heat treatment is noteworthy. The results are given in Table 1.

Table 1. Mechanical properties of Al-x Mn (x = 0.1, 0.2, 0.3) alloys

Alx-Mn (x=0.1,0.2,0.3)	Peak Load (kN)	Peak Stress (MPa)	Yield	Strain
Alx-Mn (x=0.1) without heat treatment	9.020	87.9	47.310	4.3
Alx-Mn (x=0.1) with heat treatment	7.943	101.15	59.32	18.7
Alx-Mn (x=0.2) without heat treatment	7.788	97.4	3.174	16.2
Alx-Mn (x=0.2) with heat treatment	14.188	125.4	41.884	16.4
Alx-Mn (x=0.3) without heat treatment	10.412	101.23	40.402	21.5
Alx-Mn (x=0.3) with heat treatment	6.808	106.06	44.953	22.6

Accordingly, Al-xMn (x = 0.1, 0.2, 0.3) in the amount of Mn in the alloy and heat treatment with the strength of the samples were observed to be higher.

The average hardness values of Al-xMn (x = 0.1, 0.2, 0.3) alloys were measured as 47.7, 50.8 and 53.3 for non-heat treated samples and measured as 50.2, 54.1 and 81.0 for heat treated samples, respectively. According to these results, it can be said that manganese added to aluminum positively affects the hardness together with the increasing composition value as well as the heat treatment supports this increase.

Al - xMn (x = 0.1, 0.2, 0.3) in the structural characterization of the sample containing x = 0.1 Mn  $2\theta=45^\circ$  degrees in the  $Al_6Mn$  compound is not seen after the heat treatment, at  $2\theta=65^\circ$  Al peak after the heat treatment is quite high we can say that increased. A significant increase in Al and Mn peaks was observed for the sample containing 0.2% Mn by weight. In the specimen containing 0.3% Mn by weight, the  $Al_6Mn$  peak was more pronounced after heat treatment and XRD results were obtained and given in Fig.1. In addition, the intermetallic phase of  $Al_6Mn$  with the effect of heat treatment is more pronounced in the grain boundaries and increased the mechanical and microhardness of the samples.

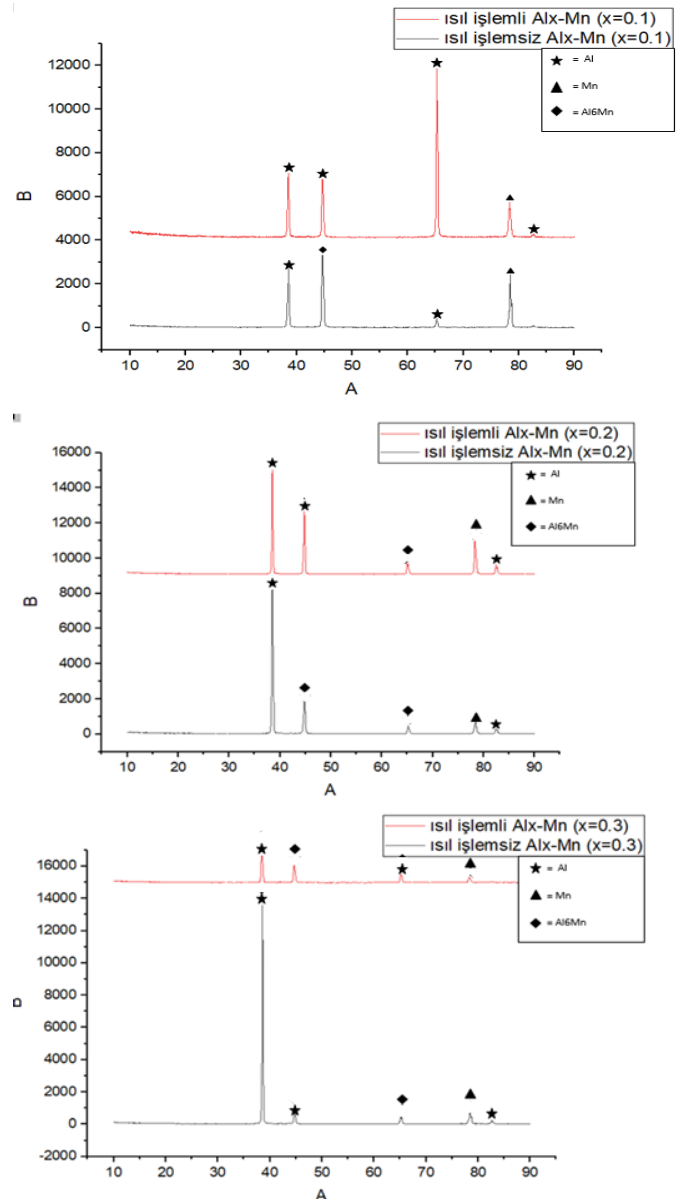


Fig. 1. XRD results of Al-x Mn (x = 0.1, 0.2, 0.3) alloys

SEM and EDX analyses of Al-xMn (x = 0.1, 0.2, 0.3) alloys are given in Fig.2. When SEM images were examined, increased Mn ratio and heat treatment resulted in more structural observed clearly at grain boundaries.

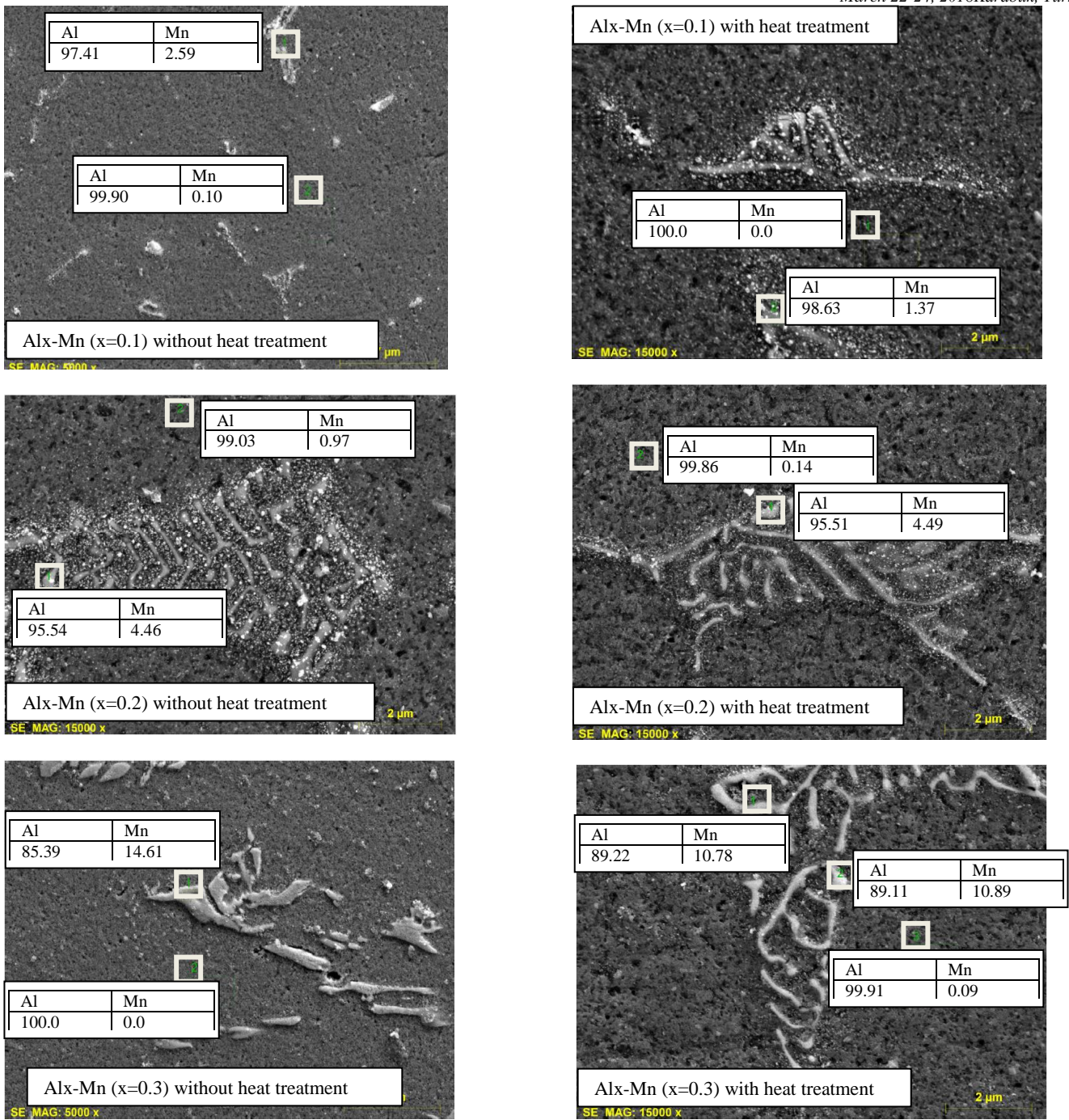


Fig. 2. SEM and EDX analyses of Al-x Mn (x = 0.1, 0.2, 0.3) alloys

ACKNOWLEDGMENT

This work was supported by TUBİTAK-2209 A (2017/2). Authors would like to thank the TUBİTAK-2209 A Project Unit for their financial support.

REFERENCES

- [1] Ian Polmear, 2005) David StJohn, Jian-Feng / *Light Alloys: Metallurgy of the Light Metals* (98-99)
- [2] K.A. Darling et al. / *Materials Science & Engineering A* 589 (2014) 57–65

- [3] *Lens et al. / Materials Science and Engineering A* 403(2005) 144–153
- [4] *M. Zamin, Al-Mn Alaşımlarının Korozyon Davranışında Mn'nin Rolü, KOROZYON. 1981;(11), 37: 627-632.*
- [5] *Ian Polmear, David StJohn, Jian-Feng / Light Alloys: Metallurgy of the Light Metals (2005) 98-201*
- [6] *(Anderson, W. A., in Aluminium, Vol. 1, K. Van Horn (Ed.), American Society for Metals, Cleveland, Ohio, 1967)*
- [7] *Sumiha Ikeshitaa, Ansis Strodahsb, Zineb Saghib, Kazuhiro Yamadaa, Pierre Burdetc, Satoshi Hatad, Ken-ichi Ikedad, Paul A. Midgleyb, Kenji Kanekoa, Hardness and microstructural variation of Al–Mg–Mn–Sc–Zr alloy, Micron, 82 (2016) 1-8.*
- [8] *N.H. Leea, P.W. Koa, T.Y. Tsengb, J.R. Sub, Effect of manganese addition on the tensile properties of cold-rolled and recovery-annealed aluminum alloy sheets, Materials Science and Engineering A 535 (2012) 297–305*

# Finite Element Analysis of Thrust Force in Drilling of Al2014 Aluminum Alloy (ISLAC'18/UHAKS18)

Mehmet Erdi Korkmaz<sup>1\*</sup>, Ramazan Çakıroğlu<sup>2</sup>, Nafiz Yaşar<sup>3</sup>, Ramazan Özmen<sup>4</sup>, Mustafa Günay<sup>1</sup>

<sup>1</sup> Makine Mühendisliği Bölümü, Karabük Üniversitesi, Karabük, 78000, Turkey

<sup>2</sup> Ostim Meslek Yüksek Okulu, Gazi Üniversitesi, Ankara, 06560, Turkey

<sup>3</sup> TOBB Meslek Yüksek Okulu, Karabük Üniversitesi, Karabük, 78000, Turkey

<sup>4</sup> Mekatronik Mühendisliği Bölümü, Karabük Üniversitesi, Karabük, 78000, Turkey

\*Corresponding author: merdikorkmaz@karabuk.edu.tr

**Özet**— Bu çalışmada, Al2014 alüminyum alaşımının kaplamasız sementit karbür takım ile delinmesinde itme kuvveti deneysel ve nümerik olarak elde edilmiştir. Çalışmanın ilk aşamasında, farklı seviyelerde kesme parametreleri (kesme hızı ve ilerleme miktarı) için itme kuvvetini ölçmek amacıyla CNC işleme merkezinde delme işlemleri yapılmıştır. İkinci aşamada, sonlu elemanlar yöntemine dayalı kesme simülasyonu yapılan ThirdWave Advantedge programıyla itme kuvveti için nümerik analizler gerçekleştirilmiştir. Değerlendirmeler sonucunda, deneysel olarak ölçülen itme kuvveti ile simülasyon sonucunda elde edilen kuvvet değerleri arasında ortalama %7'lik bir fark olduğu belirlenmiştir. Sonuç olarak, delme işleminde sonlu elemanlar yönteminin uygulanabilirliği kanıtlanmıştır.

**Anahtar Kelimeler**— Al2014, Kesme kuvveti, Sonlu elemanlar yöntemi, Simülasyon

**Abstract**— In this study, thrust force was obtained experimentally and numerically in the drilling of Al2014 aluminum alloy with uncoated cemented carbide tool. In the first phase of the study, drilling operations were performed in the CNC machining center to measure the thrust force at different levels of cutting parameters (cutting speed and feed rate). In the second stage, numerical analyzes for the thrust force were performed by using the ThirdWave Advantedge program, which is made the cutting simulations based on the finite element method. In the result of the evaluations, it was determined that there was an average difference of 7% between the experimentally measured thrust force and the force values obtained by the simulation. Consequently, the applicability of the finite element model in drilling operation was proved.

**Keywords**— Al2014, Thrust force, Finite element method, Simulation

## I. GİRİŞ

Teknoloji ve endüstrinin hızla gelişmesi ile yüksek mukavemetli, hafif ve mükemmel aşınma direncine sahip yapısal malzemelere olan talep sürekli artmaktadır [1,2]. Bu malzemelerin üretimden çıkıp son hallerini almaları için bazı plastik deformasyon işlemlerinden geçmeleri gerekmektedir. Bu işlemlerin en önemleri arasında talaşlı imalat yöntemleri

gelmektedir. Talaşlı imalat işlemleri genel olarak tornalama, delme ve frezelemeye dayanmaktadır. Delme işlemi sırasında meydana gelen talaş oluşumu kesme kuvvetlerini, kesme sıcaklığını ve dolaylı olarak deliğin yüzey kalitesini ve ölçü tamlığını etkilemektedir. Ayrıca, delme işlemleri sırasında talaşın atılabilirliği delik kalitesini doğrudan etkilemekte olup, bu süreç kesme parametrelerine (kesme hızı, ilerleme miktarı vb.) göre değişmektedir. Kesme hızı ve ilerleme miktarı delik delmedeki en önemli parametrelerdir. Bunlar kesme işlemi sırasında meydana gelen sıcaklık ve kesme kuvvetlerini doğrudan etkilemekte olup, kesici takımın (matkap ucu) performansını belirleyen unsurlardır [3,4].

Kesici takımın daha uzun süre kullanılabilmesi ve iş parçasının istenilen kalitede işlenerek hammadde israfını önlemeye yönelik olarak, kesme simülasyonları ve modellemeleri yapılmaktadır. Bu modellemeler ile talaşlı imalatın bir parçası olan delme işleminde yapılan iyileştirmeler imalat maliyetinin düşürülmesi ve rekabet edebilme şansının doğması açısından önemlidir. Yapılan her bir iyileştirme talaşlı imalatla sonuca en kısa yoldan ulaşma anlamına gelmektedir. Bu da rekabet ortamında üreticilerin rekabet edebilme şanslarını arttıracak ve malzeme israfını önlemiş olacağından ülkemiz ekonomisine katkı sağlamış olacaktır [5]. Bu bağlamda, Yang ve Sun Ti6Al4V alaşımı için üç boyutlu sonlu eleman modeline dayalı delme işlemini gerçekleştirmişlerdir. Tahmin edilen kesme kuvvetinin deneysel değerlerle karşılaştırılması sonlu eleman modelinin kullanılabilirliğini göstermiştir. Delme işlemi sırasındaki Von-Mises gerilmesi ve sıcaklığı, ilk başta artış gösterip maksimum değere ulaşmış, fakat daha sonra delme işlemi stabil hale geldiğinde, delik delinene kadar kademeli olarak azalmıştır [6]. İşbilir ve Gassamaeh, ABAQUS/Explicit ticari sonlu elemanlar yazılımı kullanarak bir 3D model geliştirmişlerdir. Önerilen model, matkap ucu ve iş parçası ile proses parametreleri arasındaki arayüzde bir temas modeli olan iş parçası malzemesinin hasar başlangıcı ve büyümesi dikkate alınarak delme işlemini simüle etmektedir. Simülasyonların sonuçları, işleme parametrelerinin delme üzerindeki etkilerini göstermektedir. Sonuçlar ayrıca delme sürecinin sonlu elemanlar simülasyonunun doğruluğunu ve avantajını doğrulamaktadır [7]. Muhammad ve arkadaşları, AISI 1010 çeliğinin delme işlemi için MSC MARC MENTAT ticari kodu kullanılarak 3 boyutlu termo-mekanik sonlu

elemanlar modeli geliştirmişlerdir [8]. Güncellenmiş Lagrangian yöntem analizi, modeldeki elasto-plastik malzeme için geçici analiz sağlamak adına kullanılmıştır. Johnson-Cook malzeme modeli elasto-plastik malzeme deformasyonu için kullanılır [9]. Modelde kesme parametrelerinin (kesme hızı, ilerleme miktarı) itme kuvveti ve tork üzerindeki etkisi incelenmiştir. Düzeltilmiş kayma sürtünme modeli, delme işlemi sırasında yağlama ve itme kuvveti üzerindeki yağlamanın etkisini araştırmak için kullanılmıştır [8]. Uçun çalışmasında, Al7075-T6 alüminyum alaşımının delme işleminde iki ve üç ağızlı matkapların performanslarını deneysel ve nümerik olarak incelemiştir. Deney aşamasında, üç farklı ilerleme miktarında (0.05, 0.1, 0.2 mm/dev) ve dört farklı kesme hızında (60, 90, 120, 150 m/dak) delme işlemleri gerçekleştirilmiştir. Delme işlemleri sırasında meydana gelen itme kuvvetleri Kistler 9257B tipi dinamometre ile ölçülmüştür. Nümerik olarak, delme işleminin 3D sonlu elemanlar modeli DEFORM-3D yazılımı ile gerçekleştirilmiştir. Delme işleminin sonlu elemanlar analizi sırasında, itme kuvvetleri sayısal olarak elde edilmiş ve deneysel itme kuvvetleri ile karşılaştırılmıştır. Ayrıca delme işleminde meydana gelen tork ve takım gerilmesi nümerik olarak belirlenmiştir. Çalışmanın sonunda, deneysel ve nümerik sonuçlar arasında yüksek oranda benzerlik olduğu vurgulanmıştır. Buna ek olarak, iki ağızlı matkap ile elde edilen itme kuvveti, tork ve takım gerilmesinin 3 ağızlı matkabinkinden daha az olduğu belirlenmiştir [10]. Gök ve arkadaşları, distal femurun Salter-Harris (SH) tip-3 epifiz kırıklarının azaltılmasından sonra stabilizasyon için Kirschner teli (K-teli) ile delme işlemi yapmışlardır. Çalışma hem deneysel hem de nümerik olarak incelenmiştir. Sayısal analizler DEFORM-3D yazılımı kullanılarak sonlu elemanlar yöntemi ile yapılmıştır. Deney sonuçları ve sonlu elemanlar analizi (FEA) sonuçları arasında iyi bir tutarlılık elde edilmiştir. Bu durum, bu modelin delme işlemlerinde güvenilir bir şekilde kullanılabileceğini göstermiştir [11]. Bu çalışmada, Al2014 alüminyum alaşımının kaplamasız sementit karbür matkap ile delinmesi sonucunda itme kuvvetinin deneysel ve sonlu elemanlar modeline dayalı delme işlemi sonuçları kıyaslanmıştır.

## II. MALZEME VE YÖNTEM

AA2014 alüminyum alaşımı için delme deneyleri ve simülasyonlarda ilerleme miktarı ve kesme hızının üç farklı seviyesi kullanılmış olup, bu seviyeler ilgili literatür çalışmaları dikkate alınarak seçilmiştir. Kesici takım olarak, iki kesme kenarlı 14 mm çapında yekpare (solid) helisel karbür matkaplar kullanılmıştır. İtme kuvvetini deneysel olarak belirlemek için Kistler 9272 tipi dinamometre ve Kistler Type 5070 amplifier kullanılmış olup, delme deneyleri Johnford VMC-550 marka CNC dik işleme merkezinde yapılmıştır.

İşleme simülasyonları için yaygın olarak kullanılan [12] Johnson-Cook malzeme modeli Eşitlik 1'de verilmektedir. Malzeme modeli ağırlıklı olarak yüksek gerilme oranı metallere deformasyon davranışı için uygundur. Genellikle plastik deformasyon süreçlerinin adyabatik geçici dinamik analizinde kullanılmaktadır. Bu modele göre sertleşme, akma

gerilmesinin  $\sigma_0$  olarak kabul edildiği belirli bir izotropik sertleşme türüdür [13]:

$$\sigma^0 = (A + B(\epsilon^p)^n) \left( 1 + C \left( \frac{\dot{\epsilon}^p}{\dot{\epsilon}_0} \right) \right) \left( 1 - \left( \frac{T - T_r}{T_m - T_r} \right)^m \right)$$

Eşitlik 1'de A, B, C, n ve m olan mekanik testler yardımıyla elde edilen malzeme parametreleri sırasıyla oda sıcaklığının altında akma gerilmesi, gerinim sertleşmesi, gerinim hızı sabiti, gerinim sertleşme sabiti ve ısıl yumuşama sabitidir. Diğer parametreler, sırasıyla eşdeğer plastik gerinim, plastik gerinme oranı, referans gerinim oranı, oda sıcaklığı, erime sıcaklığı ve referans sıcaklığı olan  $\epsilon^p$ ,  $\dot{\epsilon}^p$ ,  $\dot{\epsilon}_0$ ,  $T_r$ ,  $T_m$ ,  $T$ 'dir. Al2014 alaşımı için Johnson-Cook parametreleri ve diğer malzeme parametreleri sırasıyla Çizelge 1 ve Çizelge 2'de verilmektedir.

ÇİZELGE 1.

Al2014 alaşımının Johnson-Cook parametreleri

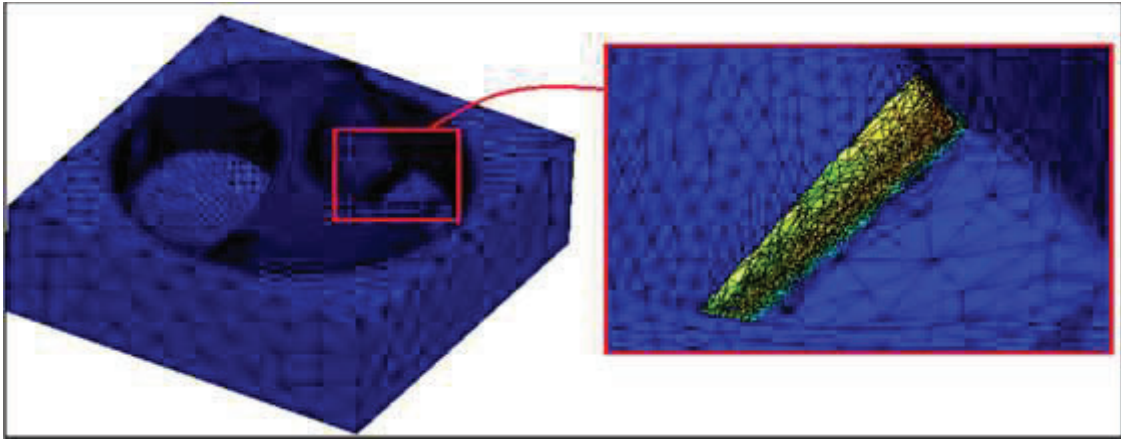
A (MPa)	B (MPa)	C	n	m	$T_r$ (°C)	$T_m$ (°C)	$\epsilon_u$
345	780	0.0083	0.17	1.7	27	638	1

ÇİZELGE 2.

Al2014 alaşımı için diğer malzeme parametreleri

Yoğunluk (g/cm <sup>3</sup> )	Poisson oranı	Elastik Modülü (GPa)	Termal İletkenlik (W/m.K)	Özgül Isı (J/kg°C)	Termal Genleşme (10 <sup>-6</sup> °C)
2.8	0.33	73.1	121	875	24.7

İtme kuvveti için delme simülasyonları Advantedge yazılımı ile sonlu elemanlar yöntemine dayalı olarak gerçekleştirilmiştir. Simülasyonun ilk aşamasında, iş parçası malzemesinin uzunluğu (17mm), genişliği (17 mm) ve yüksekliği (6 mm) belirlenmektedir. İkinci aşamada, takım geometrisi (helis açısı, uç açısı ve kesme ağız sayısı) ve takım malzemesi parametreleri tanımlanmaktadır. Son aşamada, ilerleme miktarı, kesme uzunluğu ve kesme hızı gibi gerekli delme simülasyonu parametreleri ve sürtünme katsayısı tanımlanarak delme simülasyonu gerçekleştirilmektedir. Takım ve iş parçası arasındaki arayüz durumu için Coulomb modeli kullanılmış olup, sürtünme katsayısı 0.6 olarak seçilmiştir. Mesh parametreleri sırasıyla maksimum ve minimum eleman boyutları için 0.1 mm ve 0.02 mm olarak kullanılmıştır (Şekil 1). Delme deneyleri ve simülasyonlarında kullanılan kesme parametreleri Çizelge 3'te verilmiştir. Al2014 alaşımının delinmesinde oluşan itme kuvvetlerini tahmin edebilmek için delme simülasyonlarında takım 60° döndürülerek iş parçası 7.33 mm kesilmiştir.



Şekil 1. Kesici takım ağ yapısı

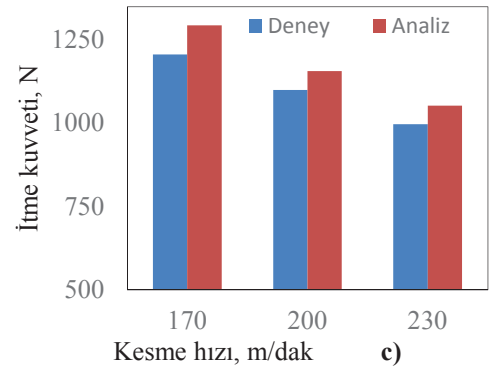
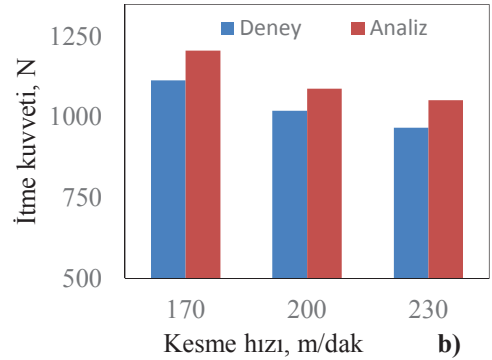
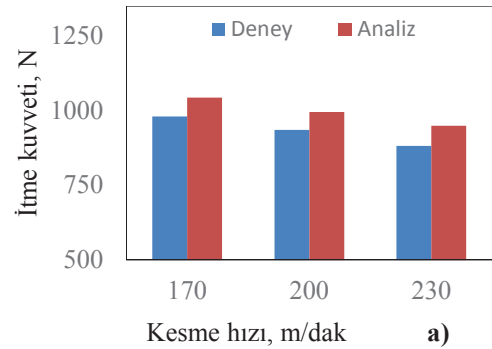
ÇİZELGE 3.  
Kesme parametreleri

Parametre	Seviye		
	1	2	3
İlerleme miktarı (f, mm/dev)	0.1	0.2	0.3
Kesme hızı (V, m/dak)	170	200	230

### III. BULGULAR VE TARTIŞMA

Belirlenen delme parametreleri ışığında gerçekleştirilen deneyler ile sonlu elemanlar modeline dayalı nümerik analizler karşılaştırıldığında, itme kuvvetleri arasında ortalama %7'lik bir fark belirlenmiştir. Şekil 2'deki grafikler incelenecek olursa, genellikle delme simülasyonu sonucunda elde edilen itme kuvvetlerinin yüksek olduğu görülebilir. Bu sonucun, büyük oranda Al2014 alaşımı Johnson-Cook malzeme modeli parametrelerine bağlı olduğu düşünülmektedir. Ayrıca, ilerleme miktarının artmasıyla itme kuvvetleri artarken, kesme hızının artmasıyla kuvvet değerlerinin azaldığı belirlenmiş olup, bu sonuç literatürle paralellik göstermektedir. Şekil 2'deki grafiklerde, deneyler ve simülasyonlar sonucunda elde edilen kesme kuvvetlerinin kesme hızı ve ilerleme miktarına göre değişimleri verilmiştir. Şekil 2a'da görüldüğü üzere, ilerleme miktarı 0.1 mm/dev iken, kesme hızının 170 m/dak'dan 230 m/dak'ya çıkarılmasıyla kesme kuvveti %10 azalmıştır. Benzer durum Şekil 2b ve 2c'de görülmüş olup, ilerleme miktarı 0.2 ve 0.3 mm/dev'de sabit tutulduğunda kesme hızı 170 m/dak'dan 230 m/dak'ya çıkarıldığında kesme kuvvetleri sırasıyla %13.2 ve %17.3 azalmıştır.

Diğer yandan, Şekil 2a-2c incelendiğinde, kesme hızının kesme kuvveti üzerinde azaltıcı bir etkisi olduğu görülmektedir. Bu grafiklere göre ilerleme miktarının etkisi değerlendirildiğinde, 170 m/dak sabit kesme hızında ilerleme miktarının 0.1 mm/dev'den 0.3 mm/dev'e artırılmasıyla kesme kuvveti %22.9 artmıştır. 200 m/dak ve 230 m/dak kesme hızlarında, ilerleme miktarının 0.1 mm/dev'den 0.3 mm/dev'e artmasıyla kesme kuvveti sırasıyla %17.6 ve %13 artmıştır. Tüm sonuçlar dikkate alındığında, itme kuvveti üzerinde ilerleme miktarının kesme hızına oranla daha etkin parametre olduğu söylenebilir.



Şekil 2. Fz'nin karşılaştırılması; a) f= 0.1 mm/rev, b) f= 0.2 mm/rev, c) f= 0.3 mm/rev

#### IV. SONUÇLAR

Bu çalışmada, Al2014 alüminyum alaşımının kaplamasız sementit karbür takım ile delinmesi sonucunda itme kuvvetinin deneysel ve simülasyon sonuçları karşılaştırılmıştır. Elde edilen sonuçlar aşağıda özetlenmiştir.

- İlerleme miktarının (f) artması ile hem deneysel hem de nümerik analiz sonuçlarında itme kuvvetinin (Fz) arttığı gözlenirken, kesme hızının artması ile itme kuvvetinin (Fz) azaldığı belirlenmiştir.
- Deneysel ve simülasyon sonuçları arasında ortalama %7'lik bir sapma olduğu tespit edilmiştir. Bu sonuç, sonlu elemanlar modeline dayalı delme simülasyonlarında itme kuvvetinin tahmin edilebileceğini göstermiştir.
- Bu sonuçlara göre, itme kuvveti tahmini için geliştirilecek matematiksel modele bağlı olarak farklı delme parametreleri için Fz değerleri hesaplanabilir.

#### KAYNAKLAR

- [1] S. V. Prasad, R. Asthana, "Aluminum metal-matrix composites for automotive applications: tribological considerations", *Tribology Letters*, 2004, 17: 445-453.
- [2] H. Raghubanshi, E. D. Dikio, E. B. Naidoo, "The properties and applications of helical carbon fibers and related materials: a review", *Journal of Industrial and Engineering Chemistry*, 2016, 44: 23-42.
- [3] Sandvik Coromant, *Modern Metal Cutting*, Sweden 1994, s. 2-61
- [4] S. Kalidas, R. E. DeVor, S. G. Kapoor, "Experimental investigation of the effect of drill coatings on hole quality under dry and wet drilling conditions", *Surface and Coatings Technology*, 2001, 117-128.
- [5] M. Arafat, "CNC delme işleminde delme parametrelerinin yüzey pürüzlülüğü açısından optimizasyonu", Yüksek Lisans Tezi, Erciyes Üniversitesi Fen Bilimleri Enstitüsü, Kayseri, 2009.
- [6] Y. Yang, J. Sun, "Finite Element Modelling and Simulating of Drilling of Titanium Alloy", *2nd International Conference on Information and Computing Science*, Manchester, UK, 21-22 May, 2009.
- [7] O. Isbilir, E. Ghassemieh, "Finite Element Analysis of Drilling of Titanium Alloy", *Procedia Engineering*, 2011, 10: 1877-1882.
- [8] R. Muhammad, N. Ahmed, Y. M. Sharif, V. Silberschmidt, "3D Finite Element Modelling of Drilling Process", *20th IWCMM*, Loughborough University, Loughborough, 2010.
- [9] M. E. Korkmaz, M. Günay, "Finite Element Modelling of Cutting Forces and Power Consumption in Turning of AISI 420 Martensitic Stainless Steel", *Arabian Journal for Science and Engineering*, 2018, 43:4863-4870.
- [10] İ. Ucu, "3D finite element modelling of drilling process of Al7075-T6 alloy and experimental validation", *Journal of Mechanical Science and Technology*, 2016, 30 (4): 1843-1850.
- [11] A. Gok, K. Gok, M. B. Bilgin, "Three-dimensional finite element model of the drilling process used for fixation of Salter-Harris type-3 fractures by using a K-wire", *Mech. Sci.*, 2015, 6, 147-154.
- [12] G. J. Johnson, W. H. Cook, "A constitutive model and data for metals subjected to large strains, high strain rates and high temperatures". *Proceedings of the Seventh International Symposium on Ballistics*, The Hague, 541-547, 1983.
- [13] A. Dorogoy, D. Rittel, "Determination of the Johnson-Cook material parameters using the SCS specimen" *Exp. Mech.* 49, 881-885, 2009.
- [14] N. Yaşar, M. E. Korkmaz, M. Günay, "Investigation on hole quality of cutting conditions in drilling of CFRP composite", *MATEC Web of Conferences*, 2017, 112: 1-7.

# Friction And Wear Properties Of T6 Treatment And As-Plated Duplex Ni-P/Ni-B Coatings On AZ91D Magnesium Alloy (ISLAC'18/UHAKS18)

Kübra Uçar <sup>1</sup>, Ugur Şen <sup>2</sup>,

Turkey

ugursen@sakarya.edu.tr

Department of Metallurgical and Materials Engineering,  
Sakarya University, Sakarya, Turkey

kubra.ucar4@ogr.sakarya.edu.tr

**Abstract:** Electroless nickel coatings can be preferred in wear resistant applications like firearms with good lubricity properties. In this study, a widely-used magnesium alloy, AZ91D both as-cast and precipitation-hardened conditions were coated with nickel phosphorus/nickel boron duplex coatings by the electroless deposition method. Solution treatment (W) of the alloy was carried out at 415 °C for 22 h in carbon powder followed by water quenched at 25 °C. Aging treatment (T6) of the solution-treated samples was performed at 216 °C for 6 h. The microstructures, elemental distributions and phase analysis of the obtained coatings were characterized by scanning electron microscopy (SEM), energy dispersive X-ray spectrometry (EDS) and X-ray diffraction (XRD) analysis. According to the XRD analysis, the obtained coatings have an amorphous character and subsequent to this, a crystallization process to the sample is carried out at 350 °C. The friction and wear properties of the coating are studied by means of ball-on-disc experiments at room temperature under 10N applied loads at 0.1 m/s sliding speed using alumina balls as counterparts. The friction coefficient of the sample was compared with each other from friction coefficient-distance graphics. The wear rates were determined by measuring the depth of the track with an 3D-optical microscope (3D-OM). Characterization of the wear tracks was performed by SEM and EDS.

**Keywords:** Electroless nickel coatings, Wear, AZ91D, electroless bath, SEM

## I. INTRODUCTION

Magnesium alloys have an important place in the defense industry and transportation sector due to their lightness and high specific strength properties (Strength / density). When unalloyed, magnesium alloys have low strength and toughness values, thus it is used by alloying. AZ91D is composed of three main phases according to Al distribution found in the structure of magnesium alloy, these are primary  $\alpha$  phase, eutectic  $\alpha$  phase (Al-rich),  $\beta$  phase which is chemical and heterogeneous depending on.  $\beta$  phase eutectic  $\alpha$  is more cathodic than primary  $\alpha$  phase.

Several studies have shown that the accumulation of Ni-P coating is nucleated on the position of  $\beta$  phase and that eutectic- $\alpha$  and primary- $\alpha$  phase are dispersed in the coating process. The initial accumulation in the electroless plating bath is severely affected by the galvanic couple between  $\beta$  phase and  $\alpha$  phase. Hence, the aging process results in the precipitation of  $\beta$  phase along the grain boundaries of the homogenized AZ91D magnesium alloy, and  $\beta$  phase acts as a physical barrier against the active cathode or corrosion. Clark reported an aging mechanism in the AZ91 series magnesium alloy, and found that both continuous and discontinuous  $\beta$  precipitates occurred [1]. For this, T6 treatment was deemed suitable before plating. The most difficult and critical part of the magnesium alloy is pretreatment to obtain high anti-corrosion resistance, substrate surface adhesion performance, mechanical properties and high-performance coating. Therefore, the oxide layer should be removed before the electroless plating process. In general, there is a superior adhesion strength when electroless coatings are applied in comparison with the electroplating method which is due to the presence of a strong metal-metal bond during plating. Electroless Ni-P alloy coating on magnesium is an effective method to change the wear and corrosion resistance of substrate materials as it shows good corrosion resistance. The Ni alloy is cathodic to the magnesium alloy base and acts as a physical barrier against corrosion of the bottom layer. However, electroless Ni-P coatings have superior properties such as high hardness, high abrasion resistance, excellent solderability and good conductivity in comparison with the Ni-B coatings. Electroless Ni-B coatings are less porous compared to electrolytic coatings. Ni-B coatings are obtained by reduction of borohydride ions or amine-borane ions, the structure and properties vary depending on the amount of boron incorporated into the coating.

For any tribology-based application, the purpose of the coating is to reduce friction coefficient and improve abrasion resistance by imparting smoothness and hardness to the surface.

Since boron is one of the most important amorphous elements, it is prepared to look for superior qualities in various alloys.

Vitry et al. thoroughly investigated the wear behaviors of extruded Ni-B coatings, but they have been extensively focused on Taber abrasion and scratching [2].

The procedure we have developed in this study is to obtain a smooth, well adherent and abrasion-resistant layer with electroless Ni-B process using uncoated T6 alloyed AZ91D and AZ91D cast alloy with coating. It has been shown that the findings improve the wear rate and durability life of the coating. Furthermore, the coating obtained on the AZ91D alloy base has a better abrasion resistance than the T6 treated uncoated alloy.

## II. EXPERIMENTAL PROCEDURE

### A. Sample Preparation

AZ91D magnesium alloy was used in the substrate of 30x20x5 mm<sup>3</sup> dimensions. Before the pretreatment, substrate was ground with metallographic operation up to by 1200 grid SiC emery paper and polished with 0.3 µm alumina. When magnesium contacts with air or water, oxide and hydroxide layer on the surface of the magnesium alloys form due to the fact that it is one of the most active metals, electrochemically. Therefore, in this study AZ91D Mg alloy was cleaned with acetone for 5 minutes, then followed by alkaline solution for 15 minutes. However, these cleaners are not enough to remove oxide and similar layers on the surface of the AZ91D Mg alloy. Hence, surfaces of samples were treated with 20 s HCl/H<sub>3</sub>PO<sub>4</sub> and 40 s HF acids in second stages. Thus, AZ91D Mg alloy matrix corrosion can be prevented by this pretreatment.

### B. Bath Preparation And Operating Conditions

Ni-P was coated in the solution of the nickel sulfate 14 gr/L, sodium hypophosphite, 15 gr/L, sodium acetate 12 gr/L, ammonium bi fluoride 8 gr/L, HF 1,8 mL, thallium acetate 0,02 gr at the temperature of 65°C for 20 min. and then Ni-B coatings was realized on the pre-NiP coated samples in the solution of nickel chloride 20 gr/L, sodium borohydride 1,05 gr/L, ethylenediamine 13.5 mL, sodium hydroxide 100 gr/L, thallium acetate 0,11 gr/L at 90°C for 90 minutes at 400 rpm magnetic stirrer. In an alkaline bath, sodium borohydride is used as a reducing agent and nickel chloride is used as a nickel source to prepare a electroless Ni-B bath. Nickel source and sodium borohydride as well as the appropriate amount of coating binder ethylenediamine is included to the coating bath. Thallium acetate is used as the stabilizer. Reduction of sodium borohydride is much higher than that of sodium hypophosphite and dimethylamine borane. The pH value of the alkaline coating bath has been increased to 12, due to the easy dissolution of sodium borohydride easily in the acidic or neutral environment. Therefore, pH value of electroless Ni-B coating bath was chosen as 13.

Zhang et.al. used thiourea as the stabilizer in Ni-P / Ni-B coating on AZ91D magnesium [3]. In the present study, thallium acetate was used in both baths and seen the same effect in the shorter time.

Table 1. Solution concentration and operation conditions of electroless coating Ni-P

<b>Bath composition</b>	
Nickel Sulfate	14 gr/L
Sodyum Hipofosfit	15 gr/L
Sodium Acetate	12 gr/L
HF	1,8 mL
Ammonium bifluoride	8 gr/L
Thallium acetate	0,02 gr
Temperature	65°C
pH	6-6,5

Table 2. Solution concentration and operation conditions of electroless coating Ni-B

<b>Bath composition</b>	
Nickel chloride	20 gr/L
Sodium borohydride	1,05 gr/L
Ethylenediamine	13,5mL
Sodium hydroxide	100 gr/L
Thallium acetate	0,11 gr/L
Operating conditions	
pH	13
Temperature	90°C

### C. Coating Characterization

SEM was used to assess the surface microstructure of Ni-P/NiB duplex coatings. Wear tracks of coatings were performed by SEM and EDS. Phase analysis of samples performed at heat treatment 350 °C for 1 h. was characterized by XRD. A ball-on-disk method was used to determine the friction and wear characteristics of un-coated and Ni-P / Ni-B dublex coated surfaces. Applied load was 10 N and sliding distance was 250 m. Sliding speed, wear scar diameter and the rotational speed of the disc was fixed at 0.1 m/s. The experiments were performed at about 35% relative humidity and 25°C heat degree.

After the wear test, the surfaces of the sample was cleaned in an ultrasonic agitator for approximately 8 minutes in acetone to remove abrasive particles on the surface. In addition, wear volume realized on the worn sample was calculated from the wear track cross-section area determined by optical profilometer and sliding distance using by eq.1

$$V = lA$$

where, l is the circumference of the wear track and A is the cross-sectional wear track area.

Wear track was examined using by Jeol 6060 Lv scanning electron microscopy (SEM). Table 2 presents the parameters used in the wear test. 3D imaging of the wear track was performed using the Huvitz HR-SPLG4 profilometer.

**Table 2** Electroless Ni-B coating conditions of the wear test.

Parameter	Ball-on-disk test
Ball diameter (mm)	10.45
Moving sample	Sample
Applied force (N)	10
Sliding velocity (m/s)	0.1
Humidity	35
Motion	Unidirectional
Temperature	25
Test length (m)	250
Test Ball	Al <sub>2</sub> O <sub>3</sub>

### III. RESULTS AND DISCUSSIONS

#### D. Coating Characteristics

The surface morphology of the Ni-P coating is shown in the Figure 1. The Ni-P coating is very compact and it has even been seen that there are no defects such as holes and cracks on the surface. As shown from the Figure 1, Ni-P coating on AZ91D magnesium alloy has been successfully carried out. There are significant boundaries in the nodules. As shown from the Figure 1 (b), coating layer includes Ni and P elements.

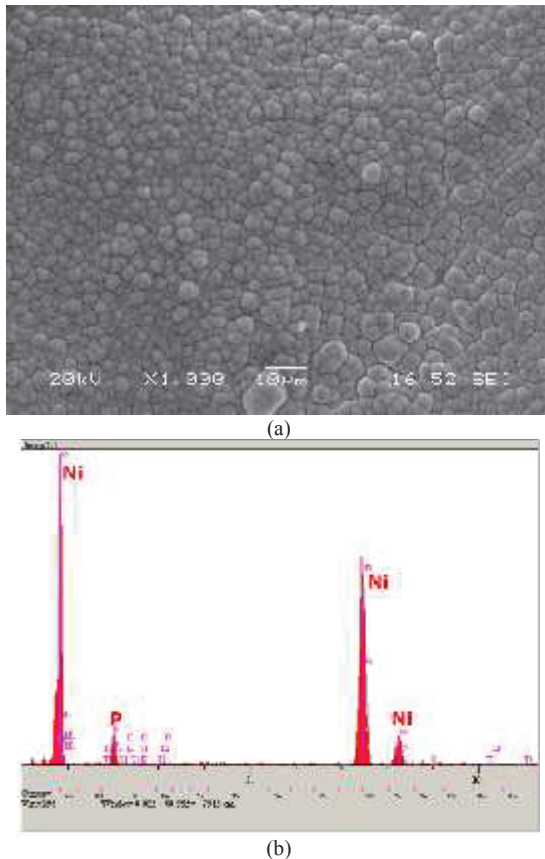


Fig. 1 (a) SEM images and (b) EDS analysis of the electroless Ni-P deposition on AZ91D substrate

A typical 'nodular-like' structure or 'cauliflower' -like structure provides a natural slippery texture in scanning

electron microscopy images of the electroless double layer Ni-P / Ni-B coatings as shown in Figure 2. It exposes a properly coated surface that includes nodules whose dimensions ranging between a few microns. On the morphological surface of the duplex coating, the Ni-B coating dominates, but the Ni-P adheres very well to the bottom layer. As can be seen from the SEM-images, the double-layer coating seems to have less porosity and rough surface. Kanta et al. observed that after coating, the surface roughness of the electroless coating was significantly higher [4].

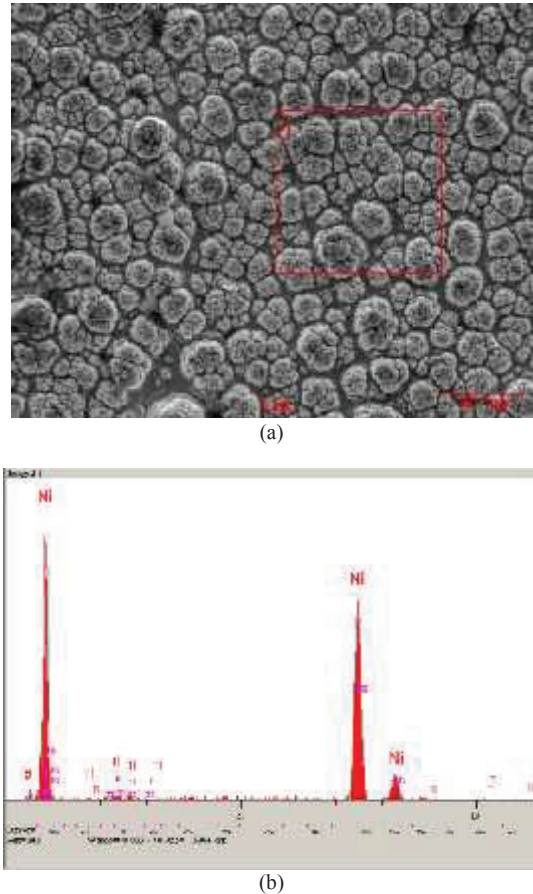


Fig. 2. (a) SEM image and (b) EDS analysis of Ni-B coatings realized on pre-NiP coated AZ91D magnesium alloy

EDS analysis was performed to determine the chemical composition of the coatings. The electroless Ni-P / Ni-B coated sample includes Ni, Ti and B elements as shown in Figure 2 (b).

Cross-sectional SEM image of the Ni-P / Ni-B coating formed on the AZ91D Mg alloy was shown in Figure 3. The coating layer was compact, porosity-free and rough. The coating layer were well bonded on the AZ91D alloy. The coating layer average thickness was  $29.3 \pm 4.2 \mu\text{m}$ .

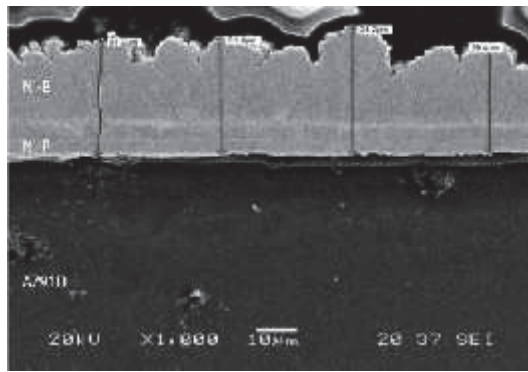


Fig. 3. The cross-sectional image of the duplex NiP/NiB coating.

The X-ray diffraction pattern of the electroless Ni-B coating shows a single broad peak indicating the amorphous nature of the coating as coat. Theoretically, an irregularity in the ordering of the atoms also manifests itself as a broad peak at the XRD. Post crystallization heat treatment caused to crystallization of the amorphous coating to be formed composite structure includes Ni matrix and Ni<sub>3</sub>B precipitates. XRD patterns of electroless Ni-B coatings post-crystallization heat treated for 1 h in 350°C, confirms the formation of Ni<sub>3</sub>B precipitate phase together with Ni matrix, see Figure 4.

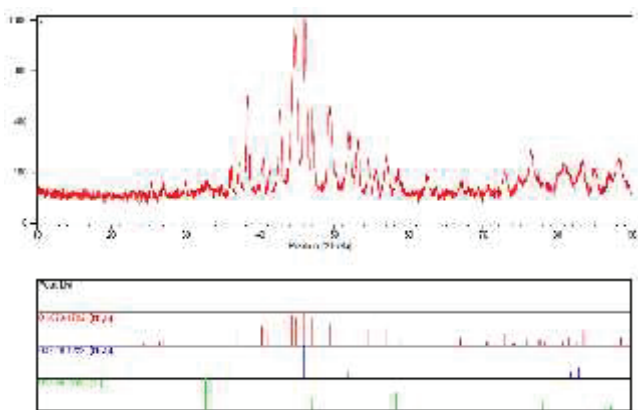
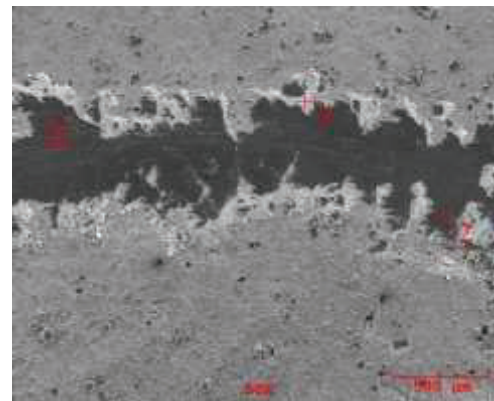


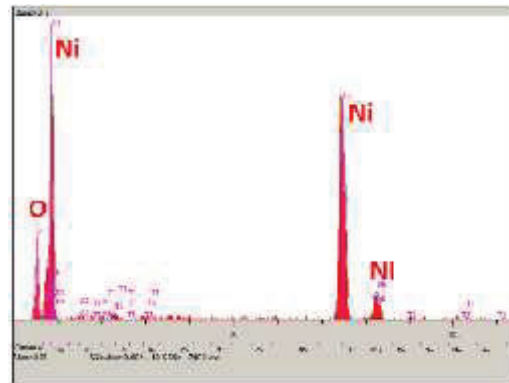
Figure 4. XRD analysis of electroless Ni-B coatings.

### E. Wear Mechanism Of The Coatings

In the Fig. 5 (a), SEM image of the Ni-P/Ni-B coating showed that wear track showed a adhesive wear with micro-abrasive scratch. Wear mod was micro abrasive adhesive coating. As seen from the Figure 5 (b-d), EDS analysis of the worn surface include oxygen besides the Ni and B elements. Wear mod of the coting was oxidative adhesive and micro-abrasive.



(a)



(b)

Fig. 5. (a) Scanning electron micrograph and (b) EDS analysis of the wear track of the NiP/NiB coating (Applied load: 10 N; Sliding distance: 250 m)

No significant adhesion is observed on the counter alumina ball during the along the wear, as can be seen in Figure 6. During the wear test, at the initial period of the test, top surface of the coating layer was polished and rough surface was getting smooth layer on the wear track. The Ni-P/Ni-B coating with a smooth surface breaks into the rough top regions during wear test in the running in 50 m sliding distance. As defined in the EDS analysis, there are partially covered oxide particles in some areas on the wear surface of the duplex coating. The presence of oxygen on the wear track is probably due to the oxidation of the Ni-B based coating during the wear test.

The friction coefficient of the T6 heat treated AZ91D alloy and Ni-P/Ni-B duplex coatings realized on the T6 heat treated samples were measured under the dry sliding conditions.

As shown from Figure 7 that T6 heat treated samples was getting steady-state behavior in the running in period of 10m. Whereas, Ni-P/Ni-B coated samples friction coefficient was getting increase slightly during the wear test. Friction behavior of the coated samples increases sharply up to 20m sliding distance and then was getting increase slightly during the all wear test. Friction coefficient of T6 heat treated samples and the coated samples were getting increase up to 0.33μm and 0.57μm, respectively. E. Correa et.al was studied about the NiB

electroless coatings' versus  $Al_2O_3$  ball for 50m sliding distance [5]. As shown from Figure 7 in the present study, friction coefficient values were similar and increase in sliding distance caused to increase during the wear test. In addition that, in the present study, wear test was applied for 250 m sliding distance and friction coefficient value increased during the wear test up to  $0.57\mu m$  value.

It was seen from the Figures 8 and 9 that the optical 3D profiles and cross-sectional view of the wear tracks of the T6 heat treated AZ91D alloy and T6 heat treated and Ni-P/Ni-B

dublex coated samples, respectively. Wear volume of the worn samples were calculated from the cross-sectional area of the worn samples wear tracks using the formula of Eq. 1. As shown from the Figure 10 that the wear rates of the dublex coating was 97.74 % lower than that of the T6 heat treated AZ91D alloy. E. Correa et.al's study showed that the wear rate of the dublex NiP/Ni-B coatings was 98,67 % lower than that of the AZ91D alloy [5].

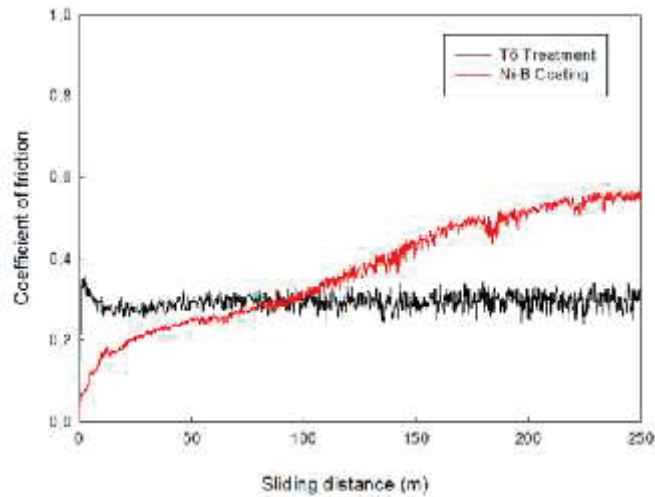


Fig. 7. Evolution of Coefficient of friction with sliding duration

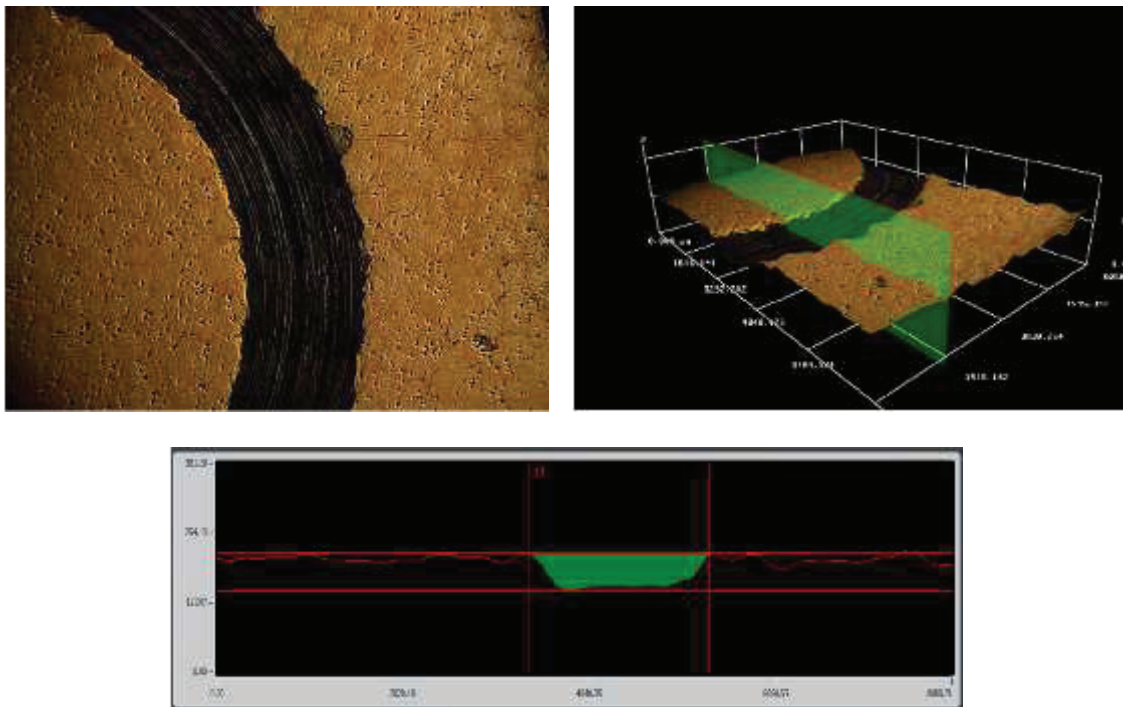


Fig 8. 3D optical profilometer image and crosssectional area of the worn track of T6 heat treated AZ91D alloy

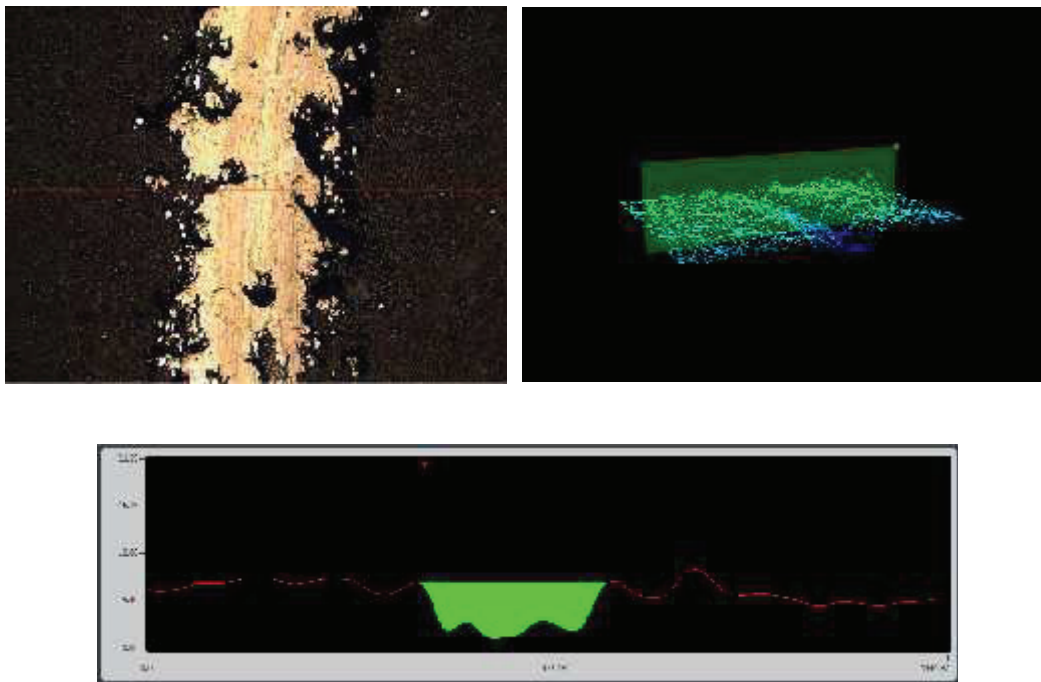


Fig 9. 3D optical profilometer image and crosssectional area of the worn track of T6 heat treated and Ni-P/Ni-B duplex coatings of AZ91D alloy

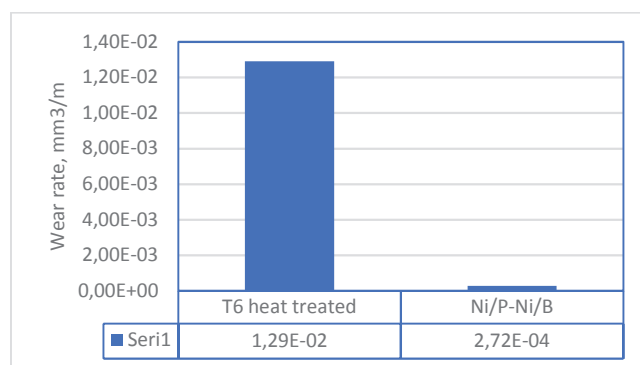


Fig 10. Wear rate values of surfaces uncoated and Ni-P / Ni-B coated

#### IV. CONCLUSIONS

It is observed that the Ni-P / Ni-B coating has a favorable as tribological effect on the T6 heat treated specimen. General results obtained without work;

1-The sample which is Ni-P/Ni-B coated exposed to the wear test, has been subjected to the a certain load but no coating is completely removed from the surface.

2-Ni-P / Ni-B coating layer is located on the entire surface of the AZ91D magnesium alloy substrate, exhibiting a partially smooth, pore-free, nodular structure.

3-The presence of abrasion residues in the undercoating conditions , confirms the adhesive wear mechanism.

4-Duplex Ni-P / Ni-B coating with the lowest wear rate increases wear resistance of T6 heat treated AZ91D alloy.

5- The wear rate of the Ni-P / Ni-B duplex coatings is lower than that from the T6 heat treated sample and not observed significant changes in the friction coefficients.

6-As wear testing results show , of the Ni-B coating is well adhered to the Ni-P layer coating and both of them exhibit coherent to each other.

#### REFERENCES

- [1] N.N. Aung,W. Zhou, "Effect of heat treatment on corrosion and electrochemical behavior of AZ91D magnesium alloy," *Journal Of Applied Electrochemistry*, 32 1397–1401, 2002.
- [2] Fatemeh Madah, Ahmad Ali Amade, Changiz Dehghanian, "Investigation on the phase transformation of electroless Ni -B coating after dry sliding against alumina ball," *Journal of Alloys and Compounds*, 658 272, 2016
- [3] E. Correa, A.A. Zuleta, L. Guerra, M.A. Gómez, J.G. Castaño, F. Echeverría , H. Liu, A. Baron-Wieche,T. Hashimoto , P. Skeldon, G.E.Thompson, "Coating development during electroless Ni –B plating on magnesium and AZ91D alloy," *Surface & Coatings Technology* 232 784,2013

- [4] Prasanta Sahoo, Suman Kalyan Das, “Tribology of electroless nickel coatings – A review,” *Materials and Design*, 32 1760,2011
- [5] E. Correa, A.A. Zuleta, L. Guerra, M.A. Gómez, J.G. Castaño, F. Echeverri, H. Liu, P. Skeldon, G.E. Thompson “Tribological behavior of electroless Ni-B coatings on magnesium and AZ91D alloy”, *Wear*, 305 115-123, 2013
- [6] Z.C. Wang, F. Jia, L. Yu, Z.B. Qi, Y. Tang, G.-L. Song “Direct electroless nickel boron plating on AZ91D magnesium alloy,” *Surface & Coatings Technology*, 206 3676-3685, 2012
- [7] Zhou-Cheng Wang, Lu Yu, Fei Jia, and Guang-Ling Song “Effect of Additives and Heat Treatment on the Formation and Performance of Electroless Nickel-Boron Plating on AZ91D Mg Alloy,” *Journal of The Electrochemical Society* 159(7), 2012
- [8] Fatemeh Madah, Changiz Dehghanian, Ahmad Ali Amadeh, “Investigations on the wear mechanisms of electroless Ni-B coating during dry sliding and endurance life of the worn surfaces,” *Surface & Coatings Technology*, 282 6-15, 2015
- [9] Zeng, Shiwei Yang, Wei Zhang, Yahuan Guo, Chuanwei Yan, “Preparation and characterization of a double-layer coating on magnesium alloy AZ91D,” *Electrochimica Acta* 55 3376–3383, 2010
- [10] J.E. Gray, B. Luan, “Protective coatings on magnesium and its alloys a critical review,” *Journal of Alloys and Compounds*, 336 88–113, 2002
- [11] Arkadeb Mukhopadhyay, Tapan Kumar Barman, Prasanta Sahoo, “Tribological behavior of sodium borohydride reduced electroless nickel alloy coatings at room and elevated temperatures,” *Surface & Coatings Technology*, 321 464-476, 2017
- [12] A.-F. Kanta, M. Poelman, V. Vitry, F. Delaunois, “Nickel-boron electrochemical properties investigations,” *Journal of Alloys and Compounds*, 505 151–156, 2010
- [13] C. Subramanian, K. Palaniradja, “Effect of Surfactant on the Electroless Ni-P/Ni-B Duplex Coatings on Aluminium 7075,” *International Journal of Metallurgical Engineering* Vol. 4 2015 No. 2,
- [14] K. Krishnaveni, T.S.N. Sankara Narayanan, S.K. Seshadri “Electroless Ni-B coatings: preparation and evaluation of hardness and wear resistance,” *Surface & Coatings Technology*, 190 115–121, 2005
- [15] L. Bonin, V. Vitry “Mechanical and wear characterization of electroless nickel mono and bilayers and high boron-mid phosphorus electroless nickel duplex coatings,” *Surface & Coatings Technology*, 307 957–962, 2016
- [16] Y.Y. Lv, Z. Liub, H. Liu, G.E. Thompson, H. Liu, “Dry sliding wear behavior and structural characteristics of laser-annealed electroless Ni-P/Ni-Mo-P duplex coatings,” *Tribology International*, 103 343-351, 2016
- [17] W.X. Zhang, N. Huang, J.G. He, Z.H. Jiang, Q. Jiang, J.S. Lian, “Electroless deposition of Ni-W-P coating on AZ91D magnesium alloy,” *Applied Surface Science*, 253 5116–5121, 2007
- [18] F. Masoumi, H. R. Ghasemi, A. A. Ziaei, D. Shahriar “Tribological characterization of electroless Ni-10% P coatings at elevated test temperature under dry conditions,” *Int J Adv Manuf Technol* 62:1063–1070, 2012

# Investigation of the Properties of Oxide Coating Layer TiO<sub>2</sub> on Ti-6Al-4V Alloy by a Thermal Oxidation Method (ISLAC'18/UHAKS18)

Mustafa Kabacan, Aysun Ayday

Sakarya University, Engineering Faculty,  
Department of Metallurgical and Materials Engineering,  
Sakarya, 54187, Turkey

\*Corresponding author: [aayday@sakarya.edu.tr](mailto:aayday@sakarya.edu.tr)

**Abstract**— TiO<sub>2</sub> coatings were fabricated by thermal oxidation on a Ti-6Al-4V alloy substrate. Thermal oxidation was carried out in varied temperature/time conditions (temperature: 600, 650 °C, time: 1-2-4-8-16-24-48-72 h). The effects of temperatures on structure properties of TiO<sub>2</sub> were studied by X-ray diffraction (XRD) and microhardness. Thermal oxidation parameters affected hardness of the obtained oxide layers, which increased along with oxidation time and temperature.

**Keywords**—Thermal oxidation, Oxide layers, Ti-6Al-4V, Rutile, Hardness.

## I. INTRODUCTION

Owing to its excellent mechanical properties and corrosion resistance, Ti-6Al-4V alloy has been widely used in different industrial fields, including aerospace components, chemical processing, and military fields [1-3]. However, titanium and its alloys limit to their various applications such as engineering components because they exhibit poor tribological properties [2,4,5]. These properties were improved by using some surface engineering to produce TiO<sub>2</sub> on alloy. There are various methods to deposit TiO<sub>2</sub> thin film such as sputtering, sol-gel, dip coating and spin coating, filtered arc deposition and laser deposition [2,6,7].

The aim of this study was to determine the influence of thermal oxidation parameters on morphology, hardness of oxide layers formed on Ti-6Al-4V alloy. The TiO<sub>2</sub> films were characterized using X-ray diffraction (XRD), scanning electron microscopy (SEM), and energy-dispersive spectrometry analyses (EDS).

## II. EXPERIMENTAL DETAILS

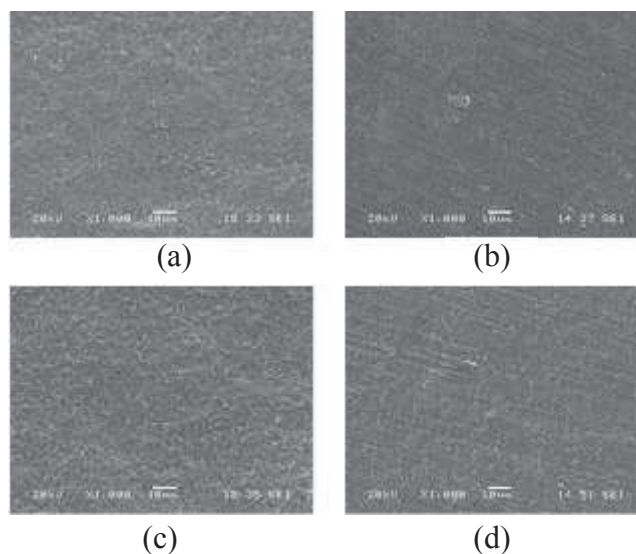
Ti-6Al-4V was used as the thermal oxidation treatment. The samples were machined to be plates with a 1 mm × 15 mm × 60 mm in dimension. The process was conducted at 600, 650 °C for 1-2-4-8-16-24-48-72 h. Before the start of the oxidation process the specimen surfaces were ground with abrasive paper with gradation up to 1200.

Phase structures of the coatings were analyzed by a Rigaku XRD-6060 X-ray diffractometer (XRD) with Cu K $\alpha$  radiation. Microstructure observation and elemental analysis of the coatings were carried out by a (JEOL 6060) scanning electron microscope (SEM) equipped and EDS analysis. The microhardness were measured using a Vickers microhardness tester with a Vickers diamond indenter under a load of 50 g.

## III. RESULTS AND DISCUSSION

The results of observations of the surface layer after thermal oxidation at 600 and 650 °C are shown in Figs. 1.

As seen in Fig. 1 for 600°C samples, the oxidized surface of specimen is relatively flat. No nodular oxide appears at the surface. The oxide layer obtained at 650 °C was composed of fine oxide particles (Fig.1f) and it covered the oxidised layer to a varying degree depending on the oxidation time. An analysis of microscope images has shown that the non-uniform oxide layer coverage of the specimen surface is especially visible after oxidation at 650 °C for 8 h.



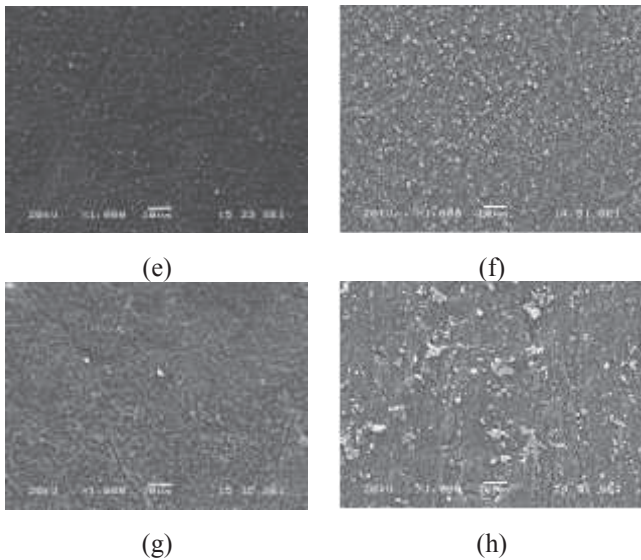


Fig. 1 SEM surface micrographs after thermal oxidation treatment (a) 600°C 1 h (b) 650°C 1h (c) 600°C 8 h (d) 650°C 8 h (e) 600°C 48 h (f) 650°C 48 h (g) 600°C 72 h (h) 650°C 72 h

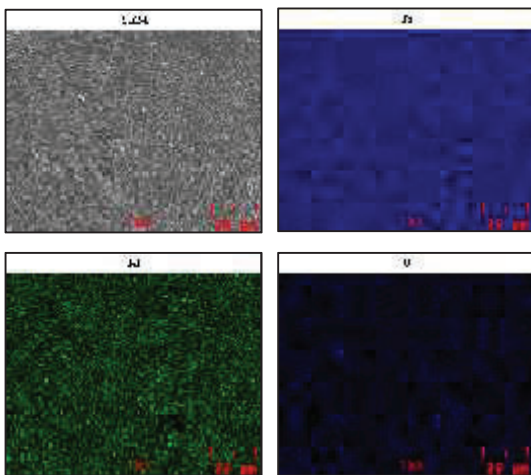


Fig. 2 EDS analysis results of the surface of 600°C-72h

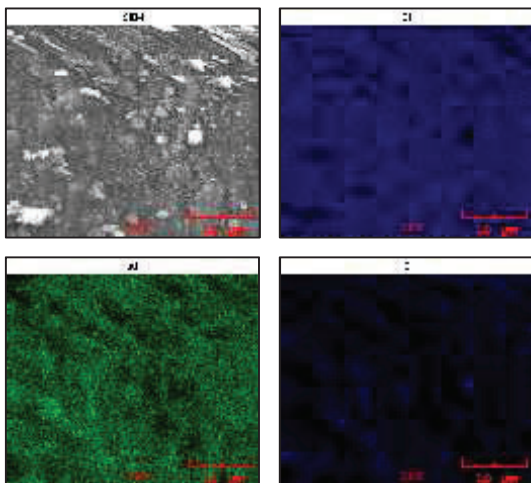


Fig. 3 EDS analysis results of the surface of 650°C-72h

The surface morphologies and elemental maps of the MAO 72 h treated coatings for 600°C and 650°C are shown in Figs. 2 and 3. The EDS result shows that the main elemental composition of the MAO coating was Ti, Al, and O elements.

The results of measurements of microhardness of oxide layers on a cross section as a function of distance from the surface, for specified oxidation parameters, are shown in Fig. 4. An analysis of the results of microhardness measurements has shown a significant influence of oxidation parameters on the hardness of oxide layers obtained on Ti-6Al-4V alloy. It has been found that hardness increases along with an increase in temperature and oxidation time. The increase in hardness was most likely caused by the formation, on the surface of the alloy, of hard oxide layers and strains evolved during the dissolution of oxygen beneath the oxide layer of the substrate.

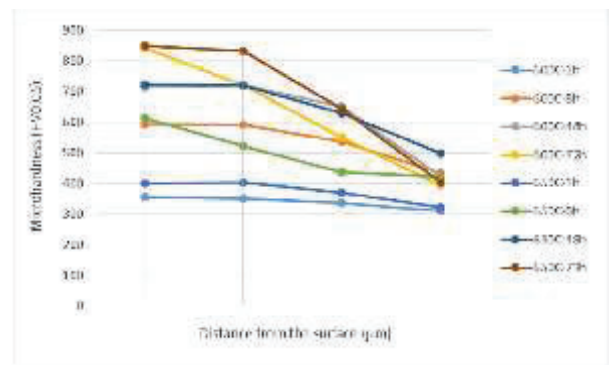


Fig. 4 Microhardness of oxide layers obtained at 600 and 650 °C (1-8-48-72h) as a function of distance from the surface

Fig. 5 presents the XRD patterns of the 48h after thermal oxidation at 600 and 650 °C, respectively. All of the coatings were composed of anatase, rutile, as well as the Ti substrate.

Both of the samples showed rutile TiO<sub>2</sub> peaks, as the oxidation temperature increased, the content of the rutile phase increased. The phase transformation from metastable anatase into stable rutile occurred during the treatment.

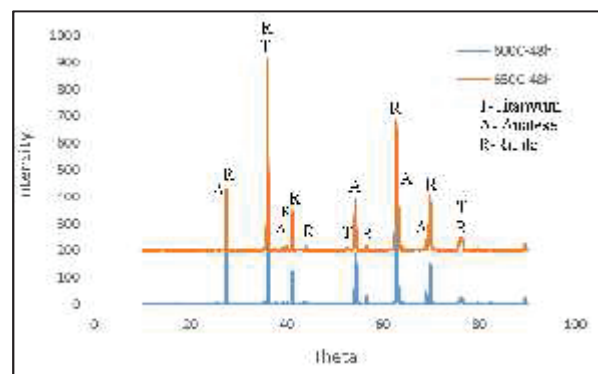


Fig. 5 XRD patterns of the samples oxidized at 600 °C and 650 °C for 48h.

#### IV. CONCLUSION

The influence of thermal oxidation parameters on morphology, thickness and hardness of oxide layers formed on the surface of titanium Ti-6Al-4V and the results were given;

Thickness of oxide layers and hardness increases along with an increase in temperature and time of oxidation. The oxide layer with the highest hardness (850 HV<sub>0.05</sub>) was obtained after oxidation at 650 °C for 72 h. Nearly 3 times increase in hardness compared to the non-oxidised Ti-6Al-4V.

Ti-6Al-4V alloy oxidized at 650 °C exhibits the formation of a thick oxide film that consists of more rutile phase and anatase whereas Ti-6Al-4V alloy oxidized at 600 °C with low intense of anatase and rutile phase peaks.

#### REFERENCES

- [1] L. Li, K. Yu, K. Zhang, Y. Liu, "Study of Ti-6Al-4V alloy spectral emissivity characteristics during thermal oxidation process", Modelling the structure and mechanical properties of oxide layers obtained on biomedical Ti-6Al-7Nb alloy in the thermal oxidation process, *International Journal of Heat and Mass Transfer*, vol.100, 1pp. 699–706, 2016.
- [2] F.M. Kgoete, A.P.I. Popoola, O.S.I. Fayomi, I.D. Adebisi, "Influence of Si<sub>3</sub>N<sub>4</sub> on Ti-6Al-4V via spark plasma sintering: Microstructure, corrosion and thermal stability", *Journal of Alloys and Compounds*, vol. 763, pp. 322-328, 2018.
- [3] Y. Zhang, G.-R. Ma, X.-C. Zhang, S. Li, S.-T. Tu, "Thermal oxidation of Ti-6Al-4V alloy and pure titanium under external bending strain: Experiment and modelling", *Corrosion Science*, vol. 122, pp. 61–73, 2017.
- [4] W. Yang, D. Xu, Q. Guo, T. Chen, J. Chen, "Influence of electrolyte composition on microstructure and properties of coatings formed on pure Ti substrate by micro arc oxidation", *Surface and Coatings Technology*, vol. 349, pp. 522–528, 2018.
- [5] V. Koshuro, Al. Fomin, I. Rodionov, "Composition, structure and mechanical properties of metal oxide coatings produced on titanium using plasma spraying and modified by micro-arc oxidation", *Ceramics International*, vol. 44, pp. 12593–12599, 2018.
- [6] J. M. Byun, H. R. Choi, S. H. Kim, M. Suk, Y. D. Kim, "Formation of nanostructured rutile TiO<sub>2</sub> synthesized on Ti powder via thermal oxidation", *Applied Surface Science*, vol. 415, pp. 43–48, 2017.
- [7] K. Aniolek, A. Barylski, M. Kupka, "Modelling the structure and mechanical properties of oxide layers obtained on biomedical Ti-6Al-7Nb alloy in the thermal oxidation process", *Vacuum*, vol. 154, pp. 309-314, 2018.

# Investigation of the Effect of Cementite Carbide Cutting Tips Coated by ALD Method on Machinability

Saim KALTAR<sup>1</sup>, Ismail KUPA<sup>2</sup>, Hakan ATES<sup>2</sup> ve Ersin BAHCECI<sup>1\*</sup>

<sup>1</sup> *Iskenderun Technical University (ISTE), Faculty of Engineering And Natural Sciences Dept. of Metallurgical and Materials Engineering, 31200, Iskederun, Hatay, TURKEY*

<sup>2</sup> *Gazi University (GU), Faculty of Technology, Dept. of Metallurgical and Materials Engineering, Ankara, TURKEY*

*\*corresponded author: ersin.bahceci@iste.edu.tr*

**Abstract**— Abrasion performans of the cemented carbide inserts coated by using Atomic Layer Deposition (ALD) and the uncoated cemented carbide inserts have been compared. Al<sub>2</sub>O<sub>3</sub> and ZnO were coated as a single layer at 10 and 150 nm thickness with ALD coating technique, which is one of the thin film synthesis methods. In order to determine of chip morphology and the effects of surface roughness on the part, machinability tests were carried out using the turning method without cooling liquid. Diamond tipped surface roughness meter was used for surface roughness tribological (abrasion, friction, lubrication) characteristics of cutting edge abrasions, which were compared by scanning electron microscope (SEM) analysis and samples were examined by using light microscope for chip morphology.

**Keywords**— ALD, Cutting Tool Coating, Machinability, Nanotechnology

## I. INTRODUCTION

Cutting tips are one of the largest inputs in determining the part costs for machining of products in the machining industry. The service life is inversely proportional to the cutting speed of the inserts, the feed rate, and the amount of wear depending on the depth of the chip in each pass. One of the methods of increasing the tribological properties of cutting inserts is to improve the coating methods. Hard-coated cutting tools are used in the manufacturing sector for more than fifty years, and in today's machining industry, about 85% of the cemented carbide cutting tools are covered cutting tools. Due to the developing technology and accordingly the use of new materials in the production industry, production processes have also been diversified [1]. Thin hard coatings have high wear resistance, low coefficient of friction and good thermal stability. While the performance of these coatings is limited due to their feasibility and cost factors, their ability has been enhanced by developing multilayer coating configurations [2].

The purpose of the coatings applied to the cutting tools is to increase the reliability of the materials and tools during the long machining process and to ensure that they are long lasting. With the development of different coating techniques, the deposition of thin hard layers with good wear resistance on

the surfaces of the cutting tools has become one of the different effective ways to improve the performance of the cutting tools. Today, the two main coating techniques that are widely used to extend the life of cutting tools and allow the deposition of protective films on cutting tools are Chemical Vapor Deposition and Physical Vapor Deposition. Atomic Layer Deposition (ALD) method used in experimental part of the study is a thin film coating method in hard structure such as chemical vapor deposition and physical vapor deposition techniques. CVD, PVD, and ALD methods vary in tribological properties depending on coating thickness, temperature and surface qualities. While the thickness of the coating made by CVD method is between 4-20 µm, the thickness of the coatings made by PVD method is 1-10 µm. However, by using ALD coating method, coatings can be achieved by forming a layer with a thickness of 10's nm. Another difference between these three methods is the coating temperature. In CVD, the coating temperature is in the range of 850-1000 °C, whereas in PVD the coating temperature requires a lower coating temperature of 150-500 °C. In the ALD method, it is possible to coat at lower temperatures (160-200 °C). Since, coating temperatures higher than 800 °C adversely affect the desired coating form due to high thermal loads and material flexibility, temperatures in ALD technique one of the advantage for obtained structures [3,4,5,6].

In recent years, ALD has been increasingly applied widely in semiconductors and nano electronics fields as well as in durability enhancement subjects. ALD technique is a kind of chemical vapor deposition method in which the reaction reaches saturation after the formation of a single atomic layer. In this way, it is possible to control the coating thickness, to achieve a homogeneous coating and to conformally coat even the most difficult geometric surfaces.

Most ALD reactions use two chemicals called precursors. This reactant reacts in a sequential manner with the precursor material surface in a self-limiting manner. A thin film is slowly deposited with repeated exposures to different precursors in succession. ALD offers advantages over other

thin film coating technologies such as chemical or physical vapor deposition (CVD / PVD) or sputtering. Other thin film methods are resource controlled accumulation and ALD is surface controlled. In the source controlled method, the antecedents react to the surface without collision. For this reason, the resulting film is not homogeneous or sufficiently protective and cannot grow properly on very small surface details such as deep cavities in silicon wafers. In addition, cracks and pores on the film prevent corrosion. Control of film thickness at atomic level by conventional methods is also impossible. ALD can enhance the quality of other films - for example, ALD can be a filler on thicker layers produced by PVD, and the underlying PVD closes the pores in the film. ALD is more sensitive to the surface than the ion bombardment-based coating [7].

The aim of the present study is to improve the machinability properties of the cutting tools by coating with the desired oxide materials. The study was carried out with parameters such as oxide type and thickness. At the end of the study, it was understood that the technique can be improved and can be applied any kind of cutting tool attachment.

## II. MATERIAL AND METHOD

In the machining experiments, AISI 1050 steel that is suitable for surface hardening was used [8]. Chemical and mechanical properties of AISI 1050 steel were given in Table 2.1 and Table 2.2.

Al<sub>2</sub>O<sub>3</sub> (Trimethylaluminum) (TMA) pre-chemically coated with nano-sized coatings. Coating parameters were determined under a vacuum (145mTorr), 200 °C and 20 sccm carrier gas flow. In order to coat the cutting tools we use the ALD system with the specially designed 3D chamber cover and specially designed specimen holders by Okyay Technology Company. Samples were coated with Al<sub>2</sub>O<sub>3</sub> at thicknesses of 10 and 250 nm. The device was a 1.29A coating standard in one cycle. These coated inserts were carried out with 770 cycles, 1923 cycles, respectively. Cutting tools with ZnO thicknesses of 10 and 250 nm were coated in ALD using DEZ (Dietilzinc) precursor at 200 °C temperature.

Turning experiments were performed for oxide coated cementite carbide tools and uncoated cemented carbide tools on lateral surface wear and performance behavior, chip morphology and surface roughness on the part without cooling liquid. ALD method, BILDONIT CNMG 120404-SM SM25 / P25 quality cementitious carbide inserts were coated with Al<sub>2</sub>O<sub>3</sub> and ZnO as single layer at 10, 250 nm thickness. VORGEN DCLNR 2525 M12 was used as the holder. The cutting speed was fixed at 120 m / min. For machining tests, AISI 1050 steel material with a length of 200 mm and a diameter of 50 mm were used with various cutting parameters (seen in Table 2.3) by using a HYUNDAI WIA L230LA model with constant feed speed of 0.1 mm /rev. The CNC lathe was also subjected to machining tests by turning one step

for 180 mm. Cutting edge abrasions were investigated by FEI QUANTA 650 Marked Electron Microscope (SEM) and their surface roughness tribological (abrasion, friction, lubrication) properties were examined using SurfTest-211 (MITUTOYO) diamond tip surface roughness meter.

TABLE 2.1  
 CHEMICAL PROPERTIES OF AISI 1050 STEEL [8].

Composition (%)				
C	Mn	Si	P	S
0,5	1	0,2-0,4	0,04	0,05

TABLE 2.2  
 MECHANICAL PROPERTIES OF AISI 1050 STEEL [8].

AISI 1050 Cold shrinkage Mechanical Properties		
<b>Dimeter (mm)</b>	13-29	29-100
<b>Tensile strenght R<sub>m</sub> (N/mm<sup>2</sup>)</b>	700-850	700-850
<b>%0.2 Yeild point Rp<sub>0.2</sub></b>	475	435
<b>% Elongation</b>	Min. 10	Min.10
<b>Hardness (HB)</b>	201-255	201-255

TABLE 2.3  
 CUTTING PARAMETERS USED IN CNC TURNING

Parameters with Baidonit cutting tool	
<b>Cutting speed</b>	120 m/min
<b>Rev count</b>	796-794
<b>Chip depth</b>	2 mm
<b>forwardness</b>	0.1 mm/rev

### III. RESULT OF DISCUSSION

SEM images of 10 nm ALD coated inserts cannot be taken clearly, because they are in very small reductions. In Fig 3.1 a-b, however, SEM images are shown without coating and after 250 nm coating. It seems that the surface of the tool is covered with sintering which is not very good quality. It was said that the coating was homogeneous.

XRD analysis was performed to determine the  $\text{Al}_2\text{O}_3$  and ZnO coating materials on the cutting edge. It can be said that the peaks shown in Fig 3.2 and Fig 3.3 represent typically  $\text{Al}_2\text{O}_3$  and ZnO coated of the surface of the material.

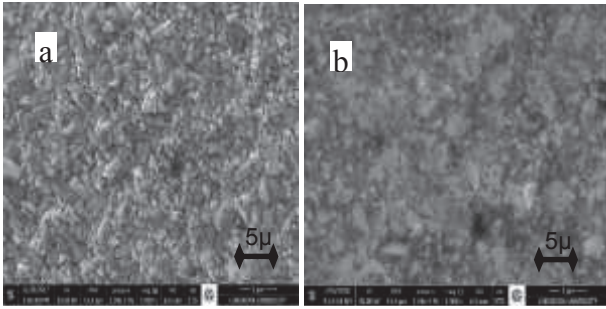


Fig 3.1. SEM image of cementitious carbide cutting tools; a) uncoated; b) 250 nm  $\text{Al}_2\text{O}_3$  coated

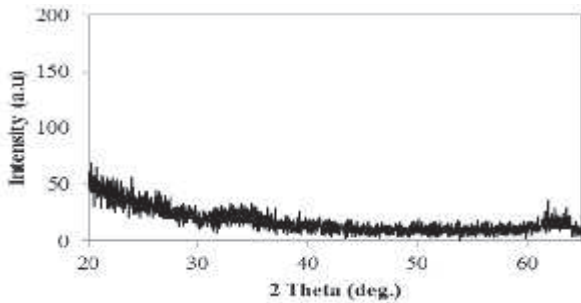


Fig 3.2. XRD diffractions of  $\text{Al}_2\text{O}_3$  coating.

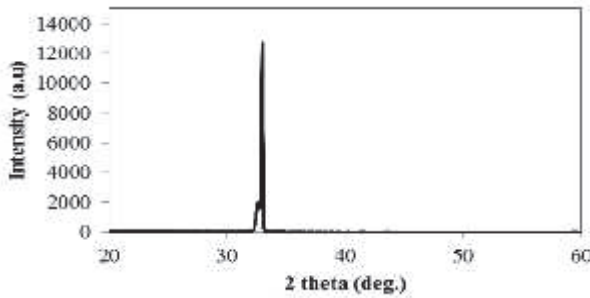


Fig 3.3. XRD diffractions of ZnO coating.

It is seen in the SEM images of the cutter side surface of the stacked chip form after machining with uncoated inserts (Fig. 3.4b). It is known that this massive sawdust, which acts as a cutting edge, changes the cutting angle [9,10,11]. Although the turning operation is performed for a short time, it is observed at the cutting edges used in the experiment that wear is started on uncoated tools. It is observed that the roughness of the surface increased due to the tool wear due to

the increase of the cutting time when  $R_a = 0,93 \mu\text{m}$  in 0,1 progression in turning operations performed for a short time.

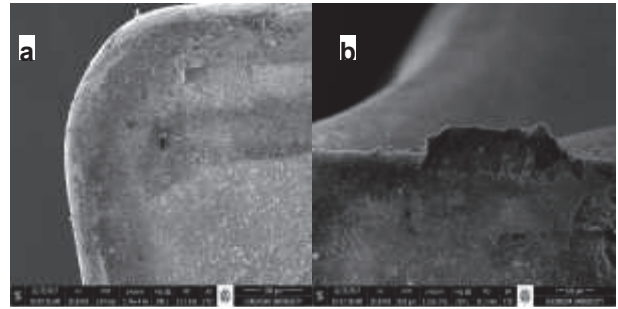


Fig 3.4. Uncoated Cementite Carbide cutting tool at a cutting speed of 120 m / min, a) top view; b) cutting side surface.

$\text{Al}_2\text{O}_3$ -coated carbide with 10 nm ALD method showed no tendency to chipping and / or sticking after cutting (Fig. 3.5a-b). No tool wear is observed on the cutting edge and side surface. No deterioration effects of the cutting edge form observed in the uncoated carbide tool were observed. 0.1 was measured to be higher than that of uncoated tools with  $R_a = 1.58 \mu\text{m}$  in surface roughness tests performed on the surface of the treated workpiece. However, the surface roughness value remained stable over standard values, as there was no wear on the tool during long turning operations. It can be considered that the coating will also provide a longer quality of the roughness quality of the work surface, depending on the time, at the cutting quality.



Fig 3.5. 10 nm  $\text{Al}_2\text{O}_3$  coated Cementite Carbide Cutting tool with a cutting speed of 120 m / min, a) top view; b) the cutting side surface

At the end of turning with a 10 nm ZnO coated insert, more agglomerated sawdust was observed from the uncoated insert (Fig. 3.6a). The cutting edge is seen in the SEM image that acts like a cutting surface, taking sharp shape due to stacking chip. (Figure 3.6b). It can be said that the machinability of ZnO with all coating thicknesses worsened by the ALD method. The surface roughness was measured as  $R_a = 1.58 \mu\text{m}$ . It is thought that the high value of this value is also contributed by the continuous winding of the piece. For this reason, processing images of ZnO coated specimens with a thickness of 250 nm were not used. Investigating the optimum values of ZnO coated tools continues by changing the feed and other parameters.

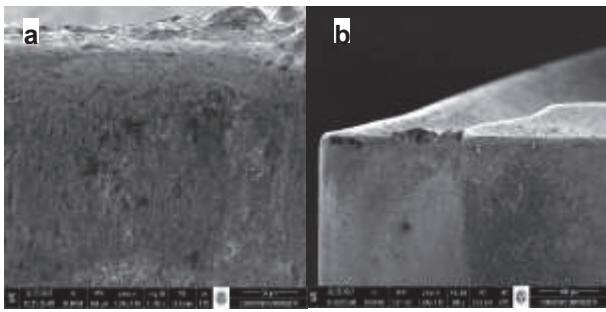


Fig 3.6. SEM image of Cutting tool with 10 nm ZnO coated cementitious carbide cutting tool turning result; a) the cutting side surface; b) the cutting tip.

It has been observed that as the coating thicknesses of the tools coated with the ALD method increase, the cutting performance decreases. As can be seen in Figures 3.7a-b, 250 nm Al<sub>2</sub>O<sub>3</sub>-coated tools were observed to accumulate agglomerate chips and cut sheet at the cutter side surface. This deteriorates the cutting properties of the cutting edge. In the ALD method, it is considered that the resistance in the oxide structure decreases by coating with about 1900 cycles. This effect is further enhanced by the fact that the surface qualities of carbide tools, which have never been cut, are not good. For this reason, this method has been observed in experimental studies in which the effect is corrected positively in smaller coating thicknesses. In surface roughness measurements, the surface roughness of the workpiece was measured as Ra = 1.70 μm with the formation of continuous sawdust similar to that of ZnO-coated materials.

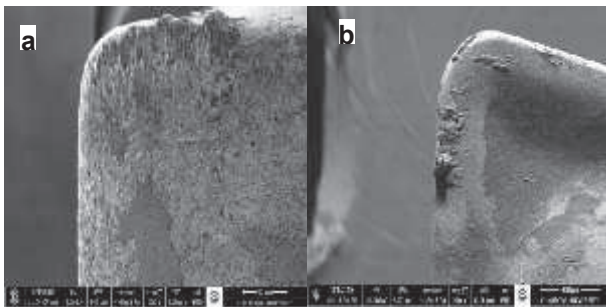


Fig 3.7. SEM image of Cutting tool with a 250 nm Al<sub>2</sub>O<sub>3</sub> coated cementitious carbide cutting tool turning result; a) the cutting side surface; b) top view.

The thickness of the coating and the shape of the chips after turning according to the type are shown in Table 3.1. The best chip forms were uncoated and processed with 10 nm Al<sub>2</sub>O<sub>3</sub> coated cutting inserts. However, continuous sawdust formation was observed due to the effect of agglomerated sawdust adhering to the tool after the turning operation with turning heads made of machining inserts without machining residue, thereby reducing the angle of the cutting plane. In the case of 10 nm Al<sub>2</sub>O<sub>3</sub> coated inserts, there was no change in the form of tool chip breaker, so the intermittent chip formation remained stable. Continuous chip formation was observed with increasing coating thickness in both Al<sub>2</sub>O<sub>3</sub> and ZnO coated inserts.

TABLE 3.1  
 MACHINING IMAGES WITH UNCOATED AND COVERED INSERTS RESULTING IN MACHINING.

Cutting tool coating material	Chip shapes after turning
Uncoated	
10 nm Al <sub>2</sub> O <sub>3</sub>	
10 nm ZnO	
250 nm Al <sub>2</sub> O <sub>3</sub>	

#### IV. CONCLUSIONS

It has been determined that coating with ALD method is easier and more advantageous than other methods. Best cutting performance was observed in 10 nm Al<sub>2</sub>O<sub>3</sub> coated tools. Short chip and surface quality have been achieved in long-term processes. Although the surface roughness is lower than uncoated tools, it has been determined that the tool cutting quality does not decrease with increasing processing time. On uncoated tools, it was observed that after machining, chips were formed and adhered to the cutting surface. For this reason, continuous chip formation was observed. It was observed that the machinability performance of the tools coated with ALD method was higher than that of uncoated tools. However, it can be said that the quality of ZnO-coated materials is poor in these processing parameters. Experimental studies have also shown that processing performance is improved by changing other processing parameters outside the ZnO coating thickness.

It can be said that it is an open method to be investigated and developed because there are already many parametric processes. Our team is continuing the oxide coating by using other oxides. In addition, the exposure mode and coating recipe will be developed in the 3D coating, and the quality and types of coating will continue to be increased.

#### ACKNOWLEDGMENT

Authors would like to thanks to Gazi University for project support namely (07/2015-08) Nanomaterial laboratory and characterize-analysis laboratory, and (07/2016-11) synthesis and investigation of electrical conductivity of higher thermal factors by ALD.

#### REFERENCES

- [1] Bobzin, Kirsten. 2017. High-performance coatings for cutting tools. *CIRP Journal of Manufacturing Science and Technology* 18, 1.
- [2] Marin, E., Guzman, L., Lanzutti, A., Fedrizz, L., Saikkonen, M., 2009. Chemical and electrochemical characterization of hybrid PVD+ ALD hard coatings on toolsteel. *Electrochemistry Communications* 11.10, 2060.
- [3] Dobrzanski, L.A., Pakula, D., Kriz A., Sokovic, M., Kopac, J. 2006. Tribological properties of the PVD and CVD coatings deposited on to the nitride tool ceramics. *Journal of materials processing technology* 175.1-3, 179.
- [4] Wei L, Quanquan C, Junjie Z, Rongxuan H, Haidong W, Ziwei W, Shanghua W 2017. PVD-CrAIN and TiAIN coated Si3N4 ceramic cutting tools 1. Microstructure, turning performance and wear mechanism. *Ceramics International* 43.12, 8999.
- [5] Alexandre Ph. Ilyuschenko, Eugene E. Feldshtein, Yuliya O. Lisovskaya, Ludmila V. Markova, Mikhail A. Andreyev, Albert Lewandowski. 2015. On the properties of PVD coating based on nano diamond and molybdenum disulfide nanolayers and its efficiency when drilling of aluminum alloy. *Surface and Coatings Technology* 270, 190.
- [6] Mattox, Donald M., 2010. Handbook of physical vapor deposition (PVD) processing. William Andrew.
- [7] Dönmez, I. 2013. Atomic layer deposition of metal oxide thin films and nanostructures. PhD Thesis. Bilkent University.
- [8] Sunay, Tolga Y., Mumin Sahin, and Sabri Altintas. 2009. The effects of casting and forging processes on joint properties in friction-welded AISI 1050 and AISI 304 steels. *The International Journal of Advanced Manufacturing Technology* 44.1-2, 68.
- [9] Özçatalbaş Y., 1998. Impact of Processing Properties of Stack Chip Formation in Low Alloy Steel, UMTIK'98, Ankara, 25.
- [10] Ozcatalbas Y., and Ercan F., 2003. The effect of heat treatment on the machinability of mild steels, *Journal of Materials Processing Technology*, 6784, 1.
- [11] Ozcatalbas Y., 2002. The effects of tool wear and mechanical properties of workpiece material on surface roughness and cutting forces, 4, special issue, 47.

# Evaluation of low-velocity impact behaviour of epoxy nanocomposite laminates modified with silica nanoparticles at cryogenic temperatures

Ahmet C. Tatar<sup>#</sup>, Halil B. Kaybal<sup>+</sup>, Hasan Ulus<sup>##</sup>, Okan Demir<sup>#</sup> and Ahmet Avci<sup>#</sup>

<sup>#</sup>Department of Mechanical Engineering, Selcuk University, Konya, Turkey  
{acaner.tatar, odemir, hasanulus, aavci}@selcuk.edu.tr

<sup>+</sup>Department of Mechanical Engineering, Amasya University, Amasya, Turkey  
hburak@amasya.edu.tr

**Abstract**— Epoxy based fiber reinforced composites are widely utilized in the aerospace application due to mechanical properties, thermal stability and, chemical resistance. However, it is known that materials become brittle and due to the poor crack resist restricts their applications at low temperatures. The purpose of this paper is to experimentally investigate the cryogenic temperatures' effect on the low velocity impact (LVI) test of composite laminates. The LVI tests were conducted at RT (room temperature), 0 °C, -50 °C, -150 °C and -196 °C (liquid nitrogen temperature) on the composite laminates to measure influence on their energy absorption capacity. LVI tests performed according to ASTM-D-7136 standard under 10, 20 and 30 J impact energy levels.

**Keywords**— Glass fiber, Epoxy composite, Cryogenic temperature, Low velocity impact

## I. INTRODUCTION

With the progress in science and technology, the use of polymer composites has become increasingly widespread for both scientific research and engineering applications. Especially, glass and carbon fiber/epoxy composites are increasingly demanding for structural applications in aerospace, automotive and marine industries due to their excellent mechanical performance and design advantages over conventional materials [1]. At the same time, the dynamic behavior of composites under impact loading is one of the major concerns in the use of the industry as it is highly susceptible to impact loads which cause significant damage such as cracking of the matrix, delamination and breakage of the fibers [2].

Fiber composites have the potential for extensive use in space applications, such as solar arrays, antennas, optical platforms and supports for cryogenic tanks [3]. However, the composites utilization and material selection for low-temperature applications is often obstructed by the inconsistency of material properties of its components [4]. Because thermal contractions of fiber and matrix due to the cool conditions on the composite structure the give rise to thermal residual stresses and strains which influence most of the mechanical properties. The general of used matrices are brittle and do not allow the release of residual stresses at low temperatures [5] and the toughness degradation induced by

low temperatures can lead to structural damages in the form of microcracks or delamination [6].

Some studies performed to investigate the impact properties of laminated composites at low temperature but the reports about lowest temperature (down to -60 °C) is scarce. Laminated composites become rigid with high stiffness at low temperatures (-50 °C to 120 °C) so as their deflections in impact tests were small [5]. Damage areas also smaller and higher perforation threshold resulted for laminates subjected to a low-velocity impact at low temperature (-60 °C to 20 °C) condition [8]. However, comparatively little work has been done to understand of the cryogenic temperatures of laminated composites. Therefore, in this work, the cryogenic behaviours of glass/epoxy composites are reported in terms of the LVI impact properties.

## II. EXPERIMENTAL

In this study, the low velocity impact (LVI) behaviors of glass/epoxy nanocomposite laminates were investigated using a drop weight impact test. Having been used for LVI tests, neat and nano SiO<sub>2</sub> (silica) added glass/epoxy laminates were produced as 10 layers. Adding 4 wt% SiO<sub>2</sub> nanoparticles were preferred as nano-reinforcements according to literature survey to perform matrix modification [12-14]. The epoxy resin system used was a bisphenol-A (DGEBA) from Momentive Hexion, Inc. Fibers was supplied from Dost Kimya Company in Istanbul, respectively. The LVI tests were repeated tree times under 10, 20, 30 Joule (J) impact energy levels and at the RT, 0 °C, -50 °C, -150 °C temperatures. In order to reach cryogenic temperature, the composite specimens were immersed in liquid nitrogen and bargain for 10 min to reach the liquid nitrogen temperature [9]. Details of experimental procedures are available in our previous studies [13-15]. Title and Author Details

## III. RESULTS AND DISCUSSIONS

Fig. 1 compares the contact force-time and force-displacement curves of the neat composite specimens with the different impact energy levels. The results show that the contact force increases significantly with the decrease of the

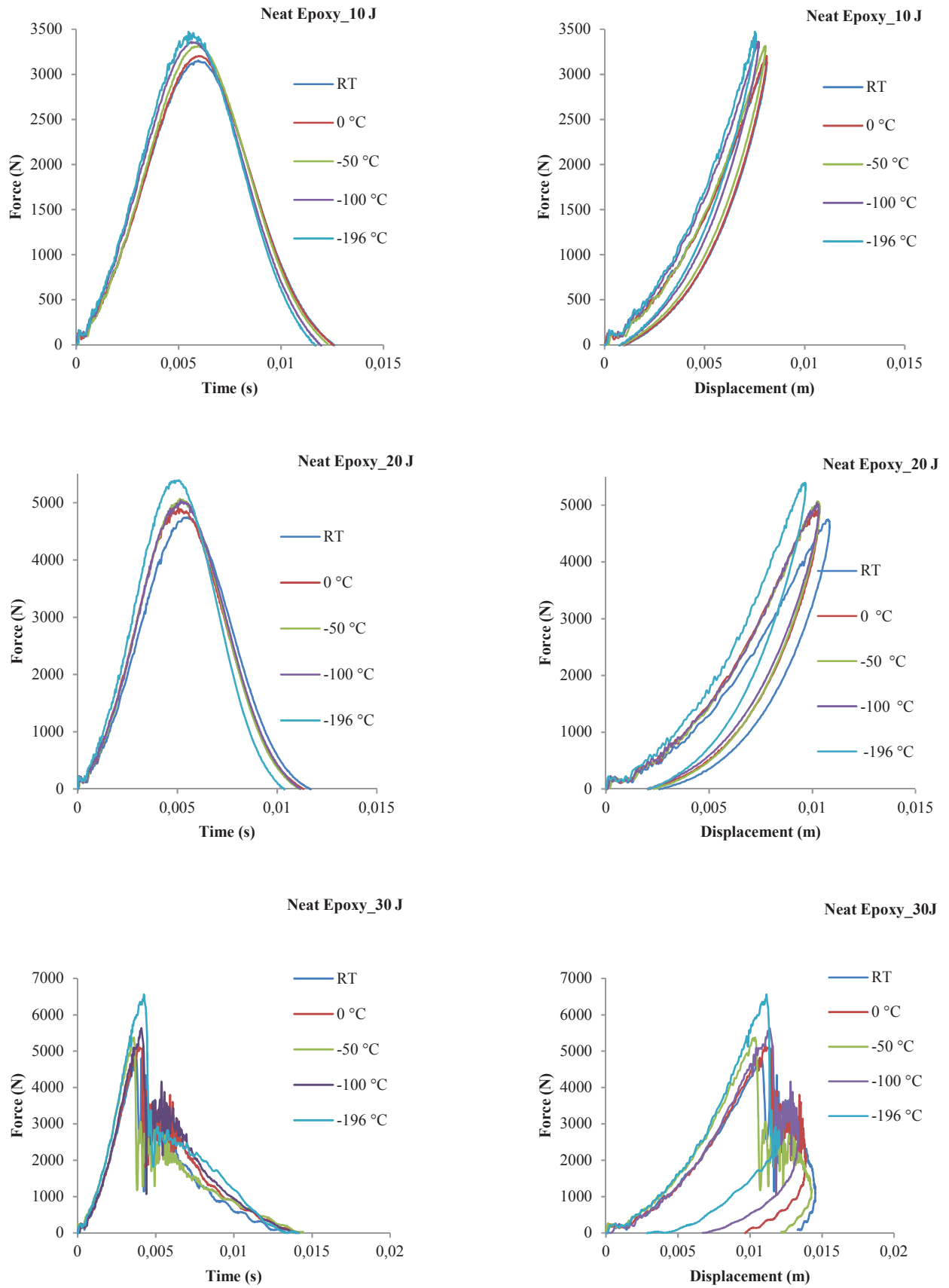


Fig. 1. Force-time and force-displacement curves at different impact energy levels

temperatures. Meanwhile, we compared the displacements of different temperatures in Fig. 2. It can be found that the displacements at liquid nitrogen temperature are reduced significantly than that of at RT. Here, diminish of displacement values occur due to the declined contact duration at low temperatures than that at RT.

The characteristic impact parameters: peak contact force and absorbed energy for composite laminate are presented in Table 1. The peak contact force at liquid nitrogen temperature is the highest for all impact energy levels. Under the 10 J impact energy, comparing at RT to 0 °C, -50 °C, -150 °C and -196 °C the energy absorption capacity are decreased by 0.3%, 13.46%, 17.53% and 25.74% respectively. On the other hand, under the 30 J impact energy comparing at room temperature, energy absorption capacity are decreased by 23.68%, 27.09%, 28.81% and 30.42% respectively.

Table 1. LVI properties of 10, 20 and 30 J impacted composites at RT, 0 °C, -50 °C, -150 °C and -196 °C.

Impact Energy	Temp. Condition	Contact Force (N)	%↑	Absorbed Energy (J)	%↓
10 J	RT	3143	-	2,95	-
	-50 °C	3198	1,75	2,94	-0,34
	-100 °C	3334	6,08	2,6	-13,46
	-150 °C	3375	7,38	2,51	-17,53
	-196 °C	3452	9,83	2,35	-25,74
20 J	RT	4700	-	9,27	-
	-50 °C	4885	3,93	9,26	-0,10
	-100 °C	4971	5,76	8,71	-6,04
	-150 °C	5043	7,29	8,1	-12,62
	-196 °C	5381	14,48	7,9	-14,77
30 J	RT	4980	-	26,13	-
	-50 °C	5185	4,12	19,94	-23,68
	-100 °C	5359	7,61	19,05	-27,09
	-150 °C	5635	13,15	18,6	-28,81
	-196 °C	6357	27,65	18,18	-30,42

Fig. 2 shows the force-time and force-displacement histories of neat and 0.4 wt% nano SiO<sub>2</sub> reinforced for different energy levels. In the graphs, no significant change was observed with the addition of SiO<sub>2</sub> nanoparticles for 10 and 20- joule energy levels while average contact force value increased significantly depending on the addition of SiO<sub>2</sub> nanoparticles for 30-joule energy level. The change in the impact properties of the nanoparticle-added specimens is given in Table 2. It is seen that peak forces are not affected much by the temperature under the low impact energy while it affected depending on temperature. The ratio of percentage change of peak contact force under the 30-joule energy level are observed 13% and 24.8% for SiO<sub>2</sub> nanoparticle added composites, respectively.

Table 2. LVI properties of 10, 20 and 30 J impacted composites at RT, 0 °C, -50 °C, -150 °C and -196 °C.

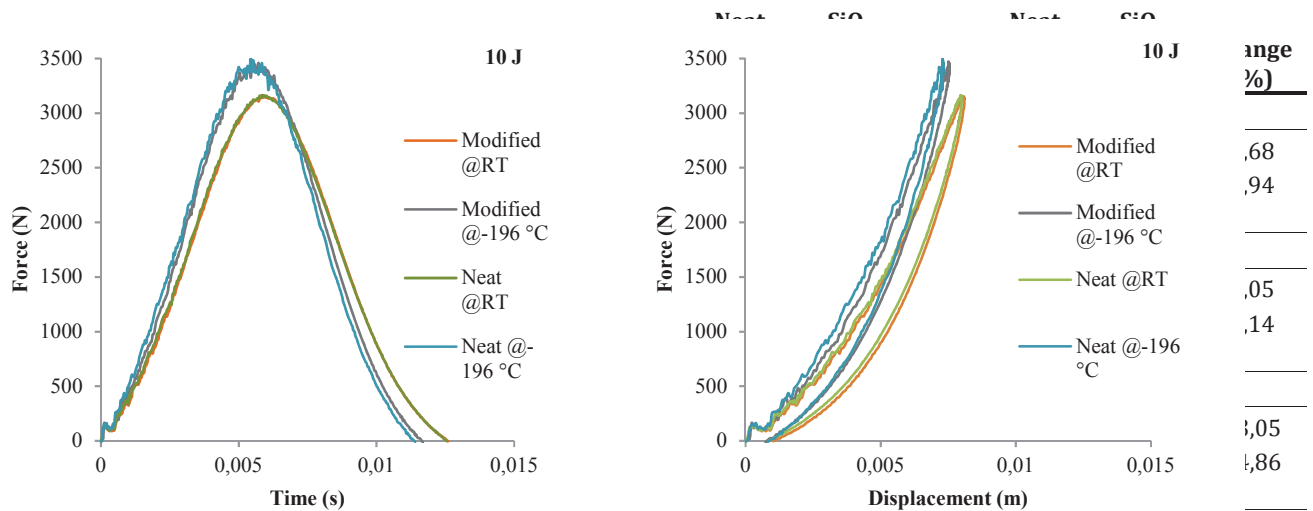


Fig. 2. Force-time and force-displacement curves of neat and modified composites at different impact energy levels

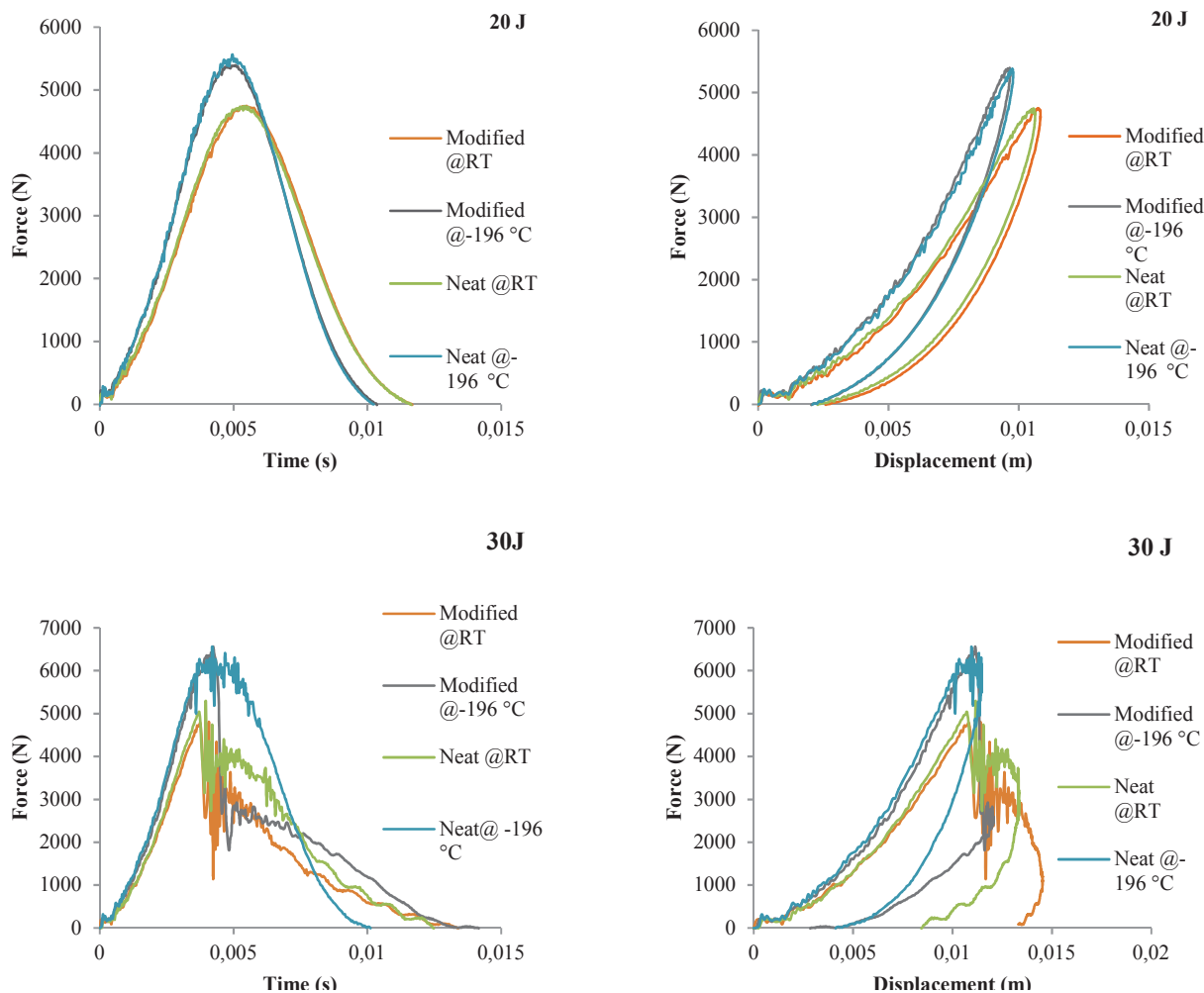


Fig. 2. Force-time and force-displacement curves of neat and modified composites at different impact energy levels (continue)

#### IV. CONCLUSION

In this study; low velocity impact responses of glass fiber reinforced neat epoxy composite and 4% (wt) SiO<sub>2</sub> modified epoxy composite laminates were investigated at different temperatures. From the results of this experimental study, the following conclusions can be drawn:

- The maximum contact forces decrease under cryogenic temperatures.
- Small energy absorptions were showed under cryogenic temperatures.
- It is clear that nanoparticle addition has an effect on slightly higher energy levels as opposed to low energy levels.

#### REFERENCES

[1] Guerrazi N, Haddar N, Elleuch K, Ayedi H. Investigations on the fabrication and the characterization of glass/epoxy, carbon/epoxy and hybrid composites used in the reinforcement and the repair of aeronautic structures. *Materials & Design* (1980-2015). 2014;56:714-24.  
 [2] El Moumen A, Tarfaoui M, Lafdi K, Benyahia H. Dynamic properties of carbon nanotubes reinforced carbon fibers/epoxy textile composites under low velocity impact. *Composites Part B: Engineering*. 2017;125:1-8. 1.  
 [3] Bansemir, H. and O. Haider, Fibre composite structures for space applications—recent and future developments. *Cryogenics*, 1998. 38(1): p. 51-59.  
 [4] Praveen, R., et al., Hybridization of carbon–glass epoxy composites: An approach to achieve low coefficient of thermal expansion at cryogenic temperatures. *Cryogenics*, 2011. 51(2): p. 95-104.

[5] Hartwig, G. and S. Knaak, Fibre-epoxy composites at low temperatures. *Cryogenics*, 1984. 24(11): p. 639-647.  
 [6] Kim, M.-G., J.-B. Moon, and C.-G. Kim, Effect of CNT functionalization on crack resistance of a carbon/epoxy composite at a cryogenic temperature. *Composites Part A: Applied Science and Manufacturing*, 2012. 43(9): p. 1620-1627.  
 [7] Salehi-Khojin, A., et al., The role of temperature on impact properties of Kevlar/fiberglass composite laminates. *Composites Part B: Engineering*, 2006. 37(7-8): p. 593-602.  
 [8] Icten, B.M., et al., Low temperature effect on impact response of quasi-isotropic glass/epoxy laminated plates. *Composite Structures*, 2009. 91(3): p. 318-323.  
 [9] Deng S, Ye L, Friedrich K. Fracture behaviours of epoxy nanocomposites with nano-silica at low and elevated temperatures. *Journal of materials science*. 2007;42(8):2766-74.  
 [10] Phonthammachai N, Chia H, He C. One-Step Synthesis of Oval Shaped Silica/Epoxy Nanocomposite: Process, Formation Mechanism and Properties. *The Delivery of Nanoparticles: InTech*; 2012.  
 [11] Sadej-Bajerlain M, Gojzewski H, Andrzejewska E. Monomer/modified nanosilica systems: photopolymerization kinetics and composite characterization. *Polymer*. 2011;52(7):1495-503.  
 [12] Kara, M., Kirici, M., Tatar, A. C., & Avci, A. (2018). Impact behavior of carbon fiber/epoxy composite tubes reinforced with multi-walled carbon nanotubes at cryogenic environment. *Composites Part B: Engineering*.  
 [13] Eskizeybek, V., et al., Static and dynamic mechanical responses of CaCO<sub>3</sub> nanoparticle modified epoxy/carbon fiber nanocomposites. *Composites Part B: Engineering*, 2017.  
 [14] Ulus, H., et al., Low-velocity impact behavior of carbon fiber/epoxy multiscale hybrid nanocomposites reinforced with multiwalled carbon nanotubes and boron nitride nanoplates. *Journal of Composite Materials*, 2016. 50(6): p. 761-770.  
 [15] Kaybal, H.B., et al., Effects of alumina nanoparticles on dynamic impact responses of carbon fiber reinforced epoxy matrix nanocomposites. *Engineering Science and Technology, an International Journal*, 2018.

# The Influence of the Grain Size of the Matrix Material on the Mechanical Properties of MMC Made Through Powder Metallurgy Route

Mutlu Karasoglu \*, Serdar Karaoglu +

\* Department of Mechanical Engineering, Eskisehir Technical University  
Eskisehir, 26555, Turkey  
mutlukarasoglu@anadolu.edu.tr

+ Department of Mechanical Engineering, Ege University  
Izmir, 35040, Turkey  
serdar.karaoglu@gmail.com

**Abstract**— In this work, two different grain sized (micro and nano) magnesium powders were utilized as matrix materials to produce silicon carbide reinforced metal matrix composite through powder metallurgy route. Nanocrystalline matrix powders were prepared by mechanical milling of microcrystalline magnesium powders. Sintering operations were carried out in a hot press machine. Two different group of samples were compared in terms of density, grain size and compression test results. Samples, produced with nano grained matrix powder, exhibited higher compressive yield strength and ductility which is attributed to high amount of grain boundaries and higher diffusion coefficient of finer grains of matrix material.

**Keywords**— Magnesium; metal matrix composites; hot press sintering; nanostructural materials; powder metallurgy

## I. INTRODUCTION

Magnesium (Mg) has a density of 1.74 g/cm<sup>3</sup>, which is known as the lightest structural metal [1]. This significant characteristic makes Mg a good candidate for potential applications in automotive and aerospace industries to reduce fuel consumption and carbon emission [2]. There are also many advantages of Mg such as good castability and machinability, high damping capacity and superior specific strength [3]-[5]. However, poor mechanical properties of Mg such as low elastic module, limited strength, low ductility, low impact toughness and creep resistance at elevated temperature, restrict application of Mg [4]. Many efforts have been made by researchers in order to improve these weak features of Mg for decades. Some of the researchers have focused on grain refinement of Mg alloys [6-8], texture [9] and magnesium matrix composites (MMC) [10]-[12].

Magnesium matrix composites have many benefits such as high strength and elastic module, excellent wear and creep resistance compared to monolithic Mg. Enhancement in strength due to the addition of particle reinforcement, usually decreases ductility of material in conventional coarse particle reinforced composites which limits application potential of MMC [13]. Although many researcher achieved increase in both strength and ductility by using nano-scaled reinforcements [14], [15], there is no attempt to reduce the grain size of the matrix in order to achieve increase in both strength and ductility.

It is well known that nanocrystalline materials have lower diffusion activation energy and much higher diffusion coefficient, it can be considered to have a potential to yield a high density and good interface bonding with reinforcements in MMC's. Nanocrystalline metals also have higher ductility than coarse grained metals, hence nanocrystalline matrix can be used to compensate the low ductility of MMC's. In this work, two different grain sized matrix materials were utilized to investigate the effect of the grain size of the matrix material on mechanical properties on MMC.

## II. MATERIALS AND METHODS

The overall procedure is summarized in the flowchart of Figure 1. Commercially pure Mg (99.1%,  $d_{\text{particle}} \sim 46 \mu\text{m}$ ) and SiC ( $d_{\text{particle}} \sim 60 \mu\text{m}$ ) powders were used as starting materials. Initially, Mg powders were subjected to mechanical milling process for 5h duration. Milling operation was carried out under argon atmosphere, with a 20:1 ball to powder weight ratio at 300 rpm in a Fritsch Pulverisette 6 planetary milling machine. Prior to milling, 2 wt. % stearic acid was added to Mg powder as a process controlling agent (PCA) to prevent excessive cold welding, and the mixture was then blended for 15 min. at 150 rpm in the absence of a milling medium. Stainless steel vial and carbon steel (100Cr6 bearing steel) balls of 15 mm diameter were used as milling medium. Subsequent to milling, Mg and SiC (10 wt. %) powders were mixed for 15 min in the milling machine without milling medium. As-received Mg and SiC powders were also blended in the same route. Both of the powder mixtures were consolidated in a hot press furnace. Sintering temperature, pressure and time were set as 500 °C, 25 MPa, 30 min., respectively. Both powders and sintered bulk samples were analysed by a Rigaku Miniflex 600 X-ray diffractometer with CuK $\alpha$  radiation ( $\lambda=1.540562 \text{ \AA}$ ) operated at 40 kV and 15 mA and a scanning rate of 0.5 °/min in order to calculate grain sizes. Grain size of milled powders and milled sintered samples were calculated by using the Scherer equation [16].

$$\beta_g(2\theta) = \frac{0.94}{d_c} \frac{1}{(\theta)} \quad (1)$$

where,  $\lambda$  is the wavelength of the X-ray radiation,  $\Theta$  is the Bragg angle,  $\beta g$  is the breadth at half the maximum intensity of the peak and  $d$  is the average grain size.

Grain size of the coarse grained ( $> 500$  nm) powders and samples reaching a grain size exceeding 500 nm after sintering couldn't be relatively calculated by the Scherer equation, due to the size limitation of the method. Thus, grain size of as-received powders (Figure 2a) and matrix of sintered samples produced with as-received powders (Figure 3a) were measured from optical microscopy images, directly by image analysing method. Optical microstructural image of the milled powders and sintered samples produced with milled powders were also displayed in Figure 2b and Figure 3b. Optical microscopy (OM) observations were carried out using a Nikon Eclipse MA100 and image analyses were performed by ImageJ software in order to measure grain sizes. Density measurements of all sintered samples were carried out geometrically. Dimensions of compression test specimens were 10 mm in diameter and 10 mm in length. Compression tests were performed with an Instron-5967 testing machine at a strain rate of 0.005 m/m.min according to ASTM E9 standard. The average of three valid tests was used to calculate the compressive strength of the samples.

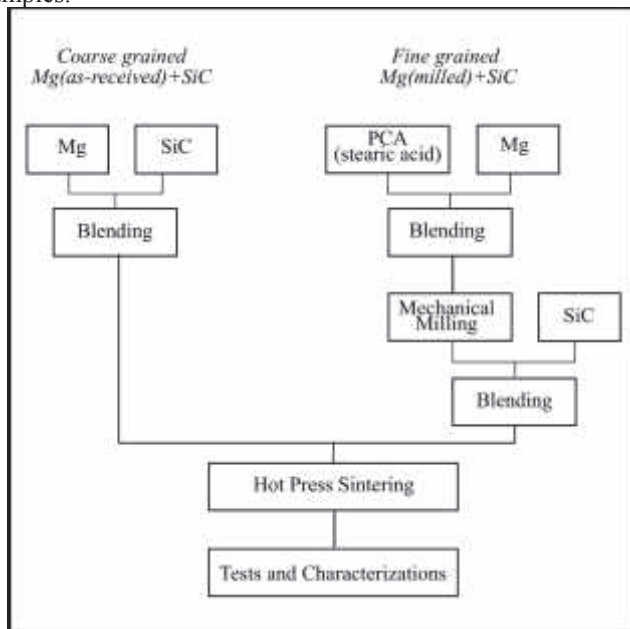


Fig. 1 Flowchart of synthesis and characterization methodology

### III. RESULTS AND DISCUSSION

XRD pattern obtained from powders and sintered samples are displayed in Figure 2. Table 1 shows grain size of Mg powders and matrix of sintered samples in addition to average amount of porosity and density of the sintered samples, respectively. It can be seen that while as-received powders have a coarse average grain size which are in microcrystalline range ( $> 1 \mu\text{m}$ ), milled powders are in nanocrystalline range ( $< 100$  nm). Coarse grains of as-received powders can be seen in Figure 3a. Although grains of milled powders unable to be seen in optical image, the microstructure of milled powders is exhibited in Figure 3b. Grain growth occurred in both as-

received and milled powders after sintering process. Post-sintering grain size calculations showed that although the 5h milled samples were no longer in the nanocrystalline range, fine grained structure was remained. Post-sintering microstructures of matrix materials are also exhibited in Figure 4.

TABLE I  
 GRAIN SIZE OF THE MAGNESIUM POWDERS AND MATRIX OF SINTERED SAMPLES, DENSITY AND POROSITY OF SINTERED SAMPLES

Matrix Type	Grain size of the powders prior to sintering (nm)	Grain size of the matrix of the sintered samples (nm)	Porosity of sintered samples (%)	Density of sintered samples (g/cm <sup>3</sup> )
As-received	8850	10800	11.02	1.71
Milled	43.27	221.94	11,00	1.71

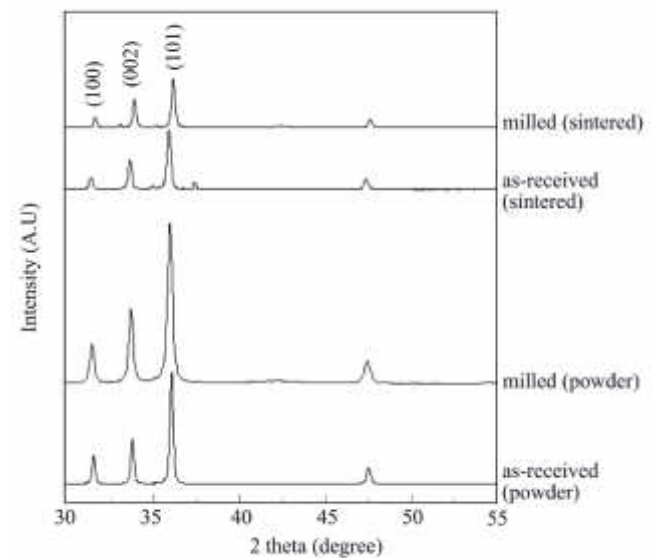


Fig. 2 XRD patterns of as-received powders, milled powders, sintered sample produced with as-received powders and sintered sample produced with milled powders

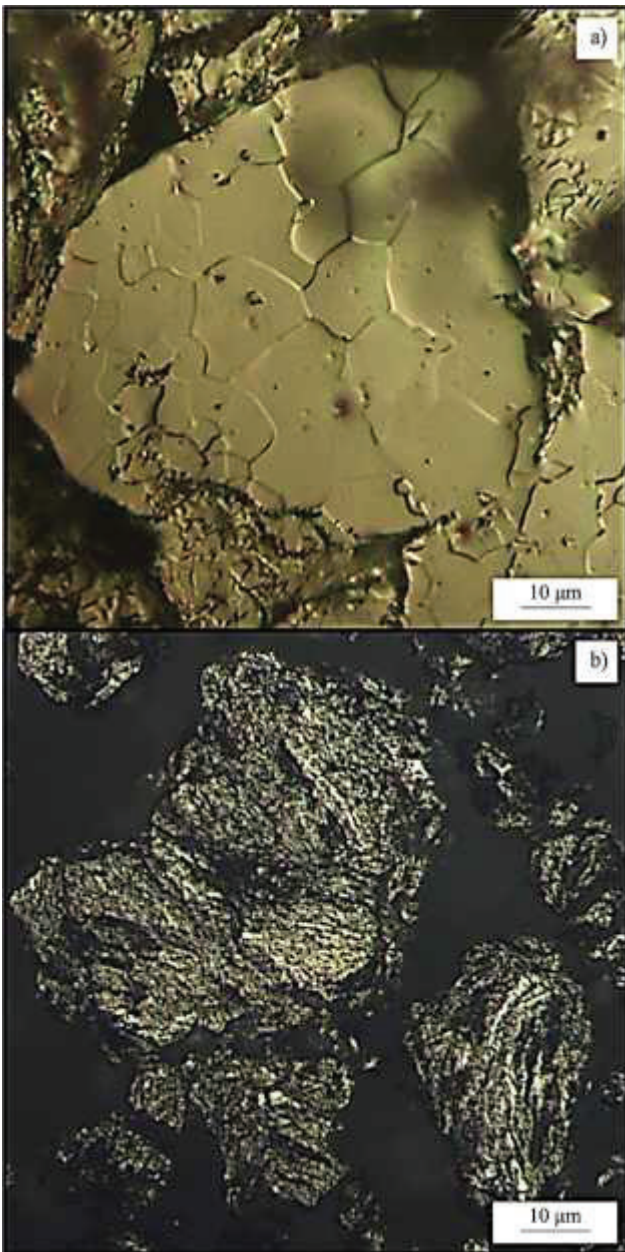


Fig. 3 Microstructure of powders; a) as-received b) milled.



Fig. 4 Microstructures of matrix of sintered samples a) as-received b) milled

According to the results of density measurement, both types of samples have similar density values accompanying high amount of porosity. Generally, high amount of porosities may be indicative of insufficient sintering parameters for achievement of nearly full densities. Further study on optimization of sintering parameters such as sintering pressure, temperature and time is necessary to improve densities. Moreover, more effective sintering methods such as spark plasma sintering, microwave sintering should be considered as potential alternatives to hot press sintering so as to improve density values with limited grain growth.

Stress-strain curves and average compressive yield strength (CYS) of the sintered samples are exhibited in Figure 5, clearly. When the stress-strain curves and yield strength of as-received and milled matrix are compared, fine grained matrix has a

remarkable effect on both CYS and ductility, obviously. It is well known that grain refinement increases yield strength of metals which is generally explained by Hall-Petch relation [17]. Grain boundaries behave as obstacles impeding further dislocation propagation. Grain refinement enhances the amount of grain boundaries in the matrix structure which means increase of the barriers against dislocation motion. Thus, finer grain size leads to higher yield strength. The relation between matrix grain size and the increase in yield strength (Hall-Petch equation) can be expressed as:

$$\sigma_y = \sigma_0 + k \cdot d^{-\frac{1}{2}} \quad (2)$$

where  $\sigma_0$  is the friction stress,  $k$  is a constant of yielding and  $d$  is the average grain size of the matrix.

Also, there are many studies showing that grain refinement increases ductility [18], [19]. Yamashita et al. reported a remarkable augmentation in both ductility and strength of pure Mg and Mg9Al alloy by grain refinement. They have attributed the increase in ductility to accompanying of increased number of grains to macroscopic plastic deformation [6]. It should be noted that grain refinement begets to suppression of twin formation during plastic deformation and lead to higher mechanical properties [7], [8,] [20]. Microstructural images of compressed samples taken from region in the vicinity of matrix demonstrate a great many of twin formations in coarse grained matrix (Figure 6a). On the other hand, twin formation cannot be seen in fine grained matrix (Figure 6b) which is consistent with literature. Therefore, one of the possible reasons for high ductility of samples with a fine grained matrix may be annihilation of twin generation throughout plastic deformation.

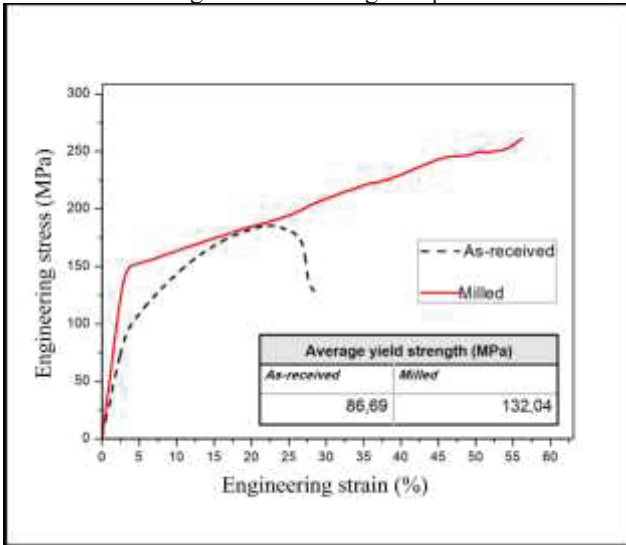


Fig. 5 Compression test results of sintered samples

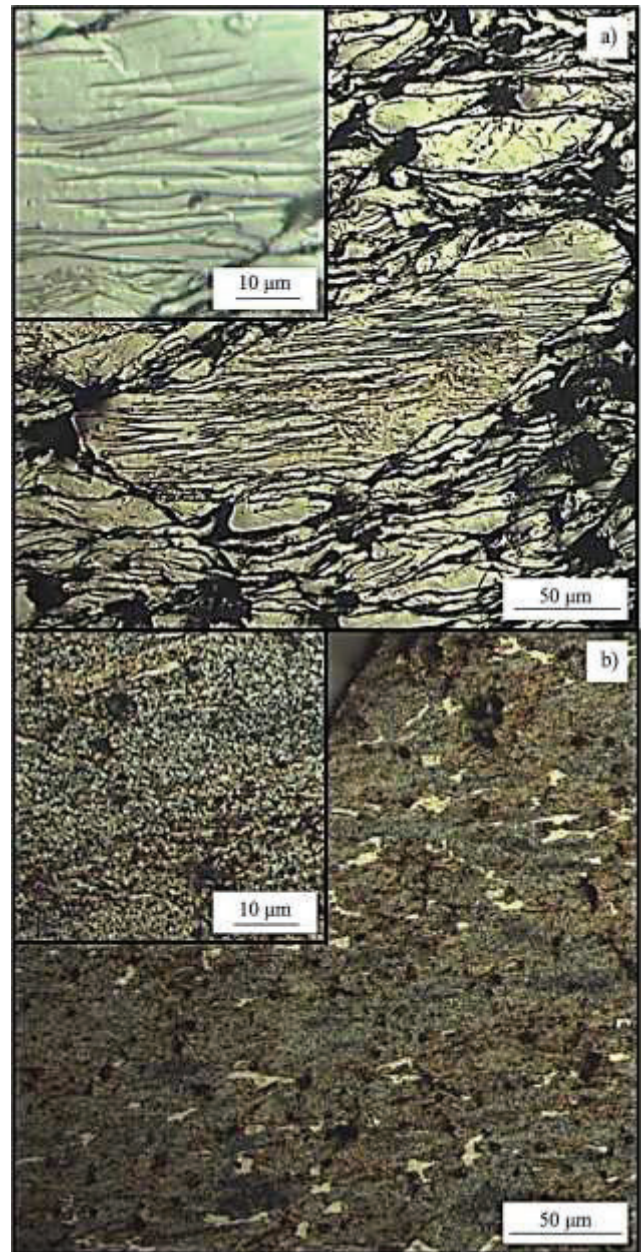


Fig. 6 Microstructures of compressed samples a) as-received b) milled

Should the interfacial bonding between matrix and reinforcement is strong, the load transfer mechanism is activated. Modified shear lag model expresses increase in yield strength by load transfer mechanism as [21]:

$$\Delta \sigma_y = 0,5 \cdot f \sigma_m \quad (3)$$

where  $f$  is volume fraction of reinforcement and  $\sigma_m$  is the yield strength of the matrix. Another possible reason for the higher mechanical properties of the milled matrix may be higher activity of load transfer mechanism. The fine grained matrix may have established a better interface bonding with the reinforcement due to its own higher diffusion coefficient compare to coarse grained matrix.

Mg is a highly chemically active metal and surface of the Mg particles are generally coated with an oxide layer which behaves as a diffusion barrier during sintering process. Beside grain refinement, mechanical milling process may have also

broken the considerably detrimental oxide layer located on the surface of the Mg particles with collisions and revealed clean metallic surfaces. In Figure 7, optical images of sintered samples of both as-received and 5h milled powders, taken from matrix-reinforcement interface, may support the idea behind the study. Milled sample exhibited a remarkable thickness of matrix-reinforcement interlayer, which may be an indicative of a high quality of interface bonding and an effective diffusion process.

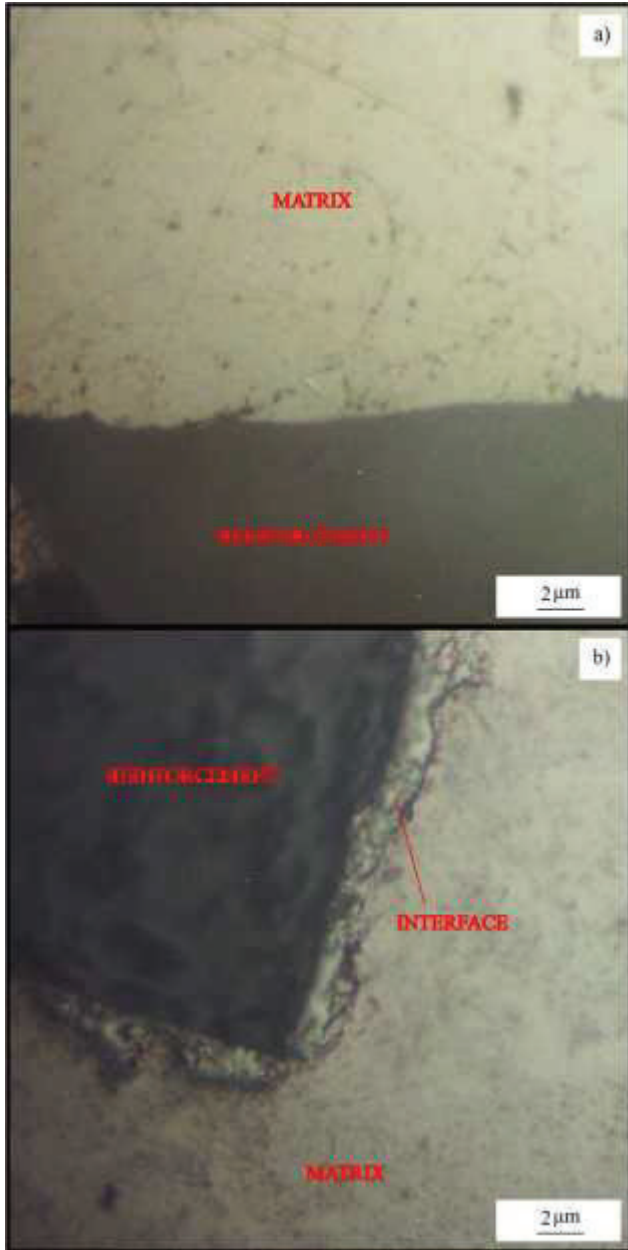


Fig. 7 Microstructures of the sintered samples a) as-received b) milled

#### IV. CONCLUSIONS

The influence of grain size of matrix on mechanical properties of silicon carbide reinforced magnesium matrix material produced through powder metallurgy route was investigated in the present study. The following conclusions can be drawn:

- 1- Nanocrystalline matrix powders with a 43.27 nm average crystal size were synthesized successfully by mechanical milling process.
- 2- Limited grain growth was observed after sintering milled samples preserved its fine grained structures.
- 3- Samples produced with nanocrystalline matrix powder gave significantly higher compressive yield strength and ductility results which are attributed to Hall-Petch effect, different deformation mode and more effective load transfer mechanism.
- 4- Microstructural investigations of compressed samples revealed that a great many of twin structures were observed in coarse grained matrix samples whereas twin formation was totally suppressed in fine grained matrix.
- 5- Samples produced with nanocrystalline matrix powder exhibited remarkable thickness of matrix-reinforcement interlayer in the microstructural images compare to coarse grained samples which may point out a high quality of interface bonding and effective diffusion process.

#### REFERENCES

- [1] I. Ostrovsky and Y. Henn, "Present state and future of magnesium application in aerospace industry", in *Proc. ASTEC'07*, 2007, p.19-22.
- [2] A. Dziubińska, A. Gontarz, M. Dziubiński and M. Barszcz, "The forming of magnesium alloy forgings for aircraft and automotive applications", *Advances in Science and Technology Research Journal*, vol.10, pp. 158-168, Sept. 2016.
- [3] M. Zheng, K. Wu and C. Yao, "Effect of interfacial reaction on mechanical behavior of SiCw/AZ91 magnesium matrix composites", *Materials Science and Engineering: A*, vol.318, pp. 50-56, Nov. 2001.
- [4] B. Mordike and T. Ebert, "Magnesium: properties—applications—potential", *Materials Science and Engineering: A*, vol.302, pp. 37-45, Apr. 2001.
- [5] P. Burke, G. Kipouros, D. Fancelli and V. Laverdiere, "Sintering fundamentals of magnesium powders", *Canadian Metallurgical Quarterly*, vol.48, pp. 123-132, July 2009.
- [6] A. Yamashita, Z. Horita and T. G. Langdon, "Improving the mechanical properties of magnesium and a magnesium alloy through severe plastic deformation", *Materials Science and Engineering: A*, vol.300, pp. 142-147, Feb. 2001.
- [7] J. Liao, M. Hotta, K. Kaneko and K. Kondoh, "Enhanced impact toughness of magnesium alloy by grain refinement", *Scripta Materialia*, vol.61, pp. 208-211, July 2009.
- [8] Q. Yang and A. Ghosh, "Deformation behavior of ultrafine-grain (UFG) AZ31B Mg alloy at room temperature", *Acta Materialia*, vol.54, pp. 5159-5170, No. 2006.
- [9] T. Mukai, M. Yamanoi, H. Watanabe and K. Higashi, "Ductility enhancement in AZ31 magnesium alloy by controlling its grain structure", *Scripta Materialia*, vol.45, pp. 89-94, Mar. 2001.
- [10] C. Li, X. Wang, W. Liu, K. Wu, H. Shi, C. Ding, X. Hu and M. Zheng, "Microstructure and strengthening mechanism of carbon nanotubes reinforced magnesium matrix composite", *Materials Science and Engineering: A*, vol.597, pp. 264-269, Mar. 2014.
- [11] C. Goh, M. Gupta, J. Wei and L. Lee, "Characterization of high performance Mg/MgO nanocomposites", *Journal of Composite Materials*, vol.41, pp. 2325-2335, Oct. 2007
- [12] R. Anish, M. Sivapragash and G. Robertsingh, "Compressive behaviour of SiC/npsc reinforced Mg composite processed through powder metallurgy route", *Materials & Design*, vol.63, pp. 384-388, Nov. 2014.
- [13] A. Dey and K. M. Pandey, "Magnesium metal matrix composites-a review", *Reviews on Advanced Materials Science*, vol.42, pp. 58-67, Mar. 2015.
- [14] M. Rashad, F. Pan, A. Tang, M. Asif and M. Aamir, "Synergetic effect of graphene nanoplatelets (GNPs) and multi-walled carbon nanotube (MW-CNTs) on mechanical properties of pure magnesium", *Journal of Alloys and Compounds*, vol.603, pp. 111-118, Aug. 2014.

- [15] C.-P. Li, Z.-G. Wang, H.-Y. Wang, X. Zhu, M. Wu and Q.-C. Jiang, "Fabrication of Nano-SiC Particulate Reinforced Mg-8Al-1Sn Composites by Powder Metallurgy Combined with Hot Extrusion", *Journal of Materials Engineering and Performance*, vol.25, pp. 5049-5054, Sept. 2016.
- [16] C. Suryanarayana and M. G. Norton, *X-ray Diffraction: a Practical Approach*, New York, Plenum Press, 1998.
- [17] E. Hall, "The deformation and ageing of mild steel: III discussion of results", *Proceedings of the Physical Society. Section B*, vol.64, pp. 747-753, Mar. 1951.
- [18] R. B. Figueiredo and T. G. Langdon, "Record superplastic ductility in a magnesium alloy processed by equal - channel angular pressing", *Advanced Engineering Materials*, vol.10, pp. 37-40, Feb. 2008.
- [19] A. Ma, J. Jiang, N. Saito, I. Shigematsu, Y. Yuan, D. Yang and Y. Nishida, "Improving both strength and ductility of a Mg alloy through a large number of ECAP passes", *Materials Science and Engineering: A*, vol.513, pp. 513-514, July 2009.
- [20] Y. Chino, K. Kimura and M. Mabuchi, "Twinning behavior and deformation mechanisms of extruded AZ31 Mg alloy", *Materials Science and Engineering: A*, vol.486, pp. 481-488, July 2008.
- [21] B. Han and D. Dunand, "Microstructure and mechanical properties of magnesium containing high volume fractions of yttria dispersoids", *Materials Science and Engineering: A*, vol.277, pp. 297-304, Jan. 2000.

# Borlanmış Fe-Mg Alaşımının Aşınma Davranışının İncelenmesi

İsmail YILDIZ<sup>1,\*</sup>, İbrahim GÜNEŞ<sup>2</sup>, Şükrü ÜLKER<sup>3</sup>

<sup>1</sup>Afyon Kocatepe Üniversitesi İncehisar Meslek Yüksekokulu Makine ve Metal Teknolojileri Bölümü, 03750, Afyonkarahisar, Türkiye; e-mail: iyildiz@aku.edu.tr

<sup>2</sup>Afyon Kocatepe Üniversitesi, Teknoloji Fakültesi, Metalurji ve Malzeme Bilimi Mühendisliği Bölümü, 03000, Afyonkarahisar, Türkiye; e-mail: igunes@aku.edu.tr

<sup>3</sup>Afyon Kocatepe Üniversitesi, Teknoloji Fakültesi, Makine Mühendisliği Bölümü, 03000, Afyonkarahisar, Türkiye; e-mail: ulker@aku.edu.tr

\*Sorumlu Yazar: iyildiz@aku.edu.tr

**Abstract**— Powder metallurgy is a method of producing material by sintering by pressing in cold press after homogenous mixing of particulate metal powders. In the study, 95% Fe and 5% Mg metal powders were homogenously mixed and sintered in tube oven at 530 °C. Sintered samples were piped in an oven atmosphere at 900 °C for 2 hours using Ekabor 2 powder. The layer thickness of the boronized sample was measured by optical microscope and found to be 11 µm. XRD analysis was performed for phase analysis of boride layer. FeB, Fe<sub>2</sub>B and Fe phases were obtained as a result of analysis. In addition, the abrasion test of the ball-type wear device was applied to the surfaces of the boronized specimens at a shear rate of 0.3 m / s at a shear distance of 2.5 N under a load of 250 and 500 m in a dry environment. As a result of the test, the wear depths of the materials were measured. It was found that the traces of the abrasion test fell below the layer, at the end of the 250 m shear distance, the average was 19.8 µm and the mean depth at the end of the shear distance was 25.3 µm. It was observed that the amount of wear increased with increasing slip distance.

**Keywords**— Powder metallurgy, sintering, boring, wear

## I. GİRİŞ

Borlama, yüzeylerinde bor tabakları oluşturmak için ana malzemenin yüzeyine bor tozlarının difüzyonunu gerçekleştiren termokimyasal bir difüzyon işlemidir [1-3]. Borlama işlemi 800-1100 °C sıcaklık aralığında, 1-12 saat süre aralıklarında katı, sıvı ve gaz ortamlarda gerçekleştirilmektedir [4-7].

Aşınma, sürtünme halindeki yüzeylerde dış etkenlerin etkisiyle zamanla meydana gelen malzeme kaybıdır [8,9]. Bu durum, çalışan mekanizmalarda istenmeyen bir durumdur. Malzemelerde aşınma problemini ortadan kaldırmak için malzeme yüzeylerine borlama gibi termokimyasal işlemler yapılmaktadır [10-12].

Borlama işlemi sonrasında malzeme yüzeyleri aşınmaya karşı dayanıklı hale gelmektedir. En çok aşınma sürtünen yüzeylerde ortaya çıkmaktadır. Bundan dolayı, toz metalurjisi yöntemiyle üretilmiş olan malzemelerin yüzeylerini borlama

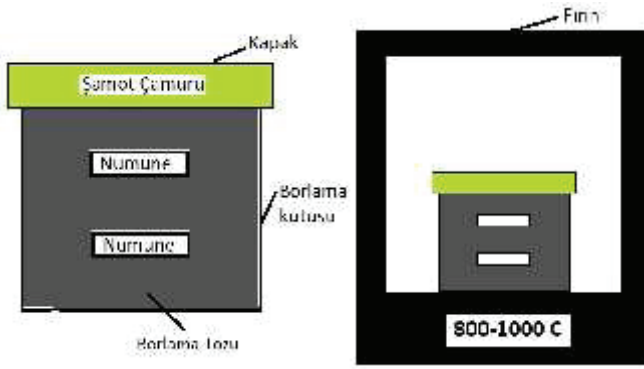
gibi yöntemlerle daha dayanıklı hale getirmek mümkündür [13-15].

Gerçekleşen bu çalışmada, toz metalurjisi yöntemiyle üretilmiş Fe-Mg alaşımlarına borlama işlemi yapılmıştır. Bu işlem sonrasında XRD ve optik mikroskop gibi metalografik analizlerin yanı sıra aşınma testi uygulanmıştır. Çalışmanın amacı ise, borlanmış Fe-Mg alaşımlarının aşınmaya karşı dayanımlarını ölçmektir.

## II. MATERYAL VE METOT

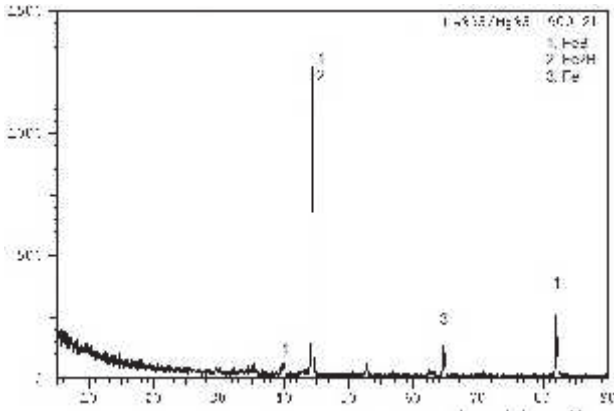
Bu çalışmada, % 95 Fe-% 5 Mg alaşım malzemelerini elde etmek için % 99 saflığa sahip Fe ve Mg metal tozları kullanılmıştır. Fe-Mg metalik tozların sinterleme sonrasında tane yapılarının iyi bir şekilde yapışması için tozlar tek fazlı karıştırıcıda 24 saat süreyle karıştırma işlemi yapılmıştır. Karıştırılan tozlar, özel olarak tasarlanmış soğuk kalıba dökülerek tek eksenli preste yaklaşık 300 bar basınç altında preslenmiştir. Preslenerek elde edilen numunelerin dayanımlarını arttırmak için koruyucu atmosferik ortama sahip tüp fırında 530 °C sıcaklıkta 2 saat süreyle sinterleme işlemi uygulanmıştır.

Sinterlenerek elde edilen numunelere borlama işlemi gerçekleştirilmiştir. Bu işlemim amacı, üretilen numunelerin dayanıklılığını arttırmaktır. Borlama işleminde, özel olarak hazırlanmış kutu bir kap kullanılmaktadır. Kabın içerisine numunelerin altına ve üzerine ticari Ekabor II toz karışımları dökülmüştür. Kabın üzeri ve kapağı şamot çamuru ile hava almayacak şekilde kapatılmıştır (Şekil 1) [16,17]. Fırın ortamında 900 °C sıcaklıkta 2 saat süre aralığında ısıtmaya tabi tutulmuşlardır. Bu süreler sonrasında numuneler fırından çıkarılarak soğumaya bırakılmıştır.



Şekil 1. Borlama işleminin yapılışı [16-17].

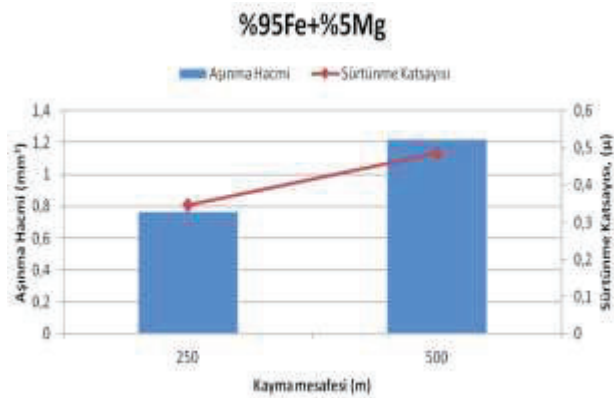
#### A. XRD Analizi



Şekil 2. Borlanmış Fe-Mg alaşımına yapılan XRD analizi

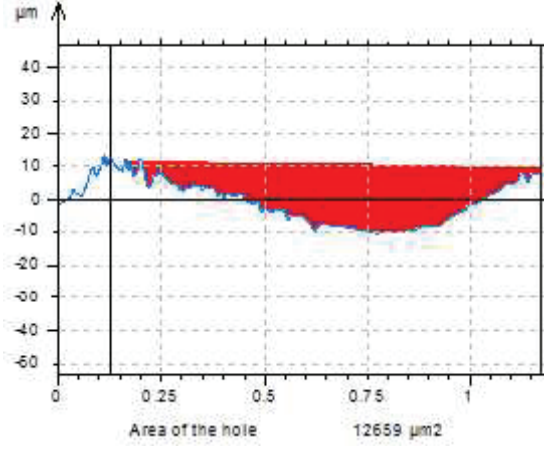
Şekil 2'de 900 °C'de 2 saat süreyle borlanmış Fe-Mg alaşımına uygulanan XRD analiz sonucu görülmektedir. En yüksek değerleri FeB ve Fe<sub>2</sub>B fazları göstermiştir. Bu değerleri takiben Fe faz değeri ortaya çıkmıştır. FeB ve Fe<sub>2</sub>B fazları borlamanın oluştuğunu göstermektedir.

#### B. Aşınma Testi

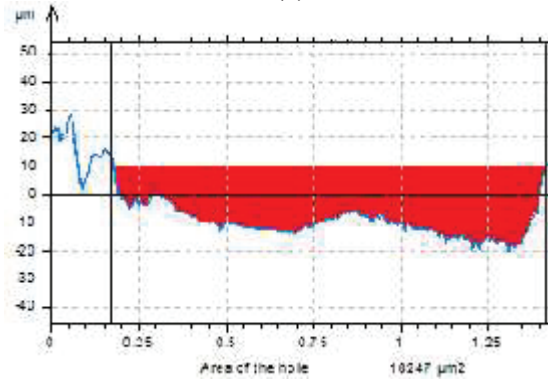


Şekil 3. Kayma mesafesine bağlı olarak aşınma hacmi ve sürtünme katsayısının değişimi.

Şekil 3'te aşınma testi sonucuna göre oluşan aşınma hacmi ve sürtünme katsayısı oranları görülmektedir. Bu grafiğe göre kayma mesafesi arttıkça Fe-Mg alaşımında meydana gelen aşınmada artmaktadır. 250 m kayma mesafesinde 0,7 mm<sup>3</sup> olan aşınma hacmi 500 m mesafede yaklaşık olarak iki katına çıkmıştır.



(a)

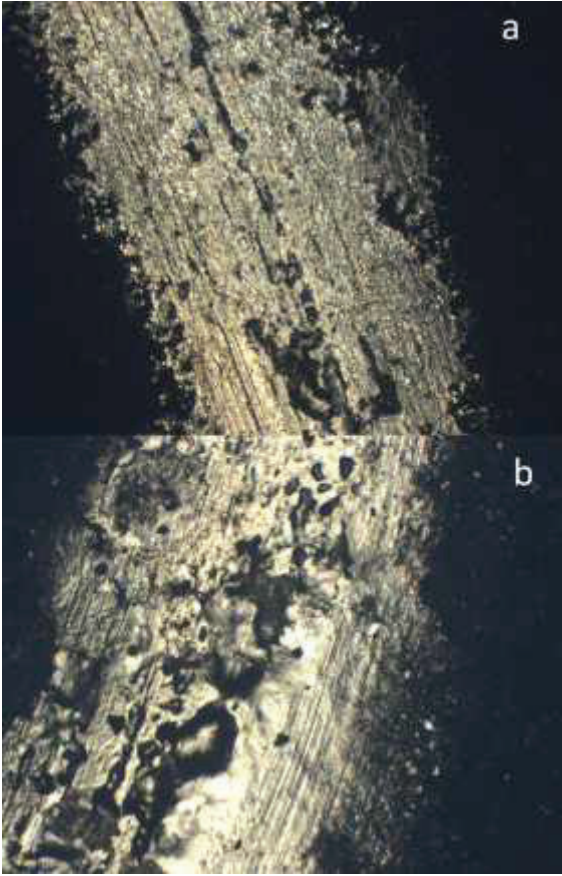


(b)

Şekil 4. Aşınma iz derinlikleri a) 250 m, b) 500 m

Şekil 4'te aşınma testi sonucu oluşan aşınma iz derinlikleri görülmektedir. Kayma mesafesi ve aşınma hacminin artmasına bağlı olarak aşınma iz derinlikleri de artış göstermiştir. 250 m kayma mesafesinde yaklaşık olarak 10 µm iz derinliği ortaya çıkarken bu değer 500 m kayma mesafesinde yaklaşık olarak 18 µm değerine kadar çıkmıştır.

#### C. Optik Mikroskop



Şekil 5. Aşınma izlerinin optik mikroskop görüntüsü, a) 250 m, b) 500 m

Şekil 5'te aşınma testi sonucu malzeme yüzeyinde oluşan aşınma izlerinin optik mikroskop görüntüleri görülmektedir. Kayma mesafesine bağlı olarak malzeme yüzeylerinde abrazyon aşınması meydana gelmiştir. Bu durum 500 m kayma mesafesinde gerçekleşen malzeme yüzeyinde daha net bir şekilde görülmektedir. Ayrıca yüzeylerde çatlaklar şeklinde oluşan delaminasyon aşınması da oluşmuştur.

### III. TARTIŞMA

530 °C'de sinterlenerek üretilen numunelere borlama işlemi sonrası elde edilen sonuçlar aşağıda verilmiştir:

- Fe %95-Mg %5 kompozisyonuna yapılan borlama işlemi sonrasında elde edilen borlama kalınlığı 11 µm olarak ölçülmüştür.
- Yapılan XRD analizi sonrasında FeB, Fe<sub>2</sub>B ve Fe faz değerleri ortaya çıkmıştır.
- Aşınma testi sonrasında 250 m kayma mesafesi ilerleme sonucunda ortalama 19,8 µm, 500 m kayma mesafesi sonucunda ise 25,3 µm iz derinliği oluştuğu tespit edilmiştir.

- Kayma mesafesinin artmasına bağlı olarak aşınma miktarının da arttığı gözlenmiştir.
- Aşınma testi sonrasında numune yüzeylerinde abrazyon aşınma ve sonrasında da delaminasyon aşınmanın olduğu ortaya çıkmıştır.

### TEŞEKKÜR

Gerçekleştirilen bu çalışma, Afyon Kocatepe Üniversitesi BAPK 17.MYO.05 no'lu proje ile desteklenmiştir. Desteklerinden dolayı Bilimsel Araştırma Projeleri Komisyonuna çok teşekkürler.

### KAYNAKLAR

- [1] D. Özyayın, "Toz Metalurjisi ile Üretilen Demir Esaslı Malzemelerde Borlamanın Mekanik Özelliklere Etkisi", *Celal Bayar Üniversitesi Fen Bilimleri Enstitüsü, Yüksek Lisans Tezi*, 2015.
- [2] F. Taştan, "Farklı Bileşimlere Sahip Çeliklerin Borlama İşlemi İle Yüzey Özelliklerinin İncelenmesi", *Celal Bayar Üniversitesi Fen Bilimleri Enstitüsü, Yüksek Lisans Tezi*, 2010.
- [3] K. Genel, " Boriding Kinetics of H13 Steel", *Vacuum*, vol. 80, pp. 451-457, June 2005.
- [4] I. Gunes, I. Yıldız, " Rate of Growth of Boride Layers on Stainless Steels", *Oxidation Communications*, vol. 38, pp. 2189-2198, April 2015.
- [5] S. Sen, U. Sen, C. Bindal, " Tribological Properties of Oxidised Boride Coatings Grown on AISI 4140 Steel", *Materials Letters*, vol. 60, pp. 3481-3486, April 2006.
- [6] T. Balusamy, T.S.N. Sankara Narayanan, K. Ravichandran , Il Song Park, Min Ho Lee, " Pack Boronizing of AISI H11 Tool Steel: Role of Surface Mechanical Attrition Treatment", *Vacuum*, vol. 97, pp. 36-43, April 2013.
- [7] I. Yıldız, I. Gunes, " Nikel Magnezyum Alaşımının Borlanmasında Magnezyum Elementinin Etkisi", *3rd International Conference on Engineering Technology and Applied Sciences (ICETAS)*, July 17-21 2018, Skopje Macedonia
- [8] D. Rai, B. Singh, J. Singh, " Characterisation of Wear Behaviour of Different Microstructures in Ni-Cr-Mo-V Steel", *Wear*, vol. 263, pp. 821-829, May 2007.
- [9] V. G. Efremenko, K. Shimizu, T. Noguchi, A.V. Efremenko, Yu. G. Chabak, " Impact-Abrasive-Corrosion Wear of Fe-Based Alloys: Influence of Microstructure and Chemical Composition Upon Wear Resistance", *Wear*, vol. 305, pp. 155-165, June 2013.
- [10] S. Senthur Prabu, S. Prathiba, Asokan M. A, D. Sai Mounish, Aditya P Vastrad, V. Sai Charan, "Experimental Study on Dry Sliding Wear Characteristics of Sintered /Forged Plain Carbon Steel (Fe-1%C) With The Addition of Titanium", *Materials Today: Proceedings*, vol. 5, pp. 12551-12558, 2018.
- [11] Niko Ojala, Kati Valtonen, Atte Antikainen, Anu Kemppainen, Jussi Minkkinen , Olli Oja, Veli-Tapani Kuokkala, " Wear Performance of Quenched Wear Resistant Steels in Abrasive Slurry Erosion", *Wear*, vol. 354-355, pp. 21-31, March 2016.
- [12] W. Wang, R. Song, S. Peng, Z. Pei, " Multiphase steel with improved impact-abrasive wear resistance in comparison with conventional Hadfield steel", *Materials and Design*, vol. 105, pp. 96-105, May 2016.
- [13] H. Ay, " Toz Metalurjisi Yöntemi İle Üretilen AA7075 Alüminyum Alaşımına Ti Ve B<sub>4</sub>C İlavesinin Aşınma Davranışı Üzerine Etkisinin İncelenmesi", *Karabük Üniversitesi Fen Bilimleri Enstitüsü, Yüksek Lisans Tezi*, 2014.
- [14] V. Koç, "Toz Metalurjisi Tekniği ile Üretilen Bir Paslanmaz Çelikte Katkı Elemanlarının Aşınma Direncine Etkileri", *Fırat Üniversitesi Fen Bilimleri Enstitüsü, Doktora Tezi*, 2006.
- [15] A. M. Ataç, " Çinko-Alüminyum (Zn) Alaşımının Toz Metalurjisi Yöntemiyle Üretimi, Karakterizasyonu ve Aşınma Özelliklerinin İncelenmesi", *Gazi Üniversitesi Fen Bilimleri Enstitüsü, Yüksek Lisans Tezi*, 2011.

- [16] A. Üçkardeşler, "Çelik Dökümlerde Borlama Isıl İşleminin Abrasif Aşınma Direnci Üzerine Etkisi", *Gazi Üniversitesi Fen Bilimleri Enstitüsü, Yüksek Lisans Tezi*, 2013.
- [17] M. Çarkçı, "Saf Nikelin Borlama Özelliklerinin İncelenmesi", *Süleyman Demirel Üniversitesi Fen Bilimleri Enstitüsü, Yüksek Lisans Tezi*, 2012.

# The Effect of Seawater Aging on the Mechanical Performance of SiO<sub>2</sub>/Epoxy Polymer Nanocomposites

Halil Burak Kaybal\*, Hasan Ulus#, A. Caner Tatar#, Okan Demir#, Ahmet Avci+

\* Department of Mechanical Engineering, Amasya University, Amasya, Turkey  
hburak@amasya.edu.tr

#Department of Mechanical Engineering, Konya Technical University, Konya, Turkey  
hasanulus@selcuk.edu.tr, acaner.tatar@selcuk.edu.tr, okandemir@selcuk.edu.tr

+ Department of Biomedical Engineering, Necmettin Erbakan University, Konya, Turkey  
aavci@selcuk.edu.tr

**Abstract**— In this study, dispersion of nano SiO<sub>2</sub> in epoxy composite aged in seawater and its effect on mechanical properties were studied. The SiO<sub>2</sub>-epoxy polymer nanocomposite materials were kept in seawater for a total of six months to be tested every two months. Tensile and bending tests were applied to composite materials as a mechanical test. According to the mechanical test results, there was less decrease in strength in SiO<sub>2</sub>-epoxy polymer nanocomposite material compared to unmodified material. In usage of seawater, the mechanical properties were observed to be the best in 2 % added SiO<sub>2</sub>-epoxy nanocomposite material.

**Keywords**— Epoxy, nanocomposites, nano SiO<sub>2</sub>, seawater, tensile, bending

## I. INTRODUCTION

Epoxy resins are thermoset materials used widely in structural and composite materials due to their properties such as high strength, low shrinkage, effective electrical insulation, excellent adhesion, chemical and solvent resistance, low toxicity and low cost. Also, epoxy resins are banally used as coatings, casting materials, binders and adhesives application [1]. The use of nanoparticles is a common method used to improve the strength of epoxy resins. Nanoparticles can enhance interfacial area between fillers and polymer [2]. Thus, an increment in performance on the properties of epoxy resin is observed [2, 3]. In the literature, boron nitride, CNT [4], nano clay [5], silica [6], graphene [7] nanoparticles are commonly used to improve composite material properties. It is known that polymeric resins can be influenced by water. The interface of filler-polymer or fiber-polymer may weaken when the resin absorbs water [8] [4]. The articles on the disintegration of polymeric composites due to water absorption can be found in the literature [9-12]. As a result, these studies have shown a decrease in mechanical properties due to water absorption.

In this research, the influence of seawater aging on the mechanical performance of epoxy nanocomposites filled with different proportions from 1 wt % to 5 wt % of nano-SiO<sub>2</sub> have been studied. The nanocomposites were submerged in seawater for up to six months at room temperature. The specimens were mechanically examined every two months.

Tensile and bending tests were evaluated as mechanical properties according to the related standard methods. The experimental results illustrate that the SiO<sub>2</sub> nanoparticles left a positive influence on the mechanical performance of the nanocomposites in the sea water conditioning.

## II. MATERIAL AND METHODS

### A. Production of Composites

Nanocomposite materials were manufactured at rates of 1 wt % to 5 wt % nano- SiO<sub>2</sub>. Epoxy and powdered nano-SiO<sub>2</sub> were mixed with the ultrasonicator for 30 minutes in the ice bath. After dispersing process curing agent was added in to epoxy and the mixture was degassed at 25 °C and 0.6 bar at approximately 20 min. Steel molds are covered with mold release in Fig 1(a). The epoxy mixture was cast into steel molds. Curing was performed firstly at 80 °C for approximately 1 h, then at 120 °C at approximately 2 h. After that it was slowly cooled to room temperature in the oven. Subsequently, the specimens were removed from the steel molds in Fig 1(b). All samples conventionally polished with SiC sandpapers with grit numbers of 800 to minimize effect stress concentration caused by sharp edges. The produced composite materials were transported to seawater environment and kept in seawater for 6 months.

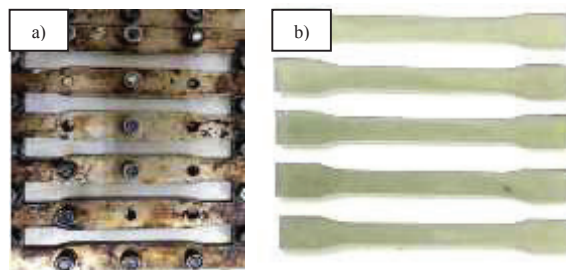


Fig. 1 a) Steel mold b) Test specimens

### B. Test procedure

Bending and tensile tests were performed as a mechanical test in the study. The ASTM D7264/ D7264M-07 standards were used for the bending test and the ASTM D4762 - 11a standards for the tensile test, respectively. The specimens were tested every two months. Shimadzu test machine which has 1 kN load cell was used for mechanical test. Tensile tests were carried out with 2 mm·min<sup>-1</sup> tensile speed and bending tests were performed under 1 mm·min<sup>-1</sup>.

### III. RESULTS AND DISCUSSIONS

In a previous study we did, reinforcement of nano-SiO<sub>2</sub> had improved the mechanical properties of epoxy composite in dry condition [13]. Tensile and Bending curves for SiO<sub>2</sub>/Epoxy nanocomposites are shown in Figure 2. Then, the composites, aged under sea water condition, were tested every two months. Figure 3 illustrated that result of tensile and bending tests for SiO<sub>2</sub>/Epoxy nanocomposite. It is clear that the nanocomposites are negatively affected by sea water when the results are examined. In spite of this situation, reinforcement of nano-SiO<sub>2</sub> tried to protect properties of the epoxy matrix. However, nanoparticle-matrix interface may be affected by sea water. According to all curves, reinforcement of 2 wt. % SiO<sub>2</sub>/Epoxy has better mechanical performance than the other difference proportions. In the end of 6th month, we did not get any results for bending test, due to excessive displacement in the nanocomposites.

Compared to 0 wt. % SiO<sub>2</sub>/Epoxy composite, the mechanical properties of 2 wt. % SiO<sub>2</sub>/Epoxy nanocomposite are presented in Table 1. Though SiO<sub>2</sub> nanoparticles are enhanced the performance of tensile strength and load bending capacity in dry condition, the particles cannot be prevented decrement of these mechanical performances after aging due to the detrimental effect of the absorbed seawater. Nevertheless, SiO<sub>2</sub> nanoparticles are succeeded in delaying the damage mechanisms when the numerical results in Table 1 are considered.

Table 1. Results of mechanical test for 0 wt. % and 2 wt. % SiO<sub>2</sub>/Epoxy nanocomposite.

Mechanical Properties	Condition				Nanocomposites
	Dry	Sea water			
		2nd	4th	6th	
Tensile Strength (MPa)	65.2	59.4	54.9	46.7	0 wt.% SiO <sub>2</sub> /Epoxy
	93.9	90.8	87.4	84.4	2 wt.% SiO <sub>2</sub> /Epoxy
Bending Force (N)	233	213.5	121.2	-	0 wt.% SiO <sub>2</sub> /Epoxy
	438.5	393.7	277.9	-	2 wt.% SiO <sub>2</sub> /Epoxy

### IV. CONCLUSIONS

Consequently, the studies on the mechanical properties show that the reinforcement of SiO<sub>2</sub> nanoparticles in the epoxy matrix polymer has significant positive or negative influences on nanocomposites for both of dry and seawater conditions. From the results of this study, the following conclusions can be drawn:

- High proportions of SiO<sub>2</sub> nanoparticles (e.g. 4-5 wt. %) have shown weak performance in load capacity due to agglomeration of particles.
- The other proportions of SiO<sub>2</sub> nanoparticles in epoxy matrix polymer are demonstrated superior properties in both of condition.
- According to result of mechanical test, sea water absorption is weakened both tensile strength and bending force. But, SiO<sub>2</sub> added nanocomposites are less affected after aging than the others.
- At the end of the sixth month of bending test results, a displacement exceeding the device capacity has occurred.

### REFERENCES

- [1] M. A. Boyle, C. J. Martin, and J. D. Neuner, "Epoxy resins," ASM Handbook Volume 21 Composites, pp. 78-89, 2001.
- [2] Y. Zheng, Y. Zheng, and R. Ning, "Effects of nanoparticles SiO<sub>2</sub> on the performance of nanocomposites," Materials Letters, vol. 57, no. 19, pp. 2940-2944, 2003.
- [3] G. Song, "Polymeric nano-metered composites," Mater Rep, vol. 4, no. 1, pp. 57-60, 1996.
- [4] H. Ulus, Ö. S. Şahin, and A. Avcı, "Enhancement of flexural and shear properties of carbon fiber/epoxy hybrid nanocomposites by boron nitride nano particles and carbon nano tube modification," Fibers and Polymers, vol. 16, no. 12, pp. 2627-2635, 2015.
- [5] L. Wang, K. Wang, L. Chen, Y. Zhang, and C. He, "Preparation, morphology and thermal/mechanical properties of epoxy/nanoclay

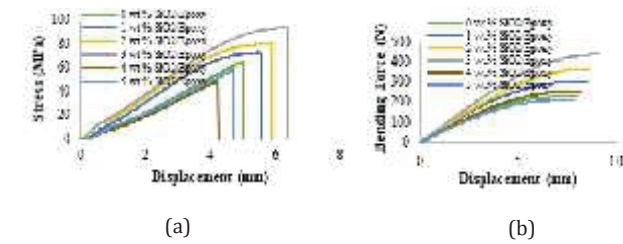


Fig 2. (a) Tensile curve (b) Bending curve in dry condition [13]

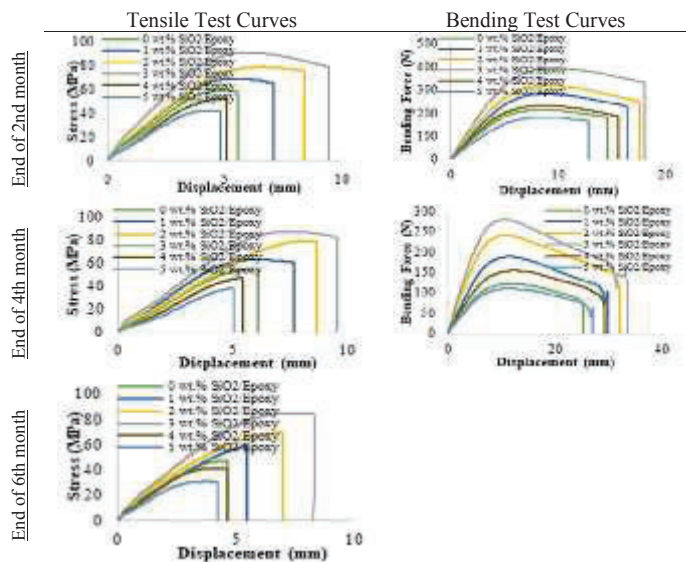


Fig 3. Tensile and Bending Curves in sea water condition for SiO<sub>2</sub>/Epoxy nanocomposite

- composite," *Composites Part A: Applied Science and Manufacturing*, vol. 37, no. 11, pp. 1890-1896, 2006.
- [6] Y.-L. Liu, C.-Y. Hsu, W.-L. Wei, and R.-J. Jeng, "Preparation and thermal properties of epoxy-silica nanocomposites from nanoscale colloidal silica," *Polymer*, vol. 44, no. 18, pp. 5159-5167, 2003.
- [7] M. A. Rafiee et al., "Fracture and fatigue in graphene nanocomposites," *small*, vol. 6, no. 2, pp. 179-183, 2010.
- [8] R. Silva, E. Aquino, L. Rodrigues, and A. Barros, "Curaua/glass hybrid composite: the effect of water aging on the mechanical properties," *Journal of reinforced plastics and composites*, vol. 28, no. 15, pp. 1857-1868, 2009.
- [9] X. Li and Y. J. Weitsman, "Sea-water effects on foam-cored composite sandwich lay-ups," *Composites Part B: Engineering*, vol. 35, no. 6-8, pp. 451-459, 2004.
- [10] P. Davies, F. Mazeas, and P. Casari, "Sea water aging of glass reinforced composites: shear behaviour and damage modelling," *Journal of composite materials*, vol. 35, no. 15, pp. 1343-1372, 2001.
- [11] N. E. Marcovich, M. M. Reboredo, and M. I. Aranguren, "Dependence of the mechanical properties of woodflour-polymer composites on the moisture content," *Journal of Applied Polymer Science*, vol. 68, no. 13, pp. 2069-2076, 1998.
- [12] R. Adams and M. Singh, "The effect of immersion in sea water on the dynamic properties of fibre-reinforced flexibilised epoxy composites," *Composite Structures*, vol. 31, no. 2, pp. 119-127, 1995.
- [13] H. B. Kaybal, H. Ulus, O. Demir, A. C. Tatar, and A. Avci, "Investigations on the Mechanical Properties of the Nano SiO<sub>2</sub> Epoxy Nanocomposite."

# Effect of Mg Addition on Al4Cu Powder Metallurgy Alloy (ISLAC'18/UHAKS18)

H. Erdem Camurlu<sup>#,\*</sup>, Vedat Bayram<sup>#</sup>

<sup>#</sup>Akdeniz University, Mechanical Engineering Department  
Dumlupınar Boulevard, Campus, Antalya, Turkey  
ecamurlu@akdeniz.edu.tr

**Abstract**— Aluminum alloys attract attention due to their lightweight and sufficient strength. Hence, they are used in aerospace and automotive industries in addition to other structural applications.

Powder metallurgy has been employed for producing parts having net shapes. In the present study, effect of Mg powder addition on microstructure and mechanical properties of Al4Cu alloy has been investigated. Mg is known to enhance sintering of aluminium alloys, by reacting with Al<sub>2</sub>O<sub>3</sub> layer which is present on the surfaces of the aluminium particles.

In the present study, Mg in powder form was added into Al, Cu (4 wt.%) powders in 1-10 wt % range. After weighing, mixing was performed in dry form. Mixed powders were shaped by pressing at 600 MPa pressure in a tool steel die. Pressed samples were sintered in nitrogen atmosphere. Sintering was conducted at 610 °C for the samples that did not contain Mg, on the other hand samples having Mg addition were sintered at 590 °C.

Sintered samples were subjected to density and hardness measurements. Optical microscope was utilized for microstructure examinations, after cutting, grinding and polishing of the samples. Three point bending tests were conducted with a Shimadzu universal testing unit.

As compared to the samples that did not contain Mg, samples having Mg presented higher density values. Density values were in 95-97 % of the theoretical density. There was a slight increase in density with the addition of Mg. This can be taken as an indication that Mg enhances sintering of aluminium particles. Hardness values of the sintered samples were about 50 HB10, without Mg addition. Mg addition was seen to increase the hardness of the sintered samples. Hardness values of samples containing 1 and 2 % Mg were in 60-70 HB10 range. Higher amounts of Mg resulted in a slight decrease in hardness. Three point bending strength values of the sintered samples were 320 MPa without Mg addition. Addition of Mg was seen to increase the bending strength. Bending strength values were 370 MPa with 1 wt. % Mg addition and 430 MPa with 5 % Mg addition.

It was seen in optical microscopy examinations that there was small amount of porosity when Mg amount was in 1-3 wt % range. However it was inferred from the microstructural examinations of the sintered samples having 5 and 10 wt% Mg that high amounts of Mg result in large pores in the structure. In addition, intermetallic compounds which are believed to be composed of Al, Cu and Mg were present in the structure of the sintered samples.

**Keywords**— Aluminum-%4 Cu alloy, Mg alloying, powder metallurgy, sintering, mechanical properties

## I. INTRODUCTION

Aluminum alloys attract attention due to their lightweight and sufficient strength. Hence, they are used in aerospace and automotive industries in addition to other structural applications [1]. In the present study, effect of Mg powder addition on microstructure and mechanical properties of Al4Cu alloy has been investigated. Mg is known to enhance sintering of aluminium alloys, by reacting with Al<sub>2</sub>O<sub>3</sub> layer which is present on the surfaces of the aluminium particles [2,3]. Aluminum is widely used as a matrix material in metal matrix composites, thanks to its lightweight and adequate mechanical properties.

Powder metallurgy was chosen for the preparation of aluminium alloy articles. Powder metallurgy has the advantage of obtaining near net shaped parts having homogeneous microstructure and high density. Powder metallurgy has widely been utilized in the production of composites also.

In the present study, Mg in powder form was added into Al, Cu (4 wt.%) powders in 1-10 wt % range. After pressing and sintering, effect of Mg addition was investigated by subjecting the products to microstructural examinations and mechanical characterization.

## II. MATERIALS AND METHODS

Preparation of the alloy samples was conducted by powder metallurgy technique that consisted of mixing, pressing and sintering of the samples. After mixing aluminium (Merck) and copper (Alfa Aesar) and Mg (Merck) in powder form, pressing was performed in a tool steel die.

Mg in powder form was added into Al and Cu (4 wt.%) powders in 1-10 wt % range. After weighing, mixing was performed in dry condition. Mixed powders were shaped by pressing at 600 MPa pressure. Pressed samples were sintered in nitrogen atmosphere for 30 minutes. Sintering was conducted at 610 °C for the samples that did not contain Mg, on the other hand samples having Mg addition were sintered at 590 °C. In the sintering operations, heating and cooling rates of 6 °C/min were employed.

Sintered samples were subjected to density and hardness measurements. Optical microscope was utilized for microstructure examinations (Nikon Eclipse LV150) after cutting, grinding and polishing of the samples. Three point

bending tests were conducted with a universal mechanical tester having 50 kN capacity (Shimadzu AG-IC). Hardness tests were performed with a Brinell hardness tester (Bulut Makina).

### III. RESULTS AND DISCUSSION

#### A. Microstructural Examinations

Microstructure of the Al4Cu alloy, which was sintered at 610 °C is presented in Figure 1. Some particles of Al<sub>2</sub>Cu intermetallic compound were observed in the microstructure of this sample. These are the darker regions, on the boundaries of Al grains. It was seen in the optical microscopy examinations that this sample contained little or no porosity.



Fig. 1 Microstructure of the Al4Cu alloy, sintered at 610 °C

Microstructures of the Al4Cu alloy containing 1 wt.% Mg is presented in Figure 2. The sizes of the intermetallic compounds, which are believed to be composed of Al, Cu and Mg [4], were seen to increase, when Mg is present in the structure (dark regions). This sample also contained little or no porosity, according to optical microscope examinations.

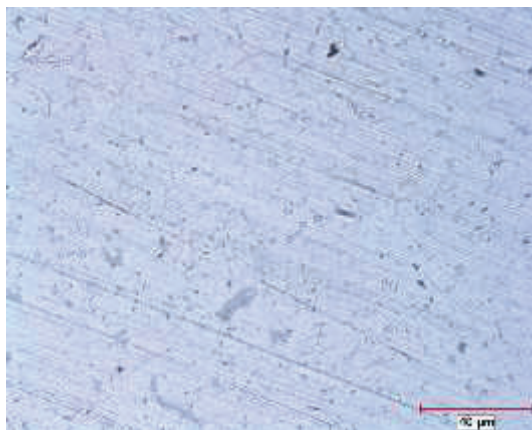


Fig. 2 Microstructure of the Al4Cu alloy, containing 1 wt.% Mg, sintered at 590 °C

Microstructures of the Al4Cu alloy containing 5 wt.% Mg is presented in Figure 3. The sizes of the intermetallic compounds were seen to increase considerably. In addition, amount of porosity in the structure increased. These pores are believed to be originated from the diffusion of Mg in aluminium.

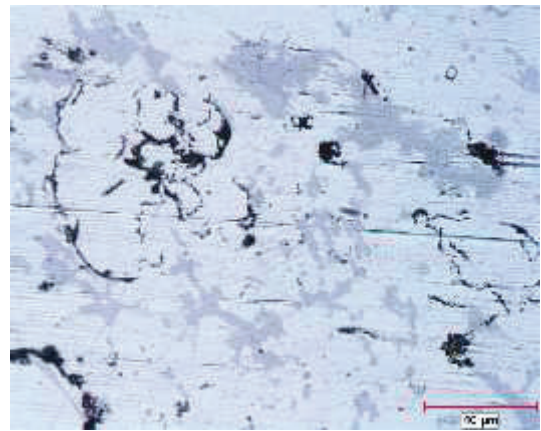


Fig. 3 Microstructure of the Al4Cu alloy, containing 5 wt.% Mg, sintered at 590 °C

Microstructures of the Al4Cu alloy containing 10 wt.% Mg is presented in Figure 4. The sizes of the pores compounds were seen to increase considerably. It can be inferred that increasing the amount of Mg particles in the starting mixture results in an increase in the size and amount of the pores.

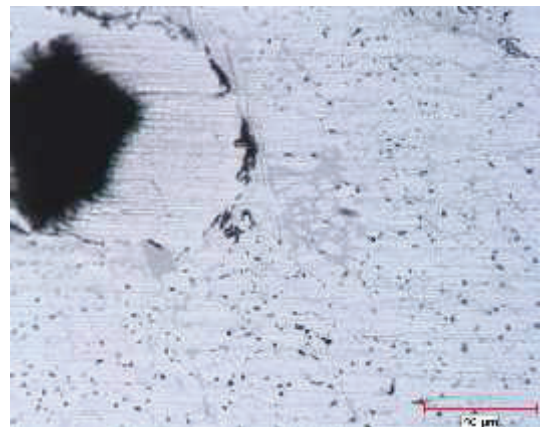


Fig. 4 Microstructure of the Al4Cu alloy, containing 10 wt.% Mg, sintered at 590 °C

#### B. Density

Percent theoretical density values of the Al4Cu samples containing 0, 1, 2, 3 and 5 wt.% Mg are presented in Figure 5. Density values of the samples were in 95-97 % range. There was a slight increase in density with the addition of Mg. On the other hand, the density of the sample containing 10 wt.% Mg could not be determined since it contained too many large pores in the structure. Nonetheless, its density is believed to be much lower than the density of the samples containing less amount of Mg.

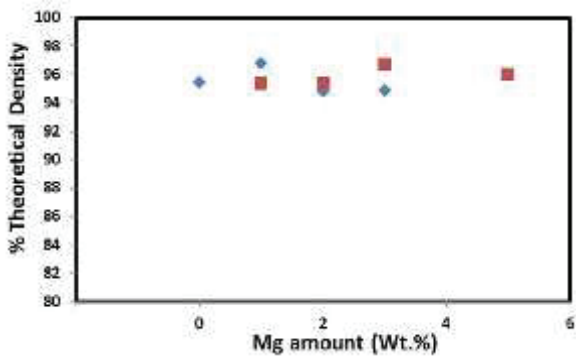


Fig. 5 Percent theoretical density values of the Al4Cu samples containing 0, 1, 2, 3 and 5 wt.% Mg

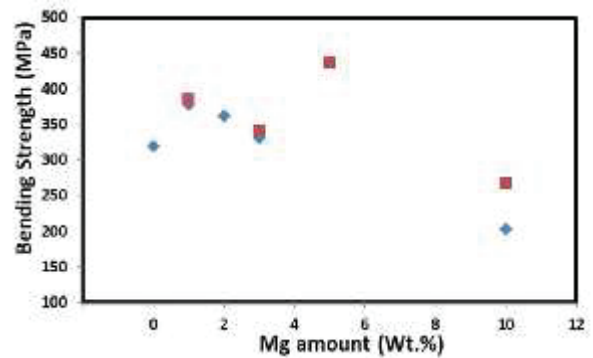


Fig. 7 Bending strength values of the Al-4Cu alloy containing 0, 1, 2, 3, 5 and 10 wt.% Mg

### C. Mechanical Properties

Al-4%Cu alloy and alloys containing 1, 2, 3, 5, 10 wt. % Mg were subjected to mechanical tests, such as hardness test and 3 point bending test.

Results of the hardness measurements are presented in Figure 6. The hardness value of the Al-4%Cu alloy was about 50 HB10. It can be seen that, hardness of the alloys increased with the addition of Mg, up to 1 wt.% Mg and then decreased. In any case, the hardness values of the alloys containing Mg were higher than the Al4Cu alloy. The highest attained hardness value was about 70 HB10.

The increase in the hardness of the alloys can be attributed to the restraint of the aluminum due to the presence of the Mg atoms or due to the presence of the intermetallic compounds containing Mg. These make the deformation of aluminium more difficult.

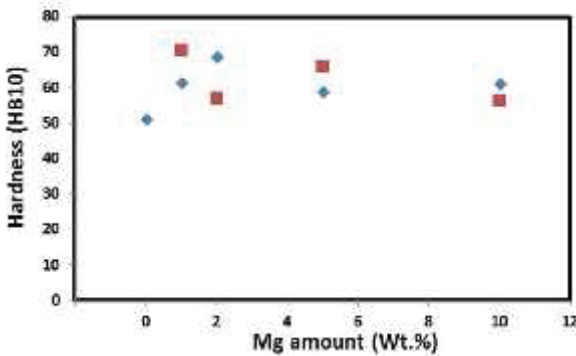


Fig. 6 Hardness values of the unreinforced Al-4Cu alloy and samples containing 1, 2, 5 and 10 wt.% Mg

Bending strength and strain values of the Al-4%Cu alloy and alloys containing 1, 2, 3, 5, 10 wt. % Mg are presented in Figures 7 and 8, respectively. Strength values were higher than Al4Cu alloy for the samples containing Mg up to 5 wt.%. Highest strength was attained in the sample having 5 wt.% Mg, with a value of about 430 MPa. The lower strength value of the sample having 10 wt.% Mg can be attributed to the presence of high amount of large pores in the structure. Bending strain values of the alloys containing Mg were slightly lower than Al4Cu alloy.

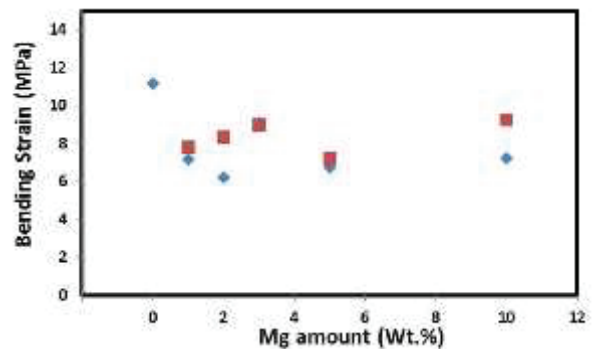


Fig. 8 Bending strain values of the Al-4Cu alloy containing 0, 1, 2, 3, 5 and 10 wt.% Mg.

Stress-strain curves of the the Al-4%Cu alloy and alloys containing 1, 2, 3, 5, 10 wt. % Mg are presented in Figures 9. These plots are obtained as a result of 3-point bending tests. It can be observed that Al4Cu alloy has a bending strength of 320 MPa. Bending strength values of the alloys can be seen to be higher in the alloys having Mg up to 5 wt.%. However, there is some loss of ductility in the alloys when Mg is present.

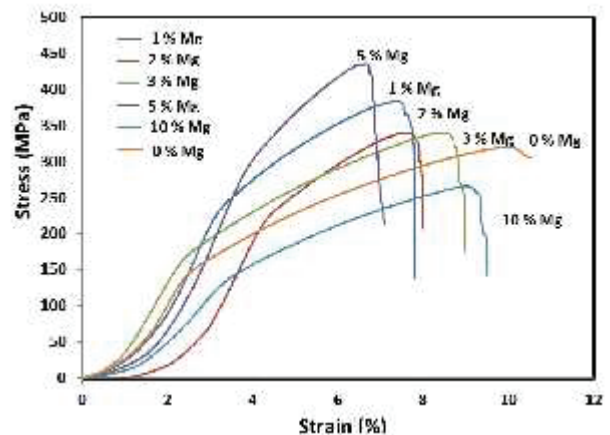


Fig. 9 Stress-strain plots of the Al-4Cu alloy containing 0, 1, 2, 3, 5 and 10 wt.% Mg.

#### IV. CONCLUSIONS

It was seen in optical microscopy examinations that there was small amount of porosity when Mg amount was in 1-3 wt. % range. However it was inferred from the microstructural examinations of the sintered samples having 5 and 10 wt% Mg that high amounts of Mg result in large pores in the structure. In addition, intermetallic compounds which are believed to be composed of Al, Cu and Mg were present in the structure of the sintered samples.

Hardness of the alloys increased with the addition of Mg. In addition, bending strength values were higher than Al4Cu when alloys contained Mg up to 5 wt.%. However, there was a slight decrease in bending strain of the alloys containing Mg, indicating some decrease in ductility.

#### ACKNOWLEDGMENT

Authors are grateful to Akdeniz University Scientific Research Projects Coordination Unit for their support.

#### REFERENCES

- [1] J. R. Davis, *Aluminum and Aluminum Alloys*, ASM International, USA, 1993.
- [2] M. C. Oh, B. Ahn, "Effect of Mg composition on sintering behaviors and mechanical properties of Al-Cu-Mg alloy", *Trans. Nonferrous Met. Soc. China*, vol. 24, pp. 53-58, 2014.
- [3] G. Xie, O. Ohashi, T. Sato, "Effect of Mg on the Sintering of Al-Mg Alloy Powders by Pulse Electric-Current Sintering Process", *Materials Transactions*, vol. 45, pp. 904-9009, 2004.
- [4] S. C. Wang and M. J. Starink, "Precipitates and intermetallic phases in precipitation hardening Al-Cu-Mg-(Li) based alloys", *International Materials Reviews*, vol. 50, pp. 193-215, 2005.

# Preparation of Al<sub>2</sub>O<sub>3</sub> Reinforced Aluminum Matrix Composites by Powder Metallurgy (ISLAC'18/UHAKS18)

H. Erdem Camurlu<sup>#,\*</sup>, Zeynep Tekyurt<sup>#</sup>

<sup>#</sup>Akdeniz University, Mechanical Engineering Department  
Dumlupınar Boulevard, Campus, Antalya, Turkey  
ecamurlu@akdeniz.edu.tr

**Abstract**— Aluminum is widely used as a matrix material in metal matrix composites, thanks to its lightweight and adequate mechanical properties. Utilization of aluminium is limited, due to its low hardness and low wear resistance. In order to improve these properties, reinforcements are introduced into aluminum generally in particulate form, forming metal matrix composites. Ceramic particles are mostly utilized as reinforcements, due to their high hardness.

In the present study, Al<sub>2</sub>O<sub>3</sub> particles were used as reinforcement in aluminum matrix. As a result, aluminum matrix composites having 0-20 vol.% Al<sub>2</sub>O<sub>3</sub> particles were obtained. Matrix alloy was aluminum having 4 wt.% Cu. Preparation of the composites via powder metallurgical routes consisted of mixing, pressing and sintering. After mixing Al<sub>2</sub>O<sub>3</sub>, aluminum and copper in powder form, pressing was performed in steel die set with 600 MPa pressure. Sintering of the pressed samples was conducted at 600 °C for 30 min in flowing nitrogen. Heating and cooling rates were about 6 °C/min.

Samples were cut, polished and were subjected to metallographic examinations with an optical microscope. Hardness tests were performed with a Brinell hardness tester. Three point bending tests were conducted with a universal mechanical tester having 50 kN capacity.

It was found by optical microscopy examinations that the Al<sub>2</sub>O<sub>3</sub> particles were homogeneously distributed in the aluminum matrix. Prepared composites had almost full density. Al<sub>2</sub>O<sub>3</sub> addition was seen to increase hardness of the obtained composites. Unreinforced Al-4%Cu alloy had a hardness of about 45 HB10 and the composite having 10 vol.% Al<sub>2</sub>O<sub>3</sub> presented a hardness value of 51 HB10. Three point bending strength was 335 MPa in the composite containing 20 vol.% Al<sub>2</sub>O<sub>3</sub>. Unreinforced sample presented higher bending strength values. Therefore, obtained composites provided an increase in the hardness values, whereas there was a reduction in the three point bending strength of the composite structures.

**Keywords**— Aluminum matrix composites, Al<sub>2</sub>O<sub>3</sub>, particulate reinforcement, powder metallurgy, sintering

## I. INTRODUCTION

Aluminum is widely used as a matrix material in metal matrix composites, as a result of its light weight and sufficient mechanical properties.

However, unreinforced aluminium has low hardness and low wear resistance, which make utilization aluminium difficult for many applications. In order to improve the hardness and wear resistance of aluminum, reinforcements are

introduced generally in particulate form, forming metal matrix composites. Ceramic particles are mostly utilized as reinforcements, due to their high hardness [1,2].

In aluminium matrix composites, matrix alloy is generally preferred as aluminum having 4 wt.% Cu. This matrix is selected since it provides liquid phase sintering, in addition to precipitation hardening.

Powder metallurgy was chosen for the preparation of Al<sub>2</sub>O<sub>3</sub> reinforced aluminum matrix composites. Powder metallurgy has the advantage of obtaining a homogenous distribution of the reinforcement particles in the metal matrix. In addition, metal matrix composites with a high range of reinforcement particle amount can be obtained by this method. Also, near net shapes can be obtained by powder metallurgy.

Liquid phase techniques such as stir casting were also employed in the literature for forming Al<sub>2</sub>O<sub>3</sub> reinforced aluminum matrix composites. In the study of Beygi, et al., nano and micron sized Al<sub>2</sub>O<sub>3</sub> particles were used as reinforcements in A386 aluminium cast alloy. There was a slight increase in tensile strength of the alloy when Al<sub>2</sub>O<sub>3</sub> micron sized particles were added [3]. Casting techniques have the disadvantages of resulting in inhomogeneous structure of the formed composite and insufficient wetting of the reinforcement particles [4].

In the present study, Al<sub>2</sub>O<sub>3</sub> particles were used as reinforcement in aluminum matrix. As a result, aluminum matrix composites having 0-20 vol. % Al<sub>2</sub>O<sub>3</sub> particles were obtained.

## II. MATERIALS AND METHODS

Preparation of the composites via powder metallurgical routes consisted of mixing, pressing and sintering. After mixing Al<sub>2</sub>O<sub>3</sub> (Merck), aluminium (Merck) and copper (Alfa Aesar) in powder form, pressing was performed in steel die set with 600 MPa pressure.

Sintering of the pressed samples was conducted at 600 °C for 30 min in flowing nitrogen. Heating and cooling rates were about 6 °C/min.

After preparation, the samples were cut, ground on emery paper (Metkon), polished and they were subjected to metallographic examinations with an optical microscope (Nikon Eclipse LV150).

Hardness tests were performed with a Brinell hardness tester (Bulut Makina). Three point bending tests were

conducted with a universal mechanical tester having 50 kN capacity (Shimadzu AG-IC).

### III. RESULTS AND DISCUSSION

#### A. Microstructural Examinations

Unreinforced Al-4%Cu alloy samples and composite samples containing Al-4%Cu matrix alloy and 5, 10 and 20 vol. %  $\text{Al}_2\text{O}_3$  were produced. Microstructure of the unreinforced Al-4%Cu alloy is presented in Figure 1. It can be seen that the microstructure is clean. In higher magnifications, intermetallic  $\text{Al}_2\text{Cu}$  phase, in the shape of rod-like particles on the grain boundaries of the aluminium grains could be observed, during the optical microscopy examinations.



Fig. 1 Microstructure of the Al-4%Cu matrix alloy, after sintering at 600 °C.

Microstructures of the composites containing 5, 10 and 20 vol. %  $\text{Al}_2\text{O}_3$  are presented in Figure 2 – Figure 4. The dark particles observed in these micrographs are  $\text{Al}_2\text{O}_3$  particles. The light, continuous structure is the Al-4%Cu matrix alloy. It can be seen that  $\text{Al}_2\text{O}_3$  particles are homogeneously distributed in the microstructure of the composites. This can be counted as an advantage of the employed powder metallurgy technique. The sizes of the  $\text{Al}_2\text{O}_3$  particles were mostly 20-25 microns. However, there were some particles smaller than 20 microns.



Fig. 2 Microstructure of the composite sample containing 5 vol. %  $\text{Al}_2\text{O}_3$ , after sintering at 600 °C.

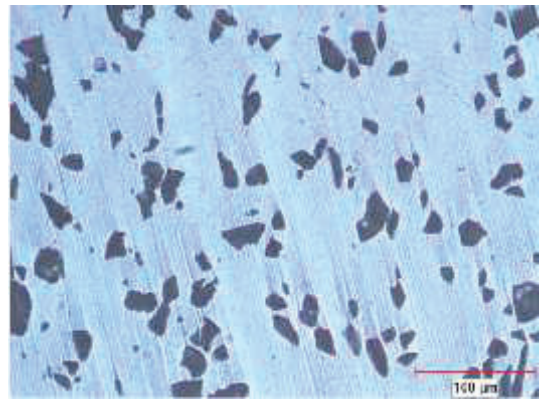


Fig. 3 Microstructure of the composite sample containing 10 vol. %  $\text{Al}_2\text{O}_3$ , after sintering at 600 °C.

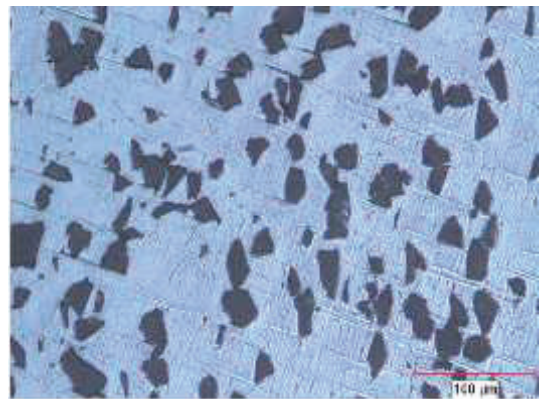


Fig. 4 Microstructure of the composite sample containing 20 vol. %  $\text{Al}_2\text{O}_3$ , after sintering at 600 °C.

#### B. Mechanical Properties

Unreinforced Al-4%Cu matrix alloy and composites containing 5, 10 and 20 vol. %  $\text{Al}_2\text{O}_3$  were subjected to mechanical tests, such as hardness test and 3 point bending test.

Results of the hardness measurements are presented in Figure 5. The hardness value of the unreinforced Al-4%Cu alloy was about 45 HB10. It can be seen that, hardness of the composites increased with the addition of  $\text{Al}_2\text{O}_3$ , until 10 %  $\text{Al}_2\text{O}_3$  addition. The highest attained hardness value was about 51 HB10.

The increase in the hardness of the composites can be attributed to the restraint of the matrix due to the presence of the  $\text{Al}_2\text{O}_3$  particles.  $\text{Al}_2\text{O}_3$  particles render the Al-4%Cu matrix harder to deform plastically.

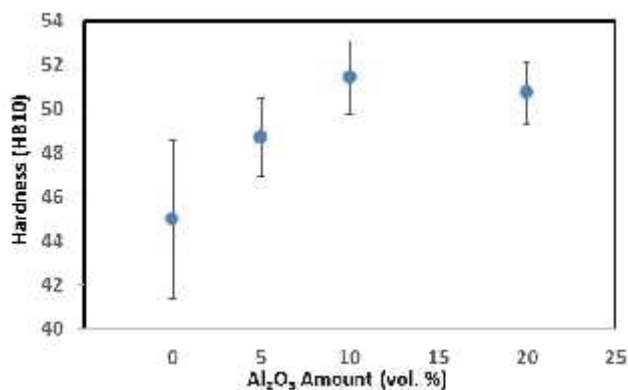


Fig. 5 Hardness values of the unreinforced Al-4Cu matrix alloy and composite samples reinforced with 5, 10 and 20 vol. % Al<sub>2</sub>O<sub>3</sub> particles.

Stress-strain curves (3 point bending) of the unreinforced Al-4%Cu alloy and composite samples containing 5, 10 and 20 vol. % Al<sub>2</sub>O<sub>3</sub> are presented in Figure 6. Three point bending strength was 335 MPa in the composite containing 20 vol.% Al<sub>2</sub>O<sub>3</sub>. Unreinforced sample presented higher bending strength values. This can be attributed to the weak interface between the aluminium matrix and Al<sub>2</sub>O<sub>3</sub> particles.

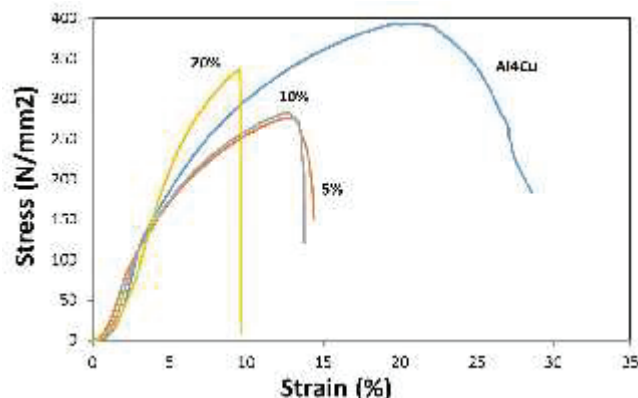


Fig. 6 Stress-strain plots of the unreinforced Al-4Cu matrix alloy and composite samples reinforced with 5, 10 and 20 vol. % Al<sub>2</sub>O<sub>3</sub> particles.

#### IV. CONCLUSIONS

Obtained Al<sub>2</sub>O<sub>3</sub> reinforced Al-4%Cu matrix composites provided an increase in the hardness values, whereas there was a reduction in the three point bending strength of the composite structures. Al<sub>2</sub>O<sub>3</sub> reinforcement is believed to enhance wear resistance of the base Al-4%Cu alloy.

#### ACKNOWLEDGMENT

Authors are grateful to Akdeniz University Scientific Research Projects Coordination Unit for their support.

#### REFERENCES

- [1] O. Yılmaz, S. Buytoz, "Abrasive wear of Al<sub>2</sub>O<sub>3</sub>-reinforced aluminium-based MMCs", *Composites Science and Technology*, vol. 61, pp. 2381–2392, 2001.
- [2] J. R. Davis, *Aluminum and Aluminum Alloys*, ASM International, USA, 1993.
- [3] H. Beygi, S.A.Sajjadi, S.M.Zebarjad, "Microstructural analysis and mechanical characterization of aluminum matrix nanocomposites reinforced with uncoated and Cu-coated alumina", *Materials Science & Engineering*, vol. A607, pp. 81–88, 2014.
- [4] H. Su, W. Gao, Z. Feng, Z. Lu, "Processing, microstructure and tensile properties of nano-sized Al<sub>2</sub>O<sub>3</sub> particle reinforced aluminum matrix composites", *Materials and Design*, vol. 36, pp. 590–596, 2012.

# Electrical Conductivity and Microstructure Properties of Cu-Mo Coatings (ISLAC'18/UHAKS18)

Serkan Islak<sup>1\*</sup>, Uğur Çaligülü<sup>2</sup>, Husain R.H. Hraam<sup>3</sup>, Cihan Özorak<sup>4</sup>, Vahdettin Koç<sup>5</sup>

<sup>1</sup> Department of Mechanical Engineering, Kastamonu University, Kastamonu, 37150, Turkey, serkan@kastamonu.edu.tr

<sup>2</sup> Department of Metallurgical and Materials Engineering, Firat University, Elazığ, 23000, Turkey, ucaligulu@firat.edu.tr

<sup>3</sup> Institute of Science, Kastamonu University, Kastamonu, 37150, Turkey, hraam.hrh@gmail.com

<sup>4</sup> Department of Metallurgical and Materials Engineering, Kastamonu University, Kastamonu, 37150, Turkey, ozorak@kastamonu.edu.tr

<sup>5</sup> Technical Sciences Vocational High School, Adiyaman University, Adiyaman, 02100, Turkey, vkoc@adiyaman.edu.tr

**Abstract**— In this study, Cu–Mo composite coatings were produced on copper substrate by plasma spray technique. Electrical conductivity and microstructure properties of the composite coatings were investigated. Microstructure and phase composition of the coatings were examined by using optical microscopy (OM), scanning electron microscope (SEM), X-ray diffraction (XRD), and energy-dispersive X-ray spectroscopy (EDS). The microhardness experiments were also performed by using a microhardness machine. The electrical conductivity properties of the coatings were evaluated with eddy current instruments. Although the electrical conductivities of the coatings are very small compared to the substrate, it has been determined that the coatings exhibit a very good hardness values in comparison to the substrate.

**Keywords**— Cu-Mo coatings; electrical conductivity; microstructure

## I. INTRODUCTION

The reason for the copper to remain as the most important engineering materials every day is; high corrosion resistance, excellent electrical and thermal conductivity, attractive appearance, high ductility and ease of forming. Pure copper is widely used in the transmission of electric current in places related to cables, wires, electrical contacts and other electrical works. Copper and some alloys are used in automotive radiators, heat exchangers, home heating systems, panels for solar energy absorption, and applications where heat is required to quickly transfer from one point of metal to another [1]. Despite the high electrical, thermal conductivity and good corrosion resistance of copper, properties such as low hardness, yield strength, creep resistance and low wear resistance limit the use of copper. Because pure copper recrystallizes at temperatures close to 500 °C, even if hardened by cold forming, and therefore quickly loses its strength. A lot of work has been done in the literature to come from above. Most of the researchers have focused on the production of ceramic reinforced copper matrix composites. In the literature, Al<sub>2</sub>O<sub>3</sub>, SiC, TiB<sub>2</sub>, TiC, B<sub>4</sub>C and WC particles are usually added to the Cu matrix [2-6]. In these previous studies, pore formation reveals the negative side of the studies. As is known, pore formation adversely affects the mechanical

properties as well as the electrical conductivity properties. Junjie et al. [7] studied the hardness and electrical conductivity of Cu-matrix nanocomposites reinforced with in-situ TiC fabricated using long-term ball milling and hot pressing. It has been detected that as the ball milling time increased, the hardness and electrical conductivity increased. Chenchen et al. [8] reported that microstructures, mechanical and electrical properties of ZrB<sub>2</sub> microparticles reinforced Cu composites prepared by hot-pressed sintering. The results indicated that the relative density and electrical conductivity of the composites decrease with increasing ZrB<sub>2</sub> content. Huanchao et al. [9] added a new generation of graphite into the copper. The Gr/Cu composites were produced by using ball milling and cold compacting sintering process. The mechanical and physicochemical properties including hardness, relative density, conductivity and oxidation resistance were tested. The relative density, hardness, oxidation weight gain and IACS of the materials obtained by the optimum process parameters were 90.0%, 53.4HB, 1.6 mg cm<sup>-2</sup> and 76.2%, respectively.

In this study, we tried to improve the hardness properties without compromising the electrical conductivity of the copper material too much. For this purpose, a Cu + Mo coating layer with different ratios was produced on copper substrate using plasma spraying method. Molybdenum is a typical refractory metal with body-centered cubic (BCC) lattice structure. The high melting point (2610 °C) is characterized by low thermal expansion coefficient and high thermal/electrical conductivity [10]. In the literature, the use of Mo in copper alloys is very limited, and coating production is not available. Plasma spraying is effectively and economically applied to various machine parts to reduce surface defects [11]. In this method, the complete or partial melting of the powders varies depending on their thermal properties. The controllability of the system at extremely high heating and cooling rates makes it possible to produce coatings made of metallic, non-metallic and ceramics and combinations with this method [12].

## II. MATERIALS AND METHODS

Pure copper plates at 20 mm x 60 mm x 5 mm and 99.9% purity were selected as the substrate. Cu and Mo powders with

-90+45  $\mu\text{m}$  and -75+45  $\mu\text{m}$  grain sizes respectively were coated on the substrate using plasma spray method. Mo was added to Cu in proportions of 10, 25 and 50% by weight. In the production of the coating layers, a Sulzer Metco F4-MB model plasma spray coating system with a power of 55 kW was used. The principle scheme of the plasma spray coating process is shown in Fig. 1. The production parameters of the coatings are summarized in Table 1. The flow rate of the argon gas used to produce the plasma beam was set at 35 l / min in all coatings. Spraying was made at a distance of 80 mm. The coating powders are injected externally into the gun. The injected powders are oriented parallel to the plasma flow. The coating powder feed rate was set to 50 g/min, the H<sub>2</sub> gas flow rate to 10 l/min and the carrier gas rate to 3 l/min.

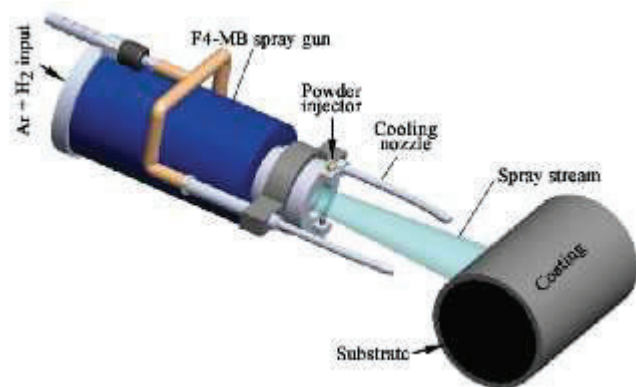


Figure 1. Sulzer Metco F4-MB model plasma spray coating system

Table 1: Production parameters

Parameters	
Gun type	Sulzer-Metco F4
Current (A)	580
Volt (V)	60-65
Ar gas flow (l/min)	35
H <sub>2</sub> gas flow (l/min)	10
Spray distance (mm)	80
The amount of powder feed (g/min)	50
Carrier gas (Ar) flow (l/min)	3.0

The microstructure and phase formation properties of the coatings were determined by SEM-EDS and XRD analyses. The hardness was measured under a load of 300 grams with a microhardness device and at a waiting time of 15 seconds by using SHIMADZU HVM-G21 model microhardness machine. The electrical conductivities of coatings (Cu-Mo) and substrate (Cu) were measured according to ASTM E1004-02 standard with eddy current principle.

### III. RESULTS AND DISCUSSION

Fig. 2 illustrates optical images of coatings. The thickness of the interlayer coating is 300  $\mu\text{m}$ . It is seen that the coating layers are homogeneous. As the Mo content increased, the porosity increased. The bond between the coating and the substrate is compatible. There is a covering layer in the appearance of a

laminated structure. In all coatings, a lamellar microstructure is observed, which is well known in thermal spray coatings and is formed by molten metal droplets impacting the substrate and continuously wetting it [13, 14]. The lamellar structure occurs in the form of impingement of molten particles on the substrate, deformation, and solidification. [15]. According to Kuroda and Kobayashi [16] the lamella is formed parallel to the substrate and the middle part of the lamella is thick and the thickness is decreased towards the end parts.

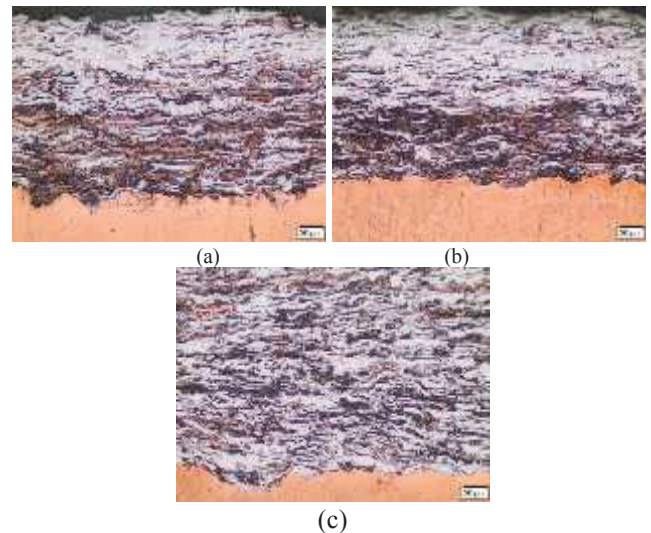


Figure 2. (a) Cu-10 Mo coating (b) Cu-25 Mo coating, (c) Cu-50 Mo coating.

The EDS analysis of the Cu-50% Mo coating produced by the plasma spray method on the Cu substrate is given in Fig. 3. The chemical compositions of different lamellae are formed in the coating. When the area from the coating layer EDS is examined, it is seen that the coating represents the Cu-50 wt.% Mo content. The MAP analysis of Fig. 4 shows that all three coatings with relatively homogeneous distribution of the elements present in the coating layer. The distribution of the elements in the coating affects the electrical conductivity and mechanical properties.

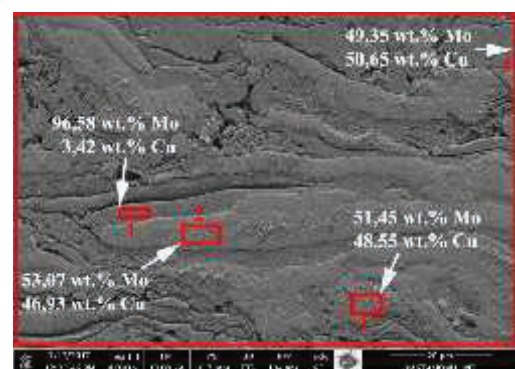


Figure 3. EDS analysis of Cu-50% Mo coating

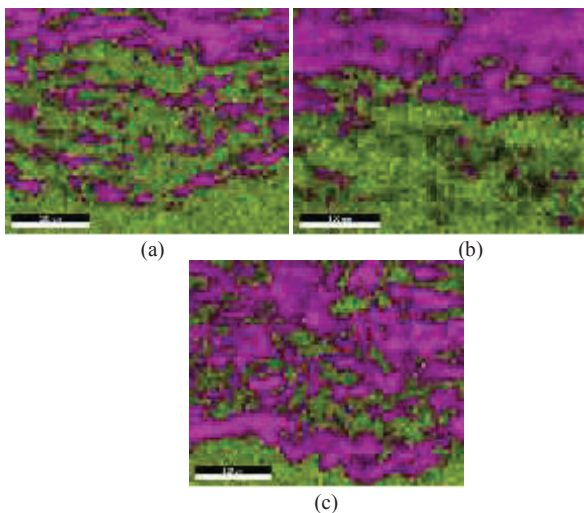


Figure 4. SEM-MAP analyses of coatings; (a) Cu-10 Mo coating (b) Cu-25 Mo coating, (c) Cu-50 Mo coating.

Fig. 5 illustrates the XRD graphic of Cu-Mo composite coatings which are produced with plasma spray. Cu and Mo phases are present in the coating layers. No oxide formation has occurred in the coatings and substrate. No phase formation occurred between Cu and Mo. According to the Cu-Mo phase diagram, this is normal. Because the Cu-Mo phase diagram is a monotectic diagram [17]. The result is that Cu-Mo coatings are mechanical mixtures of the refractory metal Mo and Cu with a face-centered cubic structure.

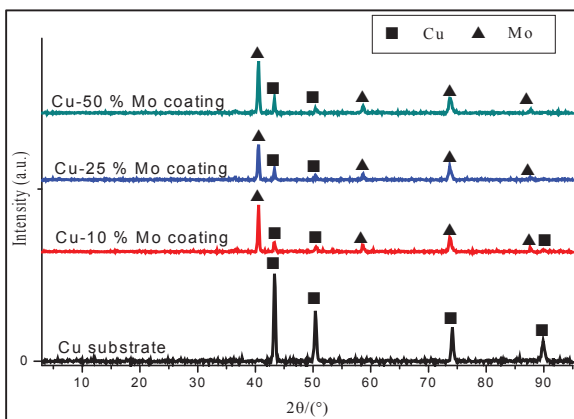


Figure 5. XRD graphic of Cu-Mo composite coatings

The hardness graph of the coatings is given in Fig. 6a. Six hardness measurements were taken from each sample. Averages of hardness were taken and evaluated. The hardness was increased by coating with Cu substrate (56-91%). As the addition of Mo increases, the hardness of the coatings increases. This is due to the natural hardness of Mo. The electrical conductivity graph of the coatings is given in Fig. 6b. With the increase of molybdenum, the electrical conductivities of the coatings decreased. This is due to the fact that the electrical conductivity of Mo is lower than that of Cu and the porosity is increased by the addition of Mo.

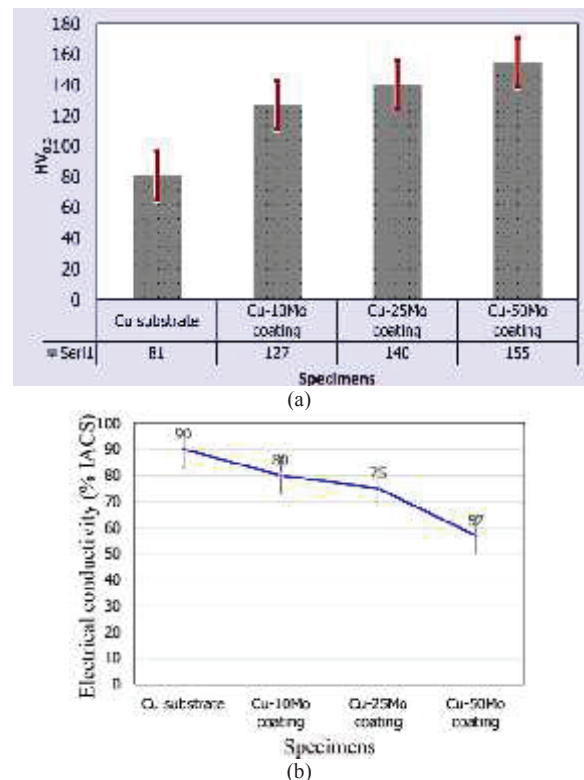


Figure 6. (a) Hardness graph and (b) Electrical conductivity graph

Coating of Cu substrate with Cu-Mo powder mixture resulted in a significant increase in the hardness. The electrical conductivity of the Cu substrate is measured as 90% IACS, while the electrical conductivities of the coatings are in the range of 57-80% IACS. These coatings can be used in areas where the electrical conductivity value is not too high than 57-80% IACS and the hardness is high.

#### IV. CONCLUSIONS

- ❖ Coating of Cu substrate with Cu-Mo powder mixture resulted in a significant increase in the hardness.
- ❖ The electrical conductivity of the Cu substrate is measured as 90% IACS, while the electrical conductivities of the coatings are in the range of 57-80% IACS.
- ❖ Although the electrical conductivities of the coatings are very small compared to the substrate, it has been determined that the coatings exhibit a very good hardness values in comparison to the substrate.
- ❖ These coatings can be used in areas where the electrical conductivity value is not too high than 57-80% IACS and the hardness is high.

#### REFERENCES

- [1] F. Akhtar, S. J. Askari, K. A. X, Shah, Du, S. Guo, *Microstructure, mechanical properties, electrical conductivity and wear behaviour of high volume TiC reinforced Cu-matrix composites*. Materials Characterization, 60: 327-336, 2009.
- [2] S. B. Chandrasekhar, S. Sudhakara Sarma, M. Ramakrishna, P. Suresh Babu, T. N. Rao, B. P. Kashyap, *Microstructure and properties of hot*

- extruded Cu–1wt% Al<sub>2</sub>O<sub>3</sub> nano-composites synthesized by various techniques. *Materials Science and Engineering: A*, 591: 46-53, 2014.
- [3] D. Božić, J. Stašić, J. Ružić, M. Vilotijević, V. Rajković, *Synthesis and properties of a Cu–Ti–TiB<sub>2</sub> composite hardened by multiple mechanisms*. *Materials Science and Engineering: A*, 528: 8139-8144, 2011.
- [4] M. R. Akbarpour, E. Salahi, F. Alikhani Hesari, A. Simchi, H. S. Kim, *Microstructure and compressibility of SiC nanoparticles reinforced Cu nanocomposite powders processed by high energy mechanical milling*. *Ceramics International*, 40: 951-960, 2014.
- [5] S. Islak, D. Kır, and S. Buytoz, *Effect of sintering temperature on electrical and microstructure properties of hot pressed cu-tic composites*. *Science of Sintering*, 46: 15-21, 2014.
- [6] T. Yener, I. Altinsoy, S. C. Yener, G. C. Efe, I. Ozbek, C. Bindal, *An Evaluation of Cu-B<sub>4</sub>C Composites Manufactured by Powder Metallurgy*. *Acta Physica Polonica A*, 127(4): 1045-104, 2015.
- [7] Junjie Ni, Jian Li, Wei Luo, Qi Han, Yibin Yin, Zhengfeng Jia, Baoxu Huang, Chengchao Hu, Zelu Xu, *Microstructure and properties of in-situ TiC reinforced copper nanocomposites fabricated via long-term ball milling and hot pressing*. *Journal of Alloys and Compounds*, Volume 755, Pages 24-28, 2018.
- [8] W. Chenchen, L. Huaijun, Z. Zhiguo, L. Wei *Fabrication, interfacial characteristics and strengthening mechanisms of ZrB<sub>2</sub> microparticles reinforced Cu composites prepared by hot-pressed sintering*. *Journal of Alloys and Compounds*, 748: 546-552, 2018.
- [9] L. Huanchao, T. Xinying, W. Weibing, W. Xiangwei, L. Jinfeng, G. Haoran, *Effect of graphene addition on properties of Cu-based composites for electrical contacts*. *Materials Research Express*, 4(6): 66506, 2017.
- [10] B. V. Cockerman, *Measuring the fracture toughness of molybdenum–0.5 pct titanium–0.1 pct zirconium and oxide dispersion-strengthened molybdenum alloys using standard and subsized bend specimens*. *Metallurgical and Materials Transactions A*, 33A: 3685–707, 2002.
- [11] E. P. Song, J. Ahn, S. Lee, N. J. Kim, *Effects of critical plasma spray parameter and spray distance on wear resistance of Al<sub>2</sub>O<sub>3</sub>-8 wt.%TiO<sub>2</sub> coatings plasma-sprayed with nanopowders*. *Surface and Coatings Technology*, 202: 3625-3632, 2008.
- [12] A. Datye, S. Koneti, G. Gomes, K. H. Wu, H. T. Lin, *Synthesis and characterization of aluminum oxide-boron carbide coatings by air plasma spraying*. *Ceramics International*, 36: 1517-1522, 2010.
- [13] C. J. Li, G. J. Yang, A. Ohmori, *Relationship between particle erosion and lamellar microstructure for plasma-sprayed alumina coatings*. *Wear*, 260: 1166-1172, 2006.
- [14] C. H. Lee, H. K. Kim, H. S. Choi, H. S. Ahn, *Phase transformation and bond coat oxidation behavior of plasma-sprayed zirconia thermal barrier coating*. *Surface and Coatings Technology*, 124:1-12, 2000.
- [15] V. Fervel, B. Normand, C. Coddet, *Tribological behavior of plasma sprayed Al<sub>2</sub>O<sub>3</sub>-based cermet coatings*. *Wear*, 230:70-77, 1999.
- [16] T. Kuroda, A. Kobayashi, *Adhesion characteristics of zirconia-alumina composite coatings by gas tunnel type plasma spraying*. *Vacuum*, 73:635-641, 2004.
- [17] P. R. Subramanian, D. E. Laughlin, *The Cu-Mo (Copper-Molybdenum) system*. *Bulletin of Alloy Phase Diagrams*, 11(2): 169-172, 1990.

# Investigation of Microstructure and Biocompatibility Properties of Ceramic Based Coatings Produced by Plasma Spray Method (ISLAC'18/UHAKS18)

Serkan Islak<sup>1\*</sup>, Nuray Emin<sup>2</sup>, Cihan Özorak<sup>3</sup>, Husain R.H. Hraam<sup>4</sup>

<sup>1</sup>Department of Mechanical Engineering, Kastamonu University, Kastamonu, 37150, Turkey, serkan@kastamonu.edu.tr

<sup>2</sup>Department of Biomedical Engineering, Kastamonu University, Kastamonu, 37150, Turkey, nurayemin@kastamonu.edu.tr

<sup>3</sup>Department of Metallurgical and Materials Engineering, Kastamonu University, Kastamonu, 37150, Turkey, ozorak@kastamonu.edu.tr

<sup>4</sup>Institute of Science, Kastamonu University, Kastamonu, 37150, Turkey, hraam.hrh@gmail.com

**Abstract**— After the implantation of a biomaterial, it is exposed to mechanical loads and body fluids continuously or periodically according to the implantation area. Hence, the most important expectancy of biomaterials is to be biocompatible; not to cause a reaction or impede natural growth of the tissue, bone and organ. Ceramic materials with excellent mechanical, corrosion and abrasion resistance is set in terms of features such as biomaterials. In this study, ceramic coatings were produced on AISI 316L stainless steel by the plasma spray method. It was aimed to investigate microstructure and biocompatibility properties of coatings. Scanning electron microscope (SEM) analysis and X-ray diffraction (XRD) phase analysis were used to determine the microstructure and phase composition properties. The biocompatibility properties of coatings have been tried to be determined by analyzing cytotoxicity and viability.

**Keywords**— Ceramic coatings, biocompatibility, microstructure

## I. INTRODUCTION

Biomaterials are natural or synthetically obtainable materials which are used for prosthetic, diagnostic or therapeutic purposes and which are in contact with tissue, blood and other body fluids within the body [1, 2]. The performances of the materials used in the body are important. The performances of the materials placed inside the body can be examined from different angles. Depending on the area in which the problem is to be solved, a classification can be made at the tissue-organ level or according to the materials used [3]. Biomaterials can be used for a long time or for a short time. The most basic feature that implants should provide is that they are not allergenic or toxic. In addition, biomaterials, designs and mechanical behaviour are important qualities. Ceramics are usually blends of metals formed by non-metallic elements. The interatomic bond is ionic or covalent. Ceramic materials have been used as medical materials for many years despite their fragility, porous structure, low tensile strength and low impact strength. With the recent development of new methods, ceramics are used in many different fields of biomolecules. Thus, ceramics and composites have begun to be applied as biomaterials instead of bone in the body. Ceramic materials

used as implants are preferred in medical applications due to their inertness to body fluids and the advantages of high compression strengths. Some carbon-based ceramics are used as heart valves because they do not interfere with blood fluid. The characteristics of bioceramics are: they are not toxic, biocompatible and have no allergic effects [4, 5].

Plasma spraying method is spraying of powder on the surface of the material to be coated at a plasma temperature which is ionized and can reach up to 15.000 °C-25.000 °C, while the diatomic gases (argon-hydrogen mixture) passing between a tungsten (cathode (-)) and a copper nozzle [6-8]. Plasma spraying is effectively and economically applied to various machine parts to reduce surface defects [9]. In this method, the complete or partial melting of the powders varies depending on their thermal properties. The controllability of the system at extremely high heating and cooling rates makes it possible to produce coatings made of metallic, non-metallic and ceramics and combinations with this method [10]. Ceramic (especially oxide based) powders are used more frequently than metallic powders in the plasma spray method due to their high chemical stability at high temperatures, excellent wear resistance and corrosion resistance [11]. Ceramic materials with high resistance to corrosive and thermal conditions, relatively low density and high hardness are preferred over polymeric and metallic materials due to their existing properties. Ceramic materials such as aluminum oxide, zirconium oxide, titanium oxide, chromium oxide, silicon oxide and yttrium oxide are widely used as surface coating materials to improve wear, erosion, cavitation and corrosion resistance of materials. Such materials are particularly needed in applications where resistance to wear and corrosion is desired [12, 13].

In this study, Al<sub>2</sub>O<sub>3</sub>, Al<sub>2</sub>O<sub>3</sub> - 40% TiO<sub>2</sub>, ZrO<sub>2</sub> - 8% Y<sub>2</sub>O<sub>3</sub> and Cr<sub>2</sub>O<sub>3</sub> - 40% TiO<sub>2</sub> oxide coatings were produced by plasma spraying on AISI 316L stainless steel surface. Microstructure and biocompatibility properties were experimentally investigated. Microstructure, microhardness and phase properties were determined by scanning electron microscopy (SEM), energy dispersive spectrometry (EDS) and X-ray

diffractogram (XRD) analyzes. The microhardness change was measured from the top of the coating layer. The biocompatibility properties of coatings have been tried to be determined by cytotoxicity and viability analysis.

## II. MATERIALS AND METHODS

AISI 316L stainless steel was used as substrate and  $\text{Al}_2\text{O}_3$ ,  $\text{Al}_2\text{O}_3$  - 40%  $\text{TiO}_2$ ,  $\text{ZrO}_2$  - 8%  $\text{Y}_2\text{O}_3$  and  $\text{Cr}_2\text{O}_3$  - 40%  $\text{TiO}_2$  were used as coating powders. A Sulzer Metco 9MB atmospheric plasma spray coating system with 80 kVA of power was used to produce the coating layer. For metallographic investigations, the samples were sanded by passing through coarse and fine sanding steps, respectively. The sanded samples were polished using diamond solutions and etched using a solution of  $\text{HNO}_3$  (40 pct.) +  $\text{C}_2\text{H}_5\text{OH}$  (60 pct.). SEM-EDS analyzes were performed to determine the chemical composition of the microstructure. X-ray analysis was carried out to determine the phases formed in the microstructure.

The hardness measurement was made with SHIMADZU HMV-G21 brand microhardness device with a waiting period of 15 sec and a load of 200 gr. The biocompatibility properties of coatings have been tried to be determined by cytotoxicity and viability analysis. Cytotoxicity tests of the prepared materials were performed by in vitro tests based on cell viability. MTT [3- (4,5-dimethylthiazol-2-yl) -2,5-diphenyl tetrazolium bromide] test, based on measuring cell viability and mitochondrial dehydrogenase activity, was used in cytotoxicity assays.

## III. RESULTS AND DISCUSSION

Microstructure images of ceramic-based coatings produced by plasma spray method are shown in Fig. 1. The coating layer is connected to the bottom material as compatible. This is a positive result of the strength of the coatings against mechanical forces. The porosity in the coating layers came to fruition. Although this is negative for mechanical properties, it is considered to be favourable in terms of biocompatibility. Pore formation is inevitable in studies carried out in the literature. Fig. 2 shows the XRD analyzes of the coatings. Phases seen in coatings represent powders before coating. Besides this, it is formed in ternary phases and binary phases.

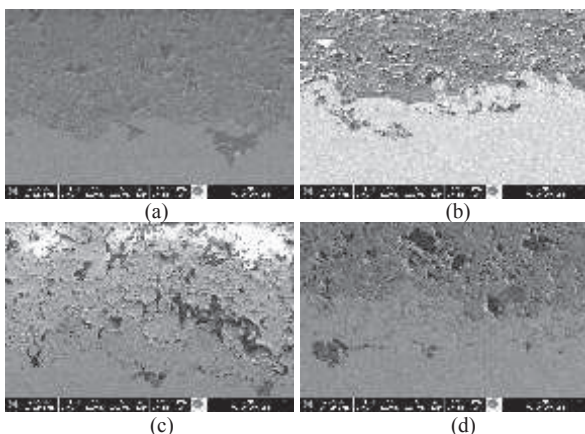


Figure 1. (a)  $\text{Al}_2\text{O}_3$  (b)  $\text{Al}_2\text{O}_3$  - 40%  $\text{TiO}_2$ , (c)  $\text{ZrO}_2$  - 8%  $\text{Y}_2\text{O}_3$  and (d)  $\text{Cr}_2\text{O}_3$  - 40%  $\text{TiO}_2$ .

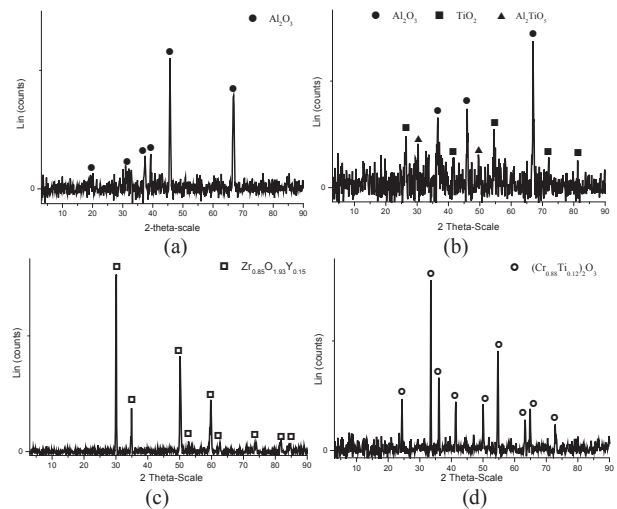


Figure 2. XRD analyzes: (a)  $\text{Al}_2\text{O}_3$  (b)  $\text{Al}_2\text{O}_3$  - 40%  $\text{TiO}_2$ , (c)  $\text{ZrO}_2$  - 8%  $\text{Y}_2\text{O}_3$  and (d)  $\text{Cr}_2\text{O}_3$  - 40%  $\text{TiO}_2$ .

In Figure 3, the microhardness values of the substrate and coating layers are given. The coating was also taken from six different regions from the layers and taken from the upper surface of the coatings. Evaluation was made by taking the average of the values received. While the hardness of the bottom layer is 215  $\text{HV}_{0.2}$ , the hardness values of the coating layers are 905  $\text{HV}_{0.2}$ , 760  $\text{HV}_{0.2}$ , 950  $\text{HV}_{0.2}$  and 1215  $\text{HV}_{0.2}$ , respectively, which are 3.5-5.6 times higher than the lower layer. These increases in hardness are due to the natural hardness of the ceramic materials. During this hardness measurement, no cracks were formed in the ceramic coatings.



Figure 3. Microhardness values of the substrate and coating layers

Mitochondrial activities and viability of the proliferating cells were followed by MTT assay. For this test, a 6-well petri dish was used depending on the size of the samples. 4.5 ml of freshly prepared medium was added to Petrin's wells and 0.5 ml MTT kit was added to provide 10% concentration. Each well was placed in a carbondioxide incubator for 4 hours with samples placed. However, one of the wells was not used as an example and the mediocre was used as blind. At the end of the incubation, the formation of formazan crystals was examined in the inverted microscope. Subsequently, the dark blue formazan crystals were dissolved in MTT solvent and the color intensity was measured at 570 nm on a UV-spectrophotometer. The MTT tests applied to the cultures were repeated three times and the mean values of three different measurements were taken and plotted against the days (Fig. 4). In general, it was

observed that cell viability did not change much in all ceramic coatings and the highest absorbance value was obtained on the 7th day. In addition, although it is clear that biocompatibility due to cell viability shows similar values for all coatings, the most compatible and consistent results in terms of cytotoxicity were obtained in the coating of aluminum oxide-titania. According to quantitative analyzes, the cell viability of the alloy with Zirconium oxide coating was generally preserved in the cell culture lasting 14 days and decreased by 35% on the 14th day. In chromium oxide titanium oxide coating, this change was calculated to be 31%, 24% for aluminum oxide-titanium oxide coating, and 13% for aluminum oxide coating.

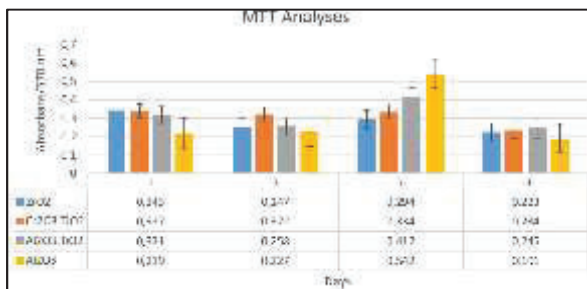


Figure 4. Change of absorbance values measured at 570 nm wavelength of ceramic coatings according to culture time.

The formazan crystals formed by the action of the MTT reagent are shown in Fig. 5. It has been observed that formazan crystals are formed on the surface of composite structures and in micropores. Besides, formazan crystals were formed in the vicinity of the flooders from weakly bonded cells on the material.

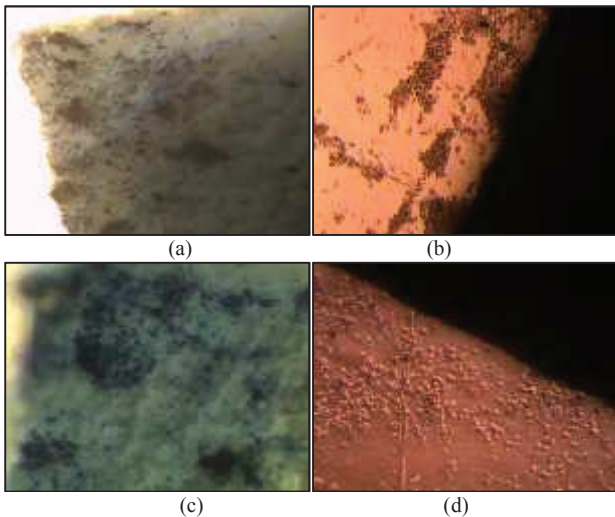


Figure 5. Formation of formazan crystals as a result of MTT analysis: (a) Al<sub>2</sub>O<sub>3</sub>, (b) Al<sub>2</sub>O<sub>3</sub>-40% TiO<sub>2</sub>, (c) ZrO<sub>2</sub>-8% Y<sub>2</sub>O<sub>3</sub> and (d) Cr<sub>2</sub>O<sub>3</sub>-40% TiO<sub>2</sub>.

#### IV. CONCLUSIONS

According to SEM studies, the coating layers are connected to the substrate in accordance. This is a positive result of the strength of the coatings against mechanical forces. The elements in the coatings are homogeneously distributed. From the XRD analysis it is understood that the phases in the coatings represent the powders before coating. Besides this, it is formed in triple phases in addition to binary phases. The hardness of the coatings varied between 760-1215 HV<sub>0.2</sub> and there was a 3.5-5.6-fold increase compared to the substrate. Although it is clear that biocompatibility depends on cell viability, similar results are obtained in all coatings, but the most compatible and consistent results in terms of cytotoxicity were obtained with aluminum oxide-titanium oxide coating.

#### ACKNOWLEDGMENT

The paper was financially supported by Kastamonu University Scientific Research Projects Unit (project number KÜBAP 01/2016-16)

#### REFERENCES

- [1] J. Y. Wong, J. D. Bronzino, *Biomaterials*, CRC Press, Taylor&Francis Group, LLC, 2007.
- [2] D. F. Williams, *Williams dictionary of biomaterials*, Liverpool University Press 1999
- [3] G. Lutišanová, E. Kuzielová, M. T. Palou, J. Kozánková, *Static and Dynamic In Vitro Test of Bioactivity of Glass Ceramics*, *Ceramics – Silikáty*, 55(2): 106-113, 2011.
- [4] H. Demirkıran, *Biyocam Takviyeli Hidroksiapatit Kompozitlerinin Geliştirilmesi*, MSc. Thesis, İTÜ Fen Bilimleri Enstitüsü, İstanbul. (2003).
- [5] K. Y. Lee, et al., *Ceramic Bioactivity: Progresses, Challenges and Perspectives*, *Biomedical Materials*, 1: R31–R37, 2006.
- [6] R. B. Heimann, *Plasma-spray coating*, VCH, New York, 1996.
- [7] L. Pawlowski, *The science and engineering of thermal spray coatings*, John Wiley & Sons, Ltd., England. 2008.
- [8] D. I. Pantelis, P. Psyllaki, N. Alexopoulos, *Tribological behaviour of plasma-sprayed Al<sub>2</sub>O<sub>3</sub> coatings under severe wear conditions*. *Wear*, 237: 197-204, 2000.
- [9] E. P. Song, J. Ahn, S. Lee, N. J. Kim, *Effects of critical plasma spray parameter and spray distance on wear resistance of Al<sub>2</sub>O<sub>3</sub>-8 wt.%TiO<sub>2</sub> coatings plasma-sprayed with nanopowders*. *Surface and Coatings Technology*, 202: 3625-3632, 2008.
- [10] A. Datye, S. Koneti, G. Gomes, K. H. Wu, H. T. Lin, *Synthesis and characterization of aluminum oxide-boron carbide coatings by air plasma spraying*. *Ceramics International*, 36: 1517-1522, 2010.
- [11] Y. Wang, S. Jiang, M. Wang, S. Wang, T. D. Xiao, P. R. Strutt, *Abrasive wear characteristic of plasma sprayed nanostructured alumina/titania coatings*. *Wear*, 237: 176–185, 2000.
- [12] Y. Sun, B. Li, D. Yang, T. Wang, Y. Sasaki, K. Ishii, *Unlubricated friction and wear behaviour of zirconia ceramics*. *Wear*, 215: 232-236, 1998.
- [13] M. Cadenas, R. Vijande, H. J. Montes, J. M. Sierra, *Wear behaviour of laser cladded and plasma sprayed WC–Co coatings*. *Wear*, 212: 244-253, 1997.

# Static Analysis of Layered Functionally Graded Square Plates (ISLAC'18/UHAKS18)

Savaş Evran\*, Yasin Yılmaz<sup>+</sup>

<sup>#</sup> Department of Machine and Metal Technologies, Vocational School of Canakkale Technical Sciences, Canakkale Onsekiz Mart University, Turkey  
sevrans@comu.edu.tr

<sup>+</sup> Department of Mechanical Engineering, Pamukkale University  
Turkey  
yyilmaz@pau.edu.tr

**Abstract** — The main purpose of this study is to analyze the bending stress and deflection behaviors of layered functionally graded square plates under clamped boundary conditions using uniform distributed loading (pressure). The layered FG plate was considered to vary according to a simple rule of mixture of composite materials in terms of the volume fractions of the constituents. Layer positions of the plates were carried out based on Taguchi L16 (4<sup>4</sup>) orthogonal array design and mechanical properties of layers were considered as control factors. Numerical bending and deflection analyses were performed using finite element software ANSYS V13 (Mechanical APDL). Optimum layers were determined using analysis of signal-to-noise (S/N) ratio in order to obtain minimum bending stress and deflection result. The layers and their percent contributions on the numerical results are evaluated using Analysis of Variance (ANOVA).

**Keywords**— Finite element method, Bending Stress, Deflection, Functionally graded materials

## I. INTRODUCTION

Plates are of major significance in the engineering fields and plates with different properties can be needed for various usage environments. A new material type named Functionally Graded Material (FGM) was presented in 1984 [1] and many studies consisting of FGM have been successfully published since that year. In literature, there are a lot of studies for static analysis of FG plates. Talha and Singh [2] observed the static and free vibration behaviors of plates prepared using FGM in which material properties vary to thickness direction and they used higher order shear deformation theory for analysis. Abrate [3] analyzed the free vibration behavior, buckling response and static deflection of plates designed using FGM. Ferreira, Batra, Roque, Qian and Martins [4] investigated the static behavior of plates formed using FGM with ceramic and metal materials and they used shear deformation theory and meshless method to perform static analysis of the plates. Zenkour [5] observed the static response of the plates formed using FGM with ceramic and metal materials under simply

supported boundary condition using a transverse uniform load. They used generalized shear deformation theory. Bhandari and Purohit [6] evaluated the static analysis of plate with FGM consisting of ceramic and metal materials under transverse load according to varying aspect ratio. Daouadji and Tounsi [7] presented a work including the static analysis of plates which having FGM with ceramic and metal materials using a new higher order shear deformation model. In this study, bending stress and deflection analysis of layered functionally graded square plates were investigated using finite element software ANSYS V13 based on Taguchi L16 orthogonal array. In addition, the effects of ceramic and metal materials on the responses were evaluated

## II. MATERIALS AND METHODS

### A. Materials

The numerical analyses were performed using two different materials. One of these materials is Alumina (Al<sub>2</sub>O<sub>3</sub>) and was used as ceramic. Other is Aluminium (Al) and was used as metal. Material properties of these materials is tabled in Table 1.

TABLE 1  
MATERIAL PROPERTIES [2]

Materials	Symbol	Unit	Al <sub>2</sub> O <sub>3</sub>	Al	Symbol
Young's modulus	E	GPa	380	70	E
Poisson's Ratio	$\nu$	-	0.3	0.3	$\nu$

### B. Methods

Bending stress and deflection analyses were carried out using layered functionally graded plates. Layer arrangements of the FG plates are modelled using Taguchi L16 orthogonal array with four control factors and four levels. Each layer considered to be the control factor. Control factors and the levels were given in Table 2.

TABLE 2  
CONTROL FACTORS AND LEVELS

Control Factors	Levels of Control Factors			
Layer 1	6% Al <sub>2</sub> O <sub>3</sub> -94% Al	12% Al <sub>2</sub> O <sub>3</sub> -88% Al	18% Al <sub>2</sub> O <sub>3</sub> -82% Al	24% Al <sub>2</sub> O <sub>3</sub> -76% Al
Layer 2	30% Al <sub>2</sub> O <sub>3</sub> -70% Al	36% Al <sub>2</sub> O <sub>3</sub> -64% Al	42% Al <sub>2</sub> O <sub>3</sub> -58% Al	48% Al <sub>2</sub> O <sub>3</sub> -52% Al
Layer 3	54% Al <sub>2</sub> O <sub>3</sub> -46% Al	60% Al <sub>2</sub> O <sub>3</sub> -40% Al	66% Al <sub>2</sub> O <sub>3</sub> -34% Al	72% Al <sub>2</sub> O <sub>3</sub> -28% Al
Layer 4	78% Al <sub>2</sub> O <sub>3</sub> -22% Al	84% Al <sub>2</sub> O <sub>3</sub> -16% Al	90% Al <sub>2</sub> O <sub>3</sub> -10% Al	96% Al <sub>2</sub> O <sub>3</sub> -4% Al

Layer 1 and Layer 4 are top layer and bottom layer, respectively. According to Table 2, each layer has different percent volume fraction of the ceramic and metal materials, based on 6% Al<sub>2</sub>O<sub>3</sub> increasing. Thus the layers have different mechanical properties. The effective material properties  $P_{ef}$  for each layer of the plates, such as Young's modulus  $E_{ef}$ , and poisson's ratio  $\nu_{ef}$ , were calculated using a simple rule of mixture of composite materials as shown in Equation 1 [8],

$$P_e = \sum_{i=1}^n P_i V_i \quad (1)$$

$P_i$  and  $V_i$  denote the mechanical properties and volume fraction of the constituent material  $i$  respectively. The sum of the volume fractions of all the constituent materials is found as one, as shown in Equation 2.

$$\sum_{i=1}^n V_i = 1 \quad (2)$$

$\nu$  was considered to be constant. Mechanical properties of the layers of the layered functionally graded plates were calculated using Equations 1 and 2 and control factors are obtained. Numerical results obtained using finite element software ANSYS V13 (Mechanical APDL) were investigated using Minitab R15 statistic software according to "smaller is better" characteristic as Equation 3 [9].

$$(\eta)_S = -10 \cdot \log \left( n^{-1} \sum_{i=1}^n y_i^2 \right) \quad (3)$$

where,  $n$  denote number of analysis in a trial and  $y_i$  illustrates investigated  $i$ th data.

### III. FINITE ELEMENT APPROXIMATION

Numerical deflection and bending analysis were performed using functionally graded square plates with 1.4 m side length. The plates were designed to be four layers along the thickness ( $z$  axis direction) and each layer has 1.4 mm thickness. Thus total thicknesses of layered functionally graded square plates were considered as 5.6 mm. All sides of the plates have clamped boundary condition. Analysis was performed under 900 Pa pressure as uniform distributed load on Layer 1 using finite element software ANSYS V13 (Mechanical APDL). In numerical analysis, UX, UY, UZ, ROTX, ROTY, and ROTZ were selected as degrees of freedom. Problem dimensionality

was determined as 3-D. SHELL181 element type for bending and deflection analysis was used with a 4 node element which having 6 degrees of freedom for each node: translations for the  $x$ ,  $y$ , and  $z$  directions, and rotations about the  $x$ ,  $y$ , and  $z$  axes. Comprehensive information for this element can be obtained from ANSYS help menu. 100x100 mesh size was used based global element sizes and mapped mesh type. Bending stresses for maximum value were carried out according to von Mises stress. The layered functionally graded square plate with all sides clamped boundary condition was shown in Figure 1.

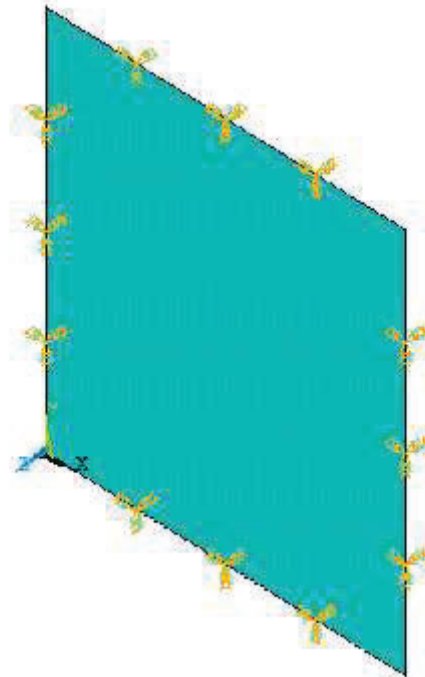


Fig. 1 Layered functionally graded square plate with all sides clamped boundary condition

### IV. RESULTS AND DISCUSSIONS

Numerical bending stress and deflection analysis of layered functionally graded square plates were carried out using finite element software ANSYS V13 parametric design language based on L16 Taguchi's orthogonal array. Bending stress and deflections results obtained were tabulated in Table 3.

TABLE 3  
 BENDING STRESS AND DEFLECTION RESULTS

Trial	Control Factors				Results			
	Layer1	Layer2	Layer3	Layer4	Numeric		S/N Ratio (dB)	
					$\sigma$ (MPa)	$\delta$ (mm)	$\eta$ for $\sigma$	$\eta$ for $\delta$
1	(Layer1) <sub>1</sub>	(Layer2) <sub>1</sub>	(Layer3) <sub>1</sub>	(Layer4) <sub>1</sub>	21.0	1.622	-26.4444	-3.19134
2	(Layer1) <sub>1</sub>	(Layer2) <sub>2</sub>	(Layer3) <sub>2</sub>	(Layer4) <sub>2</sub>	21.3	1.549	-26.5676	-2.86030
3	(Layer1) <sub>1</sub>	(Layer2) <sub>3</sub>	(Layer3) <sub>3</sub>	(Layer4) <sub>3</sub>	21.5	1.483	-26.6488	-2.33879
4	(Layer1) <sub>1</sub>	(Layer2) <sub>4</sub>	(Layer3) <sub>4</sub>	(Layer4) <sub>4</sub>	21.7	1.422	-26.7292	-2.36529
5	(Layer1) <sub>2</sub>	(Layer2) <sub>1</sub>	(Layer3) <sub>2</sub>	(Layer4) <sub>3</sub>	20.8	1.433	-26.3613	-2.47050
6	(Layer1) <sub>2</sub>	(Layer2) <sub>2</sub>	(Layer3) <sub>1</sub>	(Layer4) <sub>4</sub>	21.1	1.380	-26.4856	-2.54858
7	(Layer1) <sub>2</sub>	(Layer2) <sub>3</sub>	(Layer3) <sub>4</sub>	(Layer4) <sub>1</sub>	19.7	1.444	-25.8893	-2.15098
8	(Layer1) <sub>2</sub>	(Layer2) <sub>4</sub>	(Layer3) <sub>3</sub>	(Layer4) <sub>2</sub>	20.0	1.390	-26.0206	-2.25210
9	(Layer1) <sub>3</sub>	(Layer2) <sub>1</sub>	(Layer3) <sub>3</sub>	(Layer4) <sub>4</sub>	20.2	1.309	-26.1070	-1.57638
10	(Layer1) <sub>3</sub>	(Layer2) <sub>2</sub>	(Layer3) <sub>4</sub>	(Layer4) <sub>3</sub>	19.7	1.313	-25.8893	-1.66288
11	(Layer1) <sub>3</sub>	(Layer2) <sub>3</sub>	(Layer3) <sub>1</sub>	(Layer4) <sub>2</sub>	19.5	1.329	-25.8007	-3.19134
12	(Layer1) <sub>3</sub>	(Layer2) <sub>4</sub>	(Layer3) <sub>2</sub>	(Layer4) <sub>1</sub>	19.0	1.341	-25.5751	-2.86030
13	(Layer1) <sub>4</sub>	(Layer2) <sub>1</sub>	(Layer3) <sub>4</sub>	(Layer4) <sub>2</sub>	18.7	1.281	-25.4368	-2.33879
14	(Layer1) <sub>4</sub>	(Layer2) <sub>2</sub>	(Layer3) <sub>3</sub>	(Layer4) <sub>1</sub>	18.3	1.296	-25.2490	-2.36529
15	(Layer1) <sub>4</sub>	(Layer2) <sub>3</sub>	(Layer3) <sub>2</sub>	(Layer4) <sub>4</sub>	19.4	1.199	-25.7560	-2.47050
16	(Layer1) <sub>4</sub>	(Layer2) <sub>4</sub>	(Layer3) <sub>1</sub>	(Layer4) <sub>3</sub>	19.1	1.211	-25.6207	-2.54858
Overall Means, ( $\bar{T}$ )					20.1	1.375		

C. Detect of Optimum Layers and Their Levels

In order to carried out the optimum layer levels of layered functionally graded plate, average values of bending stress and deflection results for each level of each layer were calculated using raw data. The average data and S/N ratio value of each layer level based on bending stress and deflection behaviors were tabled in Table 4 and Table 5, respectively. According to Table 4, optimum layer levels of layered functionally graded plates for minimum bending stress value were obtained using fourth levels of Layer 1, Layer 2, and Layer 3 and first level of Layer 4. Rank and delta values demonstrate that maximum influences on the bending stress analysis was found for Layer 1. It was followed by Layer 4, Layer 3, and Layer 2. It can be seen from Table 5 that the optimum layer levels for minimum deflection value of layered functionally graded plates were determined as fourth levels of all layers. In addition, the rank and delta data values illustrate that the Layer 1 has the maximum influence on the deflection analysis and was followed by Layer 4, Layer 2, and Layer 3 in that order.

D. Effects of Layers

In order to assess the effect of each layer of layered functionally graded square plates on the bending stress and deflection behaviors, average data of bending stress and deflection behavior for each layer at all levels based on raw data were plotted in Figure 2 and Figure 3, respectively. These values were taken from Table 4 and Table 5. According to

Figure 2, the increasing of the ceramic content in Layer 1, Layer 2, and Layer 3 decreases the bending stress. But Layer 4 has opposite effect according to other layers. In order word, the increasing of the ceramic contents in Layer 4 increases the bending stress. Figure 3 shows that the increasing of the ceramic contents in all layers decreases deflection values.

E. Analysis of Variance

In order to investigate the level of importance of the layers towards the bending stress and deflection behavior, Analysis of Variance (ANOVA) at 95% confidence level is performed using raw data. ANOVA results obtained were given in Table 6. ANOVA results show that the layers on bending stress analysis are significant control parameters for  $p < 0.05$  value. Layer 1, Layer 2, and Layer 4 on deflection behavior were determined as significant control parameters for  $p < 0.05$  whereas Layer 3 is non-significant control parameter according to  $p$  value  $< 0.05$ . In addition, the percent effects of layers on the responses were shown in Figure 4. According to Figure 4, the most effective layers on the bending stress analysis were determined as Layer 1 with 82.21 %, Layer 4 with 16.29 %, Layer 3 with 0.79 %, and Layer 2 with 0.67 %, respectively. In addition, the most effective layers on the deflection analysis were found as Layer 1 with 83.33 %, Layer 4 with 10.52 %, Layer 2 with 5.43 %, and Layer 3 with 0.55 %, respectively

TABLE 4  
 RESPONSE FOR BENDING STRESS

Level	S/N Ratio (dB)				Means (MPa)			
	Layer1	Layer2	Layer3	Layer4	Layer1	Layer2	Layer3	Layer4
1	-26.6	-26.09	-26.09	-25.79	21.38	20.17	20.18	19.50
2	-26.19	-26.05	-26.06	-25.96	20.40	20.10	20.13	19.88
3	-25.84	-26.02	-26.01	-26.13	19.60	20.02	20.00	20.27
4	-25.52	-25.99	-25.99	-26.27	18.88	19.95	19.95	20.60
Delta	1.08	0.1	0.1	0.48	2.5	0.22	0.23	1.1
Rank	1	4	3	2	1	4	3	2

TABLE 5  
 RESPONSE FOR DEFLECTION

Level	S/N Ratio (dB)				Means (mm)			
	Layer1	Layer2	Layer3	Layer4	Layer1	Layer2	Layer3	Layer4
1	-3.621	-2.954	-2.783	-3.048	1.519	1.411	1.386	1.426
2	-2.994	-2.804	-2.763	-2.821	1.412	1.385	1.381	1.387
3	-2.431	-2.665	-2.719	-2.644	1.323	1.364	1.370	1.360
4	-1.911	-2.532	-2.691	-2.443	1.247	1.341	1.365	1.327
Delta	1.71	0.421	0.092	0.606	0.272	0.07	0.021	0.098
Rank	1	3	4	2	1	3	4	2

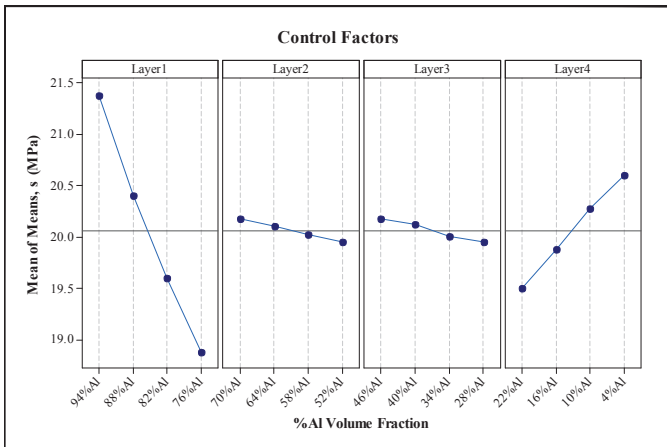


Fig. 2 Main effects plot for bending stress

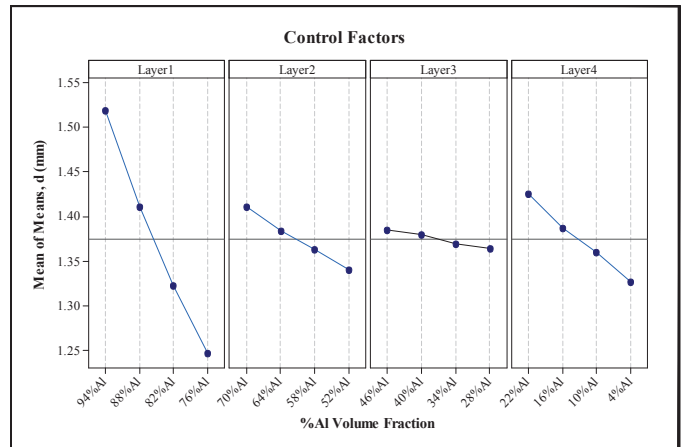


Fig. 3 Main effects plot for deflection behaviour

TABLE 6  
 ANOVA RESULTS FOR BENDING STRESS AND DEFLECTION BEHAVIOR

Source	ANOVA for Bending Stress					ANOVA for Deflection Behaviour				
	DF	Seq SS	Variance	F	P	DF	Seq SS	Variance	F	P
Layer1	3	13.8425	4.6142	1845.67	0	3	0.164954	0.054985	481.97	0
Layer2	3	0.1125	0.0375	15.00	0.026	3	0.010747	0.003582	31.40	0.009
Layer3	3	0.1325	0.0442	17.67	0.021	3	0.001083	0.000361	3.16	0.185
Layer4	3	2.7425	0.9142	365.67	0	3	0.020827	0.006942	60.85	0.003
Error	3	0.0075	0.0025			3	0.000342	0.000114		
Total	15	16.8375				15	0.197954			

S = 0.05, R-Sq = 99.96 %, R-Sq(adj) = 99.78 %      S = 0.0106810, R-Sq = 99.83 %, R-Sq(adj) = 99.14%

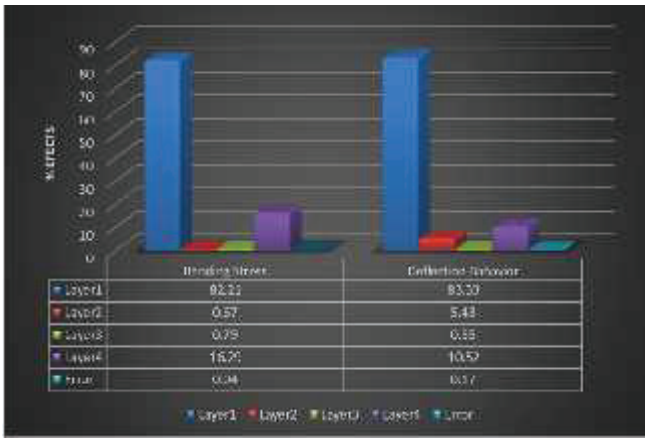


Fig. 4 The effects of layers on bending stress and deflection behavior

### F. Estimation of Numerical Results

In order to calculate the optimum results of bending stress and deflection values, optimum levels of all layers were used. The predicted results of the bending stress and deflection can be calculated based on Equation 4 and Equation 5, respectively [9].

$$\mu_{\sigma} = \text{Layer1}_{\sigma} + \text{Layer2}_{\sigma} + \text{Layer3}_{\sigma} + \text{Layer4}_{\sigma} - 3\bar{T} \quad (4)$$

where, Layer1<sub>σ</sub>=18.88, Layer2<sub>σ</sub>=19.95, Layer3<sub>σ</sub>=19.95, and Layer4<sub>σ</sub>=19.5 represent the average values of Layer1, Layer2, Layer 3 at level 4 and Layer4 at level 1, respectively. These values were obtained from Table 4.  $\bar{T}$ =20.1 refers to overall mean of 16 analysis based on L16 orthogonal array is taken from Table 3. Thus  $\mu_{\sigma}$  is calculated as 17.98 MPa.

$$\mu_{\delta} = \text{Layer1}_{\delta} + \text{Layer2}_{\delta} + \text{Layer3}_{\delta} + \text{Layer4}_{\delta} - 3\bar{T} \quad (5)$$

where, Layer1<sub>δ</sub>=1.247, Layer2<sub>δ</sub>=1.341, Layer3<sub>δ</sub>=1.365, and Layer4<sub>δ</sub>=1.327 denote the average results of Layer1, Layer2, Layer 3, and Layer4 for fourth level respectively. These values were taken from Table 5.  $\bar{T}$ =1.375 is the average result of 16 analysis using L16 orthogonal array and is taken from Table 3 and so  $\mu_{\delta}$  is calculated as 1.155 mm. Predicted results obtained Equation 4 and Equation 5 and ANSYS results were given in Table 5.

TABLE 7  
OPTIMUM RESULTS

Response	Symbol	Unit	Predicted Results	ANSYS Results	% Different
Bending Stress	σ	MPa	17.98	18.20	1.21
Deflection	δ	mm	1.155	1.18	2.12

ANSYS results obtained for bending stress and deflection analysis using optimum layers were illustrated in Figure 5. It can be said from Figure 5 that maximum bending stress was occurred middle sides of the plates. In addition, maximum deflection was detected for middle point of the plate.

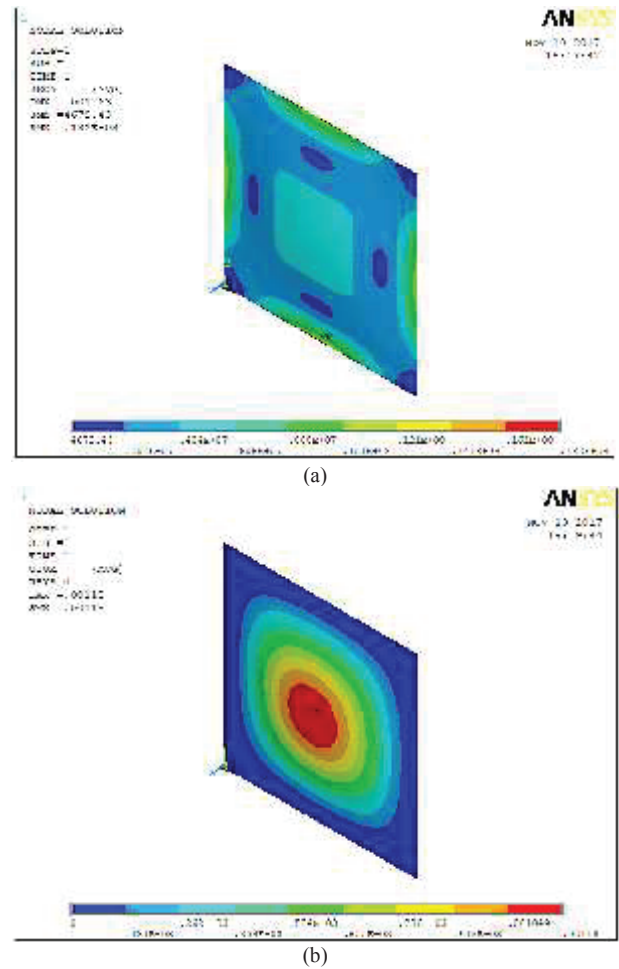


Fig. 5 Optimum results for a) bending stress and b) deflection

### V. CONCLUSIONS

Results obtained show that the increasing of ceramic contents in Layer 1, Layer 2, and Layer 3 decrease the bending stress, whereas the increasing of ceramic content in Layer 4 increases. The deflection values increase with increasing of the metal content in layers. Percent contributions of Layer 1, Layer 2, Layer 3, and Layer 4 on the bending stress analysis are carried out as 82.21 %, 0.67 %, 0.79 %, and 16.29 %, respectively. Percent contributions on deflection analysis are obtained as Layer 1 with 83.33 %, Layer 4 with 10.52 %, Layer 2 with 5.43 %, and Layer 3 with 0.55 % respectively. Percent difference between predicted and ANSYS results for bending stress and deflection are detected as 1.21 and 2.12 % respectively. According to p value < 0.05, the layers have significant effects on bending stress. Layer 1, Layer 2 and Layer 4 have significant influences on deflection analysis and Layer 3 has non-significant effect for p < 0.05. Maximum bending stress is occurred on middle side of plates, whereas middle point of the plate has maximum deflection value. Optimum levels of layers for minimum bending stress value is obtained using fourth level of Layer 1, Layer 2 and Layer 3, and first level of Layer 4, whereas minimum deflection value is found using layers with level 4.

#### REFERENCES

- [1] M. Koizumi, "FGM activities in Japan," *Composites Part B: Engineering*, vol. 28, no. 1-2, pp. 1-4, 1997.
- [2] M. Talha, and B. N. Singh, "Static response and free vibration analysis of FGM plates using higher order shear deformation theory," *Applied Mathematical Modelling*, vol. 34, no. 12, pp. 3991-4011, 2010.
- [3] S. Abrate, "Free vibration, buckling, and static deflections of functionally graded plates," *Composites Science and Technology*, vol. 66, no. 14, pp. 2383-2394, 2006.
- [4] A. J. M. Ferreira, R. C. Batra, C. M. C. Roque *et al.*, "Static analysis of functionally graded plates using third-order shear deformation theory and a meshless method," *Composite Structures*, vol. 69, no. 4, pp. 449-457, 2005.
- [5] A. M. Zenkour, "Generalized shear deformation theory for bending analysis of functionally graded plates," *Applied Mathematical Modelling*, vol. 30, no. 1, pp. 67-84, 2006.
- [6] M. Bhandari, and K. Purohit, "Static Response of Functionally Graded Material Plate under Transverse Load for Varying Aspect Ratio," vol. 2014, Article ID 980563, 11 pages, 2014.
- [7] T. H. Daouadji, and A. Tounsi, "A new higher order shear deformation model for static behavior of functionally graded plates," *Advances in Applied Mathematics and Mechanics*, vol. 5, no. 3, pp. 351-364, 2013.
- [8] H.-S. Shen, *Functionally graded materials: nonlinear analysis of plates and shells*: CRC press, Boca Raton, New York. London, 2009.
- [9] P. J. Ross, *Taguchi Techniques for Quality Engineering: Loss Function, Orthogonal Experiments, Parameter and Tolerance Design*: 2nd Edition, McGraw-Hill International Book Company, New York, 1996.

# Silikotungstik Asit Hidrat Yüklü Kitosan Hibrit Membran Sentezi Ve Sorpsiyon Performansının İncelenmesi (ISLAC'18/UHAKS18)

Derya Ünlü\*, Nilüfer Hilmioğlu†

\* Kocaeli Üniversitesi, Mühendislik Fakültesi, Kimya Mühendisliği Bölümü, 41380 Kocaeli/TÜRKİYE  
deryaunlu@gmail.com

† Kocaeli Üniversitesi, Mühendislik Fakültesi, Kimya Mühendisliği Bölümü, 41380 Kocaeli/TÜRKİYE  
niluferh@kocaeli.edu.tr

**Abstract**— In this study silicotungstic acid loaded chitosan membrane was prepared and characterized. The prepared membrane was characterized by FTIR, TGA and SEM. The presence of silicotungstic acid hydrate in the chitosan membrane was shown by FTIR analysis. TGA analysis is used to determine degradation temperatures of hybrid membrane. Structure of membrane was found stable to 200°C. In SEM analysis, the surface image of the hybrid membrane was investigated for the determination of the distribution of silicotungstic acid hydrate in the membrane. The sorption properties of different silicotungstic acid hydrate loaded chitosan membranes were first investigated on pure components water, ethanol, butanol and isopropanol. The highest sorption degree was observed in water due to the hydrophilic nature of the chitosan membrane. Then the sorption properties of the hybrid membrane were examined for binary mixtures. Separation performance of the hybrid membrane was investigated by preparing different concentrations of ethanol-water, butanol-water and isopropanol-water mixtures. Increasing the amorphous region by the silicotungstic acid results in increment of selective sorption with hydrophilicity. It is concluded that silicotungstic acid hydrate-loaded chitosan hybrid membrane is a good candidate for removing water from aqueous solutions at the end of the experimental studies.

**Keywords**— Chitosan, hybrid membrane, silicotungstic acid hydrate, sorption degree

## I. GİRİŞ

Ayırma teknolojisinde, membran prosesleri geleneksel ayırma yöntemlerine göre daha düşük maliyete sahip olmalarından dolayı son yıllarda büyük ilgi görmektedir. Membranlar seçici bir şekilde ayırmanın ve taşınımın gerçekleştiği engellerdir. Membranlarda ayırma işlemi konsantrasyon, basınç, elektriksel potansiyel gibi bir itici gücün varlığında gerçekleşir [1]. Bunun yanında ayırma, membranın morfolojik yapısına (gözenekli, asimetric, simetric, gözeneksiz vs...), ayrılacak bileşenin moleküler boyutuna ve membranın yapıldığı malzemeye bağlıdır. Membranlar gözenekli, yoğun ve kompozit membranlar olarak sınıflandırılabilir [2]. Kompozit membranlarda gözenekli alt yapının üzerinde genellikle başka bir malzemenin yapılan gözeneksiz yoğun ince bir üst tabaka

vardır ya da polimerik matris içerisine inorganik bir katkı maddesi ilave edilerek hazırlanırlar [3].

Kompozit membranlar, saf membranlara göre daha yüksek ayırma faktörüne sahiptirler ve hibrit membran olarak da adlandırılan bu membranlar ayırma işlemlerinde son yıllarda büyük ilgi görmektedirler. Bu hibrit yapılar, farklı organik-inorganik malzemeler arasındaki sinerjik etkiden yararlanarak hazırlanırlar. Zeolitler, silikalar, heteropoliasitler, hibrit membran malzemeleri için inorganik dolgu maddeleri olarak kullanılmaktadır. Fosfotungstik asit, fosfomolibdik asit ve silikotungstik asit hidrat gibi heteropoliasitler, güçlü hidrofilik ve asidik özelliklerden dolayı tercih edilmektedirler. Hibrit malzemelerin hidrofilik ve amorf bölgesi, polimer matriksine heteropoliasit ilavesiyle artar. Hidrofilite ve amorf bölge, hibrit malzemelerin sorpsiyon özellikleri için önemli noktalar [4-5].

Bu çalışmada, polimer matriks içerisine silikotungstik asit eklenmesi ile organik-inorganik hibrit membranların hazırlanması için kitosan ve silikotungstik asitin uygunluğu araştırılmıştır. Kitosan iyi film oluşturma, yüksek hidrofiliklik ve yüksek kimyasal direnç gibi özellikleri nedeniyle membran yapımında tercih edilmektedir [6]. Kitosan doğal, toksik olmayan, biyobozunur bir polimerdir. Kitosan hidroksil gruplarla birlikte büyük miktarda reaktif amin grupları içeren çok fonksiyonlu bir polimerdir. Yapısındaki bu gruplar kitosanın hidrofilik özellik kazanmasını sağlamaktadır. Bu özellik mükemmel su sorpsiyonunda ve membran arasından bileşenin difüzyonunda önemli rol oynamaktadır [7]. Kitosan membran suda şişer. Bu yüzden hem mekanik dayanımını arttırmak hem de seçiciliğini arttırmak için uygun bir ajanla çapraz bağlanmaktadır [8]. Sık sık kullanılan çapraz bağlayıcı ajanları; glutaraldehit, epiklorohidrin, sülfürik asit, dialdehit nişasta vb.dir [7].

Silikotungstik asit hidrat Keggin yapısına sahip bir heteropoliasittir. Güçlü asidite ve termal dayanıma sahiptir. Silikotungstik asit; Si, oksijen ve W<sub>3</sub>O<sub>13</sub> birimlerine sahiptir.

Su molekülleri silikotungstik asit hidratin yapısına zayıfça bağlanmışlardır [9].

Silikotungstik asit hidratin yüzeyindeki -OH grupları, kitosanın yapısındaki -OH veya -NH<sub>2</sub> grupları ile H-bağları oluşturmaktadır. Bu nedenle, kitosanın amorf bölgesi, silikotungstik asit hidratin ilavesi ile artırılabilir ve kitosan membranlarının performansı iyileştirilmiş olur [4].

Silikotungstik asit hidrat yüklü kitosan hibrit membran bu çalışmada çözültiden döküm yöntemi ile hazırlanmıştır. Membranın yapısı ve morfolojisi SEM, FTIR ve TGA ile karakterize edilmiştir. Membranın sorpsiyon özellikleri saf bileşenlerde ve ikili alkol-su karışımlarında incelenmiştir. STA içeriğinin, beslemedeki su konsantrasyonunun membranın sorpsiyon derecesine etkisi incelenerek optimum koşullar belirlenmiştir.

## II. DENEYSEL ÇALIŞMALAR

### A. Kullanılan malzemeler

Hibrit membranın hazırlanmasında kullanılan silikotungstik asit ve kitosan malzemeleri Sigma Aldrich firmasından temin edilmiştir. %99 saflıkta etanol, bütanol ve izopropanol kimyasalları ise Merck'ten tedarik edilmiştir. Ayrıca deneysel çalışmalarda yüksek saflıkta su da kullanılmıştır.

### B. Silikotungstik asit hidrat yüklü kitosan hibrit membranın hazırlanması

Silikotungstik asit hidrat yüklü kitosan hibrit membran çözültiden döküm yöntemi ile hazırlanmıştır. Kitosan ağırlıkça %2 asetik asit içeren sulu çözültide çözünerek polimerik çözelti hazırlanmıştır. Ağırlıkça %2, 4, 6, 8 ve 10 silikotungstik asit hidrat çözeltiye ilave dilip 24 saat kadar karıştırılmıştır. Homojen dağılımı sağlamak için ultrasonik karıştırıcıda da iki saat karıştırılan çözelti sonrasında polimetilmetakrilat yüzeye dökülerek 40°C'de etüvde kurumaya bırakılmıştır.

### C. Silikotungstik asit hidrat yüklü kitosan hibrit membranın karakterizasyonu

Hazırlanan membranın yapısı SEM, FTIR ve TGA yöntemleri kullanılarak karakterize edilmiştir. Taramalı elektron mikroskopları ile polimerik membran yüzeyinde oluşan yapılar incelenmiştir. Membranların SEM analizleri JEOL JSM-6335 F "Field emission scanning electron" model mikroskop ile Tübitak Marmara Araştırma Merkezi'nde yapılmıştır. Hazırlanan katkılı membranın bağ yapıları ve yapıdaki dolgu maddeleri FTIR cihazı ile analiz edilmiştir. FTIR analizi Kocaeli Üniversitesi Kimya Mühendisliği Bölümü Polimer Laboratuvarı'ndaki Perkin Elmer marka cihaz ile yapılmıştır. Malzemelerin sıcaklığa bağlı olarak kütle değişimleri ise Kocaeli Üniversitesi Kimya Mühendisliği Bölümü Polimer Laboratuvarı'nda incelenmiştir.

### D. Silikotungstik asit hidrat yüklü kitosan hibrit membranın sorpsiyon testleri

Çözücü ve membran arasındaki etkileşimi belirlemek için sorpsiyon deneyleri yapılmıştır. Membranlar küçük parçalar halinde kesilmiş ve tartımları alınmıştır. Kuru ağırlıkları belirlenen membranlar belirli zaman aralıklarında vezin kaplarından alınmış ve tartımı yapılmıştır. Bu işlem çözültideki membran ağırlığı sabit kalıncaya kadar devam etmiştir ve Eşitlik 1 kullanılarak sorpsiyon değerleri bulunmuştur.

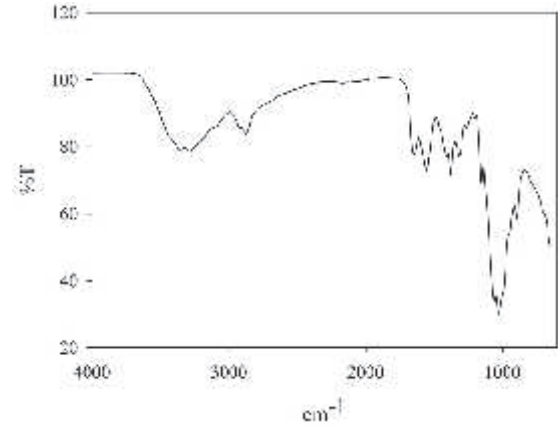
$$\text{Şişme Derecesi (\%)} = \frac{W_s - W_d}{W_d} * 100 \quad (1)$$

$W_d$ , kuru membran ağırlığı ve  $W_s$  şişmiş membranın ağırlığıdır.

## III. DENEY SONUÇLARININ DEĞERLENDİRİLMESİ

### A. Silikotungstik asit hidrat yüklü kitosan hibrit membranın karakterizasyon sonuçları

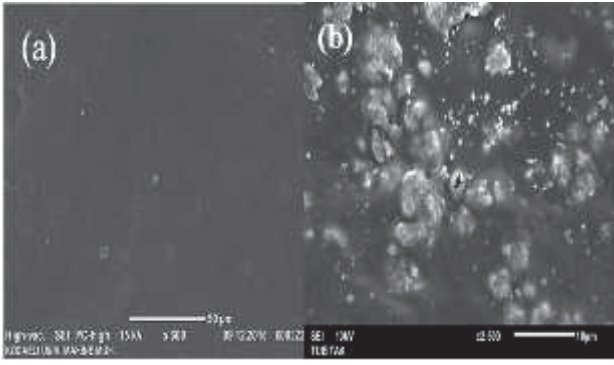
1) *FTIR*: Silikotungstik asit hidrat yüklü kitosan hibrit membranın FTIR spektrarı Şekil 1'de gösterilmektedir.



Şekil 1 Silikotungstik asit hidrat yüklü kitosan hibrit membranın FTIR spektrumu

896, 1025, 1060 cm<sup>-1</sup>'deki pikler silikotungstik asit hidrat yapısındaki Keggin birimlerini göstermektedir [4]. 3309 cm<sup>-1</sup> civarındaki pikler ise Silikotungstik asit hidrattaki OH bağlarını işaret etmektedir. N-H bağlarının absorpsansı 1555.9 cm<sup>-1</sup>'deki pikte görülmektedir. 1376.5 cm<sup>-1</sup>'deki pik ise C-H bağının spesifik absorpsanslarını göstermektedir [10-11].

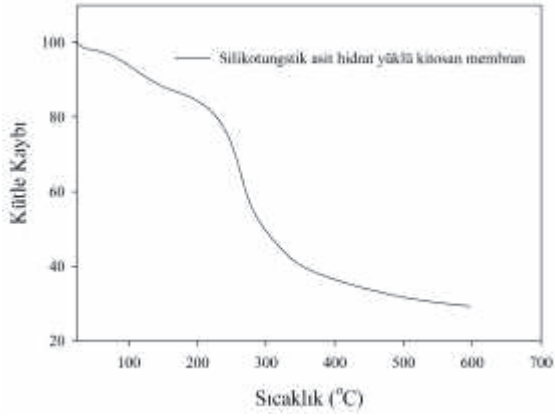
2) *SEM*: SEM analizleri, saf kitosan membran ve silikotungstik asit hidrat yüklü kitosan hibrit membrandan alınan örnekler ile yapılmıştır. Şekil 2'de saf ve katkılı membranın yüzey görüntüleri gösterilmiştir.



Şekil 2 Saf (a) ve katkılı (b) membranın yüzey görüntüleri

Şekil 2(a)'dan da görüldüğü üzere saf kitosan polimeri ile hazırlanan membranın yüzeyi oldukça düzdür. Şekil 2(b)'de ise silikotungstik asit hidrat yüklü kitosan hibrit membranın yüzeyinde silikotungstik asit hidrat dolgu maddesi açıkça görünmektedir. Yüzeyde yükleme işlemi başarı ile gerçekleştirilmiştir.

3) TGA: Silikotungstik asit hidrat yüklü kitosan hibrit membranın termal dayanımı Şekil 3'te verilmiştir.

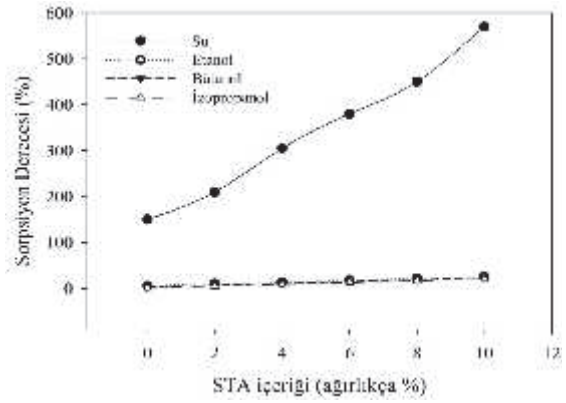


Şekil 3 Silikotungstik asit hidrat yüklü kitosan hibrit membranın TGA eğrisi

İki temel kütle kaybı yaklaşık olarak 40-200°C ve 200-600°C sıcaklık aralığında gözlenmiştir. İlk gözlenen kütle kaybı 40-200°C'de, fiziksel olarak absorblanmış su ve asetik asit gibi küçük moleküllerin buharlaşmasından ileri gelmektedir. İkinci kütle kaybı kitosanın ve silikotungstik asit hidrat katkı maddesinin bozunması ile ilgilidir. Bu bozunma polimerik ağın termal bozunması ve kitosan ve silikotungstik asit hidratın yapısal bozulması ile ilgilidir. Silikotungstik asit hidrat yüklü kitosan hibrit membran iyi termal dayanım sergilemiştir [12].

#### B. Silikotungstik asit hidrat yüklü kitosan hibrit membranın saf bileşen sorpsiyon performansının incelenmesi

Silikotungstik asit hidrat yüklü kitosan hibrit membranın saf bileşenlerdeki sorpsiyon özelliklerini belirlemek için sorpsiyon testleri yapılmıştır. Şekil 4'te silikotungstik asit hidrat (STA) yüklü kitosan hibrit membranın saf bileşenlerde şişme derecesinin STA miktarı ile değişimi verilmiştir.

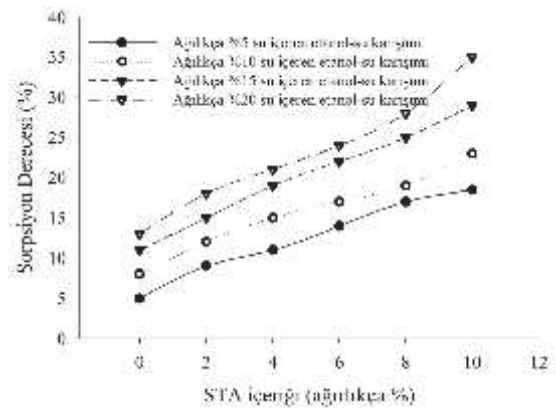


Şekil 4 Saf bileşenlerde şişme derecesinin STA miktarı ile değişimi

Membran suda en yüksek sorpsiyon derecesine sahiptir. Ardından sırasıyla etanol, bütanol ve izopropanolde şişme göstermiştir. Kitosan membranın hidrofilik özelliğinden dolayı şişme derecesi suda en yüksek değerdedir. Sudaki şişme derecesi %570 iken, etanol, bütanol ve izopropanoldeki şişme dereceleri sırasıyla %25, %23 ve %20'dir. Ayrıca STA içeriği arttıkça sorpsiyon derecesinin arttığı gözlenmiştir. Saf kitosan membranın suyu sorplama derecesi %150 iken, %10 STA yüklü membranda bu değer %570'e ulaşmıştır. STA içeriği arttıkça membranın saf bileşenleri sorplama kapasitesi yaklaşık 5 kat artmıştır. Bu durum silikotungstik asit hidrat yüklü kitosan hibrit membranın hidrofiliklik özelliğinin ve amorf bölgesinin artan STA içeriği ile arttığını göstermektedir [4].

#### C. Silikotungstik asit hidrat yüklü kitosan hibrit membranın ikili karışımlarda sorpsiyon performansının incelenmesi

1) Etanol/su ikili karışımı: Silikotungstik asit hidrat yüklü kitosan hibrit membranın etanol/su ikili karışımında besleme su miktarı ve STA içeriği ile sorpsiyon davranışı Şekil 5'te gösterilmiştir.



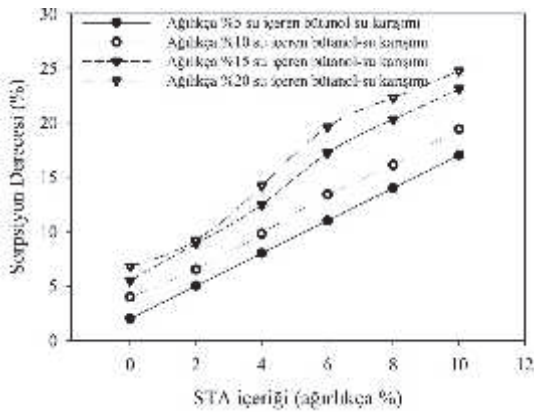
Şekil 5 Besleme su konsantrasyonunun etanol-su karışımlarında farklı STA oranlarında sorpsiyon derecesine etkisi

Membranın sorpsiyon özelliklerine beslemedeki su konsantrasyonunun etkisi ağırlıkça %5, 10, 15 ve 20 içeren etanol/su karışımlarında incelenmiştir. Besleme su konsantrasyonu arttıkça membranın sorpsiyon derecesinin arttığı görülmüştür. Kitosanın hidrofilik doğası yüksek su

sorpsiyonuna neden olmaktadır. Bunun sebebi su molekülleri ile kitosan arasında kurulan hidrojen bağlarıdır. Su konsantrasyonu arttıkça kitosan membran şişerek membranın daha fazla su sorplamasına neden olacaktır [13]. Saf kitosanda %5 su içeren besleme konsantrasyonunda membranın şişme derecesi %5 iken, %20 su içeren besleme konsantrasyonunda %13'tür.

STA'nın membrana katılması da membranın sorpsiyon performansını etkilemektedir. STA, membranın hidrofilitesini artırır [4]. Bu sebeple STA içeriği arttıkça membranın sorpsiyon derecesi artmıştır. Beslemede %5 oranında su bulunduğu koşulda gerçekleştirilen sorpsiyon deneylerinde, %2 STA içeren membranın sorpsiyon derecesi %9 iken, %10 STA içeren membranın sorpsiyon derecesi %18.5 olarak elde edilmiştir.

2) *Bütanol/su ikili karışımı*: Silikotungstik asit hidrat yüklü kitosan hibrit membranın bütanol/su ikili karışımında besleme su miktarı ve STA içeriği ile sorpsiyon davranışı Şekil 6'da gösterilmiştir.



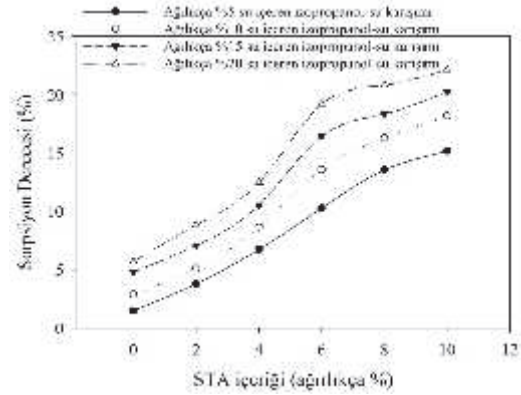
Şekil 6 Besleme su konsantrasyonunun bütanol-su karışımlarında farklı STA oranlarında sorpsiyon derecesine etkisi

Membranın sorpsiyon özelliklerine beslemedeki su konsantrasyonunun etkisi ağırlıkça %5, 10, 15 ve 20 içeren bütanol/su karışımlarında incelenmiştir. Beslemedeki su konsantrasyonu %5'ten %15'e artırıldığında membranın sorpsiyon derecesinde belirgin bir artış olduğu görülmüştür. Ancak su konsantrasyonu %15'ten %20'ye artırıldığında sorpsiyon derecesinin belirgin bir değişim gözlenmemiştir. Bu durum membranın maksimum su tutma kapasitesine ulaştığını göstermektedir. Doğunluğa ulaşan membran daha fazla şişmemektedir. Katkısız kitosan membranda beslemedeki su konsantrasyonu %15 iken sorpsiyon derecesi % 5.5 iken, su konsantrasyonu %20'ye çıkarıldığında sorpsiyon derecesi % 6.8 olarak elde edilmiştir.

STA içeriği arttıkça sorpsiyon derecesinde belirgin bir artış olduğu gözlenmiştir. Kitosanın hidrofilik özelliğinin yanında STA'nın da ilavesi membranın hidrofilikliğini arttırmış daha yüksek sorpsiyon derecesi ile sonuçlanmıştır [4]. %5 su konsantrasyonuna sahip besleme karışımında %2 STA içeren

membranın sorpsiyon derecesi %5 iken, %10 STA içeren membranın sorpsiyon derecesi %17'dir.

3) *İzopropanol/su ikili karışımı*: Silikotungstik asit hidrat yüklü kitosan hibrit membranın izopropanol/su ikili karışımında besleme su miktarı ve STA içeriği ile sorpsiyon davranışı Şekil 7'de gösterilmiştir.



Şekil 7 Besleme su konsantrasyonunun izopropanol-su karışımlarında farklı STA oranlarında sorpsiyon derecesine etkisi

Beslemedeki su miktarının sorpsiyon derecesine etkisine bakıldığında su miktarı arttıkça sorpsiyon derecesinin arttığı görülmüştür. Kitosan membran daha önce de belirtildiği gibi hidrofilik yapıdadır. Membranın yapısındaki -OH grupları ve besleme karışımındaki su molekülleri arasındaki etkileşimden dolayı sorpsiyon derecesi beslemedeki su miktarı ile artar. Beslemede artan su konsantrasyonu, membranın daha fazla şişmesi ve polimer zincirlerinin daha esnek olması ile sonuçlanır [14-15]. Saf kitosanda %5 su içeren besleme konsantrasyonunda membranın şişme derecesi %1.5 iken, %20 su içeren besleme konsantrasyonunda %5.70'tir.

Membranın hidrofiliklik özelliğini iyileştirmek için ilave edilen STA miktarının sorpsiyon derecesine etkisi incelendiğinde STA miktarı arttıkça sorpsiyon derecesinin arttığı görülmüştür. Diğer ikili alkol/su karışımlarında olduğu gibi beklenen benzer sonuçlar elde edilmiştir. %5 su içeren izopropanol-su karışımlarında %3.8 STA içeren membranın sorpsiyon derecesi %5 iken, %10 STA içeren membranın sorpsiyon derecesi %15.20'dir.

#### IV. SONUÇLAR

Bu çalışmada kitosan polimeri kullanılarak saf ve silikotungstik asit hidrat yüklü kitosan hibrit membranlar hazırlanmıştır. Çözüldüden döküm yöntemi ile hazırlanan saf ve hibrit membranlar FTIR ve SEM ile karakterize edilerek membranın yapısına ilave edilen STA'ların varlığı ispatlanmıştır. Ayrıca hibrit membranın termal dayanımı TGA analizi ile belirlenmiş ve polimer ve katkı maddesi STA'nın yüksek sıcaklıkta bozunma gösterdiği belirlenmiştir. Silikotungstik asit hidrat yüklü kitosan hibrit membranın şişme testi ilk olarak solvent absorpsiyonu yöntemi kullanılarak gerçekleştirilmiştir. Su, etanol, bütanol ve izopropanol için saf kitosan membranın şişme dereceleri

sırasıyla %150, %5, %3 ve %1 iken, %10 STA katkılı hibrit kitosan membran ile %570, %25, %23 ve %20 sorpsiyon dereceleri elde edilmiştir. Kitosanın hidrofilik yapısı gereği yapısında bulunan –OH gruplarından dolayı membran en fazla suya ilgi duyar ve bu nedenle de yüksek su sorpsiyonu elde edilir. İkili alkol/su karışımlarında da membranın sorpsiyon özellikleri incelenmiş ve su konsantrasyonu arttıkça sorpsiyon derecesinin arttığı gözlenmiştir. Bu durum su molekülleri ile kitosan arasında kurulan hidrojen bağları ile açıklanabilmektedir. STA miktarının da hibrit membranın sorpsiyon özelliklerine etkisi incelenmiştir. STA'nın membranın amorf bölgesini arttırarak, membranın hidrofilikliğini arttırdığı, bu nedenle STA içeriği arttıkça her üç ikili karışımında da sorpsiyon derecesinin arttığı görülmüştür. Çalışma sonunda silicotungstik asit hidrat yüklü kitosan hibrit membranın alkol su karışımlarının saflaştırılmasında kullanılabileceği görülmüştür.

#### KAYNAKLAR

- [1] O.S. Khaw, S. Mitra, "Pervaporation in chemical analysis", *Journal of Chromatography*, vol.1217, pp. 2736–2746, 2010.
- [2] C.S., Slater, "Membrane Technology For Energy Conservation in Traditional and Emerging Engineering Fields", *IEEE*, vol.3, pp.1731-1736, 1989.
- [3] R.W. Baker, "Membrane Technology and Applications", Second edition, Wiley, 2004, vol.212.
- [4] J.H. Chen, Q.L. Liu, A.M., Zhu, Q.G. Zhang, J. Fang, "Pervaporation separation of MeOH/DMC mixtures using STA/CS hybrid membranes", *Journal of Membrane Science*, vol.315, pp.74-81, 2008.
- [5] S. Chaudhari, Y.S. Kwon, M.Y. Moon, M.Y. Shon, Y.I. Park, S.E. Nam, "Melamine-modified silicotungstic acid incorporated into the polyvinyl alcohol/polyvinyl amine blend membrane for pervaporation dehydration of water/isopropanol mixtures", *Vacuum*, vol.147, pp.115-125, 2018.
- [6] M. Ghazali, M. Nawawi, R.Y.M. Huang, "Pervaporation dehydration of isopropanol with chitosan membranes", *Journal of Membrane Science*, vol.124, pp.53-62, 1997.
- [7] J.H. Chen, Q.L. Liu, X.H. Zhang, Q.G. Zhang, "Pervaporation and characterization of chitosan membranes cross-linked by 3-aminopropyltriethoxysilane", *Journal of Membrane Science*, vol.292 pp.125–132, 2007.
- [8] D.A. Devia, B. Smitha, S. Sridhar, T.M. Aminabhavia, "Pervaporation separation of isopropanol/water mixtures through crosslinked chitosan membranes", *Journal of Membrane Science*, vol.262, pp.91-99, 2005.
- [9] V. Vijayalekshmi, D. Khastgir, "Fabrication and comprehensive investigation of physicochemical and electrochemical properties of chitosan-silica supported silicotungstic acid nanocomposite membranes for fuel cell applications", *Energy*, vol.142, pp.313-330, 2018.
- [10] H.S. Tsai, Y.Z. Wang "Properties of hydrophilic chitosan network membranes by introducing binary crosslink agents", *Polymer Bulletin*, vol.60, pp.103–113, 2008.
- [11] C.S. Caetano, M. Caiado, J. Farinha, I.M. Fonseca, A.M. Ramos, J. Vital, J.E. Castanheiro, "Esterification of free fatty acids over chitosan with sulfonic acid groups", *Chemical Engineering Journal*, vol.230, pp.567–572, 2013.
- [12] N. Bhatt, A. Patel, "Liquid phase cyclohexylation of phenol with cyclohexene using 12-tungstosilicic acid supported onto different supports", *Journal of Molecular Catalysis A: Chemical*, vol.264, pp.214–219, 2007.
- [13] Olukman, M., Oya, S., "Synthesis of magnetite in poly (vinyl alcohol) matrix and its use in separation of acetone/water mixtures via pervaporation, vapor permeation with and without temperature difference methods", *Vacuum*, vol.120, pp.107-115, 2015.
- [14] A.A. Kittur, B.K. Jeevankumar, M.Y. Kariduraganavar, S.D.M. College, "Pervaporation separation of water-dioxane mixtures poly (vinyl alcohol)-silicone based hybrid membranes", *International Journal of Current Engineering and Technology*, vol.1, pp.148–156, 2013.
- [15] D. Sun, P. Yang, H. Sun, B. Li "Preparation and characterization of cross-linked poly (vinyl alcohol)/hyperbranched polyester membrane for the pervaporation dehydration of ethylene glycol solution", *European Polymer Journal*, vol.62, pp.155-166, 2014.

# Mechanical and Microstructure Properties of Sn-Zn Alloys Used in the Electronic Industry

Fazıl HÜSEM<sup>1\*</sup>, Fatma MEYDANERİ TEZEL<sup>1\*</sup>, Umur Can HAMUTOĞLU<sup>1</sup>, Furkan NERGİZ<sup>1</sup>, Ceyda ALBAYRAK<sup>1</sup> and Salih BEKTAŞ<sup>1\*</sup>

<sup>1</sup>Department of Metallurgy and Materials Engineering, Faculty of Engineering, Karabük University, 78050, Karabük, Turkey

\*Corresponding author: fazilhusem@karabuk.edu.tr; fatmameydaneri@karabuk.edu.tr; bektassalih25@gmail.com

**Abstract**— In this study, Sn-1 wt.% Zn, Sn-9 wt.% Zn and Sn-14 wt.% Zn alloys were cast into the kokil mould. Microstructures and composition analyses of the obtained alloys were obtained by using SEM and EDX, devices. The variation of Zn amount has a great impact on flake or needle shape distributions of Zn phase in Sn matrix result in different effects on hardness. Mechanical properties (yield, elongation, elongation and breakage) were also obtained by using a tensile tester. The tensile test results for Sn-1 wt.% Zn, Sn-9 wt.% Zn and Sn-14 wt.% Zn indicating that the sample with the best mechanical properties is Sn-9 wt.% Zn. In addition, the tensile value obtained for the Sn-9 wt.% Zn sample is 105.8 MPa, the unit strain is 12.8% and the yield stress is 85.548 MPa. Average micro hardness values of Sn-[x] wt. % Zn [x=1, 9, 14] only depend on the composition, and increase with increasing of Zn composition.

**Keywords**— Sn-Zn alloys, SEM, EDX, XRD, mechanical properties

## I. INTRODUCTION

Pb and Pb-containing compounds are prohibited to use in European Union, because of damaging the environment and human health. Limitation of lead used in the industry for more appropriate development policies to protect the environment is emphasized by most countries. In this context, great efforts for the development of lead-free alternative alloys instead of Pb-Sn eutectic solder alloy is shown [1-2]. Both economically and in terms of other physical and chemical requirements of lead-free solder alloy is required to meet. Sn-Zn eutectic alloy of lead-free solder alloy as prominently provides electronic merge without any modification and is expected to be one of the best alternatives to maintain the existing production line [3-4]. In addition, both micromechanical and metallurgical properties in terms of controlling the microstructure, strength, a casting alloy is complex in terms of silence and ductility. Thermal variables and their impact on the microstructure morphology depending on the heat transfer solidification conditions are influenced by the temperature and composition and are affected all the features as a direct result [5-7]. Since studies related to effect of temperature, Zn composition, micro hardness and used method, the electrical and thermal properties are rarely available in literature. In this study, our

purpose is examined mechanical, structural and corrosion properties and the results are discussed.

## II. EXPERIMENTAL PROCEDURE

The cavity mold is set for four cylindrical samples. The mold cavity dimensions for each sample are  $\varnothing = 20$  mm,  $h = 170$  mm Her. The amounts of the tin (Sn) and zinc (Zn) metals were calculated and melted in the melting furnace in the graphite crucible. The mold was heated more about 100 °C than the melting temperature of the sample. After mixing several times, the homogenous molten obtained was poured into the mold.

### A. Microstructure Properties

Surface morphology and composition analysis of the samples were investigated Zeiss Ultra Plus SEM and EDX spectrometer, respectively. To obtain the SEM images, Struers brand Discotom 100 and Secotom 50 devices were used to cut to samples. With Tegramin 30 automatic sanding and polishing device, transverse sections were ground flat with SiC papers and mechanically polished using 6  $\mu$ m, 3  $\mu$ m, 1  $\mu$ m, and 1/4  $\mu$ m diamond paste. Then, the etching process was performed with 49% H<sub>2</sub>O, 1% H<sub>2</sub>SO<sub>4</sub> and 2g CrO<sub>3</sub> mixture. Ratio of chemical compositions was measured by an EDX spectrometer attached to the SEM.

### B. Mechanical and Microhardness Properties

The axial and variable forces are applied to the circle or rectangular test pieces with dimensions compatible to standards by the traction device. The pulling device is mainly; It consists of two jaws that can move up and down relative to each other, two jaws to which the test piece is connected, and units that measure these two sizes, which give them movement or strength. In order to apply the tensile test to the samples, firstly, the specimen was processed to be a specimen of the tensile test, which has a diameter of ( $d_0$ ) = 10.2 mm, cross-sectional area ( $A_0$ ) = 81.71 mm<sup>2</sup>, length ( $L_0$ ) = 160 mm and round section according to the standards in the CNC machine. The tensile test of the specimen prepared according to the standards was carried out at room temperature (25 °C) with a Zwick / Roell Z600 tensile testing device.

The Vickers hardness value is the portion of the test load expressed in kg (mm<sup>2</sup>) to the trace area. Vickers hardness values of the samples were determined by QNESS Q10 A +

brand Hardness Tester. After the load is removed, the hardness value is calculated by making the measurement diagonal.

$$H_v = \frac{2F \sin(\phi/2)}{d^2} \quad (1)$$

where  $\phi$  is the indenter apex angle, F is the applied load and d is the average length of diagonals. 100 g load is applied for 15 seconds for micro hardness values.

### III. CONCLUSIONS

Surface morphologies are explored by SEM with 20.000x magnification, and presented in Fig. 1. According to the SEM analyzes, the surfaces is made up of different-sized spherically.

EDX profile and the elemental analysis, it is confirmed that the phase consisted of Sn and Zn, and presented in Fig. 1.

Microhardness measurements of Sn-[x] wt. % Zn [x=1, 9, 14] alloys were calculated to be average values of microhardness measurements of Sn and Zn phases, and Sn-Zn grain boundaries in microstructures. Solidification conditions of Sn-[x] wt. % Zn [x=1, 9, 14] alloys are same. So, microhardness values only depend on the composition, and increase with increasing of Zn composition. Average micro hardness values of Sn-[x] wt. % Zn [x=1, 9, 14] alloys were given Fig. 2. The variation of Zn amount has a great impact on the grain size, and flake or needle shape distributions of Zn phase in Sn matrix result in different effects on hardness.

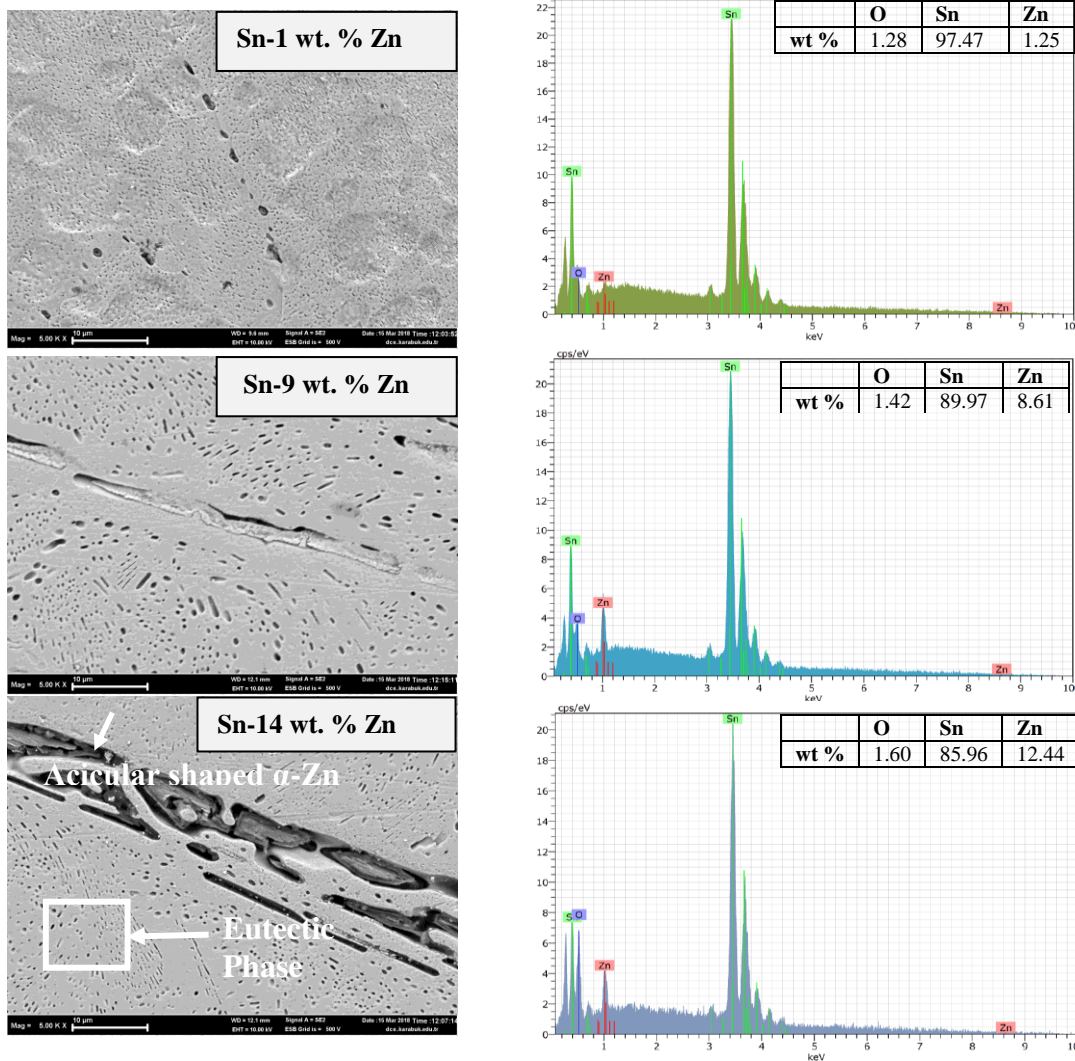


Fig. 1 SEM images and EDX analyses of Sn-x wt. % Zn (x=1, 9, 14) alloys.

grains tend to be spherical shape, and a small amount of dissolved needle-like eutectic structure, which also contains Zn phase, is located along the grain boundaries. From the

Grain sizes increased for dissolve in each other by the increase of Zn composition. The grain boundaries between two different phases also forms a barrier against the movement of

dislocations, and dislocations in the grain boundaries with large-angle are accumulated in the grain boundaries, and play an important role in increasing the microhardness of the alloy.

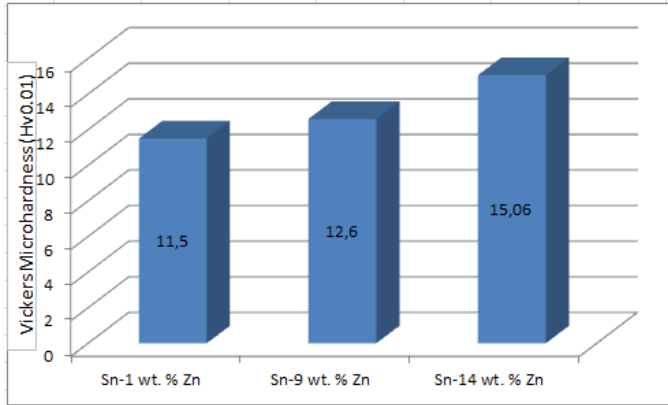


Fig. 2 Microhardness analyses of Sn-x wt. % Zn (x= 1, 9, 14) alloys.

3 tensile samples were prepared and subjected to tensile testing for each composition of the For Sn-x wt. % Zn [x= 1, 9, 14], alloys. The mechanical properties of the alloys were determined by taking the mean values of 3 separate results and given in Table 1. Accordingly, the maximum tensile strength (about 105 MPa) and the lowest elongation (about 12%) were obtained for Sn-9 wt.% Zn eutectic alloy.

Samples	Peak Load (kN)	Peak Stress (MPa)	Elongation	Yield
Sn-1 wt.% Zn	3.324	42.3	0.480	36.050
Sn-9 wt.% Zn	8.315	105.8	0.126	85.548
Sn-14 wt.% Zn	4.742	60.4	0.499	46.249

#### REFERENCES

- [1] K. Suganuma, S.H. Huh, K. Kim, H. Nakase, Y. Nakamura, *Materials Transactions*, 42 (2) (2001) 286–291.
- [2] Ünlü, S. B. ve Atik, E., “Kalay -Kurşun Esaslı Yataklardaki Alaşım Elementlerinin Aşınmaya Etkisi”, *Makine Teknolojileri Elektronik Dergisi*, 1, 1-5 (2005).
- [3] Habashi, F., “*Handbook of Extractive Metallurgy*, 2nd ed.”, Heidelberg, Germany, (1997).  
[http://works.bepress.com/fathi\\_habashi/22/](http://works.bepress.com/fathi_habashi/22/) adresinden 13.11.2017 tarihinde çevrim içi olarak erişilmiştir.
- [4] Nakashima, K., Tanaka, T., Yago, W. Yamamoto, K. ve Ichida, K., “High strength alpha brass containing Mn, Si, Co, Fe, Sn & Pb”, *United States Patent*, 5.282.298, (1994).

<https://www.google.com/patents/US5282908> adresinden 17.11.2017 tarihinde çevrimiçi olarak erişilmiştir.

[5] Akutsu, H., “Synchronizer ring in speed variator made of copper-base alloy”, *United States Patent*, 4.995.924, (1991).  
<https://www.google.com/patents/US4995924> adresinden 17.11.2017 tarihinde çevrimiçi olarak erişilmiştir.

[6] Garcia L.R., Osorio, W.R., Peixoto, L.C. ve Garcia, A., “Wetting behaviour and Mechanical properties of Sn-Zn and Sn-Pb Solder Alloy”, *Journal of Electronic Materials*, 38 :11 (2009).

[7] Meydaneri, F. Saatçi, B., Gündüz, M. ve Özdemir, M., “Determination of thermal conductivities of Sn-Zn lead-free solder alloys with radial heat flow and Bridgman-type apparatus”, *Continuum Mechanics and Thermodynamics*, 25: 6 691-704, 2012.

# An Investigation on Hardness and Tensile-Shear Stress of Friction Stir Welded Lap Joints of AA 2014 Aluminium Alloys (ISLAC'18/UHAKS18)

İbrahim Sevim\*, Mustafa Kemal Kulekci<sup>+</sup> and Ömer Uçtu\*

\*Department of Mechanical Engineering, Karamanoğlu Mehmetbey University, 70100, Karaman, Turkey  
isevim@kmu.edu.tr

<sup>+</sup>Mersin University, Manufacturing Engineering Department, 33480 Tarsus, Mersin, Turkey  
mkkulekci@mersin.edu.tr

\*Naci Topçuoğlu, Vocational School Gaziantep University, Gaziantep, Turkey  
omeructu@outlook.com

**Abstract**—The objective of this study was to determine the Tensile-Shear Stress of Friction Stir Welded (FSW) Lap Joints of Aluminium Alloys. FSW lap joints of AA 2014 aluminium alloy plates were performed on a conventional semiautomatic milling machine. Defect free FSW lap joints were produced on alloy plates. Tensile-Shear Stress of FSW lap joints were obtained from the results of shearing tensile tests.

New empirical equations were developed for Tensile-Shear Stress based on the relation between the hardness and Tensile-Shear Stress values. Tensile-Shear Stress of FSW lap joints increase exponentially as the hardness reduces. The results of the experiments showed that the amount of Si content in Al alloys affects the Tensile-Shear Stress the FSW lap joints.

**Keywords**— Friction stir welding, Lap joints, Tensile-Shear Stress, 2014 aluminium alloys

## I. INTRODUCTION

Friction stir welding (FSW) offers a new, low cost alternative to fusion welding procedures due to the low power requirements [1, 2, 3]. Aluminium alloys with good heat transfer, high strength, good formability and weight saving are being used for aerospace structure, shipbuilding, railway cars etc [4]. The specific properties that affect the welding of aluminium and its alloys are its oxide characteristics, the solubility of hydrogen in molten aluminium, its thermal, electrical and non-magnetic characteristics, and its wide range of mechanical properties and melting point [5-8].

In FSW process, the strength of the metal of the interface between the rotating tool and work piece falls below the applied shear stress as the temperature rises, so that plasticized material is extruded from the leading side to the trailing side of the tool. The tool is then steadily moved along the joint line giving a continuous weld [9, 10]. The plates to be welded are secured to prevent the butted joint faces from being forced apart as the probe passes through and along the seam. The

heat affected zone is much wider at top surface (in contact with shoulder) and tapers down [11].

In literature there are some studies which explain the mechanical properties of FSW. However, there are only a few them, which investigates the shear tensile stress of FSW joints. Lack of comprehensive study for assessing the shear tensile stress of FSW joints has led to the present work to be carried out. In this study, shear tensile stress of lap joints that obtained with FSW was investigated. FSW joints that investigated were performed on similar and dissimilar Al alloys. Fracture performance of FSW weld joints was assessed with the account of the test results.

## II. EXPERIMENTAL

Commercial AA 2014 and AA 6063 aluminium alloy materials were used in this study. The thicknesses of these aluminium alloy plates were 4.35mm for AA2014 and 5.44 mm for AA6063. The plates were machined out in 200 mm lengths and 100 mm widths. The composition Table I and mechanical properties of the studied material are listed in Table II.

The shoulder diameter and threaded pin height of the tool were 15 and 6 mm, respectively. The diameter of the threaded pin was 5 mm (M5 screw). The shoulder was formed as a straight surface. Schematic illustration of the FSW tool and lap joint application, which was used in this study, is given in Fig. 1(a). The pre-machined plates were fixed rigidly on the table of the vertical semiautomatic milling machine for lap joint FSW as seen in Fig. 1 (b) and (c). Then tool was moved along the joint line. All of the FSW lap joints were obtained with 1200 rpm tool rotation and 60 mm/min traverse speed. Lap joints were welded as AA2014+ AA2014, AA6063+ AA6063 and AA6063+ AA2014 combinations. Ten shearing samples were extracted from the lap welded plates.

A special tensile shearing test device was designed as seen in Fig. 2 (a) and (b) and manufactured to perform shearing

tensile tests on FSW lap joints. The dimensions of the shearing tensile test specimens that were machined from the FSW lap welded joints are given in Fig. 3 and 4. Surface of the weld was cleaned by milling. The thicknesses of

aluminium alloy plates used in the study were 4.35mm (t1), for AA 2014 and 5.44mm (t2) for AA 6063. D is the diameter of the pin (M5 = 5mm).

TABLE I  
 CHEMICAL PROPERTIES OF ALUMINIUM ALLOYS.

Chemical Composition wt. %										
	Al	Mg	Si	Mn	Zn	Fe	Ti	Cu	Cr	Sn
AA 2014	Balance	0.68	0.83	0.58	-	0.24	-	4.4	0.04	0.03
AA 6063	Balance	0.7	0.4	0.1	0.1	0.35	0.1	0.1	0.1	-

TABLE II  
 MECHANICAL PROPERTIES OF ALUMINIUM ALLOYS.

Mechanical Properties				
Materials	Yield strength (MPa)	Ultimate tensile strength(MPa)	Relative elongation(%)	Vickers HardnessHV, (MPa)
AA 2014	360	410	7	105
AA 6063	130	170	8	26

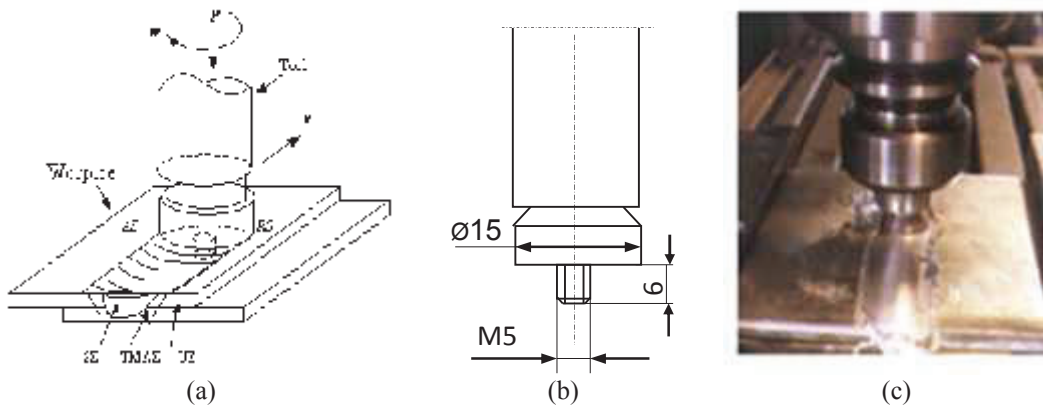


Fig. 1 Schematic illustration of FSW lap joints and FSW application on conventional vertical milling machine, (a) Schematic illustration of FSW lap joints performed in the study (SZ: stirring zone, TMAZ: thermo-mechanically affected zone – transition zone, UZ: unaffected zone – base metal, AS: advancing side, RS: retreating side), (b) Dimensions of the FSW tool, (c) FSW application on conventional vertical milling machine and fixed plates

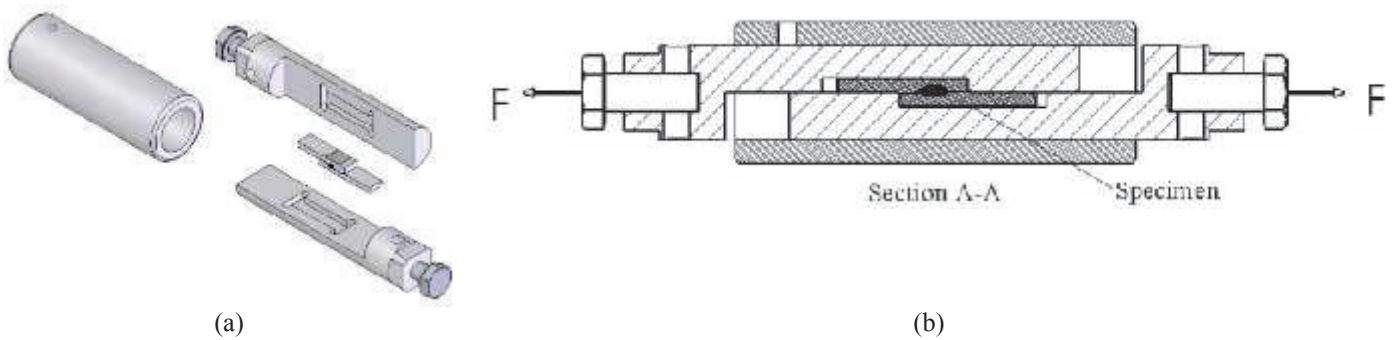


Fig. 2 Shearing tensile test device; (a) Three-dimensional model, (b) Sectional view of shearing tensile test device

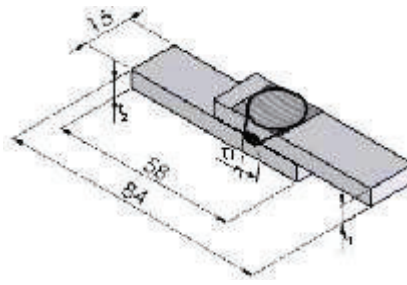


Fig. 3 Lap welded joint specimen (The thicknesses of aluminium alloy plates used in the study were 4.35mm (t1), for AA 2014 and 5.44mm (t2) for AA 6063. D is the diameter of the pin (M5 = 5mm))

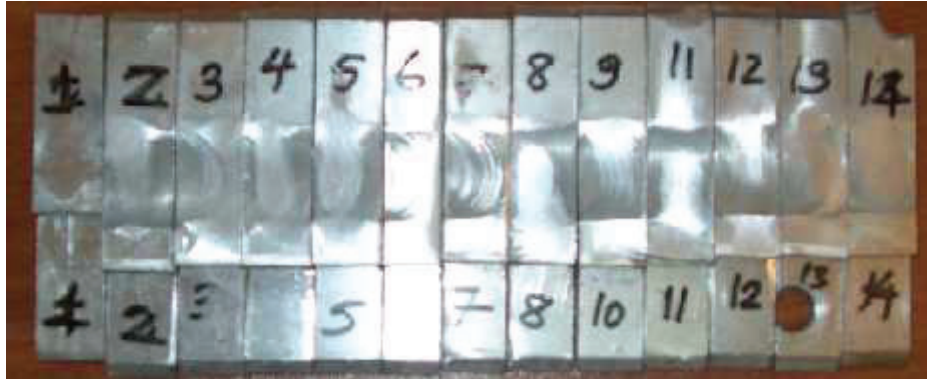


Fig. 4 Shearing tensile test specimens machined out from FSW lap joints. All of the FSW lap joints were obtained with 1200 rpm tool rotation and 60 mm/min traverse speed (1,2,3,4 samples are AA2014+ AA2014; 5,6,7,8,9 samples are AA6063+ AA6063 and 11,12,13,14 samples are AA6063+ AA2014 combinations)

Hardness of FSW joints were measured on the weld centre of sheared surfaces after shearing tensile tests. The sheared surfaces were polished with 80 – 1000 mesh abrasive paper and etched using Keller's etching then the hardness was measured with Vickers hardness tester using 1.96N (HV<sub>0.2</sub>). The metal of the welded plates is stirred up at the interface of the plates. Stirring of two metal caused hardness difference at the joint interface of two metals. Hardness difference can be explained with the different stirring effect between advancing side and retreating side of welding. Hardness values of studied materials before welding are given in Table 2. Hardness values measured on the sheared surfaces of joints are given in Fig. Fig. 5, 6, 7, 8 and 9.

### III. RESULTS

The variation of shear tensile stress with the Vickers hardness HV<sub>0.2</sub> measured on the sheared surface is given in Fig. 5, 6, 7, 8 and 9. The metal of the welded plates is stirred up at the interface of the plates. This situation explains that the stirring of the metal at the interface of the two plates affects the hardness of the stirred metal.

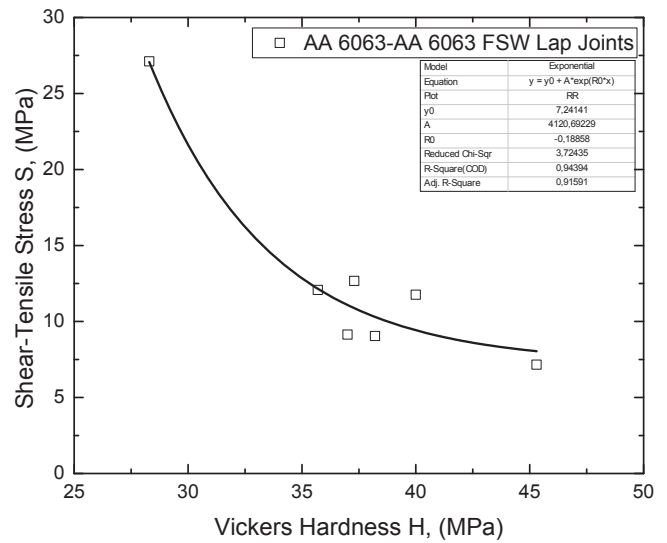


Fig. 5 Shear tensile stress variation with hardness in FSW lap joints of AA 6063-AA 6063

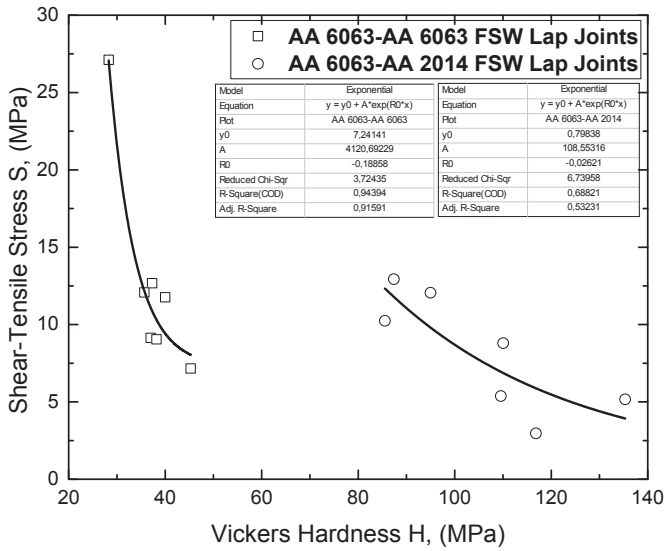


Fig. 6 Shear tensile stress variation with hardness in FSW lap joints of AA 6063-AA 6063 and AA 6063-AA 2014

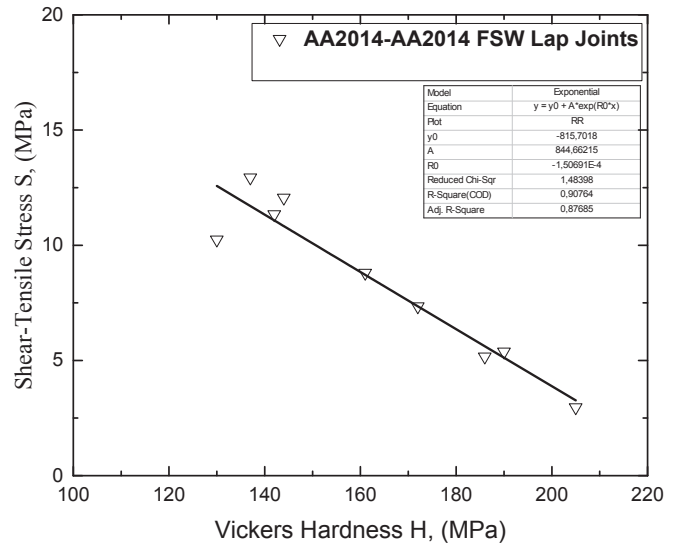


Fig. 8 Shear tensile stress variation with hardness in FSW lap joints of AA 2014-AA 2014

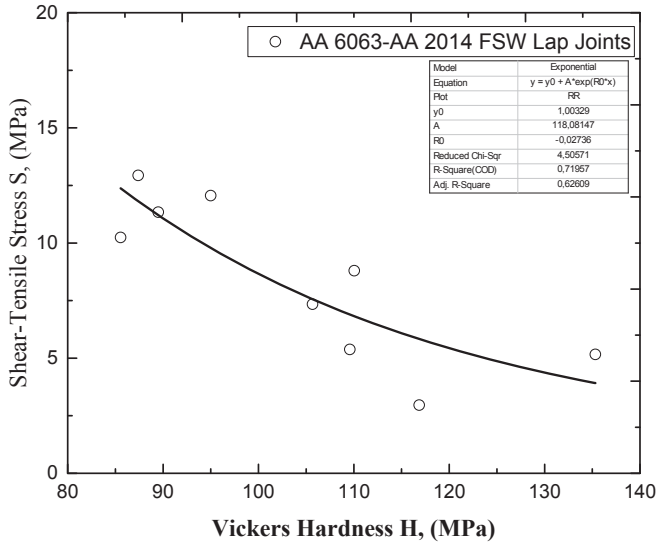


Fig. 7 Shear tensile stress variation with hardness in FSW lap joints of AA 6063-AA 2014

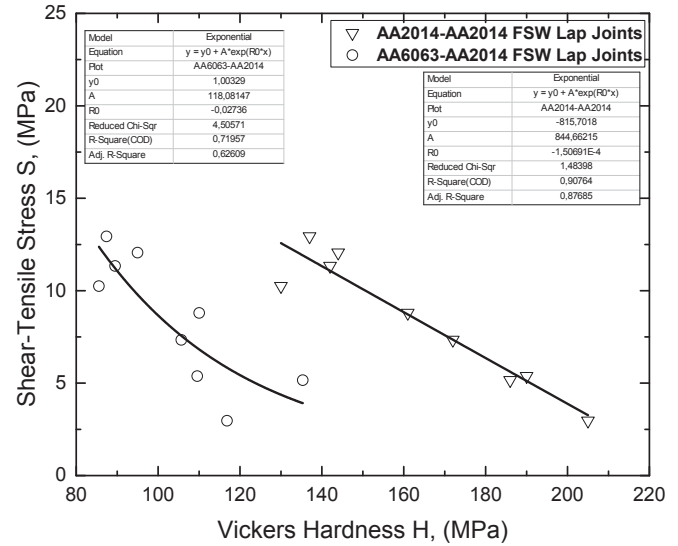


Fig. 9 Shear tensile stress variation with hardness in FSW lap joints of AA 2014-AA 2014 and AA 6063-AA 2014

#### IV. CONCLUSIONS

From the results given above, the following conclusions can be drawn.

- The amount of Si alloy element affects the shear tensile stress of the FSW lap joints.
- Increase in the Si ratio in Al alloy reduces the shear tensile stress.
- Stirring of the materials at the interface of welded plates affects the shear tensile stress of lap joints.

#### REFERENCES

- [1] S.R. Ren, Z.Y. Ma, L.Q. Chen "Effect of welding parameters on tensile properties and fracture behavior of friction stir welded Al-Mg-Si alloy", *Scripta Materialia*, vol. 56(1), pp. 69-72, 2007.

- [2] S.R. Ren, Z.Y. Ma, L.Q. Chen “Effect of welding parameters on tensile properties and fracture behavior of friction stir welded Al–Mg–Si alloy”, *Scripta Materialia*, vol. 56(1), pp. 69-72, 2007.
- [3] M.K.Kulekci, F. Mendi, İ. Sevim, O.Basturk, “Shear tensile stress of friction stir-welded joints of AlCu4SiMg aluminium alloy”. *Metallurgija*, vol. 44(3), pp. 209-213, 2005.
- [4] S.R. Ren, Z.Y. Ma, L.Q. Chen “Effect of welding parameters on tensile properties and fracture behavior of friction stir welded Al–Mg–Si alloy”, *Scripta Materialia*, vol. 56(1), pp. 69-72, 2007.
- [5] H. Uzun, C.D. Donne, A. Argagnotto, T. Ghidini, C. Gambaro, “Friction stir welding of dissimilar Al 6013-T4 To X5CrNi18-10 stainless steel”, *Materials & Design*, vol. 26(1), pp. 41-46, 2005.
- [6] S.Rajakumar, C. Muralidharan, V. Balasubramanian, “Influence of friction stir welding process and tool parameters on strength properties of AA7075-T-6 aluminium alloy joints”, *Materials & Design*, vol. 32(2), pp. 535-539, 2010.
- [7] K. Colligan, “Material flow behaviour during Friction Stir Welding of Aluminium”, *Welding Research*, vol. 78(7), pp.229-237, 1999.
- [8] M.K. Kulekci and A.Sik, “Effects of tool rotation and traverse speed on fatigue properties of friction stir welded AA 1050-H18 aluminium alloy”, *Archives of Metallurgy and Materials*, vol. 51(2), pp.213-216, 2006.
- [9] J.Q. Su, T.W. Nelson, R. Mishra, M. Mahoney, “Microstructural investigation of friction stir welded 7050-T651 aluminium”, *Acta Materialia*, vol. 51(3), pp.713, 2003.
- [10] M.K. Kulekci, E.Kaluc, A. Sik, O.Basturk, “Experimental Comparison of Mig and Friction Stir Welding Processes for EN AW-6061-T6 (Al Mg-1 Si Cu) Aluminium Alloy”, *Arabian Journal for Science and Engineering*, vol.35(1B), pp. 321-330, 2010.
- [11] W.M., Thomas, K.I.Johnson, C.S. Wiesner, “Friction stir welding – recent developments in tool and process technologies”, *Advanced Engineering Materials*, vol. 5(7), pp.485-490, 2003.

# Tufalin Çelik Plaka Yüzeylerinin Temizlenmesinde Kumlama Malzemesi Olarak Kullanılabilirliği Üzerine Bir Araştırma (ISLAC'18/UHAKS18)

Mustafa Kemal Kulekci\*, Ugur Eşme<sup>+</sup>, İbrahim Sevim\*, Onur Duman<sup>+</sup>

\*Manufacturing Engineering Department, Mersin University  
33480 Tarsus, Mersin, TURKEY  
mkkulekci@mersin.edu.tr

<sup>+</sup>Manufacturing Engineering Department, Mersin University  
33480 Tarsus, Mersin, TURKEY  
esme@mersin.edu.tr

\*Mechanical Engineer Department, Karamanoglu Mehmetbey University  
Karaman, TURKEY  
isevim@kmu.edu.tr

<sup>+</sup>Manufacturing Engineering Department, Mersin University  
33480 Tarsus, Mersin, TURKEY  
mkkulekci@mersin.edu.tr

**Özet**—Dökümhanelerde, haddehanelerde sıcak slab ve kütük yüzeyinin soğutulması sırasında yüksek sıcaklık ve oksitleyici ortam nedeniyle kütük, slab ve ingot yüzeylerinde oksit tabakası oluşmaktadır. Demir çelik fabrikalarına yüzeyinde tufal tabakasıyla gelen hammaddeler veya yarı mamül malzemeler belirli metodlarla yüzeyleri temizlenerek tufalden arındırılmaktadır. Atık olarak kabul edilen tufal fabrikaların belirli yerlerinde biriktirilerek bedelsiz veya çok az bir fiyata fabrikadan uzaklaştırılmaktadır. Bu çalışmada, tufalin makine imalat sanayinde yüzey temizleme işlemlerinden birisi olan kumlama tekniğinde, aşındırıcı malzemesi olarak kullanılabilirliği araştırılmıştır. Deneysel çalışmada, çelik plaka yüzeyleri kumlama malzemesi olan Al<sub>2</sub>O<sub>3</sub> ve tufal ile kumlama tekniği ile temizlenmiştir. Temizlenen yüzeylere boyama uygulaması yapılarak boyalara yapışma mukavemeti testi (ASTM D4541 - 09e1) uygulanmıştır. En iyi boya yapışma dayanımı tufal ile temizlenen yüzeylerde elde edilmiştir. Yapılan çalışmanın sonuçları, atık malzeme niteliğinde olan tufalin yüzey temizleme tekniği olan kumlama işleminde aşındırıcı olarak kullanılarak değerlendirilebileceğini ortaya koymaktadır.

**Anahtar Kelimeler**—Kumlama, Tufal, Yüzey temizleme, Boya yapışma testi

**Abstract**— During the cooling of the hot slab and the billet surface in the casting mills, oxide layers are formed on the billet, slab and ingot surfaces due to the high temperature and oxidizing environment. Scale layer on the surface of raw materials or semifinished materials coming from iron industry are cleaned by certain methods.

The scale, which is accepted as waste, is collected at certain places of the factories and is removed without charge or very little price. In this study, the usability of scale as abrasive material in sandblasting technique which is one of the surface

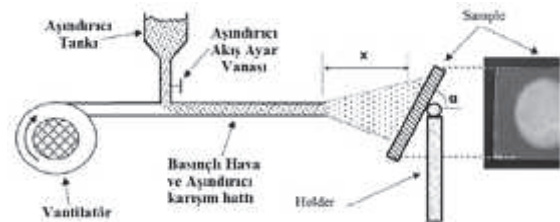
cleaning processes in the machine manufacturing industry was investigated.

In the experimental work, the steel plate surfaces were cleaned with blasting technique using Al<sub>2</sub>O<sub>3</sub> and scale abrasives. The paint adhesion test (ASTM D4541 - 09e1) was applied to the cleaned surfaces. The best paint adhesion strength is obtained on the surfaces cleaned with scale abrasives. The results of the study show that scale which is a waste material can be evaluated as abrasive in sandblasting techniques.

**Keywords**— Sand blasting, Scale, Surface cleaning, Paint pul off test

## I. GİRİŞ

Kumlamanın amacı, malzemelerin üzerinde biriken kir, yağ, pas boya ve tufal gibi atıkları yüzeyden arındırmak veya malzeme yüzeyini boyama işlemine hazırlık için arzu edilen formda pürüzlendirmektir. Malzeme yüzeyinin temizlenmesi ve pürüzlendirilmesi, aşındırıcının malzeme yüzeyine belirli bir basınç ve açı ile püskürtülmesi ile gerçekleştirilir. Kumlama yaygın, etkin ve ekonomik olması nedeniyle en çok kullanılan yüzey temizleme yöntemlerindedir [1]. Şekil 1 de kumlama tekniğinin uygulaması verilmiştir.



Şekil 1 Kumlama tekniğinin uygulaması [2]

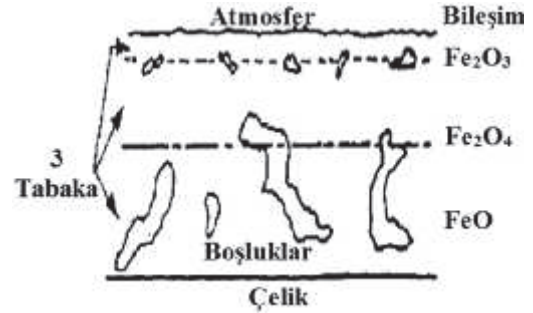
Çelik yapıların yüzeyleri kumlama tekniği ile temizlenirken, elde edilecek yüzeyin özellikleri aşındırıcı çeşidi, büyüklüğü, fırlatma basıncı veya hızı, püskürtme açısı, iş parçası ilerleme değeri, kumlama süresi vb. gibi parametrelere bağlıdır [3]. Kambham ve arkadaşları, yapmış oldukları çalışmada işleme parametrelerinin yüzey kalitesine etkisini belirlemek için aşındırıcı olarak bakır cürufu kullanmışlardır [4]. Çalışmalarında, kumlama işlemlerinde aşındırıcı cürufun püskürtme basıncını 80, 100 ve 120 PSI, fırlatma miktarını ise 180, 240 ve 360 kg/saat olarak kullanmışlardır. Yapmış oldukları deneyler sonucunda, aşındırıcı püskürtme basıncı ve fırlatma miktarı arttıkça yüzey pürüzlülüğünün arttığını belirlemişlerdir. Abrasif püskürtme yöntemleri basınçlı havanın itici etkisiyle püskürtme ve bir türbin vasıtasıyla santrifüj etkisiyle püskürtme olmak üzere iki şekilde yapılmaktadır. Bu çalışmada basınçlı hava ile püskürtme yöntemi kullanılmıştır. Basınçlı hava ile püskürtmede, basınçlı havanın basınç enerjisinin, basınç düşümüyle kinetik enerjiye dönüşmesi sonucu beraberinde taşıdığı aşındırıcı partiküllere kinetik enerji kazandırması yoluyla olmaktadır. Aşındırıcı partiküller genellikle havanın itici etkisiyle Şekil 1 de şematik gösterimi verilen sistem boyunca taşınmakta ve bir nozul vasıtasıyla püskürtülmektedir. Kumlama işleminde elde edilecek yüzey özelliklerine etki eden en önemli parametre aşındırıcı olarak kullanılan malzemenin fiziksel özellikleridir. Hazırlanacak yüzey özellikleri dikkate alınarak aşındırıcı tanelerinin sertliği temizleme hızına, temizlenmesi gereken malzemenin özelliklerine, istenen yüzey pürüzlülüğüne ve belirlenen işletme giderlerine göre değişiklik gösterir [5]. Fırlatılan taneciklerin sertliği arttıkça daha az oranda deforme olurken, parça yüzeyi üzerinde daha fazla iş yaparlar. Şekil 2 de görüldü gibi kumlanacak malzemeye de bağlı olarak belirli bir sertliğin altındaki aşındırıcıların kumlama amacıyla kullanılmaması gerekir [5]. Kumlama işlemi için uygun aşındırıcı püskürtme hızı 80 m/sn dir. Basınçlı hava ile kumlamada uygun aşındırıcı hızını temin etmek için nozuldaki hava basıncı 5 bar olmalıdır [6].



Şekil 2 Aşındırıcı sertliğine bağlı olarak aşındırıcı partikül ve parça yüzeyi arasındaki ilişki[5]

Tufaller, çelik üretimi yapılan tesislerde tavlama sonucu oluşan ince oksit tabakadır. Basınçlı su püskürtülmesiyle üründen ayrıştırılır. Tavlamanın sıcaklığına, fırın atmosferine ve süresine bağlı olarak isimlendirilmektedir [7]. Tufal; haddehanelerde yanma olayında gereğinden fazla olarak verilen hava, yanmanın anormal olmasını, fırının soğumasını,

yakıt tüketim miktarının artmasına neden olmaktadır. Sıcaklık-zaman ve oksijen ölçüsü başta olmak üzere çelik malzemenin oksidasyonuna birtakım nedenler etkindir. Fe-C alaşımlarının tavlama sırasında yüzeyde oluşan 3 ayrı demir oksit fazı katmanlı bir yapı oluşturarak meydana gelecek metalden ayrılmaya çalışırlar. Bu tabaka Tufal olarak tanımlanmaktadır. Türkiye'deki haddehanelerde miktarı tam olarak bilinmemekle birlikte üretilen çeliğin %4-5'i oranında tufal olduğu varsayılmaktadır. En basit tufal demir oksit (FeO)'dur. Isıtılan yüzey sıcaklığı 900 °C yi geçtiği anda tufalleşme de hızlanır. Meydana gelen tufal kalınlığının %80 wüstit, %18 Manyetit ile %2 si  $\alpha$ -Hematit'tir. Şekil 3 de demir esaslı malzemelerin yüzeyinde oluşan tufal tabakası ve yapısı gösterilmektedir [8].



Şekil 3 Tufal tabakası ve yapısı[8]

Tufal düşük ısı iletkenliğinden dolayı çelik yarı mamulün ısı kaybını azaltmak için izolasyon rolü oynar. Tavlama çelik yarı ürünün yüzeyindeki küçük hatalar oluşan tufal ile kaybolur [9].

Metal yüzeyinden itibaren sırasıyla aşağıda belirtilen tabakalar oluşmaktadır.

Wüstit (FeO); metale en yakın yüzeyde oluşan, düşük oksijen miktarına sahip olan oksit tabakasıdır. Tufaldeki miktarı sıcaklık artmasıyla artmaktadır. Çelik yüzey sıcaklığı 700 °C yi aştığında tufal tabakasının %95'ini ihtiva eder. Çelik ve tufalin diğer fazlarına göre 1370-1425 °C düşük ergime fazlarına sahiptir. Tabakanın çelik yüzeyinde erimesi, tufalleşme hızını arttırarak yüzey kalitesini bozar aynı zamanda yakıt sarfiyatını arttırarak fırın verimliliğini azaltır.

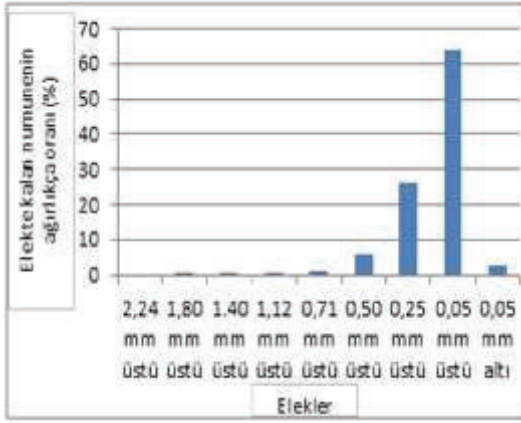
Manyetit (Fe<sub>2</sub>O<sub>4</sub>); tufal katmanlarında bir ara fazdır. Çelik yüzey sıcaklığı 500 oC altında olduğunda tufal ağırlıklı olarak manyetitten oluşur. Sıcaklık 700 °C nin üstüne çıktığında wüstit oluşumu başlar. Yüksek sıcaklıklarda manyetit, tufal yapısının %4 ünü oluşturur. Manyetit Wüstitten daha aşındırıcıdır ve serttir.

Hematit (Fe<sub>2</sub>O<sub>3</sub>); tufalin dış yüzey tabakasıdır. Hematit, çelik yüzey sıcaklığı 880 °C'ye eriştiği zaman oluşur. Tufal tabakasını %1'ini oluşturur. Manyetit gibi, hematit de sert ve aşındırıcıdır [10].

Bu çalışmada makine imalat sanayinde kumlama tekniğinde kullanılan aşındırıcı malzemelere alternatif olarak tufal adını verdiğimiz belirli bir sertlikteki atk malzemenin kullanılabilirliği araştırılmıştır.

## II. MATERYAL VE YÖNTEM

Çelik üretim tesislerinde, döküm, tavlama ve haddeleme sırasında malzeme yüzeyinde oluşan tufal tabakası, malzeme kullanılmadan önce yüzeyinden uzaklaştırılır. Atık madde olarak elde edilen tufalın geri dönüşümünü sağlayan herhangi bir entegre tesis bulunmamaktadır. Bu çalışmada atık madde tufalın kuşlama malzemesi olarak kullanılabilirliğinin çalışmaları yapılmıştır. Bu amaçla demir esaslı filmaşinlerin üzerinde bulunan tufal tabakaları incelenmiştir. Filmaşin üzerinde oluşan atık madde tufaldan örnek alınıp boyut ve kimyasal analizleri yapılmıştır. Analiz sonuçları Şekil 4 de verilmiştir. Yapılan kuru elek analizi; konileme dörtleme yöntemi ile 100 gr malzeme tartılarak, Retzsch marka AS200 basic model sarsıcı elek cihazında elekler kullanılarak yapılmıştır. Elekler 80 Hertz frekansı ile 15 dakika sürekli titreşimle gerçekleştirilmiştir. Bu analize göre tufalın tane boyutunun 0,05 ile 0,50 mm aralığında olduğu görülmüştür.



Şekil 4 Elekte kalan numunelerin ağırlıkça oranları

Tufalın kimyasal analizi için SHIMADZU XRD-6000 cihazı ile Cu X-Işını tüpü ( $\lambda=1.5405$  Angstrom) kullanılmıştır. Kalitatif ve kantitatif analiz sonuçlarına göre tufal ürün dağılımı aşağıda gibi tespit edilmiştir. Tufal tabakalarının oluşumuna göre sertlik değerleri çizelge 1 de verilmiştir.

- 1- Wüstit, FeO %35,2
- 2- Magnetit Fe<sub>2</sub>O<sub>4</sub> %53,1
- 3- Hematit, Fe<sub>2</sub>O<sub>3</sub> %11,7

### ÇİZELGE 1

TUFAL TABAKALARIN SERTLİK DEĞERLERİ

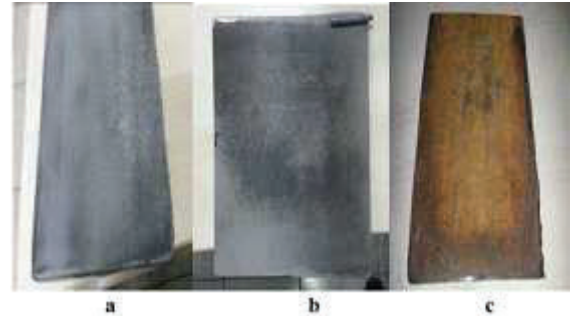
Wustit	50-55 HRC
Magnetit	60-65 HRC
Hematit	60-65 HRC

Atık madde olarak ortaya çıkan tufalın kuşlama malzemesi olarak kullanılabilirliğini araştırmak amacıyla piyasada kuşlama yapmak için yaygın olarak kullanılan havalı kuşlama Şekil 5 de verilen kuşlama makinesi kullanılmıştır.



Şekil 5. Havalı Kuşlama Makinesi

Bu makinenin depo kısmına aşındırıcı kuşlama malzemesi doldurulur ve basınçlı hava yardımıyla pastan, kirden arındırılmak istenen yüzeye aşındırıcı malzeme yollar. Böylece parça yüzeyinde istenilen temizlik elde edilmiş olur. Bu çalışmada aynı ebatlarda kesilen 3 adet yüzeyi paslı plakanın birincisini havalı kuşlama makinesi kullanılarak kuşlama malzemesi olan alüminyum oksit (Al<sub>2</sub>O<sub>3</sub>) kullanılarak temizlenmiştir. İkinci paslı plaka kuşlama malzemesine alternatif olarak kullanacağımız atık madde tufal kullanılarak temizlenmiştir. Üçüncü paslı plakaya hiçbir işlem uygulanmamıştır. Şekil 6 de atık madde tufal ile temizlenmiş a parçasının, kuşlama malzemesi olan alüminyum oksit ile temizlenmiş b parçasının, ve üzerinde hiçbir işlem uygulanmamış c parçasının resimleri verilmiştir.



Şekil 9 (a) tufal ile temizlenmiş, (b) alüminyum oksit ile temizlenmiş (Al<sub>2</sub>O<sub>3</sub>), (c) hiçbir işlem uygulanmamış parça resimleri

Yüzey temizliği işlemi yapıldıktan sonra aynı oranlarda boyama işlemine tabii tutulmuş sac levhalar üzerindeki boyalara ASTM D4541 - 09e1 standardına göre, boya yapışma mukavemeti testi uygulanmıştır. Şekil 7 de boyama işlemine tutulmuş parçaların resimleri verilmiştir.



Şekil 7. a) Tufal ile temizlenerek boyama işlemine tabii tutulmuş parça

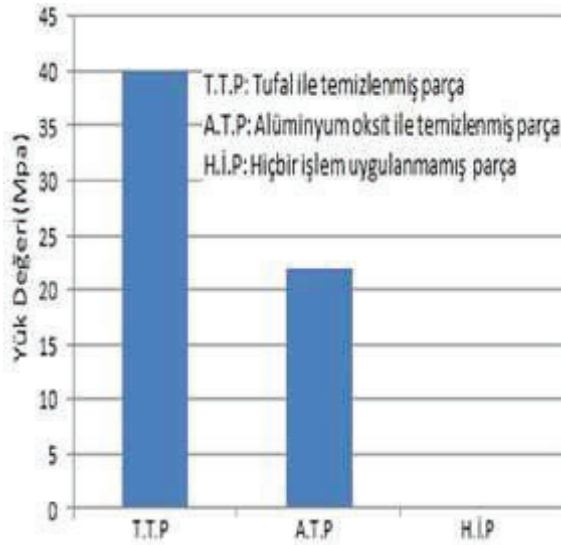


Şekil 7. b) Alüminyum oksit ile temizlenerek boyama işlemine tabi tutulmuş parça



Şekil 7 c) Hiçbir işlem uygulanmadan boyama işlemine tabi tutulmuş parça

Boya yapışma mukavemeti testi cihazı, kaplamaların, metal, ahşap, beton ya da benzer yüzeyler üzerindeki yapışmalarını test eder. Tufal ile temizlenmiş numuneye 40 MPa değerinde bir yük uygulandığında boyanın kalktığı saptanmıştır. Alüminyum oksitle temizlenmiş numunede ise 22 MPa'lık bir kuvvete maruz kaldığında boyanın kalktığı saptanmıştır. Üzerinde herhangi bir kumlama işlemine tabi tutulmamış paslı levhada ise boyamaya elverişliliği son derece kötü ve okunan değer 0 MPa olduğu görülmüştür. Yapılan deneyin sonuçları şekil 8 de gösterilmiştir.



Şekil 8 Boya yapışma mukavemeti test sonuçları

### III. TARTIŞMA VE SONUÇ

Ülkemizde çelik üretim tesislerinde döküm tavlama ve haddelme sırasında açığa çıkan tufalin geri dönüşümünü sağlayan herhangi bir entegre tesis bulunmamaktadır. Yapılan boya yapışma mukavemet test sonuçlarına göre işletmelerde ortaya çıkan ve kullanılmayan atık madde olan tufalin

kumlama malzemesi olarak kullanılan alüminyum oksitten daha etkili olduğu ortaya çıkmıştır. Tufal ile temizlenen çelik sac yüzeyine uygulanan boyanın yapışma mukavemet değeri 40 MPa, Al<sub>2</sub>O<sub>3</sub> ile temizlenen yüzeydeki boyanın yapışma mukavemet değeri 20 MPa'dır. Deneysel çalışmanın sonuçları tufalin yüzey temizleme işlemlerinde kullanılan aşındırıcılar yerine kullanılarak değerlendirilebileceğini göstermektedir.

### TEŞEKKÜR

Güney Çelik Hasır ve Demir Mam. San. Tic. A.Ş.'ye çalışmaya vermiş oldukları destek için teşekkür ederiz.

### REFERANSLAR

- [1] US Army Corps of Engineers. "Surface Preparation Painting," New Construction and Maintenance, Washington, ABD., 4-15, 1995.
- [2] The Researchgate website (18.04.2017). [Online]. Available: [https://www.researchgate.net/profile/Nourredine\\_Bouaouadja/publication/248455726/figure/fig2/AS:298300168261636@1448131710606/fig-2-Schematic-representation-of-the-used-sandblasting-apparatus.png](https://www.researchgate.net/profile/Nourredine_Bouaouadja/publication/248455726/figure/fig2/AS:298300168261636@1448131710606/fig-2-Schematic-representation-of-the-used-sandblasting-apparatus.png)
- [3] Çelik Granül Sanayii A.Ş., "Etkin temizlik için aşındırıcı seçimi," Çelik Granül Sanayii A.Ş. Teknik Bülten, 2: 1-4, 2002.
- [4] K.Kambham, S. Sangameswaran, S.R. Datar, B. Kura, "Copper slag: Optimization of productivity and consumption for cleaner production in dry abrasive blasting." Journal of Clean Production, 15: 465-473, 2007.
- [5] M. E. Satici, "Kumlama işleminin ve bu işleme etkiyen parametrelerin incelenmesi," Yüksek Lisans Tezi, İstanbul Teknik Üniversitesi, Türkiye, 2004.
- [6] The Guide to Impact Treatment, Metabrasive Limited Manufacturers of High Performance Metallic Abrasives Carponfield Works, Bilston, West Midlands, England
- [7] A. O. Saud, "Recycling steel mill scale as fine aggregate in cement mortars," European Journal of Scientific Research ISSN 1450-216X Vol.24 No.3, pp.332-338, 2008.
- [8] Ö. L. Çakıroğlu, Sanayi tav fırınlarında çelik yüzey oksidasyonu ve verimliliğe etkileri, İstanbul Teknik Üniversitesi doktora tezi, 1995.
- [9] W.Haitao, Reduction Kinetics of Iron Ore Concentrate Particles Relevant to A Novel Green Ironmaking Process, 2011.
- [10] G., Önkibar, Entegre demir-çelik tesisi tufalinden doğrudan redüklenme yöntemi ile ham demir üretimi, Yüksek Lisans Tezi, Sakarya Üniversitesi, 2006.

# Thermal Energy Storage Properties of Vermiculite Based-Composite PCM With Carbon Nanotubes Additive For Thermoregulation of Buildings

Ahmet SARI<sup>a,b,\*</sup>, Gökhan HEKİMOĞLU<sup>a,\*</sup>, Alper BİÇER<sup>c</sup>

<sup>a</sup>Karadeniz Technical University, Metallurgical and Material Engineering, 61080, Trabzon, Turkey

<sup>b</sup>Centers of Research Excellence, Renewable Energy Research Institute, KFUPM, 31261, Dhahran, KSA

<sup>c</sup>Department of Chemistry, Gaziosmanpaşa University, 60240 Tokat, Turkey

\*Corresponding authors: ghekimoglu@ktu.edu.tr; G. Hekimoğlu; ahmet.sari@ktu.edu.tr (A.Sari)

**Abstract**—As different from the literature, our challenge is to find an effective key for leakage problem and low thermal conductivity drawback without noticeably changing LHTES capacity of fatty acid eutectic mixture (FAcEM) (capric acid(CA)-stearic acid(SA)) used as phase change material (PCM). Expanded vermiculite (ExpV) was selected as good supporting material for this PCM because of many advantageous properties such as high surface area, excellent compatibility, light weightness, porosity and low cost etc [34-36]. The effects of CNTs additive on the chemical/morphological structures and LHTES properties of the thermal enhanced composite PCMs (CPCMs) were investigated by SEM, FT-IR, and DSC techniques. The DSC results showed that the ExpV/FAcEM/CNTs have melting temperature in the range of 24.35-24.64°C and latent heat between 76.32 and 73.13 J/g. The thermal conductivity of the ExpV/FAcEM/CNTs was increased as 83.3%, 125.0% and 258.3% by CNTs doping, 1, 3 and 5 wt%. The enhanced thermal conductivity also reduced appreciably the heat charging and discharging times of the CPCMs without notably influencing their LHTES properties. Furthermore, the thermal cycling test and TGA findings proved that all fabricated composites had admirable thermal durability, cycling LHTES performance and chemical stability. In addition to these beneficial properties, the ExpV/FAcEM/CNTs produced as CPCMs can be integrated with ordinary construction materials to produce different building elements used in radiant floor heating systems, insulation and ceiling panels or walls for passive solar cooling purposes depending on the climatic circumstances.

**Keywords**—Fatty acid, eutectic mixture, CNTs, expanded vermiculite, PCM, thermal conductivity, thermal energy storage

## I. INTRODUCTION

In recent years, with the rapid economic development, energy shortage and environmental issues have become increasingly serious. Therefore, it is an important topic to improve energy utilization efficiency and protect environment. Energy storage is an essential method to match the thermal energy supply and demand in time or space. Latent heat thermal energy storage (LHTES) can achieve a higher energy storage density a smaller size of the system and a narrower temperature range during the melting and freezing process of phase change materials (PCMs). PCMs have attracted much attention for their various thermal energy storage (TES) applications in

building energy efficiency, solar heating systems and air-conditioning systems [1,2].

Fatty acids or eutectic mixtures of them have been preferred as organic PCMs for passive solar TES applications because of their favored and re-obtainable LHTES properties [3]. However, direct operation of these PCMs not only allows chemical interaction with near environment but also leads to leakage problem during solid-liquid phase change. To avoid this intricacy, they have been prepared in macro or microcapsule [4]. However, the synthesis of such type capsule materials is relatively more complex and needed high cost and generally resulted in PCMs with low LHTES capacity. Another option is creating leakage-resistive composite PCMs by combination of them with lightweight, porous and low cost construction materials. On the other hand, another drawback of fatty acids is low thermal conductivity (0.16-0.20 W/mK), which strongly influences their heat charging-discharging rates [5]. Moreover, their incorporation with especially clay based-building matrixes in stabilized form can cause a significant decrease in thermal conductivity. Therefore, the doping of such a type composite with high thermal conductivity materials is an effective approach in terms of enhancing its thermal conductivity. On the other hand, low density, large surface, high stability and resistance for corrosion and ultrahigh thermal conductivity (reach up 4000 /m.K for Single-walled CNTs (SWCNTs) and 2000 W/mK for multi-walled CNTs (MWCNTs) play important role on their usage as doping agents for heat transfer enhancement within PCMs or composite PCMs [6].

In this work, the effects of CNTs additive on the chemical/morphological structures and LHTES properties of the ExpV/FAcEM/CNTs prepared as thermal enhanced composite PCMs (CPCMs) were investigated. The fabricated CPCMs were characterized by SEM, FT-IR, and DSC techniques. The thermal conductivity of the ExpV/FAcEM/CNTs was increased by CNTs doping, 1, 3 and 5 wt%. The enhanced thermal conductivity was also also verified by comparing heat charging and discharging times of the CPCMs with/without CNTs. Furthermore, the thermal cycling test was subjected to the CPCMs and thermal cycling reliability and chemical stability were studied.

## II. EXPERIMENTAL

In the first stage, the ExpV/FAcEM/CNTs composites were prepared using vacuum impregnation method in different mass fractions of FAcEM from 20 to 50%. The maximum holding ratio of FAcEM was determined by applying leakage test. After this test, the maximum mass fraction of FAcEM into the prepared form-stable CPCMs corresponds to 40wt%.

In the second step, the ExpV/FAcEM/CNTs composites were prepared. The CNTs in the specified amount was dispersed in acetone under intensive ultrasonic treatment. Then, the previously prepared form-stable ExpV/FAcEM composite was added to CNTs/acetone suspension. To guarantee the dispersion of CNTs uniformly into ExpV/FAcEM composite, the suspension was continually stirred for 3 h with a magnetic stirrer. In order to remove the acetone thoroughly, the obtained mixture was maintained in an oven at 60°C for 6h. Three kind of composite PCM were prepared ExpV/FAcEM/CNTs (1wt%), ExpV/FAcEM/CNTs(3wt%) and ExpV/FAcEM/CNTs (5wt%) by arranging the amount of the added CNTs. The leakage test results confirmed that the composite PCM including 40 wt% FAcEM did not show any leakage behavior.

The chemical characterizations of the ExpV, the developed FAcEM, ExpV/FAcEM and ExpV/FAcEM/CNTs composites were made by using Jasco 430 model FT-IR spectrometer. The sample was prepared by mixing the composite with KBr. The spectrum was obtained at wavenumber range between 4000 and 400  $\text{cm}^{-1}$  with resolution of 4  $\text{cm}^{-1}$ .

The microstructures of the prepared CPCMs were investigated by using a LEO 440 model SEM instrument. Before the SEM analysis, tiny amount of sample was adhered on a copper SEM stub by conductive adhesive and gold-coated in a high vacuum evaporation coating machine.

The LHTES properties of the eutectic mixture and the fabricated ExpV/FAcEM/CNTs were measured at the same heating/cooling rate of 3°C  $\text{min}^{-1}$  by DSC technique (Perkin Elmer-JADE model). The measurement was repeated three times and the accuracy in the temperature and enthalpy data was calculated as  $\pm 0.01^\circ\text{C}$  and  $\pm 0.61 \text{ J/g}$ , respectively.

By using a thermal cycler (BIOER TC-25/H model), the developed CPCM was subjected to a thermal cycling test including 500 melting/freezing cycles. After 500 cycling treatments, the DSC analyses for CPCMs were repeated under the same analysis conditions applied for the uncycled composite samples. The possible changes in the LHTES properties after the cycling test were determined by DSC analysis. To have information about the chemical stability of CPCMs, the FT-IR spectrum bands taken before and after the cycling test were compared.

## III. RESULTS AND DISCUSSIONS

### A. Characterization of the CPCMs

Figure 1 (a-c) shows that the SEM analysis results of SF and CPCM doped with 5.0 wt% CNT.

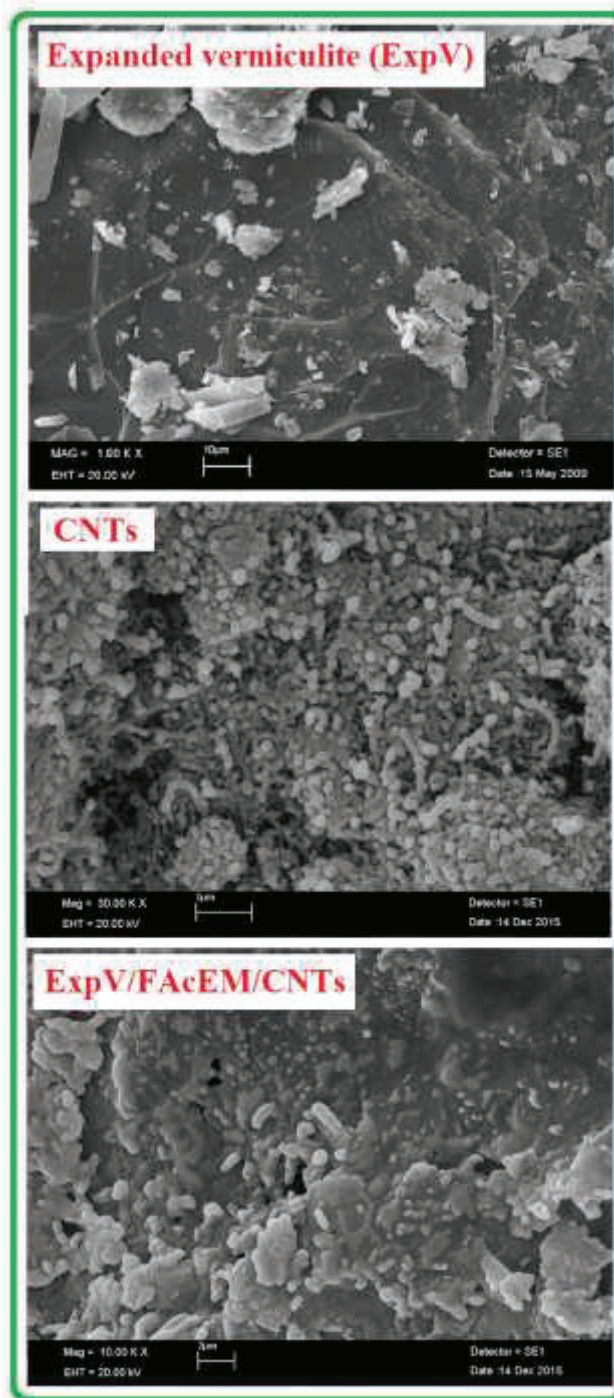


Fig. 1. SEM photographs of (a)ExpV, (b)CNTs (c) ExpV/FAcEM/CNTs

As shown in Fig. 1, the ExpV surface is mainly composed of micro- and nano-sized cracks and pores. As can be clearly seen from the microstructure of CPCMs containing 5.0 wt.% CNTs. FAcEM has effectively holded into the cracks of the structure of ExpV and no leakage was observed despite the sample being heated as a result of electron beams during SEM analysis. Thus, the hybrid structure consisted of SF and CNTs to prevent FAcEM leakage due to capillary and surface tension forces between them.

Figure 2 shows the FT-IR spectra of the prepared CPCMs and its pure components. According to the ExpV spectrum, the characteristic peaks observed at  $3200-3600\text{ cm}^{-1}$  and  $1652\text{ cm}^{-1}$  are considered to be the stretching and bending vibrations of the OH group, respectively. The stretching vibration bands of Si-O and of Si-O-Si are detected at  $1096\text{ cm}^{-1}$  and  $463\text{ cm}^{-1}$ . As clearly observed from the spectrum of FAcEM, the peaks at  $2938\text{ cm}^{-1}$  and  $2876\text{ cm}^{-1}$  are attributed to the symmetrical stretching bands of  $-\text{CH}_3$  and  $-\text{CH}_2$  bands, respectively.

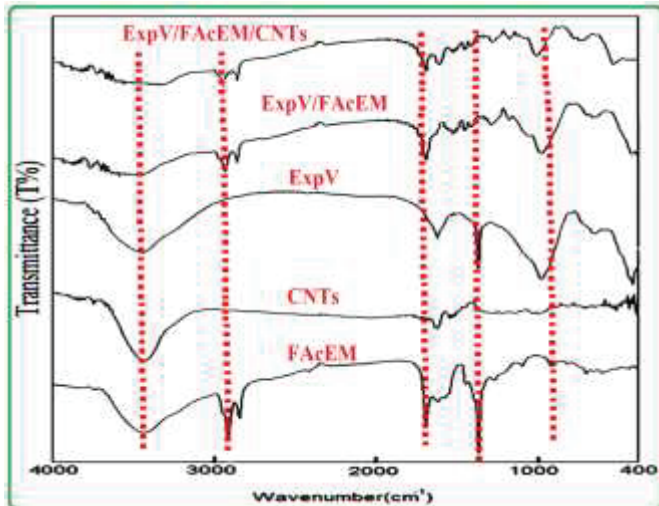


Fig. 2. FT-IR spectra of the CPCMs and its pure components

The symmetrical stretching vibration band at  $1712\text{ cm}^{-1}$ , while the peaks at  $1469$  and  $1318$  and  $942\text{ cm}^{-1}$  are related with C=O group. In the spectrum of CNTs, the bands at  $3456\text{ cm}^{-1}$ ,  $2842\text{ cm}^{-1}$  and  $2921\text{ cm}^{-1}$  are evaluated by the symmetric and asymmetric stretching vibration of O-H and C-H groups. Furthermore, the peaks at  $1628\text{ cm}^{-1}$  and  $1032\text{ cm}^{-1}$  refer to asymmetric stretching vibrations of the  $-\text{C}=\text{C}-$  and C-O groups. The minor changes in the wave length of some characteristic bands are due to poor physical electrostatic attractions. Moreover, there is no new peak, suggesting that there is no chemical reaction between the components of the CPCMs.

#### B. LHTES properties and cycling reliability of the CPCMs

Fig. 4 shows the DSC curves of DSC curves of FAcEM and ExpV/FAcEM/CNTs. According to the DSC thermograms and Table 1, the melting and freezing temperatures of the prepared CPCMs were measured in the range of  $24.35-24.54^\circ\text{C}$ . Compared with FAcEM, the phase change temperatures of ExpV/FAcEM and ExpV/FAcEM/CNTs were slightly decreased because of the interaction forces between FAcEM molecules and ExpV [8-10]. As also seen from the LHTES data in Table 1, its latent heat capacity was measured in the range of about  $73-76\text{ J/g}$ . Consequently, the LHTES properties make them suitable materials for regulating/controlling indoor temperature of buildings.

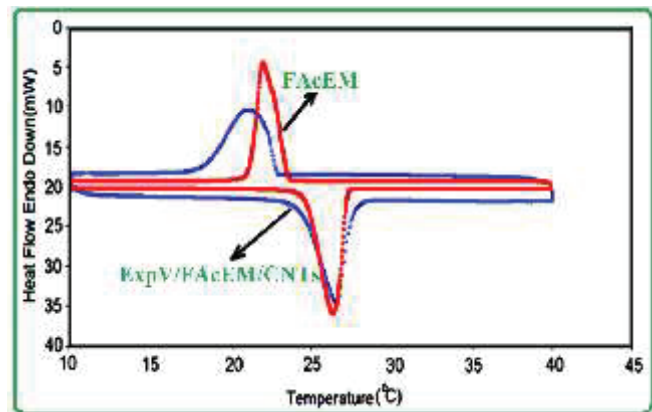


Fig. 3. DSC curves of FAcEM and ExpV/FAcEM/CNTs

TABLE 1.  
 The measured LHTES data of ExpV/FAcEM and ExpV/FAcEM/CNTs

Material	Melting temperature (°C)	Latent heat of melting (J/g)	Freezing temperature (°C)	Latent heat of freezing (J/g)
FAcEM	24.72	184.43	23.12	-183.12
ExpV/FAcEM	24.54	76.32	23.01	-74.56
ExpV/FAcEM/CNTs	24.35	73.13	23.71	-72.27

On the other hand, when compared with other composites reported in literature, it can be remarkably noted that the ExpV/FAcEM/CNTs have higher latent heat capacity than most of the prepared CPCMs in this work.

#### C. Long-term thermal and cycling stability of the CPCMs

After the cycling test including 500 heating/cooling processes, the chemical structure, phase change temperatures and latent heat capacities of the the ExpV/FAcEM/CNTs were compared by examining the FTIR and DSC results.

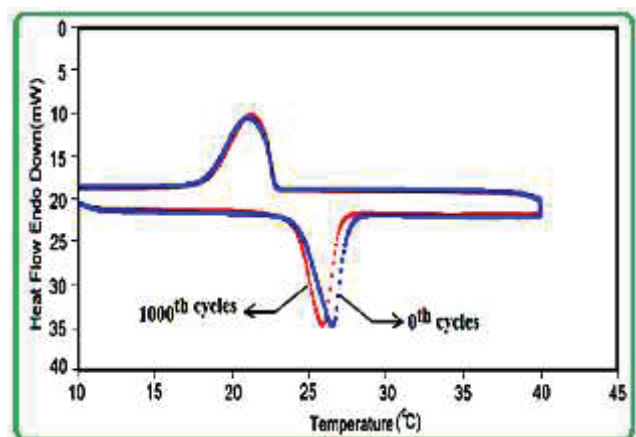


Fig. 4. DSC results of the ExpV/FAcEM/CNTs after thermal cycling

Figure 4 and Figure 5 shows the FT-IR results of the ExpV/FAcEM/CNTs obtained after 500 thermal cycling, respectively.

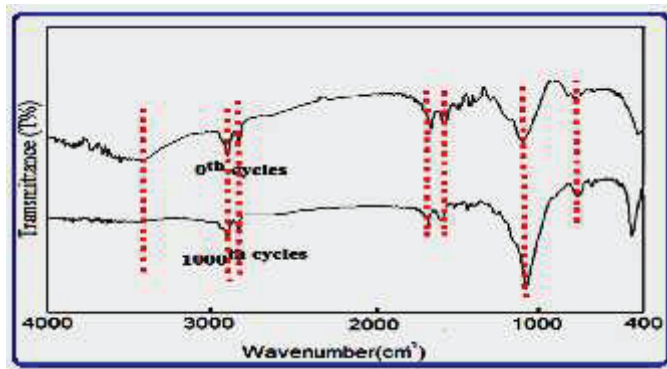


Fig. 5. FT-IR results of ExpV/FAcEM/CNTs after thermal cycling

Based on Figure 4, it was remarkably noted that the changes occurred in the LHTES after cycling process are not in considerable level for building TES applications. Moreover, As seen from the FT-IR spectra of the ExpV/FAcEM/CNTs, it was observed no change in the wavenumber values and shape in the main characteristic bands meaning that it has excellent chemical structure stability.

#### D. Thermal conductivity enhancement and its verification

Considering this fact, ExpV/FAcEM composite was doped by CNTs in three different mass fractions of 1.0, 3.0 and 5.0 wt%. The thermal conductivity was measured as 0.15 W / mK for FAcEM; 0.22, 0.37 and 0.43 W/mK for ExpV/FAcEM/CNTs (1.0% by weight), ExpV/FAcEM/CNTs (3.0 wt%) and ExpV/FAcEM/CNTs(5wt%), respectively. This further development could be attributed to the high thermal conductivity of the CNTs.

TABLE 2.

The reductions occurred in the heating charging and discharging times of the CPCMs with CNTs

	ExpV/FAcEM	CNTs (1.0%)	CNTs (3.0%)	CNTs (5%)
Charging Times (s)	300	225	200	180
Discharging Times (s)	350	260	170	90

On the other hand, in order to evidently see the influence of the increment in the thermal conductivities on the heat absorbing and releasing times of CPCMs were recorded vs

time (Table 2). Compared to the CPCM, the reductions occurred in the times are clear evidence of the enhancement in their thermal conductivities.

#### IV. CONCLUSIONS

The FAcEM eutectic mixture was impregnated into ExpV in maximum fraction of 40 wt% by vacuum technique. Three kinds of thermal enhanced CPCMs (in mass fraction of 1, 3 and 5 wt%) were prepared by doping CNTs. The composite PCM with/without CNTs exhibited worthy cycling chemical stability and LHTES performance. The thermal conductivity of form-stable CPCM was increased significantly. It was also concluded that especially fabricated thermal enhanced CPCMs have a great potential for the fabrication of new construction materials in different types for thermoregulation of building envelopes.

#### ACKNOWLEDGMENT

Authors would like to thank Scientific Research Project Commission of the Gaziosmanpaşa University (Project Number: 2016/75). Authors would also like to thank Karadeniz Technical University and King Fahd University of Petroleum & Mineral University because of their laboratory facilities during the handling this work.

#### REFERENCES

- [1] V.V. Tyagi, D. Buddhi, PCM thermal storage in buildings: A state of art, *Renewable & Sustainable Energy Reviews*, 11, 1146-1166, (2007).
- [2] A. Sharma, V.V. Tyagi, C.R. Chen, D. Buddhi, Review on thermal energy storage with phase change materials and applications. *Renewable & Sustainable Energy Reviews* 13, 318-45, (2009).
- [3] M. Kenisarin, K. Mahkamov, Solar Energy storage using phase change materials. *Renewable & Sustainable Energy Reviews*, 11, 1913-65, (2007).
- [4] Y. Yuan, N. Zhang, W. Tao, X. Cao, Y. He, Fatty acids as phase change materials: A review, *Renewable & Sustainable Energy Reviews* 29, 482-498, (2014).
- [5] D. Rozanna, T.G. Chuah, A. Salmiah, T.S.Y. Choong, M. S a'ari, Fatty acids as phase change materials (PCMs) for thermal energy storage: a review. *International Journal of Green Energy*; 1, 495-513, (2004).
- [6] V. Kumaresan, R. Velraj, S.K. Das, The effect of carbon nanotubes in enhancing the thermal transport properties of PCM during solidification. *Heat Mass Transfer*, 48, 1345-55, (2012).
- [7] B. Xu, H. Ma, Z. Lu, Z. Li, Paraffin/expanded vermiculite composite phase change material as aggregate for developing lightweight thermal energy storage cement-based composites. *Applied Energy* 160, 358-367, (2015).
- [8] A Sari, A Karaipekli. Preparation, thermal properties and thermal reliability of palmitic acid/expanded graphite composite as form-stable PCM for thermal energy storage. *Sol. Energy Mater. Sol. Cells* 93. 571-576 (2009).
- [9] D. Zhang, Z. Li, J. Zhou, K. Wu. Development of thermal energy storage concrete. *Cem. Concr. Res.* 34:927-34 (2004).
- [10] S. Memon, W. Liao, S. Yang, H. Cui, S. Shah. Development of composite PCMs by incorporation of paraffin into various building materials. *Mater.* 8:499-518 (2015).

# Form-Stable Attapulgite/PCM Composite For Thermal Energy Storage in Building Envelopes

Ahmet SARI<sup>a,b,\*</sup>, Gökhan HEKİMOĞLU<sup>a,\*</sup>, Alper BİÇER<sup>c</sup>

<sup>a</sup>Karadeniz Technical University, Metallurgical and Material Engineering, 61080, Trabzon, Turkey

<sup>b</sup>Centers of Research Excellence, Renewable Energy Research Institute, KFUPM, 31261, Dhahran, KSA

<sup>c</sup>Department of Chemistry, Gaziosmanpaşa University, 60240 Tokat, Turkey

\*Corresponding authors: ghekimoglu@ktu.edu.tr; G. Hekimoğlu; ahmet.sari@ktu.edu.tr (A.Sari)

**Abstract-** The integration of a eutectic mixture of two fatty acids with a lightweight traditional construction material in form-stable combination results in a composite PCM with TES ability in solar heating and cooling aims in building envelopes. In this sense, this study presents the preparation of eutectic mixture of capric acid (CA) and lauric acid (LA) and then impregnation of them into attapulgite acted as supporting material by means of vacuum technique. The chemical and morphological properties of newly developed attapulgite/(CA-LA) composites were investigated using XRD analysis, SEM and FTIR techniques. The LHTES properties and thermal reliability of the fabricated form-stable composite PCMs (F-SCPCMs) were analyzed by differential scanning calorimetry (DSC). The chemical and morphological results indicate that the attapulgite provided well capillary to the fatty acid eutectics for uniformly adsorption. The optimum absorption ratio of CA-LA was confined by attapulgite in the mass fraction of 46 wt% without observing their melted leakage. The eutectic mixture was hold into the attapulgite by only physical attraction instead of any chemical reaction. As seen from Fig. 1, the DSC analysis results revealed that the produced melting temperatures of the attapulgite/(CA-LA) composite PCM were measured as 21.97°C and the latent heat capacities of them were determined 66.24 J/g. These LHTES properties were suitable for heating and cooling purposes in buildings. The produced F-SCPCM shows good thermal and chemical reliability after 500 times thermal cycling test. Based on all results, it was also concluded that the created three type F-SCPCMs are considered an effective LHTES building materials to reduce energy consumption.

**Keywords**—Lauric acid, Capric acid, eutectic mixture, PCM, thermal energy storage

## I. INTRODUCTION

Solar energy can be used through a thermal storage medium like phase change material (PCM) and decrease active energy consumption through heating, ventilation and air conditioning (HVAC) systems in buildings. This could be possible by applying the best suitable thermal energy storage technique (TES) to building envelopes or compartments of building such as floors, walls and ceilings [1]. TES can be applied in the form of chemical energy using latent heat and a reversible chemical reaction using phase-changeable media, which makes sense by using solid or liquid media. Precise heat storage by heating or cooling of materials is easy to do, but its use is limited to low heat storage capacity and the large

weight or volume requirement of the material used; Chemical energy storage has not yet been widely applied in practice due to both technical and economic issues. To date, most research and promising applications of TES are based on latent heat storage using PCMs.

Fatty acids as solid-liquid (S-L) PCMs are gaining attraction for TES applications in buildings because of good latent heat thermal energy storage (LHTES) characteristics such as high latent heat, suitable S-L phase change temperature, good thermal stability and thermal reliability, no phase separation, slightly subcooling, relatively little corrosivity and low price [2]. The eutectic mixtures of such type PCMs allow for tailoring their phase change temperatures according to different passive solar TES targets. Moreover, the addition of a two-fatty acid mixture with a light traditional building material into a form-stable combination aims at creating envelopes resulting in a composite PCM with TES ability to heat and cool with solar energy [3,4].

This study presents the preparation of the eutectic mixture of capric acid (CA) and lauric acid (LA) and then impregnating it into the attapulgite, which acts as a support material with the vacuum technique. Chemical and morphological properties of newly developed attapulgite / (CA-LA) composites were investigated using XRD analysis, SEM and FTIR techniques. LHTES properties and thermal reliability of form-stable composite PCMs (F-S CPCMs) were analyzed by differential scanning calorimetry (DSC).

## II. EXPERIMENTAL

### A. Materials

Capric acid (CA) and lauric acid (LA) were obtained from Sigma-Aldrich Company (Germany). Attapulgite was obtained by Karaman mines Company (Turkey). According to the manufacturer, it has weight composition of 83.4% SiO<sub>2</sub>, 5.60% Al<sub>2</sub>O<sub>3</sub>, 1.0% CaO, 1.0% Fe<sub>2</sub>O<sub>3</sub>, 0.7 % and other mineral oxides (K<sub>2</sub>O, Na<sub>2</sub>O, TiO<sub>2</sub>). The clay sample was sieved through 150 mesh. It was dried at 105 °C for 24 h before use.

### B. Preparation of attapulgite/(CA-LA) as F-SCPCMs

In the first stage of the experimental procedure, the attapulgite/(CA-LA) composite was prepared by conducting

vacuum infiltration process. The experimental procedure was shown schematically in Fig. 1.

Firstly, the specified amount of attapulgite is placed in a bottle connected to a vacuum pump. Vacuum treatment was maintained at 0.18 MPa for 30 minutes; The eutectic mixture in liquid state (CA-LA) was flowed gradually into the flask using a funnel. The vacuum was then broken and allowed to air for 30 minutes to provide easy infiltration. The prepared attapulgite/(CA-LA) composite was cooled to 10 °C to ensure complete crystallization of CA-LA to the porous attapulgite network. This procedure ranged from 15 to 40% for different weight combinations. In the second stage, leakage test was performed and optimal infiltration rate was established. The prepared composite was placed on a filter paper and heated above the melting temperature of the considered eutectic mixture. The leakage condition of the Attapulgite / (CA-LA) composite was controlled by controlling the filter paper by heating.

### C. Characterization of Attapulgite / (CA-LA)

Chemical characterization of Attapulgite and developed attapulgite/(CA-LA) composites was performed using the Jasco 430 model FT-IR spectrometer. The microstructures of the prepared F-S CPCMs were investigated using a LEO 440 model SEM. X-ray diffraction (XRD) analyzes of the produced attapulgite/CA-LA composites were made using a PANalytical X'Pert3 powder diffractometer (45 kv, 40 mA) with a width Cu ( $K\alpha = 1.5406 \text{ \AA}$ ). The LHTES properties of the eutectic mixture and the manufactured F-SCPCM were measured by the DSC technique at the same heating/cooling rate as  $3 \text{ }^\circ\text{C min}^{-1}$  (Perkin Elmer-JADE model). The measurement was repeated three times and the accuracy in the temperature and enthalpy data were calculated to be  $\pm 0.012 \text{ }^\circ\text{C}$  and  $\pm 0.59 \text{ J/g}$ , respectively.

By using a thermal cycler (BIOER TC-25/H model), the developed CPCM was subjected to a thermal cycling test including 500 melting/freezing cycles. To have information about hermal cycling reliability and chemical stability of F-SCPCMs, the DSC and FT-IR analysis were conducted again.

## III. RESULTS AND DISCUSSIONS

### A. Characterization of the CPCMs

The photographs of the prepared attapulgite/(CA-LA) composite are shown in Fig. 1. As shown form the photograph images, the maximum absorption of CA-LA by the attapulgite in the mass fraction of 46 wt% without observing their melted leakage. Thus, this composite was called as F-S CPCM. The microstructures of attapulgite and the prepared F-SCPC were shown on in Fig. 2. As seen from the SEM photographs, the surface of attapulgite is consisted of the arbitrary-shaped particles and most of them have needle structure.

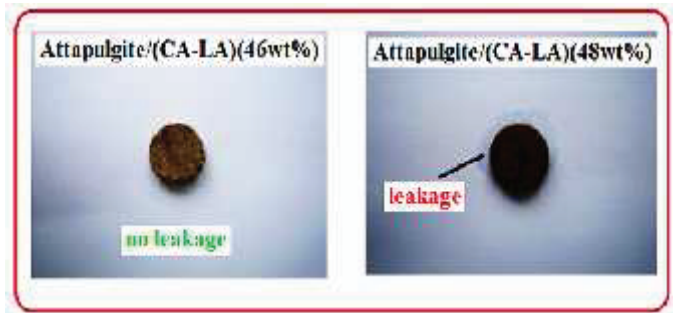


Fig. 1. The photographs of composites above/below the form-stable combination ratio

As also seen from the SEM images of the F-SCPCM, the CA-LA eutectic mixture was homogenously dispersed throughout the surface. It was due to the structural resistance of cement and the capillary/surface tension forces in whole matrix. These results proved the existence of excellent physical compatibility among the component of the F-SCPCM.

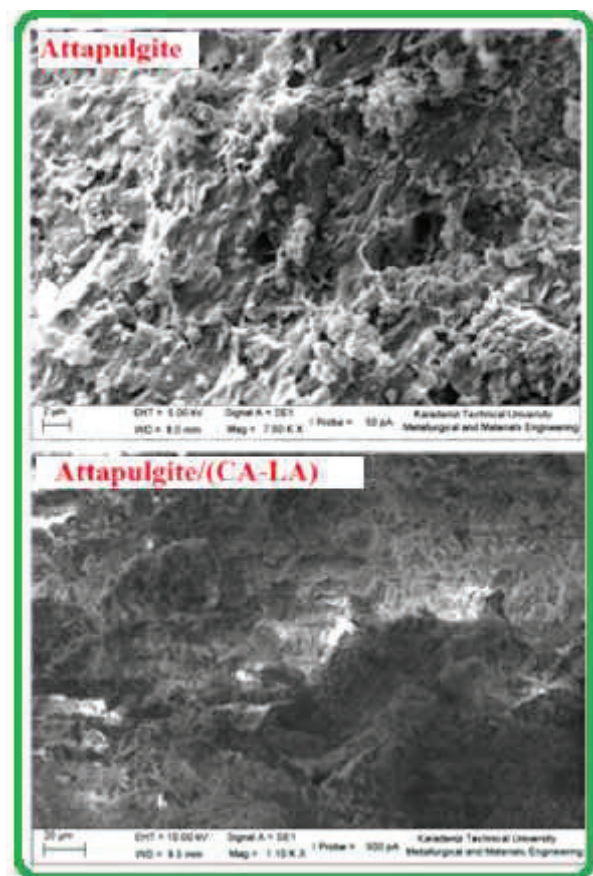


Fig. 2. The microstructures of the attapulgite and F-SCPCM

The FTIR analysis was performed to describe the probable specific interactions between attapulgite and CA-MA eutectic mixture. As seen from the FT-IR spectrum of attapulgite in Fig. 3, the band in the range of  $3200\text{-}3750 \text{ cm}^{-1}$  is assigned by the asymmetrical stretching of hydrogen bonded OH groups. The band in the range of  $1090 \text{ cm}^{-1}$  is characterized as stretching vibrations of Si-O-Si and bending vibrations.

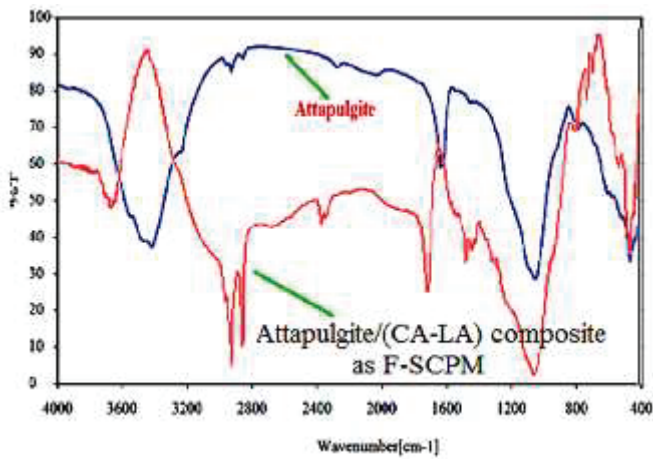


Fig. 3. The FT-IR spectrum of attapulgite and F-SCPCM

In case of the attapulgite/CA-LA composite, the stretching vibration and bending vibrations of Si-OH bands are seen at about 3200-3700  $\text{cm}^{-1}$  and 1046  $\text{cm}^{-1}$ . These bands are the presence of the attapulgite component of the composite PCM. Moreover, in the FT-IR spectrum of the eutectic mixtures, the bands at 3100-3600  $\text{cm}^{-1}$  was regarded with the stretching vibration of OH group as the bands at 933  $\text{cm}^{-1}$  and 732  $\text{cm}^{-1}$  are due to the bending vibration of this group. The asymmetrical and symmetrical stretching bands at 2980-2850  $\text{cm}^{-1}$  and 1470  $\text{cm}^{-1}$  are responsible for the alkyl groups (-CH<sub>2</sub> and -CH<sub>3</sub>). The bands in the range of 1704  $\text{cm}^{-1}$  are identified as at the stretching band of C=O. The stretching band of C-O groups at was over layered by bending vibrations of Si-O, Mg-O and Si-O-Al groups). These results are attributed to the characteristic groups of the CA-LA eutectic mixture components of the composite PCM. Additionally; any new peak is not monitored in the spectrum. This result confirms the fact that any chemical reaction is not carried out between the components of F-SCPCM. However, the little shifts observed in some characteristic bands of the F-SCPCM can be attributed to the probable intermolecular physical attractions between the characteristics groups of CA-LA eutectic mixture and attapulgite.

The XRD patterns of the attapulgite/CA-LA composite prepared as F-SCPCMs are shown in Fig. 3. As seen from these findings, the XRD patterns of the attapulgite/CA-LA composites prepared as F-SCPCM contains all crystal diffraction peaks of its pure components. Moreover, some of the peaks are overlapped because their  $2\theta$  values are close each other.

On the other hand, the little shifts in  $2\theta$  values were observed and the change in peak intensities of the CA-LA eutectic mixture. It does not mean that its crystal structure is not destroyed after impregnation process and these results may be due to the capillary and the tension forces.

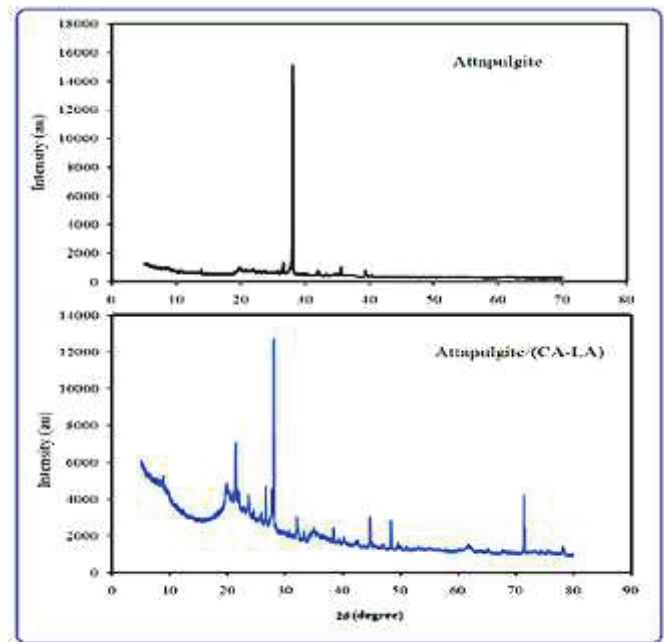


Fig.4. The XRD results of the attapulgite and F-SCPCMs

### B. The LHTES characteristics of the developed F-S CPCMs

By taking account of these considerations in the DSC thermograms (Fig. 5) the eutectic weight composition, melting temperature and the latent heat capacity of the CA-LA mixture were determined as 43:57 wt% 22.88°C and 147.21, respectively.

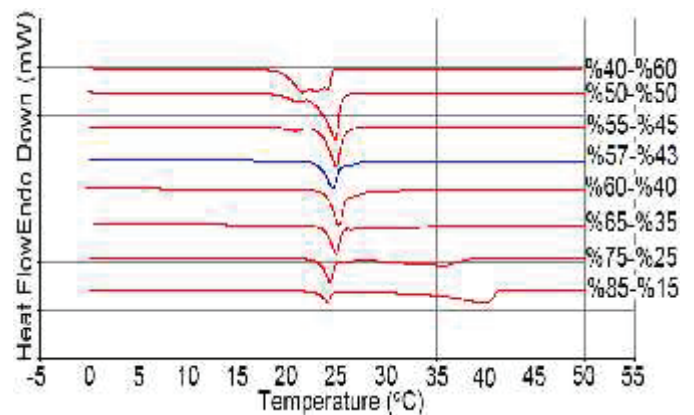


Fig. 5. DSC thermograms of CA-LA mixtures prepared at different weight combinations

TABLE 1.  
The LHTES properties of form-stable attapulgite/CA-LA composite

PCM	Melting temperature (°C)	Solidification temperature (°C)	Heat of fusion (J/g)	Heat of solidification (J/g)
CA	31.04	30.94	190.21	-188.65
LA	43.97	43.27	200.18	-198.34
CA-LA	22.88	22.39	147.21	-145.12
F-SCPCM	21.97	66.24	22.77	-65.74

Fig. 6 indicated the DSC thermogram of the fabricated attapulgite/(CA-LA) composite with combination of 46 wt%, respectively. The LHTES data derived from this thermogram

was also presented in Table 1. As clearly observed from these results, the prepared form-stable attapulgite/(CA-LA) composite melts and solidifies at 21.97 °C and 22.77 °C, respectively. Moreover, its melting and freezing LHTES capacity were measured to be 66.24 and -65.74 J/g, respectively.

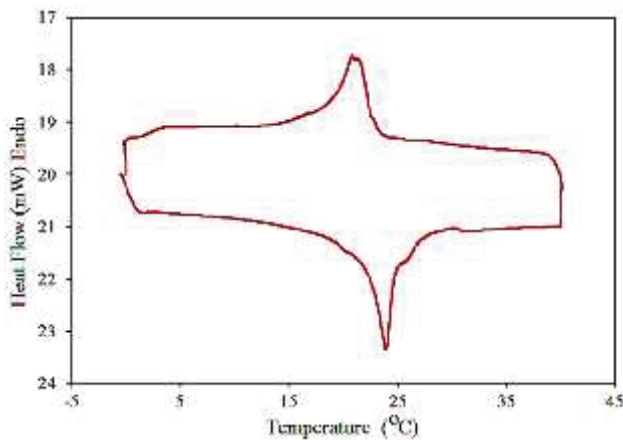


Fig. 6. DSC thermogram of F-SCPCM

On the other hand, when compared to the CA-LA eutectic mixture, the phase change temperature of the F-SCPCM decreased as -0.91°C for melting and 0.38 °C for freezing process. Although little deviations were observed in the phase change temperatures, the F-SCPCM can be evaluated as fitting LHTES material to regulate indoor temperature of building envelopes.

### C. Thermal and chemical cycling stability of the F-S CPCM

For practical building applications, it is important to investigate the thermal cycling stability of the F-SCPCM within their operating temperature range [5-8]. Therefore, the accelerated melting/freezing experiments were conducted to investigate the thermal cycling stability of the fabricated F-SCPCM. After the cycling test including 500 heating/cooling processes, the chemical structure, phase change temperatures and latent heat capacities of the F-S CPCM were compared by examining the FTIR and DSC results.

As seen from the FT-IR spectra (Fig. 7), in the wavenumber values and shape of the main characteristic bands any change were not observed after cycling period. This means that the long-term cycling process has no damage effect on the chemical structure of F-SCPCM. The melting and freezing temperatures of the attapulgite/(CA-LA) composite PCM was diminished in the range of -0.06-0.12°C. 0 as its LHTES capacity was decreased as little as 4.1-5.7%. Based on these results that the changes occurred in the LHTES of the prepared F-SCPCM cycling are not in considerable level for building TES applications even they are subjected to repeated 500 cycles.

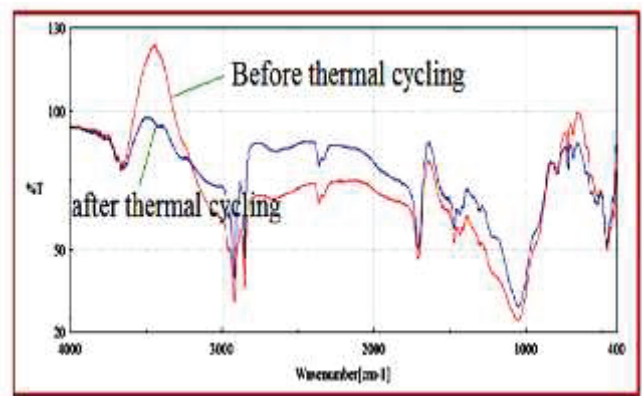


Fig. 7. The FTIR analysis results of F-SCPCM after 500 thermal cycling

## CONCLUSIONS

The CA-LA eutectic mixture was impregnated into attapulgite by vacuum technique. The DSC analysis results revealed that the produced melting temperatures of the attapulgite/(CA-LA) composite were measured as 21.97 °C and the latent heat capacity as 66.24 J/g. These LHTES properties were suitable for heating, cooling ventilating and air conditioning (HVAC) purposes in building envelopes. The produced F-SCPCM shows good thermal and chemical reliability after thermal cycling test. Based on all results, it was also concluded that the created F-SCPCM is considered an effective LHTES building material to reduce energy consumption.

## ACKNOWLEDGMENT

Authors would like to thank Scientific Research Project Coordination Unit of the Karadeniz Technical University (Project Number: FBA-2017-6863). Dr. A. Sarı would also like to thank KFUPM because of their laboratory facilities during the handling this work.

## REFERENCES

- [1] H. Zhang, J. Baeyens, G. Caceres, J. Degreve, Y. Lv, Thermal energy storage: recent developments and practical aspects, *Prog. Energy Combustion Science*, 53 1–40, (2016).
- [2] Y. Yuan, N. Zhang, W. Tao, X. Cao, Y. He, Fatty acids as phase change materials: A review, *Renewable & Sustainable Energy Reviews* 29, 482-498, (2014).
- [3] V.V. Raa, R. Parameshwarana, V.V. Ram, PCM-mortar based construction materials for energy efficient buildings: A review on research trends, *Energy and Buildings*, 158, 95–122, (2018)
- [4] R. Parameshwaran, S. Kalaiselvam, S. Harikrishnan, A. Elayaperumal, Sustainable thermal energy storage technologies for buildings: a review, *Renewable & Sustainable Energy Reviews*, 16 2394–2433, (2012).
- [5] Farid, M.M.; Khudhair, A.M.; Razack, S.A.K.; Al-Hallaj. S. A review on phase change energy storage: Materials and applications. *Energy Conv. Manage.* 45. 1597–1615 (2004).
- [6] H. Akeiber, P. Nejat, M.Z.A. Majid, M.A. Wahid, F. Jomehzadeh. I. ZeynaliFamileh. J.K. Calautit, B.R. Hughes, S.A. Zaki. A review on phase change material (PCM) for sustainable passive cooling in building envelopes. *Renew. Sustain. Energy Rev.* 60 1470-1497 (2016).
- [7] Sharma, A.; Tyagi, V.V.; Chen, C.R.; Buddhi. D. Review on thermal energy storage with phase change materials and applications. *Renew. Sust. Energy. Rev.* 13. 318–345 (2009).
- [8] S.A. Memon. Phase change materials integrated in building walls: a state of the art review. *Renew. Sustain. Energy Rev.* 31 870–906 (2014).

# PATERN KAYNAK YÖNTEMİ İLE 15N20 VE 1075 KALİTE ÇELİKLERİ KULLANILARAK ÜRETİLEN DAMASCUS ÇELİĞİNİN EĞMELİ YORULMA DAVRANIŞININ İNCELENMESİ

Furkan ACAR<sup>1</sup>, Fatma KÖZ<sup>1</sup>, Hayrettin AHLATCI<sup>1\*</sup>, Sait ÖZÇELİK<sup>1</sup>, Yavuz SUN<sup>1</sup>, Yunus TÜREN<sup>1</sup>, Süleyman YAŞIN<sup>1</sup>, Emre DEMİRCİ<sup>1</sup>, Hakan KIRDAN<sup>1</sup>,

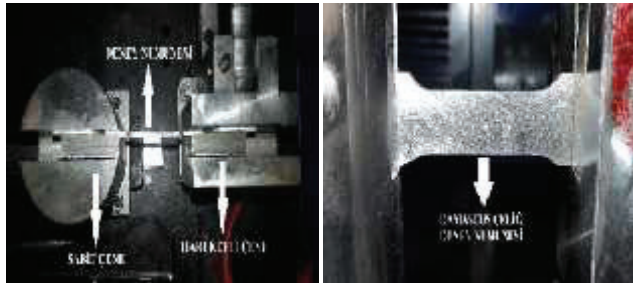
Karabük Üniversitesi, Metalurji ve Malzeme Mühendisliği Bölümü, Karabük 78000 Turkey

\*Corresponding author: [hahlatci@karabuk.edu.tr](mailto:hahlatci@karabuk.edu.tr)

**Abstract-** In this study, microstructure analysis, vickers hardness values, pulse-notch energy values and endless fatigue life and wöhler curve obtained from fatigue tests with samples prepared by standards were determined.

## I. GİRİŞ

İncelenen damascus çeliği korozyon dayanımları ve mekanik özellikleri birbirinden farklı olan 1075 ve 15N20 kalite çeliklerinden patern kaynağı yöntemiyle imal edildiğinden dolayı tabakalı çelik-çelik kompozit bir yapıya sahiptir [1-6]. Yüksek mukavemetli çeliklerin alternatifi olarak düşünülebilecek damascus çeliğinin harelî (tabakalı) yapısının dinamik yükler karşısında sergileyeceği yorulma davranışının belirlenmesi amacıyla plaka yorulma deneyi şuana kadar başka bir çalışmada yapılmamıştır



Şekil 1. Plaka Yorulma Test Cihazının Üstten ve Önden Görünüşü.

Günümüzde üretilen ve bu çalışma kapsamında kullanılan damascus çeliklerinin büyük çoğunluğu katlamalı teknik ile üretilmektedir. Bu teknikle damascus çeliği üretebilmek için korozyon dayanımları farklı iki tip çelik kullanılır. Korozyon dayanımlarının farklı olmasındaki amaç asitleme işleminden sonra oluşacak harelîleri belirgin kılmaktır.

## II. DENEYSEL ÇALIŞMALAR

Kullanılan bu çelikler hem patern kaynağına uyumlu hem de korozyon dayanımları farklı olması gerektiği için üretilen damascus çeliklerinde genellikle 1075 ve 15N20 çelik türleri kullanılmıştır. Damascus çeliğinin imalinde kullanılan bu iki

Tablo 1. 1075 ve 15N20 Kalite Çeliklerin Kimyasal Kompozisyonları çelik türünün kimyasal kompozisyonları da Tablo.1'de verilmiştir (Tablo 1).

	C	Mn	Ni	P	S	Si
1075	% 0,7	%0,4-0,7	-	% 0,04 max	% 0,05 max	-
15N20	% 0,7	% 0,4	%2	%0,025 max	%0,01 max	%0,25

### A. Mikroyapı Karakterizasyonu

Üretilen Damascus çeliğinin mikroyapı karakterizasyonu için numuneler standart metalografik aşamalar olan zımparalama ve parlatma kademelerinden geçirildikten sonra hidroklorik asit ve nitrik asitin 3:1 oranında göre karıştırılmasıyla elde edilen kral suyu ile dağlama gerçekleştirildi. Ardından Leica marka optik mikroskop ile 5X, 10X, 20X ve 40X büyütmelerde görüntüler alındı.

### B. HV Sertlik Ölçümleri ve Çekme Deneyi

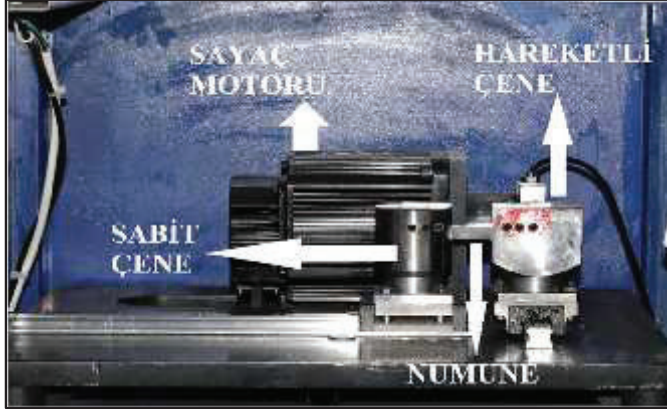
Sertlik değerleri için Shimadzu marka HMV2 Mikro Sertlik Deney Cihazı kullanılmıştır. Testlerde vickers HV 10 skalası kullanılmıştır. Sertlik değerleri, en az 5 ölçümün ortalaması alınarak tespit edilmiştir.

Mekanik özellikleri ASTM 6891-1 ve ASTM 6892-2 standartlarına göre 100 KN kapasiteli MTS marka çekme test cihazı ile belirlenmiştir. Çekme testi oda sıcaklığında yapılmıştır.

### C. Düzlemsel Eğme Gerilmeli Yorulma Deneyi

Yorulma testleri düzlemsel eğme gerilmeli yorulma test cihazı (Şekil 1-2) kullanılarak ASTM E 466 standartlarca hazırlanan dikdörtgen kesitli numunelerin tekrarlı eğme gerilmelerine maruz bırakılmasıyla yapılmıştır.

Her bir numune için farklı birim yer değiştirme (sehim) parametreleri altında yorulma testleri gerçekleştirilmiş olup çeliğin yorulma dayanım sınırı, % deformasyon oranları ve S-N eğrisi belirlenmiştir (Tablo 2).



Şekil 2. Düzlemsel Eğme Gerilmeli Yorulma Deney Cihazı

Tablo 2. Deneylerin Yapıldığı Ortalama Test Frekansı ve Sehim Parametreleri

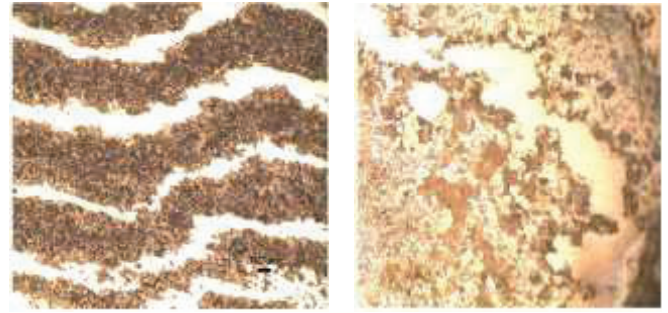
Ortalama Test Frekansı (Hertz)	Sehim (Y)
3,5 Hz	0,40 mm
	0,50 mm
	0,60 mm
	0,87 mm
	1,25 mm

Damascus çeliği katlamalı bir teknikle dövülerek üretildiğinden dolayı yorulma deneyinin yapıdaki harelere (kat) etkisini görmek için Karabük Üniversitesi Demir-Çelik Enstitüsü bünyesinde kırık yüzey üzerinde SEM-EDX çalışması yapılmıştır.

### III. DENEYSEL ÇALIŞMALARIN SONUÇLARI

#### A. Mikroyapı Karakterizasyonu Sonuçları

Damascus çeliğinin mikro yapısı, ferritik ve perlitik yapılardan oluşmaktadır. Çok yüksek C içeren 1075 kalite çelik perlitik yapı sergilerken yüksek Ni içeren 15N20 kalite çelik ferritik yapı sergilemektedir. Bu çalışmada 1075 ve 15N20 kalite çelikleri birbirine patern kaynağı yöntemiyle kaynatılmış ve farklı desenler oluşturmak için belli katlama yöntemleri kullanılmıştır. Mikro yapı görüntülemesi sırasında 1075 çeliğe ait kısımlar yüksek C içerdiğinden dolayı daha koyu, 15N20 çeliğe ait olan kısımlar ise Ni içerdiğinden daha parlak ve açık renkli görülmüştür (Şekil 3).



Şekil 3. Damascus Çeliğinin 5X ve 10X Büyütmedeki Mikroyapı Görüntüleri.

#### B. Sertlik Ölçümleri ve Çekme Deney Sonuçları

Patern kaynak yöntemiyle 1075 ve 15N20 kalite çelikleri kullanılarak imal edilmiş damascus çeliğinin Vickers sertlik ölçümleri ve değeri ile birlikte çekme deneyinden belirlenen akma-çekme dayanımları Tablo 3'de belirtildiği gibidir. Daha önce de belirtildiği üzere damascus çeliği iki farklı çelik türü olan 1075 ve 15N20 kalite çeliklerinin bileşiminden oluştuğundan dolayı harelitabakalı bir yapıya sahip olup bu harelere sertlik değerleri birbirinden bağımsız olarak belirlenmiştir

Tablo 3. 15N20 ve 1075 Kalite Çeliklerinden İmal Edilen Damascus Çeliğinin Sertlik-Darbe/Çentik-Çekme Deneylerinden Elde Edilen Veriler.

	Sertlik(HV10)	Akma Dayanımı (Mpa)	Çekme Dayanımı (Mpa)	Uzama (%)
15N20(Ferritik)	749,2	472,09	863,43	3,15
1075(Perlitik)	253,8			

#### C. Düzlemsel Eğme Gerilmeli Yorulma Deneyi Sonuçları

Düzlemsel eğme gerilmeli yorulma deney cihazından elde edilen veriler ışığında aşağıda belirtilen formüller yardımıyla numunelerin deney sırasında maruz kaldığı gerilimler ve oluşan deformasyonlar hesaplanmıştır.

Denklem 1 : Max Gerilme Değerinin Hesabında Kullanılan Denklem

$$\sigma_{max} = 1,5 * \frac{P_{(max \& min)} * L}{B * H^2}$$

$P = \text{Kuvvet(N)}$   
 $L = \text{Ölçü Boyu(mm)}$   
 $B = \text{Numunenin Eni(mm)}$   
 $H = \text{Numune Kalınlığı(mm)}$

Denklem 2 : Yorulma Deney Sırasında Oluşan % Deformasyon Miktarı

$$\epsilon (\%Def) = \frac{6 * Y * H}{L^2} * 100$$

$Y = \text{Sehim(mm)}$   
 $H = \text{Numune Kalınlığı}$   
 $L = \text{Ölçü Boyu}$

Max. ve min. gerilme değerlerini hesaplamak için numuneye uygulanan max. ve min. kuvvetler üzerinden ayrı ayrı hesaplar yapılmıştır.



# Comparison of Different Production Methods and Recycled CuSn10 Chips

Aydın Güneş<sup>1\*</sup>, Handan Demirel<sup>2</sup>, Emin Salur<sup>1</sup>, Abdullah Aslan<sup>1</sup>, Ömer Sinan Şahin<sup>1</sup>

<sup>1</sup>Selçuk University, Mech. Eng. Dept., Konya-Türkiye

<sup>2</sup>Çankırı Karatekin University, Mach. Met. Tech Dept., Çankırı-Türkiye

\*Sorumlu yazar: [aydingsn@hotmail.com](mailto:aydingsn@hotmail.com)

**Abstract**— In this study, waste bronze chips were recycled by using different methods. The mechanical properties of the transformed metal matrix composite materials were determined and compared with each other. Cold pressing post sintering method which is widely known as the production method and hot pressing methods under high pressure have been used. Pore, density and micro vickers (HV) hardness values were taken into consideration in determining the mechanical properties. As a result of the mechanical tests, more porous structures were obtained in the sintering method and values close to each other were obtained.

**Keywords**— metal matrix composite, recycle, bronze, hot pressing, sintering.

## I. INTRODUCTION

With the increase of the world population, the dependence on energy increases. The evaluation of waste materials after these uses is very important nowadays. The recycling of waste metals is generally based on the melting method. During this process, the high energy consumed and the occurrence of unwanted wastes reduce the efficiency [1-3]. In this study, the mechanical properties of bronze chips recycled by different production methods were compared with cast bronze. Hot pressing and sintering methods are used as production

methods. These two production methods are used in a wide area today [4,5]. Different production methods can be selected depending on the production costs and the conditions of use of the produced materials [6-8]. Production by hot pressing was carried out at a temperature of 450 ° C and a pressure of 820 MPa. In the sintering method, pre-forming before sintering was applied first by pressure of 955 MPa and then by 1146 MPa in reverse direction [9]. Sintered at 875 ° C after compression. The mechanical properties of bronze materials produced by two different methods were compared with cast bronze.

## II. MATERIALS AND METHODS

In this study, CuSn10 tin bronze was used as bronze material. Two different production methods were used in the production of waste bronze chips. Bronze chips are arranged by means of ball mills and sieves before production. Then weights are weighed in the weights determined by precision scales. Figure 1 shows the production units used for the recycling of waste bronze materials. Fig. 1a also shows the ash furnace sintered to the bronze chips compressed by the one-way press. In Fig.1b there is a production unit where bronze chips are produced by hot pressing. Prior to the

sintering process shown in Figure 1a, the bronze chips were first pressed to 955 MPa and then inverted at a pressure of 1146 MPa and heat treated. In the other production method, this process was carried out with the help of double acting press under high pressure and temperature without sintering process.

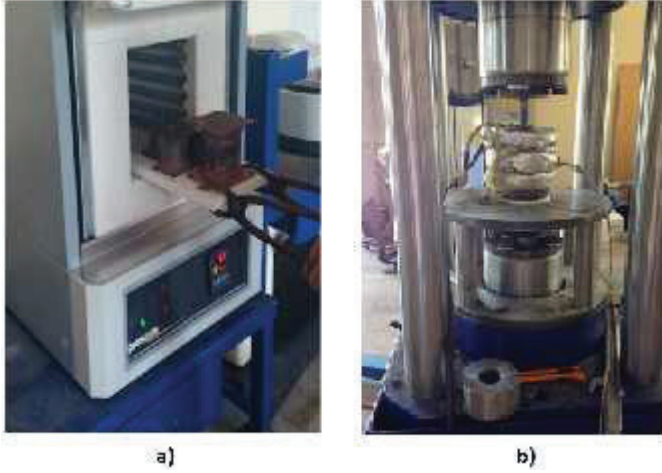


**Figure.1** Different production units for the production of waste bronze chips

### III. RESULTS AND DISCUSSIONS

The mechanical properties of the produced bronze chips are shown in Table.1. In determination of mechanical properties, porosity, density and hardness values were taken into consideration. The porosity and density tests of the produced bronze materials were carried out via the Archimedes' scale. After the measurements, the hardness values of the materials were determined in the microvickers hardness instrument. When the data in Table.1 are examined, there is no significant difference in the hardness of the materials. When we look at the pore and density values, it is much more than the porosity of the bronze produced by hot pressing in the pore amounts of the materials produced by sintering. Again, density amounts change in this context, density decreases as the pore increases. The

reason for this can be explained as the effect of hot and pressure on materials due to production methods [10].

**Tablo.1** Üretilen malzemelerin mekanik özellikleri

	Gözeneklilik (%)	Yoğunluk (gr/cm <sup>3</sup> )	Brinell Sertlik (HV)
Döküm Bronz	%1-3	8,7	245-255
Sıcak Presleme		400°C	
	5,70%	8,2 gr/cm <sup>3</sup>	219-224
Sinterleme		875 °C	
	10,59%	7,779	221-230

### IV. ACKNOWLEDGEMENTS

This work was financially supported by the Scientific and Technological Research Council of Turkey (TUBITAK, No. 113M141).

### V. REFERENCES

- [1] Abdullah Aslan, Aydın Güneş, Emin Salur, Ömer Sinan Şahin, Hakan Burak Karadağ, Ahmet Akdemir, Mechanical Properties and Microstructure of Composites Produced by Recycling Metal Chips, International Journal of Minerals, Metallurgy and Materials, 2018
- [2] Aslan A, Sahin O.S, Salur E., Gunes A., Karadağ H. B., Akdemir, A, A New Method for Recycling of Metal Chips, Journal of Selçuk University Natural and Applied Science Vol:4 No:1, 2015
- [3] Karadağ, H.B., Çelik/Bronz Talaş Kompozitin Üretimi ve Mekanik Özellikleri, (Doktora Tezi), Selçuk Üniversitesi Mühendislik Fakültesi, 2012.
- [4] Ömer Sinan Şahin, Aydın Güneş, Abdullah Aslan, Emin Salur, Hakan Burak Karadağ, Ahmet Akdemir, Low Velocity Impact Behavior of Porous Metal Matrix Composites Produced by Recycling of Bronze and Iron Chips, Ir. Journal of Science and Tech., Transactions of Mechanical Engineering, 2017
- [5] Fogagnolo, J.B. Ruiz-Navas, E.M., Simón, M.A. Martinez M.A., Recycling of aluminium alloy and aluminium matrix composite chips by pressing and hot extrusion, Journal of

Materials Processing Technology, 143–144, 792–795, 2003.

[6] Mindivan, H., Kayalı, E.S., Çimenoglu, H., Recycling Of Aluminum Machining Chips, 12th International Materilas Symposium (IMSP'2008), Denizli, 109-113, 2008.

[7] Abdullah Aslan, Emin Salur, Aydın Güneş, Ömer Sinan Şahin, Hakan Burak Karadağ, Ahmet Akdemir, Production And Mechanical Charecterization of Prismatic Shape Machine Element By Recycling of Bronze And Cast Iron Chips, Journal of the Faculty of Engineering and Architecture of Gazi University, 2018.

[8] Aydın Güneş, Ömer Sinan Şahin, Ahmet Akdemir, "Characterization of Cusn10 Metal Chips by Using Recycling without Melting", International Porous and Powder Materials Symposium and Exhibition, İzmir, Türkiye, 2015.

[9] Demirel, H., "Dökme Demir/Bronz Talaş Kompozitin Toz Metalurjisi Esaslarıyla Üretimi Ve Mekanik Özellikleri", Selçuk Üniversitesi Fen Bilimleri Enstitüsü, 2017.

[10] German, R.M. Toz Metalürjisi ve Parçacıklı Malzeme İşlemleri, Çeviri Editörleri: S.Sarıtaş, M.Türker, N.Durlu, Ankara, Pp:38, 2007.

# Investigation of Energy Absorption Capacities of DP600 Steel with Al 2024 and AZ31 Light Metal Alloys (ISLAC'18/UHAKS18)

Selcuk Karagoz\*, Huseyin Beytut\*, Mehmet Kivanc Turan\*

\*Department of Mechanical Engineering, Bursa Technic University, Bursa, 16330, Turkey

\*Corresponding author: [huseyin.beytut@btu.edu.tr](mailto:huseyin.beytut@btu.edu.tr)

**Abstract**— Automobile is an indispensable tool of our lives and crash box is important safety part of automobile. In this study, materials and geometry effects on the crash performance of crash box were investigated. DP600, AZ31, Al 2024 were used.

**Keywords**— Automobile, Thin-Walled Structure, Crash box, Crash performance, Safety components

## I. INTRODUCTION

Automobiles had been beginning to enter our lives in the early 20<sup>th</sup> century, was becoming widespread in the middle, and from the end of 20<sup>th</sup> century, has become an indispensable tool of our lives. As a result, the automotive industry is one of the biggest industries of our era. As the other sectors, the trend in the automobile industry is determined by needs and consumer demands. At the end of the 20th century, fuel consumption problems arose in the automotive industry. Because of environmental awareness and CO<sub>2</sub> emission effect on the global warming, automobile manufactures started investigate to reduce of automobile weight. Because reduction in automobile weight also reduce fuel consumption. For this reason, automobile manufactures tend to low density materials such as aluminium, titanium, magnesium, composite instead of steel. For example, Audi uses significant amount of aluminium components in A8 [1]. Nowadays, automobile designers focus on two issues when designing security components ; reduce the weight, increase the performance of safety. In this study, the effects of utilization of low density metals and different geometries on the crash performance of crash box were investigated.

## II. CRASH BOX

Crash box is one of the important safety components. The main task of crash box is to return kinetic energy to deformation energy at low and medium speed accidents. Nowadays, many different types of crash box are used, such as cylinder, hexagon, rectangular, square. Cylindrical model is most widely used. For assessing the performance of crash box, five important criteria are used. These are, total absorbed energy, specific energy, maximum force, mean force and efficiency of crash force [2].

### A. Total Absorbed Energy

The total amount of energy that the collision box absorb during the collision [2-3].

$$EA = \int (x) dx$$

### B. Specific Energy

The total absorbed energy by unit weight(kg) [2-3].

$$SEA = E / m$$

### C. Maximum Force

The maximum force in the crash direction. If this force reaches to critical value, crash box can't absorb energy, total of force is transmitted to body [2-3].

### D. Mean Force

Mean force is ratio of total absorbed energy and amount of crush [2-3].

$$P = E / \int (x) dx$$

### E. Efficiency of Crash Force

Efficiency of crash force is ratio of mean force and maximum force [2].

$$\eta = F_{\text{mean}} / F_{\text{max}}$$



Fig.1 Crash box.

## III. MATERIAL AND METHOD

In this study, three different metal materials were used (table 1), these are DP600, AZ31 and Al 2024[4-6]. Five different types of crash box(cylinder, hexagon, square, rectangular, triangle) were investigated. Crash box dimensions were chosen equally. Quad mesh type was used, mesh size was 2mm\*2mm.

TABLE I  
 PROPERTIES OF MATERIALS

Material	DP600	AL2024-T4	AZ31
Young Modulus(GPa)	205	73.1	44.8
Poisson	0.3	0.33	0.35
Yield Strength(MPa)	400	324	200
Density(g/cm <sup>3</sup> )	7.86	2.78	1.77

Analysis was performed explicit and non-linear.

IV. RESULTS

Analysis results is showed bottom (figure 2-7, table 2).

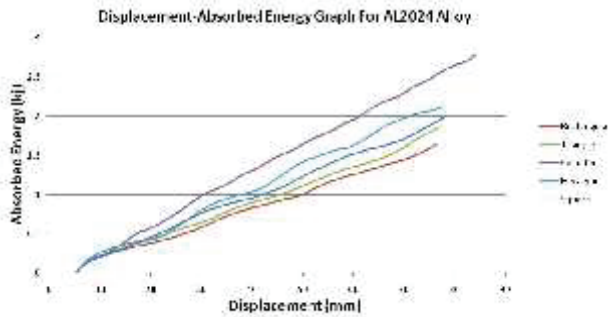


Fig.2 Displacement-total absorbed energy graph Al 2024.

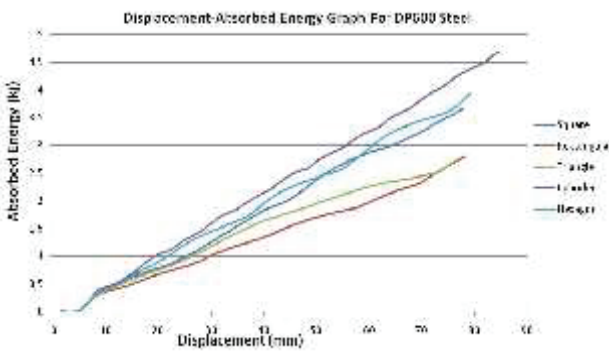


Fig.3 Displacement-total absorbed energy graph for DP 600

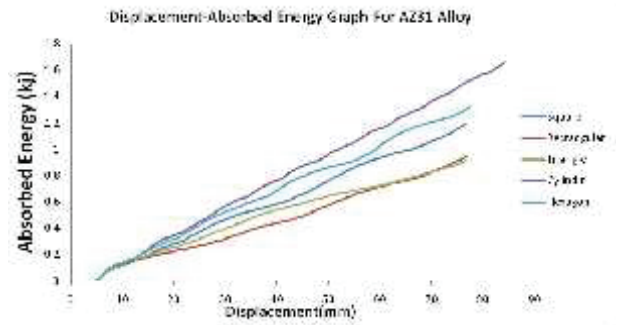


Fig.4 Displacement-total absorbed energy graph AZ31.

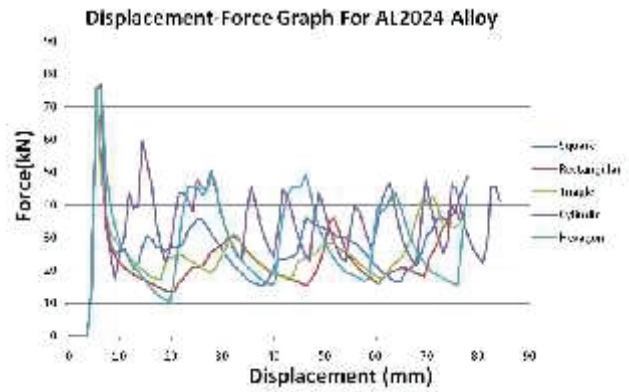


Fig.5 Displacement-force graph Al 2024

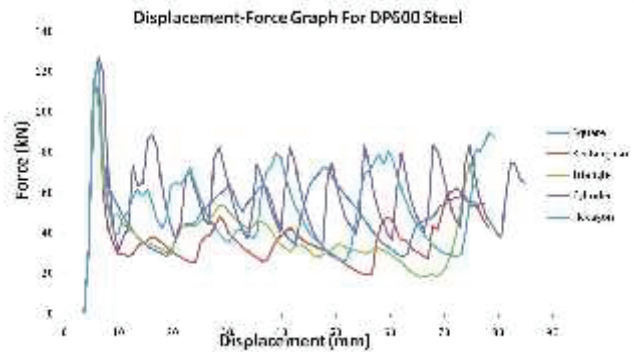


Fig.6 Displacement-force graph for DP 600.

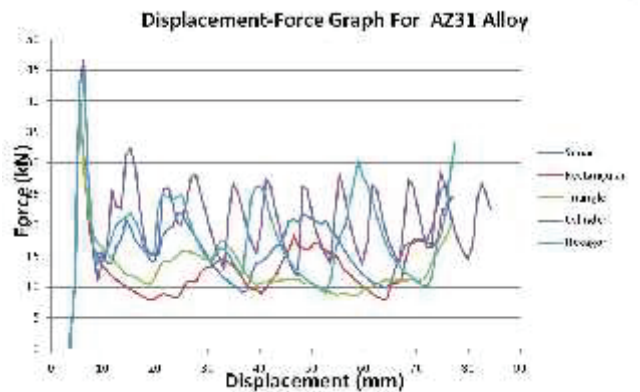


Fig.7 Displacement-force graph for AZ31.

TABLE II.  
SAMPLE DATA AND ANALYSIS RESULTS

Material	Thickness	Mass	Geometry								
			Cylinder			Square			Hexagon		
			TAE(kJ)*	SE(kJ)**	MF(kN)***	TAE	SE	MF	TAE	SE	MF
DP600	1.2	150	4.69	31.24	127.08	3.65	24.33	114.25	3.86	25.73	123.05
AL2024	1.2	53.5	2.79	52.15	77.10	1.99	37.20	74.80	2.10	39.40	74.80
AZ31	1.2	33.9	1.66	48.97	46.51	1.19	35.10	42.10	1.32	38.94	44.40

#### IV. CONCLUSIONS

Results show that cylindrical model gave the best outcome in all material types. DP 600 has the largest total absorbed energy capacity, on the other hand Al 2024 has the largest specific energy. In addition AZ31 has larger specific energy than DP 600 too. Also maximum force values of Al 2024 and AZ 31 lower than DP 600. As a result, aluminum and magnesium have very important characteristics for performance of crash therefore these materials are alternative to steel. In the future, these low density materials replace steel in the automotive industry highly likely.

#### REFERENCES

- [1] T.A. Baser, "Aluminyum Alasımları ve Otomotiv Endustrisinde Kullanımı", *Muendis ve Makina*, vol 635, pp 51-58, 2013.
- [2] S. Karagoz, "Development of High Performance Vehicle Safety Systems", Bursa Technical University, Bursa, Turkiye, 2016.
- [3] S. Karagoz and H. Beytut, "Tasıtlarda Kullanılan Enerji Yutuculardaki Geometrik Degisikliklerin Carpisma Performansına Etkisinin Incelenmesi", International Conference on Multidisciplinary, Science, Engineering and Technology, Bitlis, Turkiye, Oct 27-29, 2017.
- [4] B. Aydemir, H.K. Zeytin, G. Guven, A. Gungor, " Investigation of mechanical properties of DP 600 steels at elevated temperatures", 2<sup>nd</sup> International Symposium on Innovative Technologies in Engineering and Science, Karabuk, 1333-1339, 2014.
- [5] <http://asm.matweb.com/search/SpecificMaterial.asp?bassnum=MA2024T4>, Kasım, 2017.
- [6] J.S. Kim, D.H. Lee, S.P. Jung, K.S. Lee, K.J. Kim, H.S. Kim, B.J. Lee, Y.W. Chang, J. Yuh, S. Lee, "Novel strip-cast Mg/Al clad sheets with excellent tensile and interfacial bonding properties", *Scientific Reports*, 2016.

# Recycling of Waste Bronze Wood Chips by Powder Metallurgy

Aydın Güneş<sup>1\*</sup>, Handan Demirel<sup>2</sup>, Ömer Sinan Şahin<sup>1</sup>

<sup>1</sup>Selçuk University, Mech. Eng Dept., Konya-Türkiye

<sup>2</sup>Çankırı Karatekin University, Machine and Metals Tech. Dept, Çankırı-Türkiye

\*Corresponding Author: [aydingns@hotmail.com](mailto:aydingns@hotmail.com)

**Abstract**— In this study, waste bronze (CuSn10) chips were recycled and their mechanical properties were investigated together with pure bronze casting. Then, the recycled bronze material was compared with the cast bronze material. Powder metallurgy method, which is widely used in the recycling of waste chips, has been used after cold pressing sintering method. In determining the mechanical properties, the porosity, density and hardness values of the materials were taken into consideration. In addition to these mechanical tests, the materials produced by microscopy were compared. After evaluations, it was determined that the recycled bronze materials had mechanical properties close to pure bronze material.

**Keywords**— metal matrisli kompozit, bronz, recycle, sintering, cold pressing

## I. INTRODUCTION

Nowadays, many metal materials are found as waste after machining. It is very important to recycle these materials and develop different production techniques [1-7]. In the recycling of waste chip, common melting method is used. However, due to the low efficiency in the use of this method, the losses are very high.

The most common materials used in the process starting with industrialization, especially metals, aluminum, steel, bronze and iron are the most common method of recycling methods of melting. The scrapes recovered from the factories are reused according to the application areas and according to the desired properties, melting in the furnace (melting in the

pot, melting in the cupola, melting in the flame furnace, melting in electric arc furnaces, melting in induction furnaces, melting in induction furnaces in electric resistance furnaces) are re-used. However, these processes require very large energy and are a very inefficient process. One of the main reasons for this inefficiency is that the oxide layers on the surface behave as thermal insulator on the material and reduce the heat conduction. In addition, the air pockets between the material also make the heat conduction very difficult. This makes it difficult to melt the material. In addition to energy inefficiencies, toxic gases released from melting (cutting fluids used during machining) are released directly into the atmosphere, which adversely affects the ecological balance. On average, 10% of the chips used in a melting process can be recycled to 8% cast iron waste, 18% on extrusion losses and 10% on melting losses.

## II. MATERIALS AND METHODS

In the studies, composite materials were produced by cold pressing and sintering at the determined pressures after turning the waste bronze (CuSn10) chips into appropriate dimensions [8]. It has been passed through the sieves after homogenous mixing of waste bronze chips with different diameters. Sieves were selected by means of 1mm and 2 mm sieves. Then, as shown in Figure 1, the one-way cold press was used to pre-deform the bronze chips in the cylindrical mold by first pressing 955 MPa, then inverted at 1146 MPa. After the cold pressing process, sintering processes were performed in the ash furnace. The sintering time was determined based on the literature and it was determined that the desired temperature should be at 45 min for one hour and then allowed to cool in the oven. It took about 12 hours for the sample in the oven to cool to room temperature.



Figure.1 Production steps

## III. RESULTS AND DISCUSSIONS

The density, brinell hardness, porosity and microstructure properties of the materials were examined and compared with the bronze produced by the casting method. A second active parameter is observed in the recycling of waste bronze shavings made at three different sintering temperatures together with bronze chips. As can be seen in Table.1, there was a significant increase in pore quantities due to the reproduction of waste bronze chips compared to cast bronze materials. As the amount of pores increased, the density values decreased. The determination of the appropriate

sintering temperature and the expected mechanical properties of the produced materials are important [9]. When we look at the hardness results, the hardness values increased with increasing sintering temperature. It is observed that the bronze material produced by the sintering at 875 ° C is quite close to the hardness values of the bronze material produced in the cast form.

Table.1 Mechanical properties of materials

Döner Bıçak	Göreceli Yoğunluk (%)		Yoğunluk (g/cm <sup>3</sup> )		Sinter Sıcaklığı (°C)				
	800	850	875	900	950	1000	1050	1100	1150
Görünüm	20,202	19,250	18,900	18,477	17,970	17,477	16,977	16,477	15,977

Furthermore, when we look at the microscope images in Figure 2, it is seen that the decrease in pore amounts is observed with increasing temperature. The sintering process at increasing temperatures causes this decrease in the pore amount.

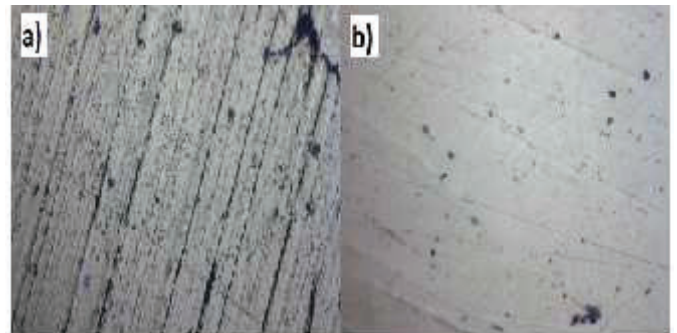


Figure.2. Microstructure of MMC material after sintering  
 a) B100D0-T800/500x b) B100D0-T875/1000x

## IV. Acknowledgements

This work was financially supported by the Scientific and Technological Research Council of Turkey (TUBITAK, No. 113M141).

#### IV. REFERENCES

- [1] Gronostajski J.Z., Kaczmar J.W., Marciniak H., Matuszak A., Direct Recycling of Aluminum Chips into Extruded Product, *Journal of Materials Processing Technology*, 64, 149-156, (1997).
- [2] Karadağ, H.B., Çelik/Bronz Talaş Kompozitin Üretimi ve Mekanik Özellikleri, Selçuk Üniversitesi Fen Bilimleri Enstitüsü, (2012).
- [3] Gronostajski J., Marciniak H., Matuszak A., New Methods of Aluminum and Aluminum Alloy chips Recycling, *Journal of Materials Processing Technology*, 106,34-39, (2000).
- [4] Gronostajski J., Matuszak A., The Recycling of Metals by Plastic Deformation: An Example of Recycling of Aluminum and its Alloy's Chips, *Journal of Materials Processing Technology*, 92-93,34-41, (1999).
- [5] Abdullah Aslan, Aydın Güneş, Emin Salur, Ömer Sinan Şahin, Hakan Burak Karadağ, Ahmet Akdemir, 2018, Mechanical Properties and Microstructure of Composites Produced by Recycling Metal Chips, *International Journal of Minerals, Metallurgy and Materials*
- [6] Ömer Sinan Şahin, Aydın Güneş, Abdullah Aslan, Emin Salur, Hakan Burak Karadağ, Ahmet Akdemir, 2017, Low Velocity Impact Behavior of Porous Metal Matrix Composites Produced by Recycling of Bronze and Iron Chips, *Ir. Journal of Science and Tech., Transactions of Mechanical Engineering*
- [7] Abdullah Aslan, Emin Salur, Aydın Güneş, Ömer Sinan Şahin, Hakan Burak Karadağ, Ahmet Akdemir, 2018, Production And Mechanical Charecterization of Prismatic Shape Machine Element By Recycling of Bronze And Cast Iron Chips, *Journal of the Faculty of Engineering and Architecture of Gazi University*
- [8] Demirel, H., "Dökme Demir/Bronz Talaş Kompozitin Toz Metalürjisi Esaslariyla Üretimi Ve Mekanik Özellikleri", Selçuk Üniversitesi Fen Bilimleri Enstitüsü, (2017).
- [9] German, R.M. Toz Metalürjisi ve Parçacıklı Malzeme İşlemleri, Çeviri Editörleri: S.Sarıtaş, M.Türker, N.Durlu, Ankara, Pp:38, (2007)

# PATLAMALI KAYNAK YÖNTEMİ İLE BİRLEŞTİRİLEN ALÜMİNYUM-DEMİR- ALÜMİNYUM TABAKALI KOMPOZİTİN YORULMA DAVRANIŞININ İNCELENMESİ

Sakine OBUZ, İlayda ŞAHİN, Fikri GÜNSÜR, Gülcan ÇETİN, Yunus TUREN, Yavuz SUN, Sait ÖZÇELİK,  
Süleyman YAŞIN, Mustafa ACARER, Hayrettin AHLATCI\*

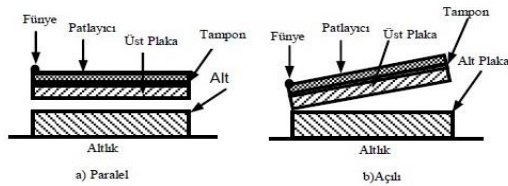
Karabük Üniversitesi, Metalurji ve Malzeme Mühendisliği Bölümü, Karabük 78000 Turkey

\*Corresponding author: hahlatci@karabuk.edu.tr

**Abstract** In this study, the mechanical properties and fatigue behavior of the aluminium-steel-aluminium layer composite produced by explosive welding technique will be examined. In the construction of composites, 1110 grade steel sheet with 0.5 mm thickness and 1050 grade aluminum sheet with 1.0 mm thickness were used. Layered composite materials to be investigated are provided for the project work and it is seen that aluminum-steel-aluminum layered composite has a flat interface at macro size in the micro structure studies carried out during preliminary studies. It is expected to exhibit much higher yield and tensile strength than 1050 grade aluminum without significant reduction in composite ductility and impact resistance.

## I. GİRİŞ

Patlamalı kaynak tekniği genel olarak, ucuz bir malzeme yüzeyini nispeten daha pahalı bir malzemeyle kaplama işlemidir. Geleneksel kaynak yöntemleriyle belirlenemeyen farklı metallerin kaynağı bu yöntemle yapılabilmektedir. Metal yüzeylerin çarpışması sonucu yeterli bir çarpışma enerjisi meydana geldiğinde, bu yüzeyler oluşan ilk temaslarını birbirleri üzerinde bir akış sergileyerek devam ettirirler ve sonuçta bir katı hal birleşmesi meydana gelir.



Şekil 1. Patlamalı kaynak yöntemi

Bu yöntemle elde edilen ısı değiştiriciler herhangi bir sızıntı olmaksızın en zor koşullarda da çalışabilme

yeteneğine sahiptir. Kaynak bölgesi en az ana malzemenin dayanımı kadar bir dayanıma sahiptir ve en zor çalışma gerilmelerine karşı mukavemet özellikleri iyidir [1].

Bilindiği gibi alüminyum alaşımları, uygulanan tekrarlı yüklemeler karşısında sürekli azalan bir ömür sergilerken çelikler belirli bir gerilmeden sonra sonsuz ömre sahiptirler. Bu proje sayesinde Türkiye sektöründe patlamalı kaynakla üretilen alüminyum-çelik- alüminyum tabakalı kompozitin yorulma ömrünü inceleyerek Türk imalat sektöründe kullanılması amaçlanmıştır [2].

Bu çalışmada, patlamalı kaynak tekniği ile üretilmiş alüminyum-çelik-alüminyum tabakalı kompozit numunelerin, plaka yorulma cihazı ile yorulma davranışı incelenmiştir. Tabakalı kompozitlerle imal edilen plaka parçalar dinamik yüklemelere maruz kaldığı için yorulma davranışının bilinmesi önem arz etmektedir.

## II. DENEYSEL ÇALIŞMALAR

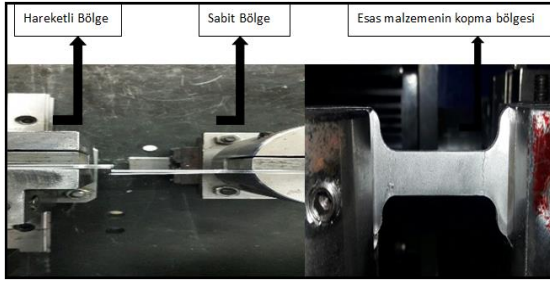
Kompozit yapımında, 0.5 mm kalınlığında 1110 kalite çelik sac ve 1.0 mm kalınlığında 1050 kalite alüminyum sac kullanılmıştır.



Şekil 2. Patlamalı kaynak yöntemiyle üretilen kompozit.

Metalografik prosedür, numuneleri 180, 400, 600, 800, 1000 ve 1200 mesh zımparalarla zımparalama ve ardından elmas solüsyonla parlatma işlemleri yapılmıştır. Mikro yapı çalışması, Leica marka DM ILM model optik ışık mikroskobunda dağlanmamış numuneler üzerinden çekilmiştir. Metalografik olarak incelenen numuneler 500 gramlık bir yük altında Shimadzu marka mikro sertlik test cihazı ile sertlik ölçümü gerçekleştirilmiştir.

İleri geri eğmeli plaka yorulma deneyi, bölümümüz tarafından tasarlanan ve imal edilen çalışma mekanizması sayaç motoru, sabit ve hareketli çeneden oluşan (Şekil 3) test cihazı kullanılmıştır. Deneyler sırasında ortalama frekans değerleri kullanılıp ileri-geri yüklemelerin etki ettiği deformasyon miktarı 0.2-0.9 aralığındadır. Cihaza bağlı olan loadcell yardımıyla etki eden yükler okunmuştur.



Şekil 3. Yorulma deney cihazı

### III. DENEYSEL SONUÇLAR

#### A. MİKROYAPI SONUÇLARI

Patlamalı kaynak yöntemi ile üretilen 1050 Al-1110 çelik-1050 Al tabakalı kompozitin kesit mikro yapısı Şekil 4'de görülmektedir. Al-çelik-Al tabakalı kompoziti düz bir birleşme ara yüzeyi sergilemektedir.

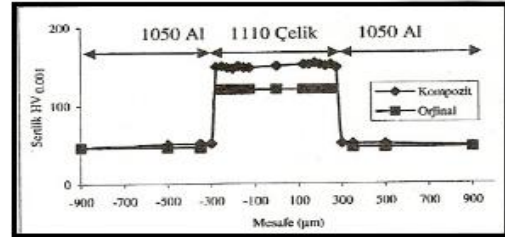


Şekil 4. 1050 Al-1110 çelik-1050 Al tabakalı kompozitin kesit mikro yapısı

#### B. SERTLİK SONUÇLARI

Şekil 5'de malzeme kesitinde yapılan sertlik taraması verilmiştir. Bu tarama neticesinde

kompozitlerin mekanik olarak farkları net bir şekilde görülmektedir. Orijinal durumda Al alaşımı ve çeliğin sertlikleri sırasıyla 46HV ve 120HV'dir. Birleşme ara yüzeyine yakın bölgelerde Al alaşımının sertliği 50HV ve çeliğin sertliği 150HV değerlerinde olup, Al alaşımının sertliğinde %10 ve çeliğin sertliğinde %25 oranında bir artış gözlemlenmiştir. Sertliklerdeki bu artış patlama işlemi sırasında Al ve çeliğin soğuk plastik deformasyona uğramasından kaynaklandığı düşünülmektedir [1].



Şekil 5. İncelenen kompozitin sertlik deneyi sonuçları

#### C. AKMA VE ÇEKME SONUÇLARI

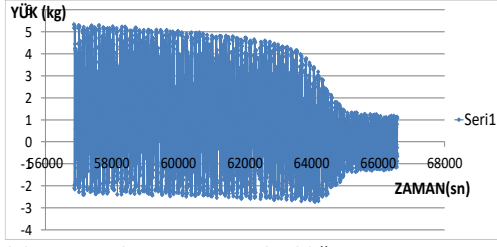
Tablo 1'de incelenen kompozitin çekme deneyi sonrası elde edilen akma ve çekme mukavemeti değerleri verilmiştir. Bu tablodan görüleceği üzere yoğunluğu 2,64 gr/cm<sup>3</sup> olan 1050 alüminyum ve yoğunluğu 7,75 gr/cm<sup>3</sup> olan 1110 çelik malzemeden üretilen kompozit malzeme 3,38 gr/cm<sup>3</sup> gibi düşük yoğunluğuna rağmen yüksek bir mukavemet sergilemektedir [3].

Tablo 1. İncelenen kompozitin mukavemet değerleri

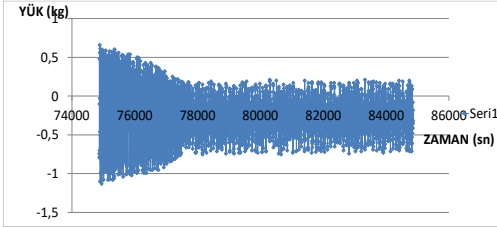
Malzeme	Akma Mukavemeti (MPa)	Çekme Mukavemeti (MPa)
1050	90	115
1110	250	340
<b>Kompozit</b>	<b>145</b>	<b>195</b>

#### D. YORULMA SONUÇLARI

Belirli bir yer değiştirme miktarına karşılık zaman ile ölçülen yük grafiği Şekil 6-7'de verilmiştir. Şekillerden gözlendiği gibi yorulma deneyleri sırasında önce 1050 kalite Al sac malzemesi hasara uğramakta olup, ardından 1110 kalite çelik malzemesi kırılarak ayrılmıştır. Test başlangıcında kompozit malzeme +5,5/-2,5 kg yük aralığında çevrimsel zorlamaya maruz kalmakta iken, kompozitin alüminyum bileşeni kırıldığında zamana karşılık okunan yük çevrimi +0,7/-1,2 kg'dır. Diğer yüklemeler için de çevrim sayıları ölçülmüştür.

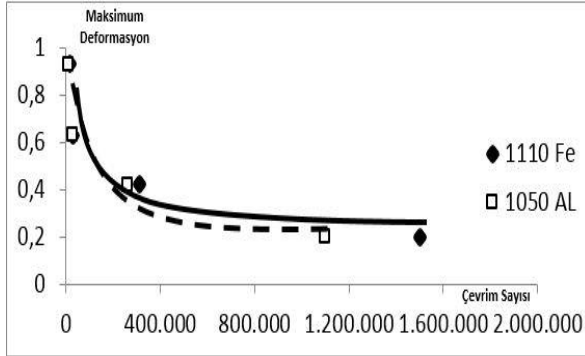


Şekil 6. 1050Al numunesinin kırıldığı anını gösteren Yük (kg)-Zaman (sn) grafiği



Şekil 7. 1110Fe numunesinin kırıldığı anını gösteren Yük (kg)-Zaman (sn) grafiği

İncelenen kompozitin yorulma deneyleri sonrası elde edilen S-N (Wöhler) eğrisi Şekil 8'de gösterilmiştir.



Şekil 8. İncelenen kompozitlerin S-N eğrisi

Bu diyagram, farklı sabit gerilmeler altında malzemenin kaç çevrim sonunda çatlayacağını veya kırılacağını gösteren bağıntıyı verir. Şekil 8'in üzerinde kesikli çizgi kompozitin alüminyum bileşenin kırıldığı çevrimi gösterirken düz çizgi ise kompozitin çelik bileşenin kırıldığı çevrim sayısını verir. Test başlangıcında kompozit malzeme +5,5/-2,5 kg yük aralığında çevrimsel zorlamaya maruz kalmakta iken kompozitin alüminyum bileşeni kırıldığında zamana karşılık okunan yük çevrimi +0,7/-1,2 kg'dır.

#### REFERANSLAR

- [1] Prof. Dr. Selahaddin ANIK Yrd. Doc. Dr. Murat VURAL Özel kaynak yöntemleri (İTÜ MAKİNA FAKÜLTESİ)
- [2] Mustafa ACARER Patlamalı kaynakta patlayıcı oranı ara boşluk mesafesi altlık cinsinin çelik/çelik birleştirilmesi kalitesini etkisi (SAKARYA ÜNİVERSİTESİ-MAKİNE EĞİTİMİ)
- [3] Yakup KAYA Patlamalı kaynak yöntemi ile üretilen grade a gemi sacı-paslanmaz çelik kompozitlerin mikroyapı, mekanik ve korozyon özelliklerinin incelenmesi (KARABÜK ÜNİVERSİTESİ)

## Failure Analysis of Adhesively Patch Repaired Composite Plates

Abdullah ÇELİK<sup>1</sup>, Kadir TURAN<sup>2</sup>, Yusuf ARMAN<sup>1</sup>,

<sup>1</sup>Department of Mechanical Engineering, Dokuz Eylül University, İzmir, Türkiye

<sup>2</sup>Department of Mechanical Engineering, Dicle University, Diyarbakır, Türkiye

**Abstract**— In this study, the failure analysis of adhesively-patch repaired notched composites were investigated experimentally. In the experimental study, eight-layered woven glass fiber reinforced epoxy resin matrix composite plates and epoxy based adhesive were used as materials. Notch types variations, double side repair and single side repair were used as a parameter. The composite plates and patches were used from same materials and the fiber reinforced angle and layer arrangement was taking as  $[0^0]_8$ . Four notch types were used in the experimental study. Double side patch application on edge notched samples have more increasing strength comparing to double side application on central notched samples.

**Keywords**— **Laminar composite plates, progressive failure analysis, repair with patch and adhesive.**

### I. Giriş

This template, modified in MS Word 2007 and saved as a Günümüzde artan malzeme ihtiyacı ve azalan kaynaklardan ötürü malzeme talebini karşılamak amacıyla, gelişen teknolojiyle uyumlu yeni malzemelerin keşfine ihtiyaç duyulmuştur. Farklı malzemelerin istenilen özelliklere uyacak şekilde bir araya getirilmesiyle elde edilen kompozit malzemeler günümüz ihtiyaçlarını tam olarak karşılamaktadır. Çünkü kompozitler sınırsız taleplere sınırsız üretim seçenekleriyle cevap vermektedir. Kompozit malzemeler; güçlü, sert fiberlerin daha zayıf ve daha az katı matris malzemeler içerisinde sıkıca sarılmasıyla elde edilir. Bu birleşim sonucunda güçlü, sert ve sıklıkla düşük yoğunlukta yapılar oluşur.(1)

Kompozitler istenmeyen dış etmenlerden kaynaklı veya yapı elemanı olabilmek için çentiklere maruz kalabilir. Çentikler gerilme yığılması gibi büyük bir problemi de beraberinde getirir. Çentik geometrisi ve kompozitlerin fiber takviye açıları hasar oluşumunda en belirleyici etkenlerdendir. Soutis ve Hu (1997) yama ile tamir edilmiş

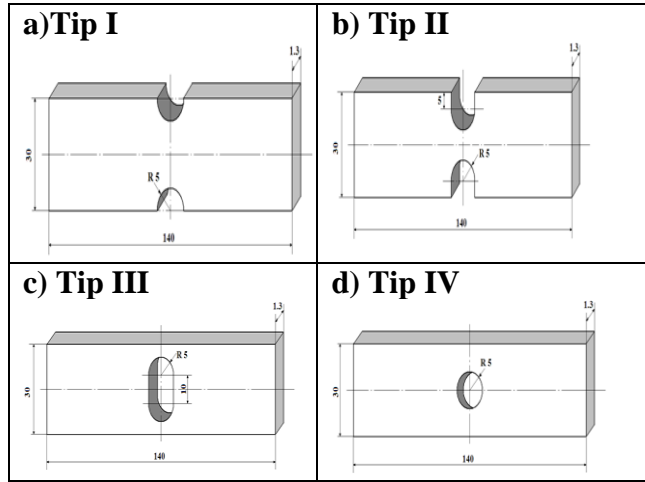
kompozit levhaların basma yükü altında mekanik davranışlarını incelemişlerdir. Kritik bağlantı parametrelerini belirlemek için çift tesirli bağlantı üzerinde lineer olmayan gerilme analizi uygulamışlardır. Yapmış oldukları deneysel ve sayısal çalışmalar sonucunda, tamir edilmiş hasarlı kompozit levhaların mukavemetinin sağlam kompozit levhaların mukavemetine % 80 oranında yaklaştığını gözlemlemişlerdir. (2) Charalambides ve ark. (1998) dış kısımdan yama ve yapıştırıcı kullanılarak tamir edilmiş kompozit levhaların hasar davranışlarının dış etmenlere bağlı analizini deneysel ve sayısal yöntemlerle gerçekleştirmişlerdir. Hem yapıştırıcı hem de kompozit levhalar için lineer elastik ve lineer elastik-plastik olmak üzere iki farklı model kullanmışlardır Lineer elastoplastik modelin lineer elastik modelden hasar tahmini için daha doğru sonuç verdiğini görmüşlerdir. Yapmış oldukları çalışmayla deneysel ve sayısal hasar tiplerinin hasar yüklerini tespitinde benzer sonuçlar verdiklerini ortaya koymuşlardır. (3) Charalambides ve ark. (1998) epoksi film (redux319) yapıştırıcı kullanılarak yapılandırılmış karbon fiber takviyeli epoksi reçineli levhaların (T300/914) tamir bağlantılarını statik ve yorulma yükleri altında çalışmışlardır. Tamir bağlantıları 50 C0'de 16 ay süresince damıtılmış suda bekletilmiş ve sıcak/nemli çevrenin statik ve yorulma mukavemetleri üzerindeki etkileri incelenmiştir. Bu çalışmada uygulanan parametrelerin tamir edilmiş kompozit levhaların statik çekme mukavemetleri üzerine büyük bir etkisinin olmadığı tespit edilmiş fakat hasar tiplerinde değişimler gözlenmiştir. (4) Her ve ark. (1999) tek ve çift tesirli yapışma bağlantılarının hasar davranışlarını araştırmışlardır. Tek ve çift tesirli yapıştırıcı bağlantısını modellemek için basitleştirilmiş tek boyutlu bir yaklaşım geliştirilmiştir. Basit bir sayısal çözüm elde edilmiş ve iki boyutlu sonlu eleman sonuçlarıyla karşılaştırılmıştır. Sonuçların uyumlu olduğu görülmüştür. Kullanılan yaklaşımın basit ama doğru sonuçlar veren bir yaklaşım olduğu, bundan dolayı bağlantı türünün seçimi için çok önemli olduğu vurgulanmıştır. (5) Achour ve ark. (2003) yanal yarım daire çentikli kompozitlerin boron epoksi yama ile tamirini gerilme yığılmalarını azaltmaya yönelik çalışmışlardır. Yapıştırıcı özelliklerinin çentik uç kısımlarında gerilme yığılması üzerindeki etkileri incelenmiştir. Yapıştırıcı özelliklerinin yama tamirinin performansını arttırmada büyük bir etken olduğu belirtilmiştir. Yapıştırıcı seçimi gerilmeyi yamaya taşıyacak ve yapıştırıcı seviyesindeki gerilmeyi arttırmak için

adhezyon hasarından kaçınacak şekilde olması gerektiği vurgulanmıştır (6)

Bu çalışmada tek ve çift yüzünden tamir edilmiş merkezi çentikli ve kenar çentikli kompozit levhaların hasar davranışları deneysel olarak çalışılmıştır. [0o]8 cam fiber takviyeli epoksi matrisli kompozit levhalar çekme yükü altında incelenmiştir. Geometrik parametre olarak dört farklı çentik tipi, tek ve çift yüzünden yama işlemi seçilmiştir. Yapılan deneyler sonucunda merkezi çentik tipinin yamasız ve yama tamiratlı numunelerinin çekme mukavemet değerlerini çok fazla etkilediği görülmüştür.

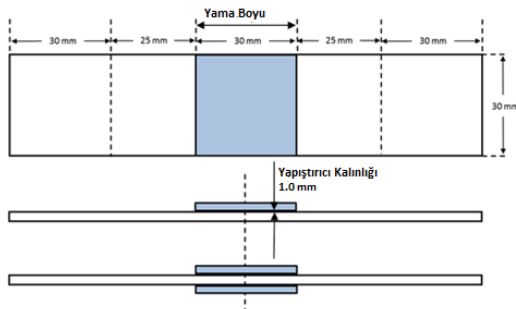
## II. DENEYSEL ÇALIŞMA

Deneysel çalışmada örgülü cam elyaf takviyeli epoksi matrisli reçineli 180 mm uzunluğunda ve 30 mm genişliğinde kompozit levhalar kullanılmıştır. Hasarı modellemek için öncelikle levhaların merkezlerine ve kenarlarına şekil 1 'de görüldüğü gibi çentikler açılmıştır. Şekil 1 'de görüldüğü üzere çentik türlerine göre numuneler Tip1, Tip2, Tip3 ve Tip4 olarak isimlendirilmiştir



Şekil 1. Deneysel çalışmada kullanılmak üzere üretilen çentik tipleri [8,9].

Şekil 2'de deneysel çalışmada kullanılan yama işlemleri uygulanmış numuneler ve ölçüleri görülmektedir. Tek ve çift yüzünden yama işlemi TY ve ÇY olarak isimlendirilmiştir. Tamir için aynı kompozit malzemeden 30mm x 30mm boyutlarında yamalar ve epoksi esaslı yapıştırıcı kullanılmış olup yapıştırıcı kalınlığı  $T_{ha} = 1.0$  mm olarak alınmıştır. Her bir parametre için eşit koşullarda üçer adet numune üretilmiştir.

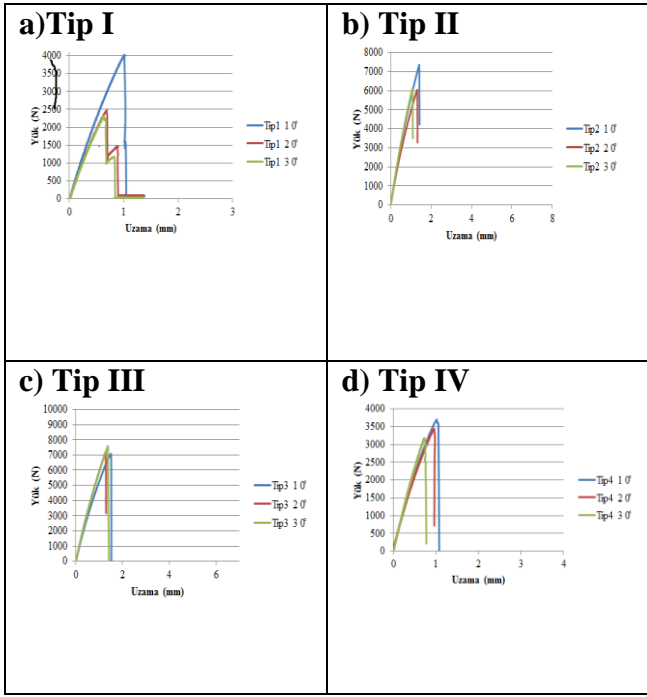


## Şekil 2. Yama uygulamaları ve problemin tanımı. [8]

Bütün numuneler uç kısımlarından çenelere sabitlenerek Şekil 3'deki 100 KN'luk instron çekme cihazıyla ASTM (1982) standartlarına göre oda sıcaklığında çekme testine tabi tutulmuştur.(7) Ortam neminin malzeme özellikleri üzerinde etkisinin olmadığı kabul edilmiştir. Çekme testi için hız 1 mm/dk uygulanmıştır. Test cihazının üstteki çenesi sabit ve alttaki çenesi hareketlidir. Numuneler bağlanırken eksenlemeye dikkat edilmiş ve çene basınçları eşit uygulanmıştır. Her bir numunenin çekme testi esnasında şekil değişimleri, soyulmaları ve kırılmaları gözlemlenmiş, yapılan gözlemler not edilmiştir. Numuneler test edilirken hasar yükleri ve yer değiştirmeler bilgisayara otomatik olarak kaydedilmiş ve bu veriler istenilen grafiklerde kullanılmıştır.

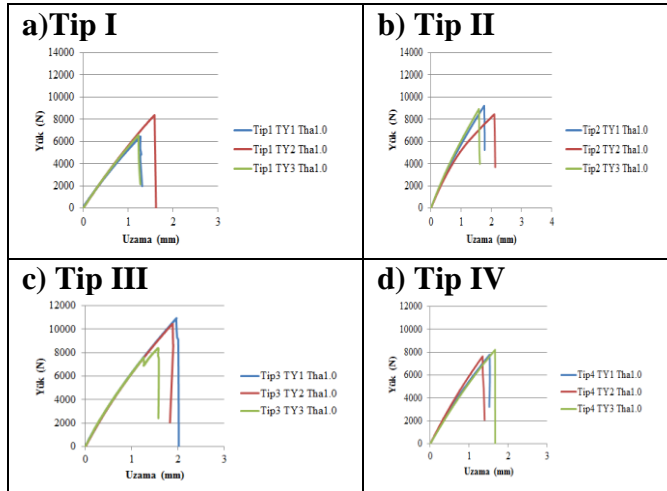


Deneysel sonuçta, tamir edilmemiş çentikli, tek yüzünden tamir edilmiş ve çift yüzünden tamir edilmiş numuneler için elde edilen yük-uzama grafikleri Şekil 4'te sunulmuştur. [0o]8 fiber takviye açılı numunelerde grafik eğrileri lineer olarak artmakta ve anlık kırılmayla levhalar hasara uğramaktadır.



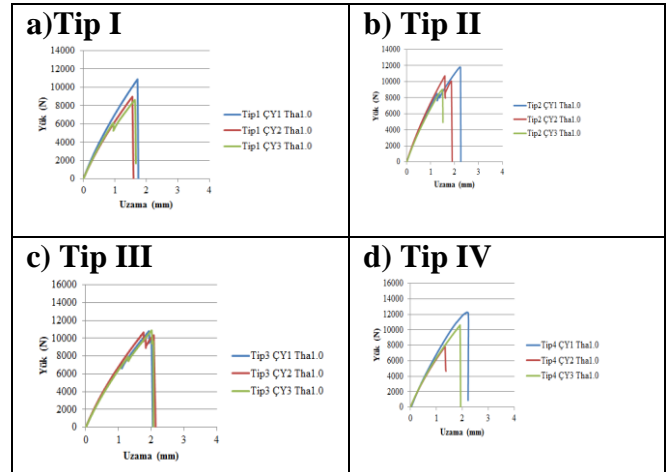
Şekil 4 . Yamasız çentikli numunelerin deneysel çalışma yük-uzama grafikleri [8,9].

Yamasız çentikli numuneler yamalı numunelere göre grafiklerde daha doğrusal bir eğim vermektedir.



Şekil 5 . Tek yüz yamalı numunelerin deneysel çalışma yük-uzama grafikleri[8,9].

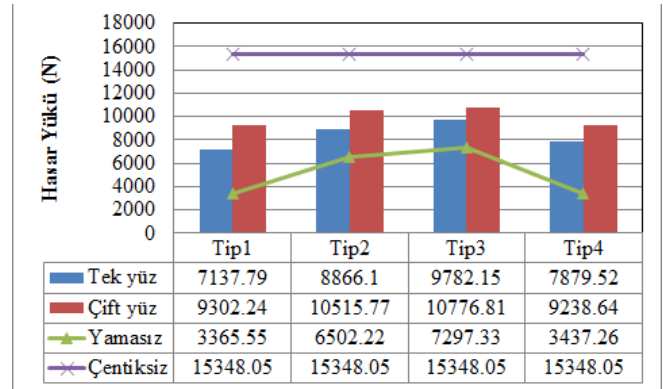
Şekil 5'te görüldüğü üzere tek yüz yama bağlantılı numunelerde kademeli kırılma gerçekleşmemiştir. Bütün tiplerde yamanın bulunduğu bölgede çekme esnasında iç bükey eğilme meydana gelmiş ve yama uçlardan soyulmaya başlayıp tamamen işlevini kaybettiği anda kırılma gerçekleşmiştir.



Şekil 6 . Çift yüz yamalı numunelerin deneysel çalışma yük-uzama grafikleri [8,9].

Şekil 6'da yer alan grafiklerden görüldüğü üzere tamir edilmemiş levhalar belirli bir yük değerinde aniden kırılarak hasara uğramıştır. Tek ve çift yüzünden tamir edilmiş levhalarda ise yüklerin belirli bir değerinde yükler aniden düşüş gösterdikten sonra tekrar yükselmeye devam etmektedir. Deneyin başlaması ile birlikte yama ve levha arasındaki yük transferi yapıştırıcı üzerinden gerçekleşir. Yükün belirli bir değere ulaşması ile yapıştırıcı hasara uğradığı için yükler düşer fakat henüz levha kırılmamış olduğu için yükler artmaya devam eder ve belirli bir yük değerine ulaşıldığında levha ile yapıştırıcı hasara uğrar. Levha kırıldığı içinde yükler aniden düşüş gösterir.

### III. SONUÇLAR VE TARTIŞMA



Şekil 7. [0o]8 Tip1,2,3,4 tek yüzünden ve çift yüzünden tamir işleminin hasar yükü üzerine etkisi grafiği [8,9].

Şekil 7'de çentikli numunelere yama uygulamalarının hasar yükü olarak etkileri görülmektedir. En büyük hasar yükü değeri Tip3 çift yüz yama uygulaması için 10776.81 (N) olarak ölçülürken en düşük hasar yükü Tip1 tek yüz yama uygulaması için 7137.79 (N) olarak ölçülmüştür.

Tamir Tipi	Karşılaştırma	Çentik Tipi			
		Tip1	Tip2	Tip3	Tip4
Tek yüzünde n tamir edilmiş	Çentiksiz Levhaya göre	-% 53	- %42	- %36	-%48
	Çentikli Yamasız Levhaya göre	+% 112	+%3 6	+%3 4	+% 12 9
Çift yüzünde n tamir edilmiş	Çentiksiz Levhaya göre	-% 39	- %31	- %29	-%39
	Çentikli Yamasız Levhaya göre	+% 17 6	+%6 1	+%4 7	+% 16 8

**Tablo 8.** [0o]8 Tip1,2,3,4 tek yüzünden ve çift yüzünden tamir edilmiş levha için elde edilen hasar yükleri artış oranları tablosu. [8,9].

Tablo 8'de tek yüz yama tamiratında çentiksiz levhalara kıyasla hasar yükünde en büyük düşüş oranı Tip1 çentik türü tek yüz yama uygulaması için %53 olarak ölçülürken en küçük düşüş oranı Tip3 çentik türü tek yüz yama uygulaması için % 36 olarak ölçülmüştür. Tek yüz yama tamiratında çentikli levhalara kıyasla hasar yükünde en büyük artış oranı Tip4 çentik türü tek yüz yama uygulaması için %129 olarak ölçülürken en küçük artış oranı Tip3 çentik türü tek yüz yama uygulaması için %34 olarak ölçülmüştür.

Çift yüz yama tamiratında çentiksiz levhalara kıyasla hasar yükünde en büyük düşüş oranı Tip1 ve Tip4 çentik türü çift yüz yama uygulaması için %39 olarak ölçülürken en küçük düşüş oranı Tip3 çentik türü tek yüz yama uygulaması için % 29 olarak ölçülmüştür. Çift yüz yama tamiratında çentikli levhalara kıyasla hasar yükünde en büyük artış oranı Tip1 çentik türü çift yüz yama uygulaması için %176 olarak ölçülürken en küçük artış oranı Tip3 çentik türü tek yüz yama uygulaması için %47 olarak ölçülmüştür.

#### IV. DEĞERLENDİRMELER

- Levhalara açılan çentikler çentiksiz levhalara göre %40 ile %78 arasında değişen oranlarda hasar yükünü düşürmüştür.
- Küçük boyutlu orta çentikli levhaların hasar yüklerinin küçük boyutlu kenar çentikli levhaların hasar yüklerinden büyük olduğu belirlenmiştir.

- Büyük boyutlu kenar çentikli levhaların hasar yüklerinin büyük boyutlu orta çentikli levhaların hasar yüklerinden büyük olduğu belirlenmiştir.
- Çift yüz yama uygulaması kenar çentiklerde merkezi çentiklere göre daha fazla oranda mukavemet artışı sağlamıştır.
- Tip2 ve Tip3 çentik alanı olarak eşit fakat farklı konumlarından dolayı farklı hasar yüklerine ulaşmışlardır. Tip3 merkezi çentik olduğundan bu levhaların hasar yükleri Tip2'den daha yüksektir.
- Tip1 ve Tip4 çentik türleri arasındaki ilişkinin benzeri Tip2 ve Tip3 çentik türlerinde de mevcuttur. Tip1 levha merkezinde yer alan bir çentiği gösterirken Tip4 kenarda yer alan bir çentik türünü göstermektedir. Çentik boyutları aynı olmasına rağmen Tip1 merkezi çentik olduğundan daha yüksek hasar yüküne ulaşması beklenirken tam tersi Tip4 daha yüksek hasar yüküne ulaşmıştır.

Yama bölgesinde çekmeyle beraber eğilme ve şekil değişimi başlamaktadır. Yamayı tutan yapıştırıcının işlevini tamamen yitirdiği anda yama herhangi bir hasara uğramadan yerinden çıkmakta ve kırılma sonlanmaktadır.

#### V. KAYNAKLAR

1. Mallick, P., Fiber Reinforced Composites, Department of Mechanical Engineering University of Michigan-Deaborn, Michigan, 1993.
2. Soutis, C., Zu, F.Z., Design and Performance of Bonded Patch Repairs of Composite Structures, Department of Aeronautics, Imperial College of Science, Technology and Medicine, London 1997; Proc Instn Mech Engrs Vol 211 Part 3.
3. Charalambides, M.N., Hardouin, R., Kinloch, A.J., Mathews, F.L., Adhesively-bonded Repairs to Fibre-composite Materials I: Experimental, Composites Part A 29A 1998; 1371– 1381..
4. Charalambides, M.N., Kinloch, A.J., Matthews, F.L., Adhesively-bonded Repairs to Fibre-composite Materials II: Finite Element Modelling, Composites Part A 29A 1998; 1383–1396.
5. Her, S.C., Stress Analysis of Adhesively-bonded Lap Joints, Elsevier, Composite Structures 47 1999; 673-678.
6. Achour, T., Bouiadjra, Serier, B., Numerical Analysis of the Performances of the Bonded Composite Patch for Reducing Stress Concentration and Repairing Cracks at Notch, Computational Materials Science 28 2003; 41–48.

7. ASTM-D. 3039-76, 1982.

8. YL tezi: Çelik A., Yama ve yapıştırıcı kullanılarak tamir edilmiş çentikli kompozit levhaların hasar davranışlarının araştırılması , Dicle Üniversitesi Fen Bilimleri Enstitüsü, Diyarbakır, 2015.

9. Tez yayını: Çelik, A, Turan, K. (2015). Çentikli kompozit levhaların hasar davranışlarının incelenmesi, Dicle Üniversitesi Mühendislik Fakültesi Mühendislik Dergisi, vol. 6, pp 73-82.